Supplementary Information (SI) for Dalton Transactions.
This journal is © The Royal Society of Chemistry 2024

Supporting information

Supramolecular bidentate rhodium(I) or iridium(I) phosphine and oxazoline amino acid bioconjugates as selective catalysts for enantioselective reactions

Marija Bakija[a], Saša Opačak[a], Berislav Perić,[a] Soumyadeep Chakrabortty[b], Andrea Dell'Acqua[b], Eszter Baráth[b], Johannes de Vries[b], Sergey Tin[b,*], Srećko I. Kirin[a,*]

[a] Ruđer Bošković Institute, Bijenička c. 54, HR-10000 Zagreb, Croatia
[b] Leibniz Institut für Katalyse e.V., Albert-Einstein-Straße 29A, DE-18059 Rostock, Germany

* Authors to whom the correspondence should be addressed.
(E-mail: Sergey.Tin@catalysis.de, Srecko.Kirin@irb.hr)

Table of Contents

1. Compounds synthesis schemes

1.1. Ligands

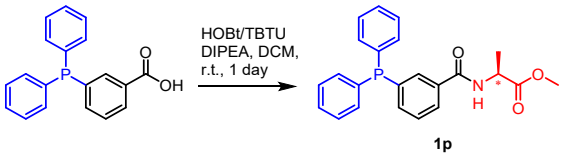

Scheme S1. Reaction conditions: (a) HOBt/TBTU, DIPEA, CH_2Cl_2, 1 day. [1]

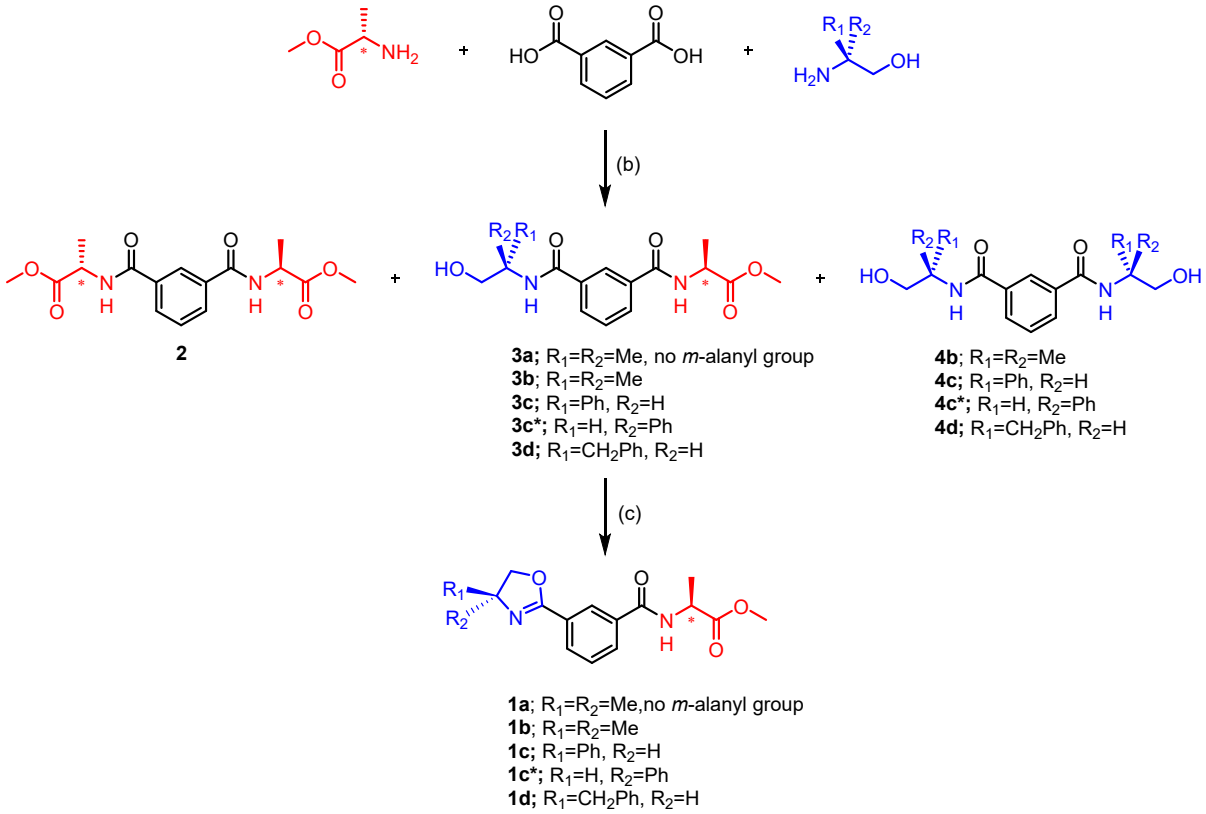

Scheme S2. Reaction conditions: (b). HATU, DIPEA, CH_2Cl_2/DMF, 2 days.[2] **1a** was obtained using HOBt/TBTU. c) DAST, dry CH_2Cl_2, K_2CO_3, -75°C (dry ice in acetone).[3]

1.2. In situ generated precatalyst complexes

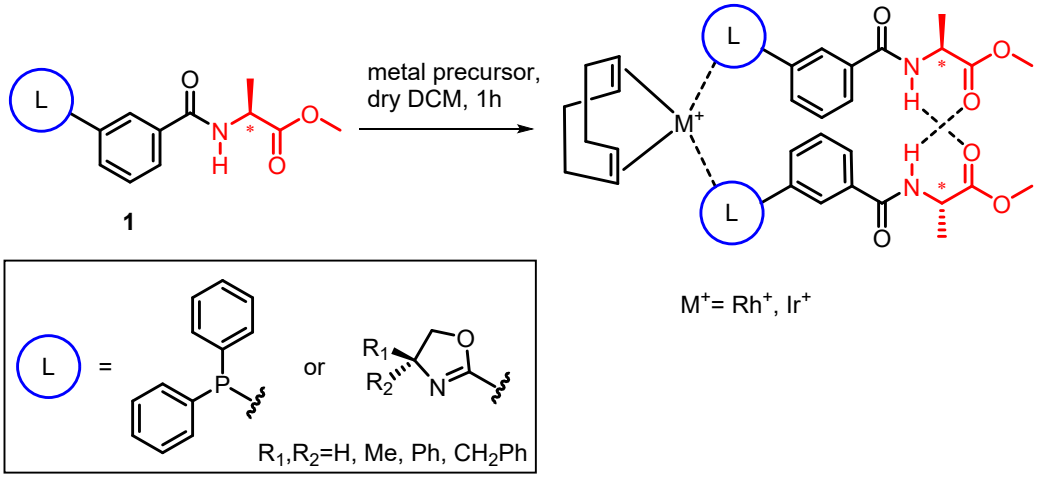

Scheme S3. Proposed structure of complexes with homo- and hetero-combinations of phosphine and oxazoline ligands, generated *in situ* from $[MCOD_2]^+$ derivatives and ligands by stirring in dry CH_2Cl_2 under argon atmosphere for 1 hr.

2. Compounds overview

2.2. Ligands

Chart S1. Types of ligands used in this publication

a) Achiral	b) Chirality placed several bonds away from the donating atom	c) Chiralities placed near the donating atom and several bonds away
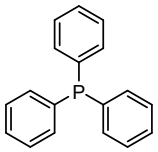 **PPh_3**	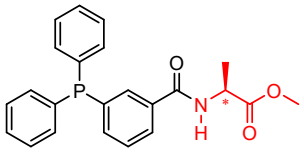 **1p**	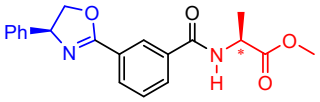 **1c**
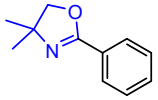 **1a**	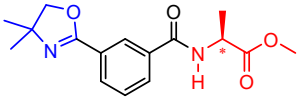 **1b**	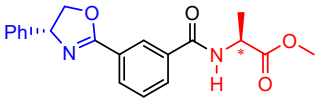 **1c*** 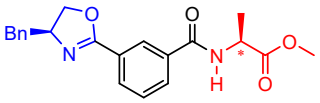 **1d**

2.2. „One pot“ products

Chart S2. One pot products obtained in this publication

	2	3	4
a		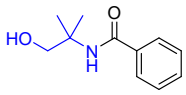 3a	
b		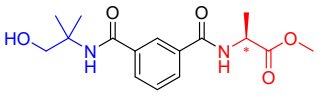 3b	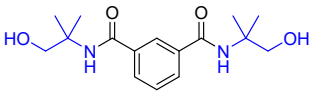 4b
c	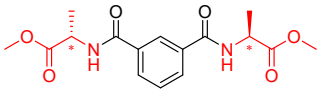 2	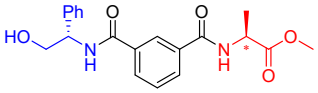 3c	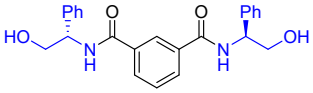 4c
c*		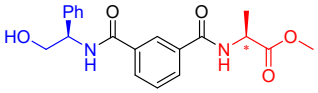 3c*	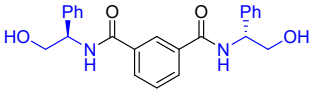 4c*
d		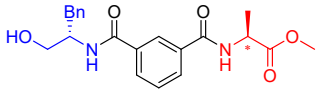 3d	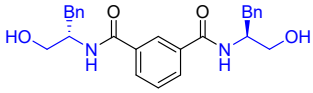 4d

2.3. Hydrogenation Substrates

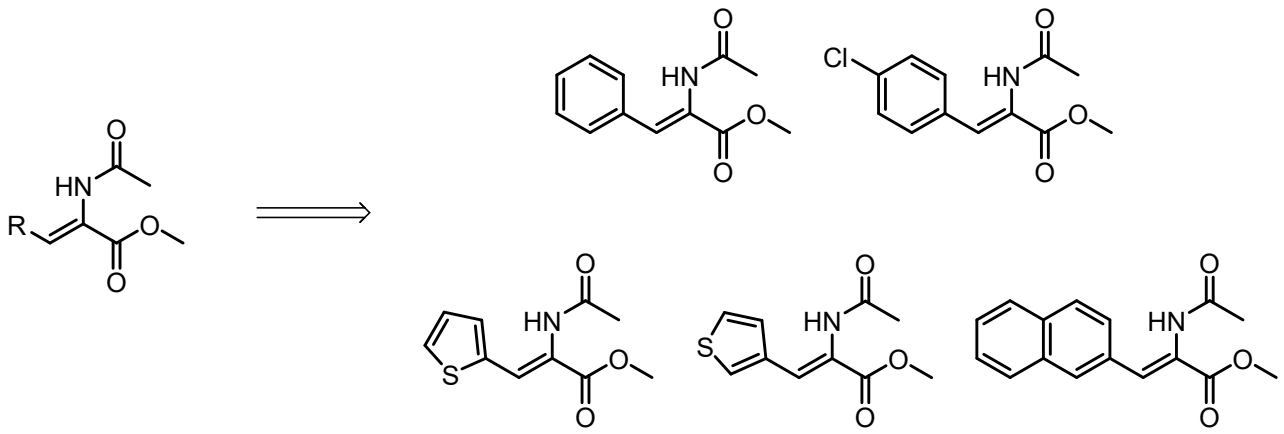

Figure S1. Dehidroamino acid substrates for hydrogenation; R = phenyl, 4-chloridophenyl, 2-thionyl, 3-thionyl or 2-naphthyl.

2.3. Hydroformylation Substrates

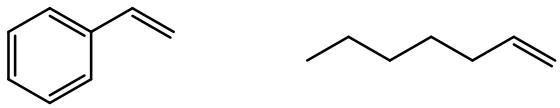

Styrene 1-octene

Figure S2. Substrates for hydroformylations; styrene, 1-octene

3. NMR Spectra

Table S1. Selected differences in ^{1}H NMR (CD_2Cl_2) peak shifts of complexed and free ligand peaks, calculated as *δ(complex) - δ(free ligand)*.

Δδ / ppm	**–N–H**	**isolated '=C–H (arom., C6H4)**	**=C–H (arom., C6H5)**	**–O–CH3**	**–CH–CH3**	**–CH2– (Ox.)**	**–CH– (Ox.)**
Rh : 1p = 1 : 2	1.18	0.1	≥ -0.18	0.08	0.04	-	-
Rh : 1p : 1c* = 1 : 1: 1	0.69 (**1p**) 0.68 (**1c***)	0.57 (**1p**) 1.90 (**1c***)	n.d.a	0.09 (**1p**) -0.01 (**1c***)	0.10 (**1p**) 0.11 (**1c***)	-0.38 0.15	-0.54
Rh : 1c* = 1 : 2	0.74	1.67	≥ -0.36	0.02	0.14	-0.77 -0.69	-1.43
Ir : 1p = 1 : 2	1.30	n.d.	≥-0.21	0.10	≤0.01	-	-
Ir : 1p : 1c* = 1 : 1: 1	≤0.47 (**1p**) ≤0.36 (**1c***)	n.d. (**1p**) 1.29 (**1c***)	n.d.	0.10 (**1p**) 0.00 (**1c***)	0.05 (**1p**) 0.07 (**1c***)	n.d.	-0.50
Ir : 1c* = 1 : 2	0.15	1.67	≥-0.33	0.08	0.12	-0.95 -0.28	-1.32

[a] not determined

3.1. Phosphorus compounds

^{1}H NMR (600 MHz, $CDCl_3$) of **Ph_2P-*m*-C_6H_4-COOH**.

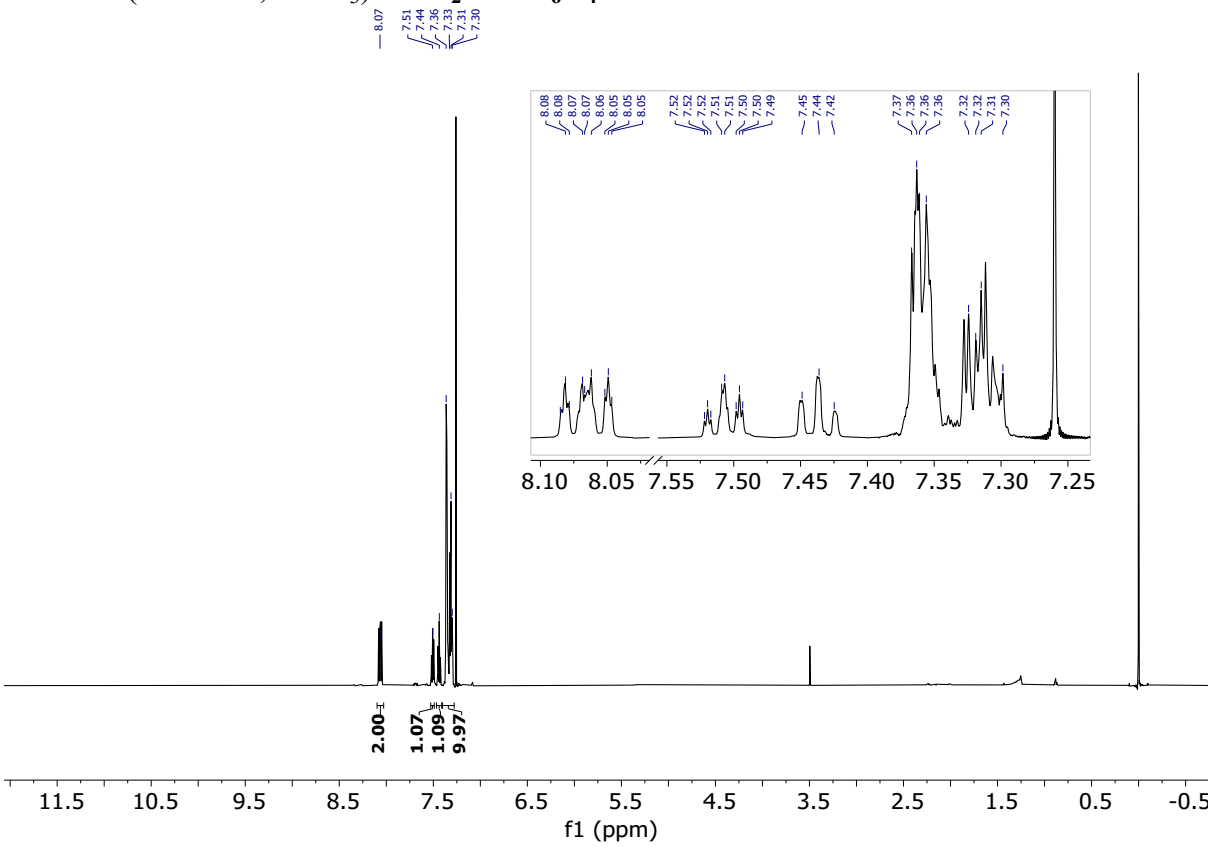

^{31}P NMR (243 MHz, $CDCl_3$) of **Ph_2P-*m*-C_6H_4-COOH.**

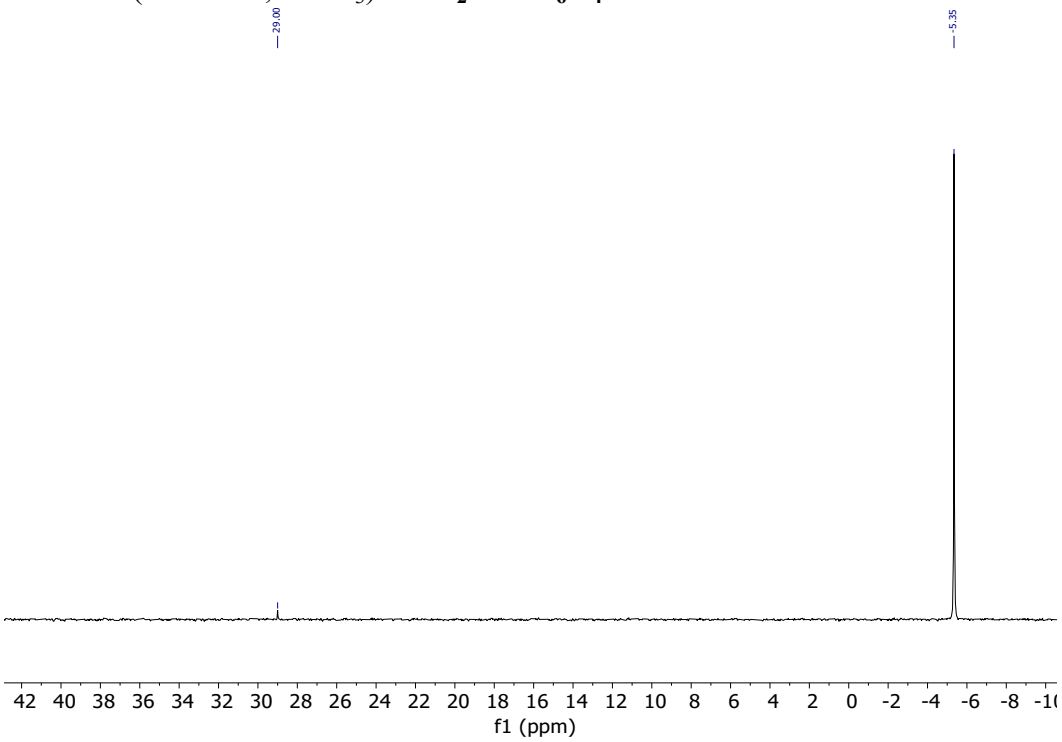

^{1}H NMR (300 MHz, CD_2Cl_2) of **Ph_2P-*m*-C_6H_4-(*S*)-Ala-OMe (1p).**

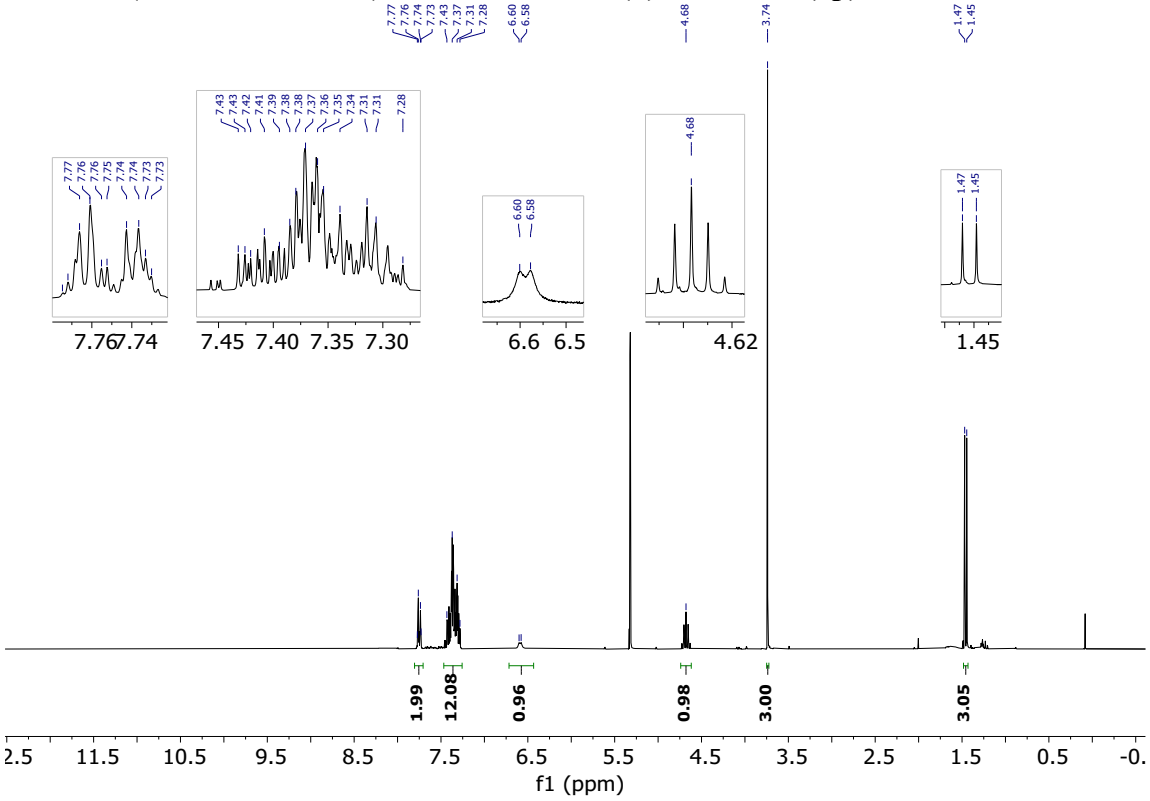

^{31}P NMR (122 MHz, CD_2Cl_2) of **1p**.

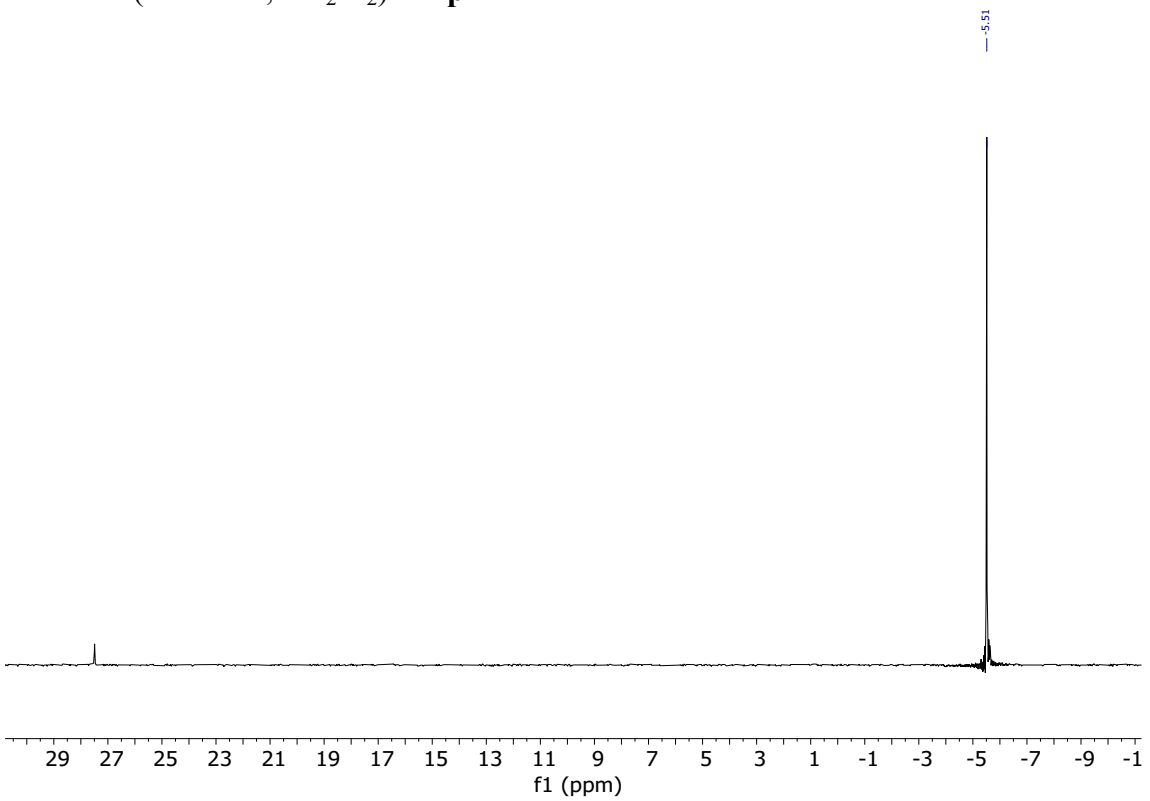

^{13}C NMR (75 MHz, CD_2Cl_2) of **1p**.

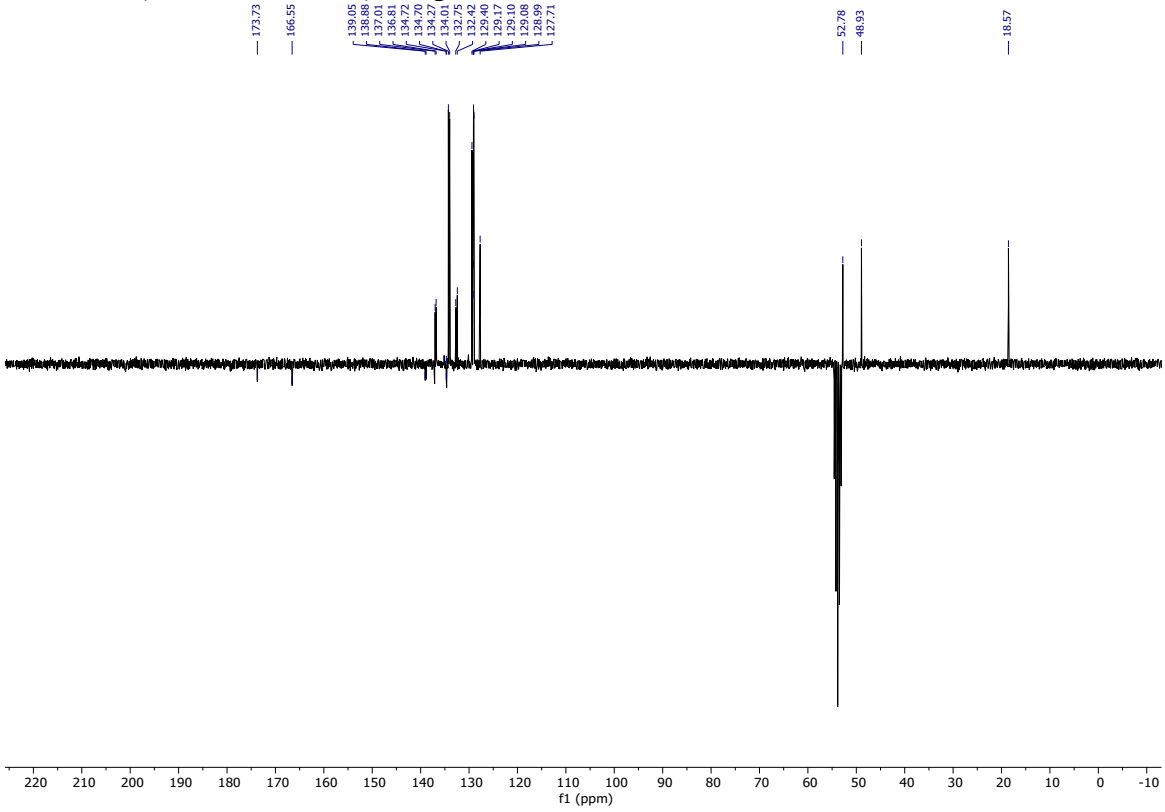

3.2. Oxazoline comounds

^{1}H NMR (300 MHz,CD_2Cl_2) of **1a**.

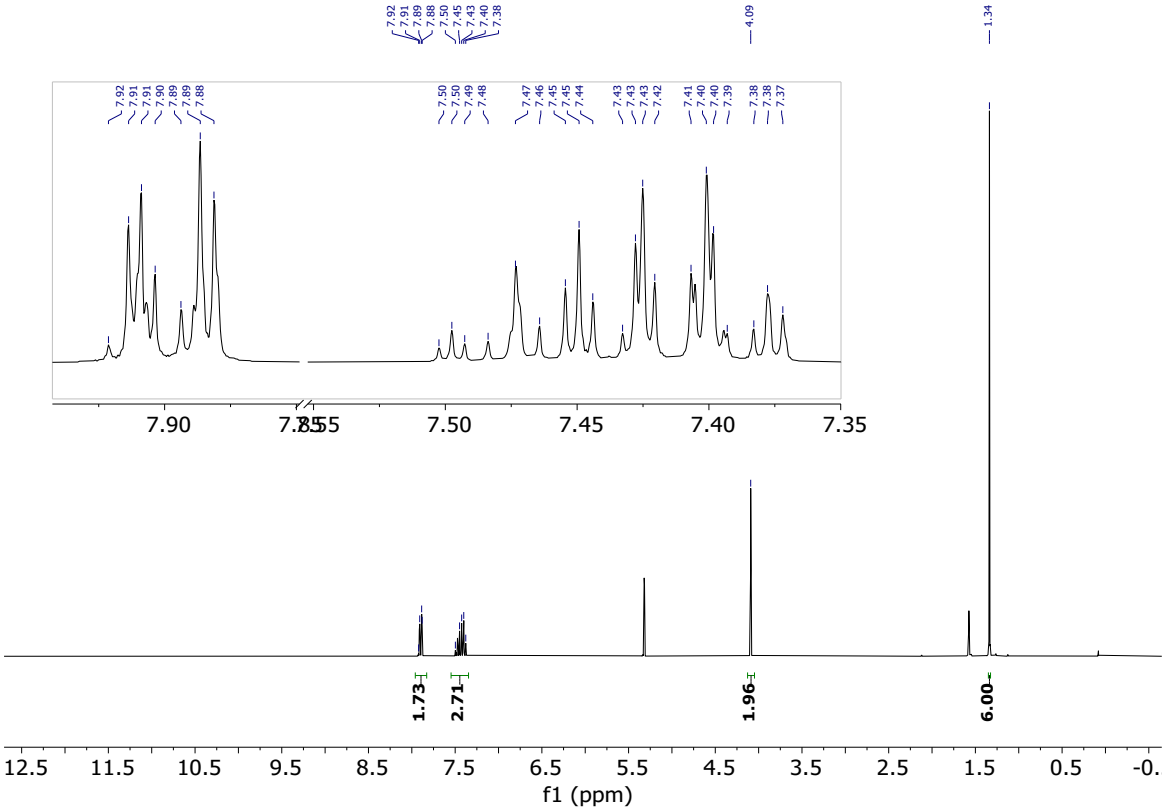

^{13}C NMR (75 MHz, $CDCl_3$) of **1a**.

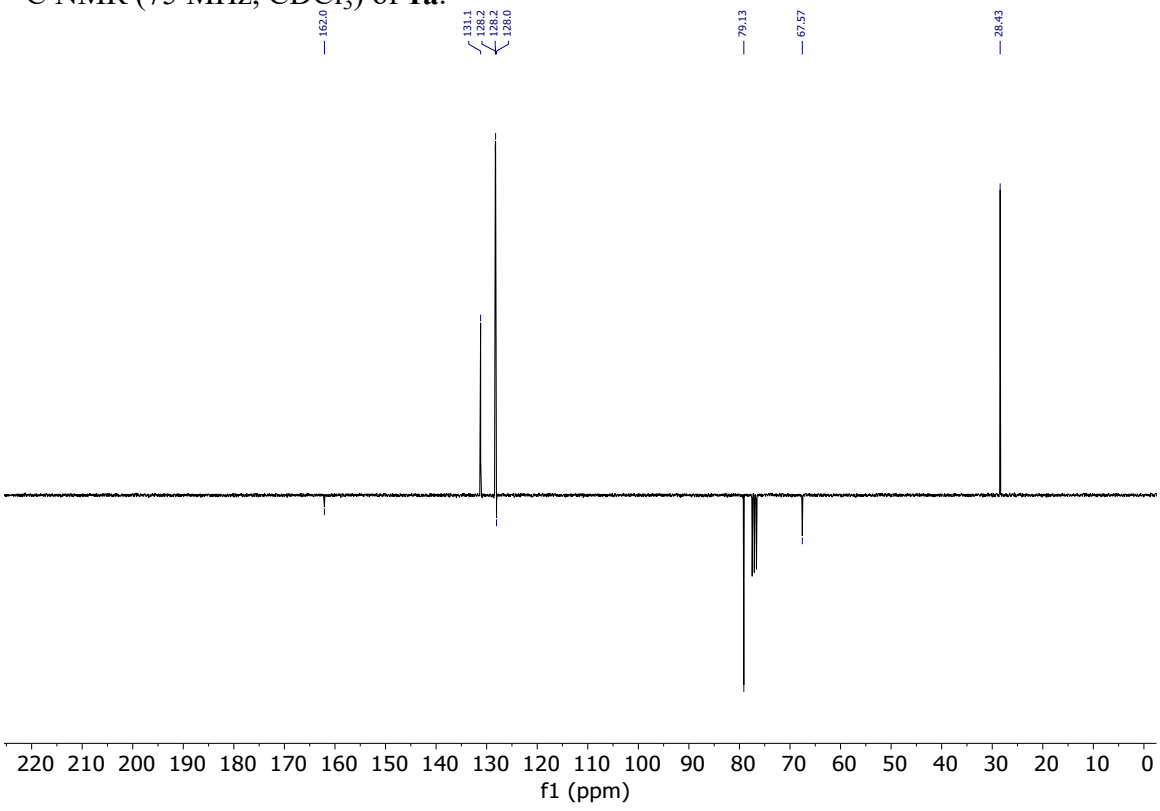

^{1}H NMR (300 MHz, CD_2Cl_2) of **1b**.

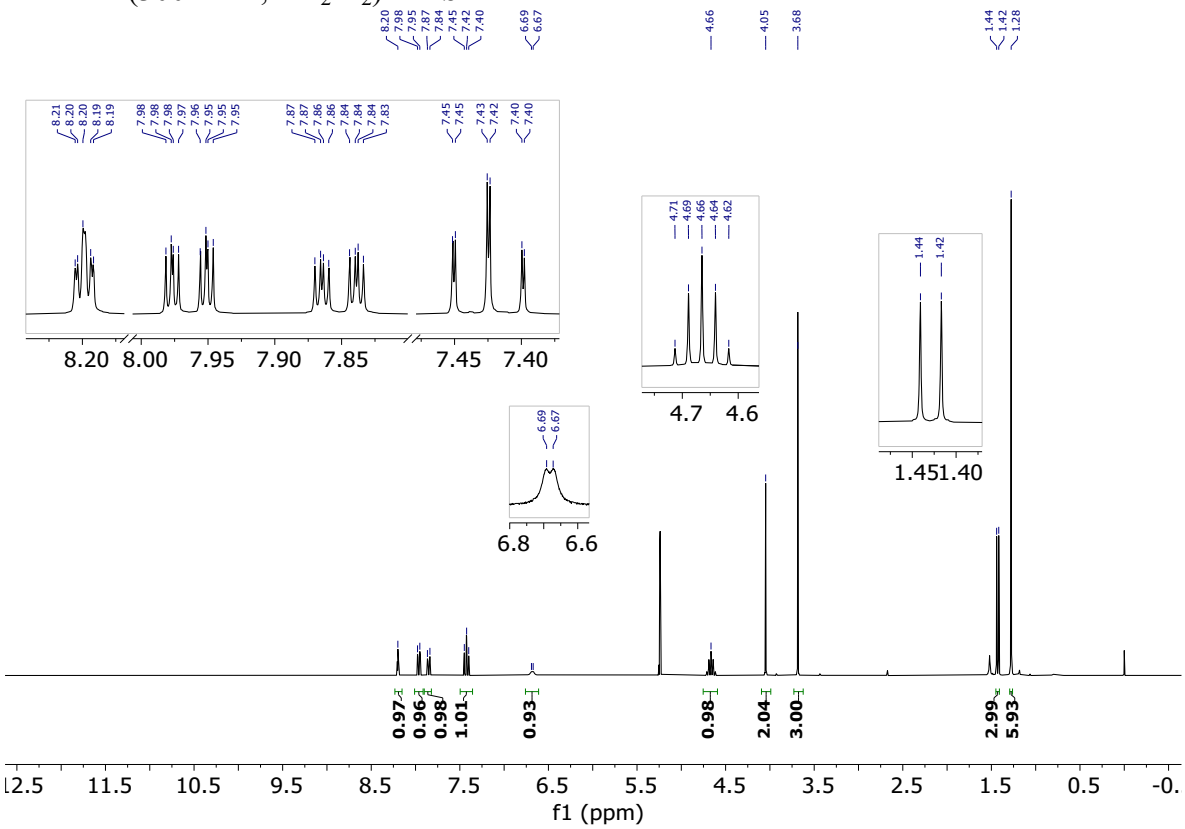

^{13}C NMR (75 MHz, CD_2Cl_2) of **1b**.

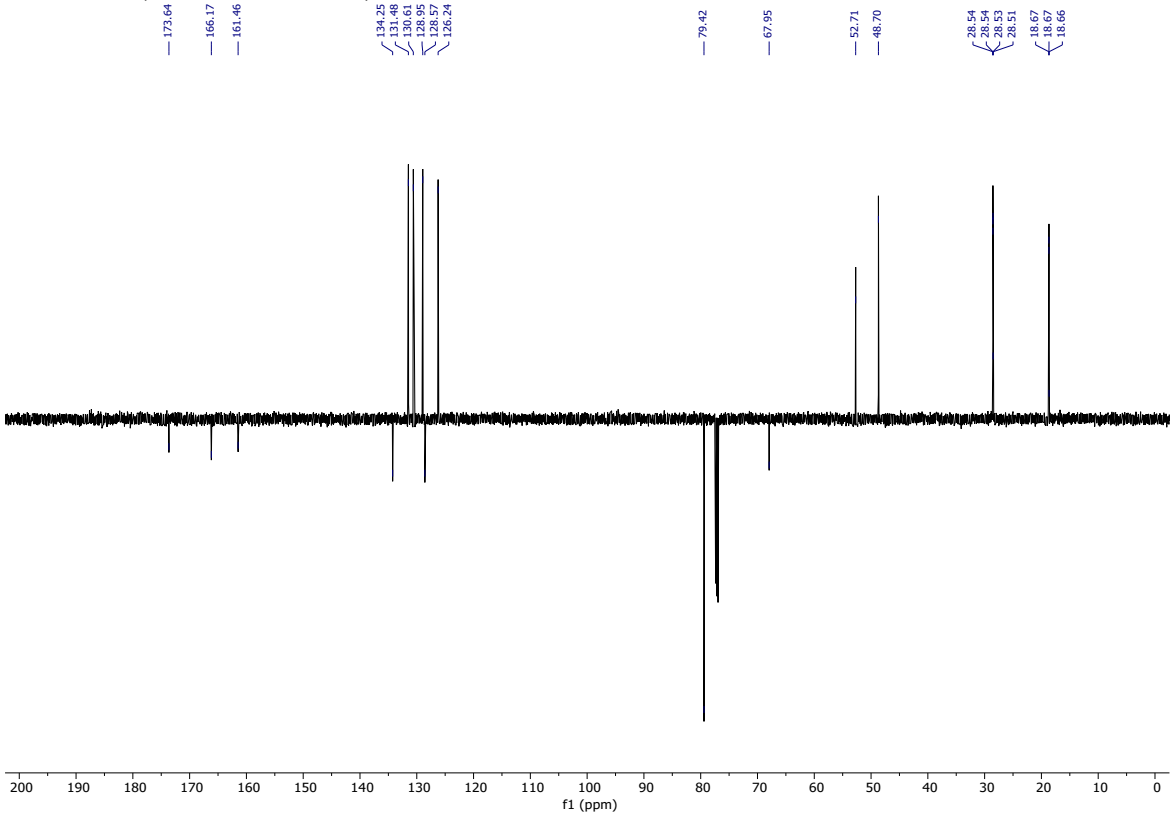

^{1}H NMR (300 MHz, $CDCl_3$) of **1c**.

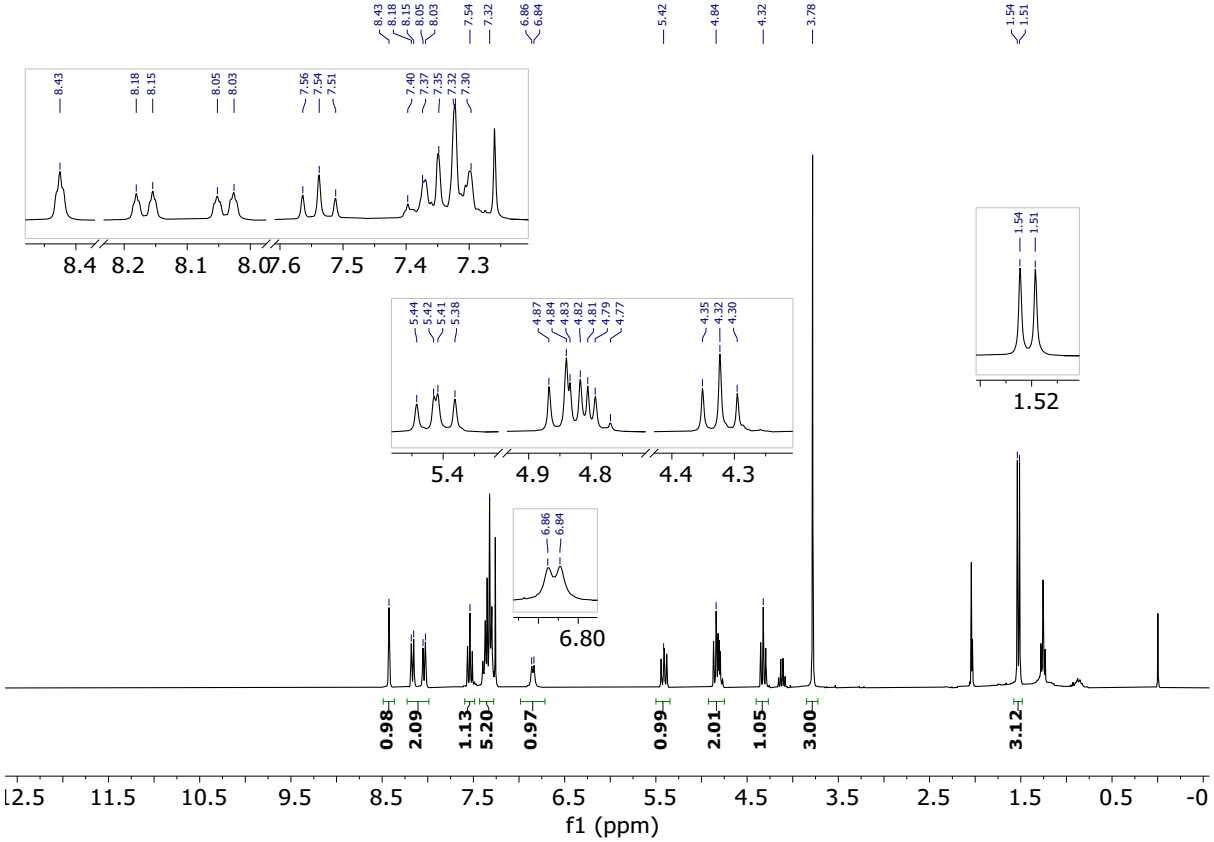

^{1}H NMR (600 MHz, CD_2Cl_2) of **1c**.

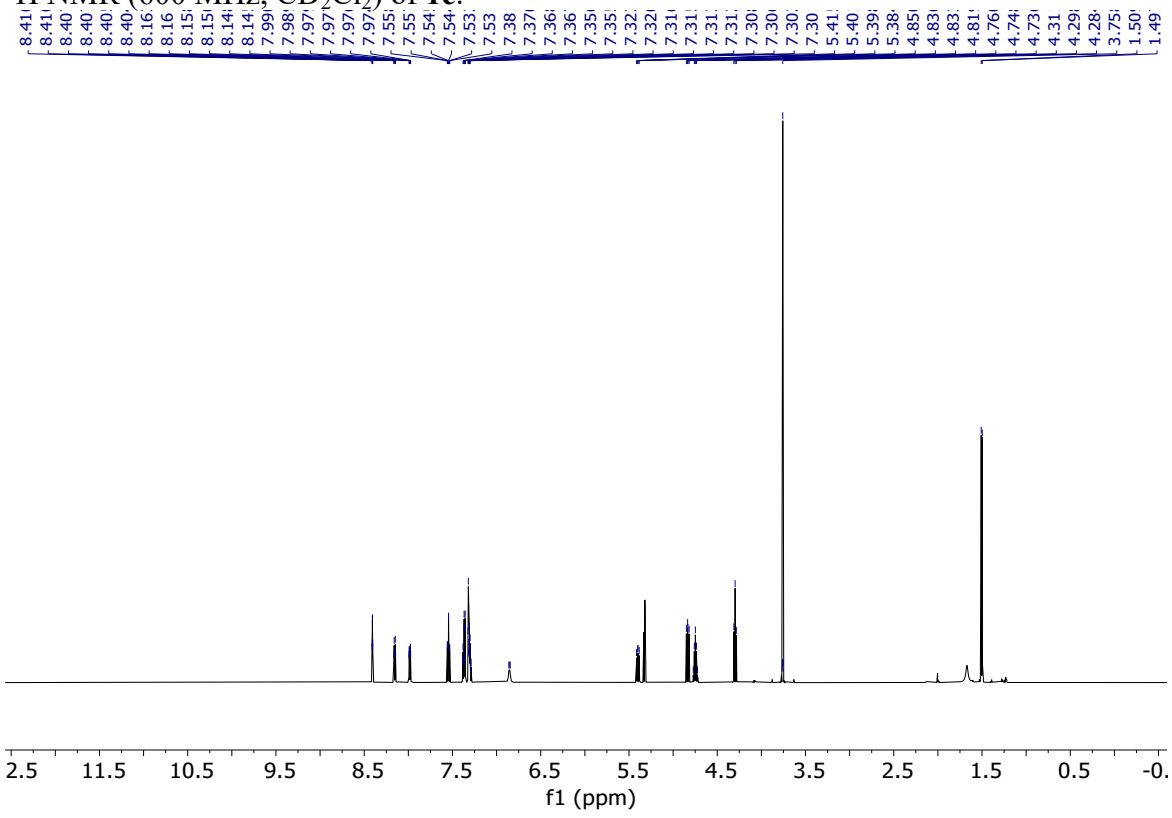

^{13}C NMR (151 MHz, $CDCl_3$) of **1c**.

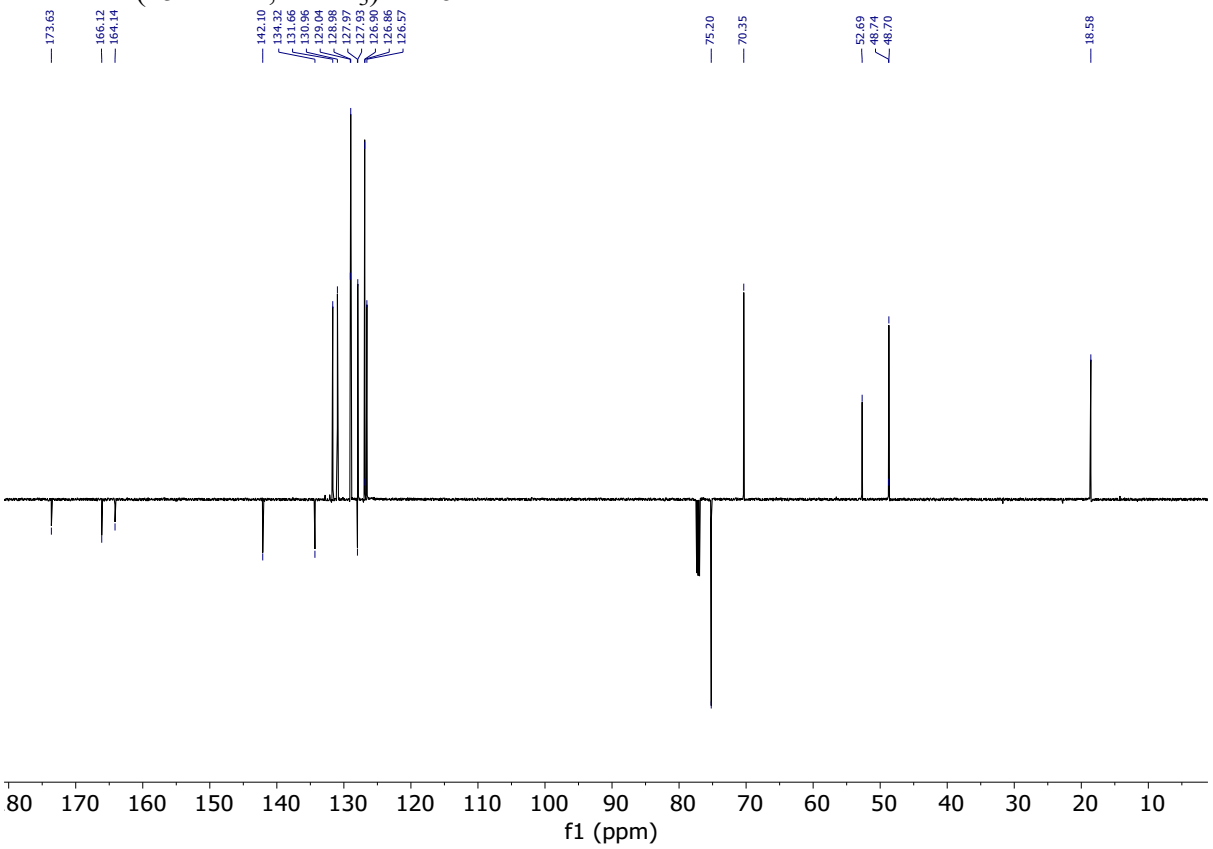

^{1}H NMR (300 MHz, $CDCl_3$) of **1c***.

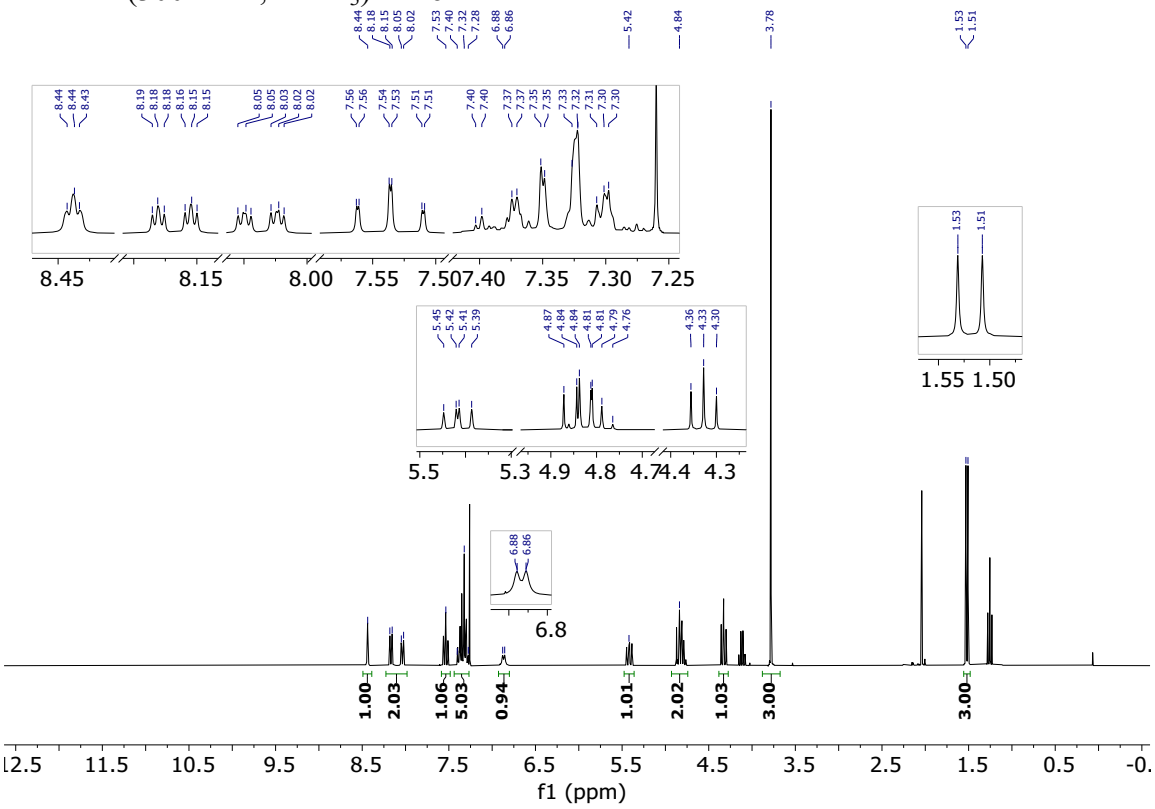

^{13}C NMR (75 MHz, $CDCl_3$) of **1c***.

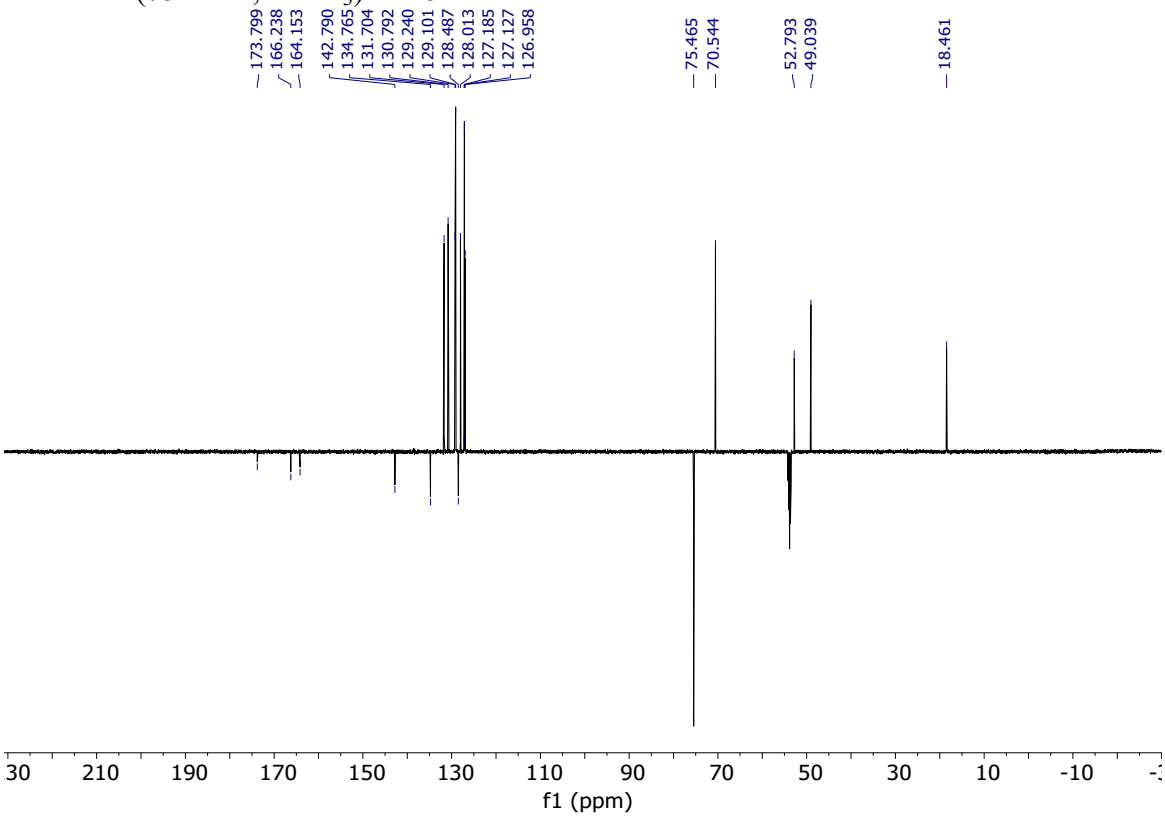

^{1}H NMR (300 MHz, $CDCl_3$) of **1d**.

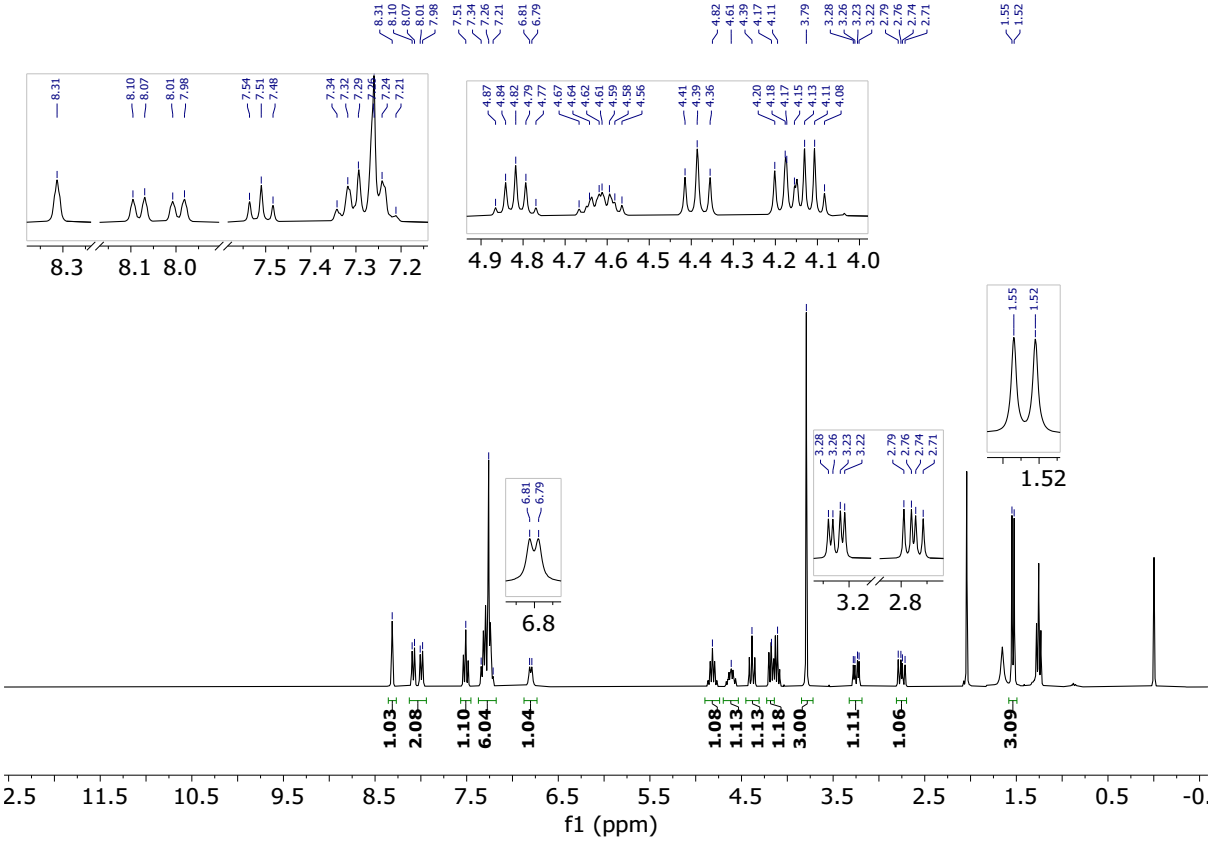

^{13}C NMR (151 MHz, $CDCl_3$) of **1d**.

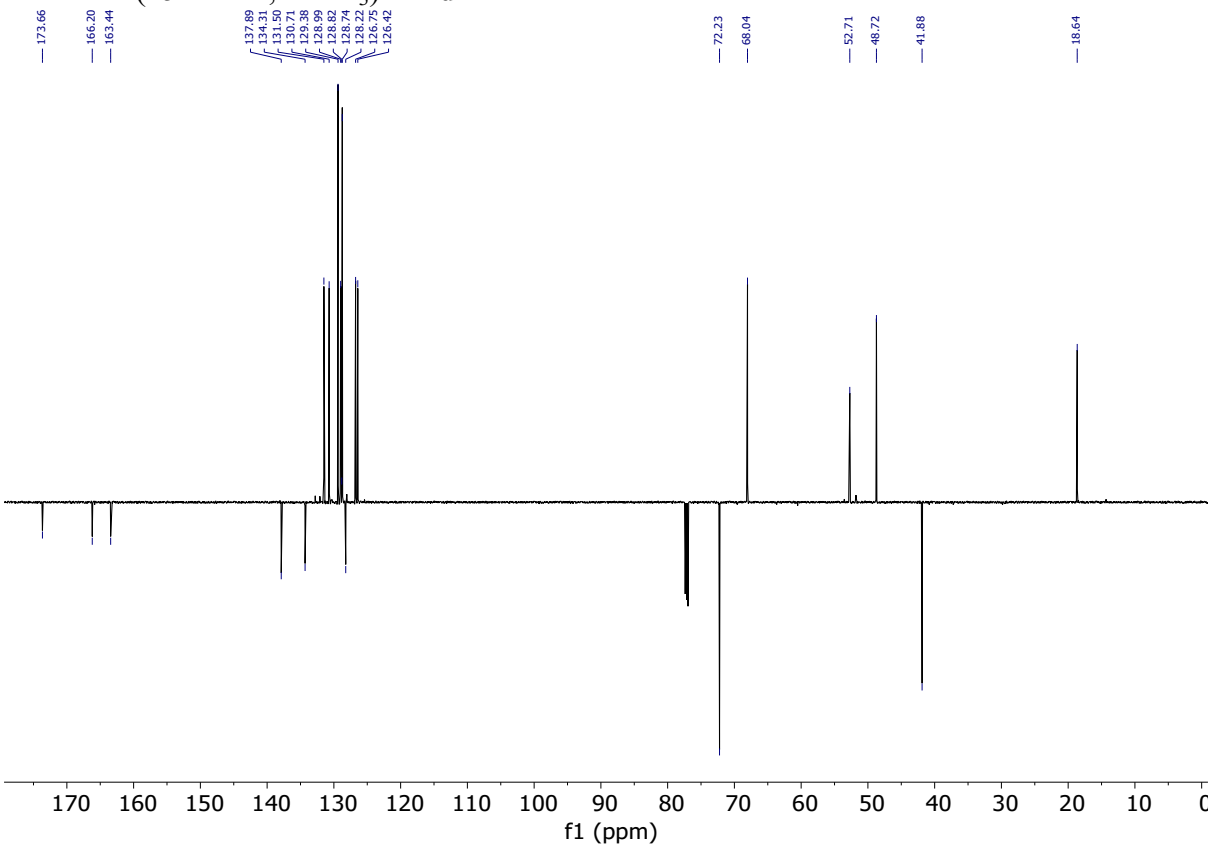

^{1}H NMR (300 MHz, $CDCl_3$) of **AMP-C_6H_5 (3a)**.

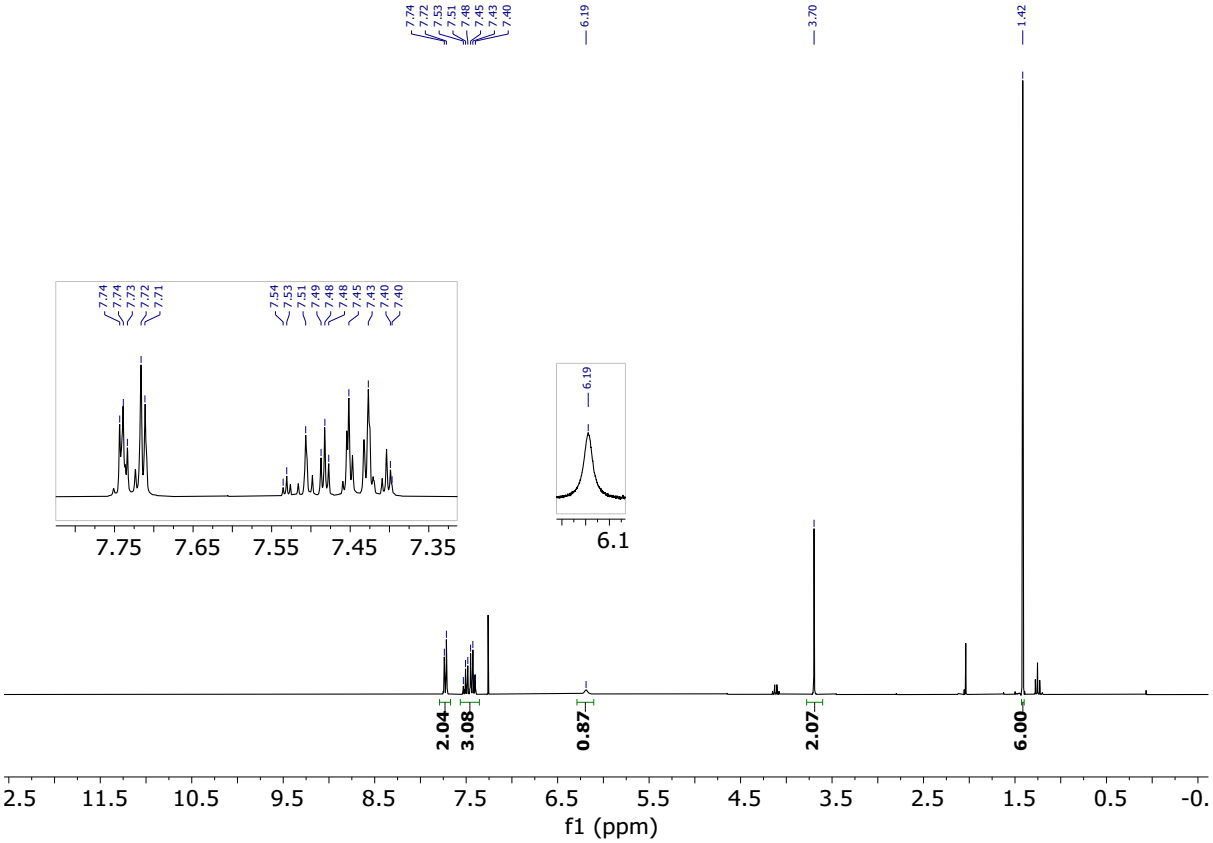

^{13}C NMR (75 MHz, $CDCl_3$) of **AMP-C_6H_5 (3a)**.

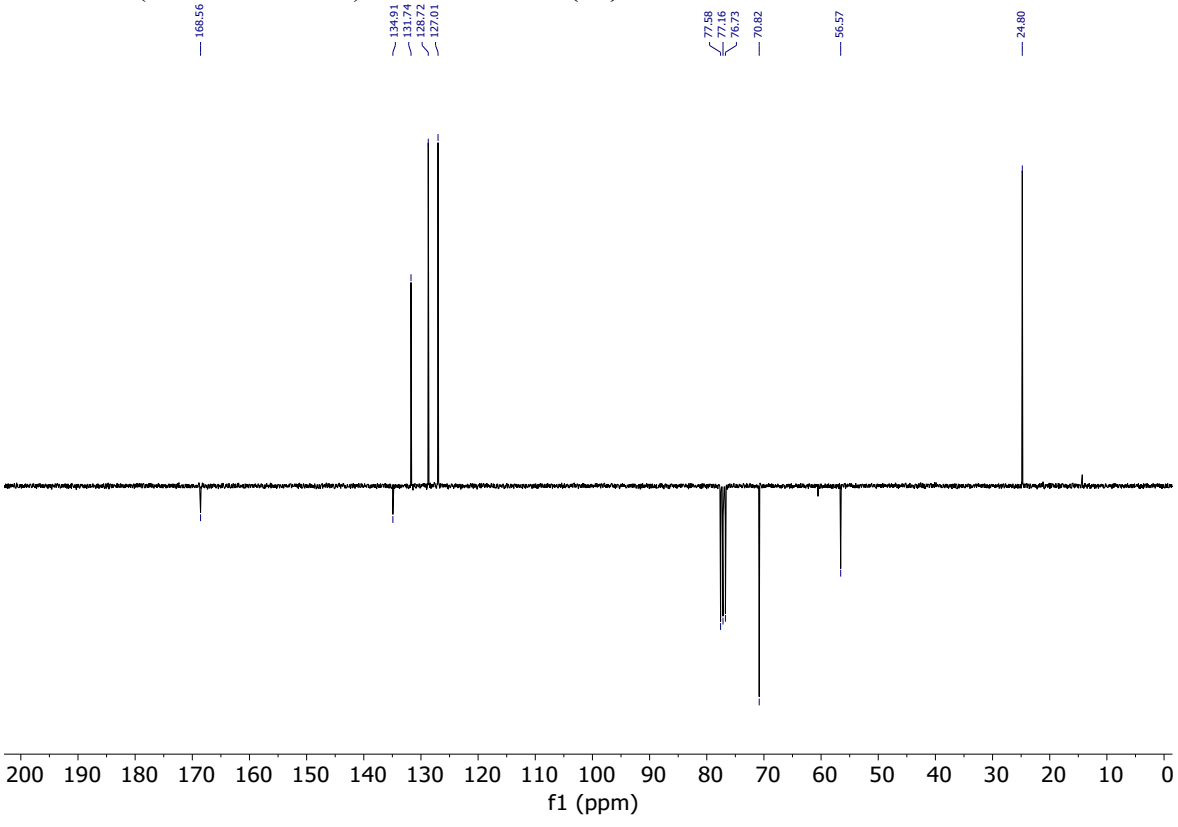

^{1}H NMR (600 MHz, $CDCl_3$) of **3b**.

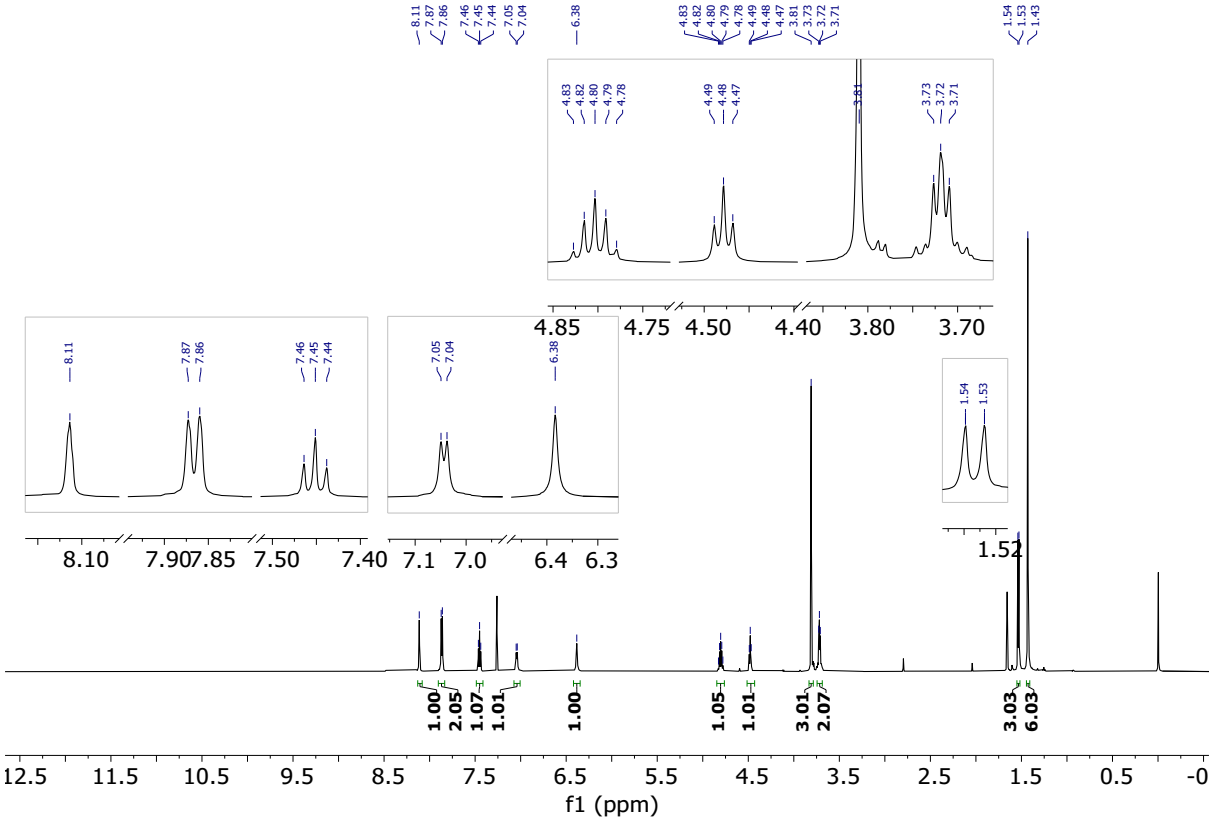

^{13}C NMR (151 MHz, $CDCl_3$) of **3b**.

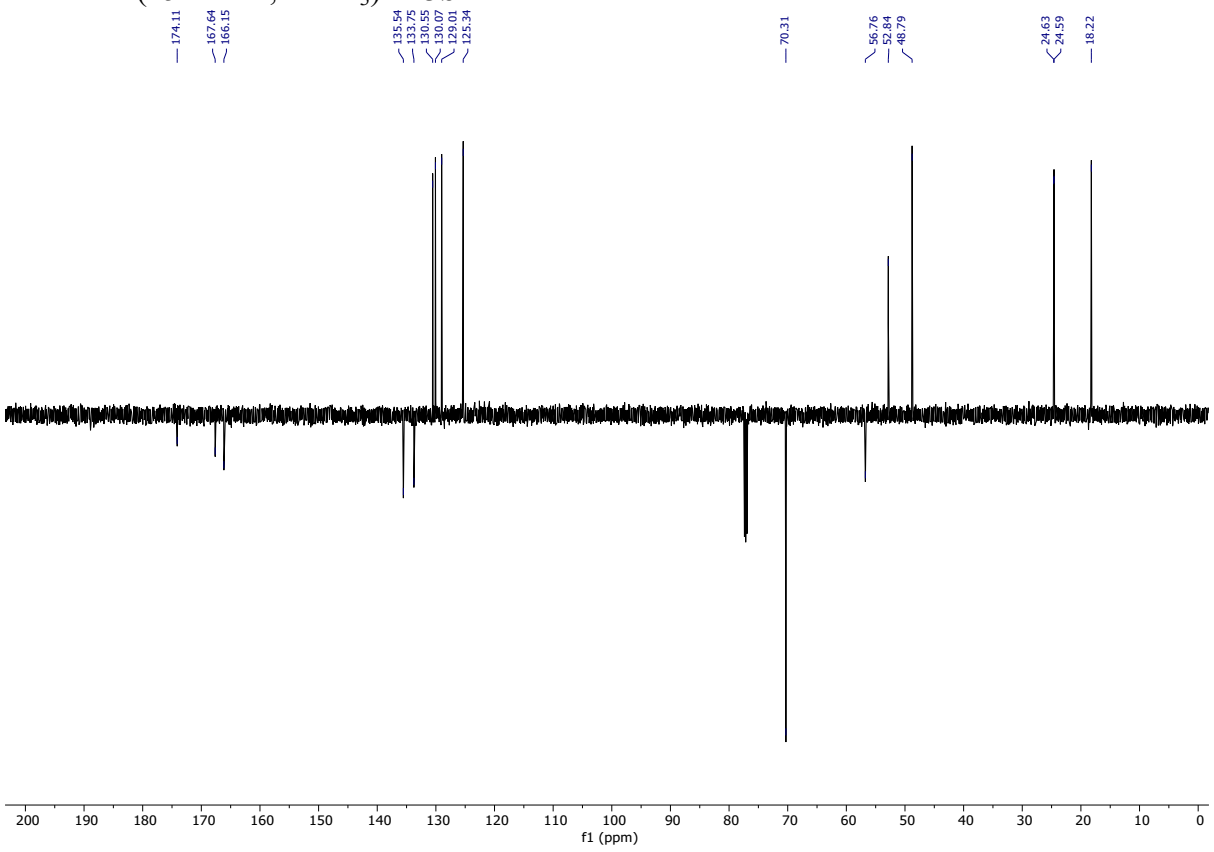

^{1}H NMR (300 MHz, $CDCl_3$) of **3c**.

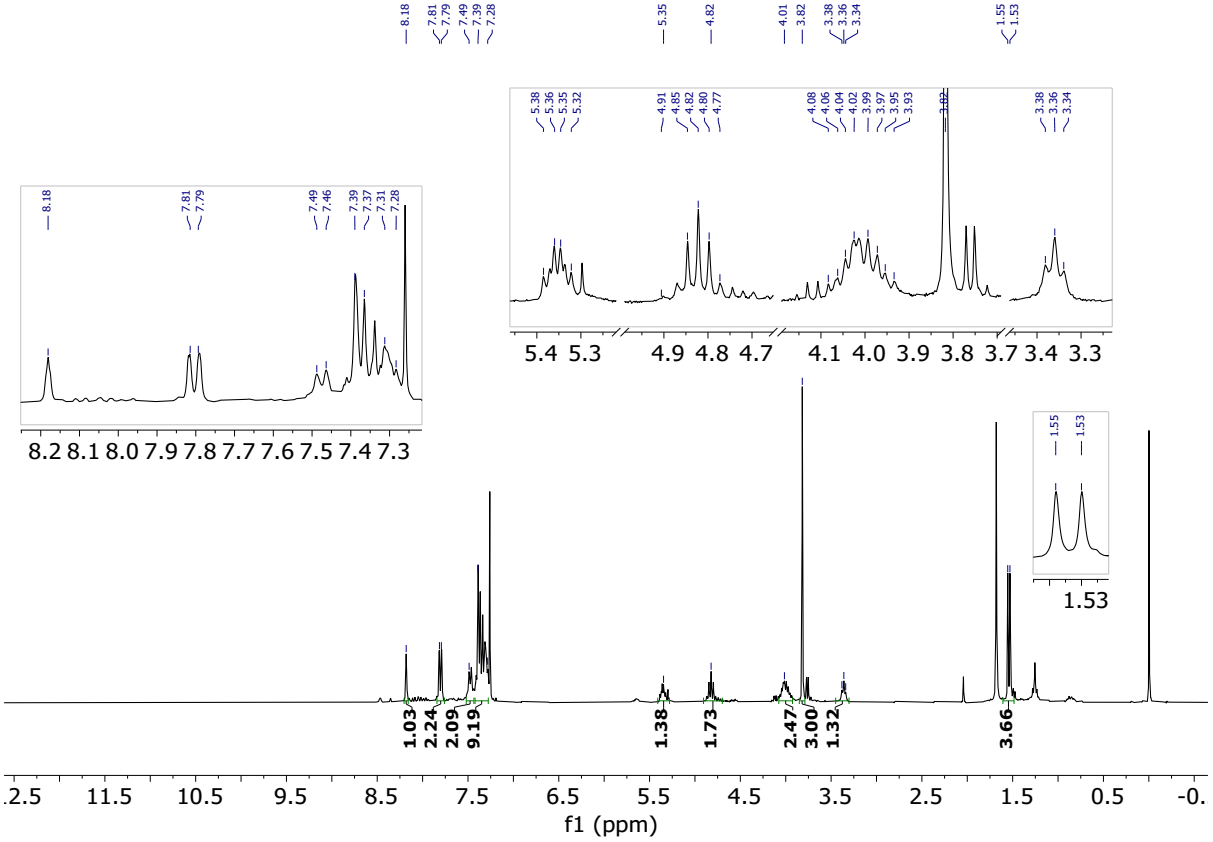

^{1}H NMR (300 MHz, $CDCl_3$) of **3c***.

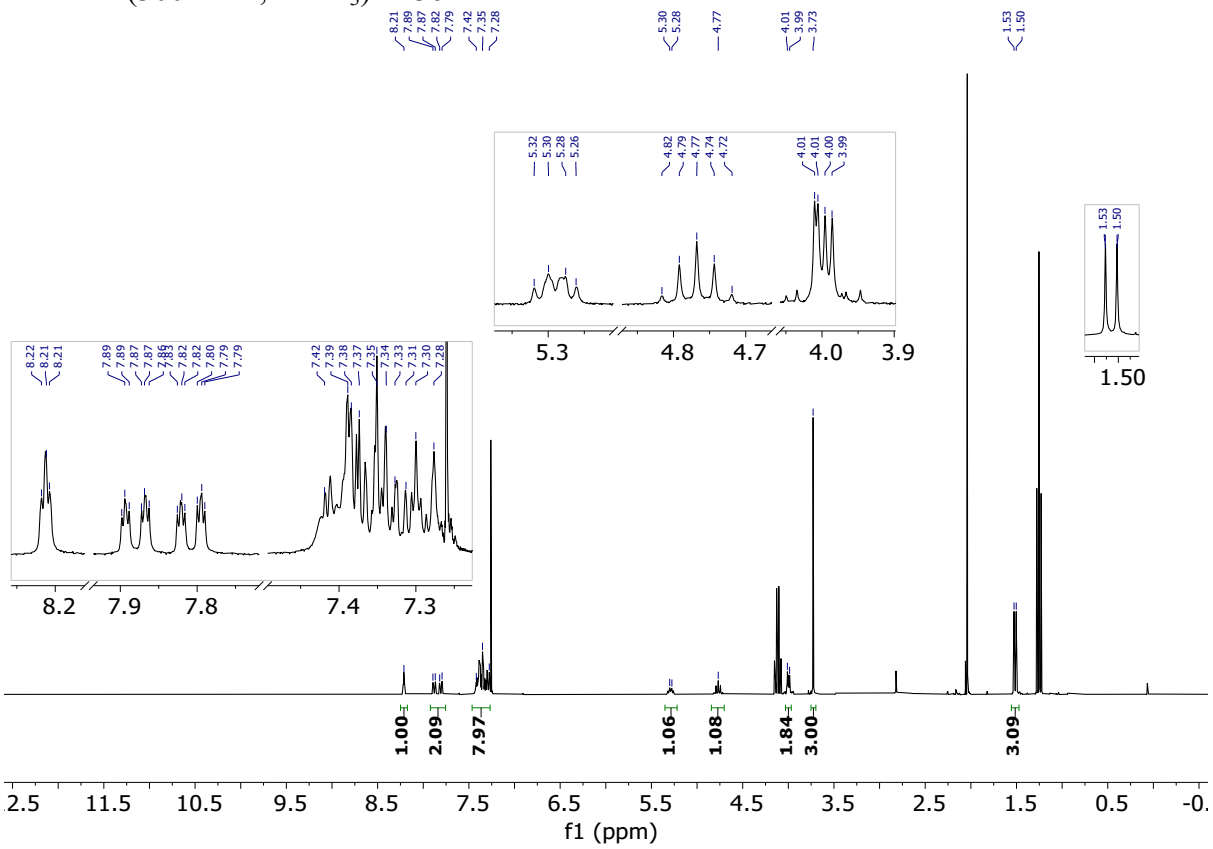

^{13}C NMR (75 MHz, $CDCl_3$) of **3c***.

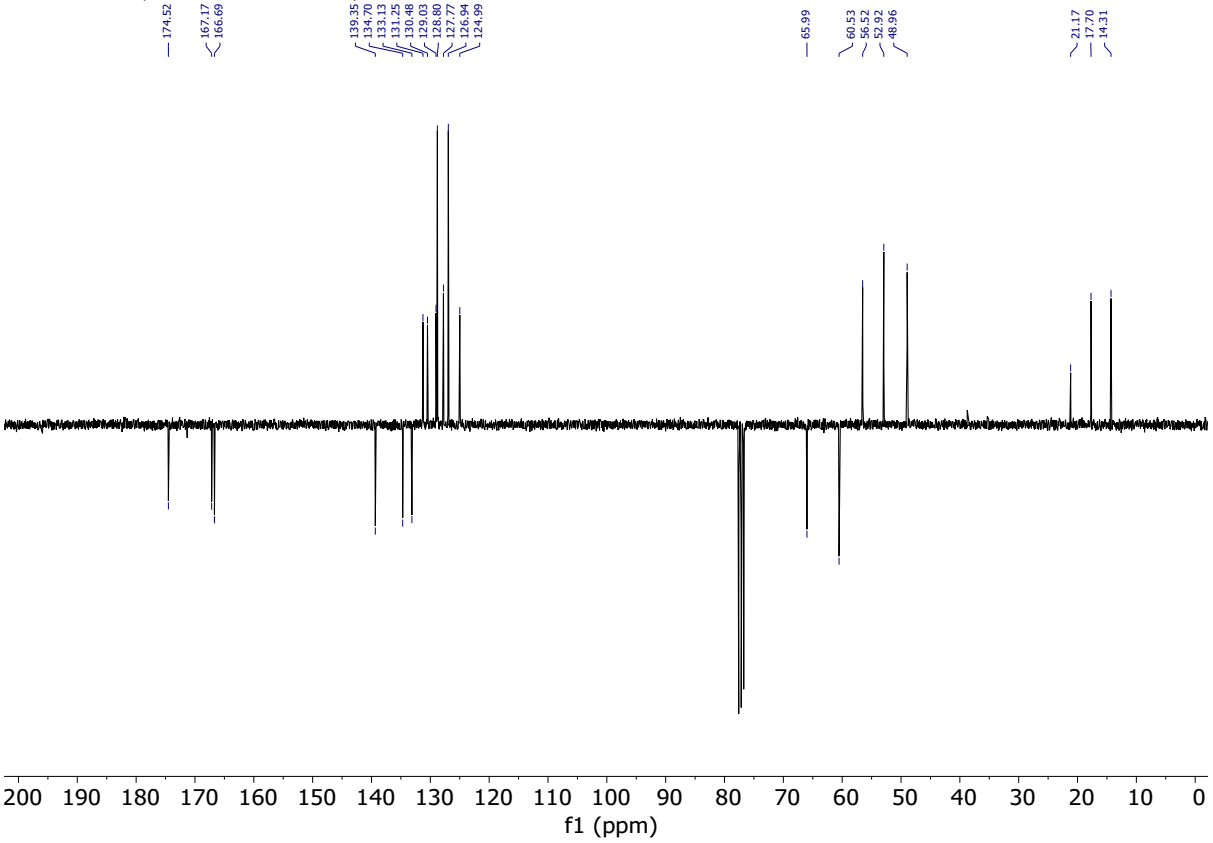

^{1}H NMR (300 MHz, $CDCl_3$) of **3d**.

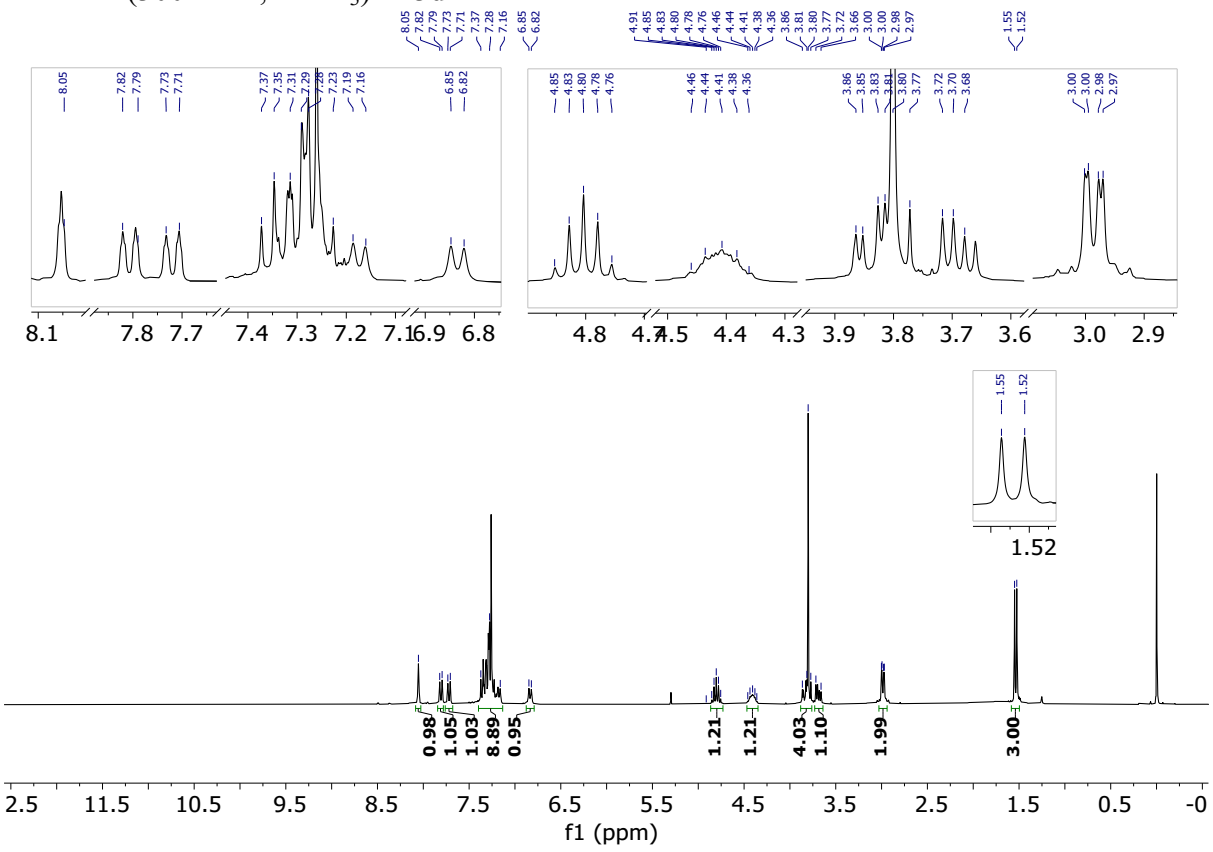

3.3. Metal complexes

3.3.1. Ir:1p = 1:1

^{1}H NMR (300 MHz, CD_2Cl_2)

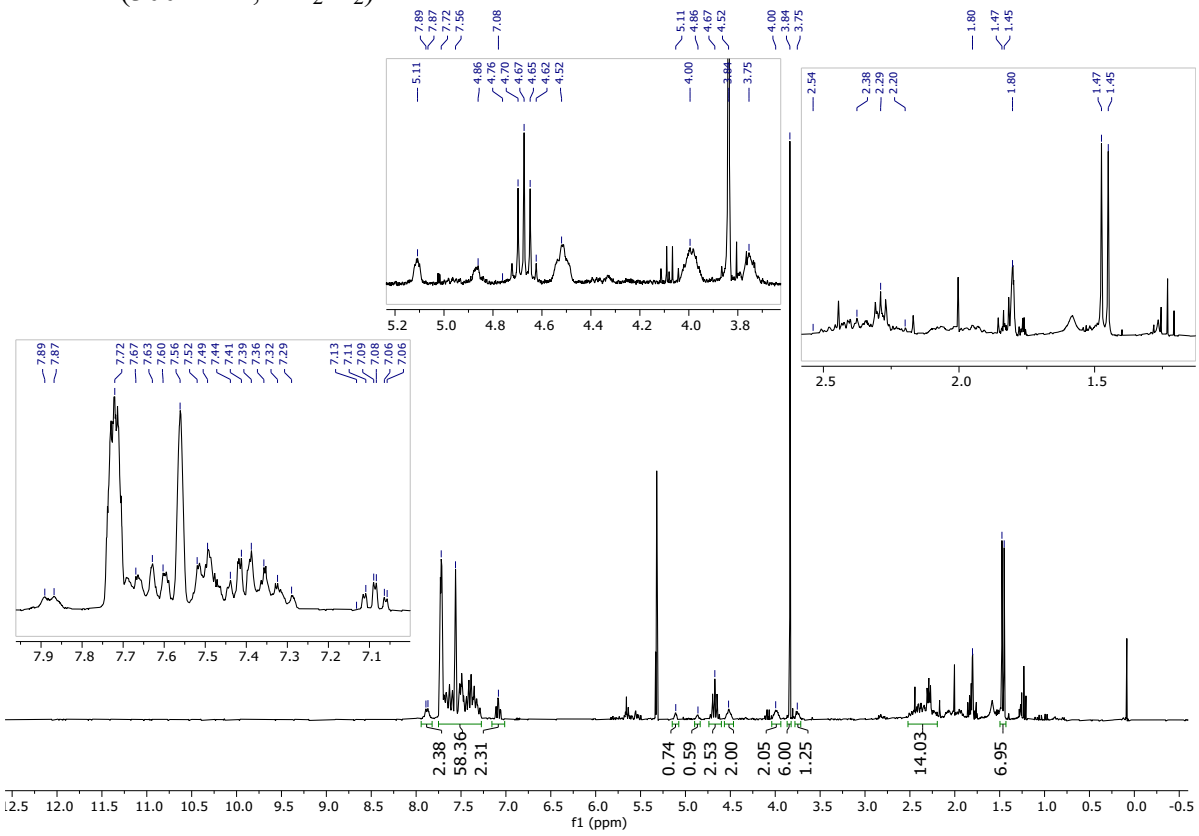

^{31}P NMR (122 MHz, CD_2Cl_2)

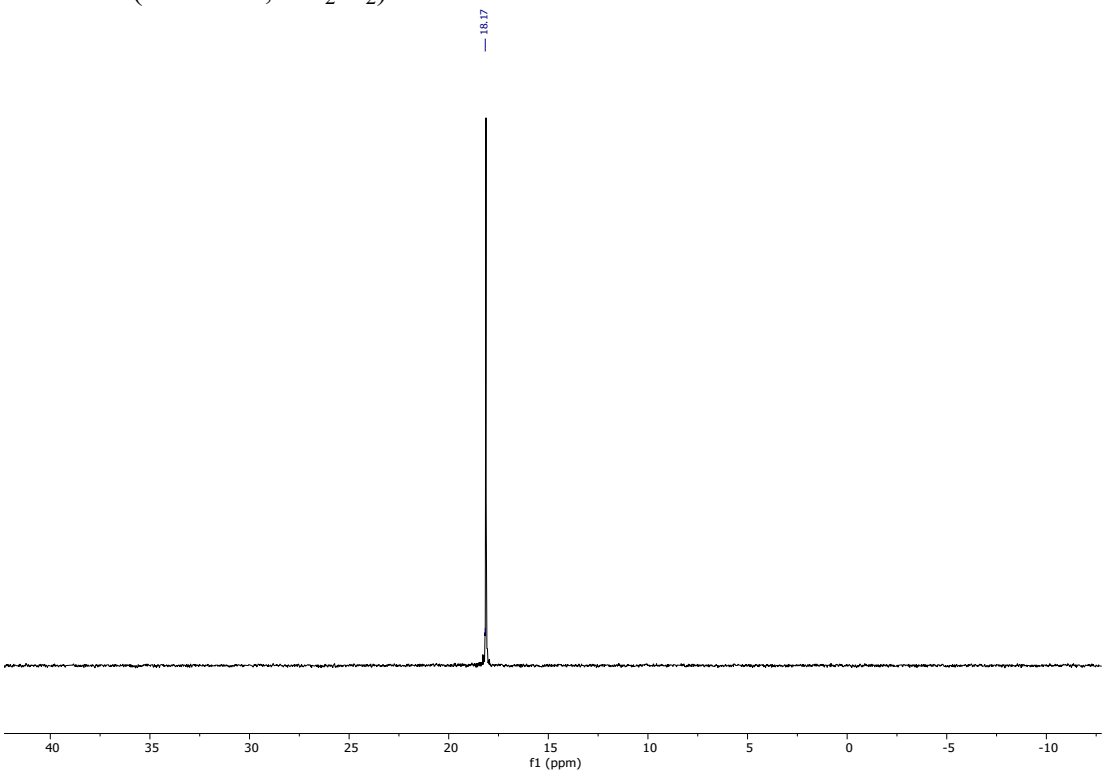

^{13}C NMR (151 MHz, CD_2Cl_2)

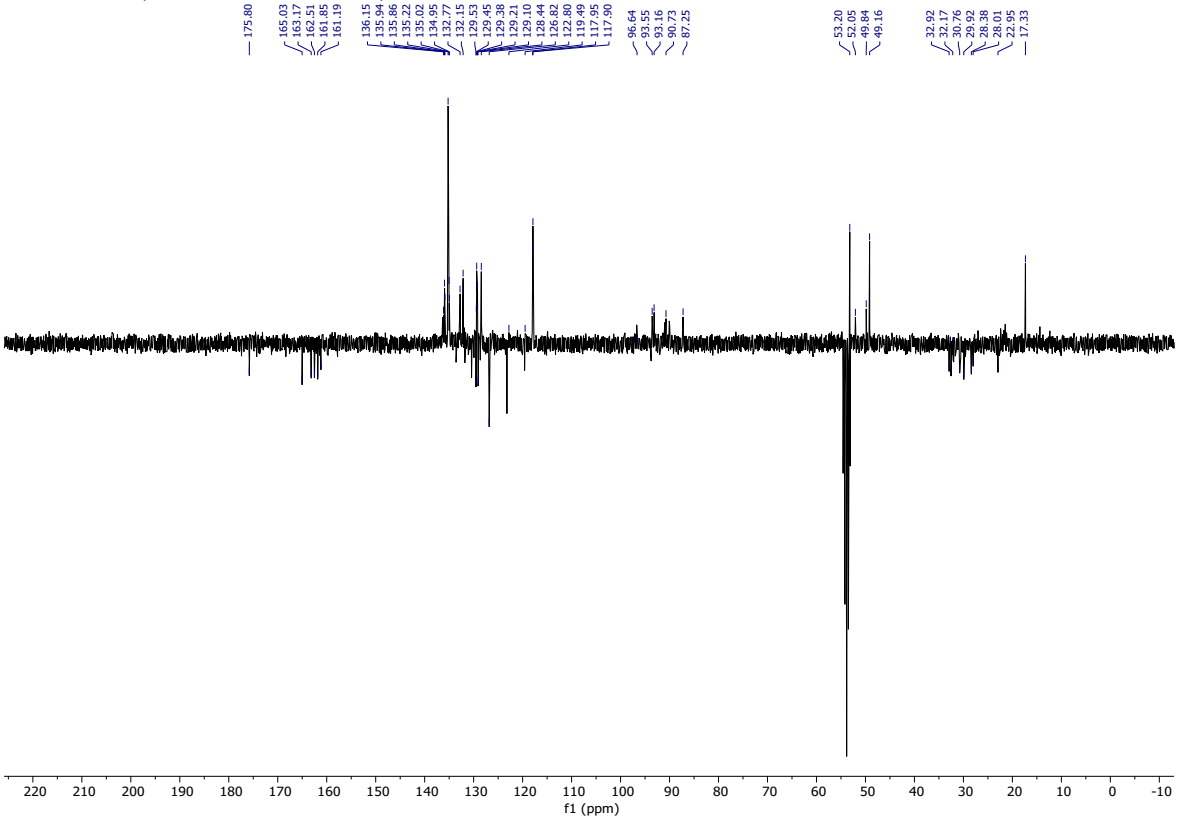

3.3.2. Ir:1p = 1:2,

^{1}H NMR (300 MHz, CD_2Cl_2)

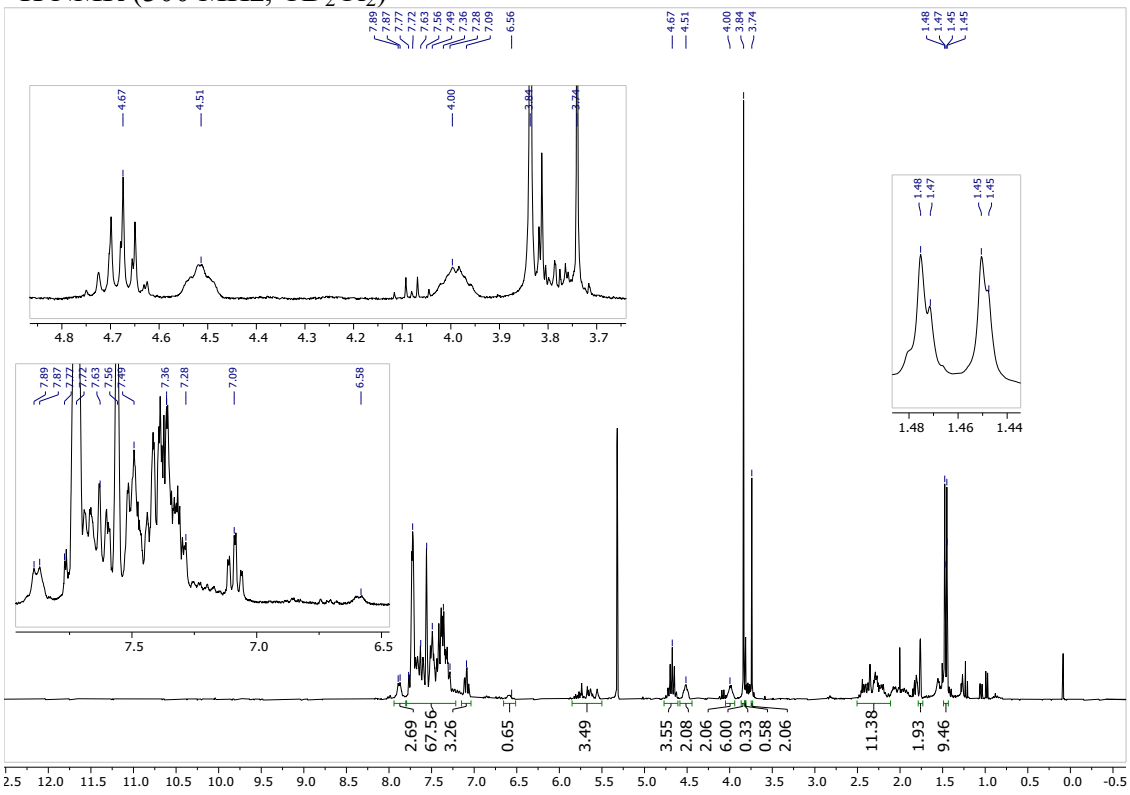

^{31}P NMR (122 MHz, CD_2Cl_2)

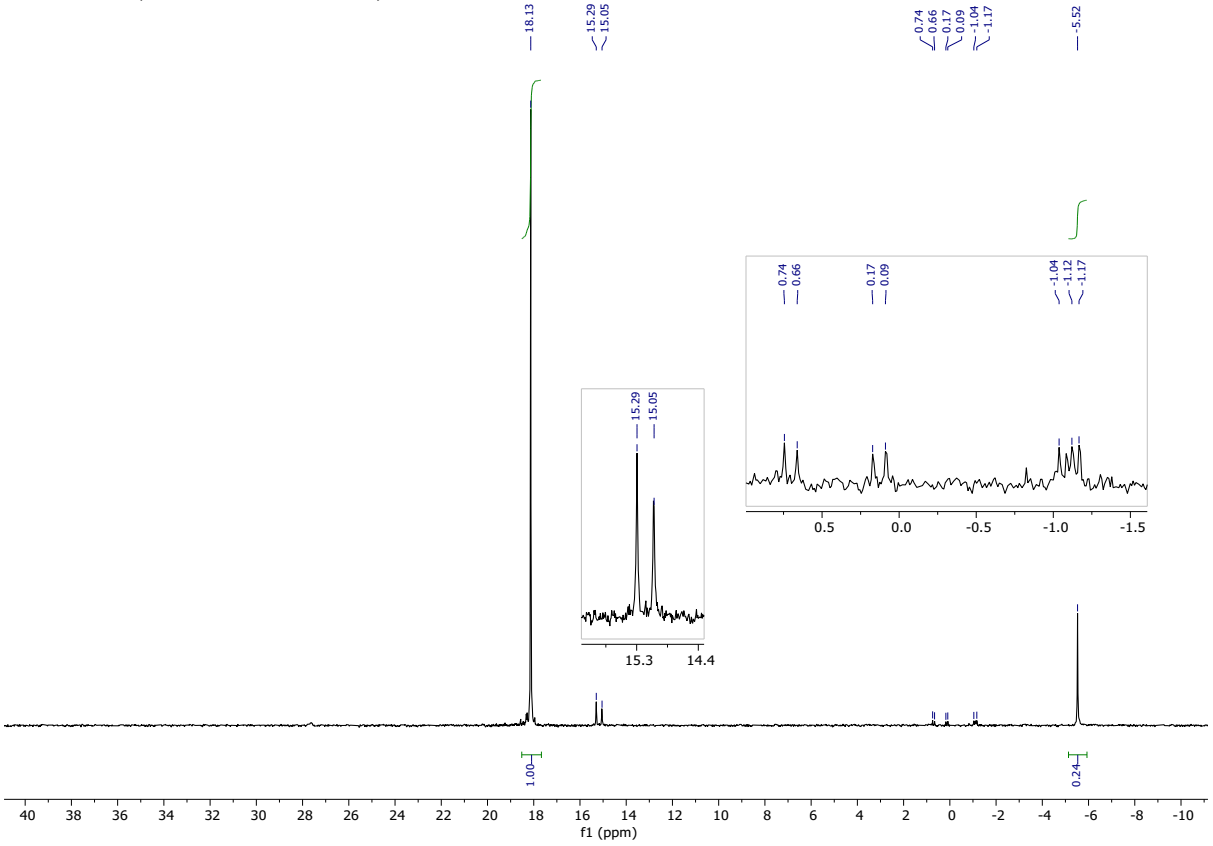

^{13}C NMR (151 MHz, CD_2Cl_2)

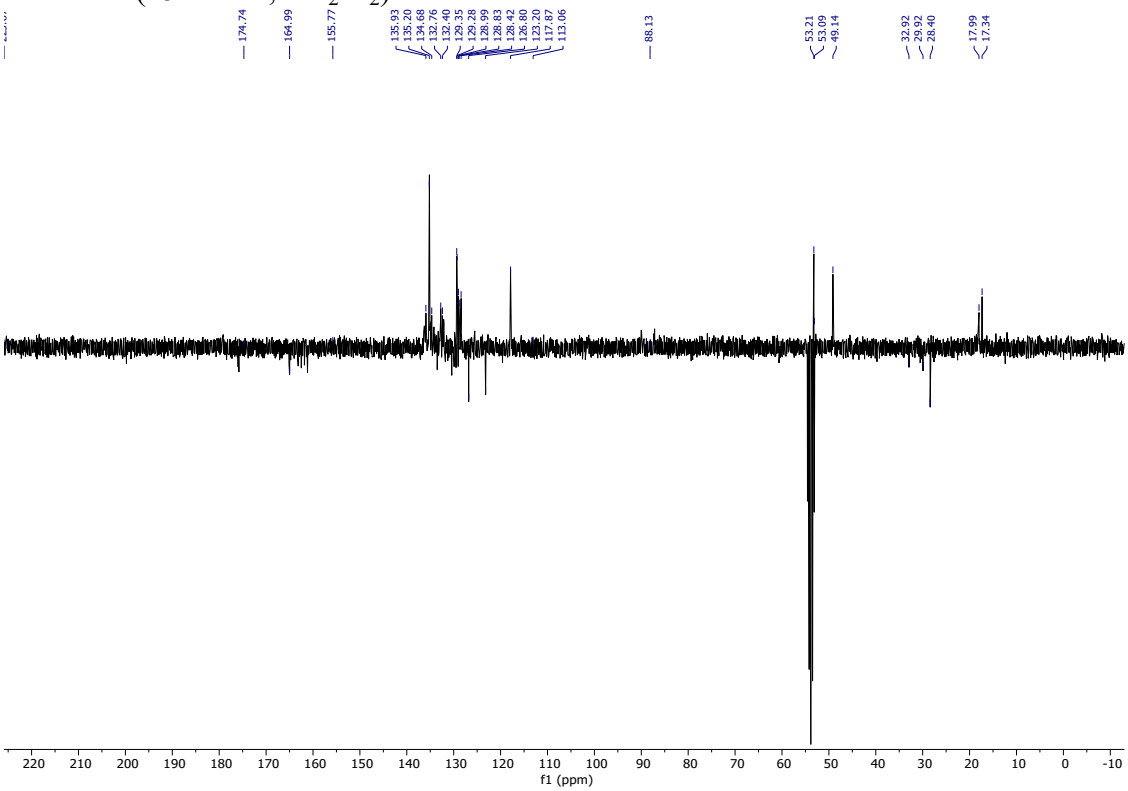

3.3.3. Ir:1p = 1:3

^{1}H NMR (300 MHz, CD_2Cl_2)

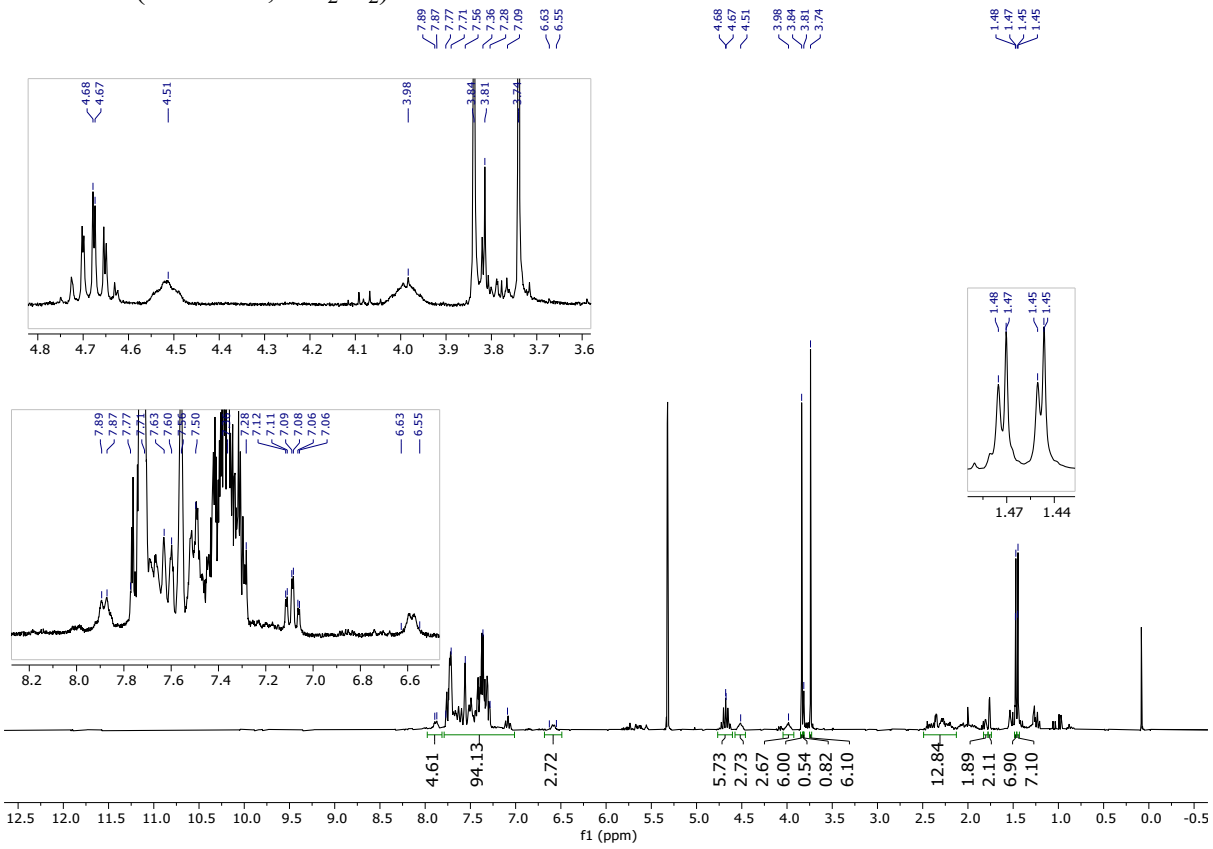

^{31}P NMR (122 MHz, CD_2Cl_2)

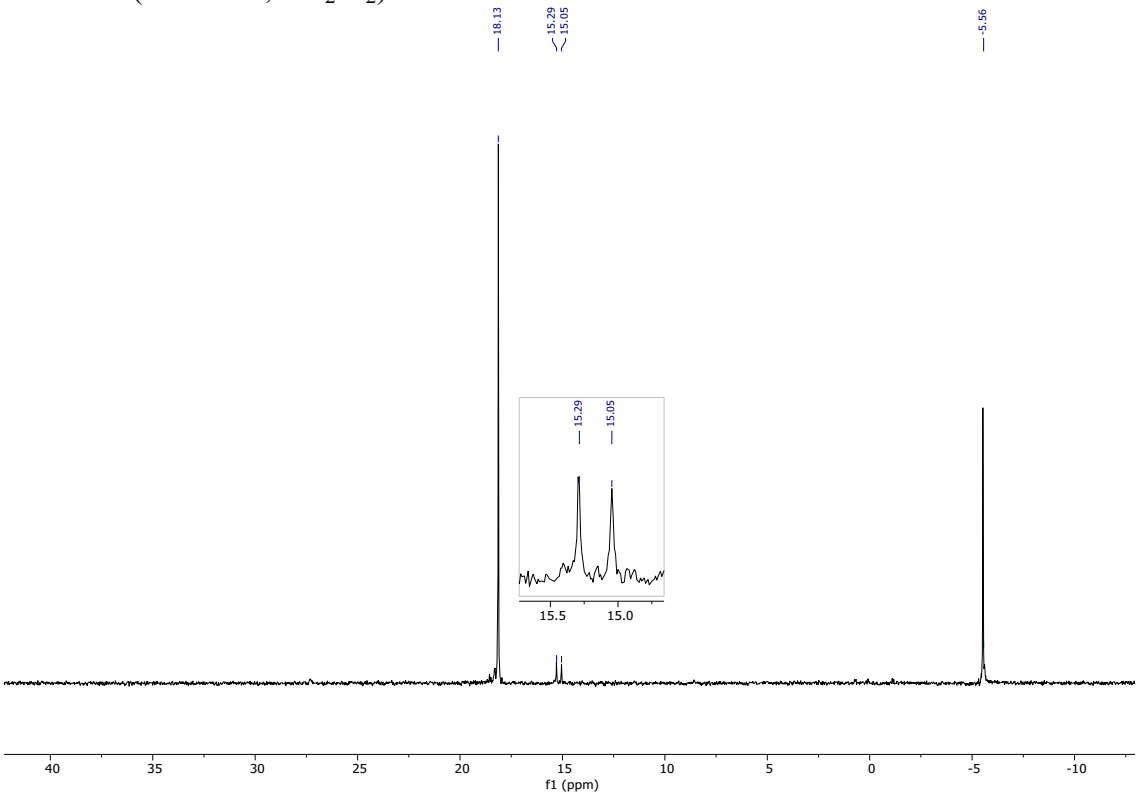

3.3.4. Ir:1b = 1:2

^{1}H NMR (600 MHz, CD_2Cl_2)

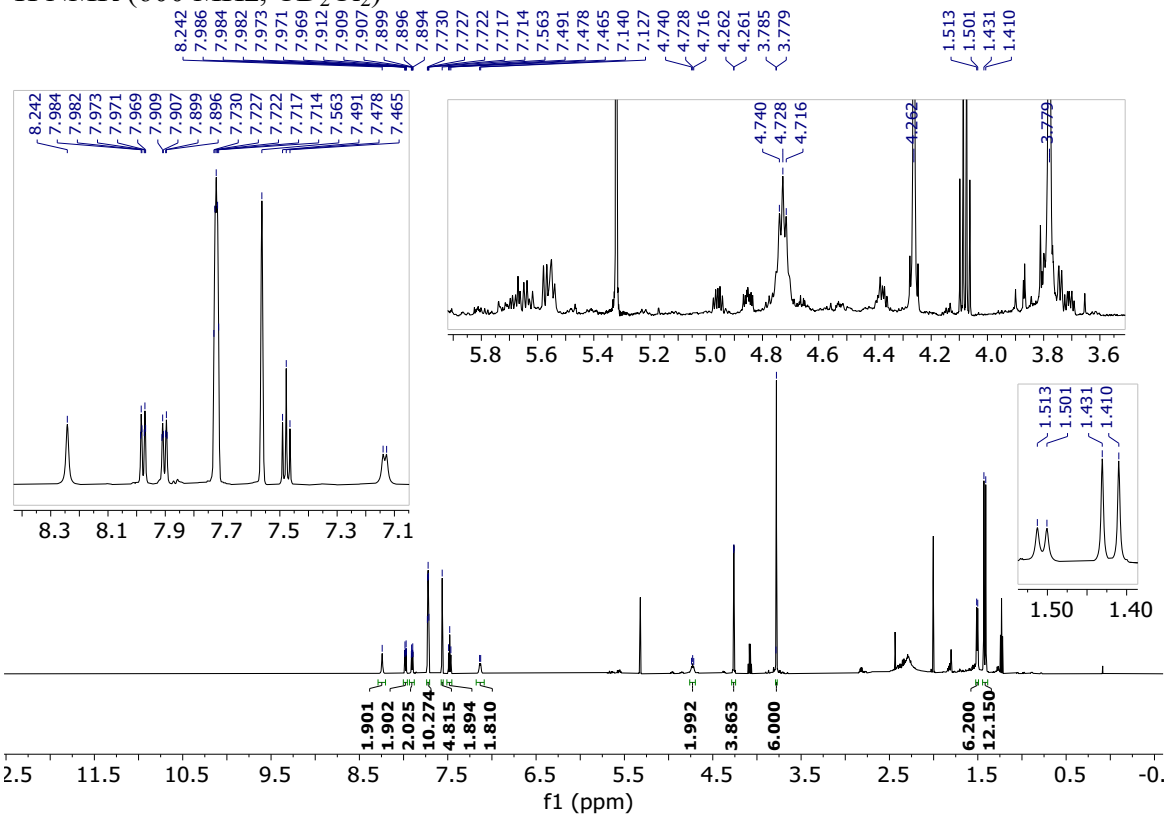

^{13}C NMR (151 MHz, CD_2Cl_2)

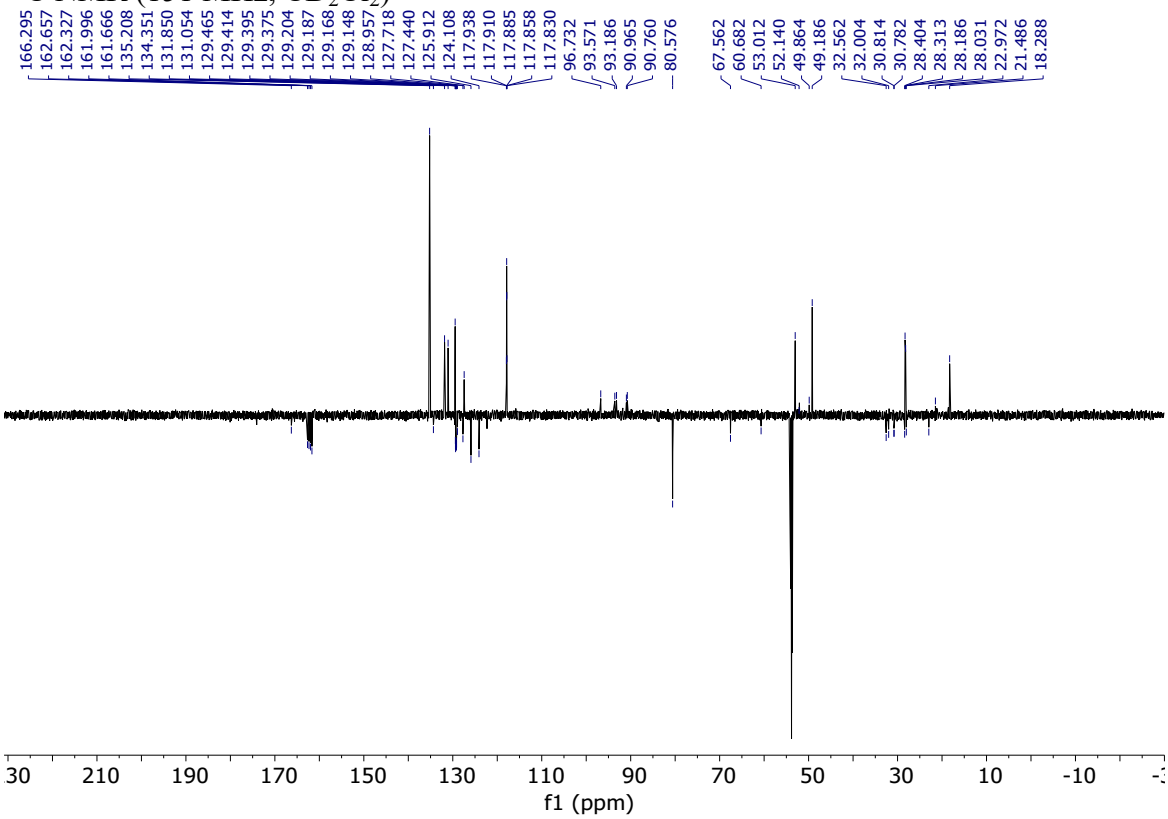

3.3.5. Ir:1p:1b = 1:0.5:0.5

^{1}H NMR (300 MHz,CD_2Cl_2)

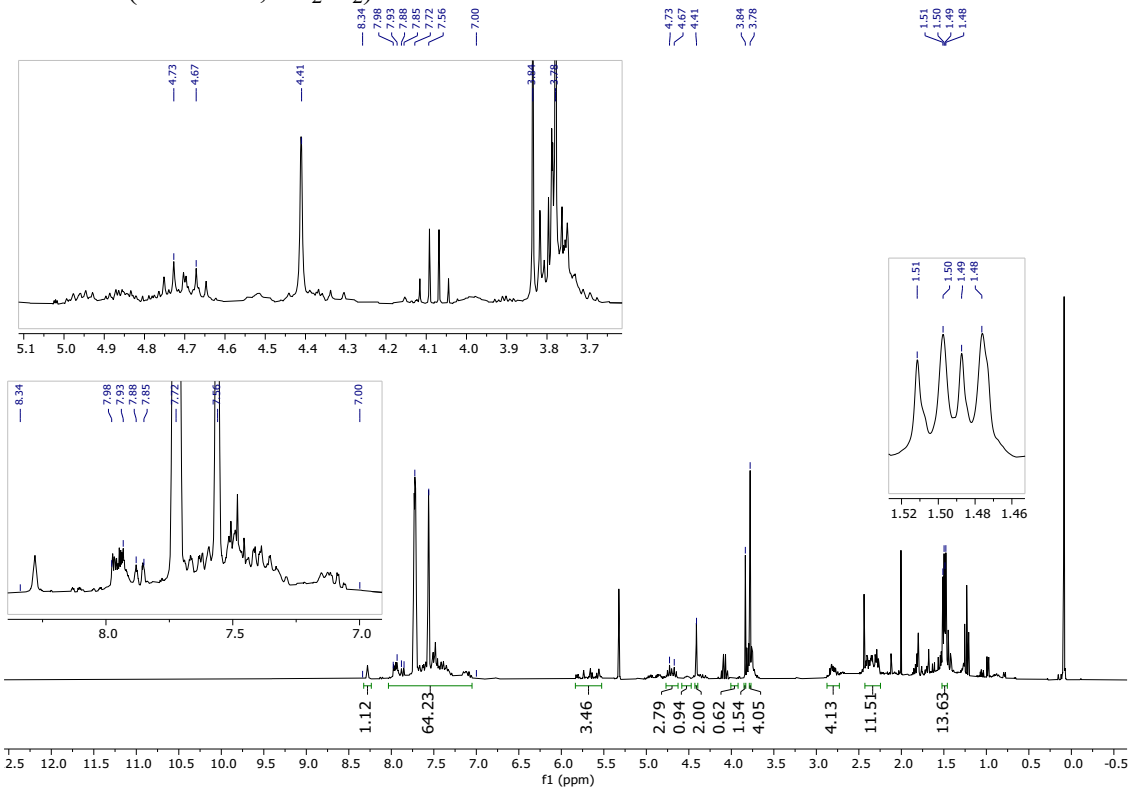

^{31}P NMR (122 MHz, CD_2Cl_2)

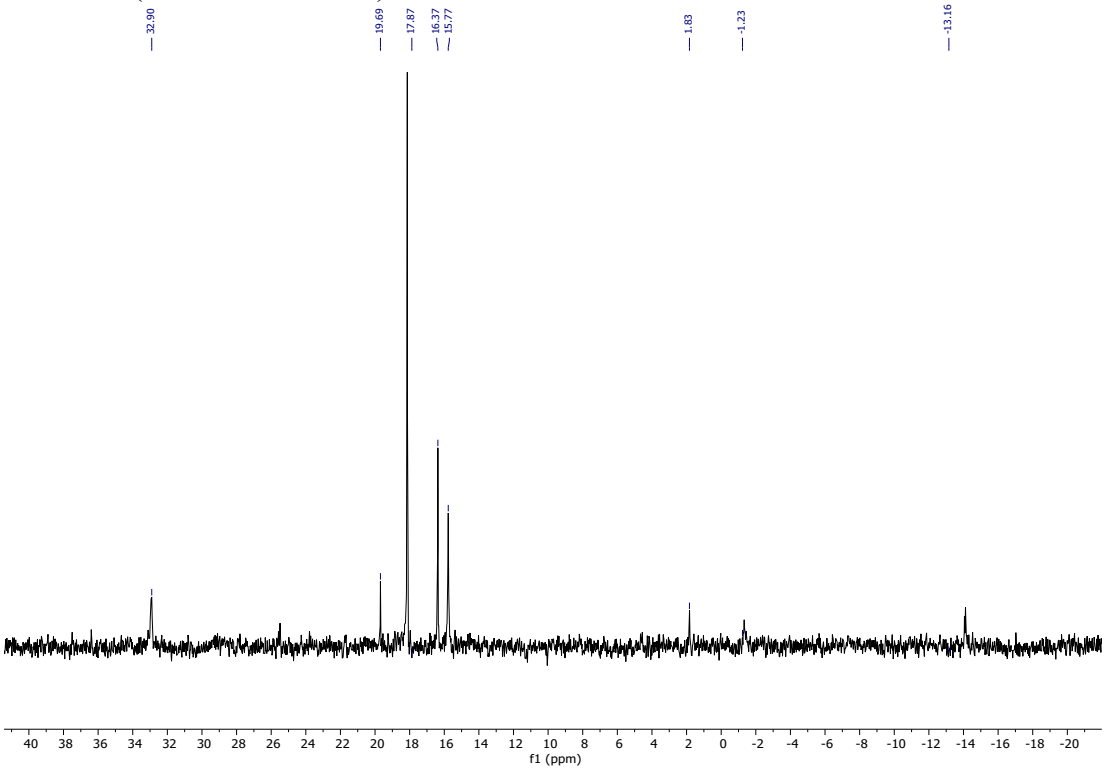

3.3.6. Ir:1p:1b = 1:1:1

^{1}H NMR (300 MHz, CD_2Cl_2)

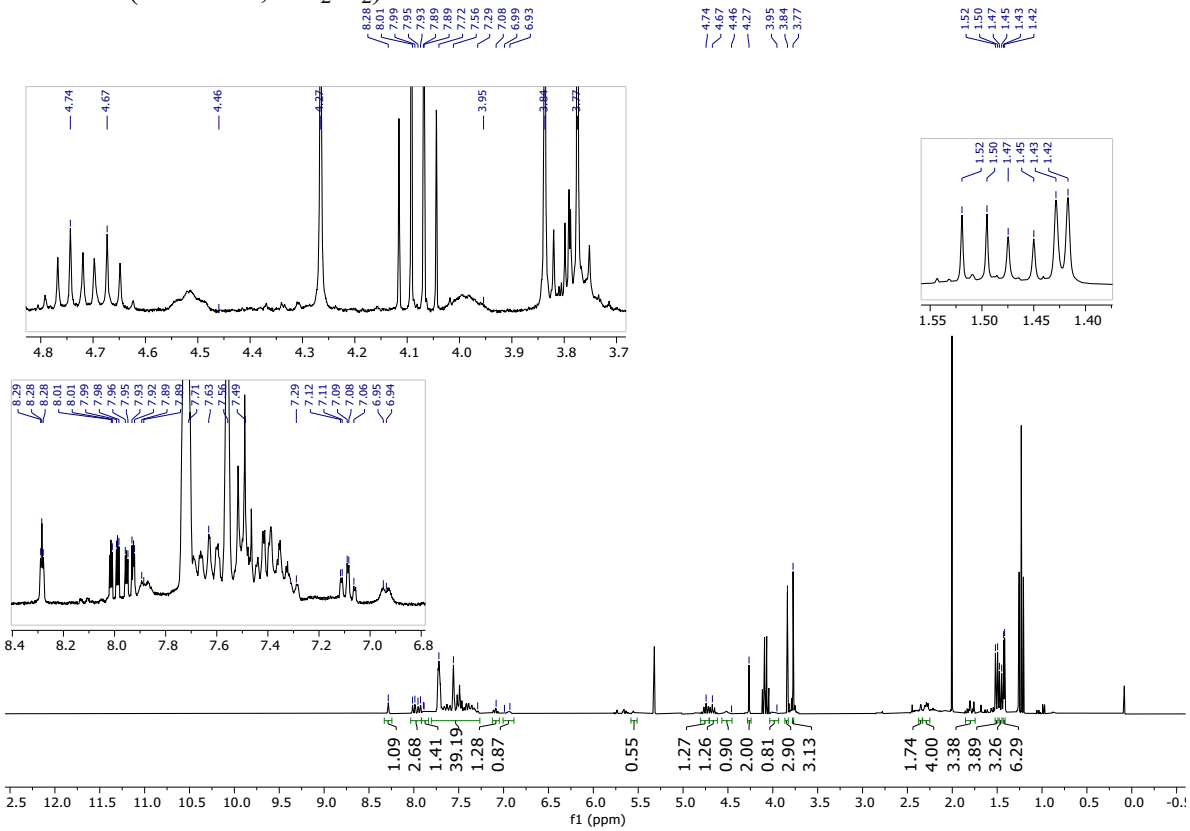

^{31}P NMR (122 MHz, CD_2Cl_2)

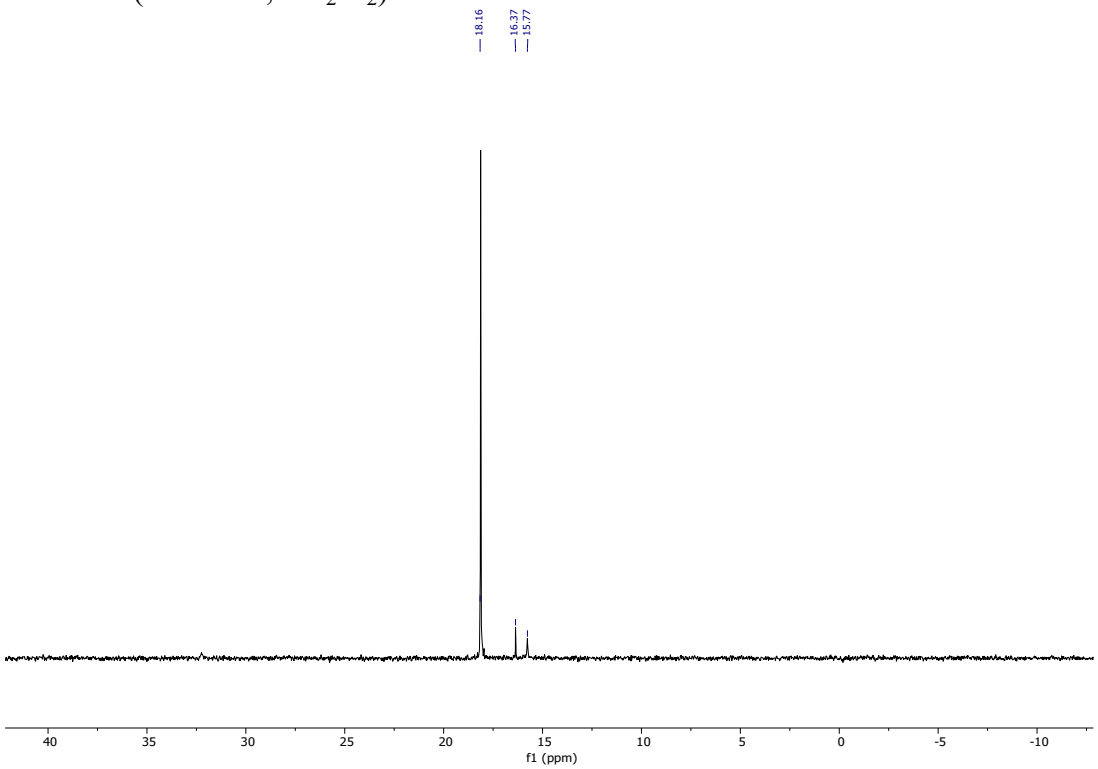

^{13}C NMR (151 MHz, CD_2Cl_2)

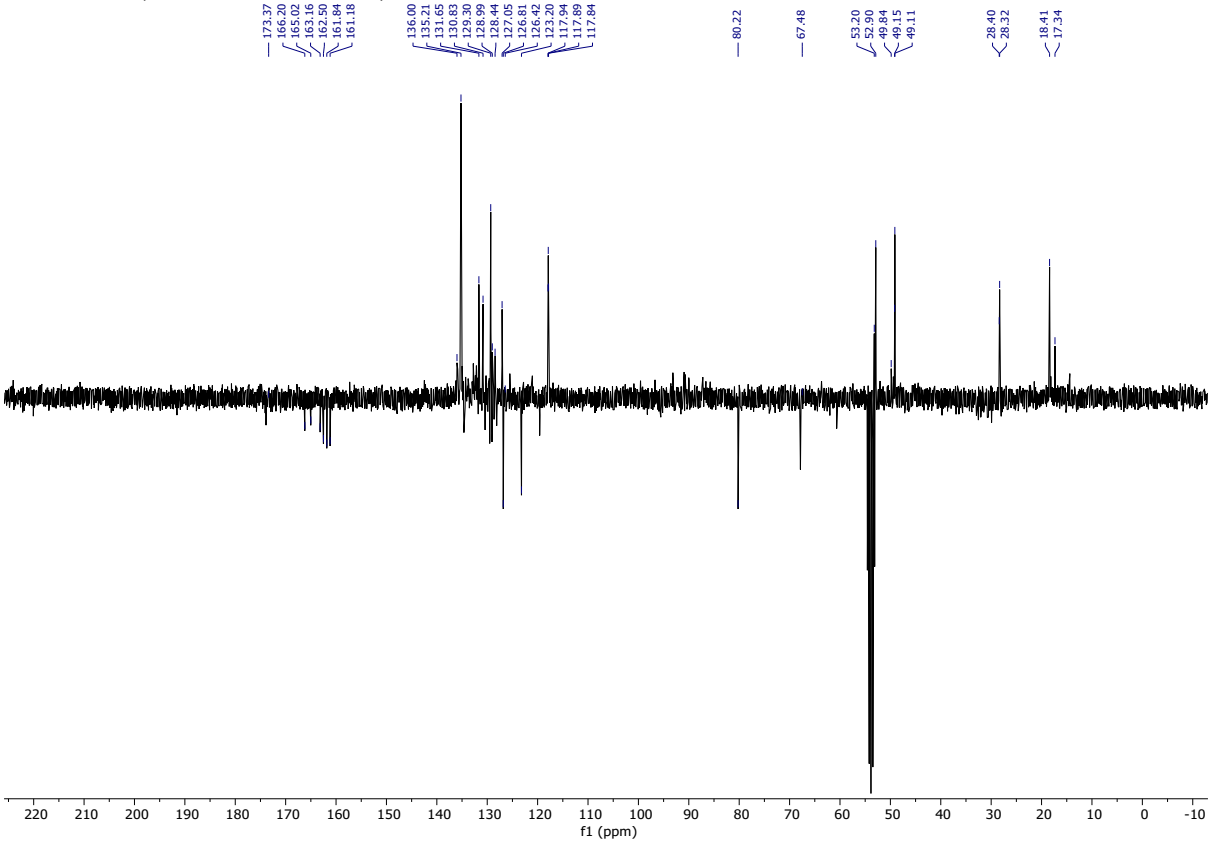

3.3.7. Ir:1p:1b = 1:1:2 ([Ir(COD)Cl]$_2$ was used)

^{1}H NMR (300 MHz, CD_3Cl)

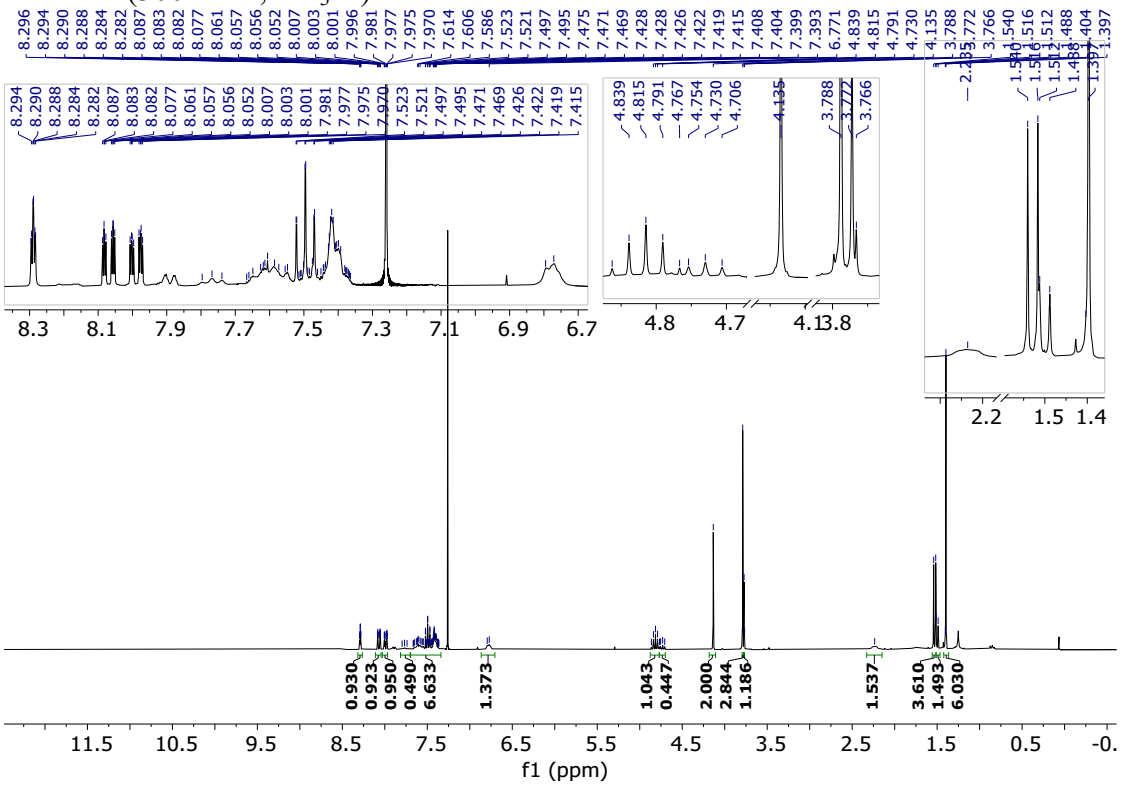

^{31}P NMR (122 MHz, CD_3Cl)

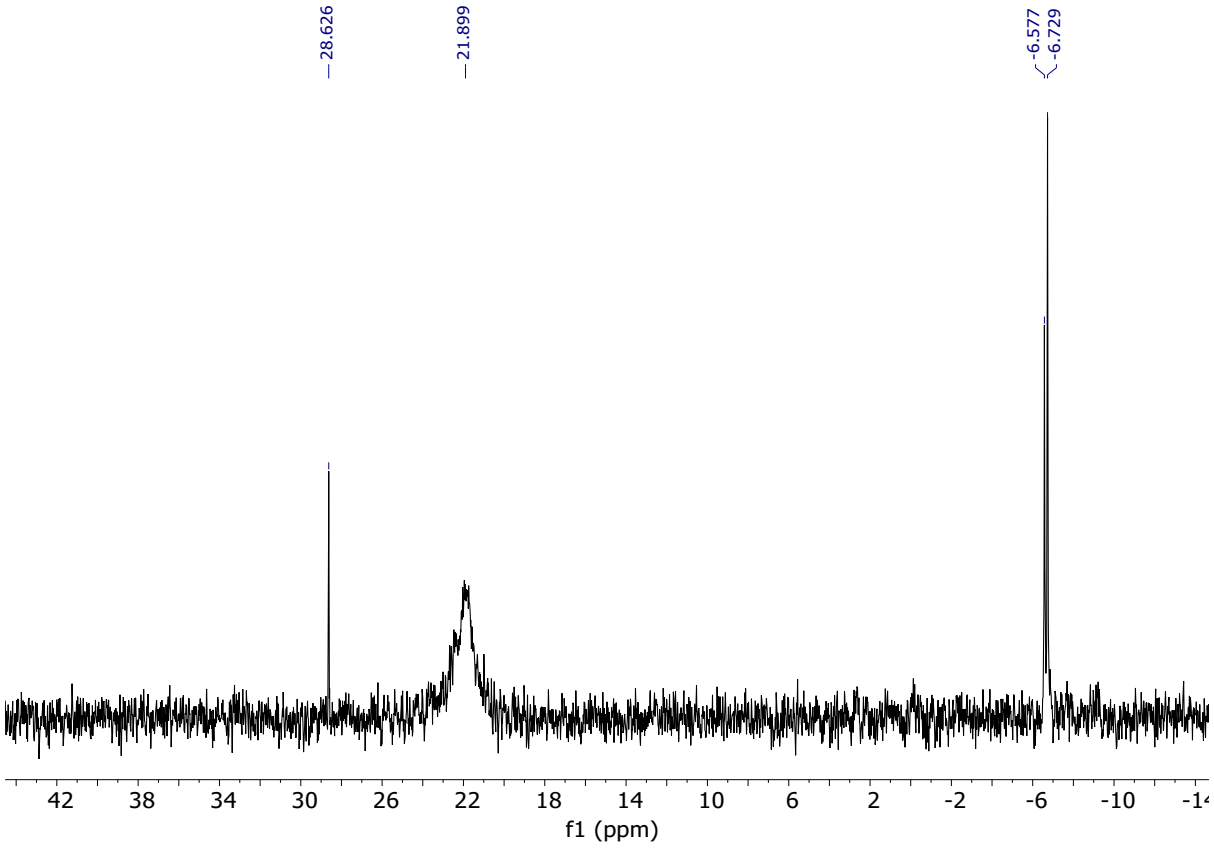

3.3.8. Ir:1c = 1:2

^{1}H NMR (600 MHz, CD_2Cl_2)

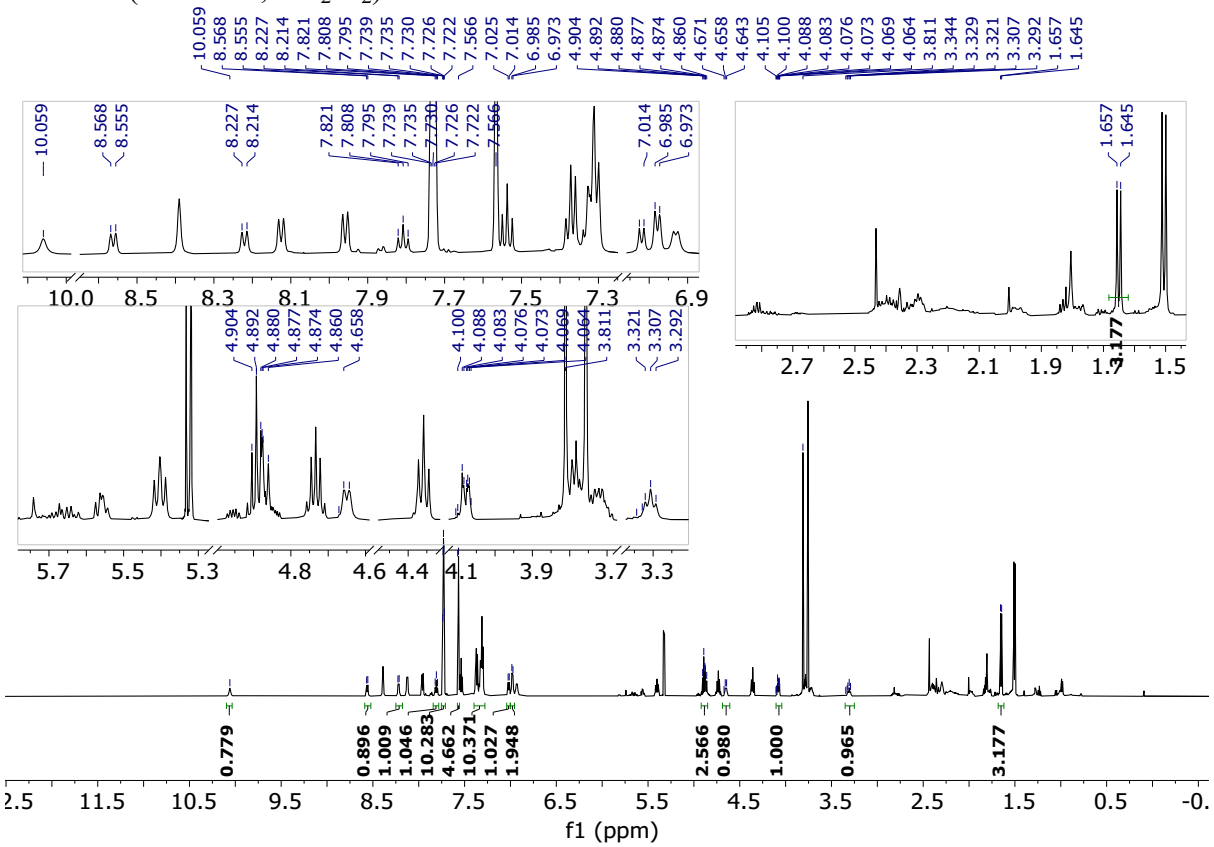

^{13}C NMR (151 MHz, CD_2Cl_2)

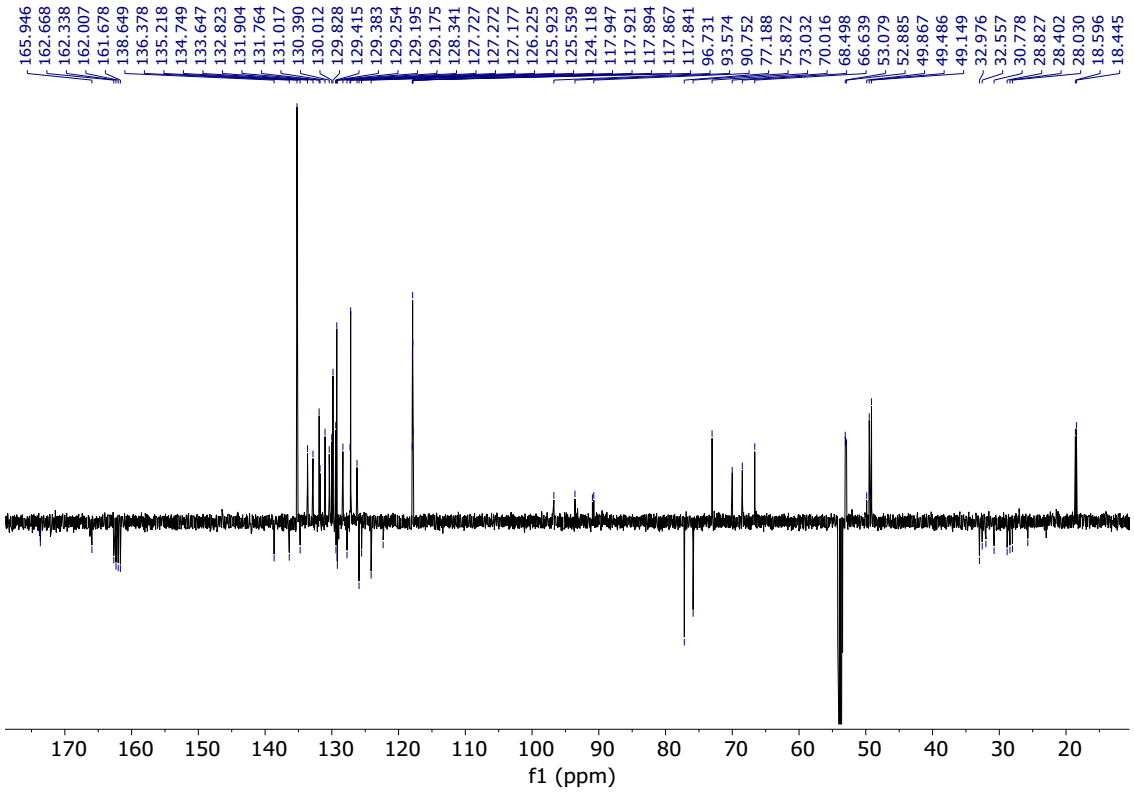

COSY NMR in CD_2Cl_2

a) whole spectra

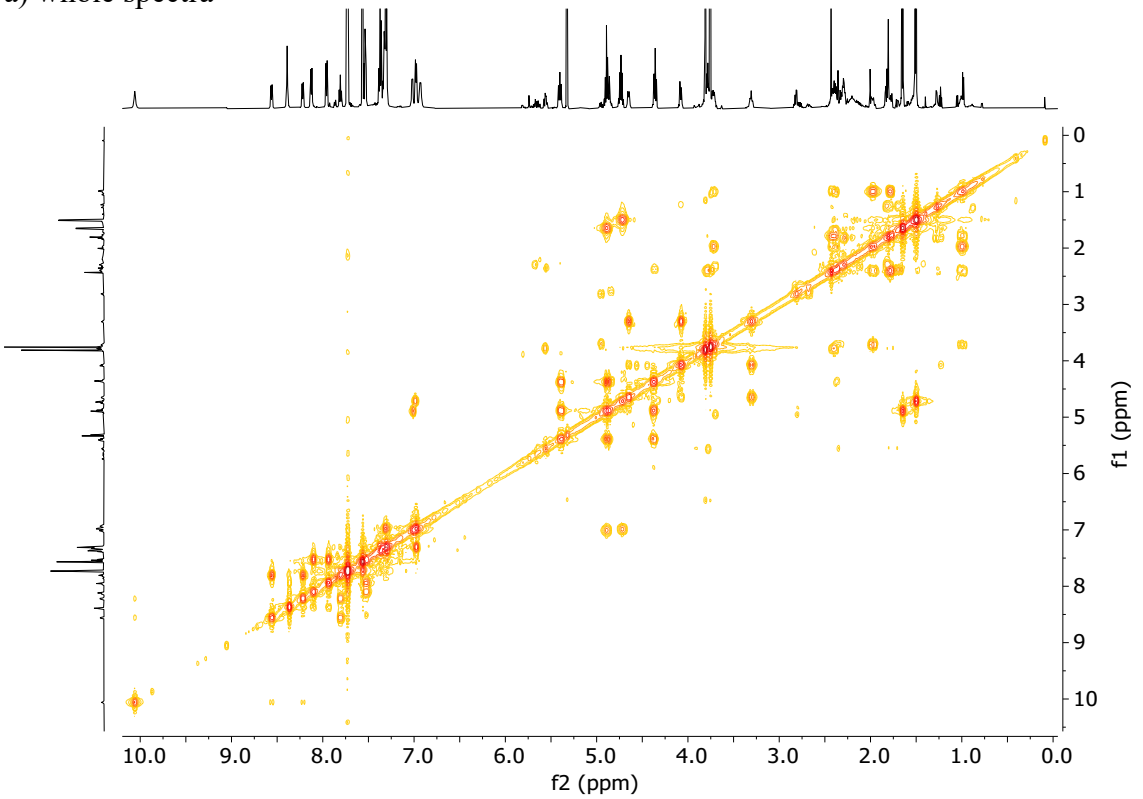

b) aromatic region

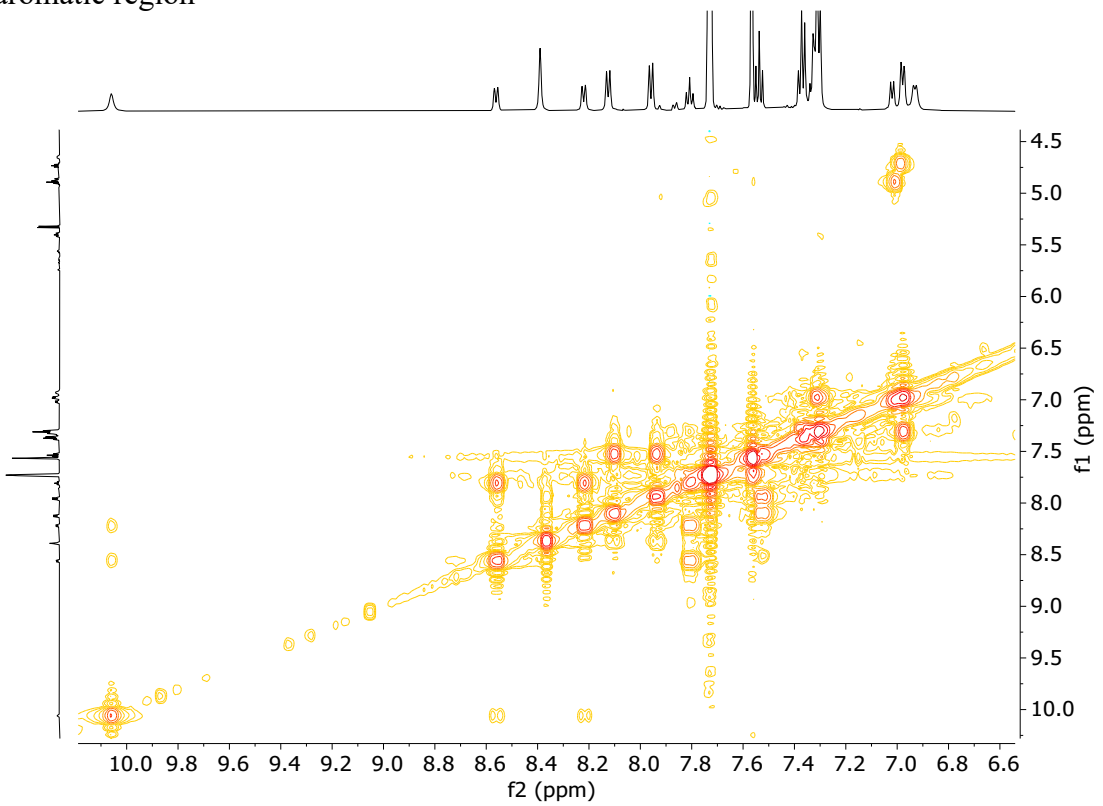

c) Functional group region

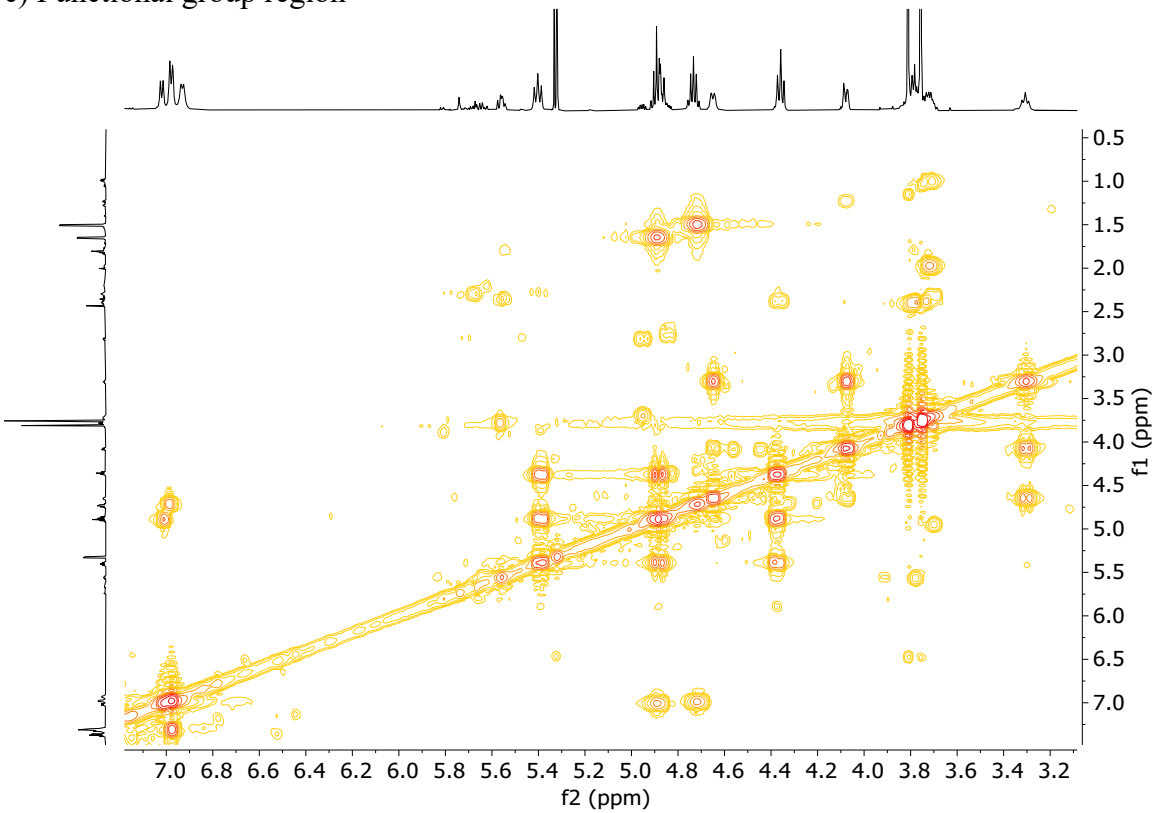

d)Aliphatic group region

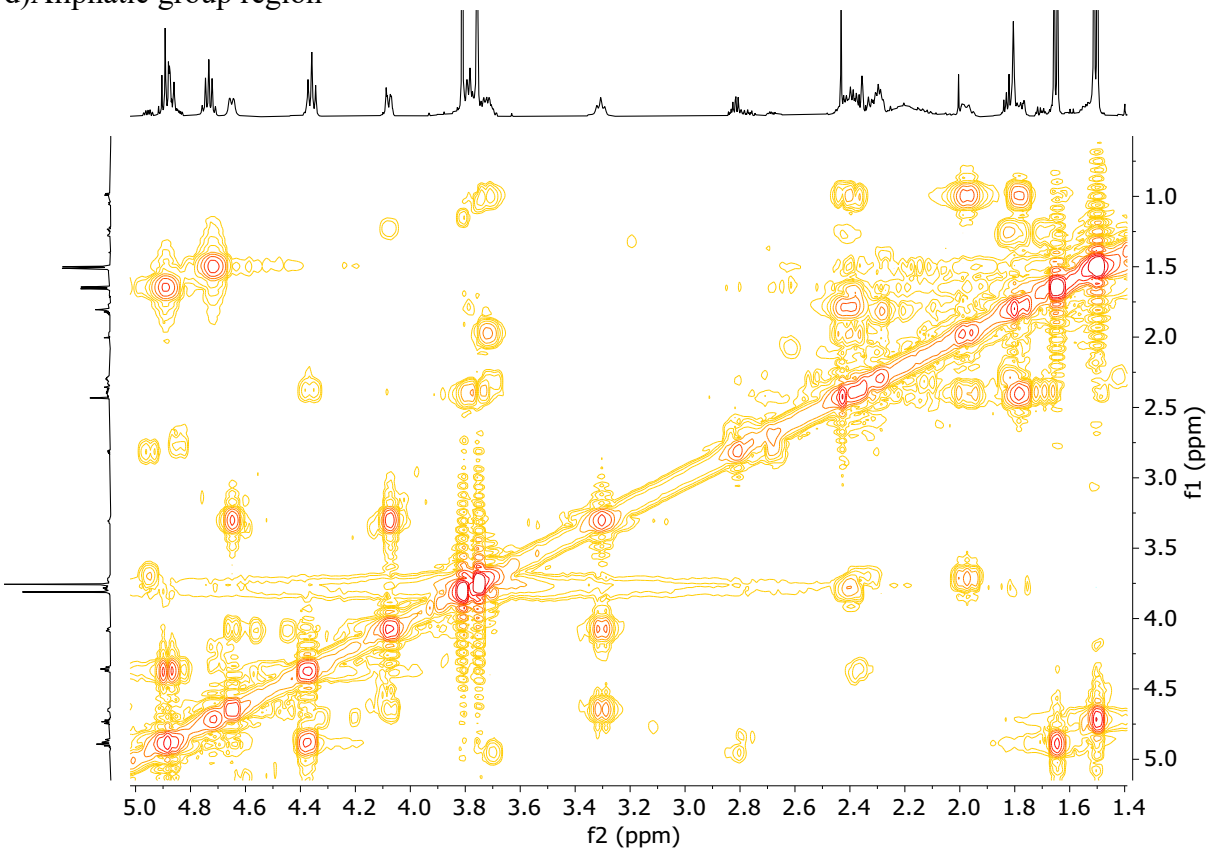

3.3.9. Ir:1c* = 1:2

^{1}H NMR (600 MHz, CD_2Cl_2)

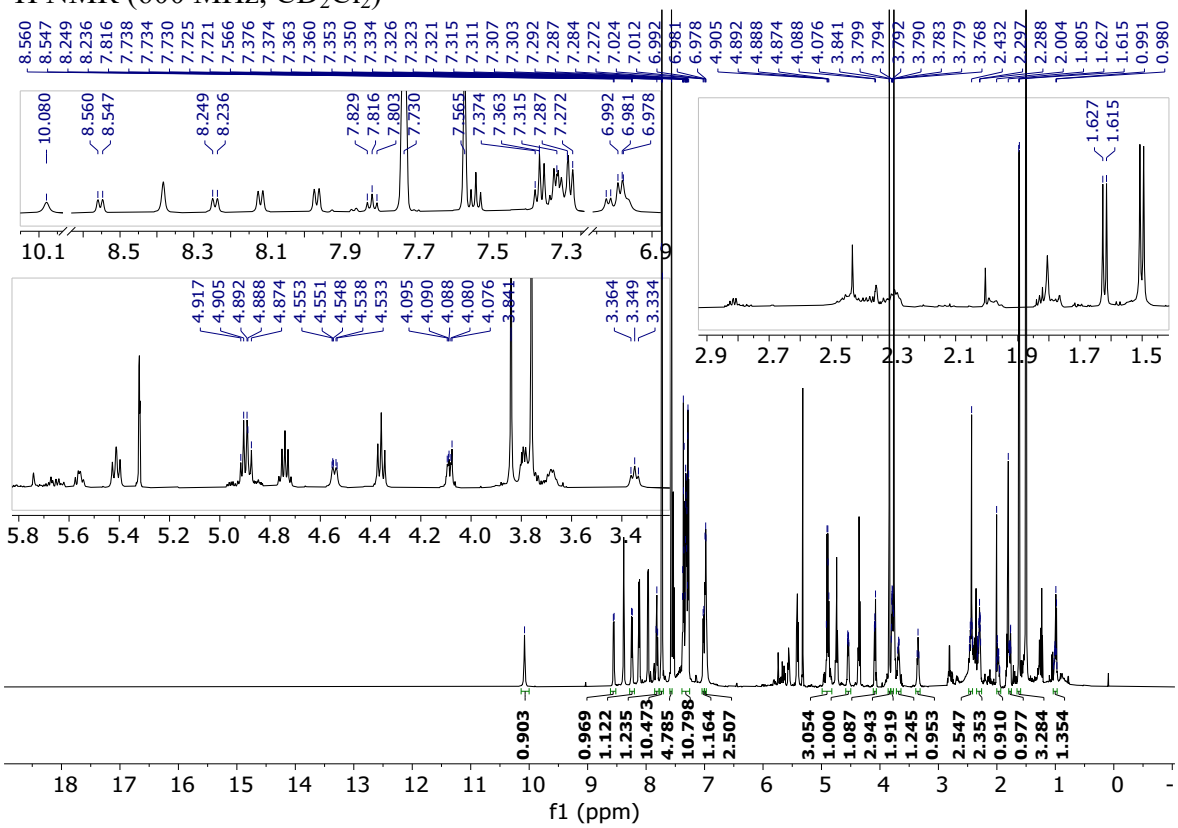

^{13}C NMR (151 MHz, CD_2Cl_2)

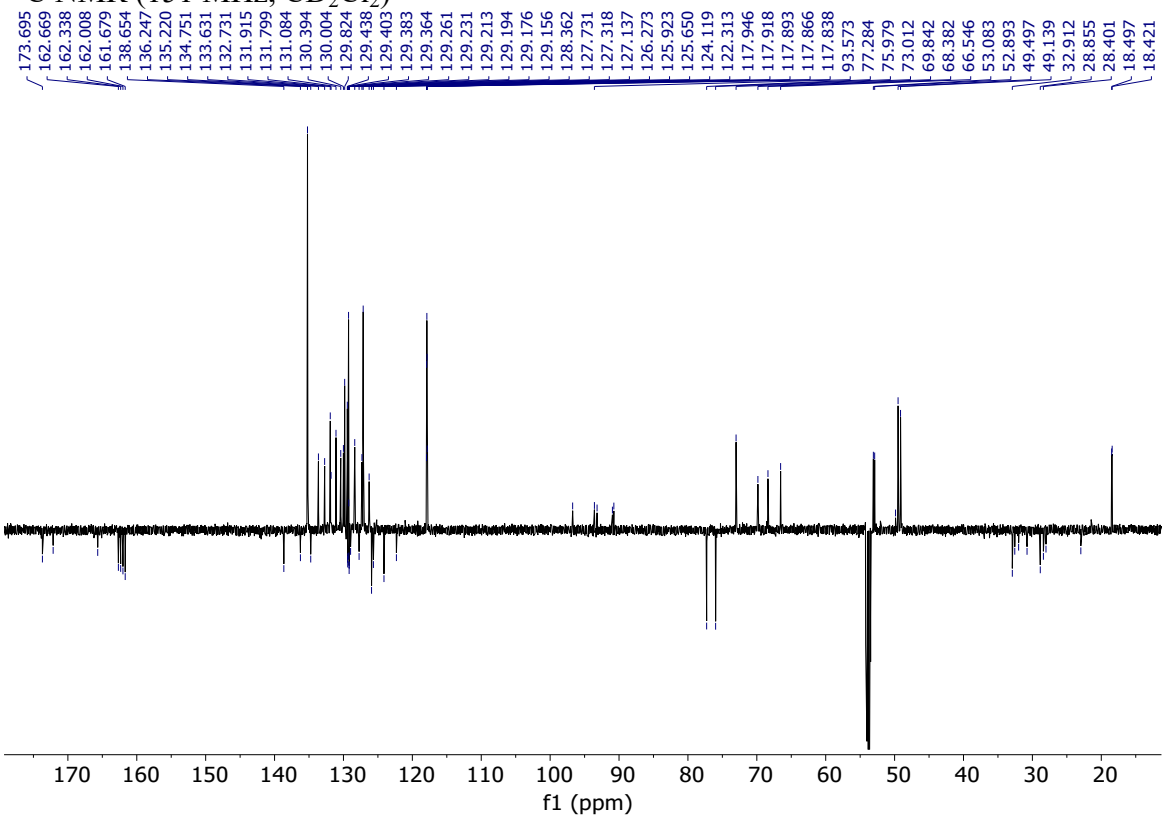

COSY NMR in CD_2Cl_2

a) whole spectra

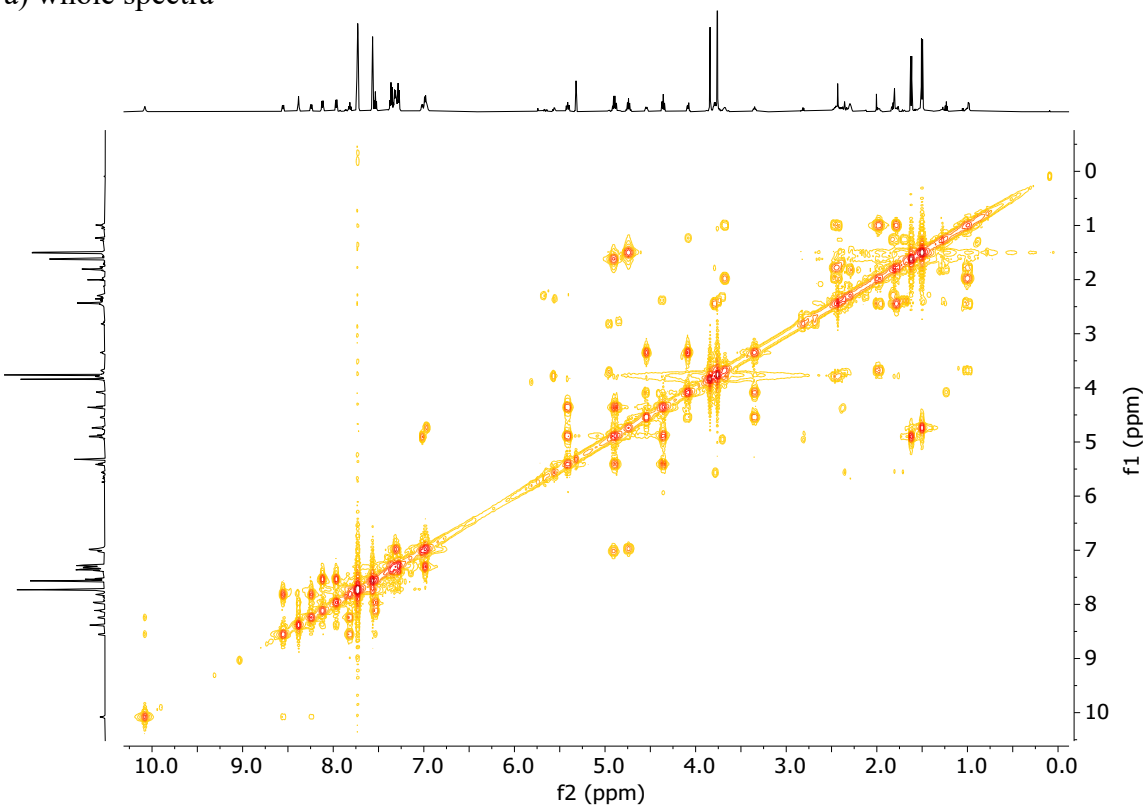

b) aromatic region

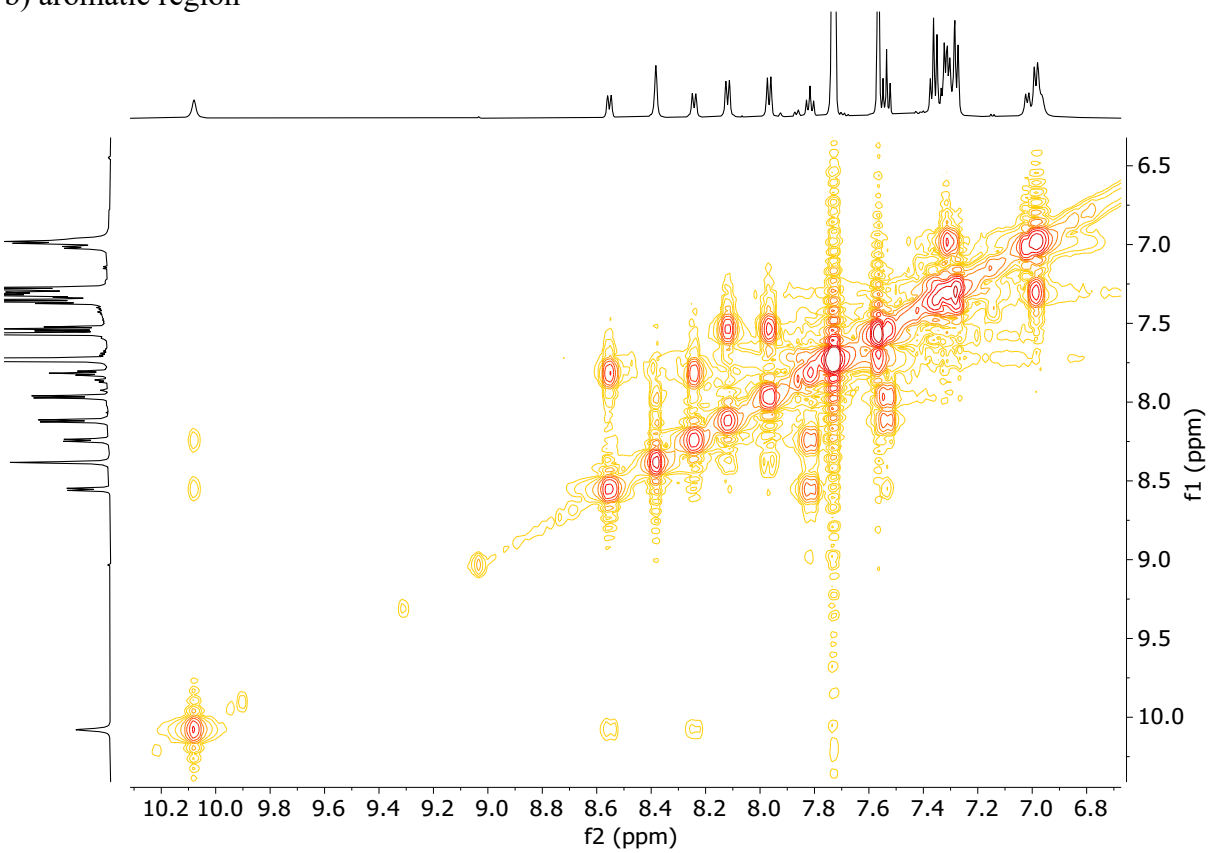

c) Functional group region

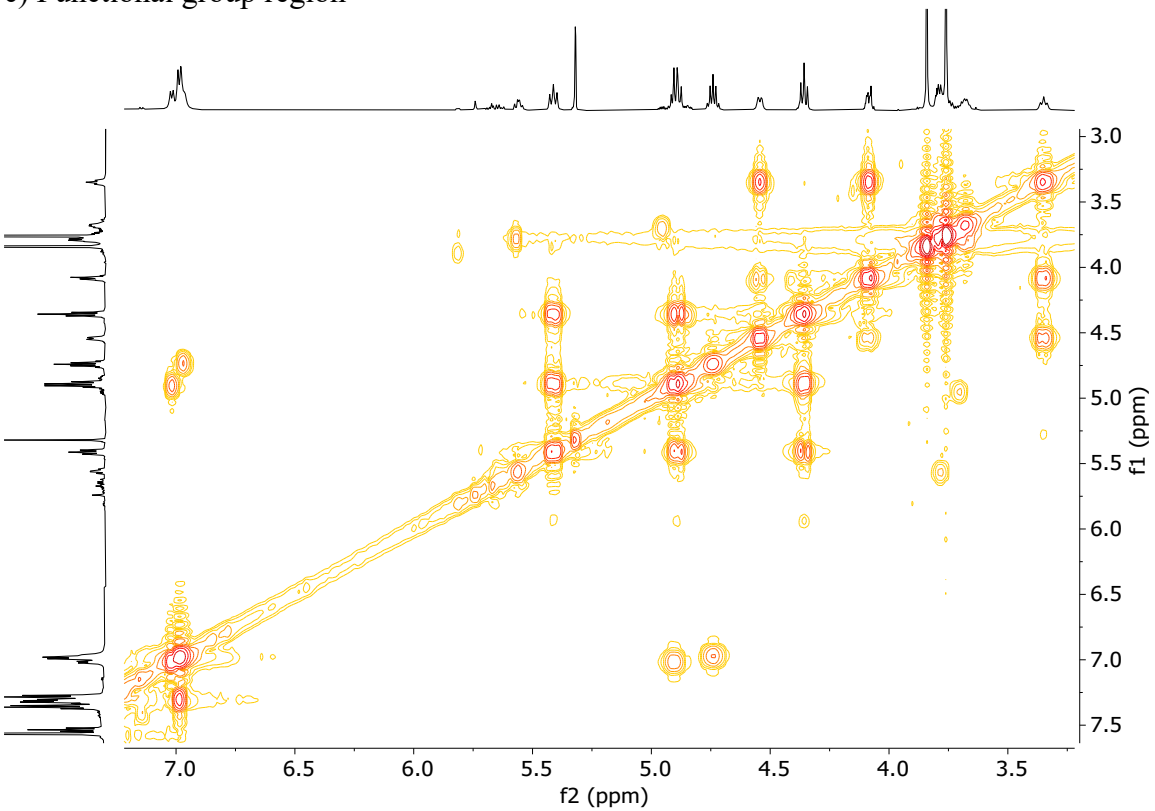

d)Aliphatic group region

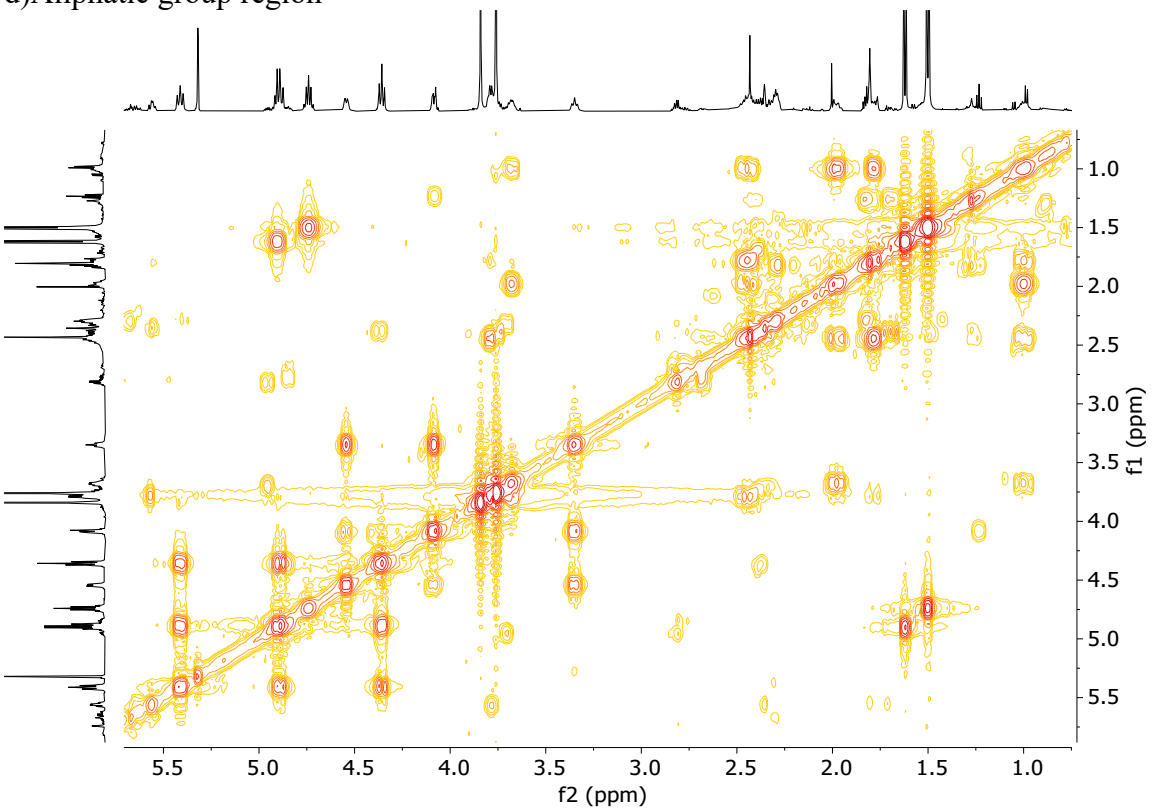

3.3.10. Ir:1p:1c* = 1:1:1

^{1}H NMR (600 MHz, CD_2Cl_2)

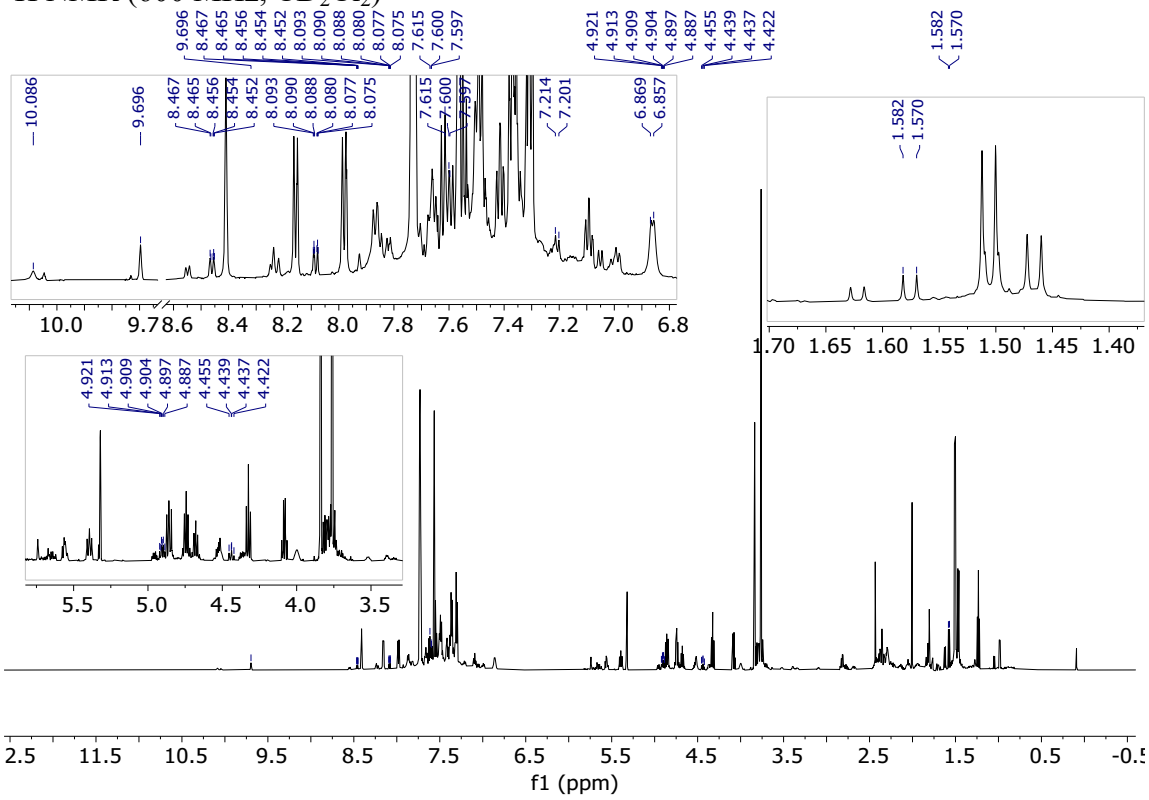

^{31}P NMR (243 MHz, CD_2Cl_2)

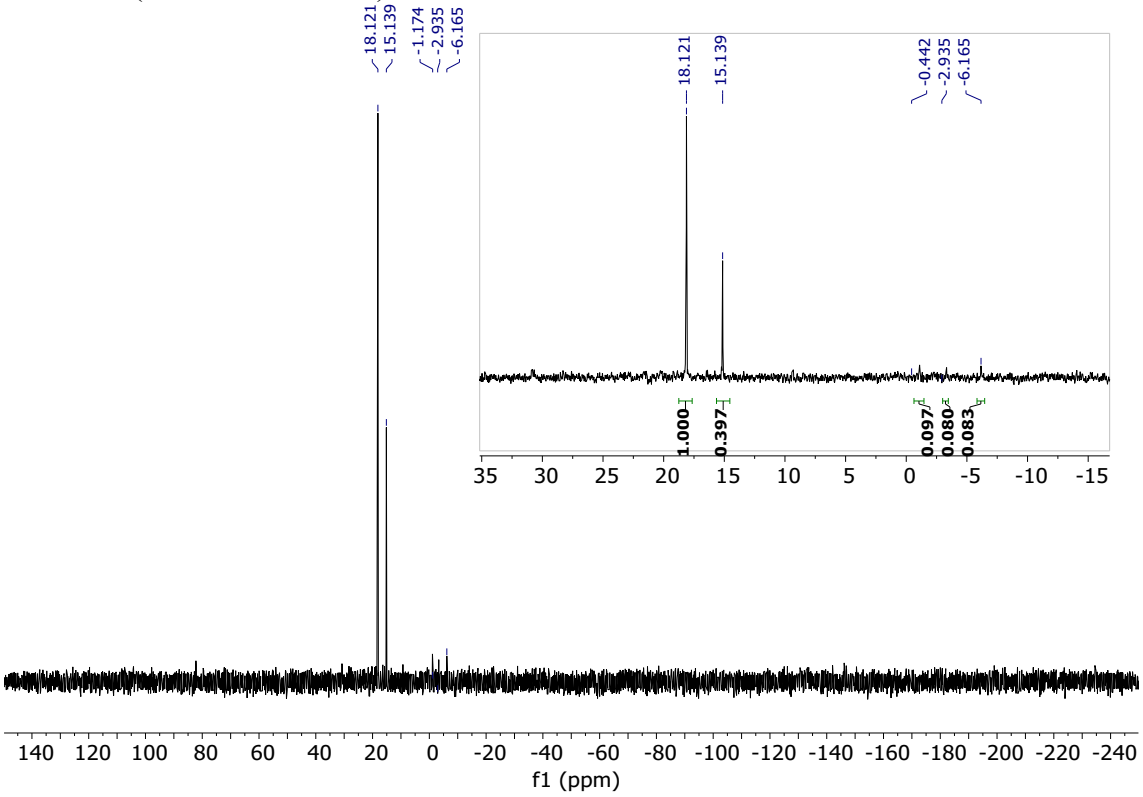

^{13}C NMR (151 MHz, CD_2Cl_2)

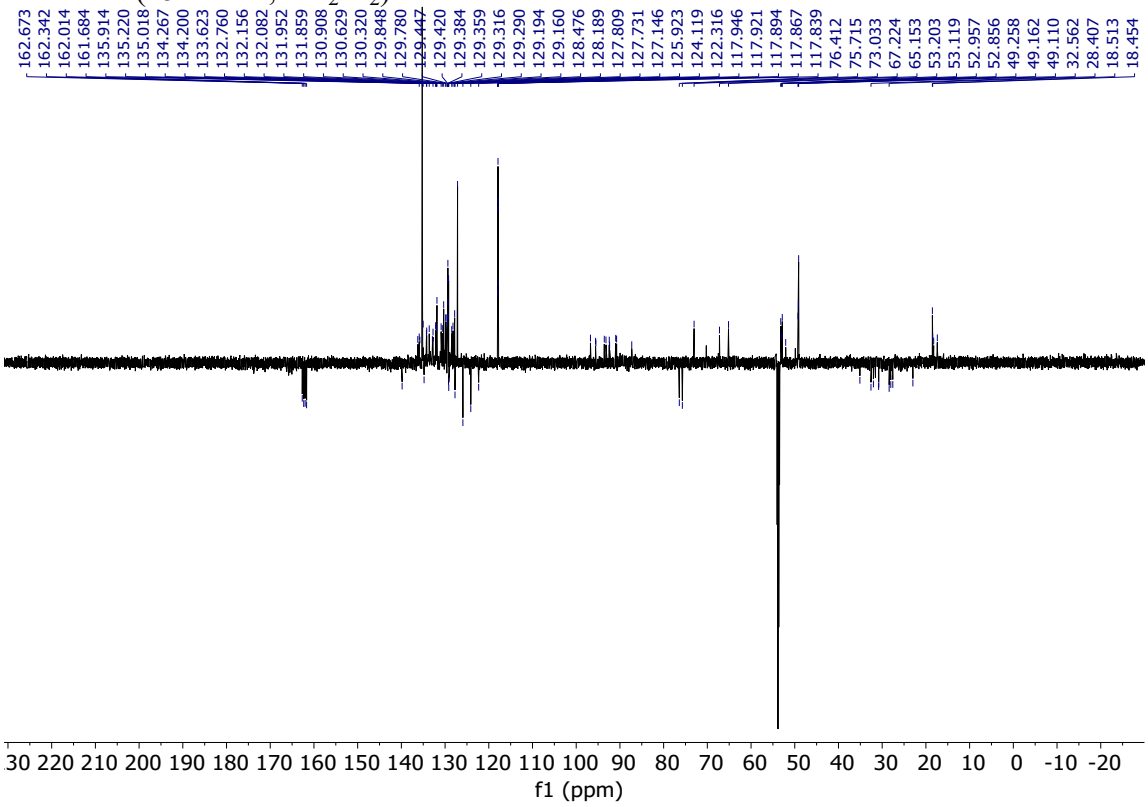

COSY NMR in CD_2Cl_2

a) whole spectra

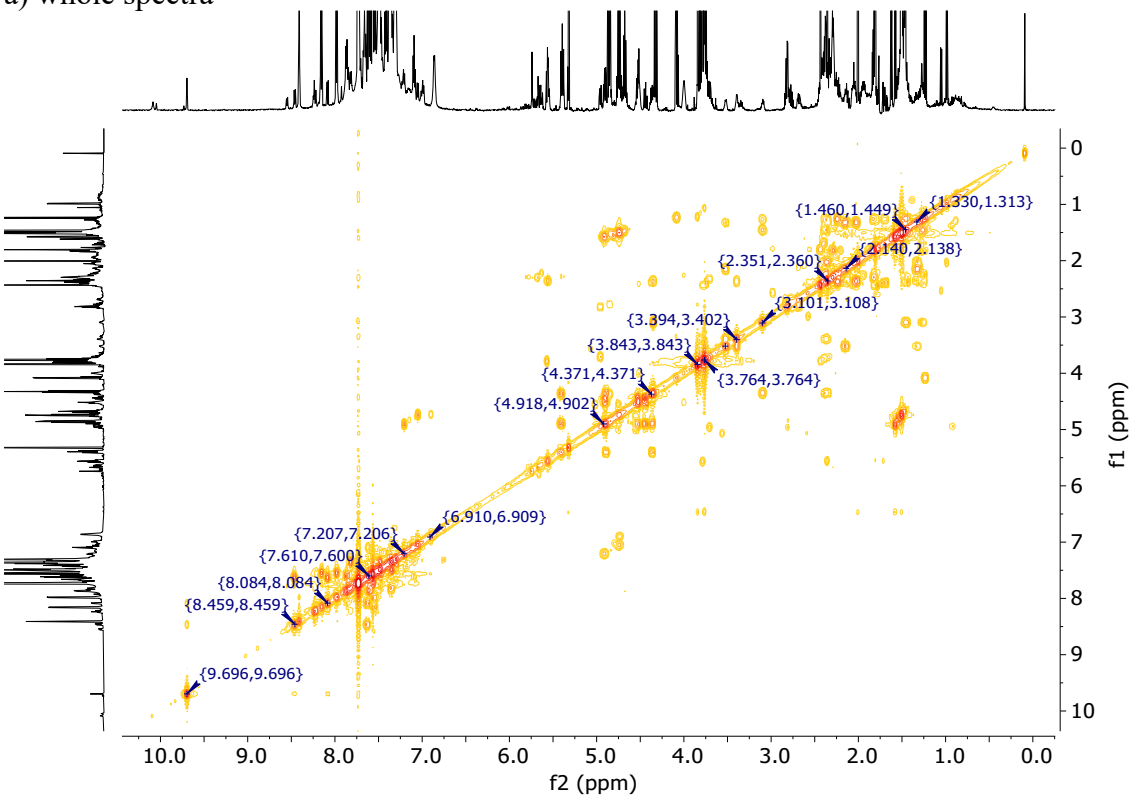

b) aromatic region

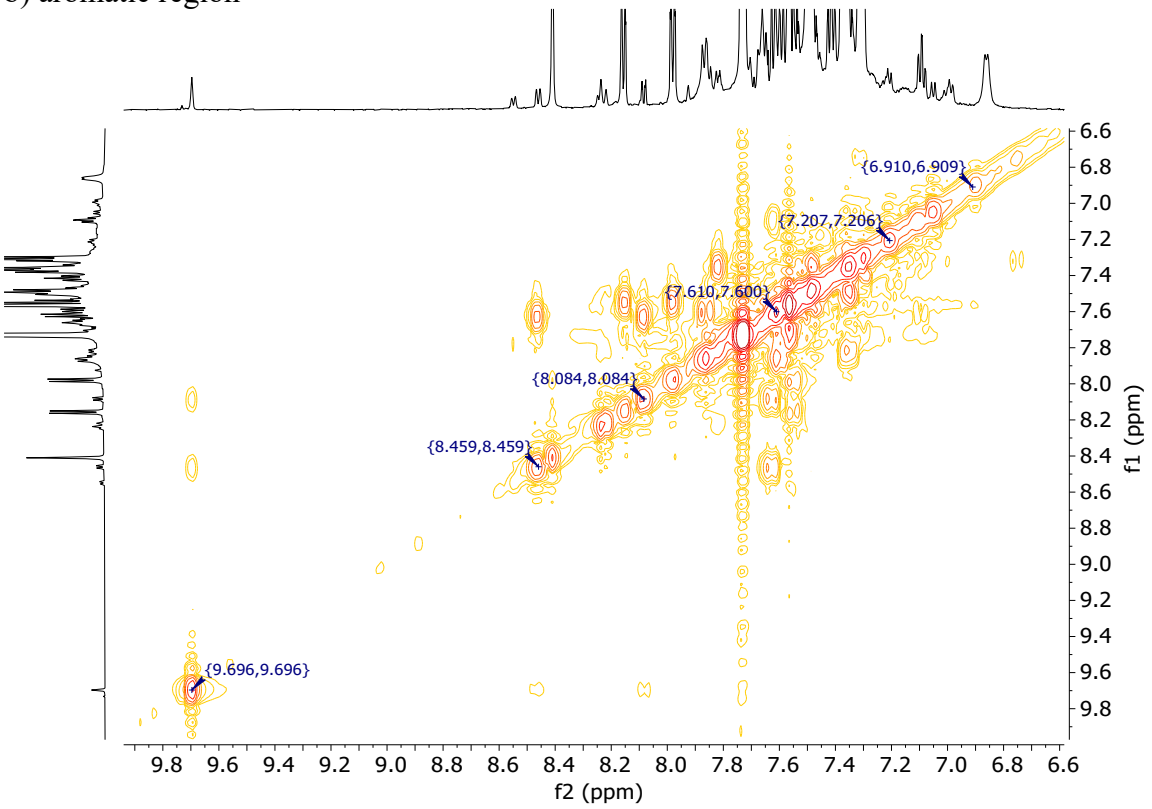

c) Functional group region

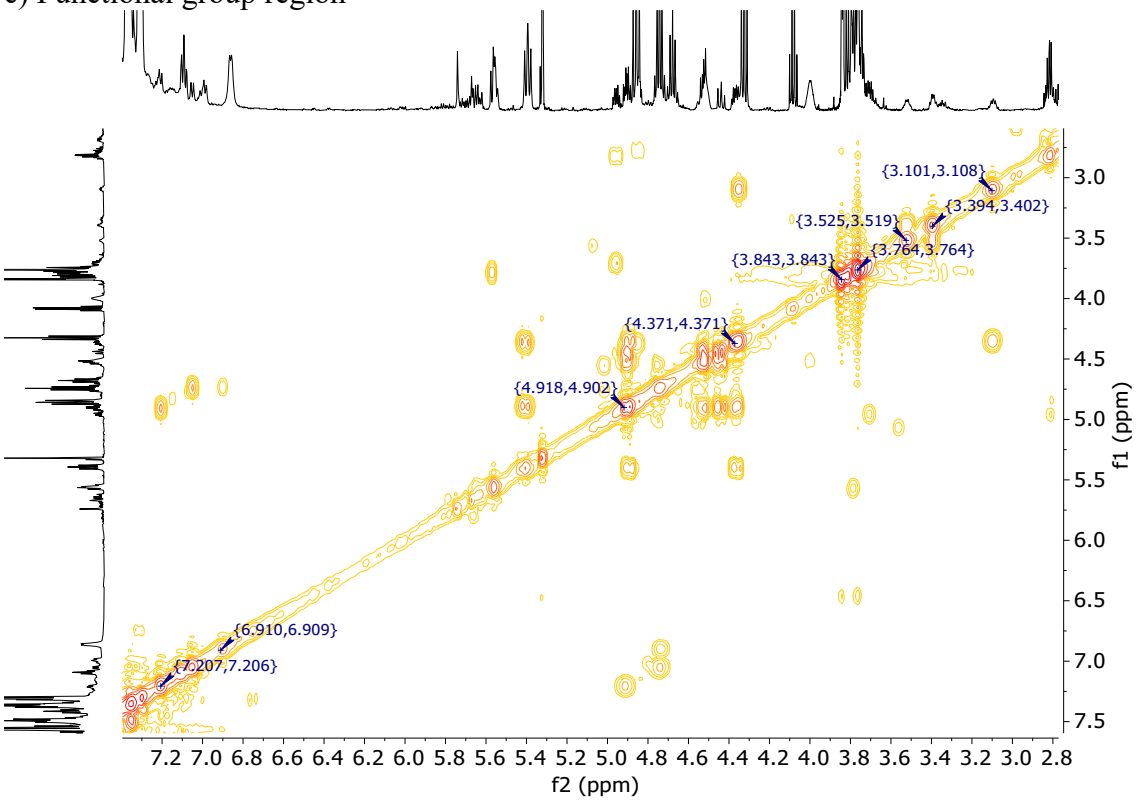

d)Aliphatic group region

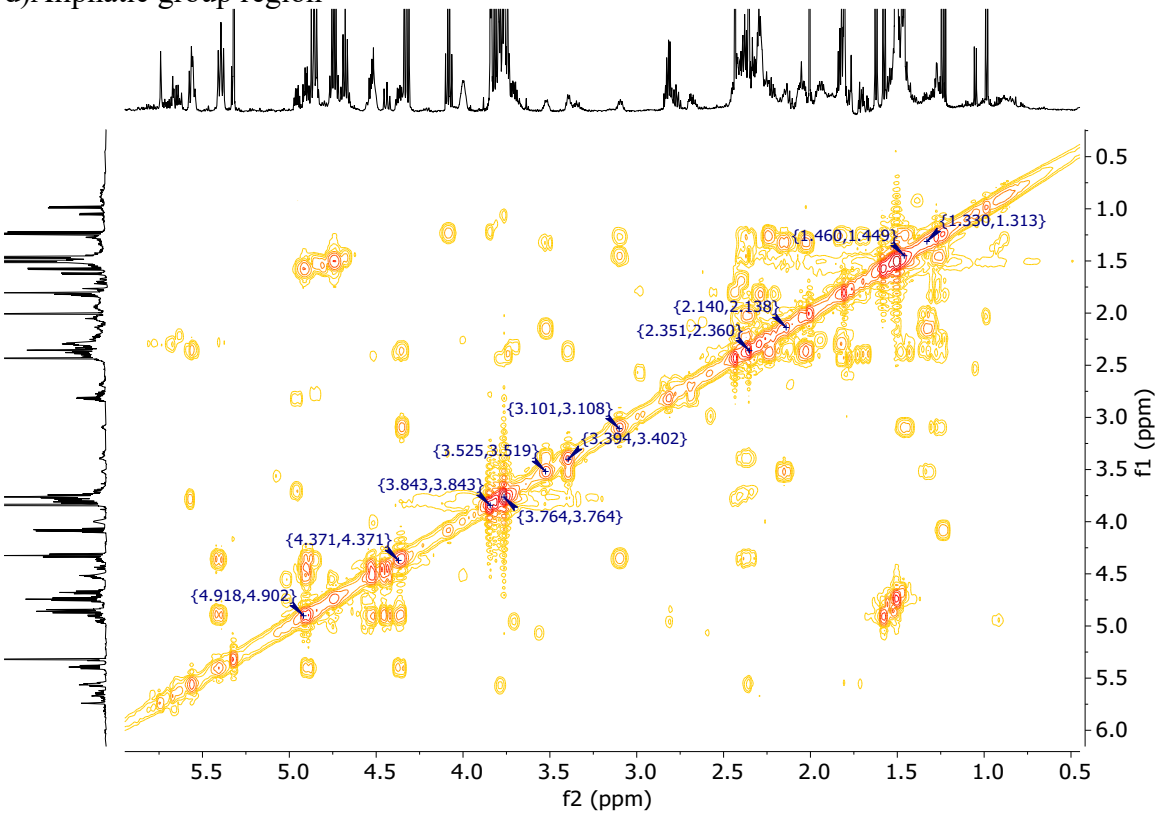

3.3.11. Rh:1p = 1:2

^{1}H NMR (600 MHz, CD_2Cl_2)

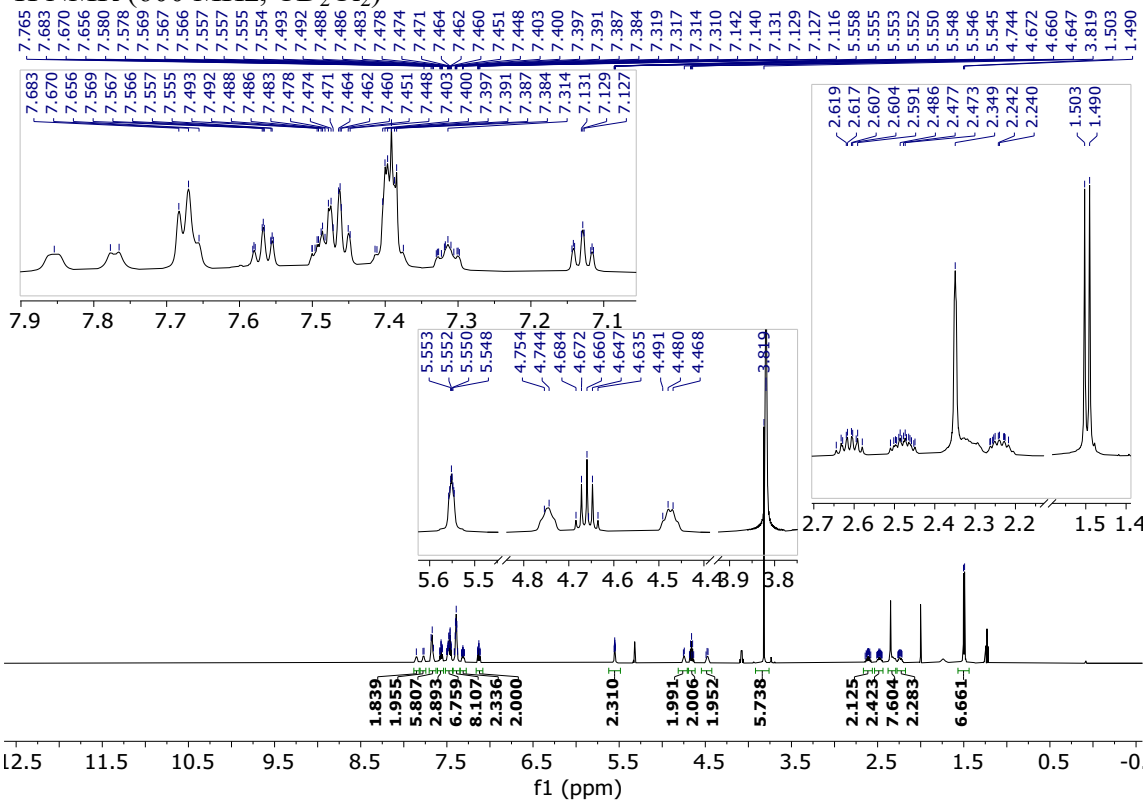

^{31}P NMR (243 MHz, CD_2Cl_2)

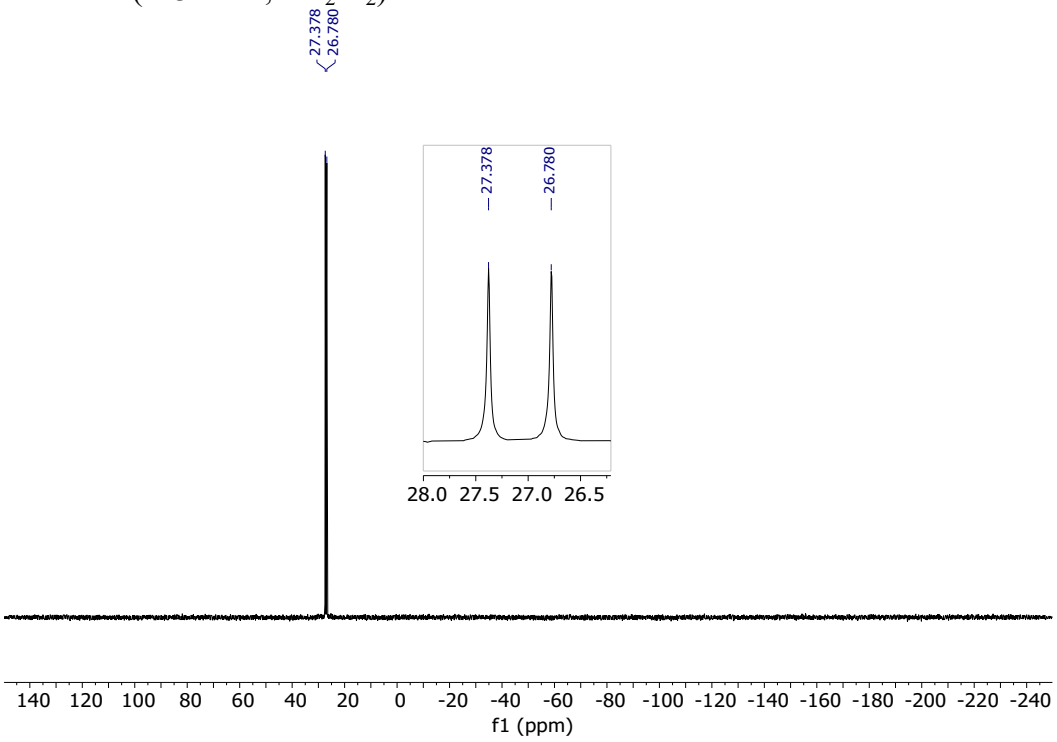

^{13}C NMR (151 MHz, CD_2Cl_2)

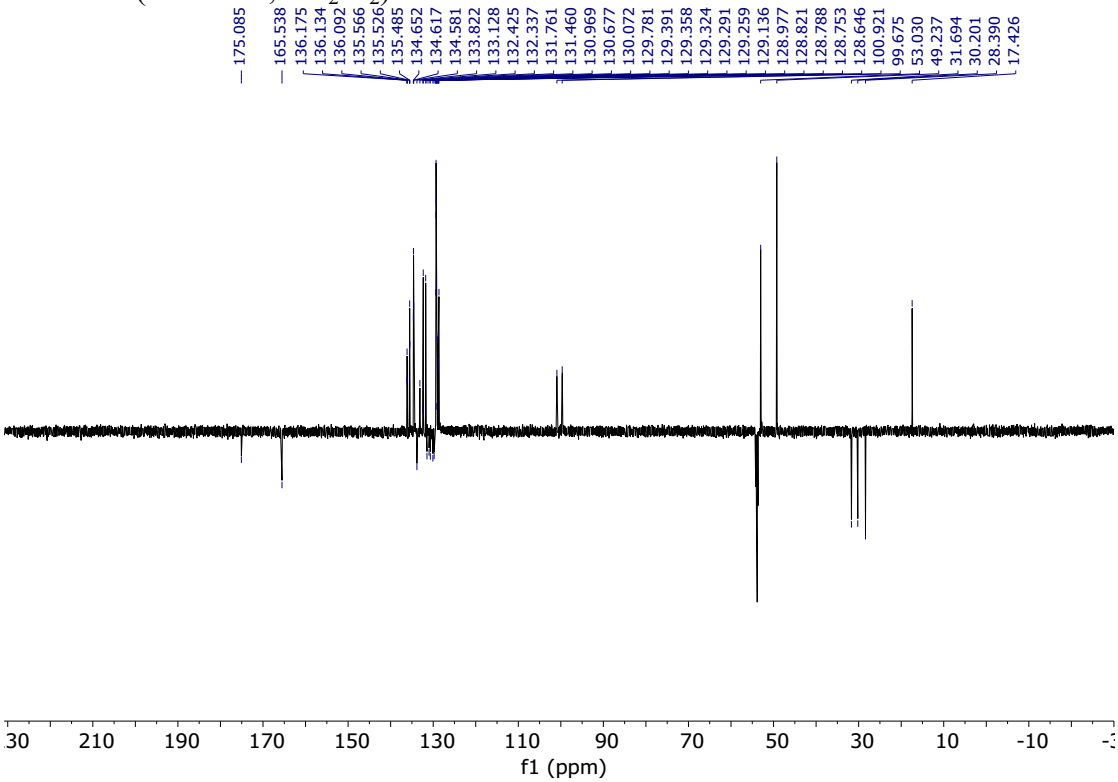

COSY NMR in CD_2Cl_2

a) whole spectra

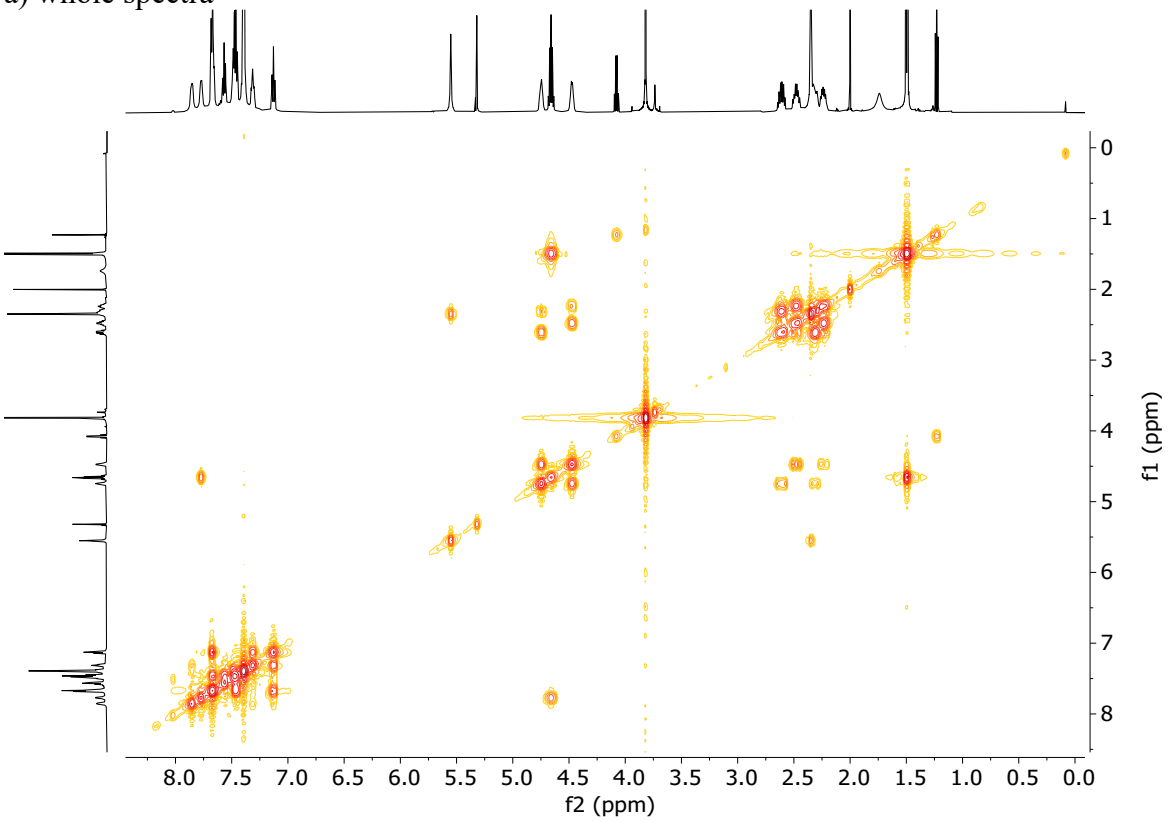

b) aromatic region

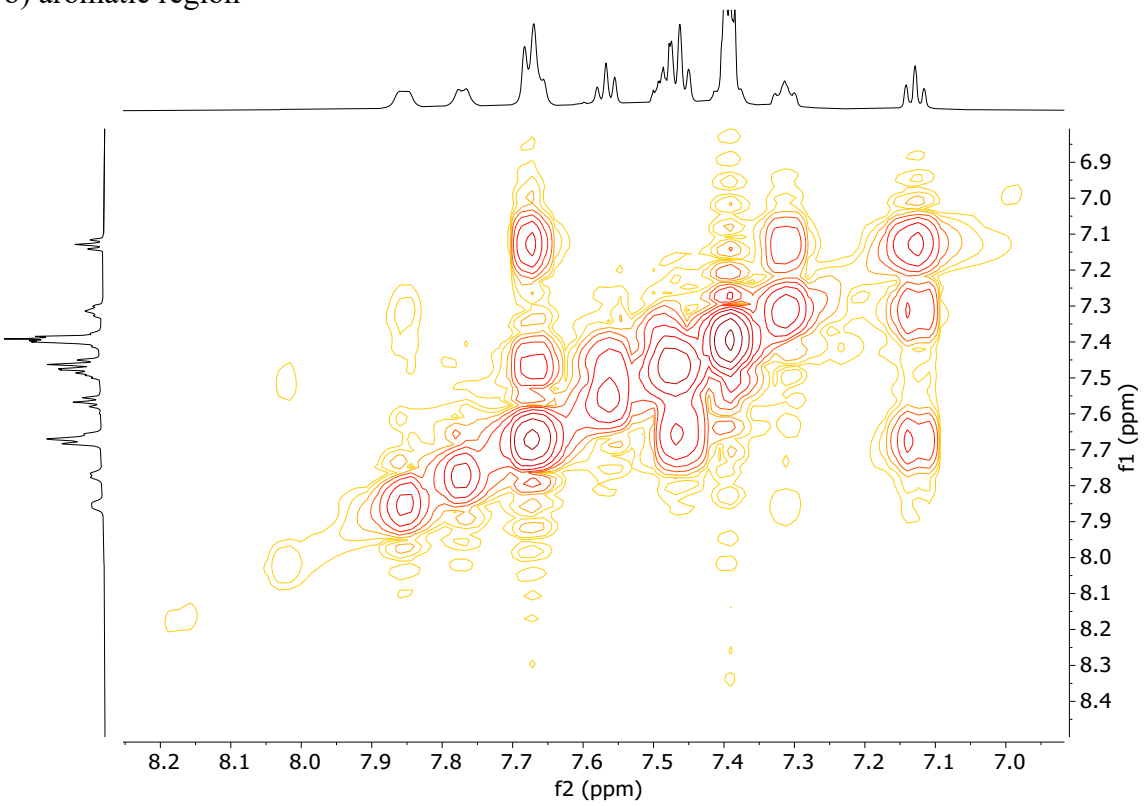

c) Functional group region

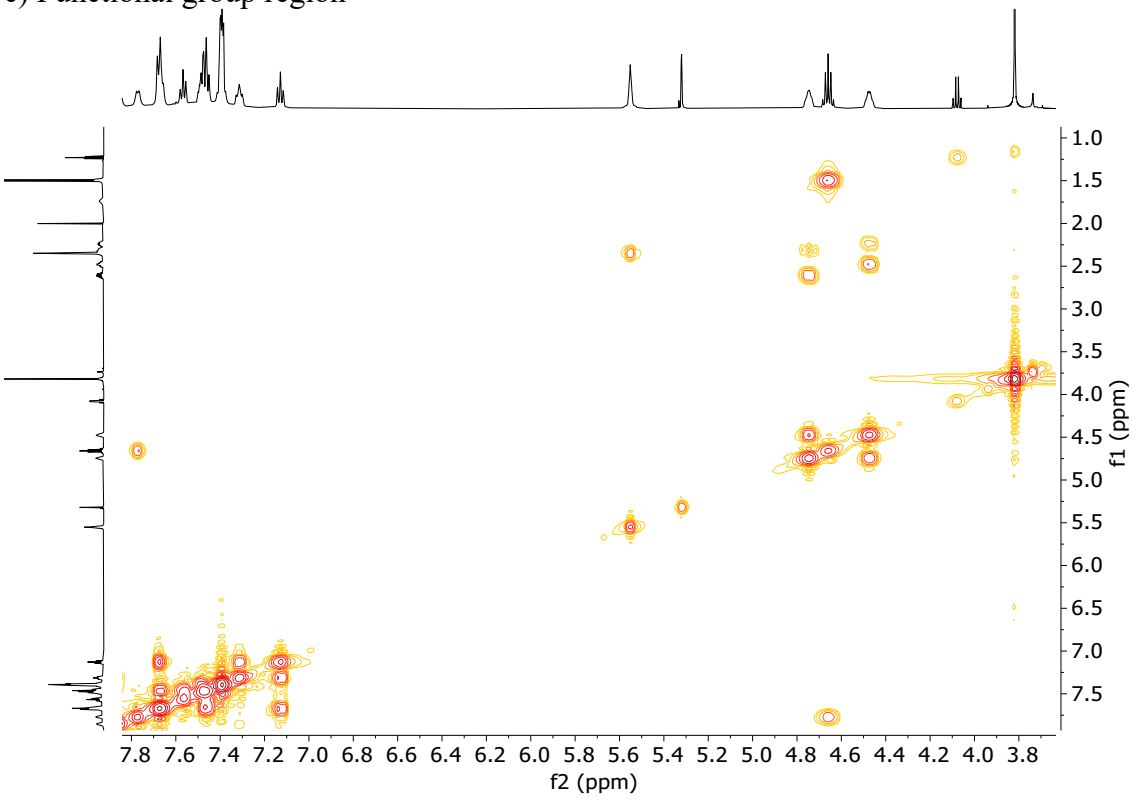

d)Aliphatic group region

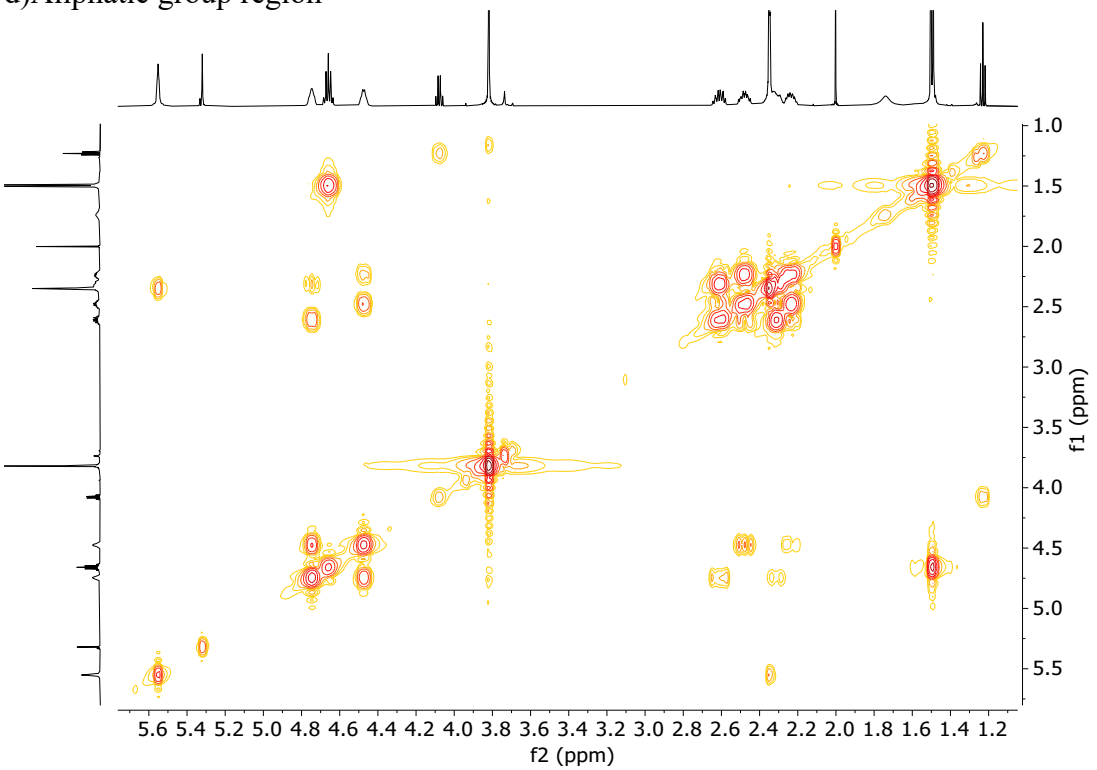

3.3.12. Rh:1c* = 1:1

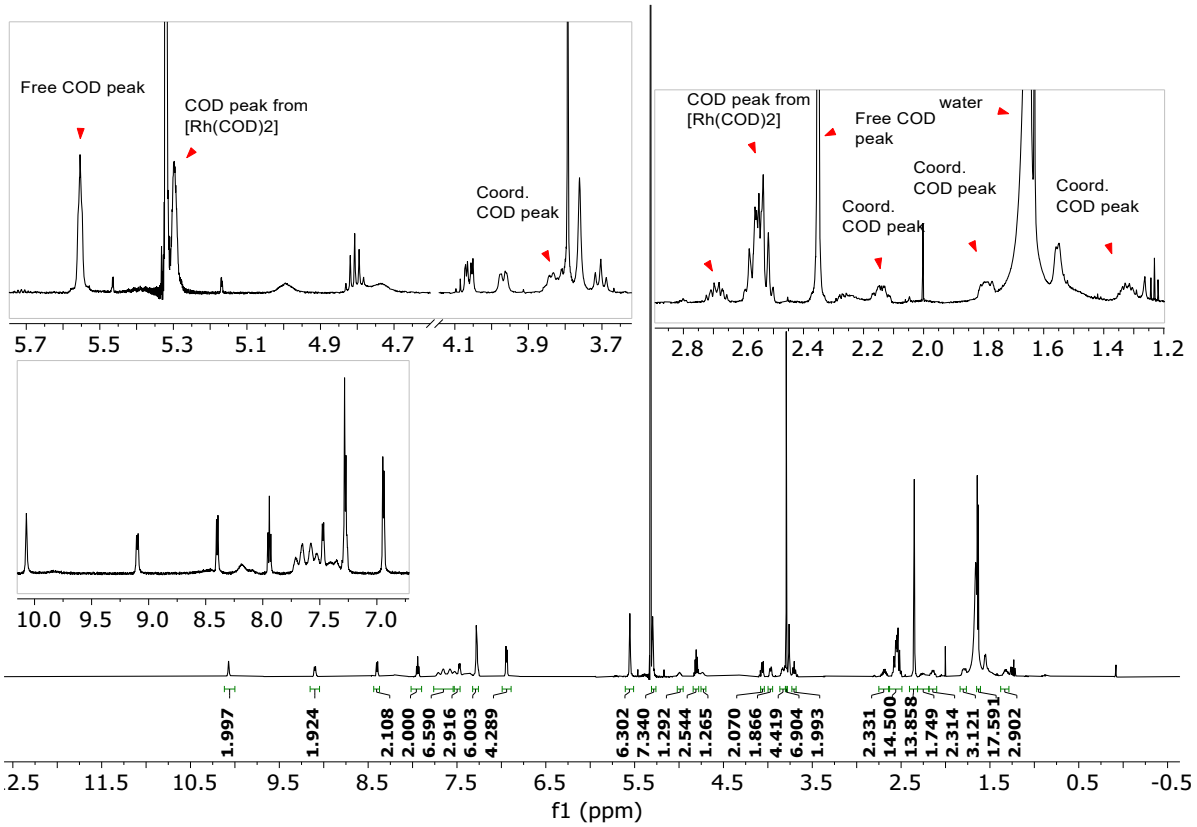
Free COD peak
COD peak from [Rh(COD)2]
Coord. COD peak
COD peak from [Rh(COD)2]
Free COD peak
water
Coord. COD peak
Coord. COD peak
Coord. COD peak
1.997
1.924
2.108
2.000
6.590
2.916
6.003
4.289
6.302
7.340
1.292
2.544
1.265
2.070
1.866
4.419
6.904
1.993
2.331
14.500
13.858
1.749
2.314
3.121
17.591
2.902
f1 (ppm)

3.3.13. Rh:1c* = 1:2

^{1}H NMR (600 MHz, CD_2Cl_2)

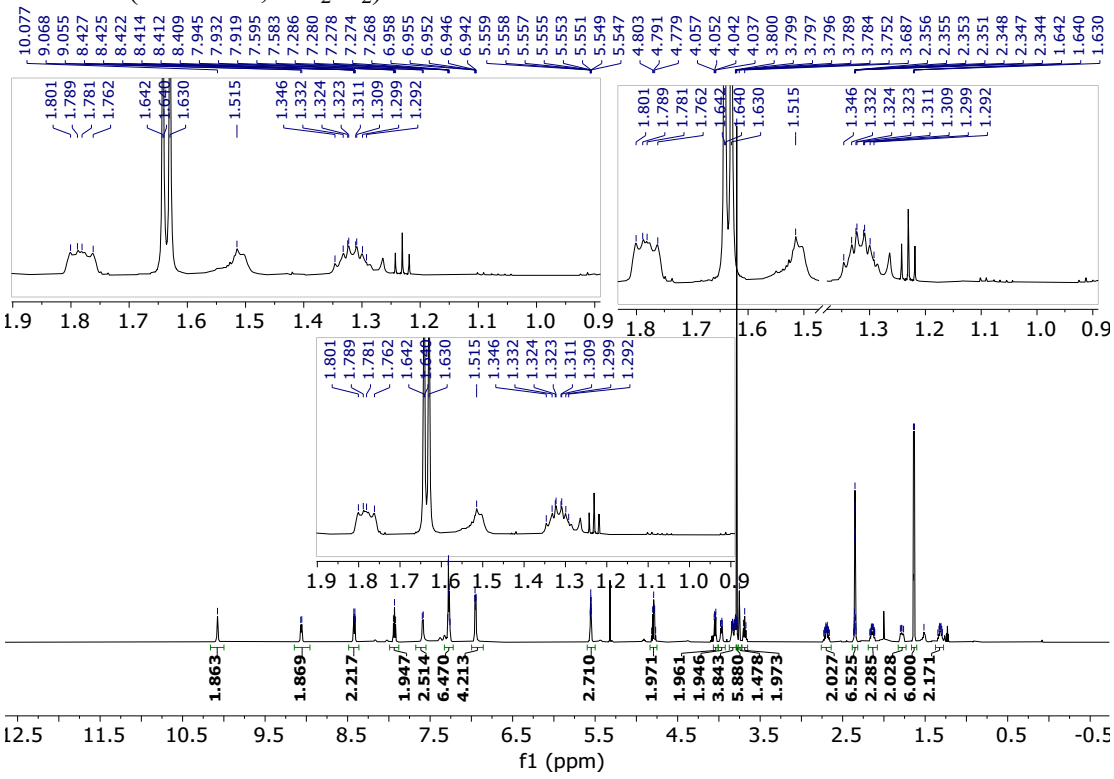

^{13}C NMR (151 MHz, CD_2Cl_2)

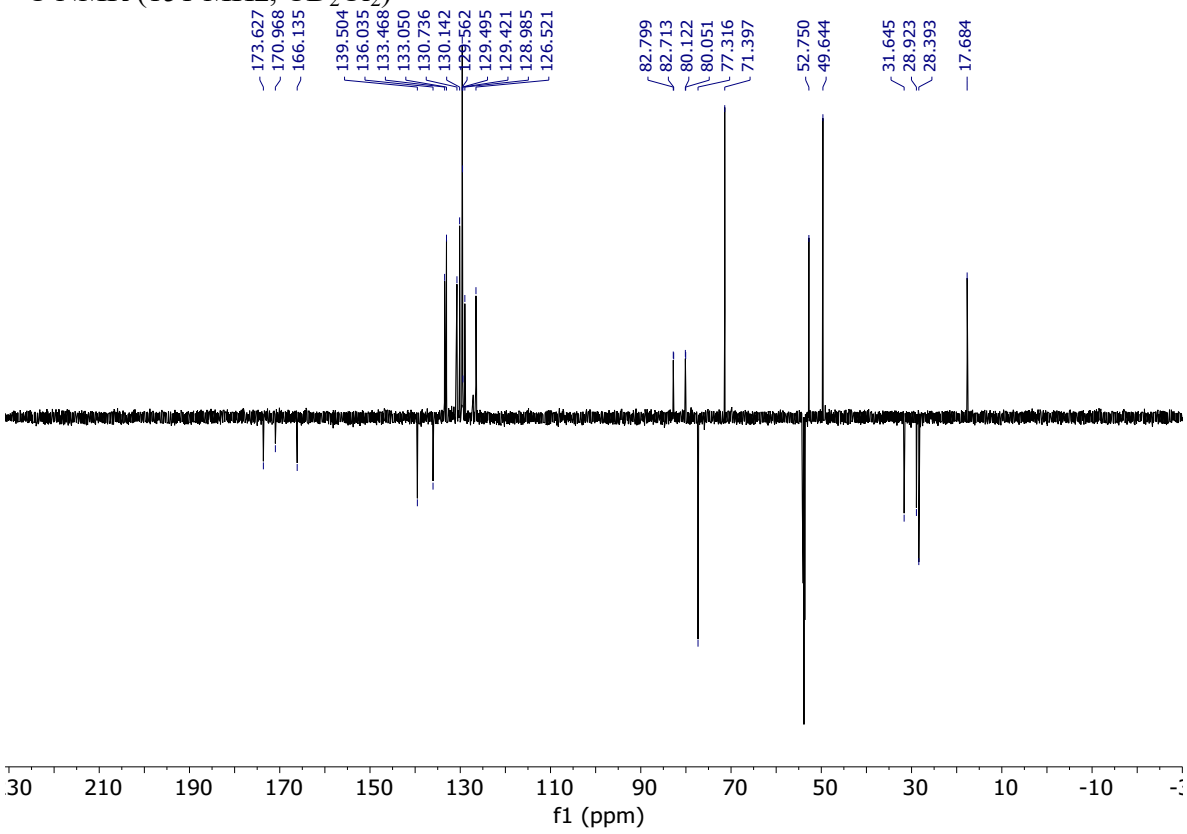

COSY NMR in CD_2Cl_2

a) whole spectra

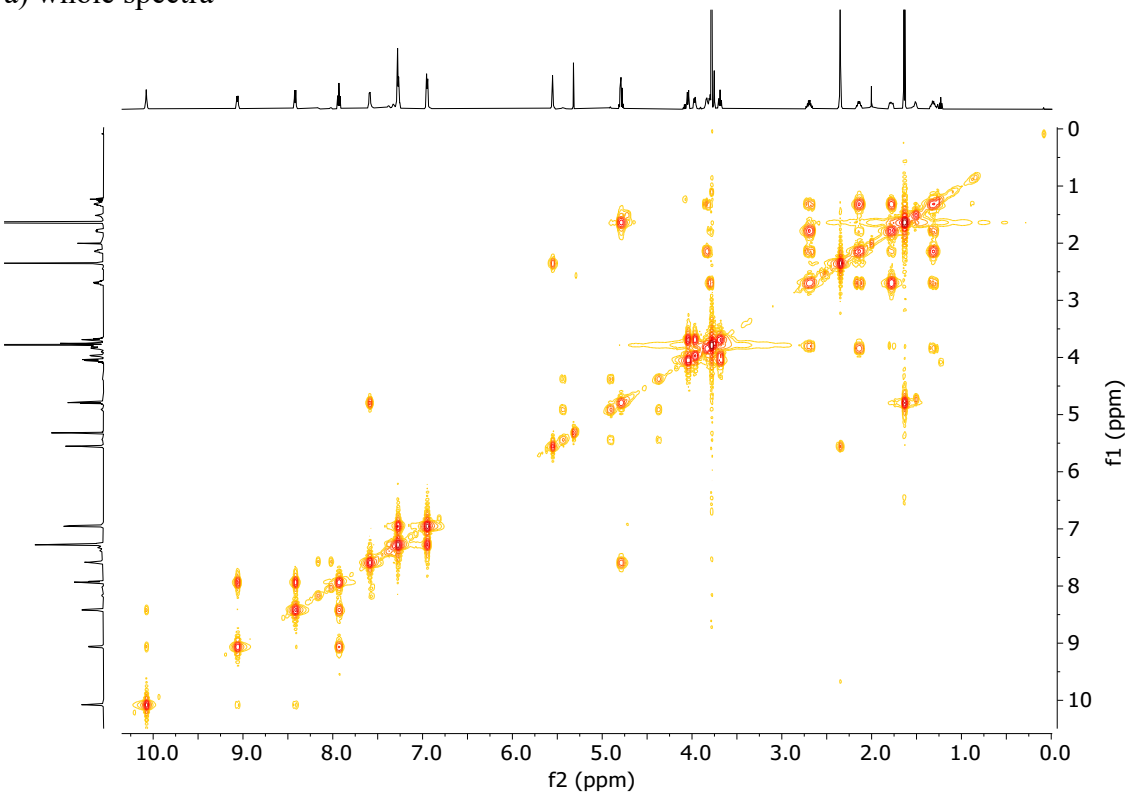

b) aromatic region

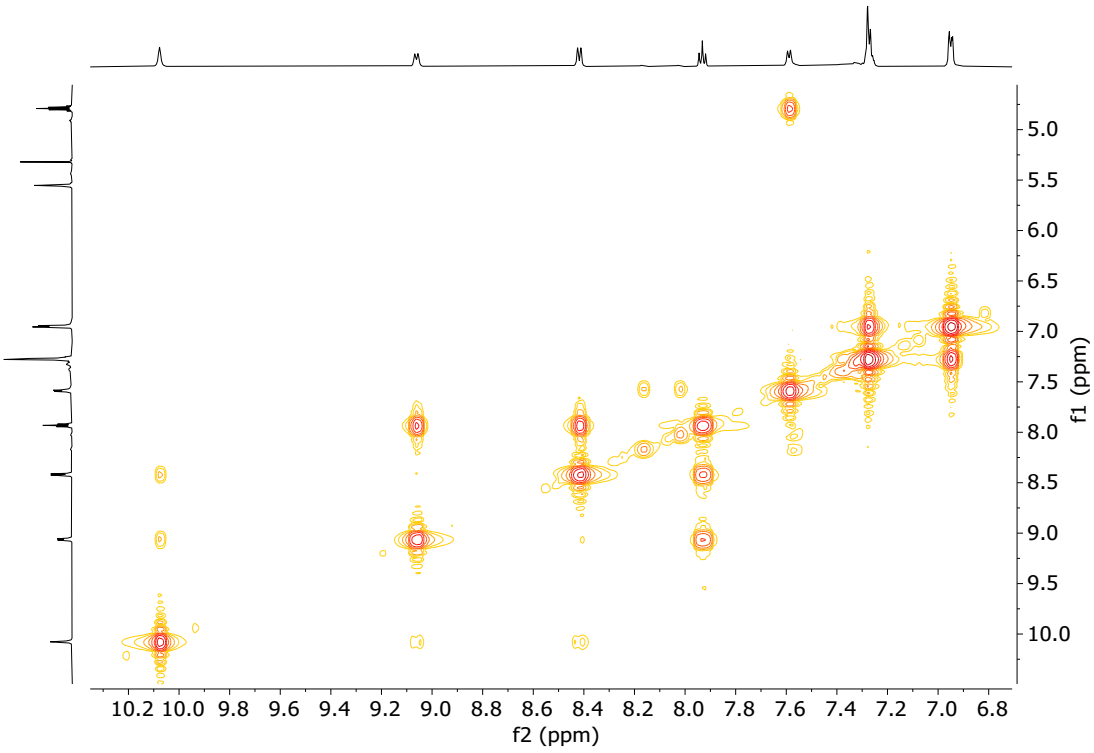

c) Functional group region

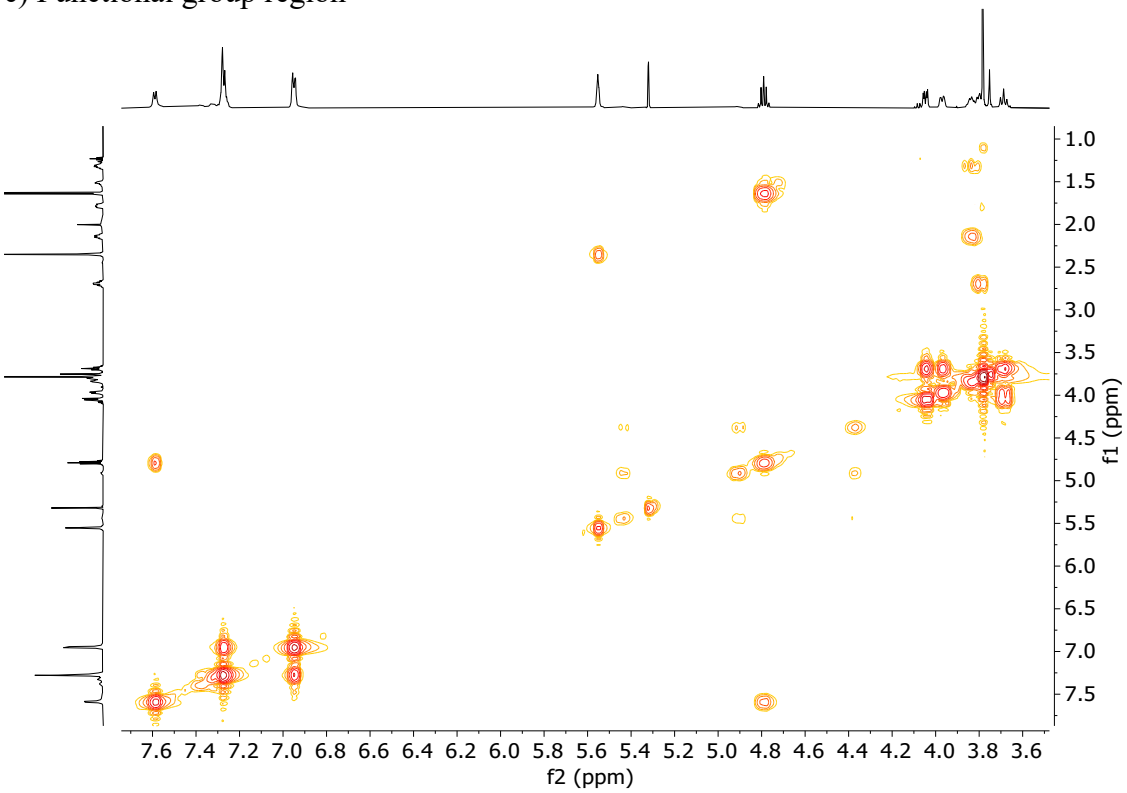

d)Aliphatic group region

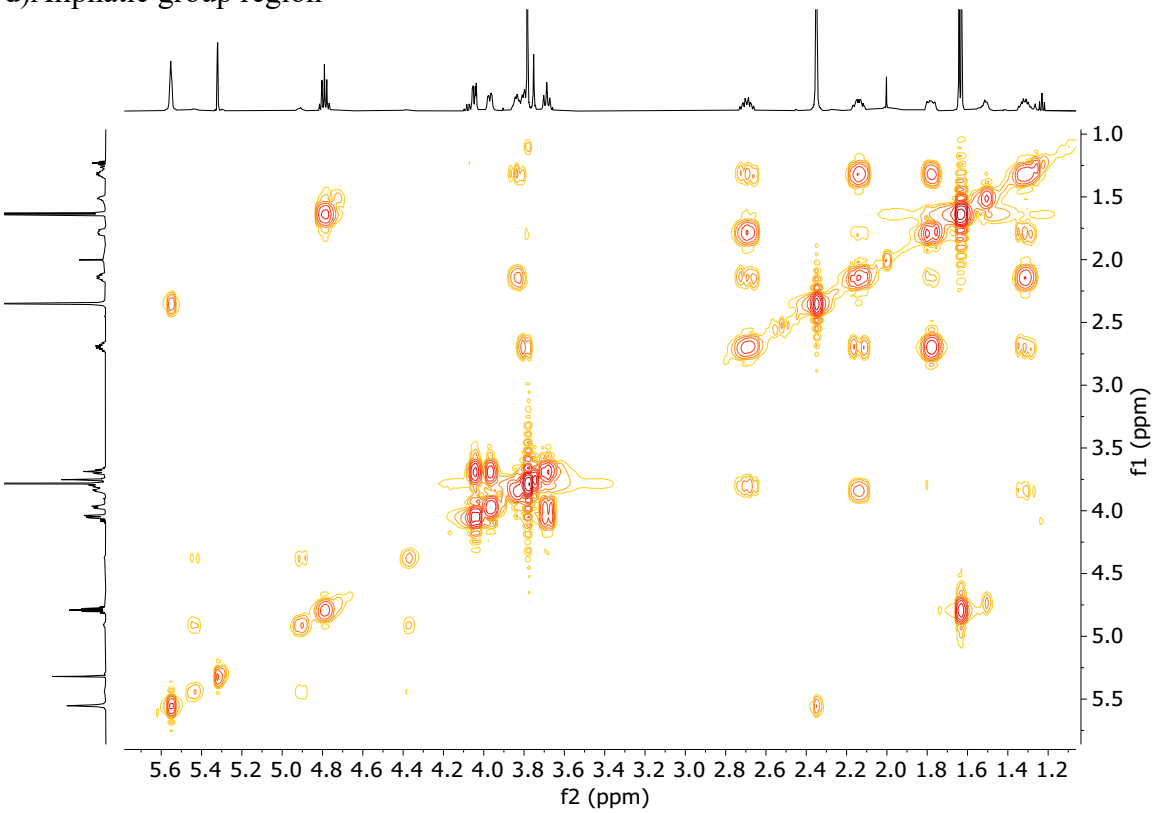

HSQC in CD_2Cl_2

a) whole spectra

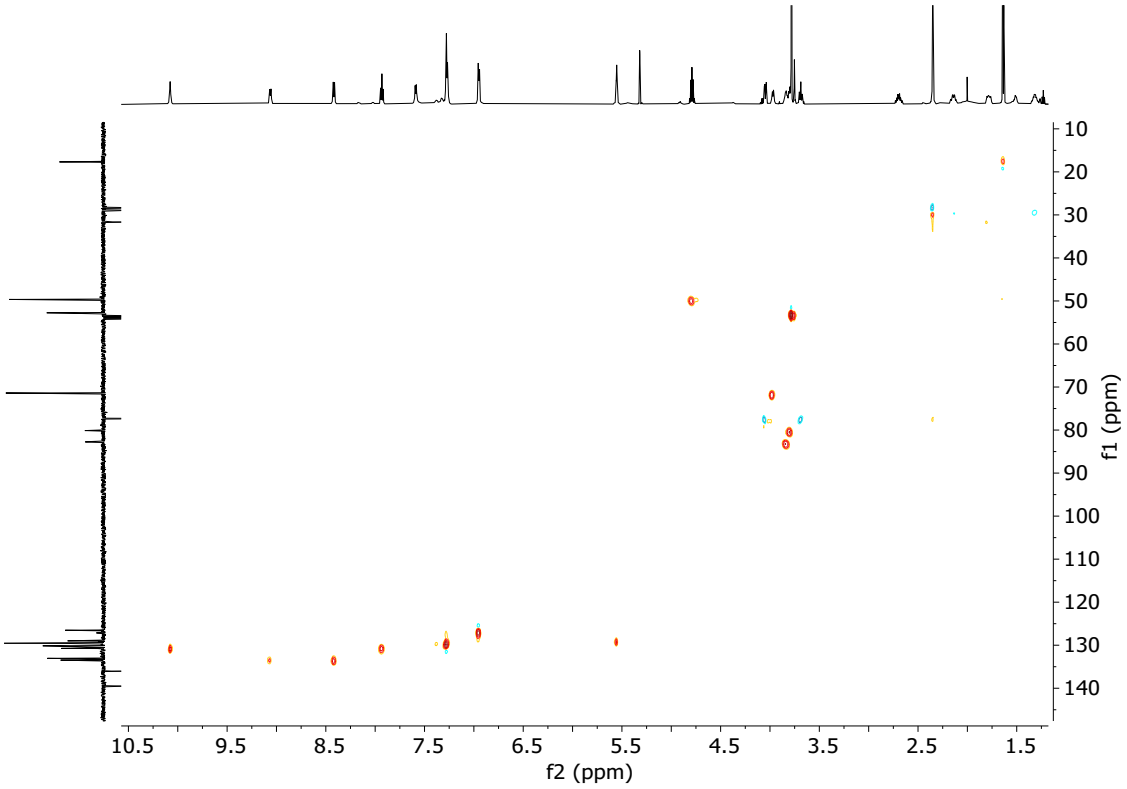

b) Aromatic region

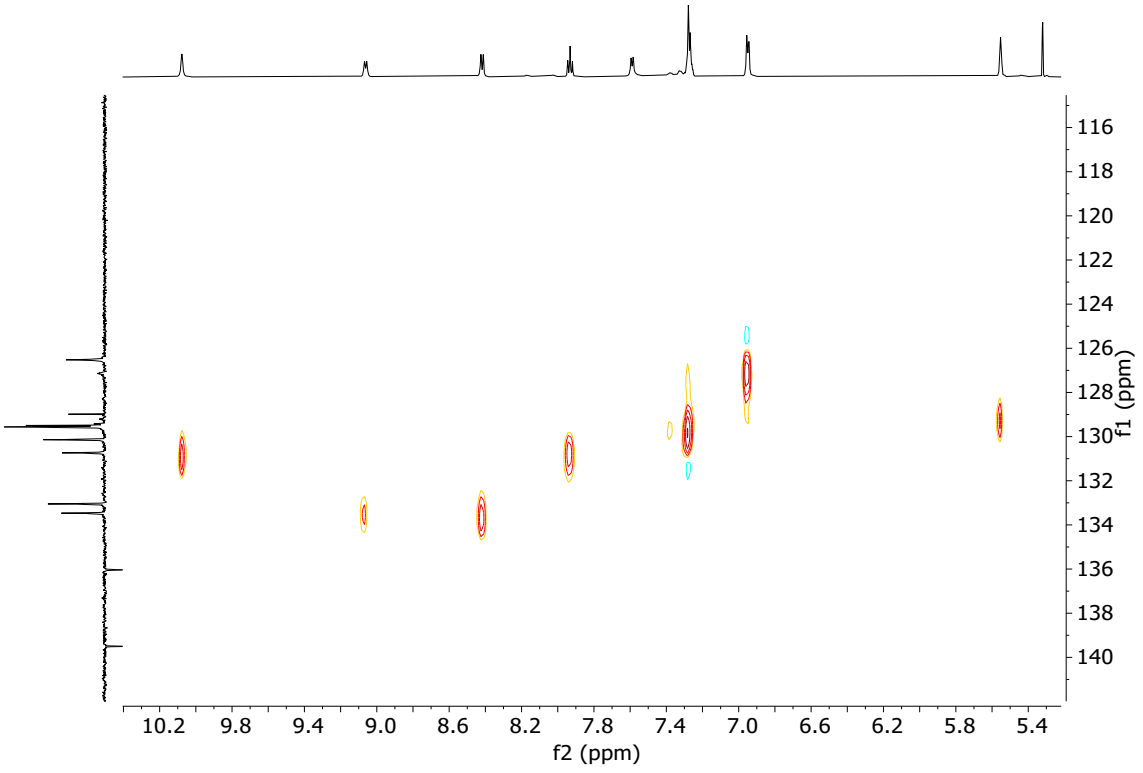

b) Functional group region

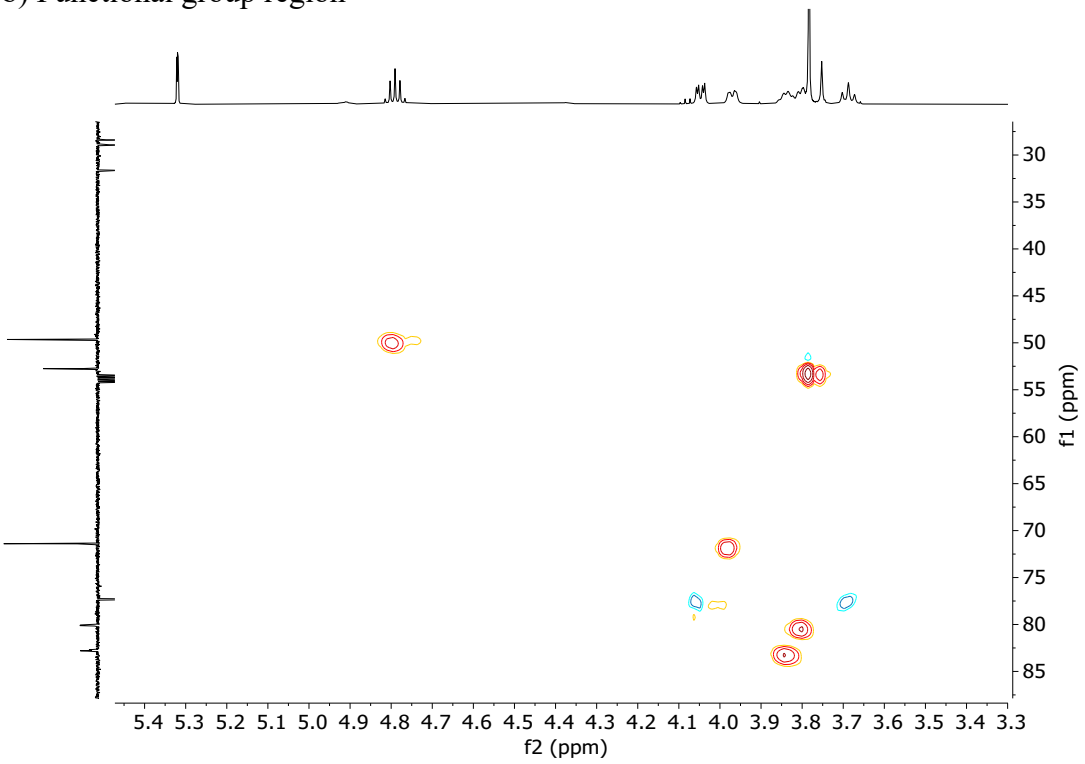

c) Aliphathic group region

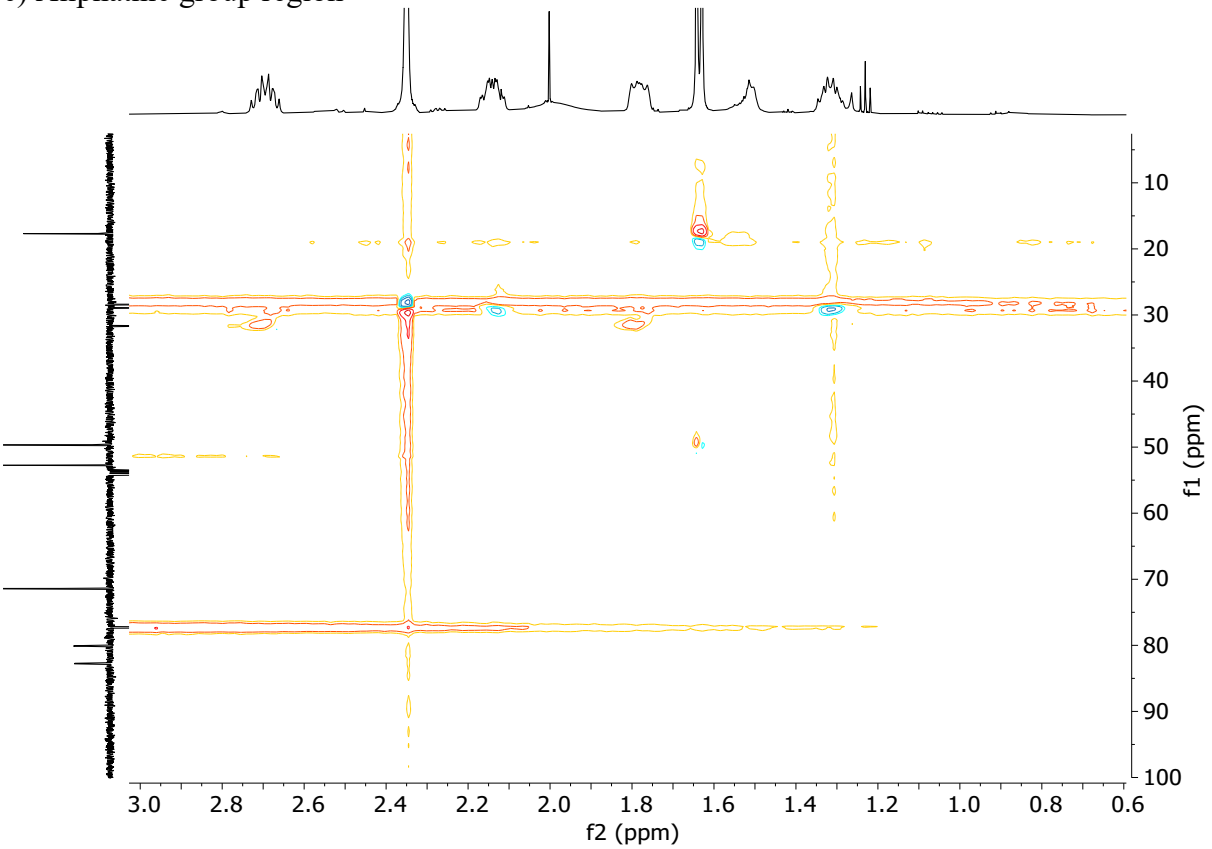

3.3.14. Rh:1p:1c* = 1:1:1

^{1}H NMR (600 MHz, CD_2Cl_2)

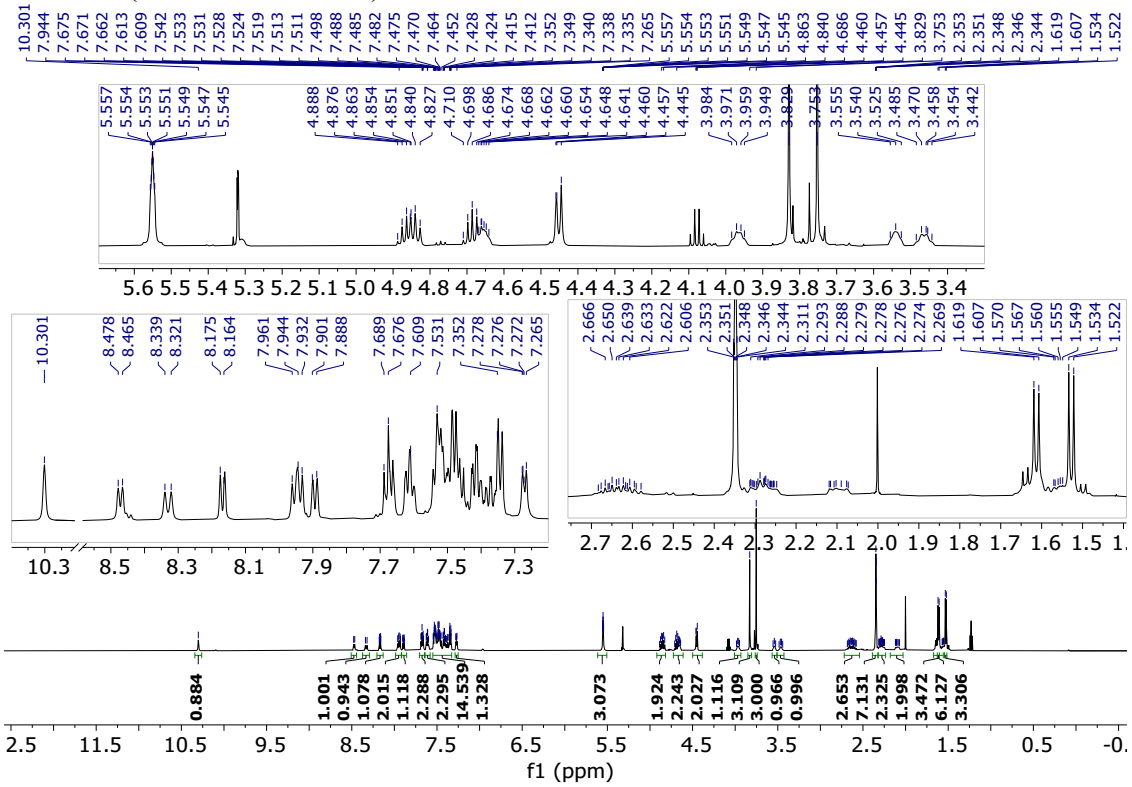

^{31}P NMR (243 MHz, CD_2Cl_2)

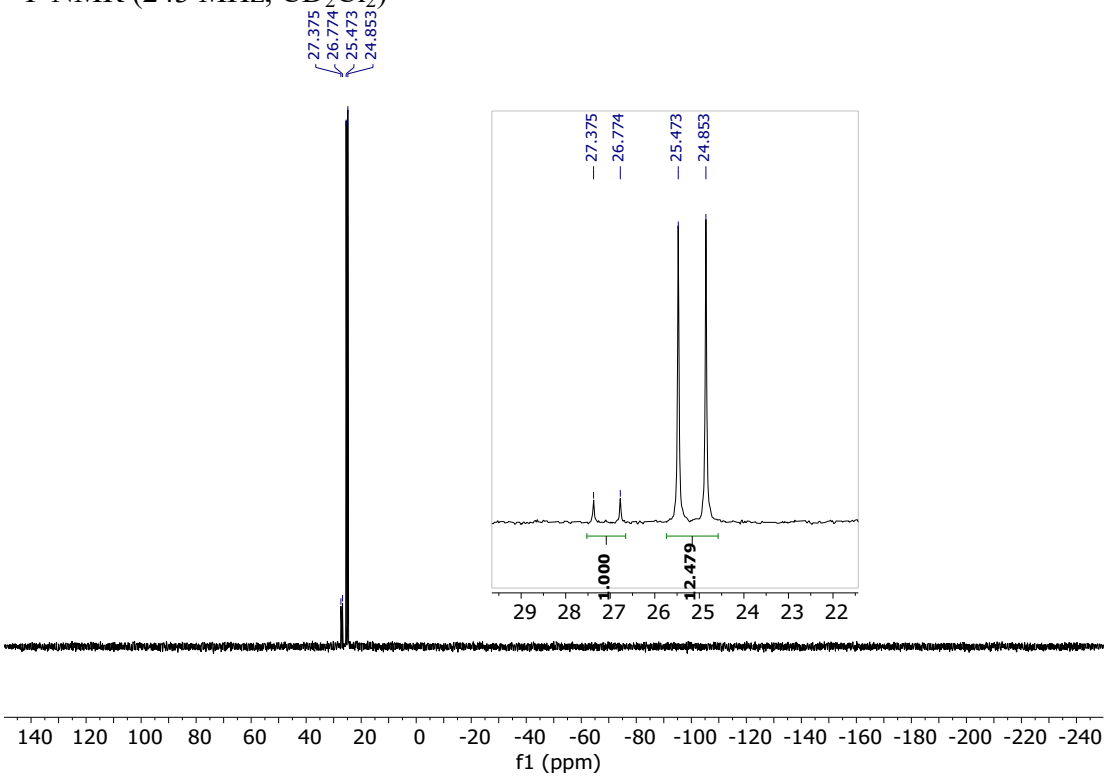

^{13}C NMR (151 MHz, CD_2Cl_2)

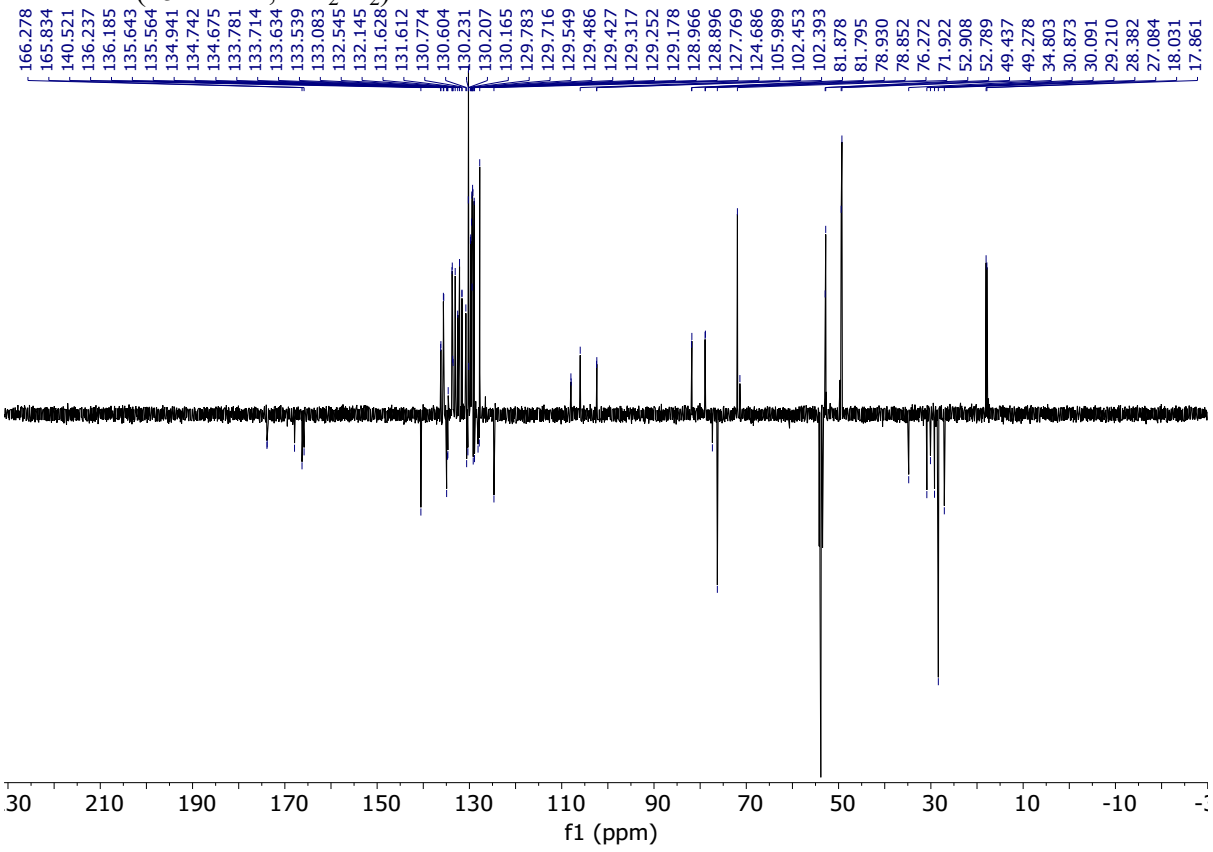

COSY NMR in CD_2Cl_2

a) whole spectra

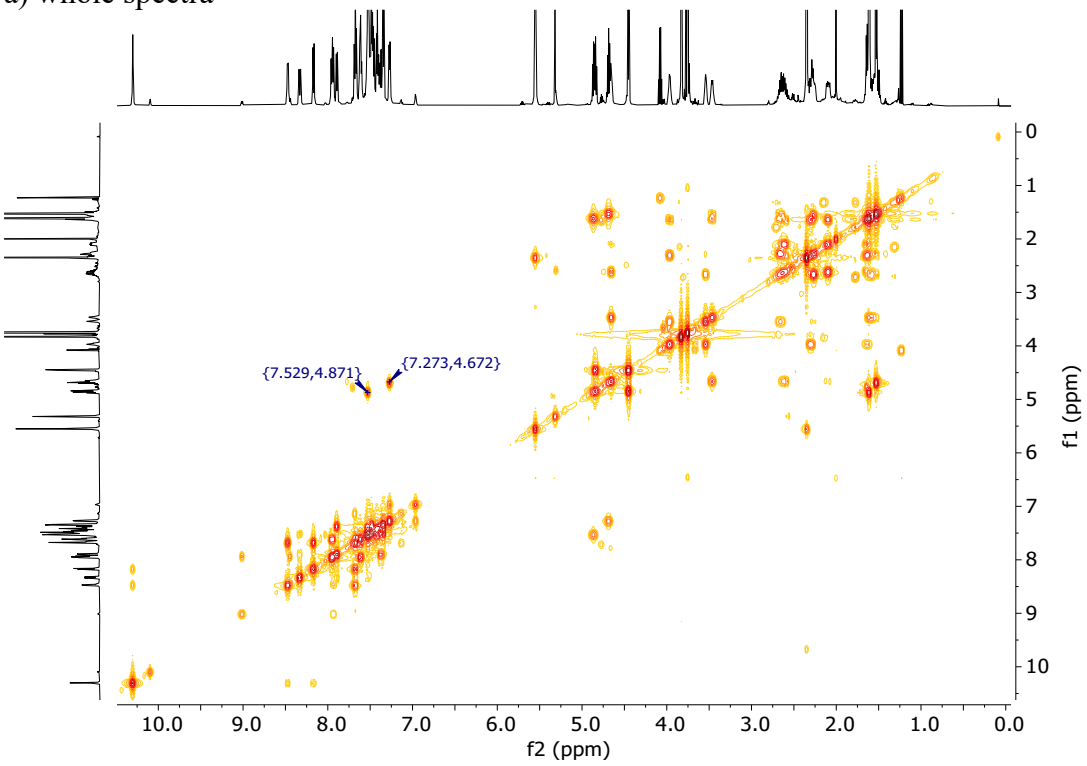

b) aromatic region

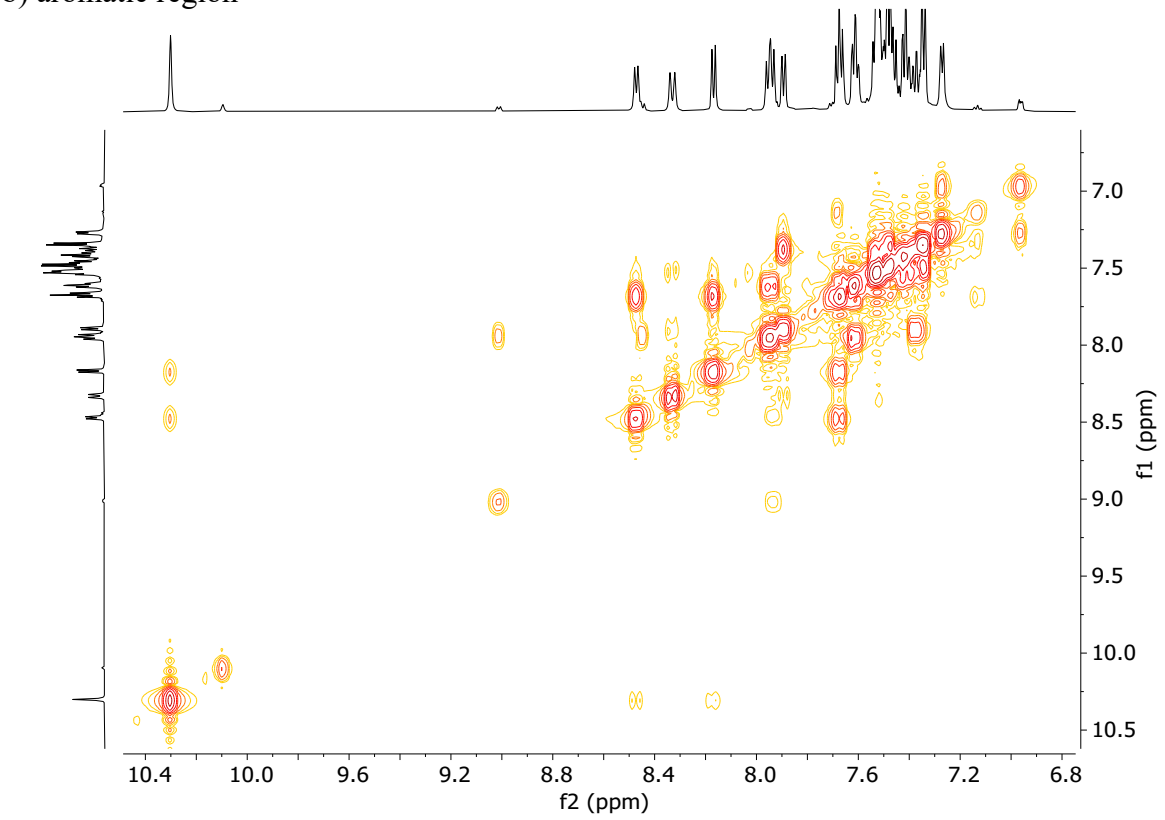

c) Functional group region

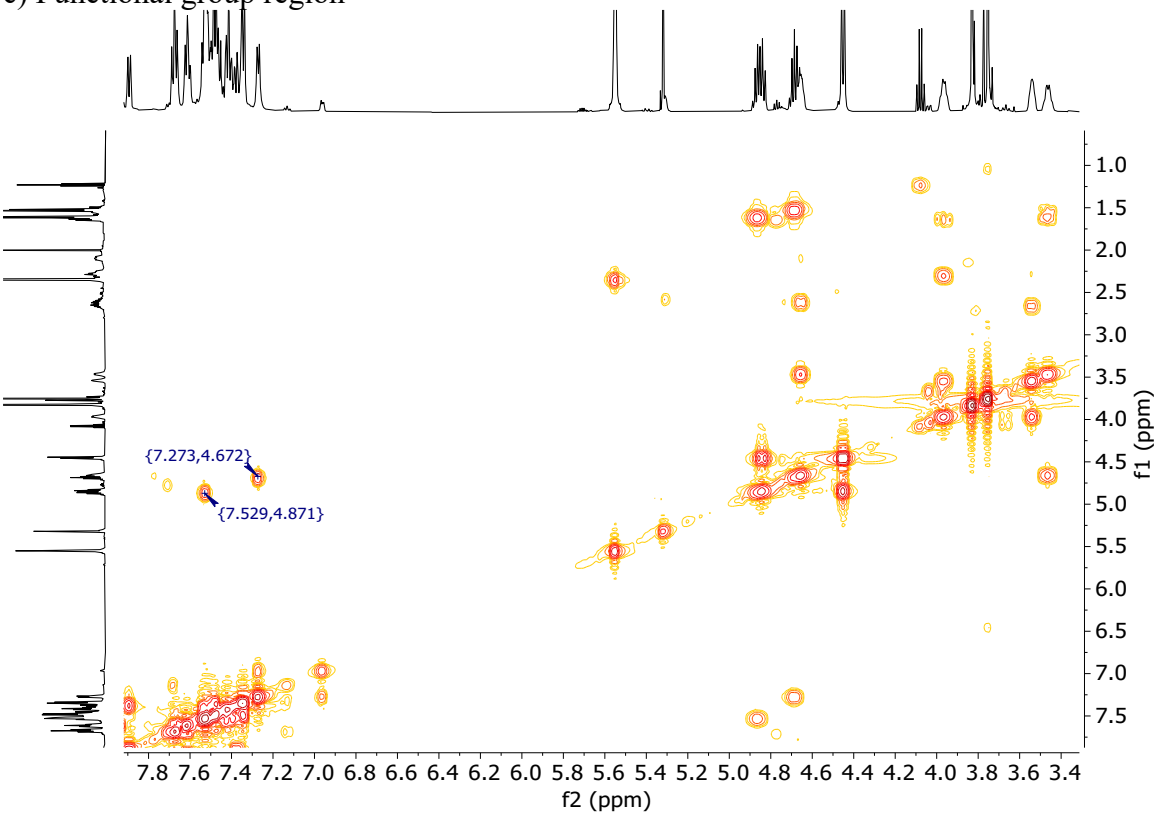

d)Aliphatic group region

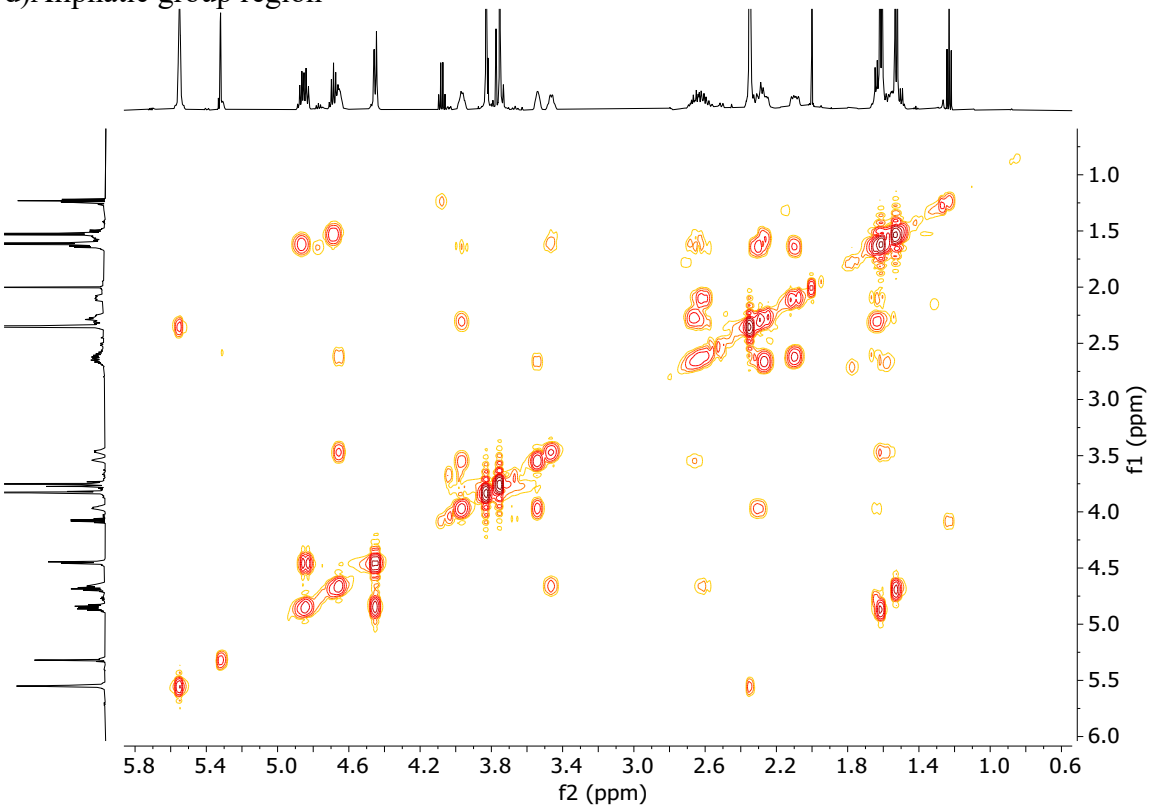

3.3.15. Rh:1p = 1:2 (Quantitative)

^{1}H NMR (600 MHz, CD_2Cl_2)

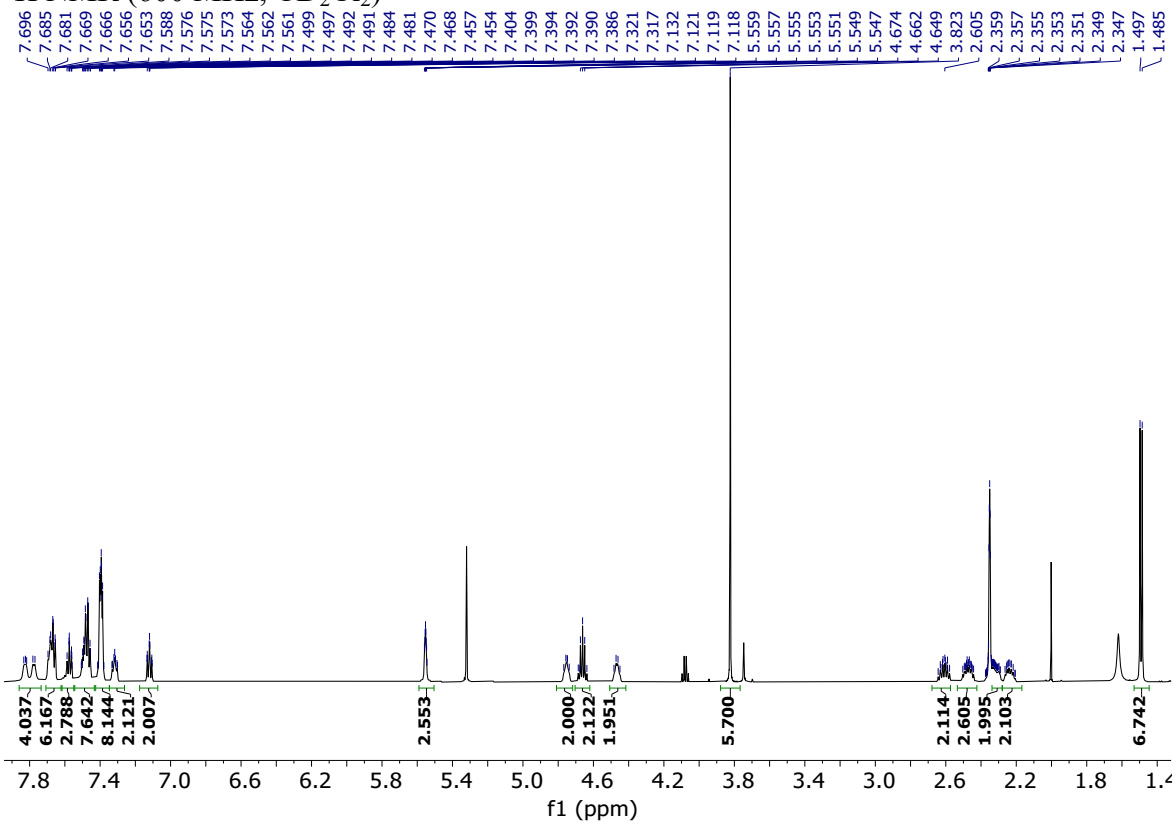

^{31}P NMR (243 MHz, CD_2Cl_2)

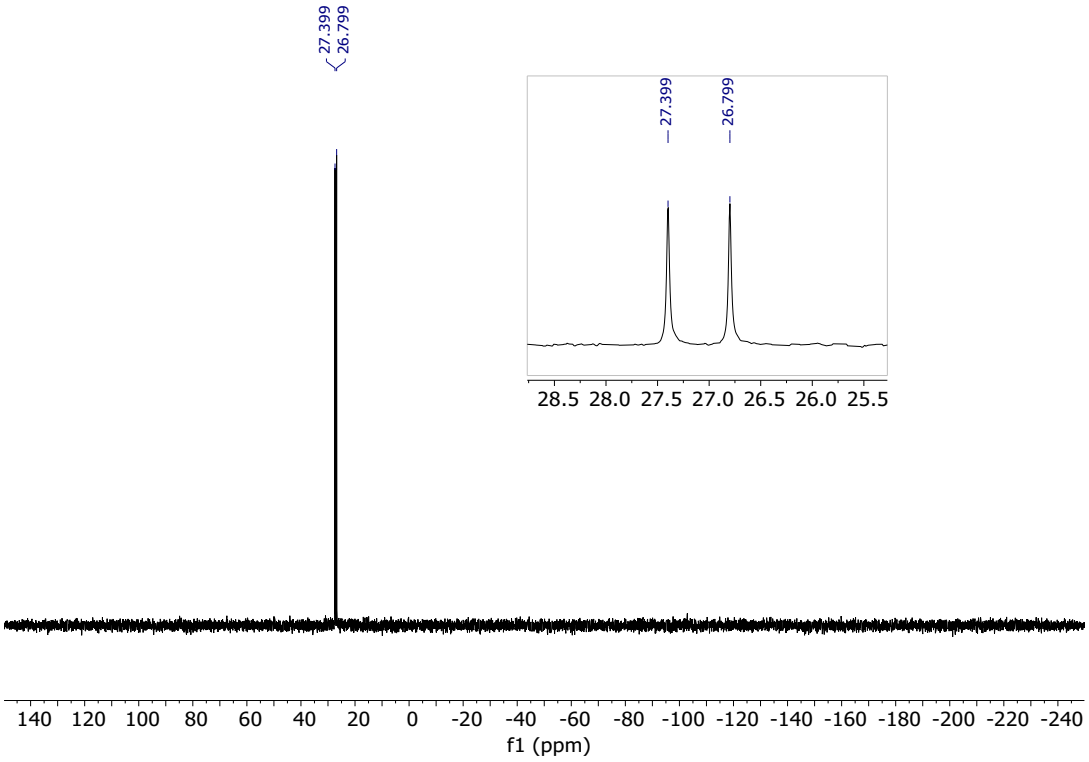

3.3.16. Rh:1p:1c* = 1:1:1 (Quantitative)

^{1}H NMR (600 MHz, CD_2Cl_2)

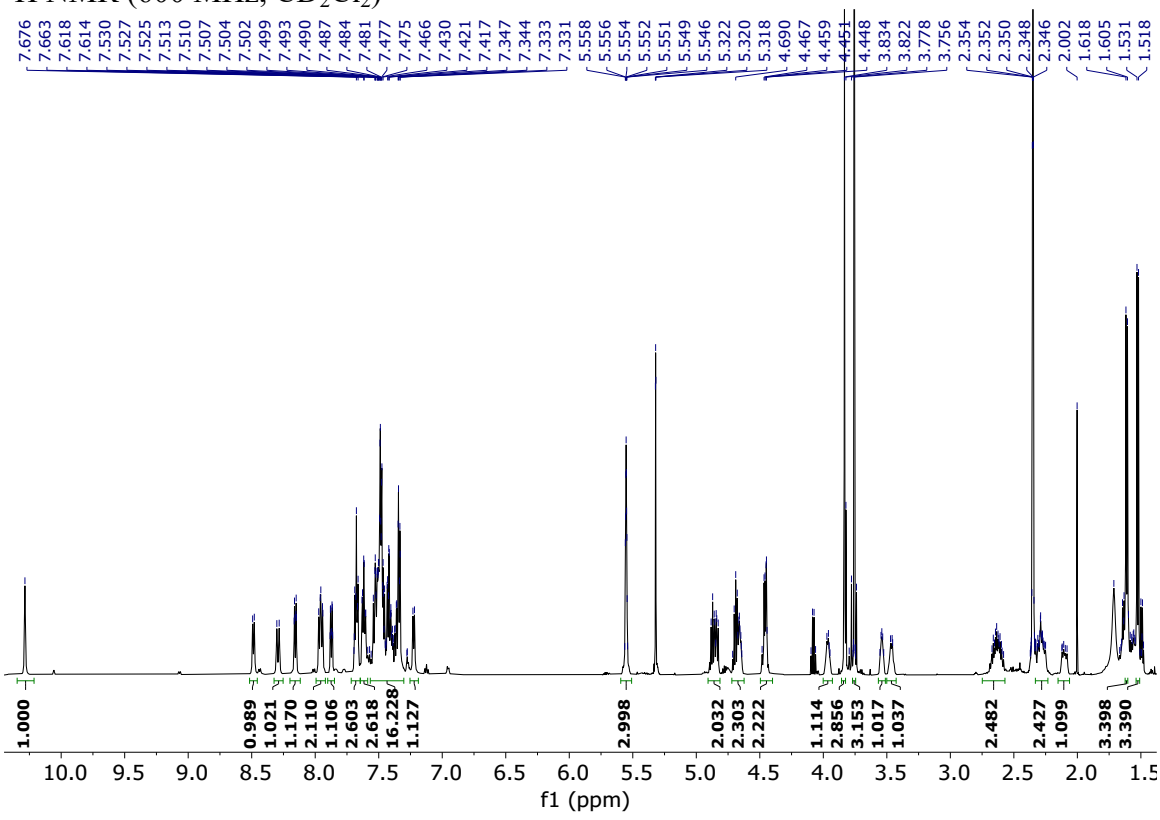

^{31}P NMR (243 MHz, CD_2Cl_2)

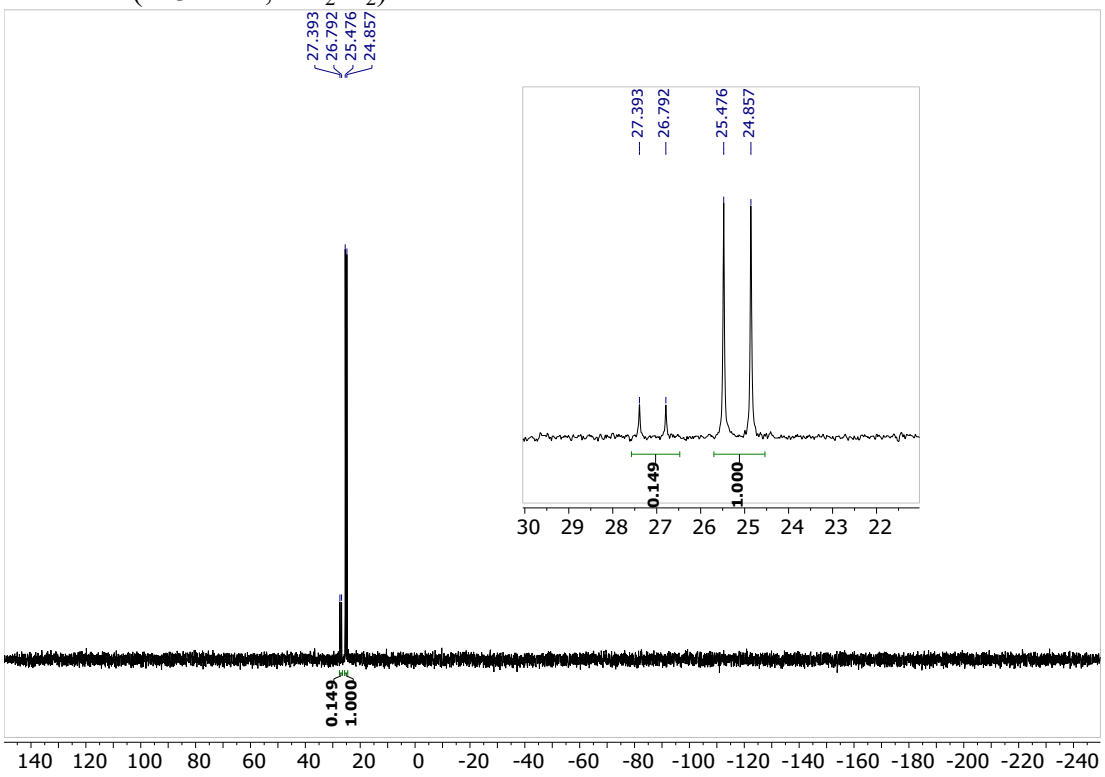

3.3.17. Ir:1p = 1:2 (Quantitative)

^{1}H NMR (600 MHz, CD_2Cl_2)

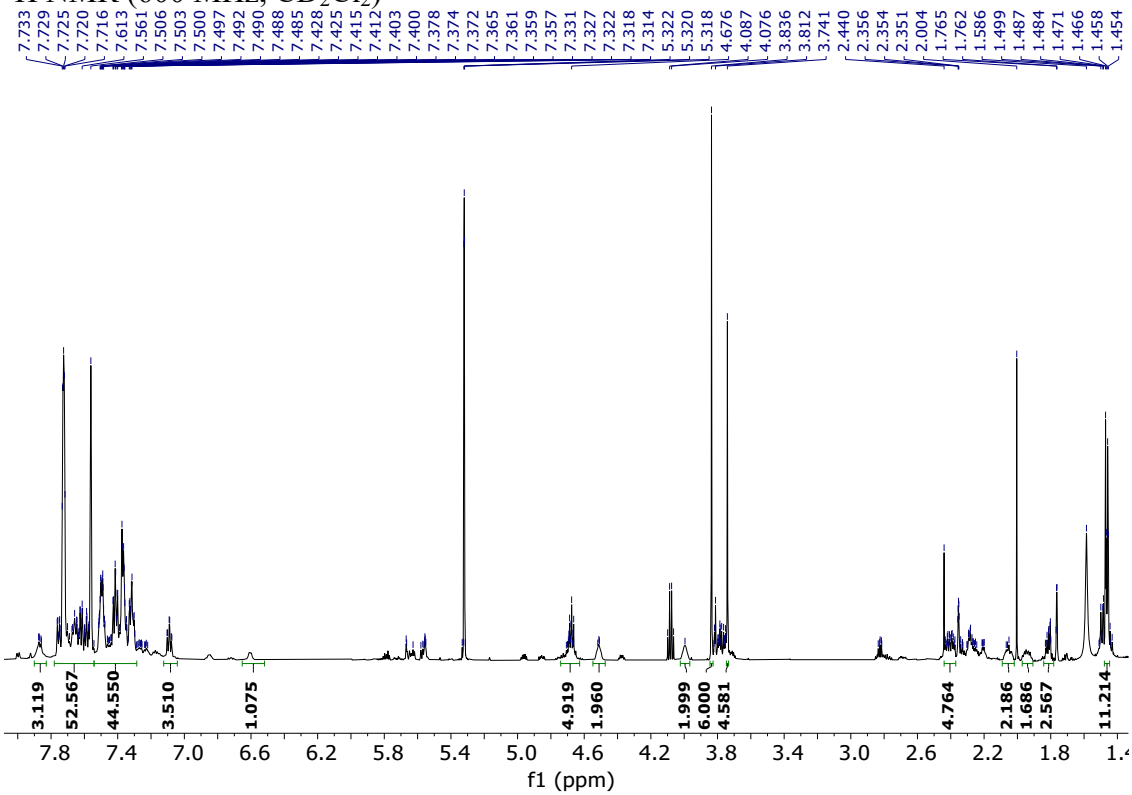

^{31}P NMR (243 MHz, CD_2Cl_2)

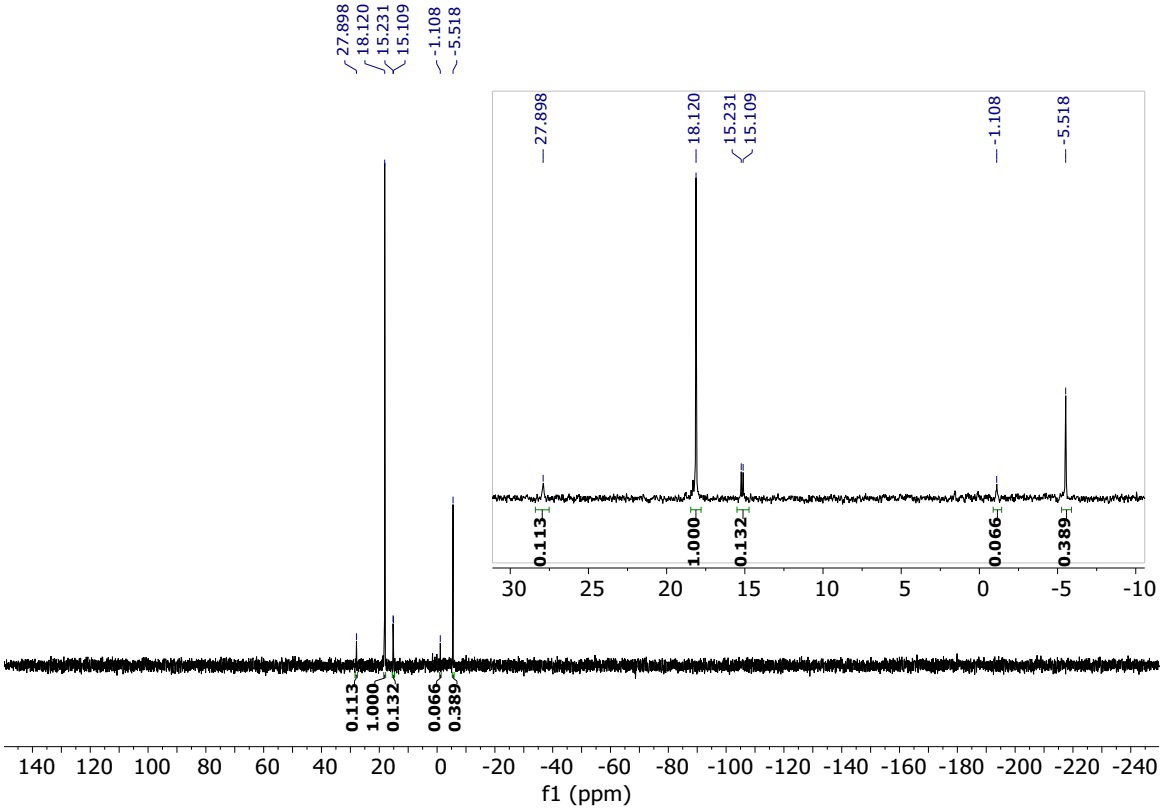

3.3.18. Ir:1p:1c* = 1:1:1 (Quantitative)

^{1}H NMR (600 MHz, CD_2Cl_2)

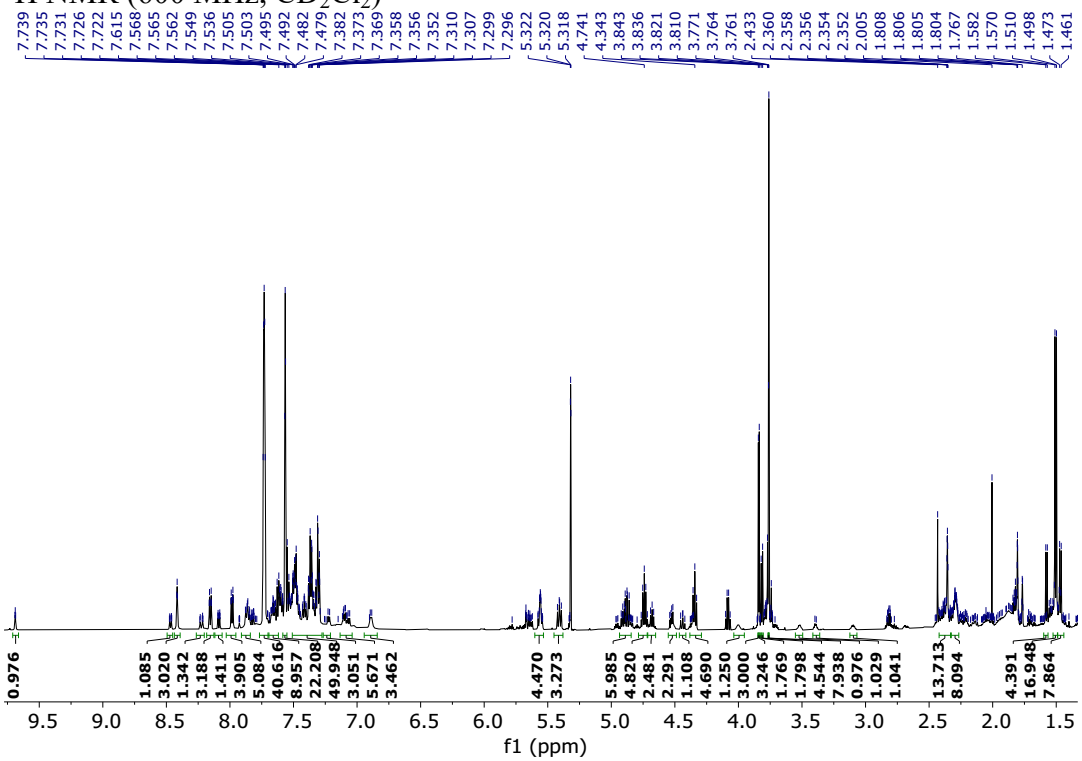

^{31}P NMR (243 MHz, CD_2Cl_2)

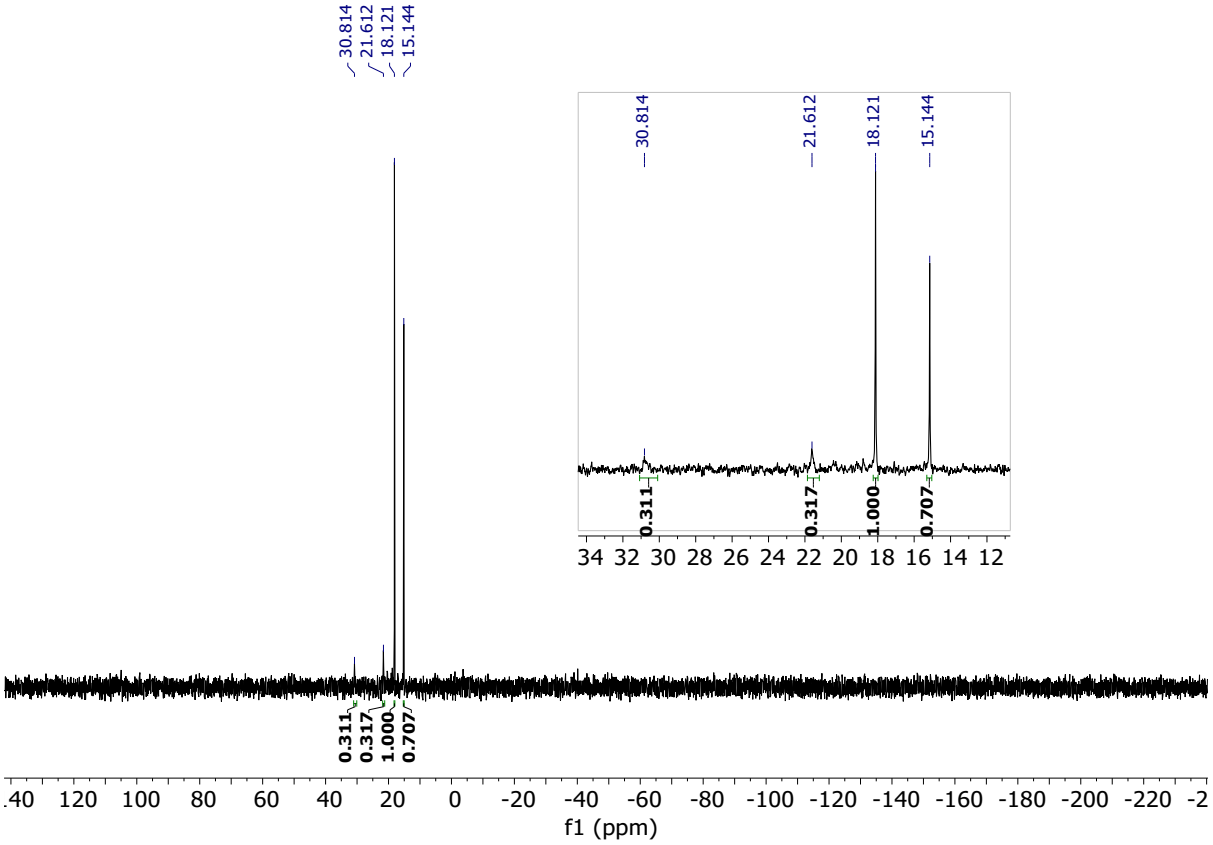

3.4. Stacked NMR spectra of precatalyst solutions

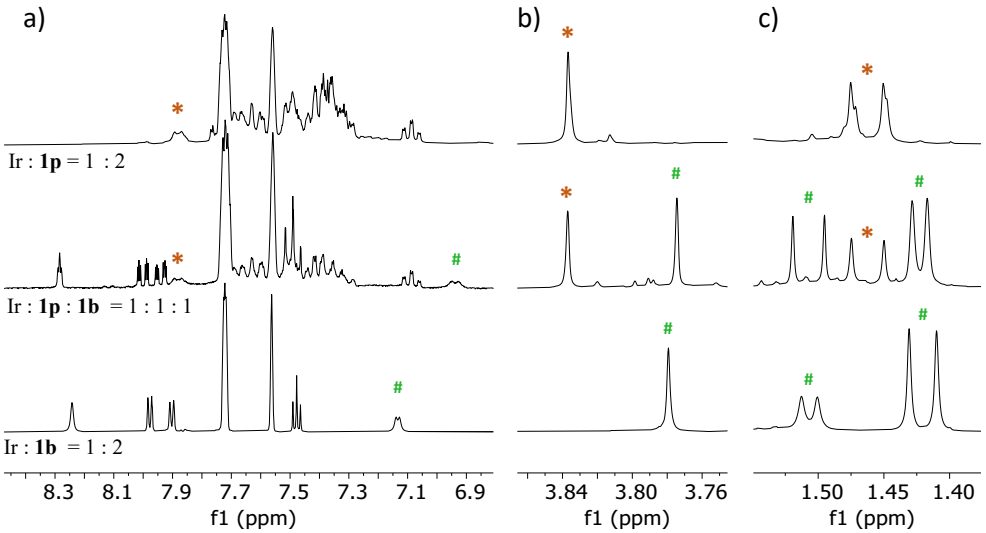

Figure S3. ^{1}H NMR stacked spectra of solutions with various ratios of Ir(I) precursor to **1p** ligand(*) and **1b** ligand (#): a) aromatic region, b) functional group region, c) aliphatic region.

NMR spectroscopy. *In situ* formation and the presence of supramolecular interactions in precatalyst homoleptic and heteroleptic complexes of [Ir(COD)$_2$]BARF with ligands **1a**, **1b**, **1p** and **PPh$_3$** (triphenylphosphine) in CH_2Cl_2 has been studied by ^{1}H, ^{13}C and ^{31}P NMR spectroscopy (Figure S3, ESI sections 3.3. and 3.4.). The amide peaks of non-coordinated ligands appear below 7.00 ppm, indicating no significant hydrogen bonding under given conditions for both individual **1p** and **1b** ligands (ESI sections 3.1. and 3.2.), and their mixture in 1:1 ratio (ESI section 3.6). The ^{1}H NMR spectrum of the homoleptic **1p** iridium complex (Ir : **1p** = 1 : 2, Figure S3, first row) exhibits a large downfield shift of the alanine amide peak ($\Delta\delta$ ~ 1.30 ppm) and a smaller downfield shift of the ester methyl group peak (~ 0.10 ppm) along with non-coordinated **1p** peaks. Excess ligand addition to the mixture mainly increases intensity of the non-coordinated **1p** peaks (ESI sections 3.3. and 3.4.). The NMR spectrum of the homoleptic **1b** iridium complex (Ir:**1b**=1:2, Figure S3, third row) shows a small downfield shift of the alanine amide peak ($\Delta\delta$ ~ 0.36 ppm) indicating weak hydrogen bonding, and a downfield shift of the ester methyl group peak ($\Delta\delta$ ~ 0.10 ppm), similar to the **1p** derivative. Interestingly, the dimethyl group of the non-coordinated ligand shows as a singlet peak at 1.28 ppm (ESI section 3.2, **1b**), while the same group shows as two peaks in the metal complex solution, at 1.41 and 1.43 ppm, resepctively (ESI section 3.3.4). This indicates that the oxazoline faces are no longer equivalent. A similar observation has been reported in our previous article for a similar oxazoline bioconjugate.[2] However, in that report no such observations have been made for ligand **1b**, even at elevated concentrations of 60 mM. This strongly suggests that changes in the NMR spectrum of the homoleptic iridium **1b** complex indeed occur as a result of complexation.

3.4.1. Ir:1p, ^{1}H NMR in CD_2Cl_2

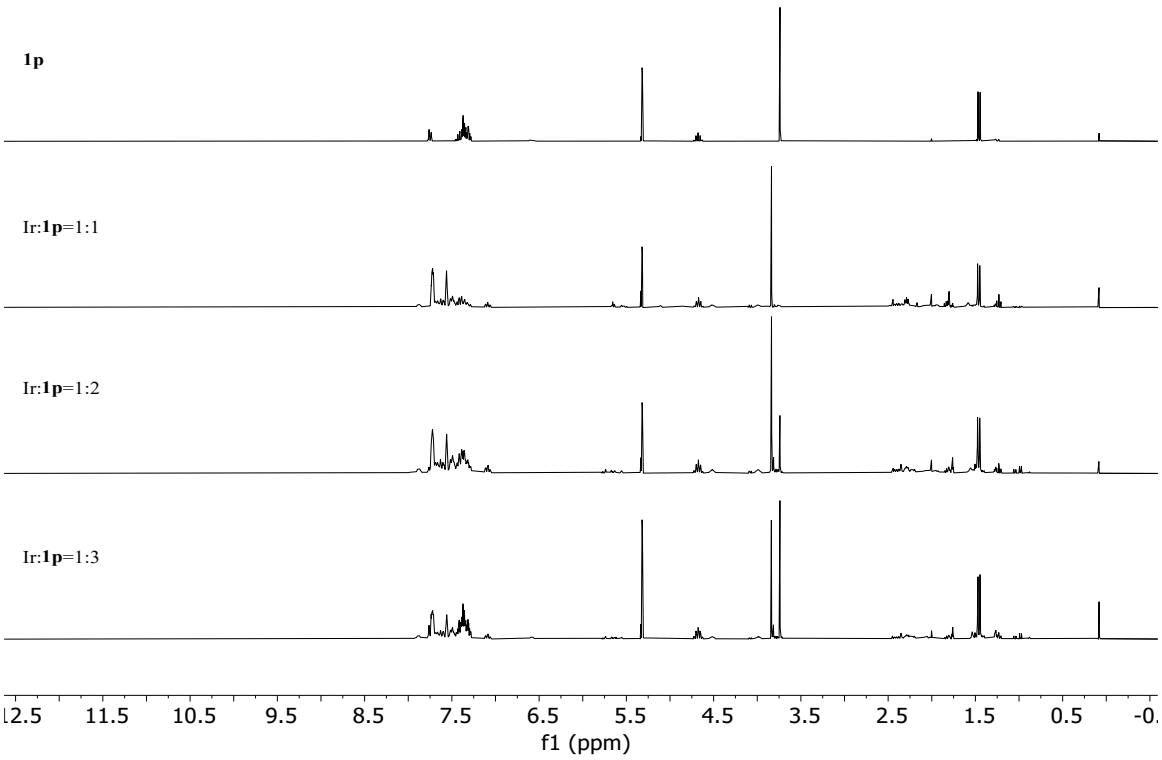

Aromatic group area of Ir:1p, ^{1}H NMR inCD_2Cl_2

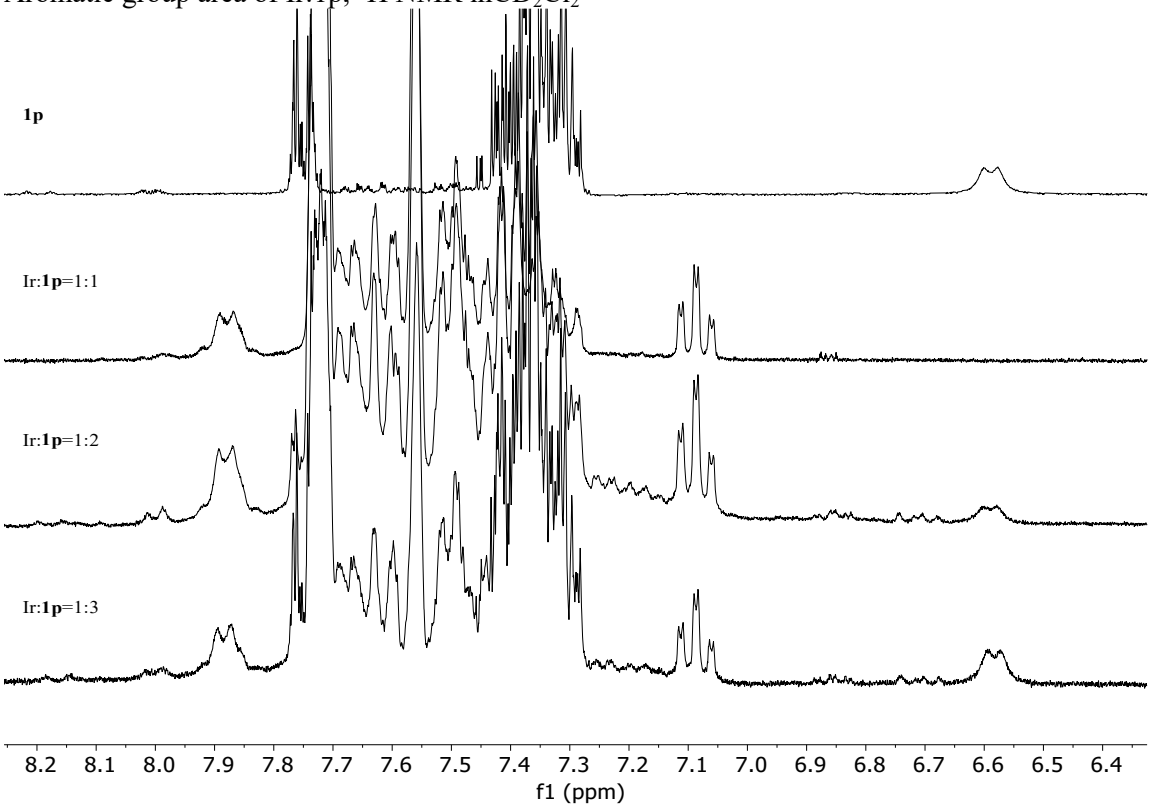

Functional group area
a)Lowered intensitiy

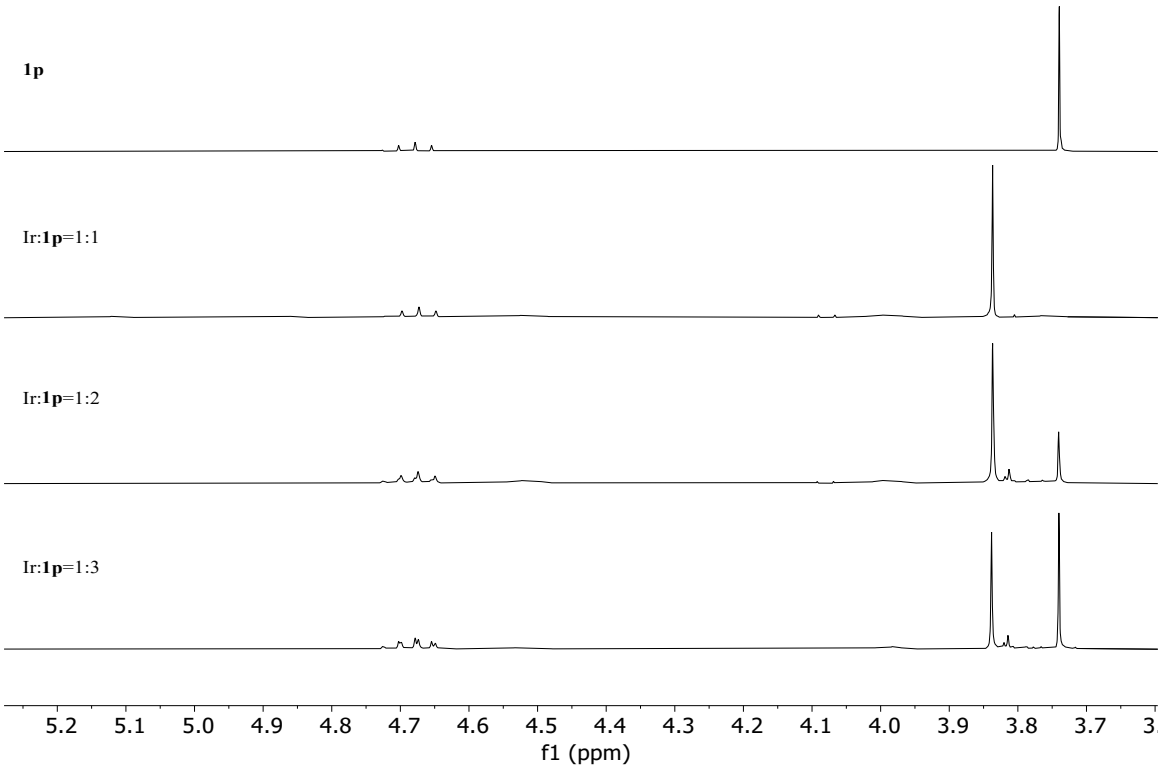

b) Increased intensity

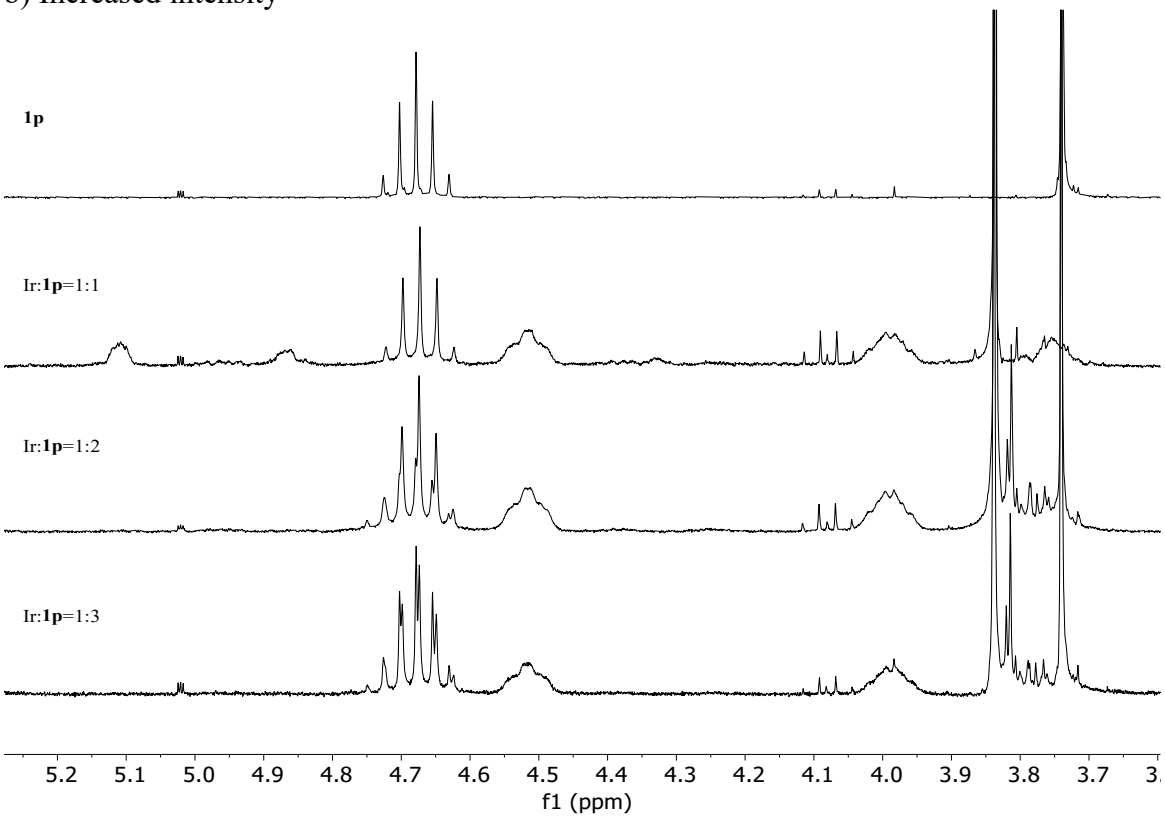

Aliphatic group area

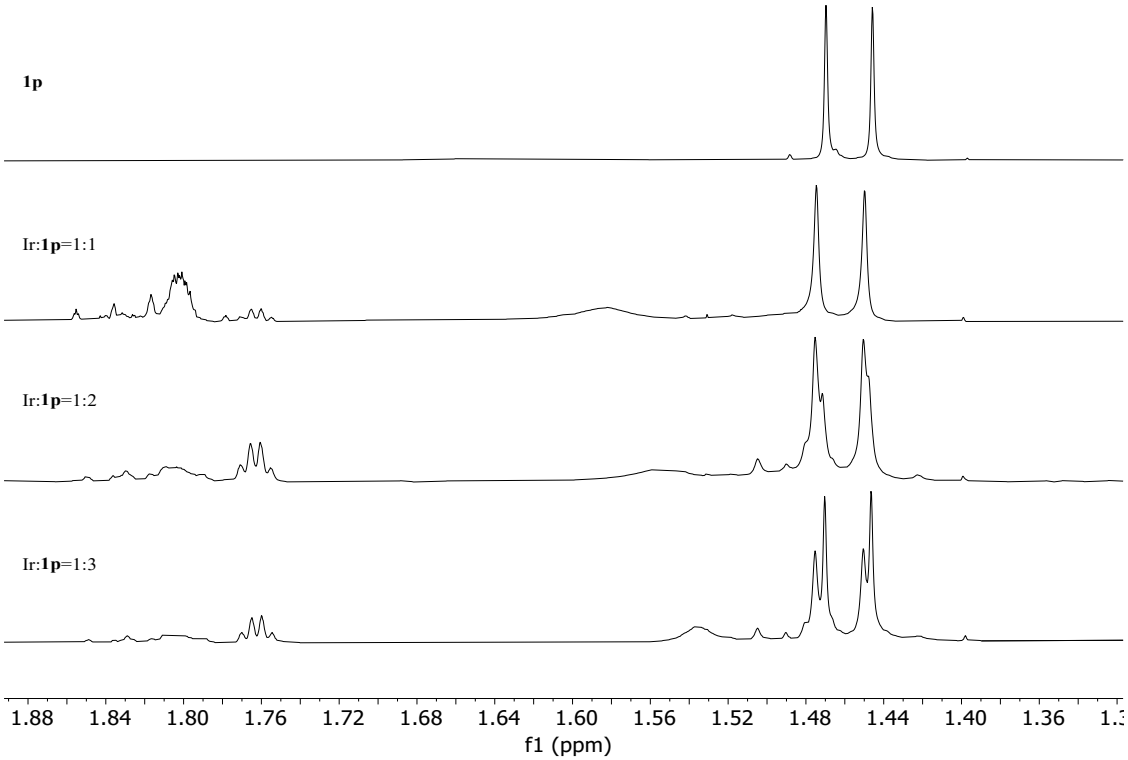

3.4.2. Ir:1p, ^{31}P NMR inCD_2Cl_2

a)Lowered intensity

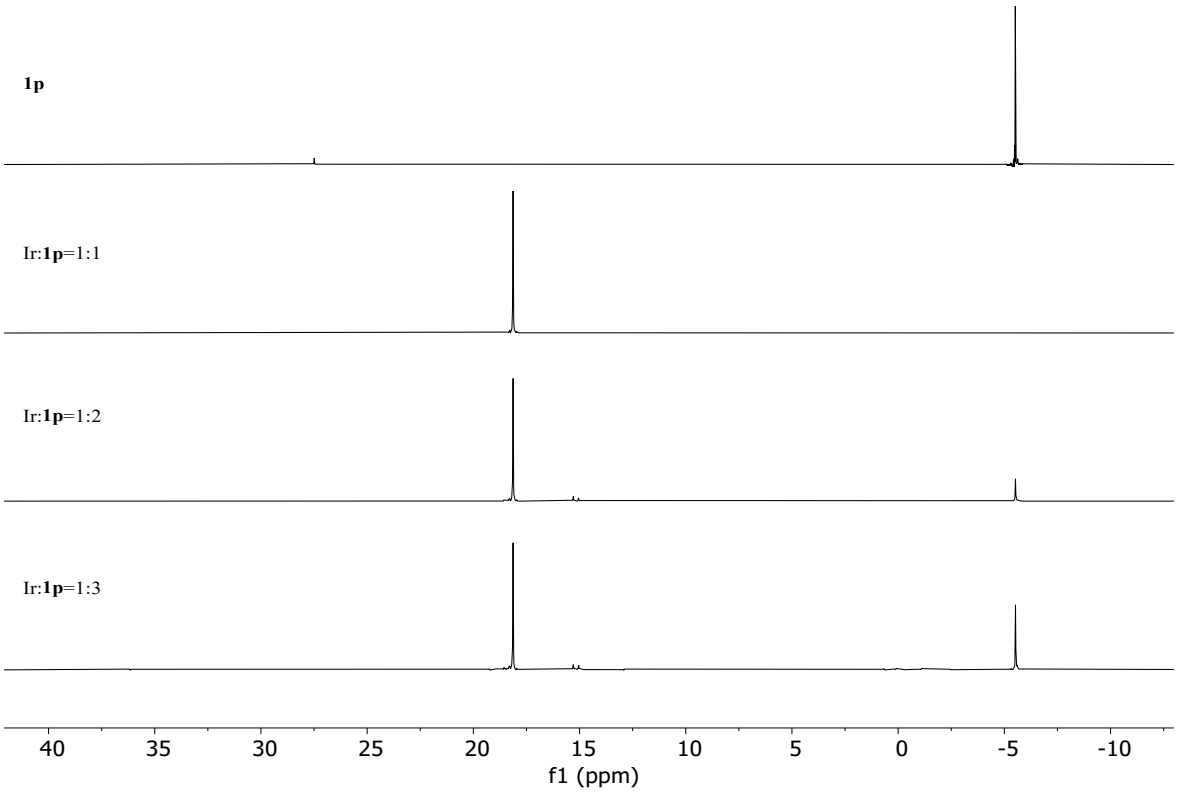

b) Increased intensity

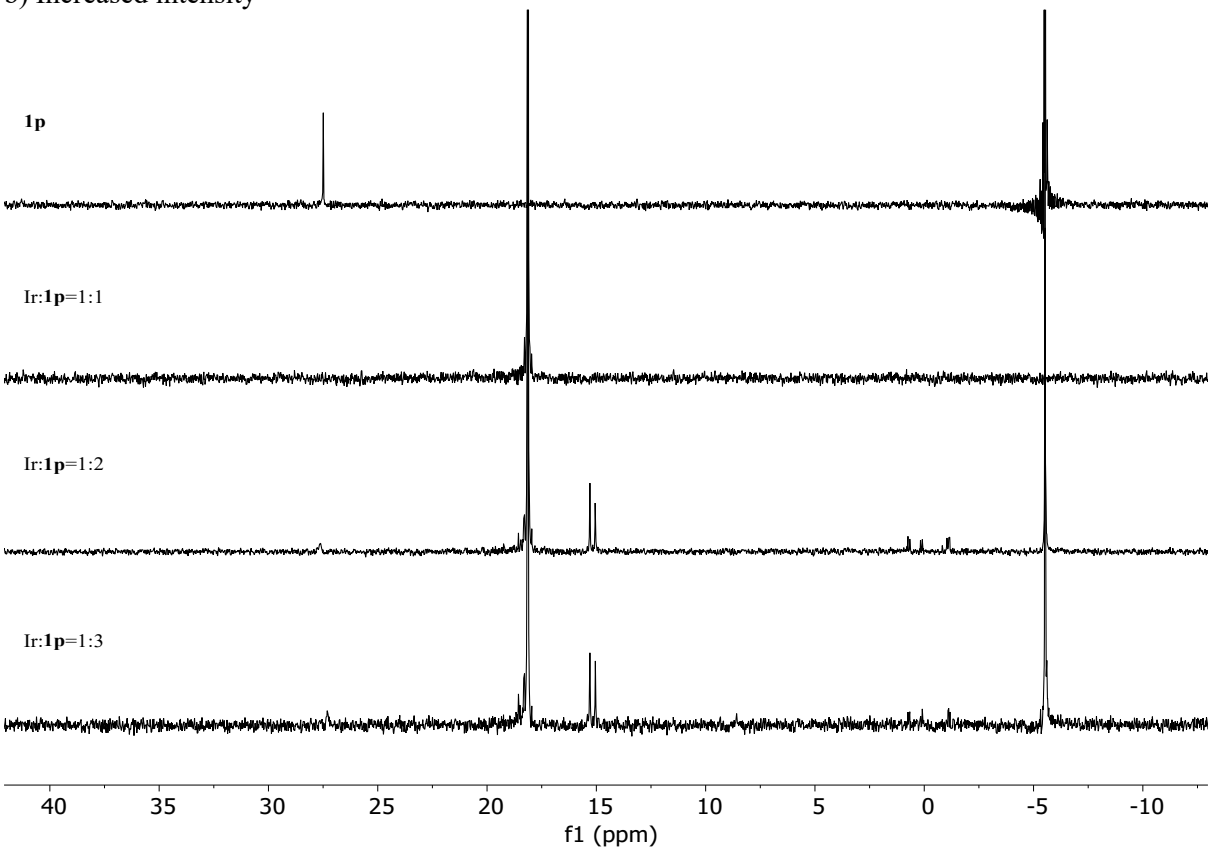

3.4.3. Ir:1p, ^{13}C NMR in CD_2Cl_2

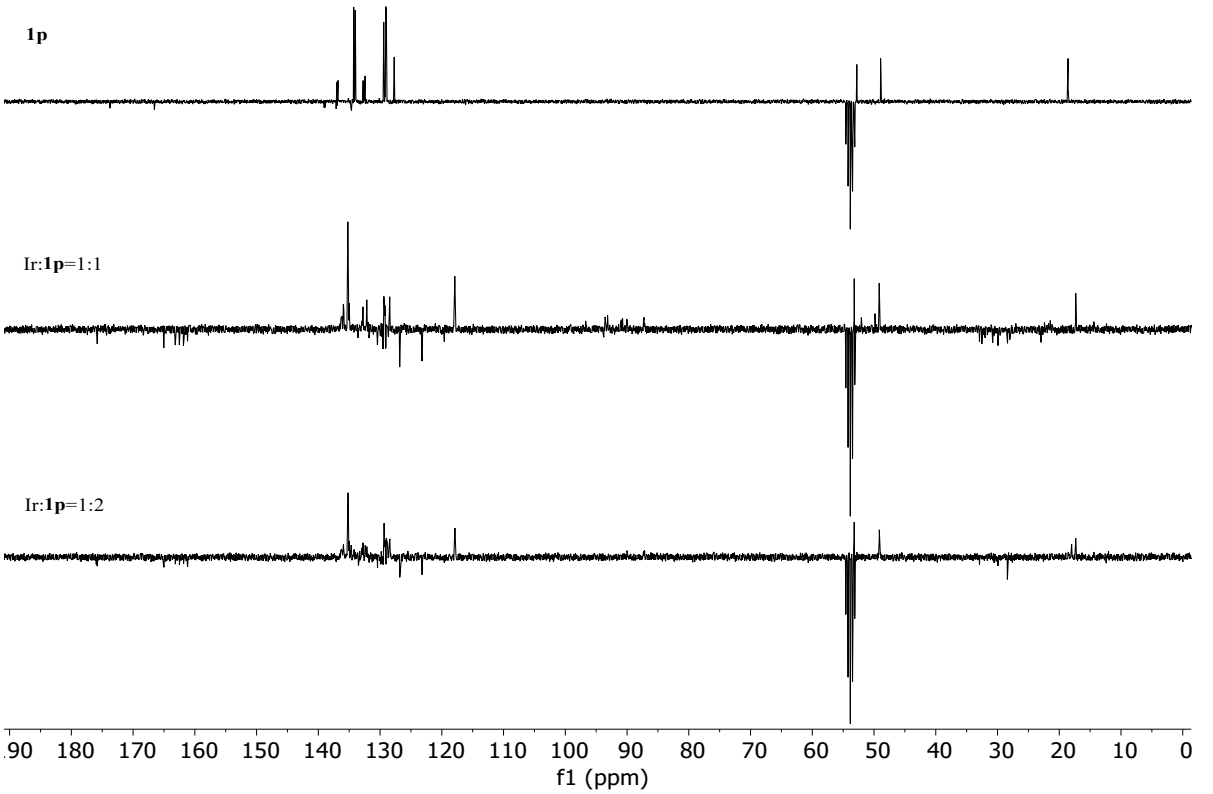

Amide/ester group area

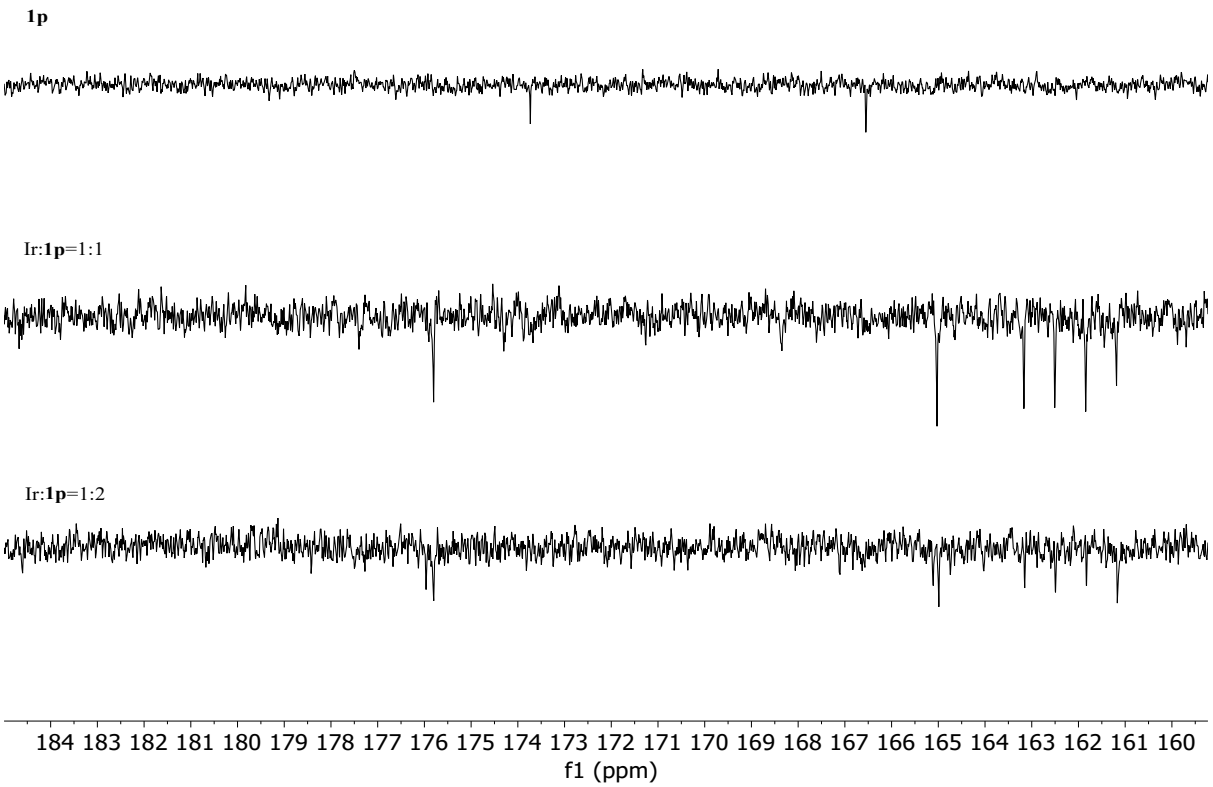

Aromatic group area

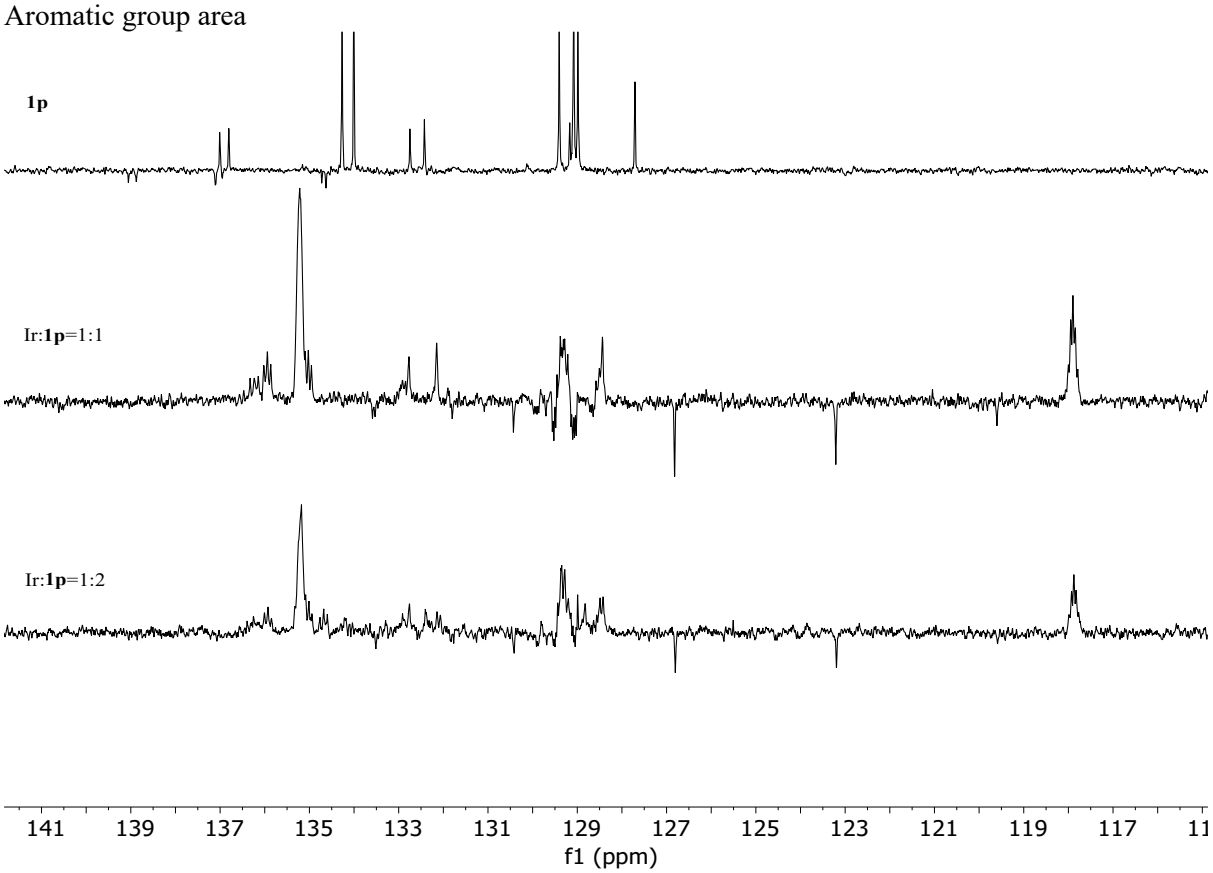

110ppm-80ppm

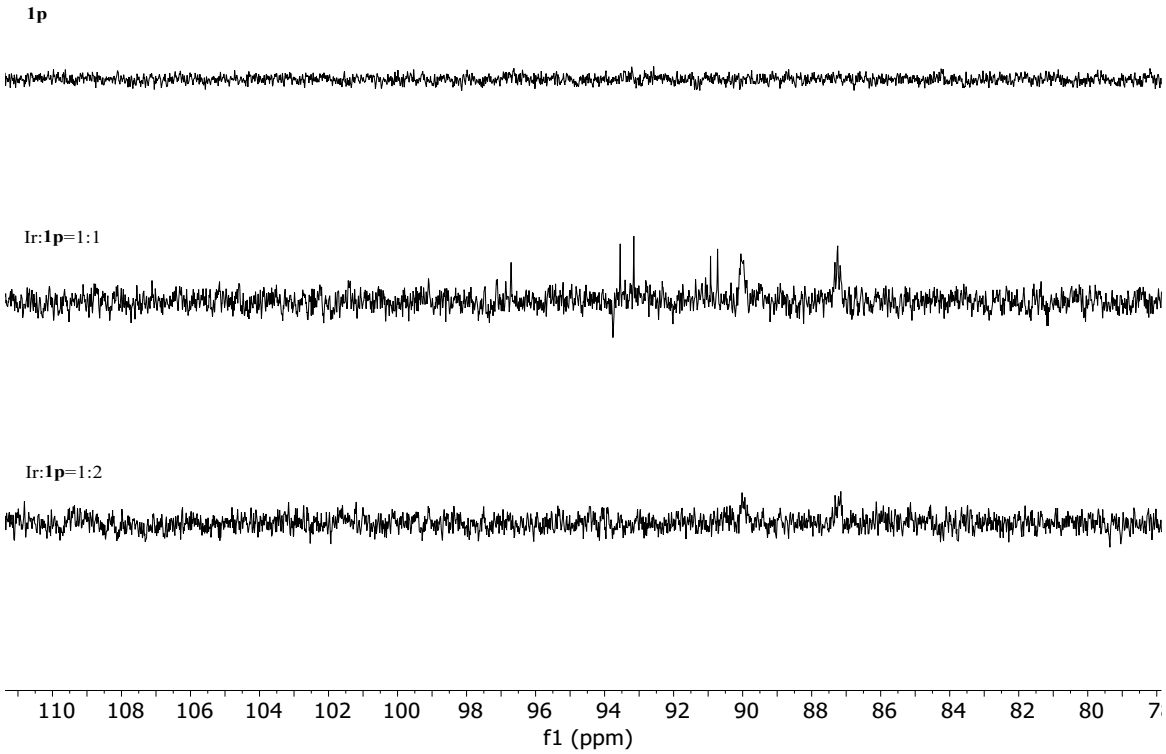

Functional group area

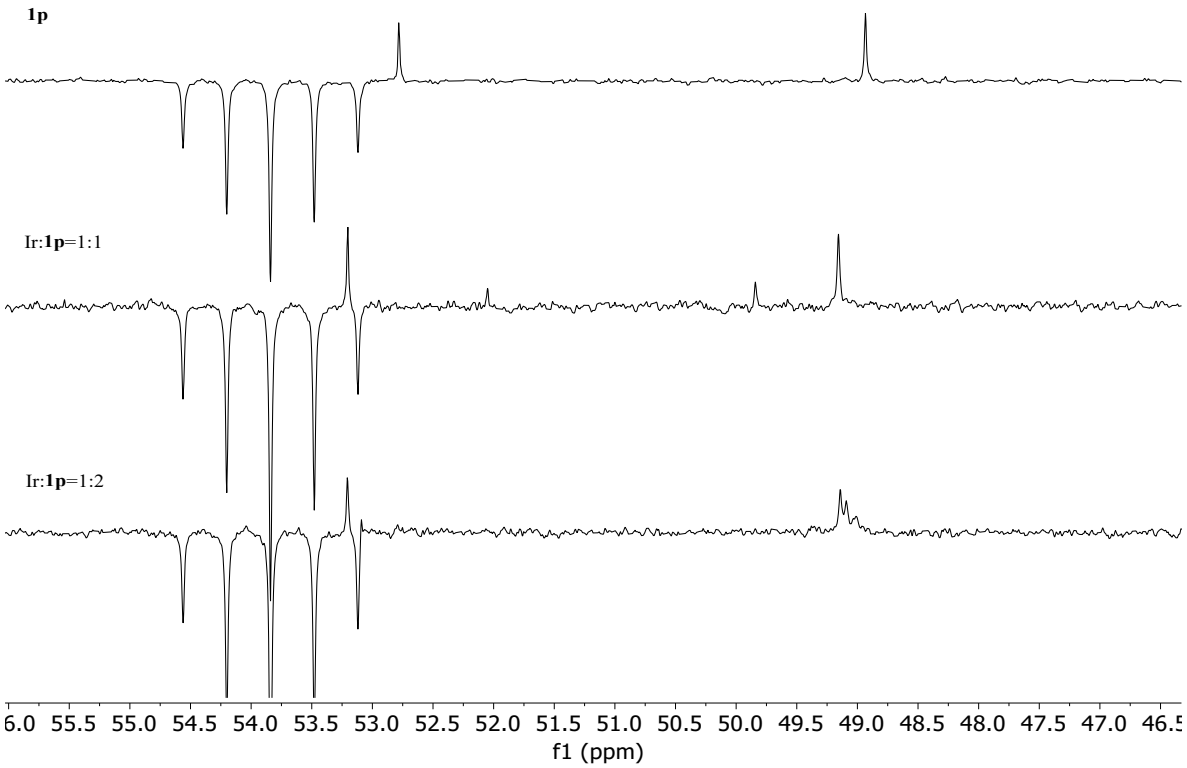

Aliphatic group area

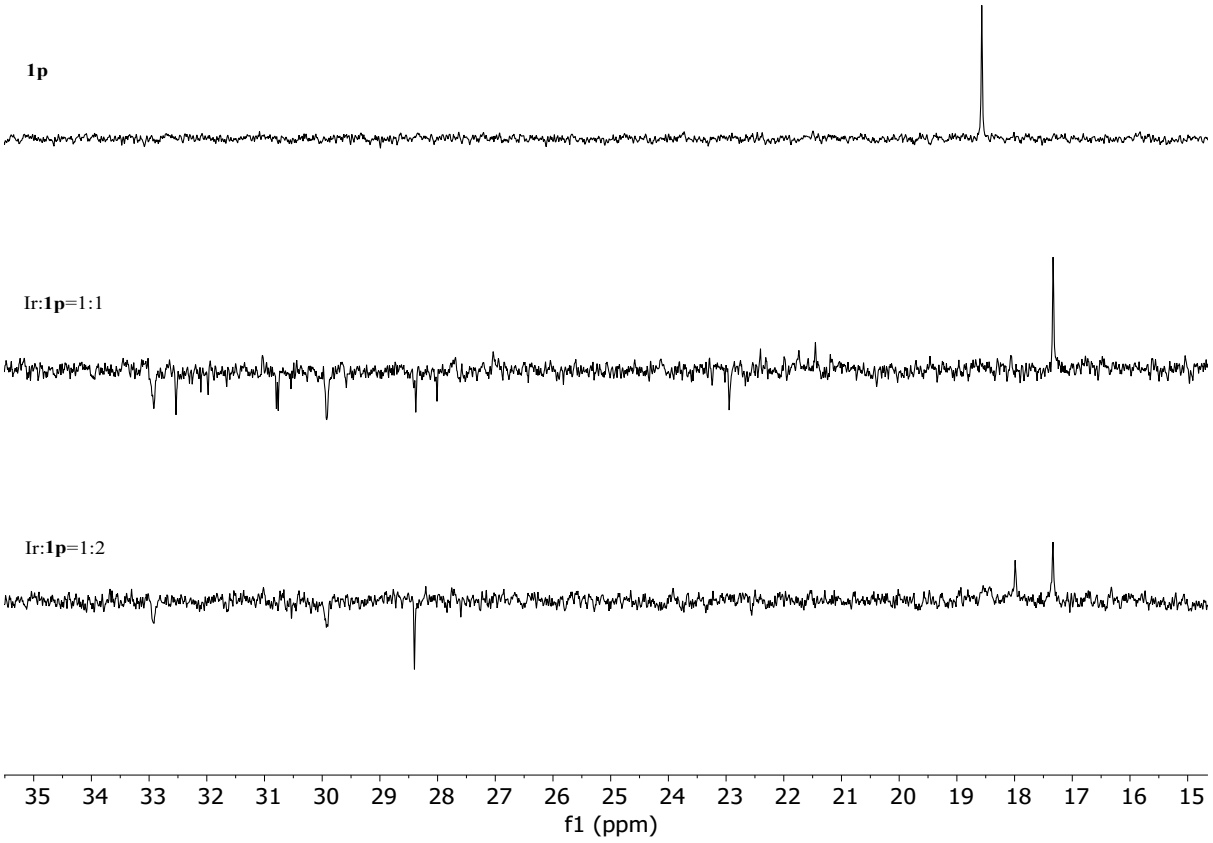

3.4.4. Ir:1b, ^{1}H NMR in CD_2Cl_2

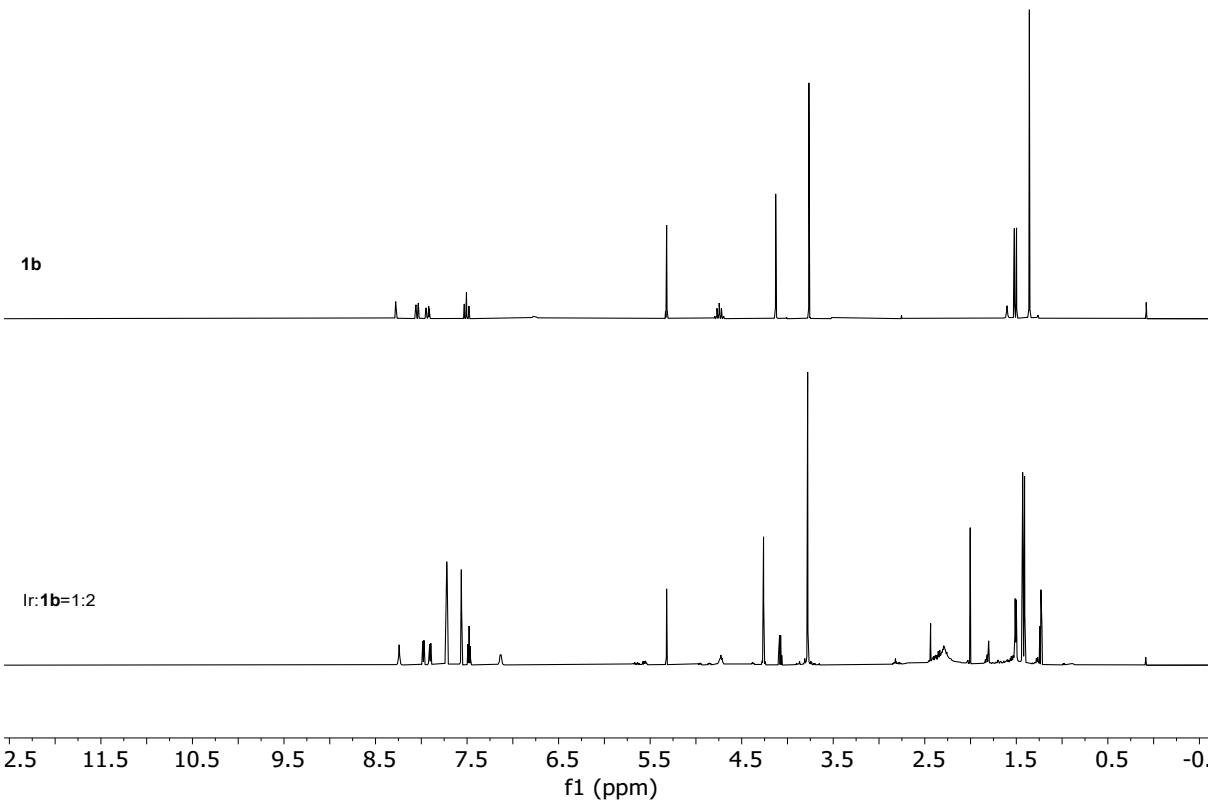

Aromatic group area

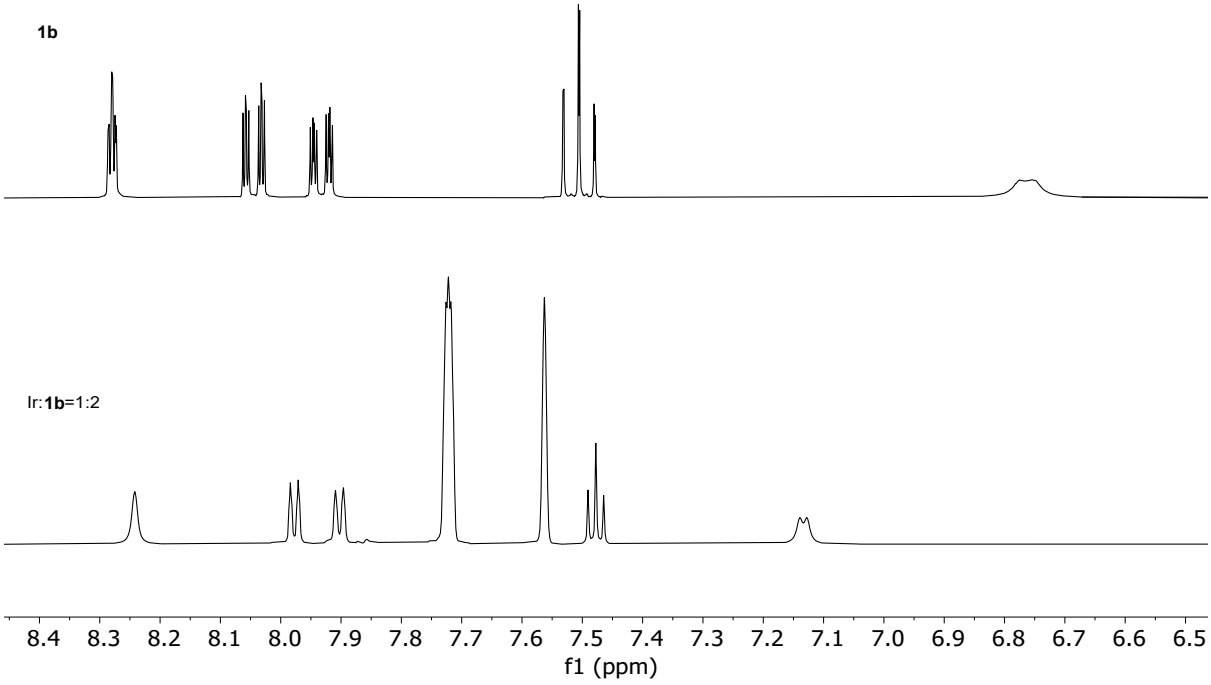

Functional group area

a) Lowered intensity

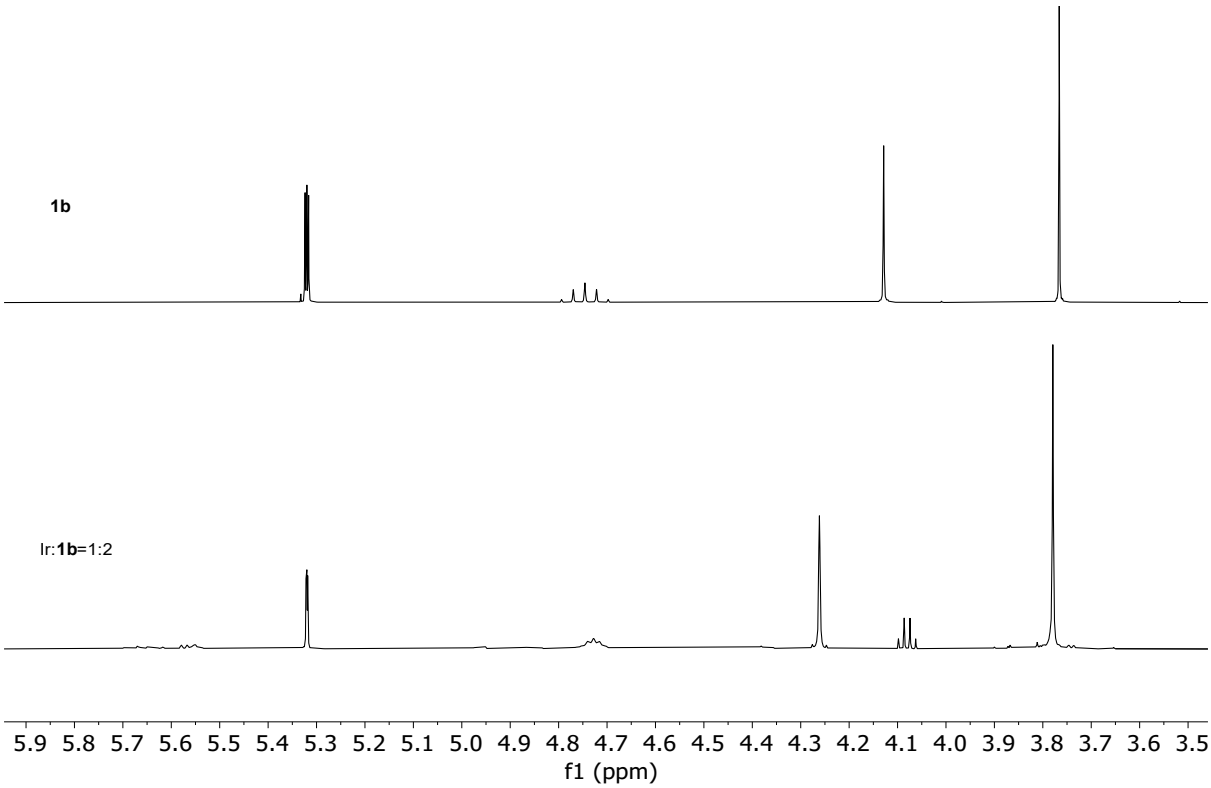

b) Increased intensity

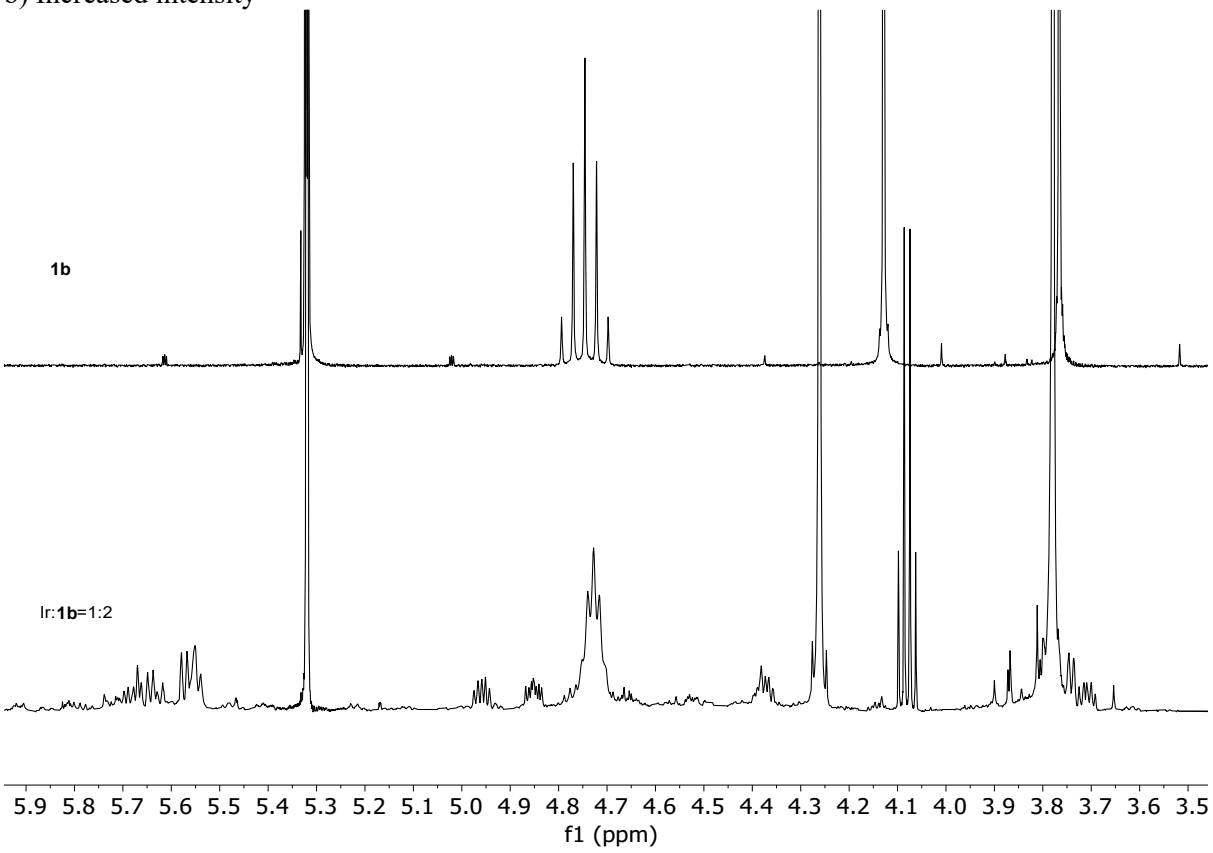

Aliphatic group area

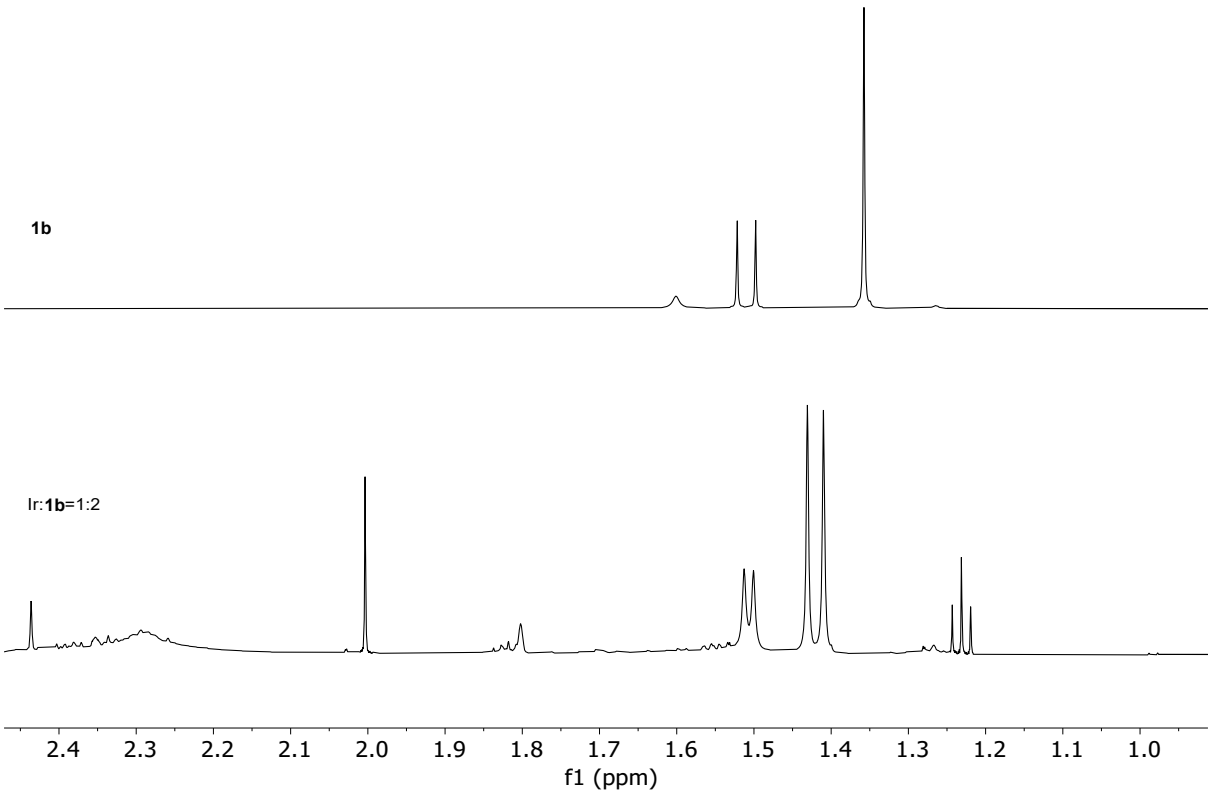

3.4.5. Ir:1b, ^{13}C NMR in CD_2Cl_2

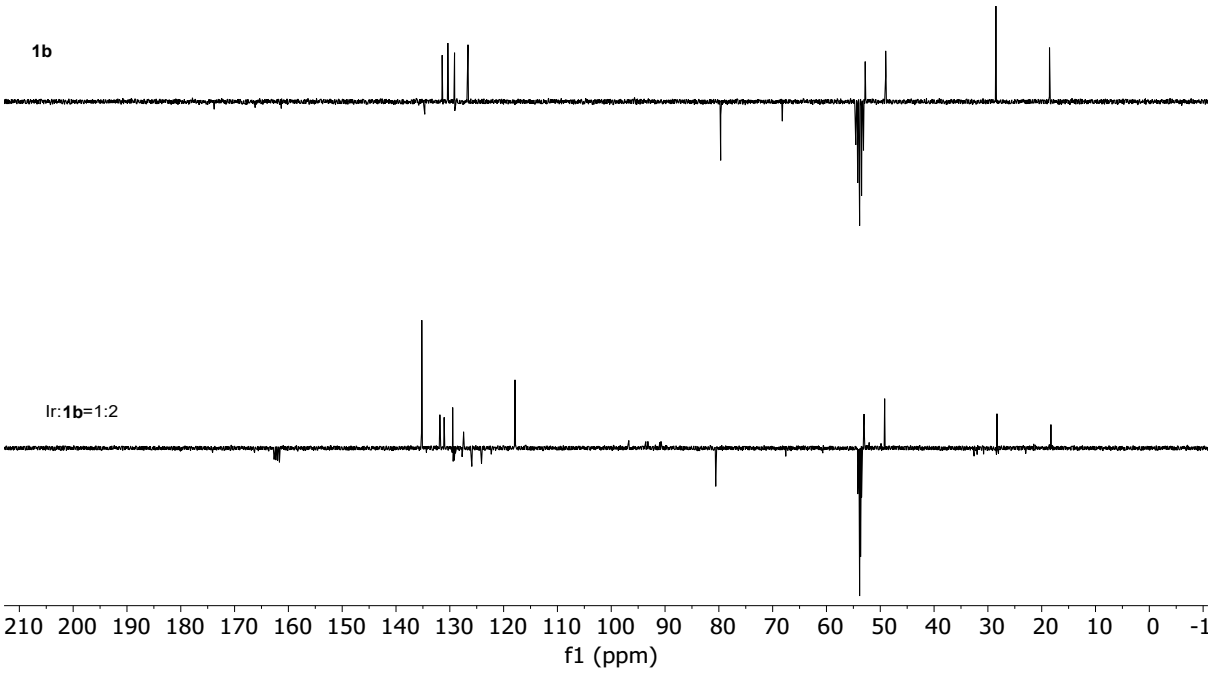

Amide/ester group area

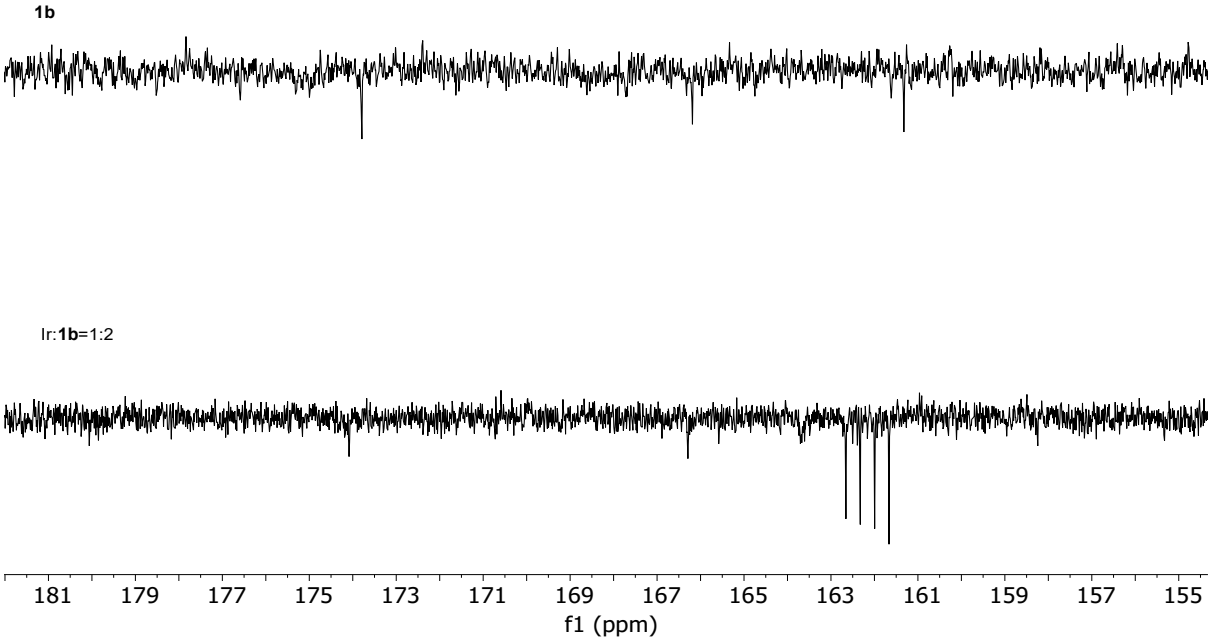

Aromatic group area

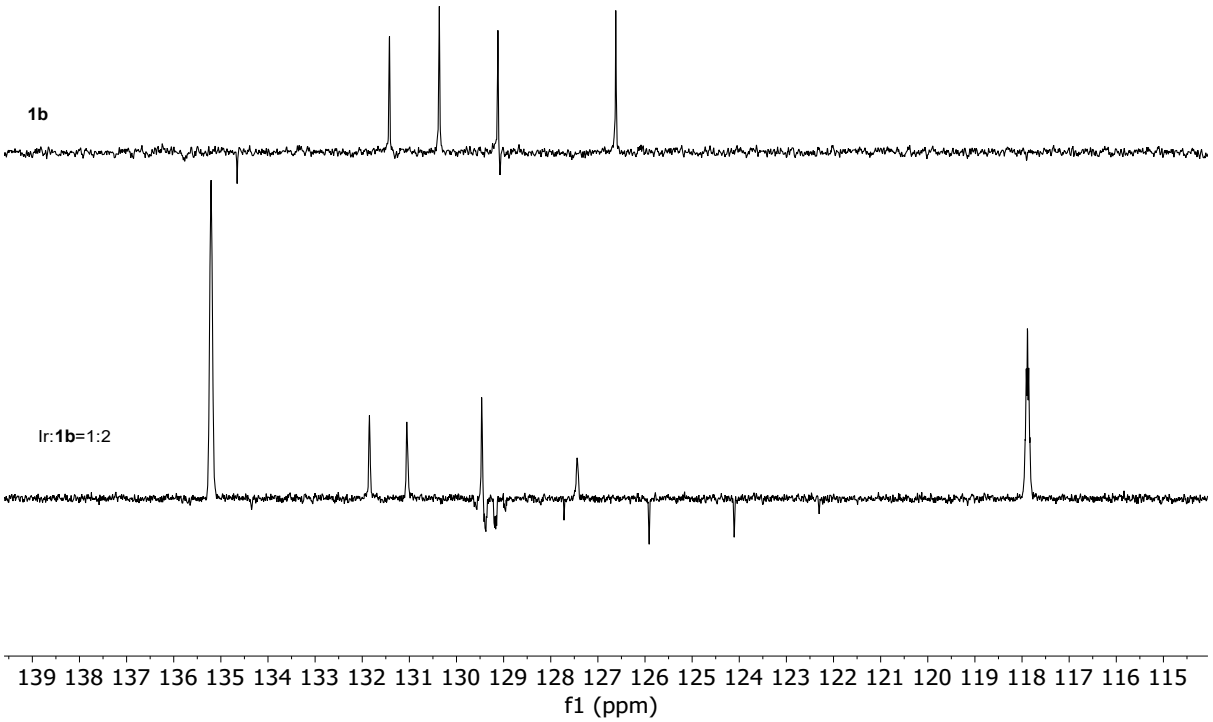

110ppm-80ppm

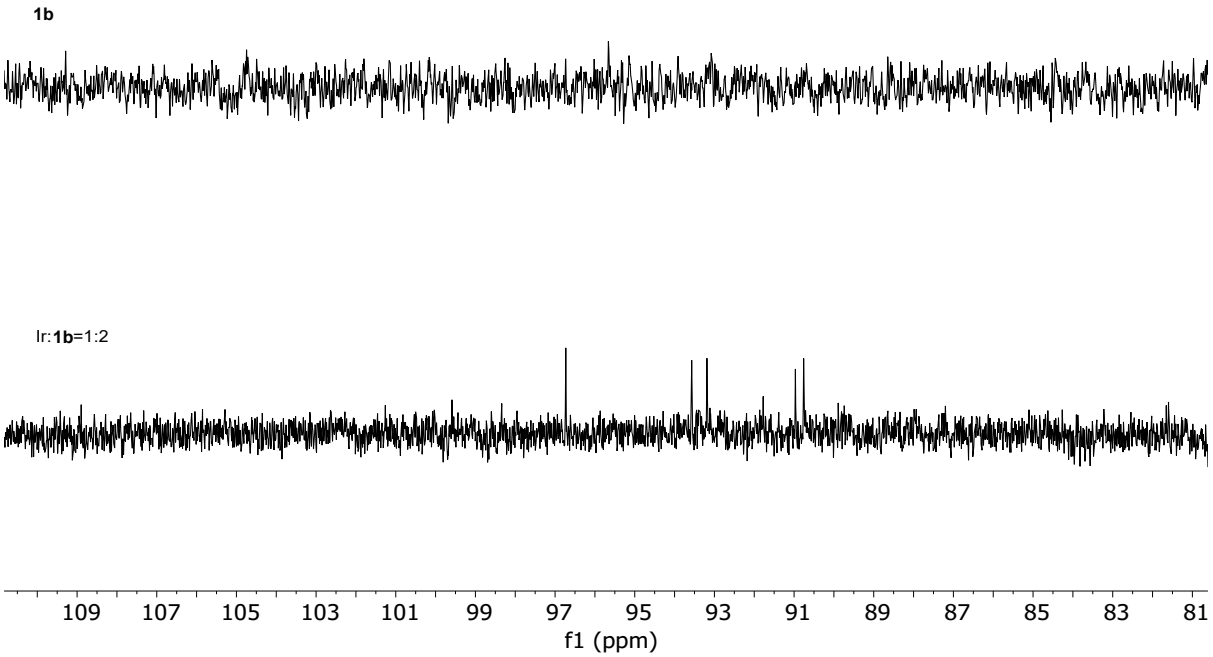

Functional group area

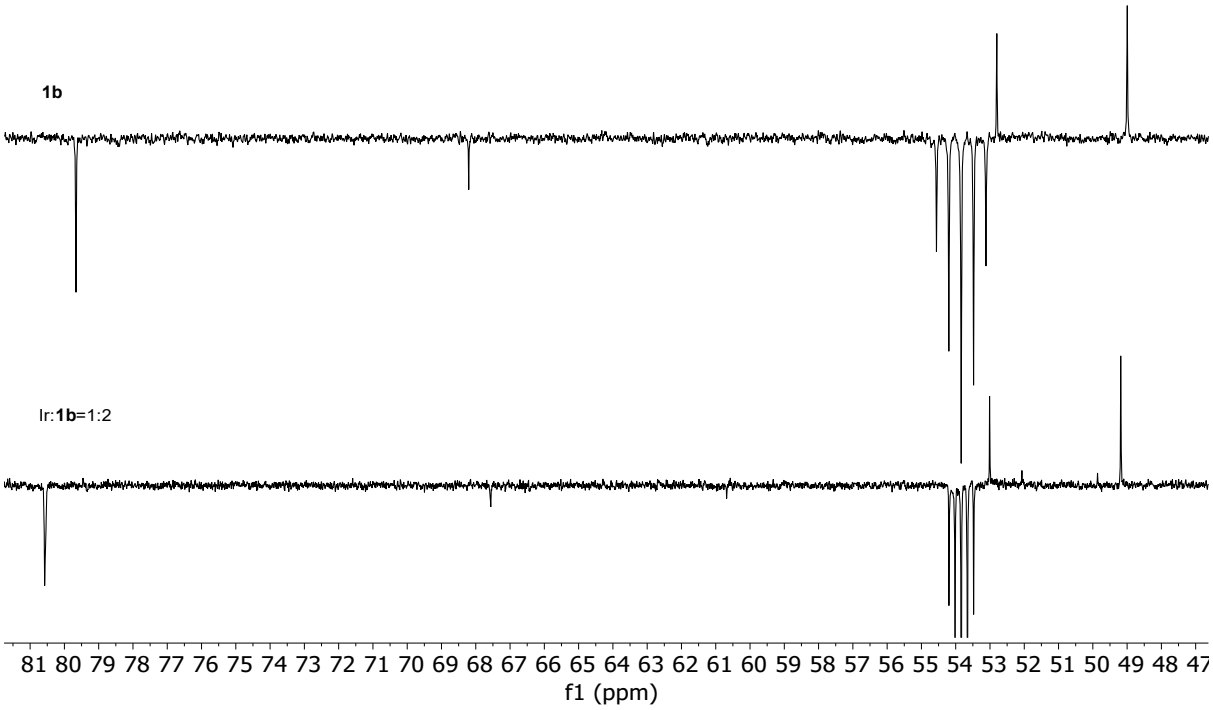

Aliphatic group area

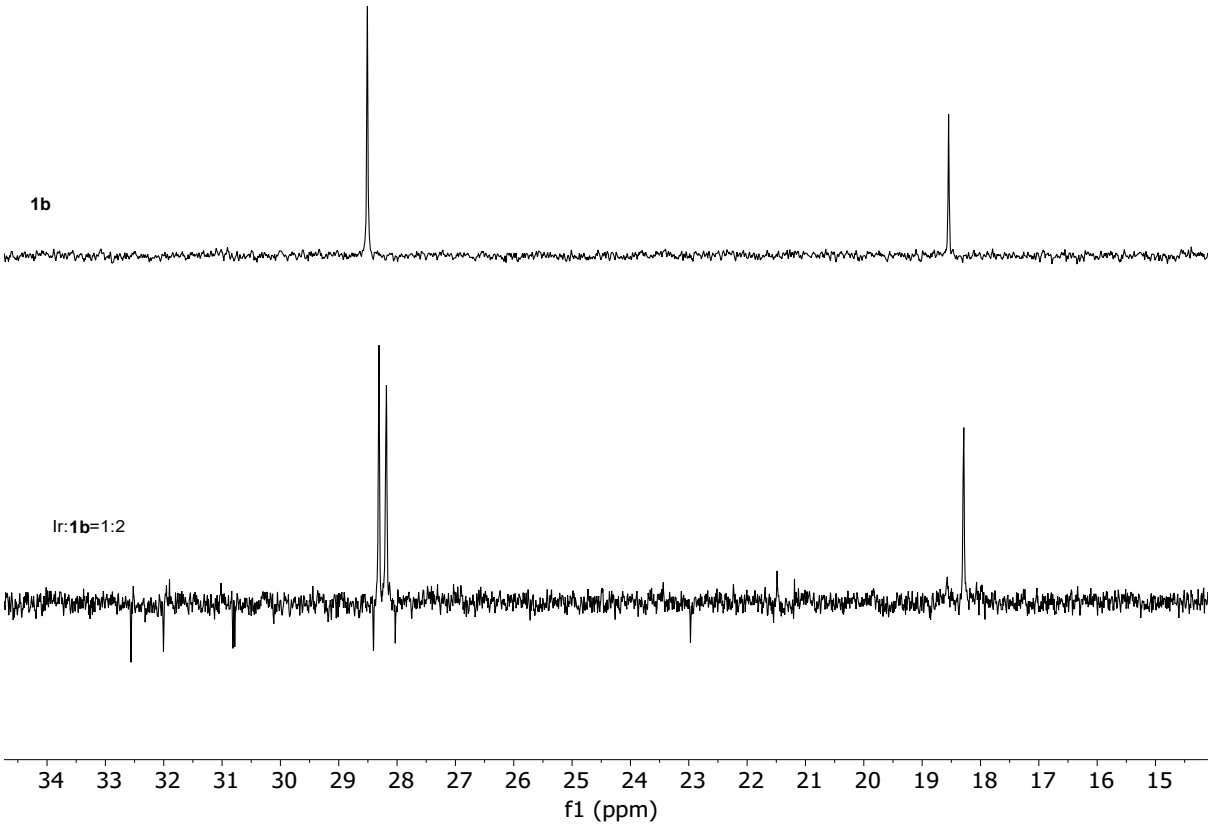

3.4.6. Ir:1p:1b, ^{1}H NMR in CD_2Cl_2

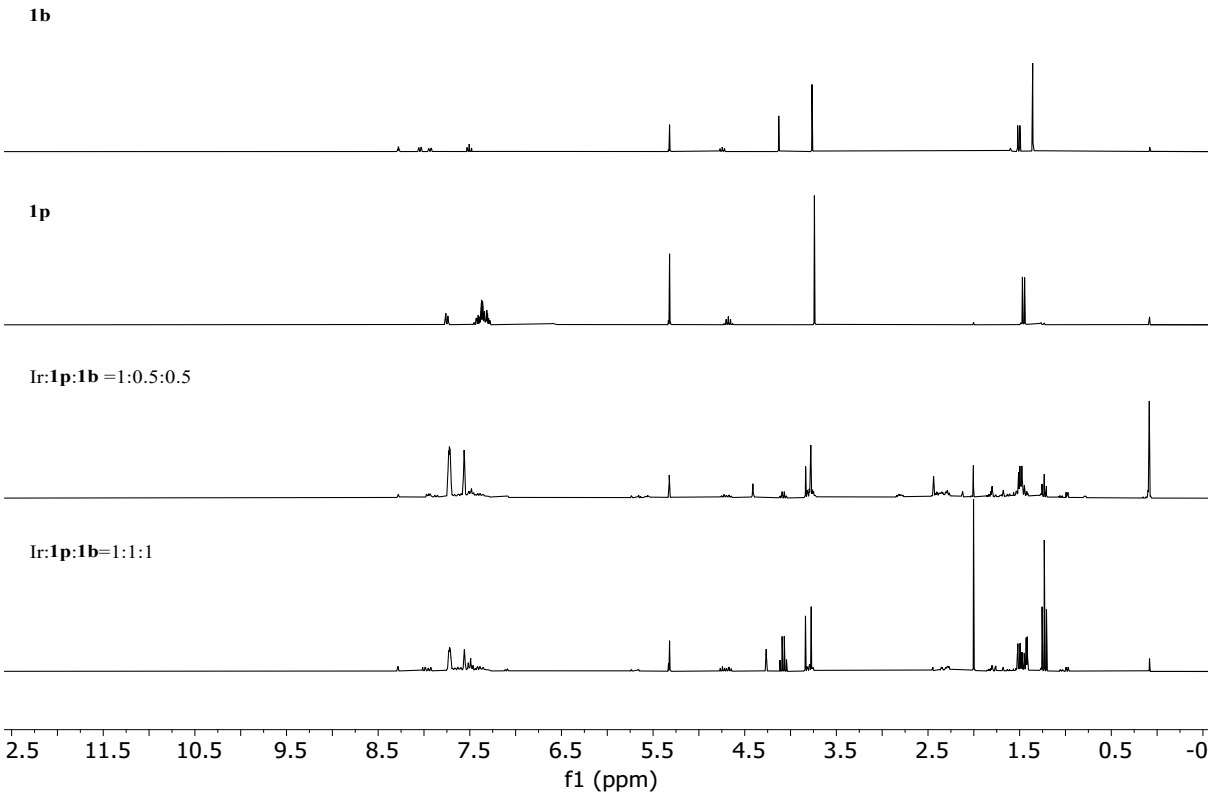

Aromatic area

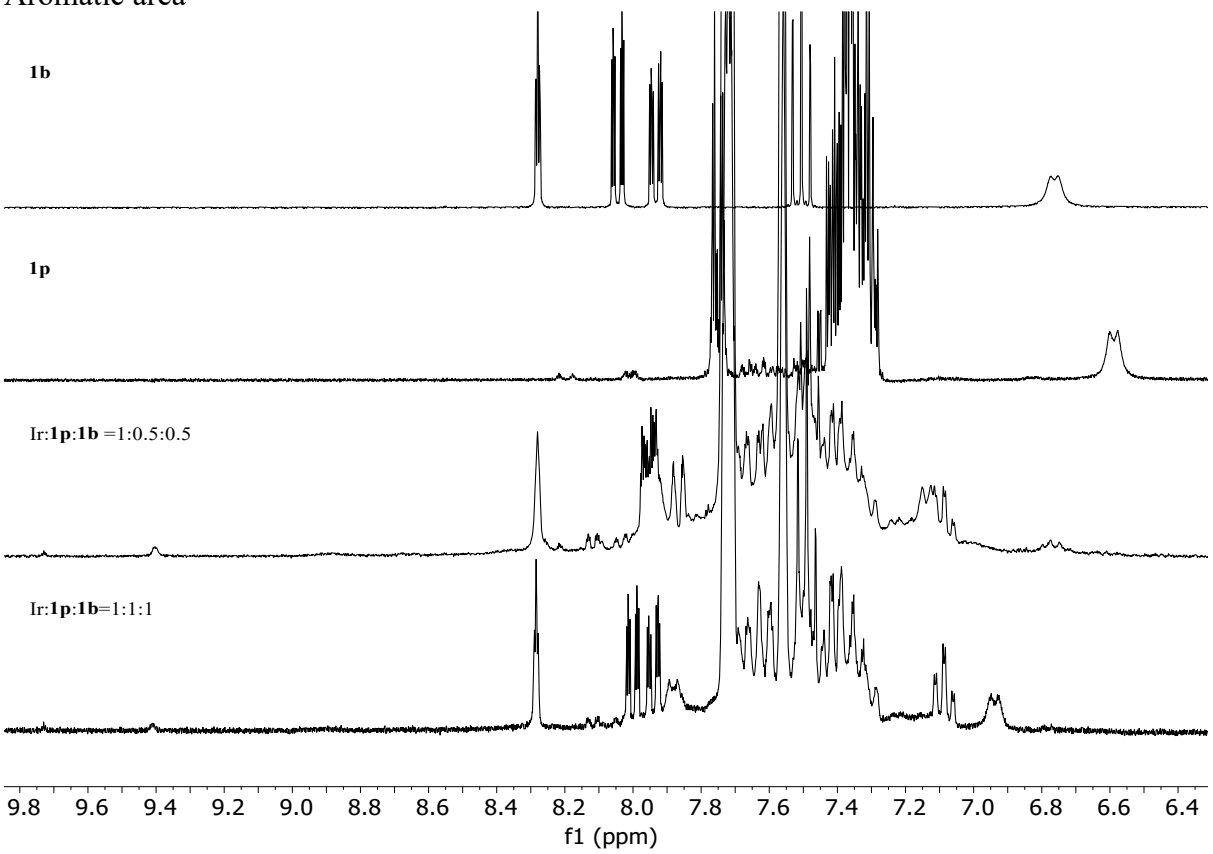

Functional group area

a) Lowered intensity

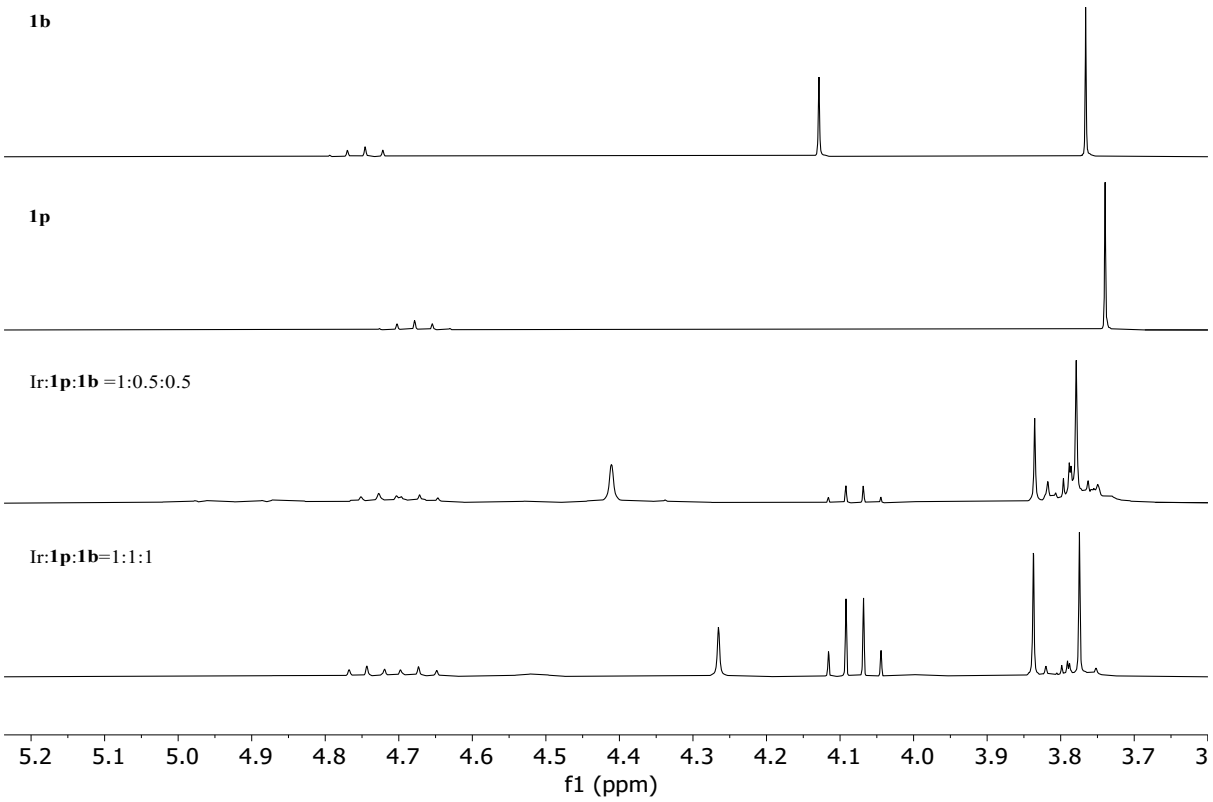

b) Increased intensity

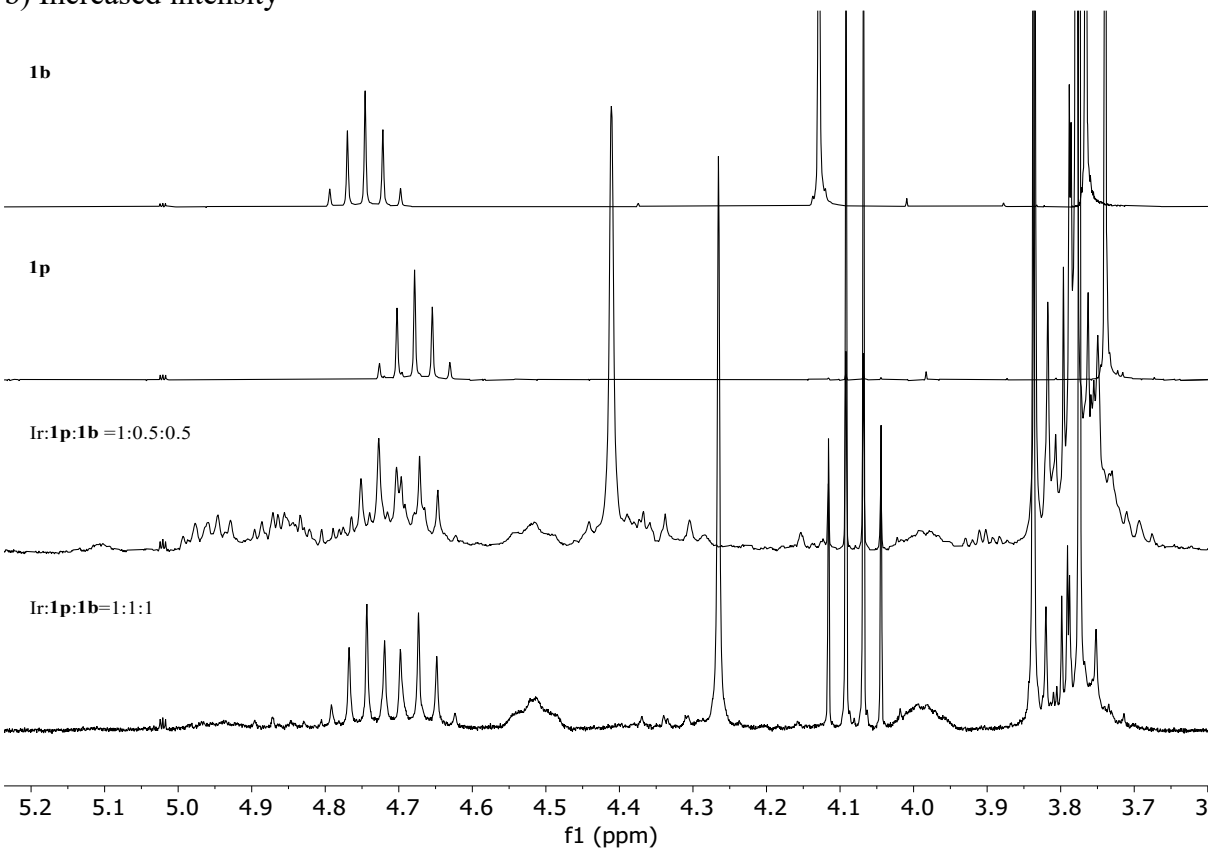

Aliphatic group area

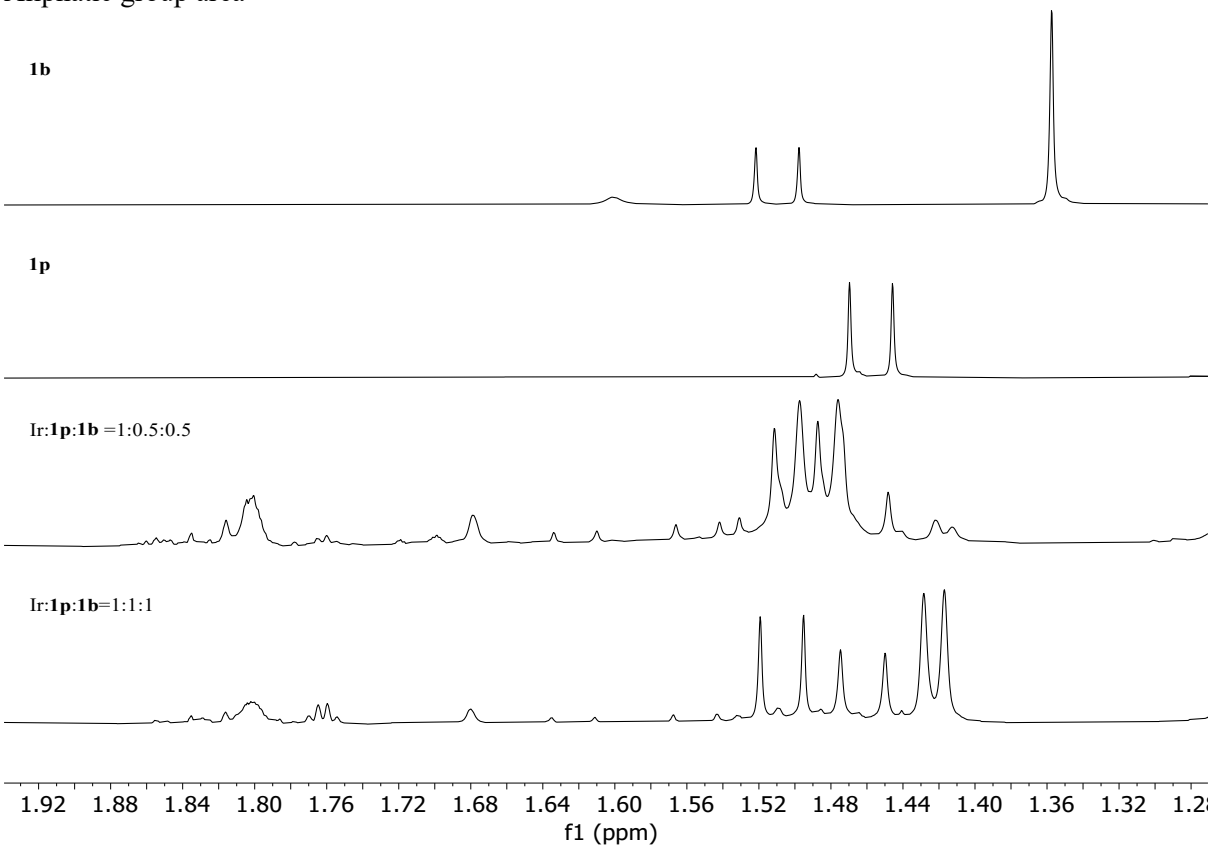

3.4.7. Ir:1p:1b, ^{31}P NMR in CD_2Cl_2

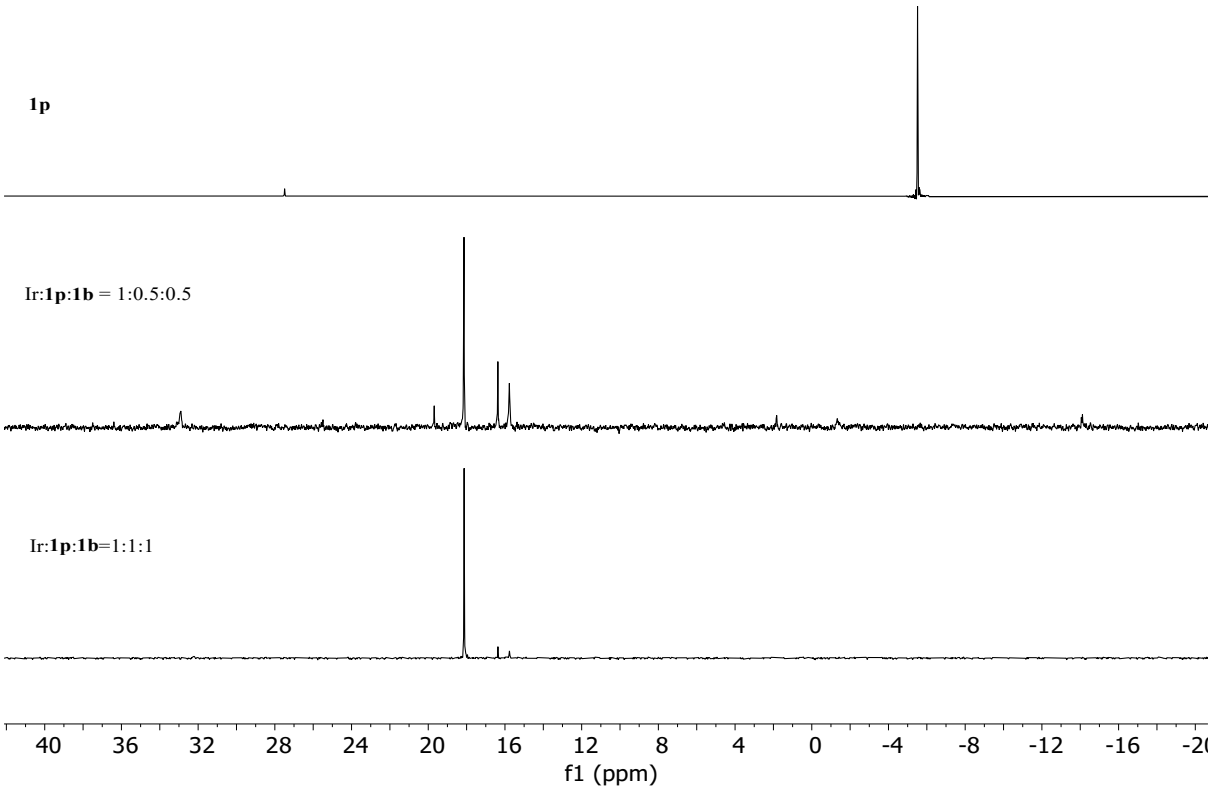

3.4.8. Ir:1p:1b, ^{13}C NMR in CD_2Cl_2

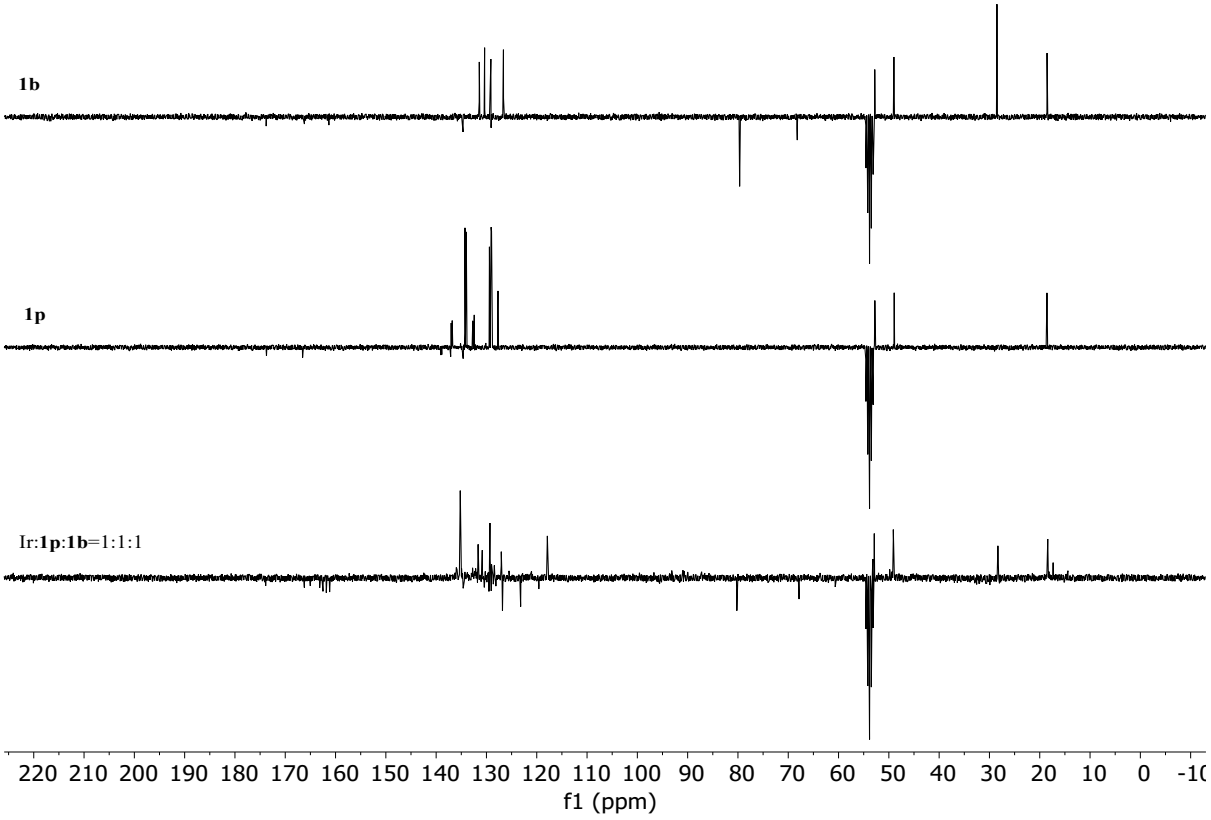

Amide/ester group area

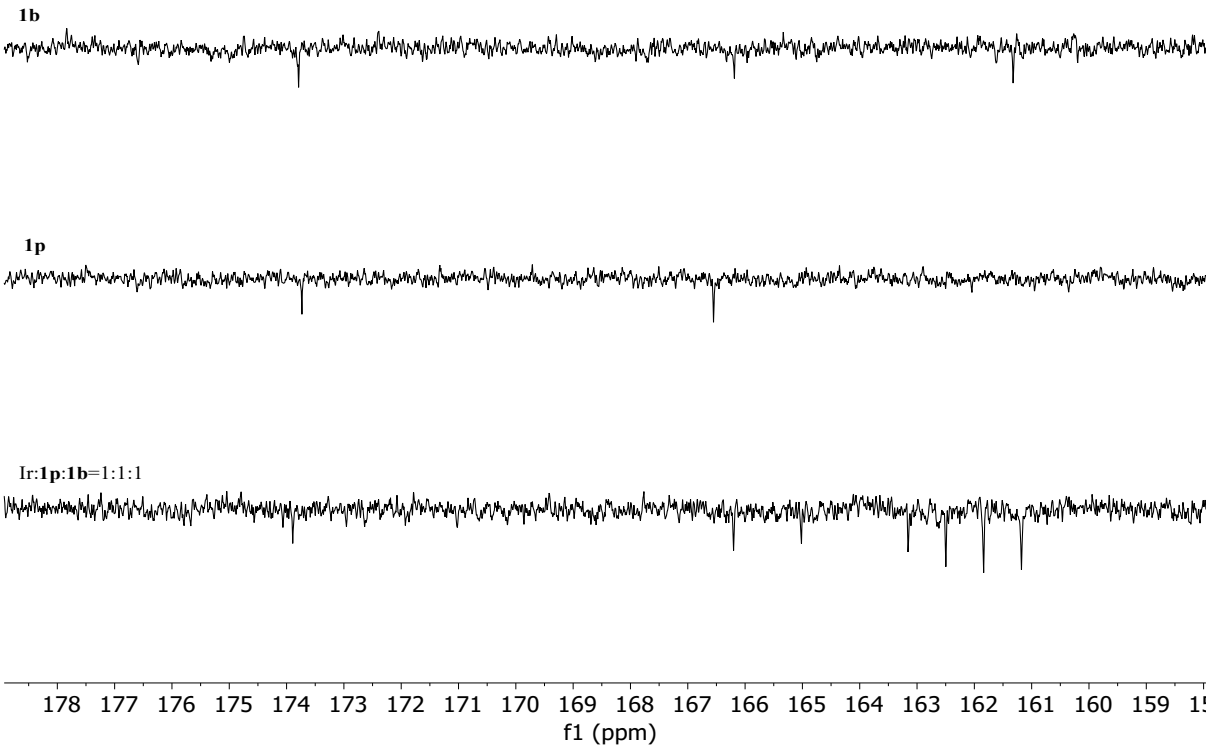

Aromatic group area

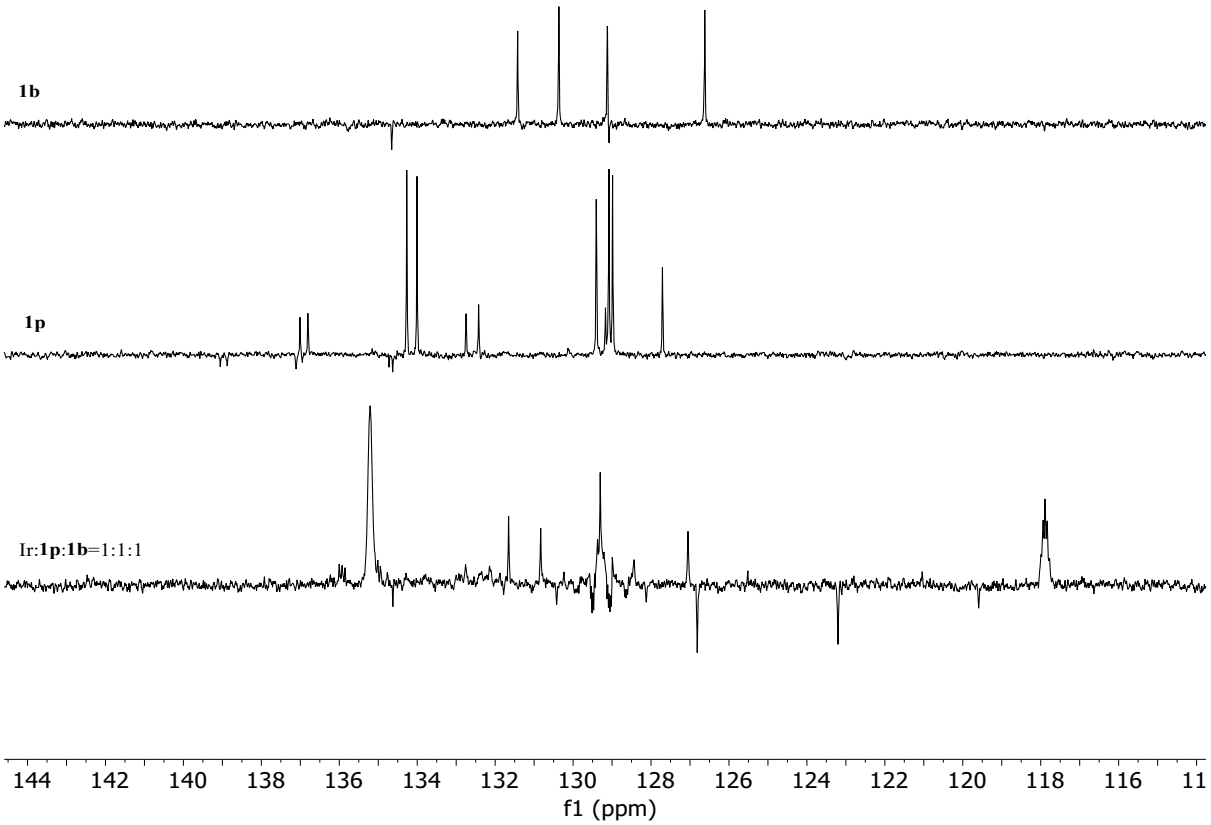

110ppm-60ppm

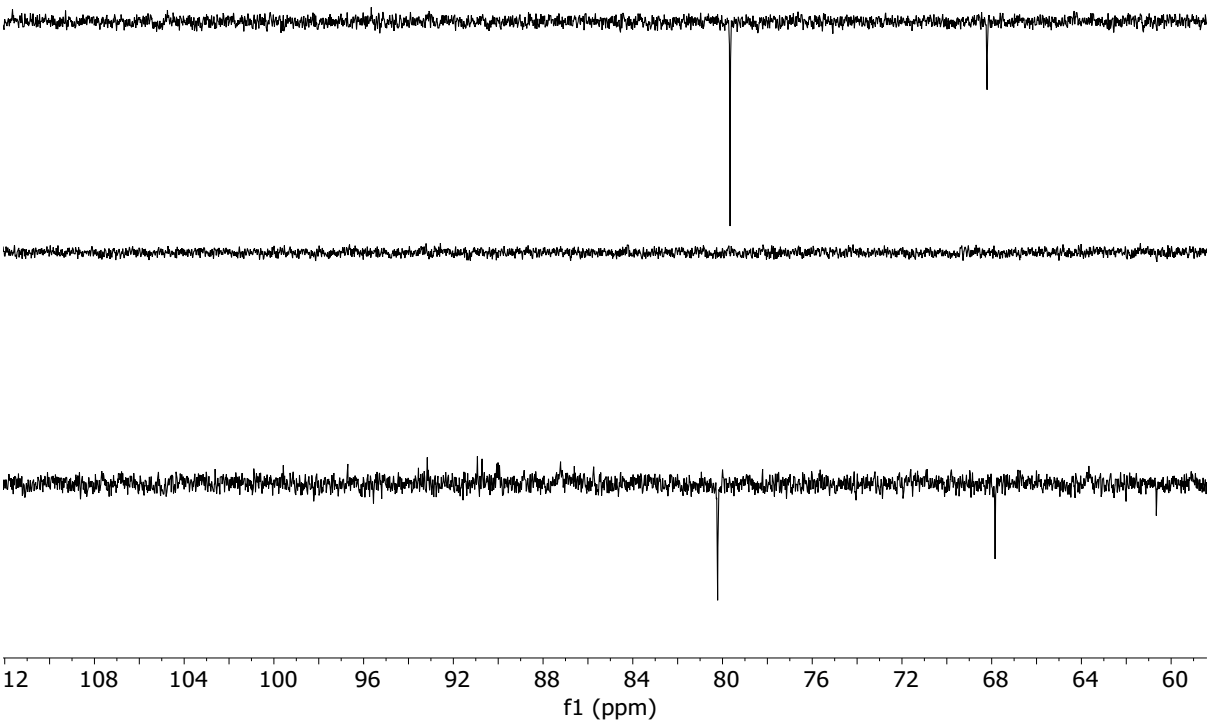

55-48ppm

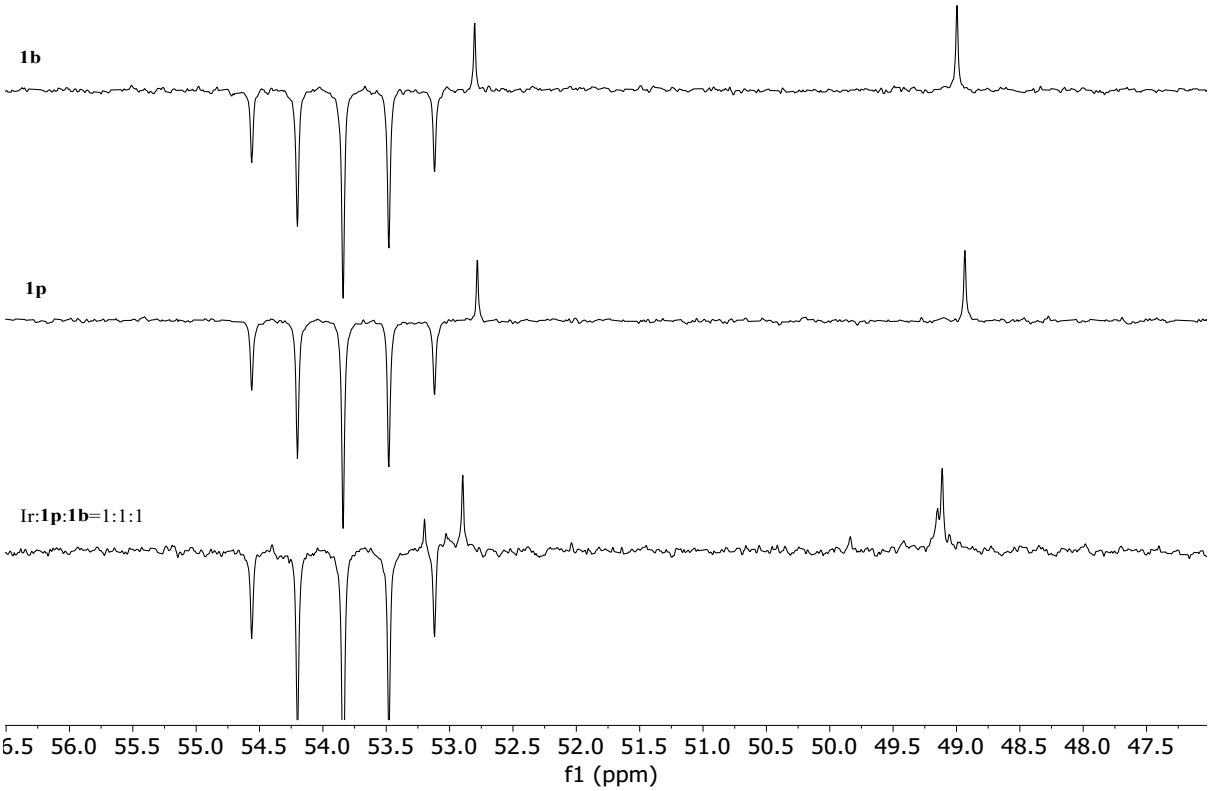

Aliphatic group area

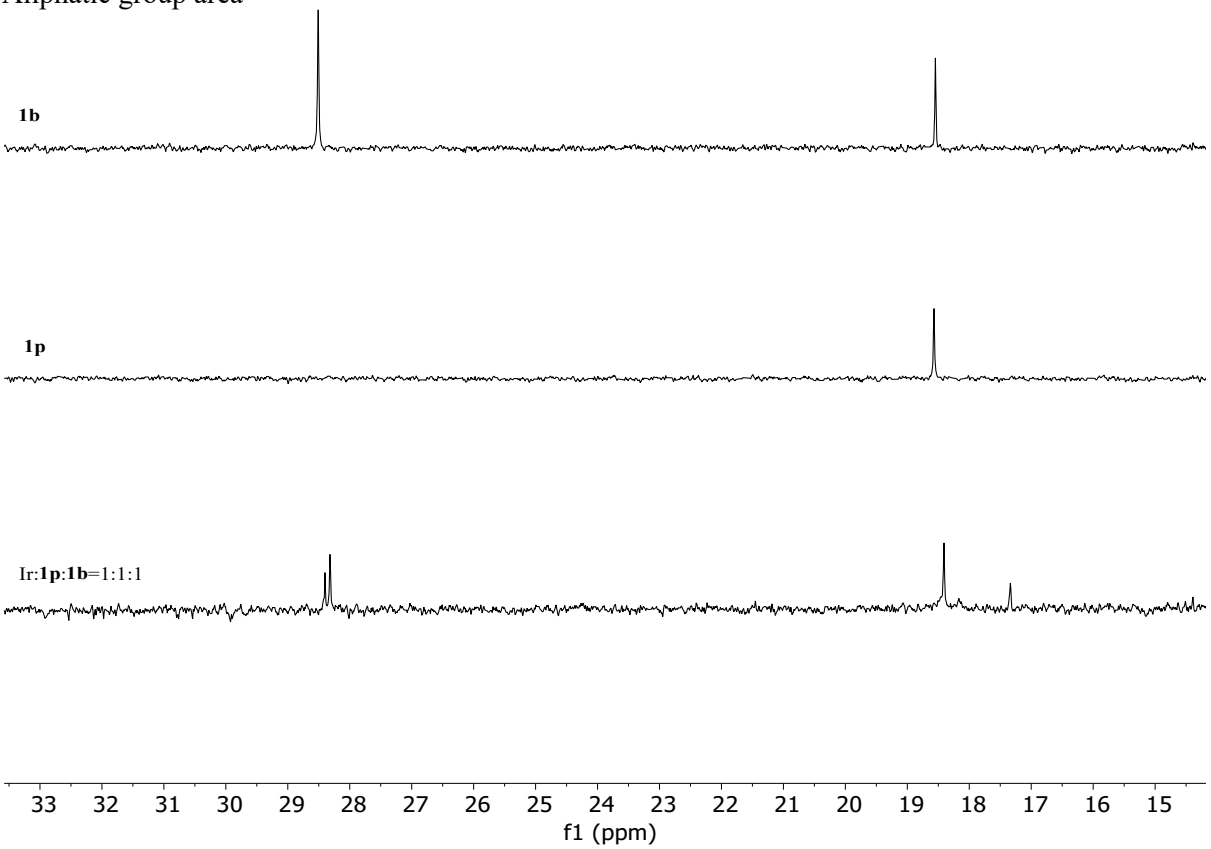

3.4.9. Ir:$TPPH_3$, ^1H NMR in CD_2Cl_2

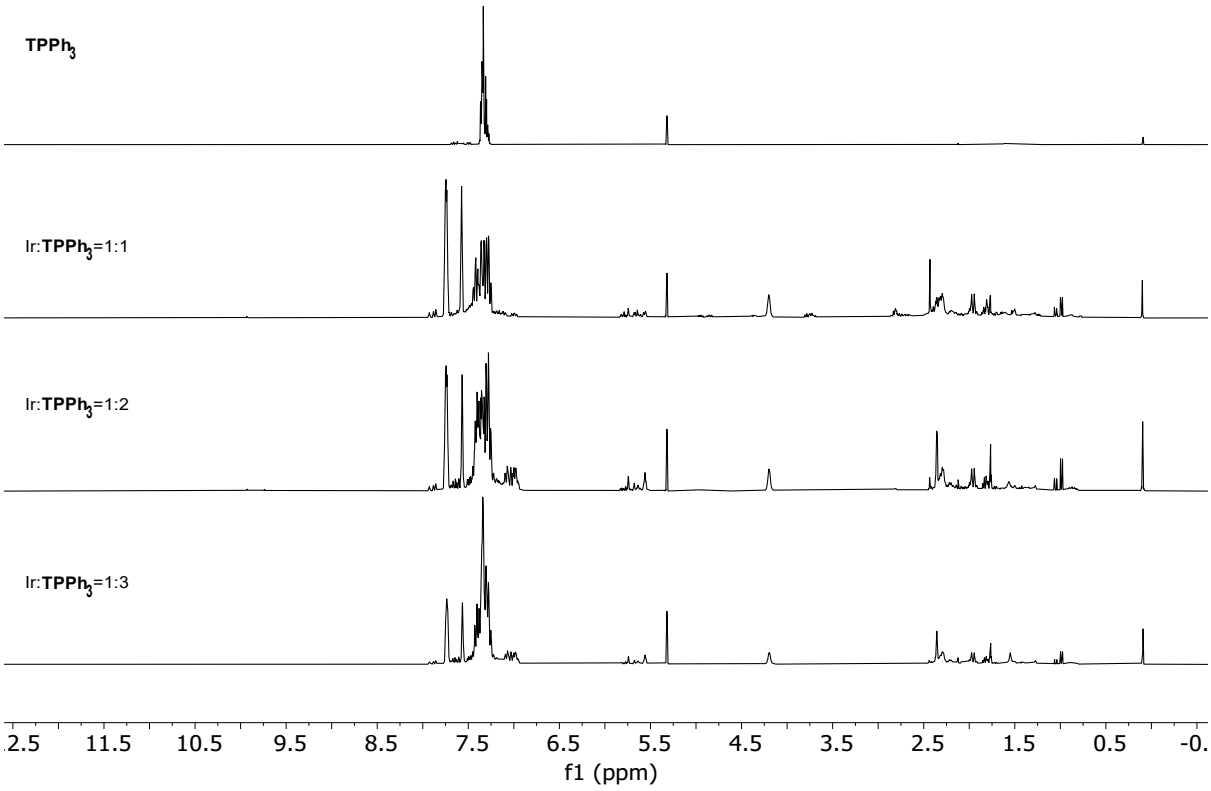

3.4.10. Ir:$TPPH_3$, ^{31}P NMR in CD_2Cl_2

a) Whole spectrum

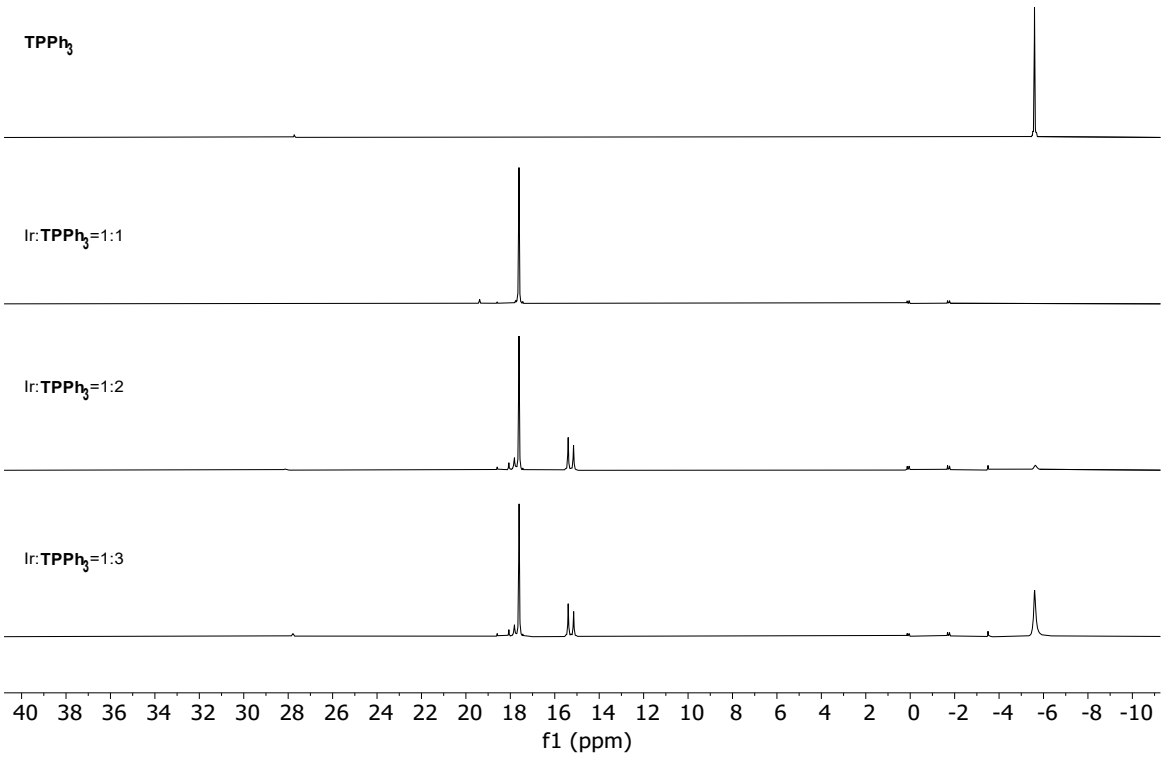

b) Lowered intensity

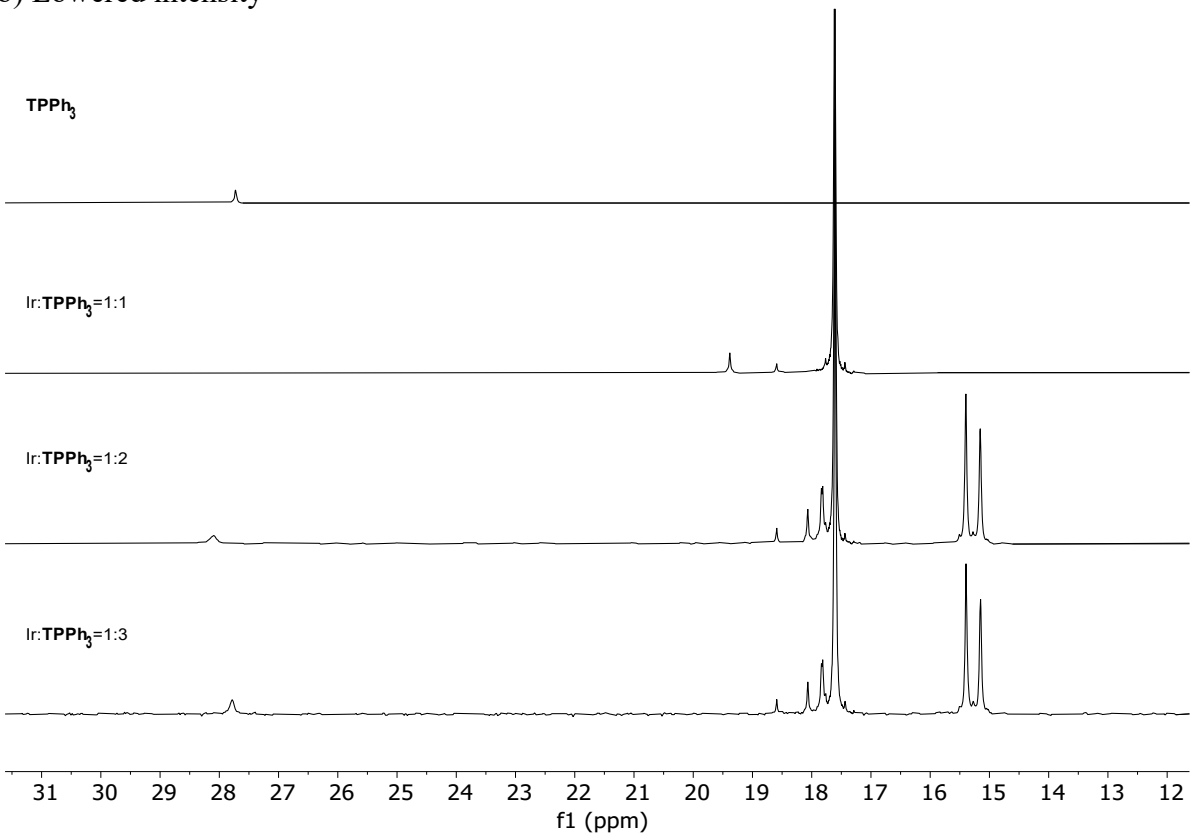

c) Increased intensity

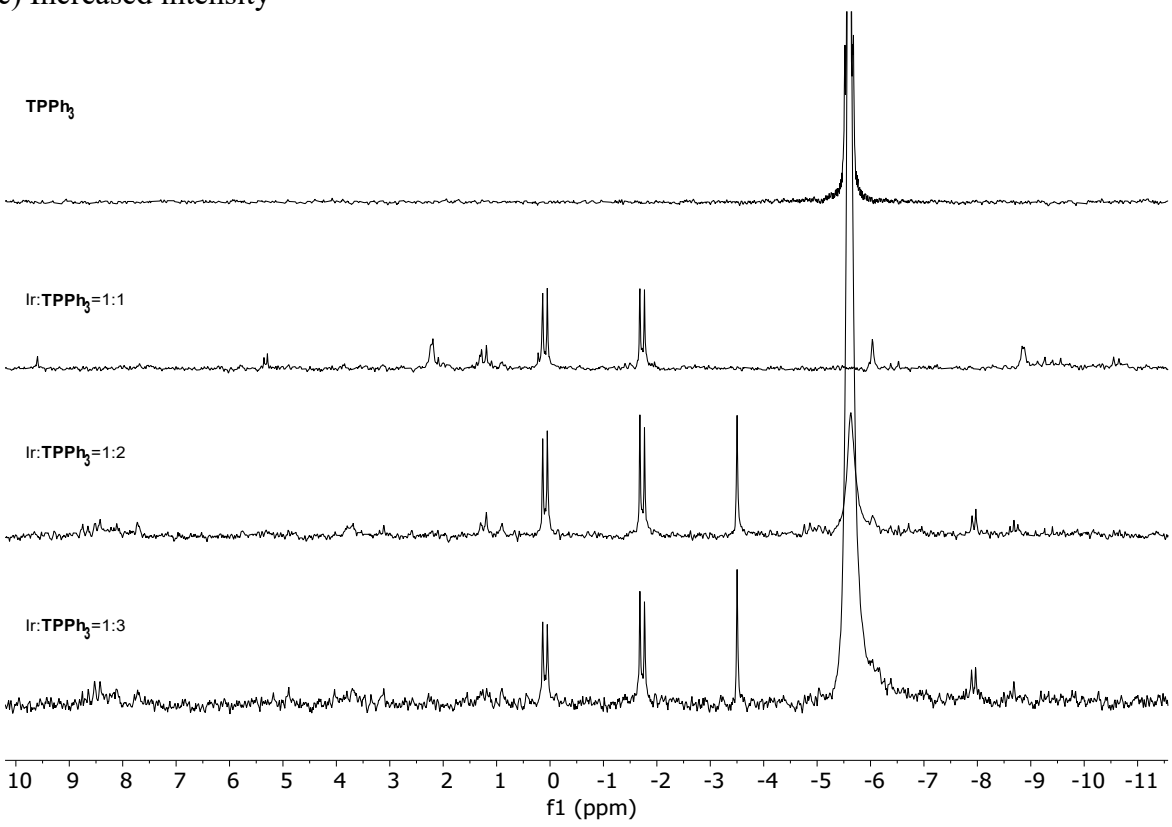

3.4.11. Ir:$TPPH_3$, ^{13}C NMR in CD_2Cl_2

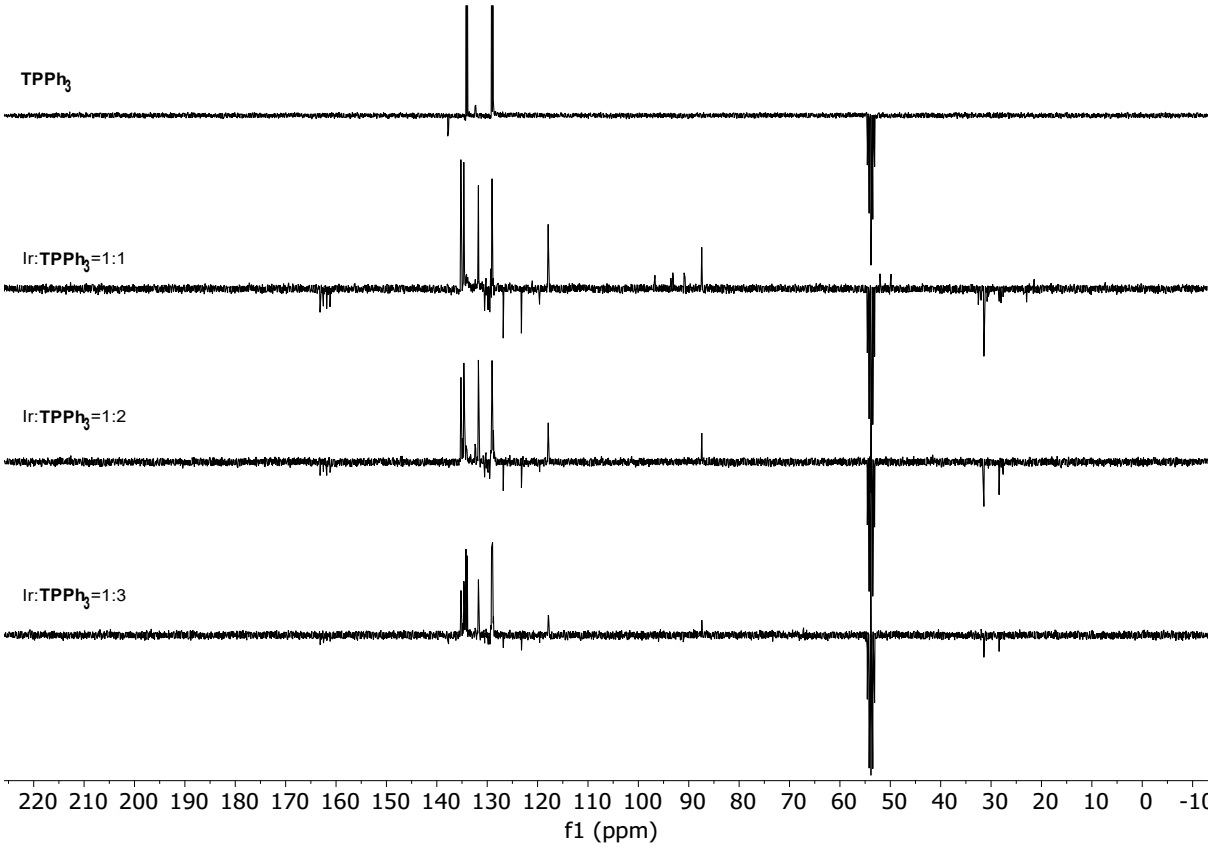

3.4.12. Ir:1p:$TPPH_3$, ^{1}H NMR in CD_2Cl_2

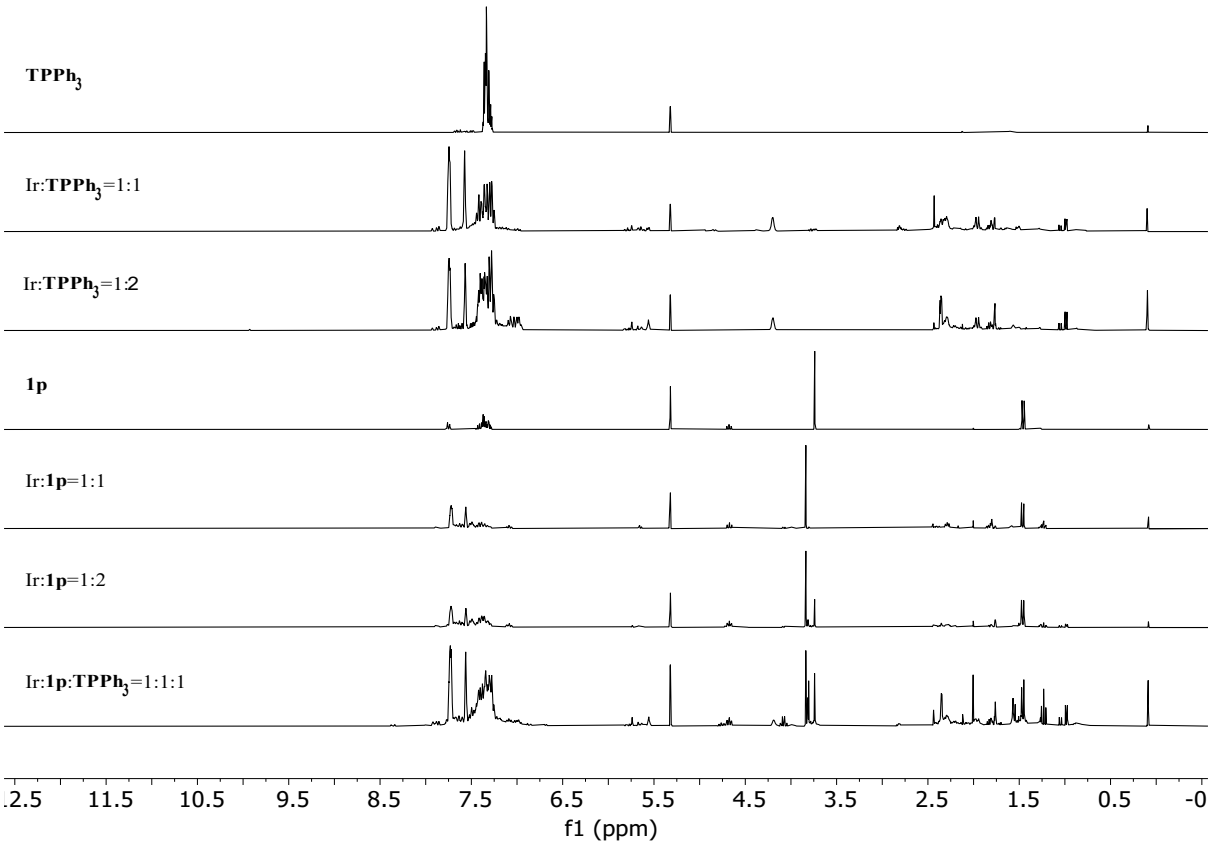

Functional group region:
a) Lowered intensity

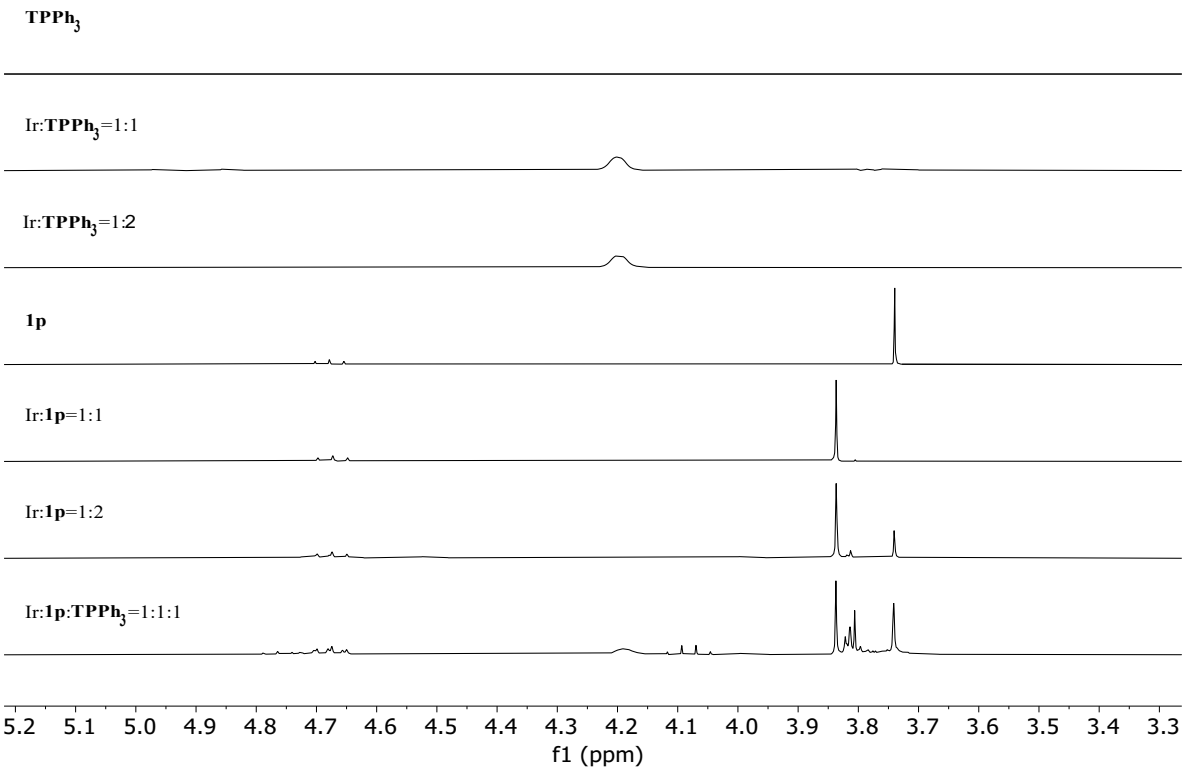

b) Increased intensity

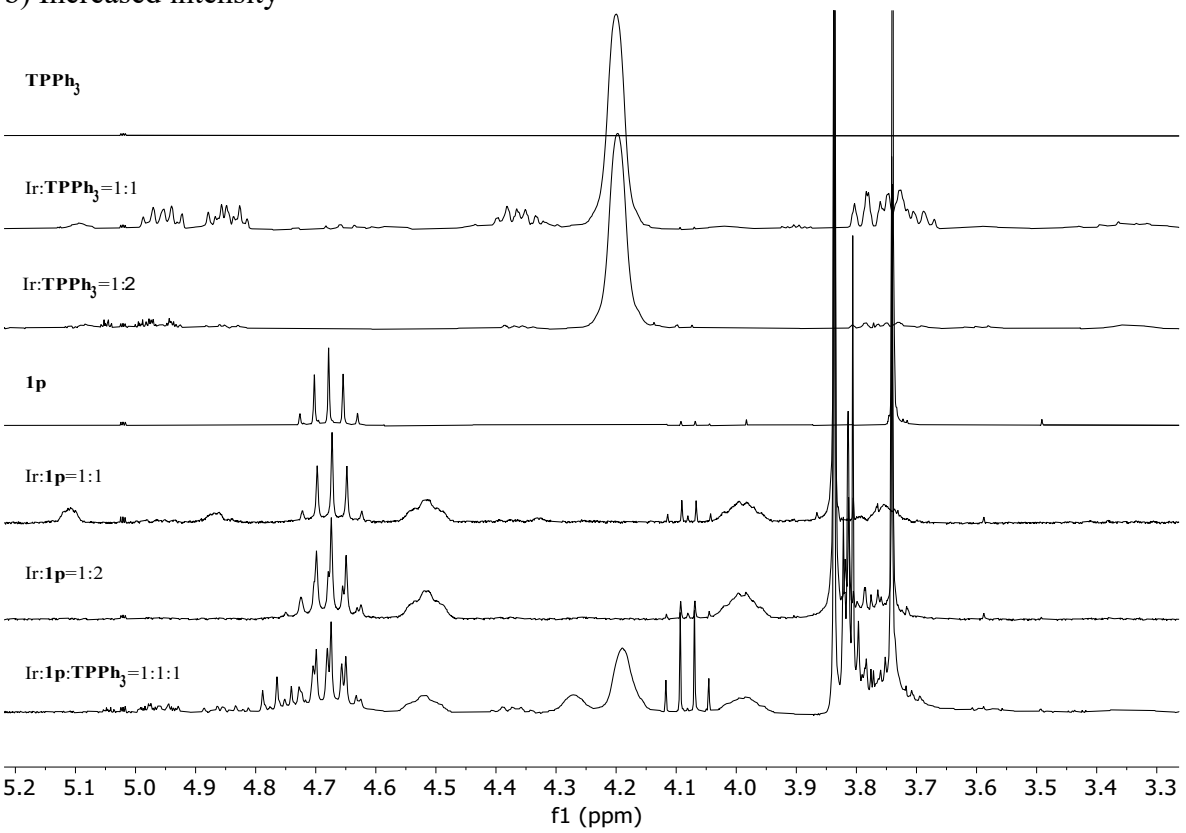

Aliphatic group region

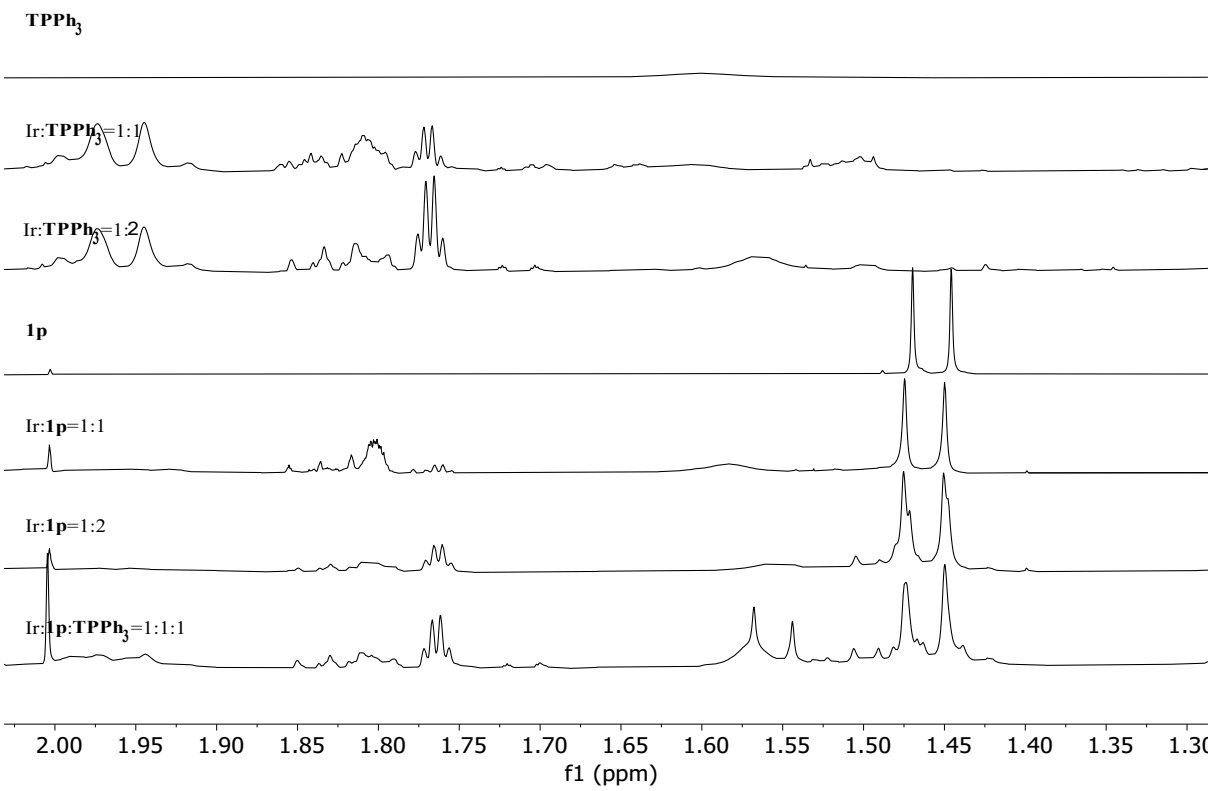

3.4.13. Ir:1p:TPPH$_3$, ^{31}P NMR in CD_2Cl_2

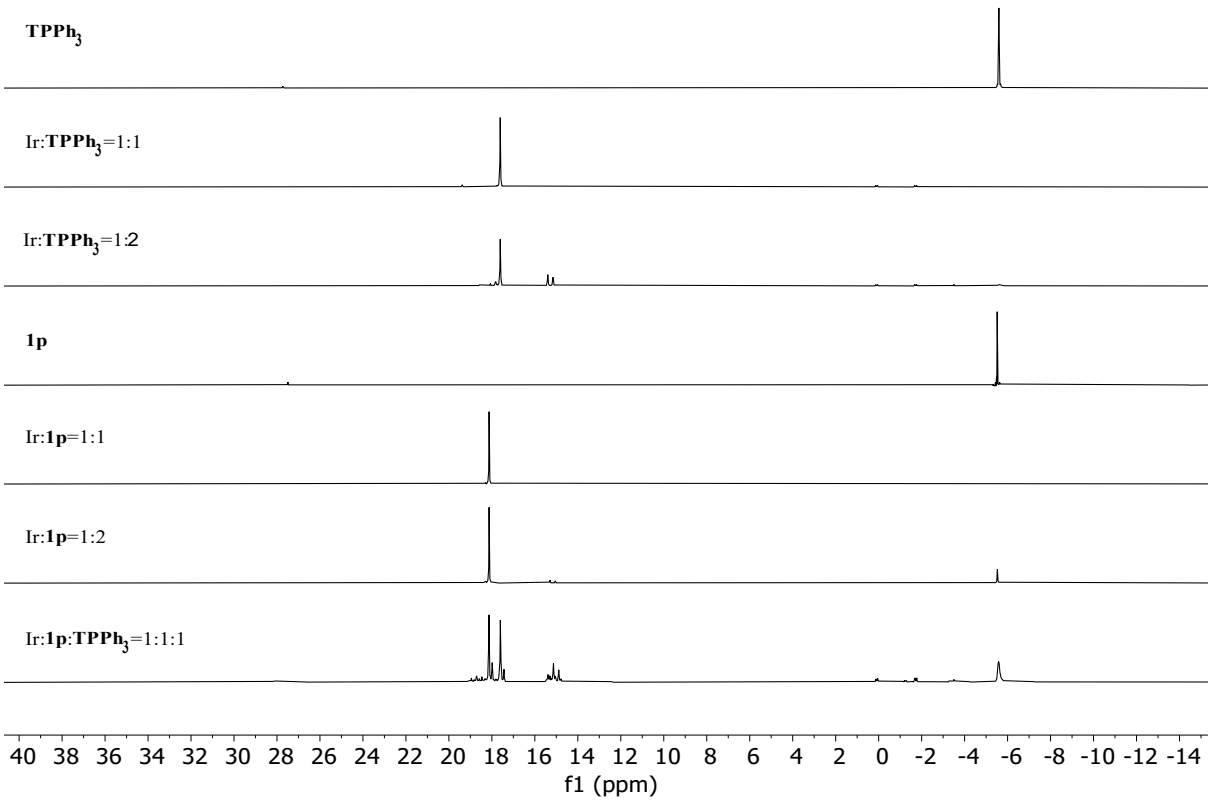

a)

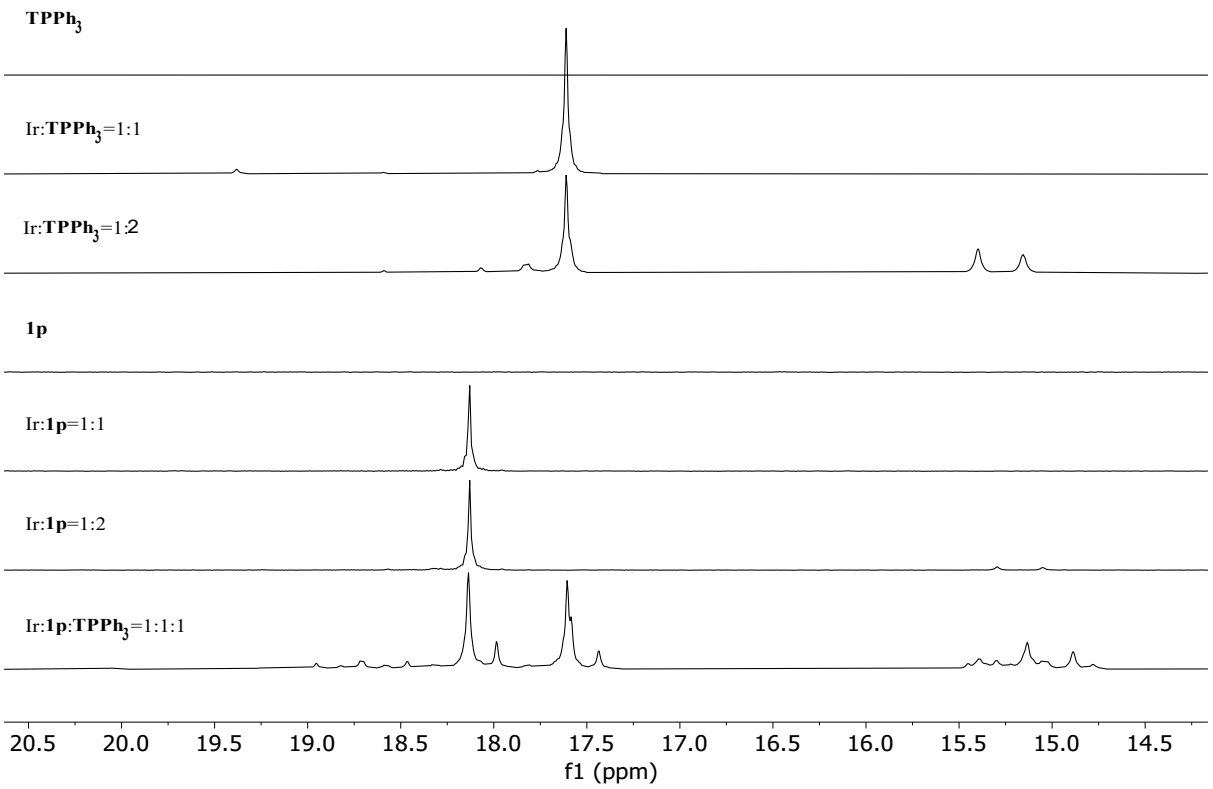
TPPh3
Ir:TPPh3=1:1
Ir:TPPh3=1:2
1p
Ir:1p=1:1
Ir:1p=1:2
Ir:1p:TPPh3=1:1:1
20.5 20.0 19.5 19.0 18.5 18.0 17.5 17.0 16.5 16.0 15.5 15.0 14.5
f1 (ppm)

b)

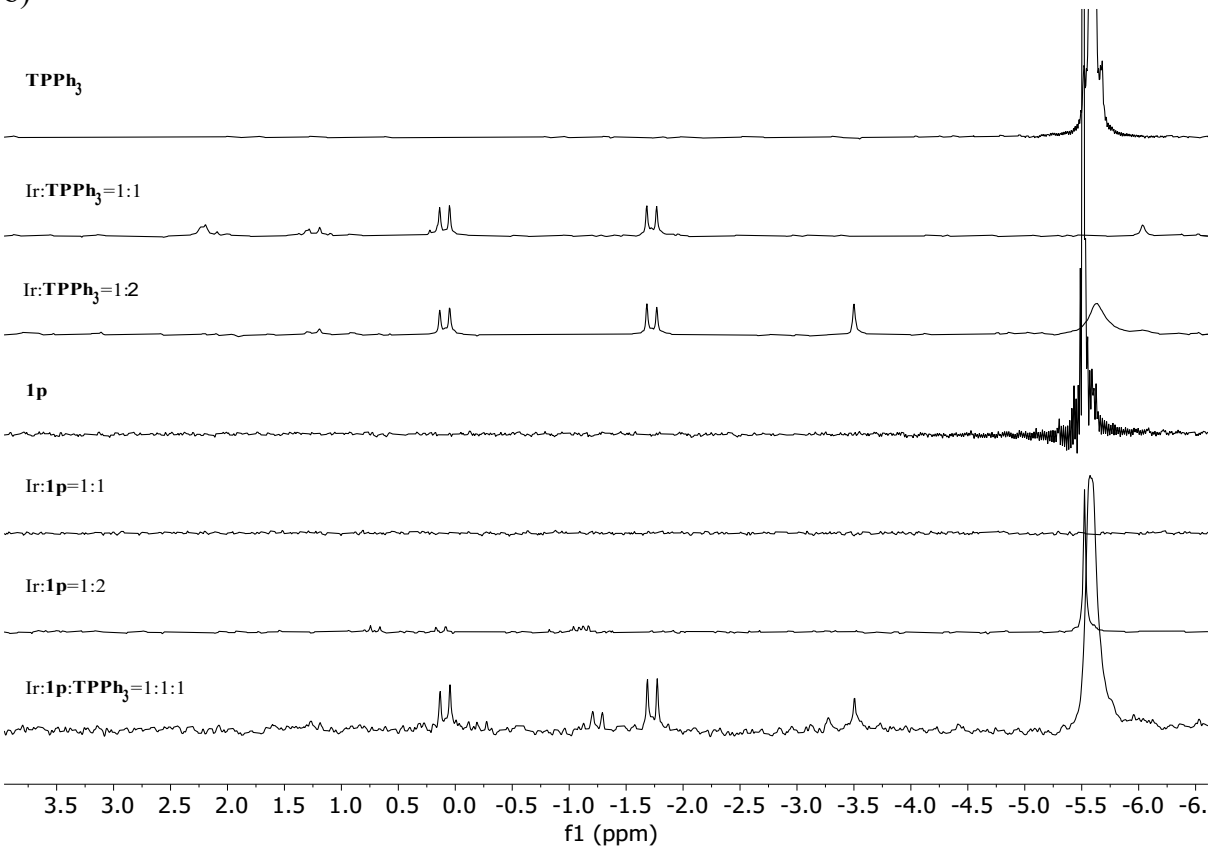
TPPh3
Ir:TPPh3=1:1
Ir:TPPh3=1:2
1p
Ir:1p=1:1
Ir:1p=1:2
Ir:1p:TPPh3=1:1:1
3.5 3.0 2.5 2.0 1.5 1.0 0.5 0.0 -0.5 -1.0 -1.5 -2.0 -2.5 -3.0 -3.5 -4.0 -4.5 -5.0 -5.5 -6.0 -6.
f1 (ppm)

3.4.14. Ir, 1p, $TPPH_3$, 1a, 1b, ^{31}P NMR in CD_2Cl_2

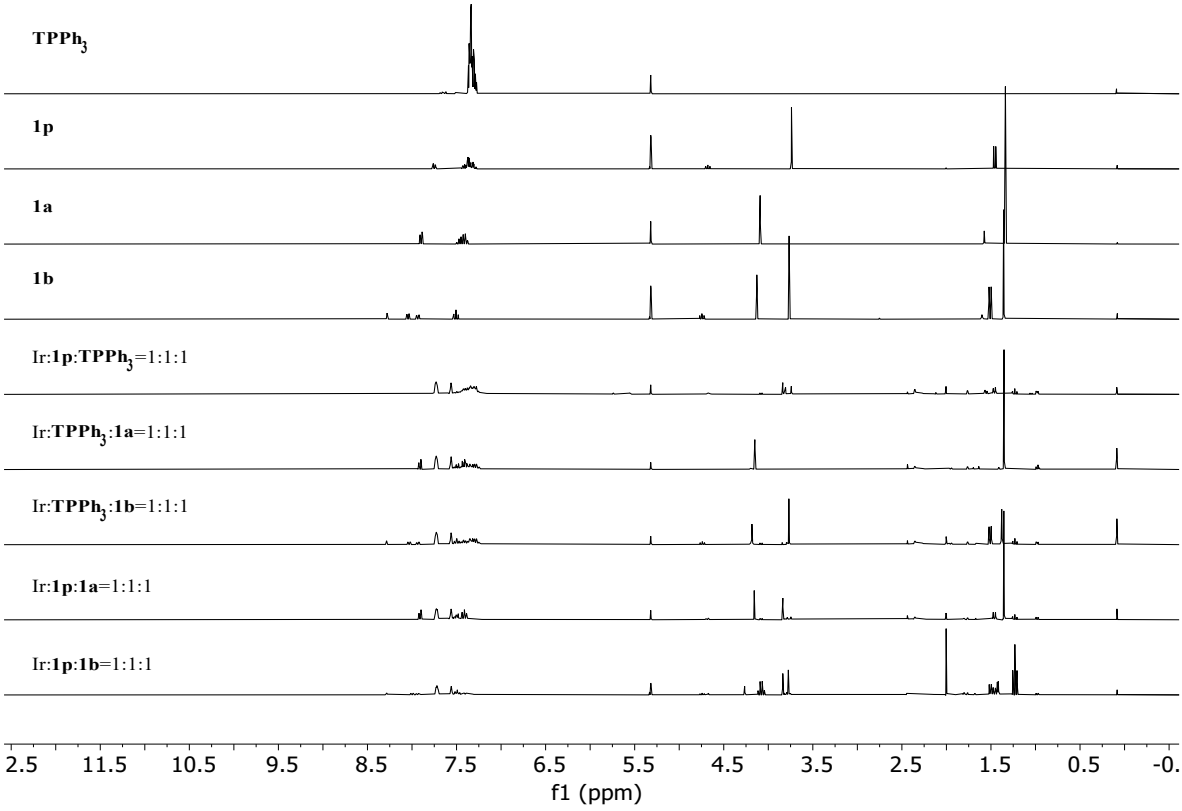

Aromatic region:

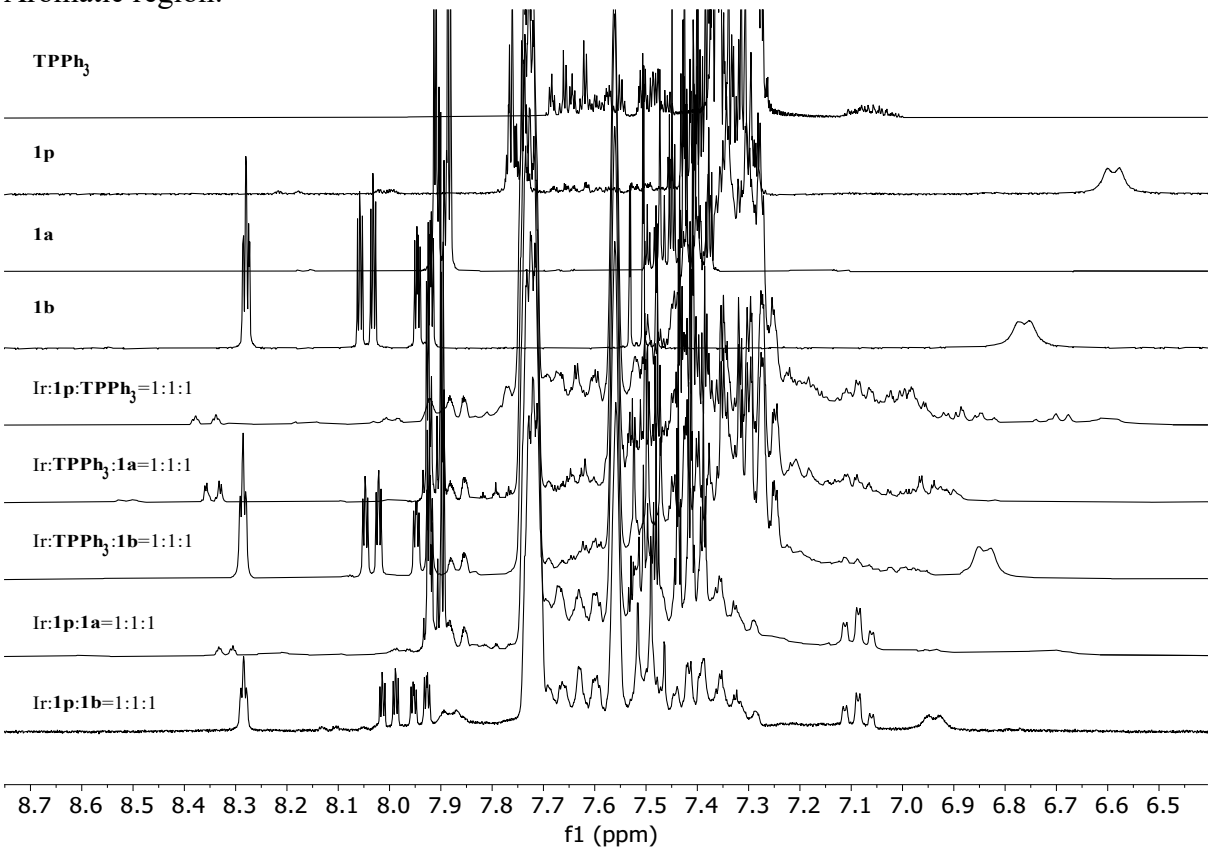

Functional group region

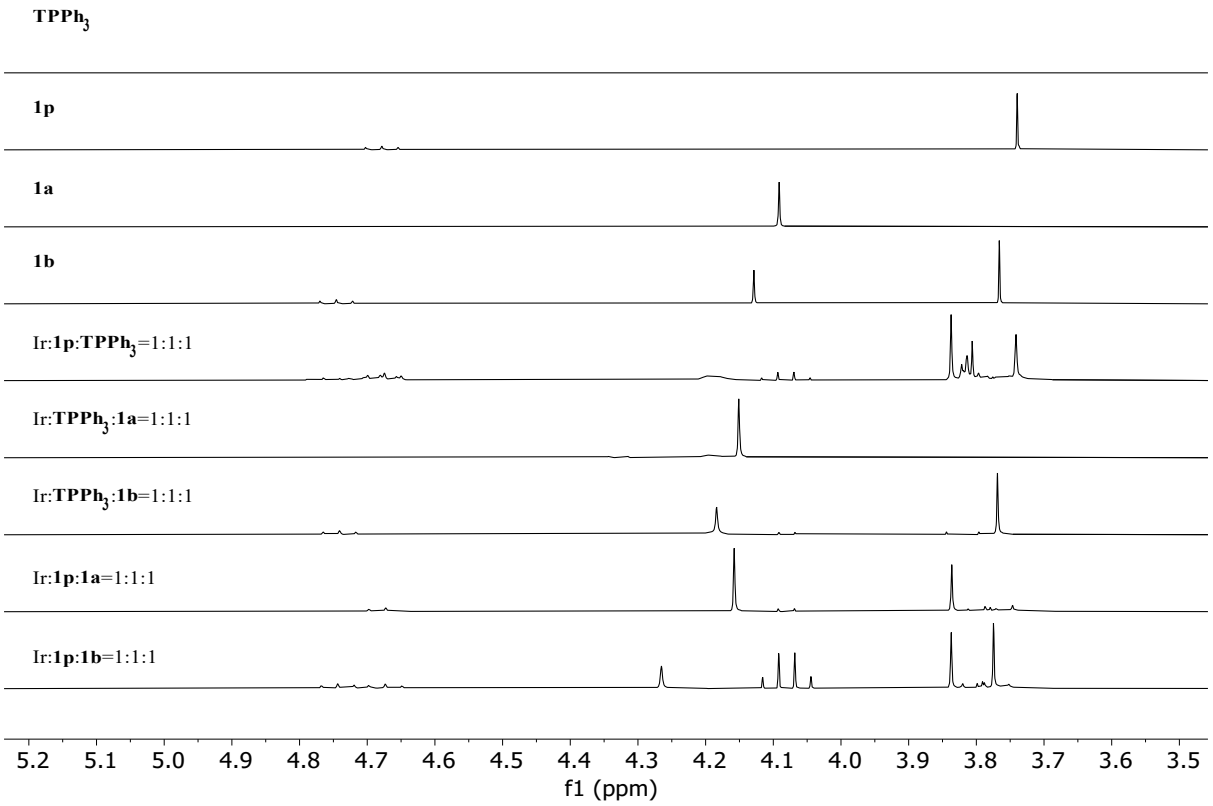

Aliphatic group region:

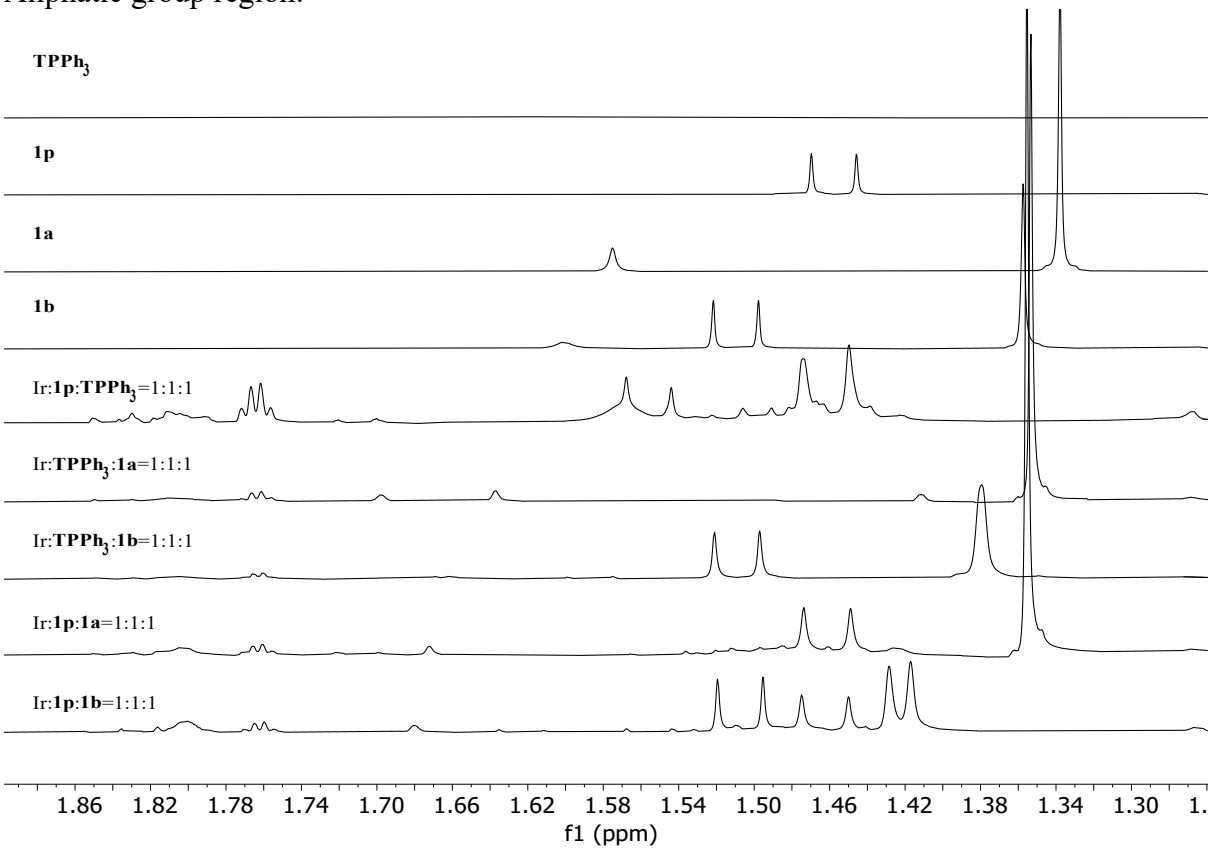

3.4.15. Ir:1p:$TPPh_3$, ^{31}P NMR in CD_2Cl_2

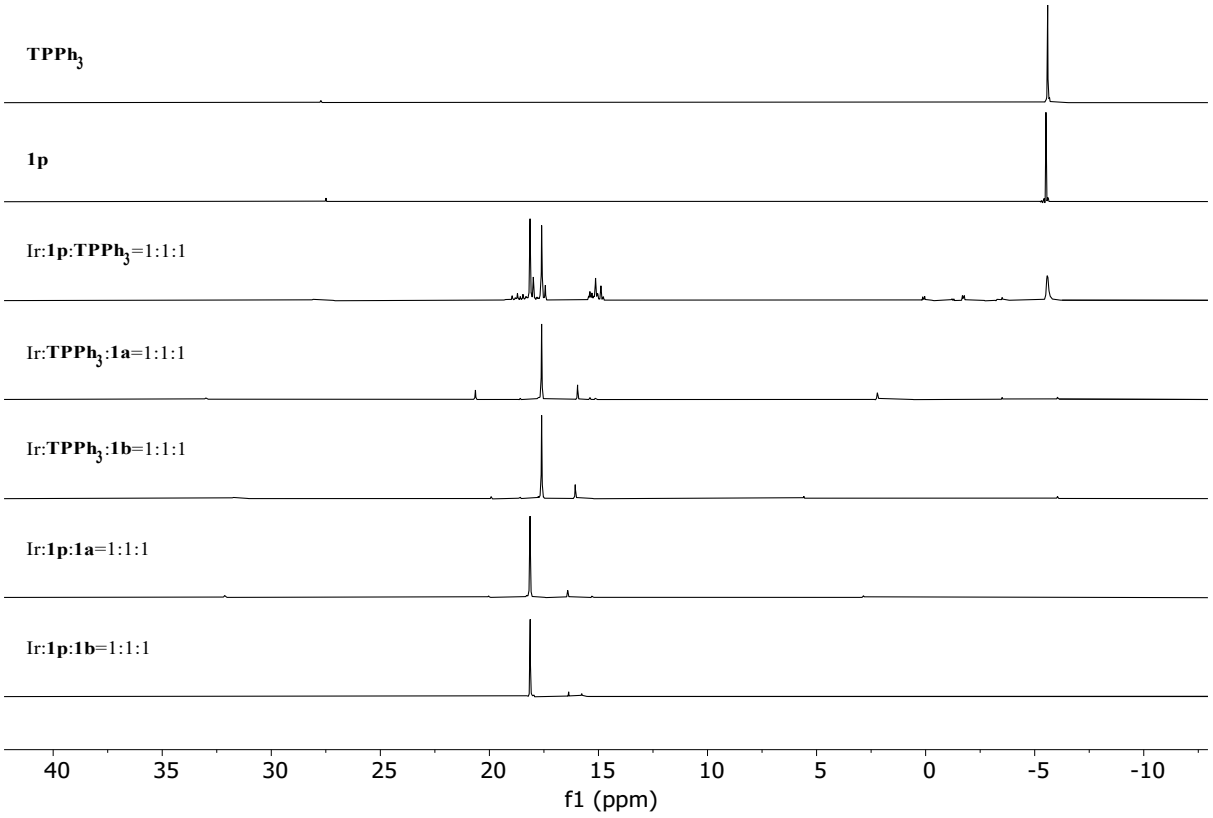

a)

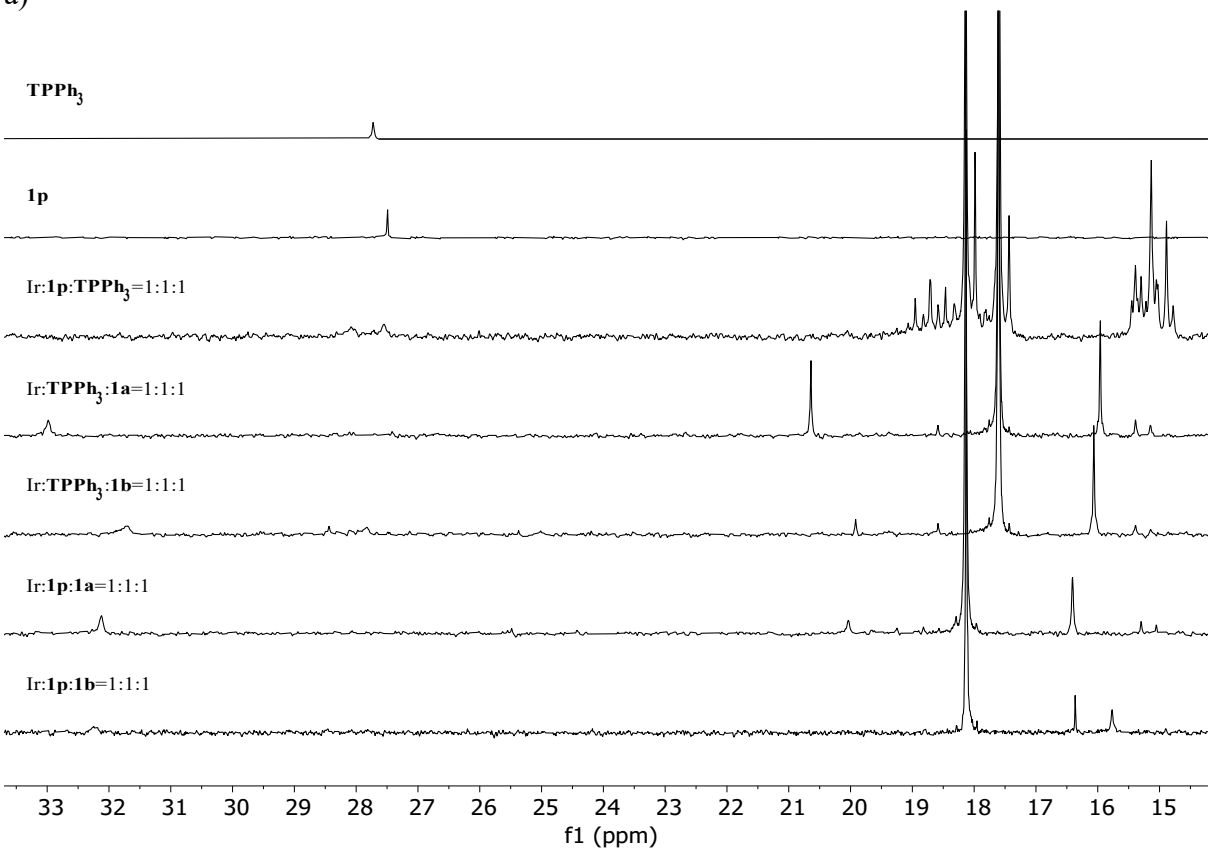

b)

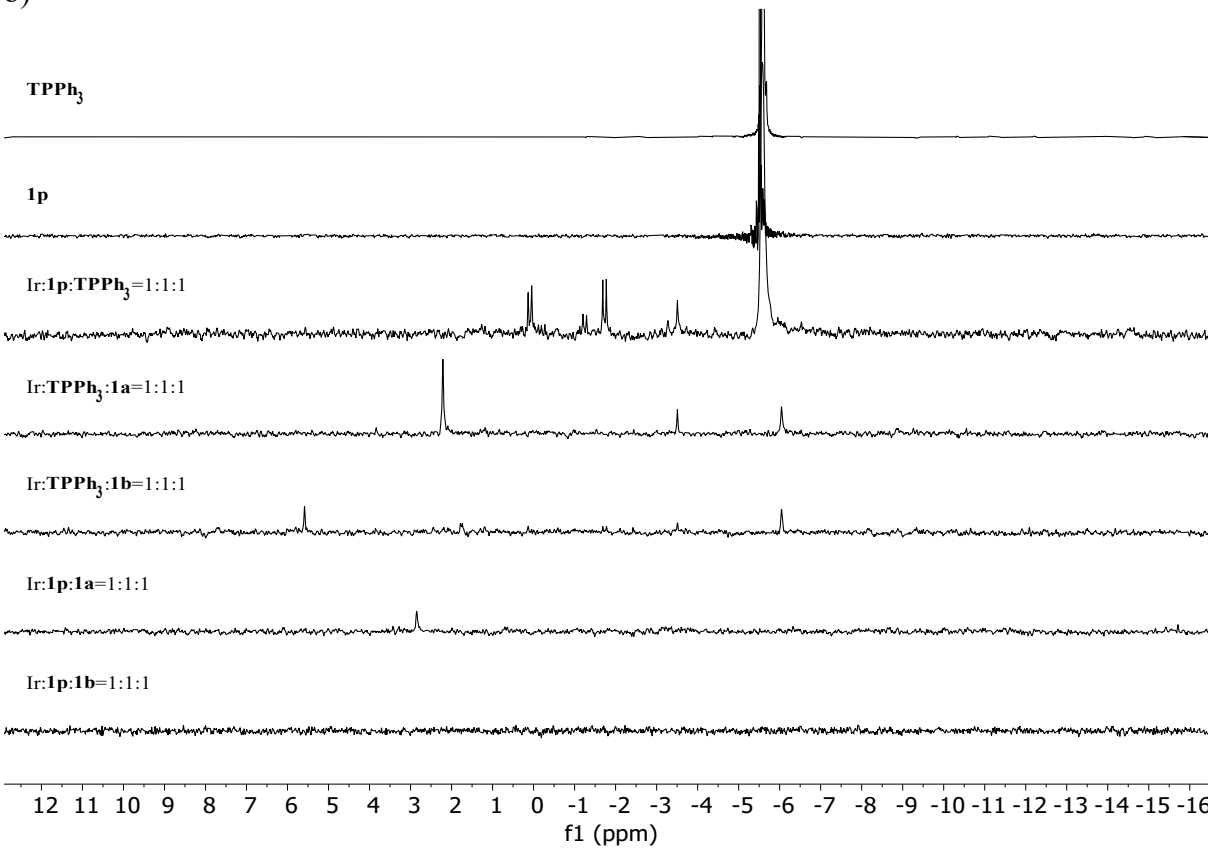

3.4.16. Ir:1c, ^{1}H NMR in CD_2Cl_2

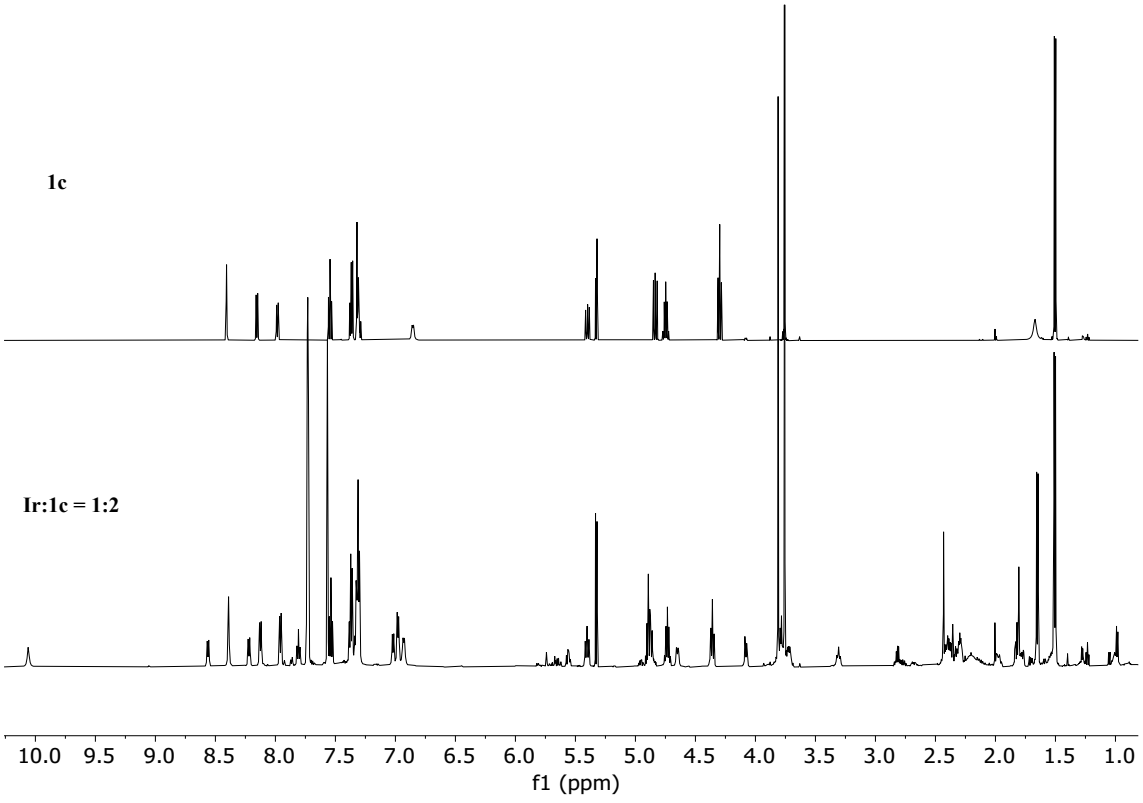

Aromatic group area of Ir:**1c**, ^{1}H NMR in CD_2Cl_2

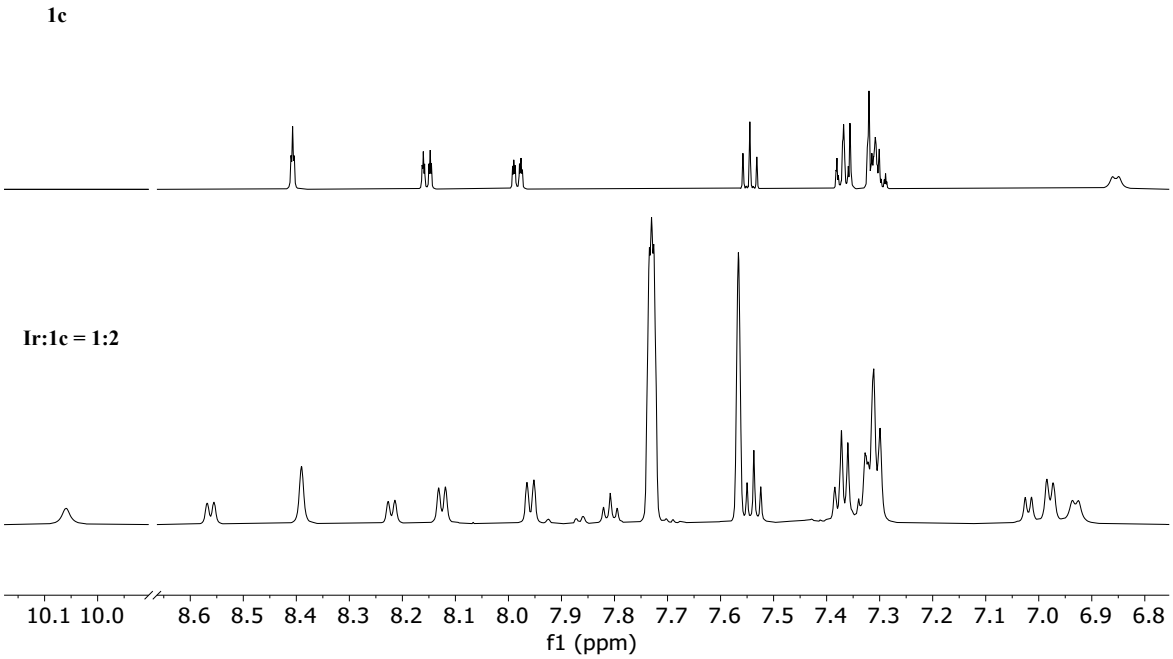

Functional group area
a) Lowered peak intensity

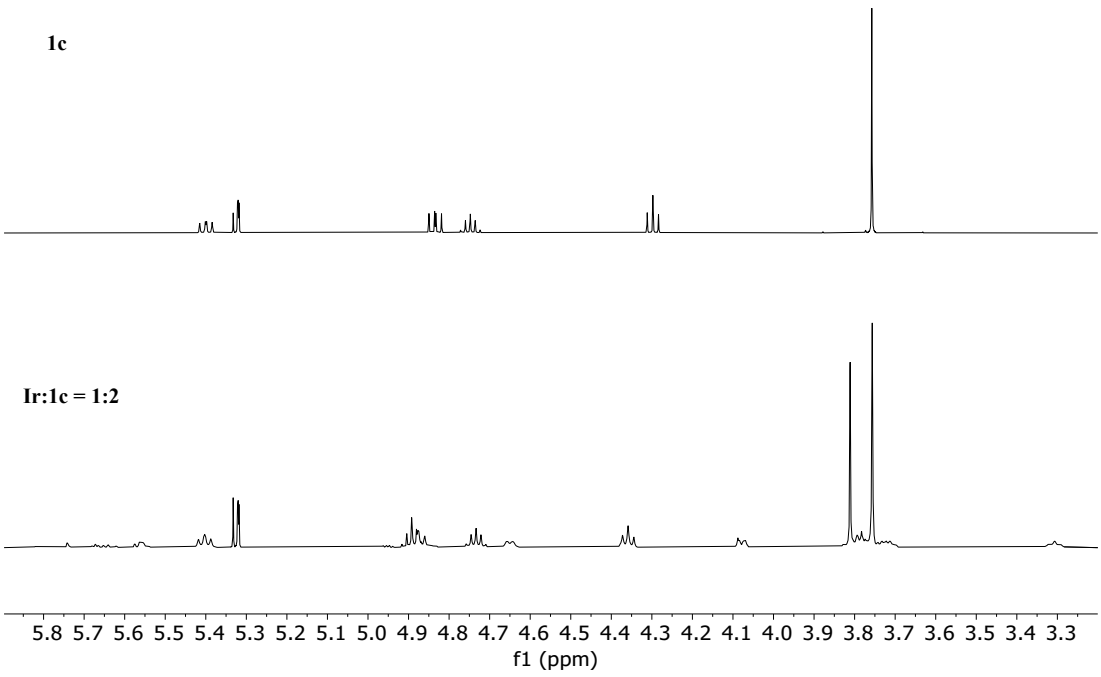

b) Increased peak intensity

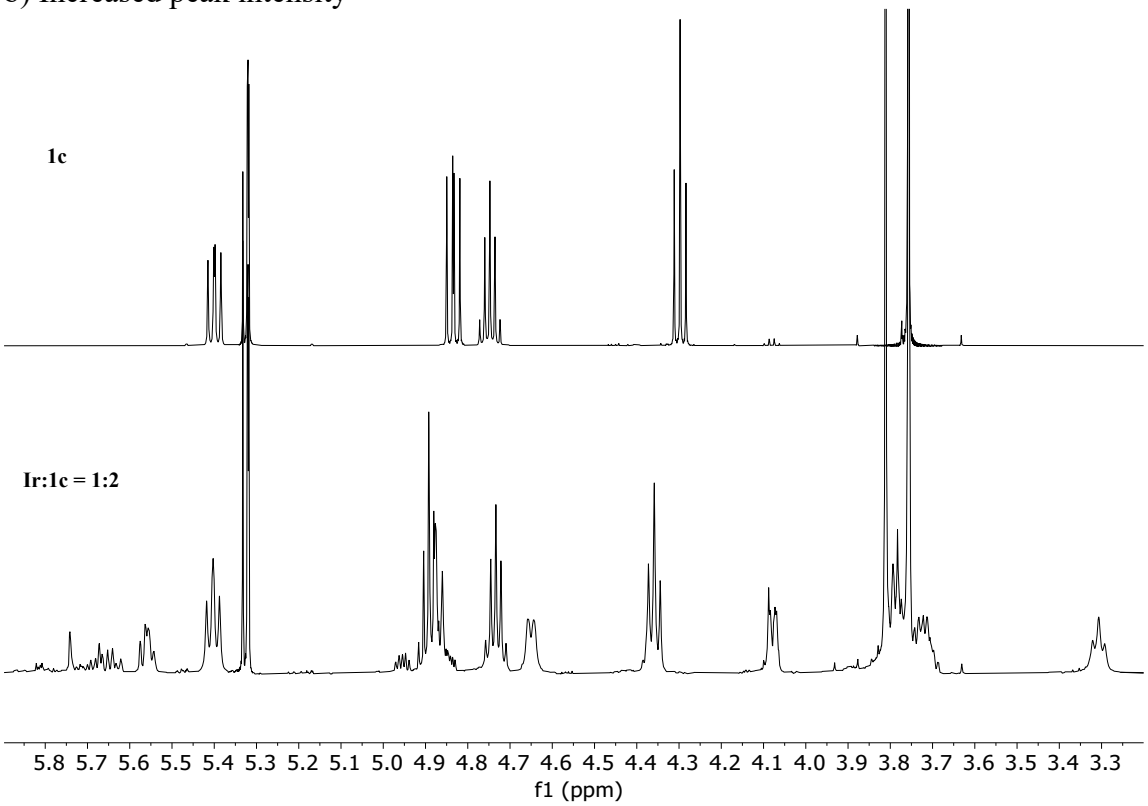

Aliphatic group area

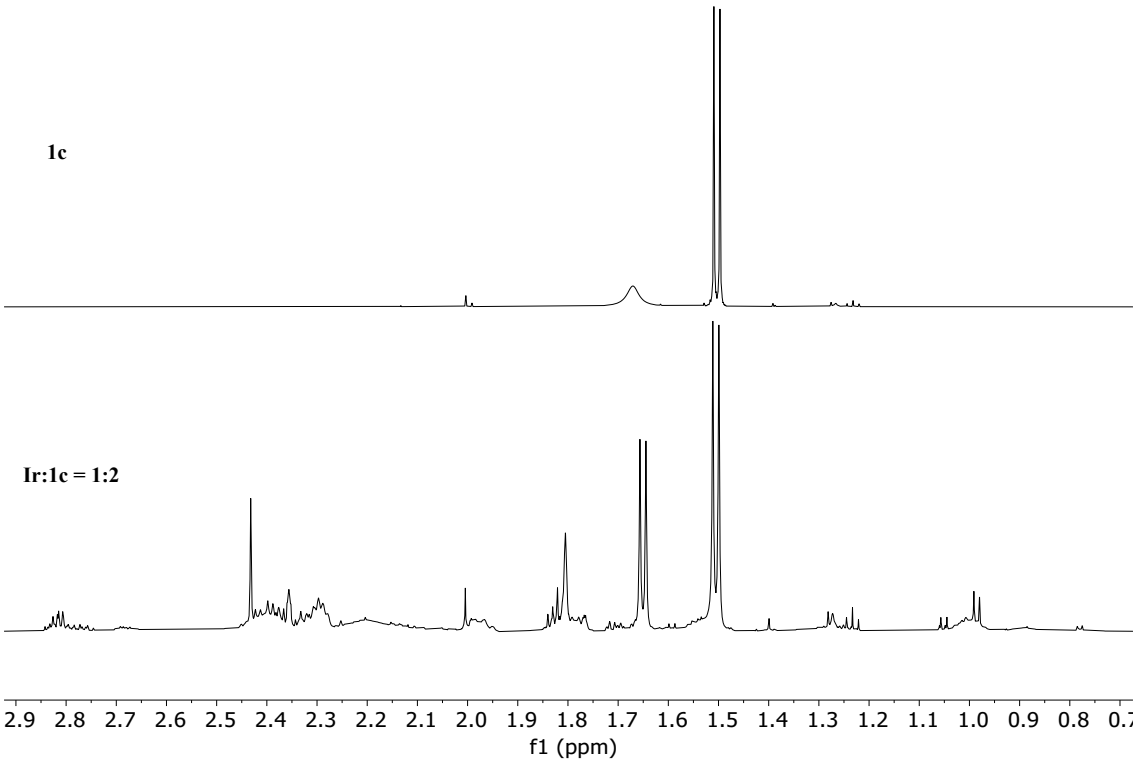

3.4.17. Ir:1c*, 1H NMR in CD_2Cl_2

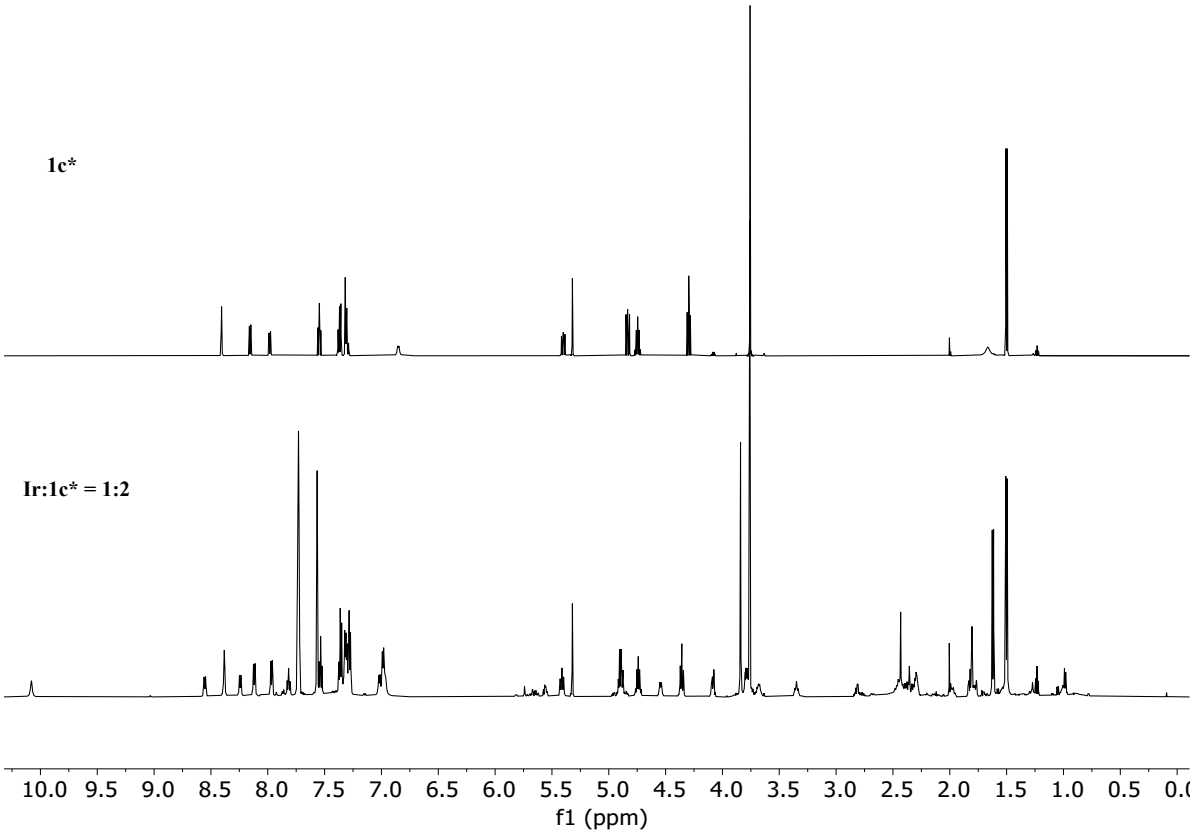

Aromatic group area of Ir:**1c**, ^{1}H NMR in CD_2Cl_2

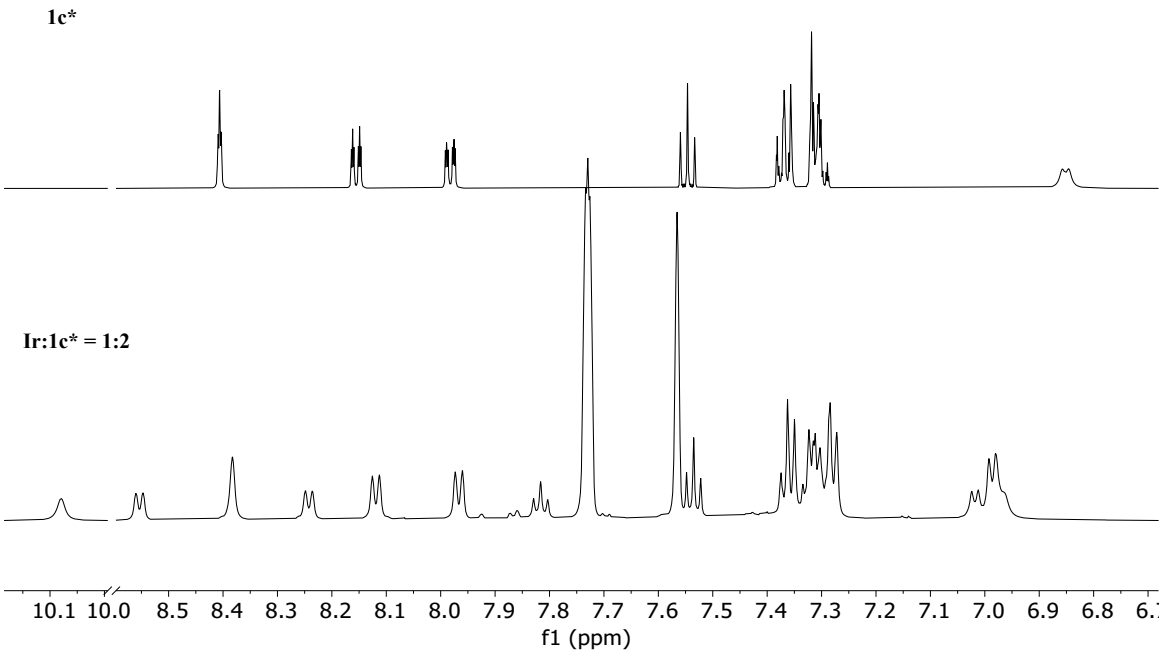

Functional group area

a) Lowered peak intensity

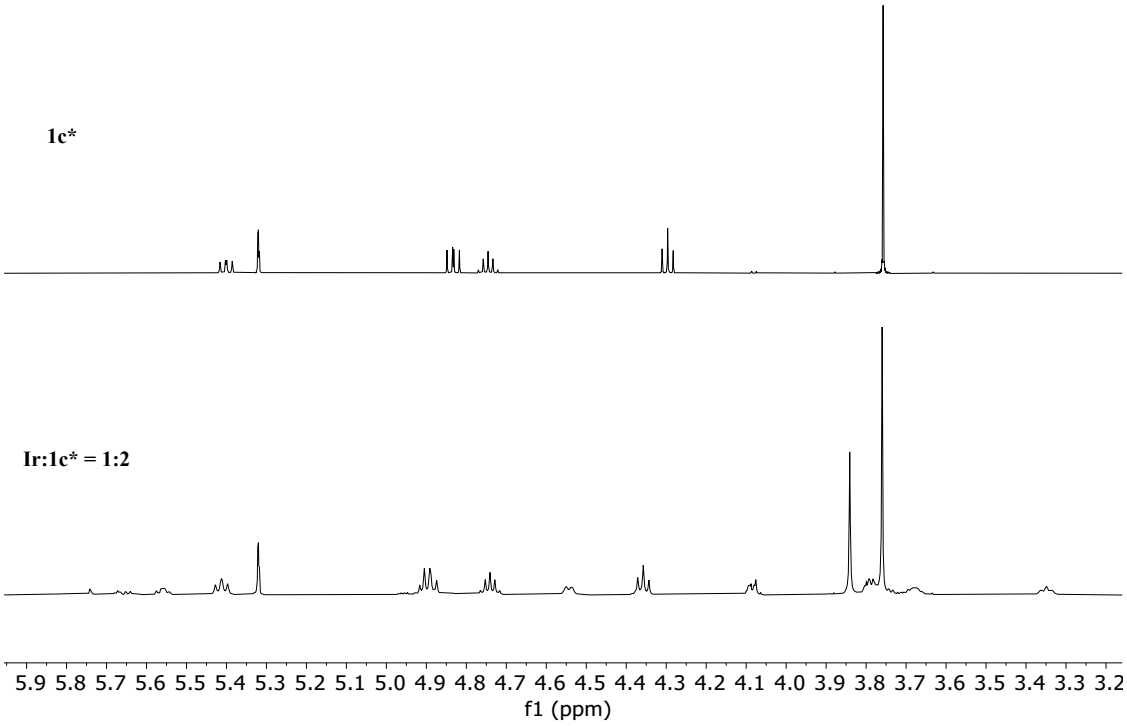

b) Increased peak intensity

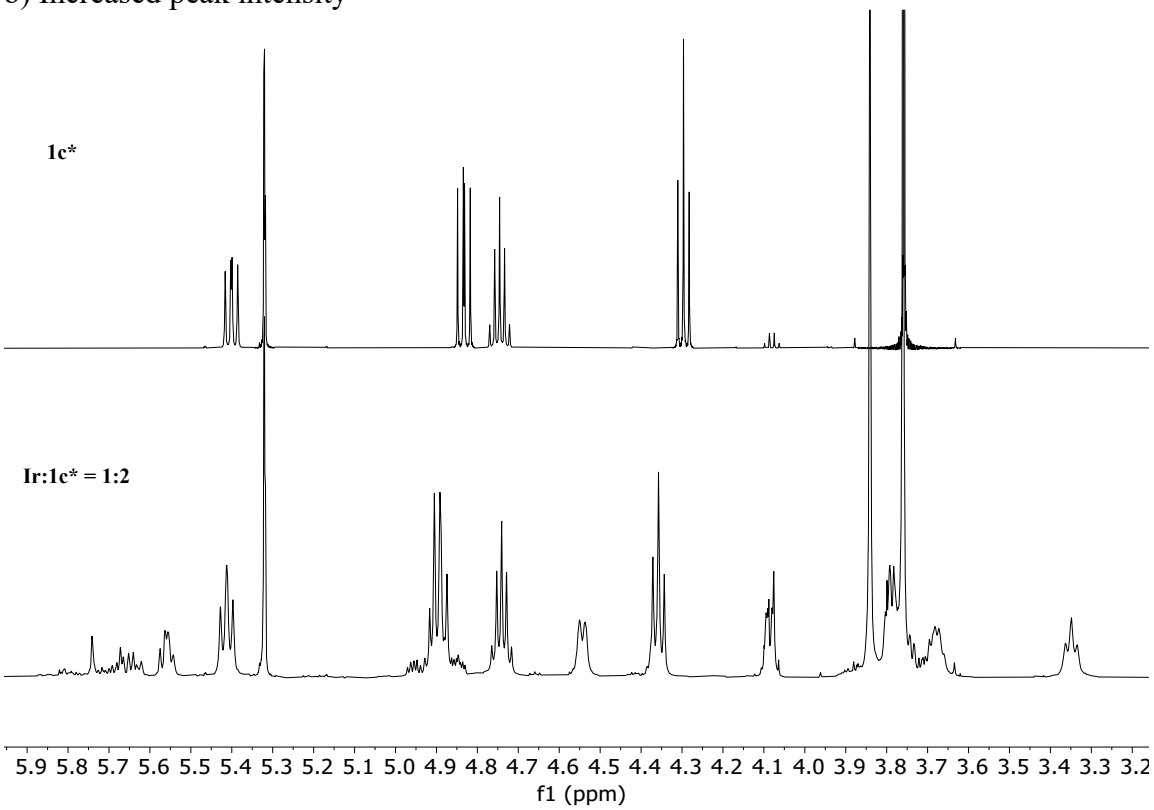

Aliphatic group area

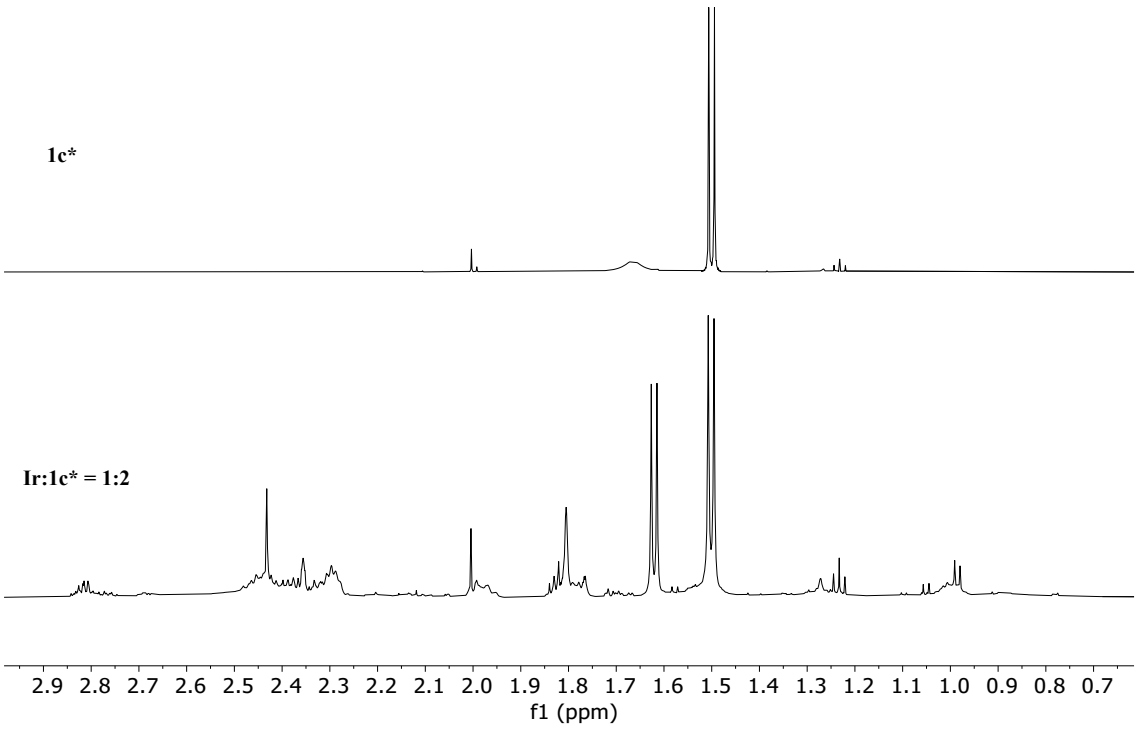

3.4.18. Ir:1c*, ^{13}C NMR in CD_2Cl_2

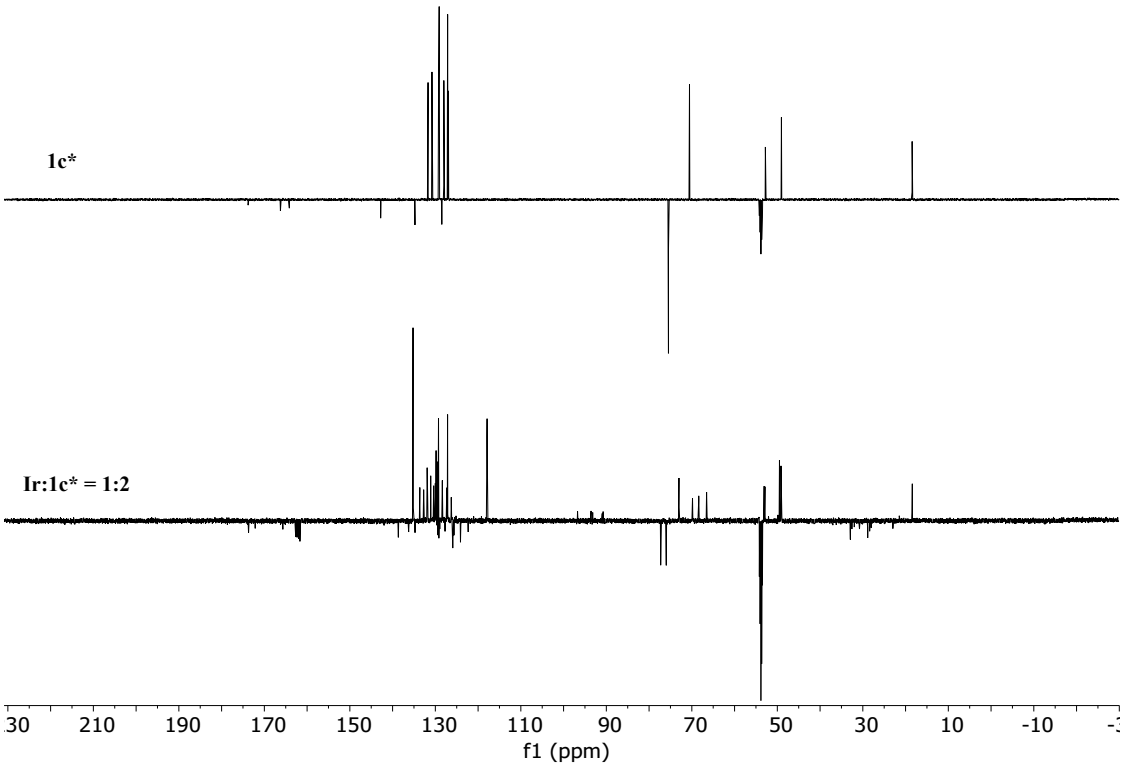

Amide/ester group area

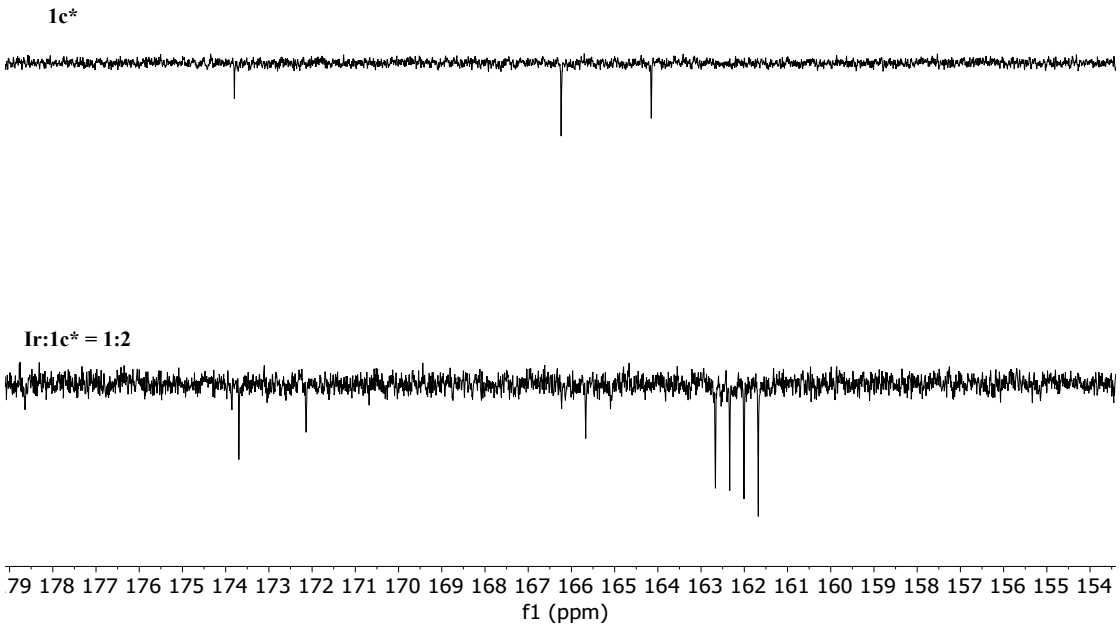

Aromatic group area

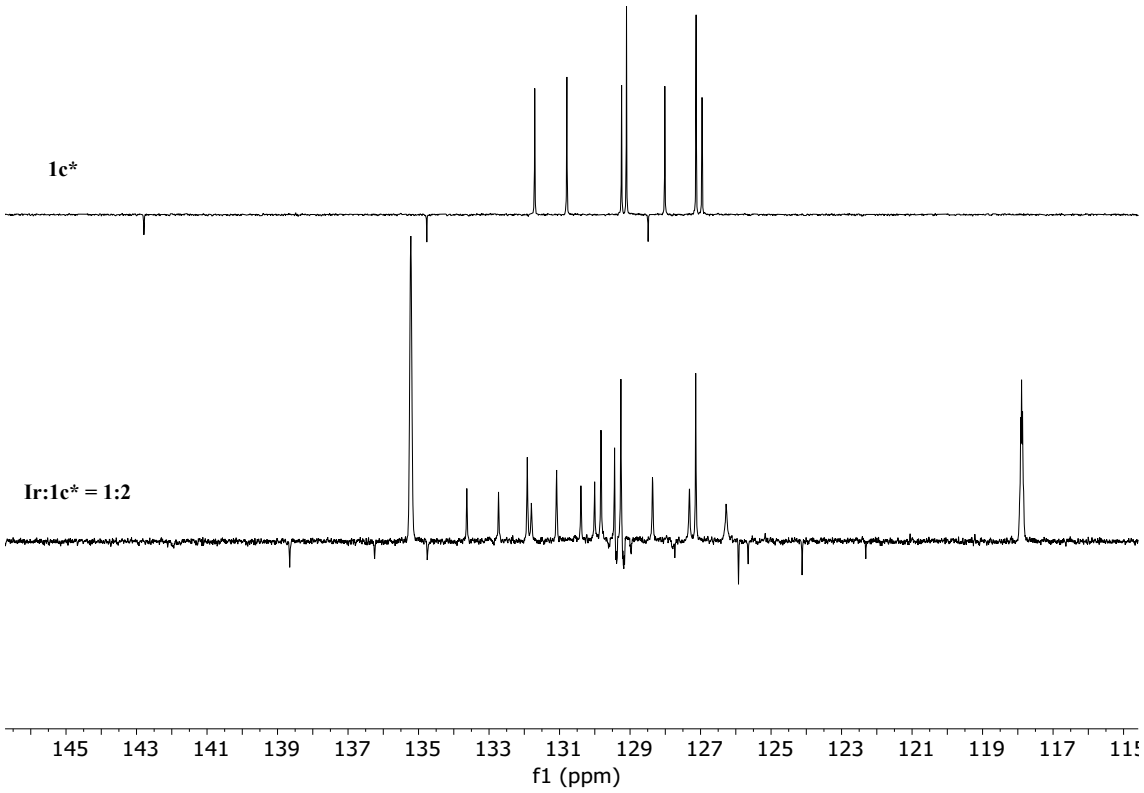

110ppm-80ppm

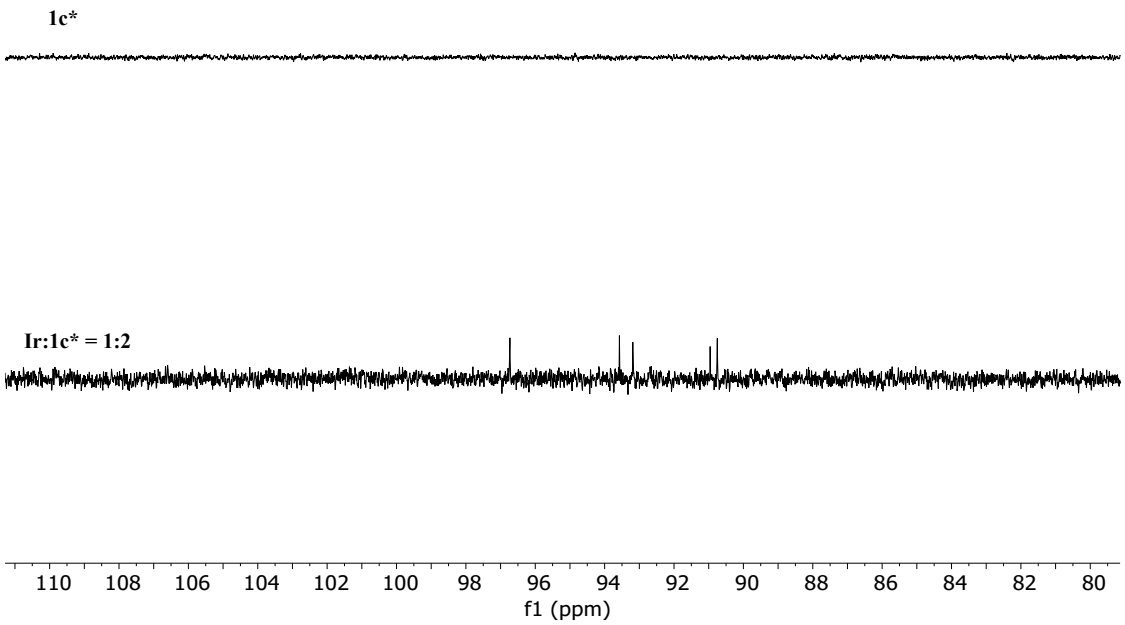

Functional group area

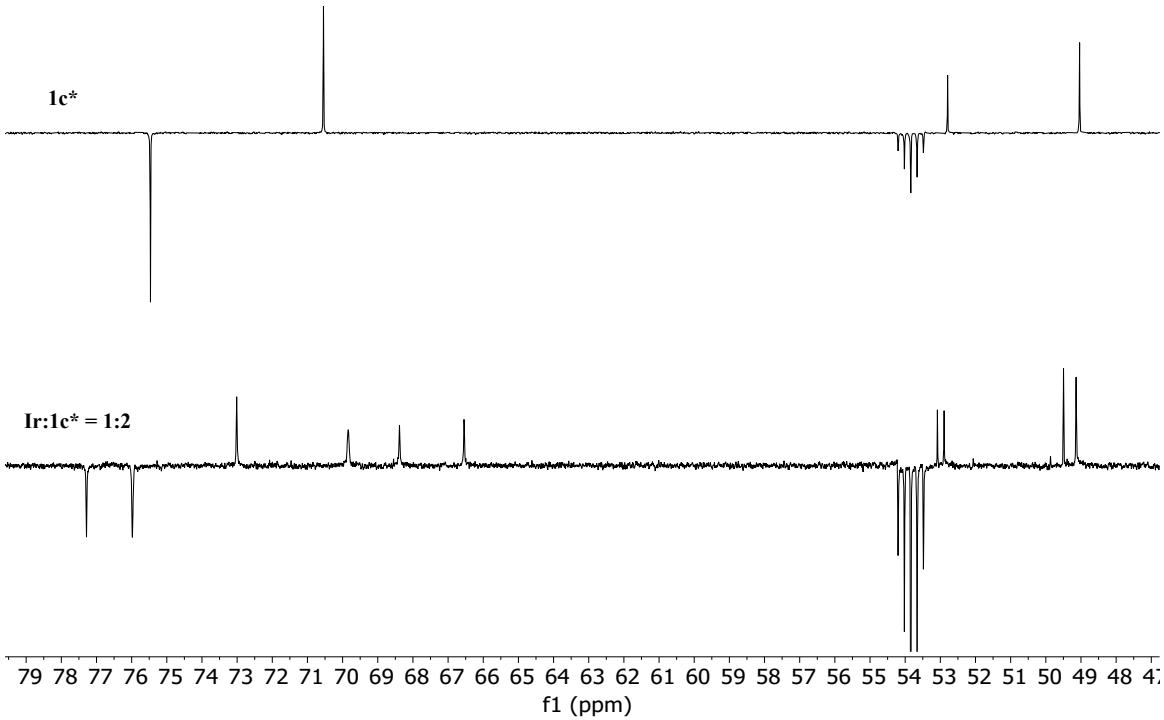

Aliphatic group area

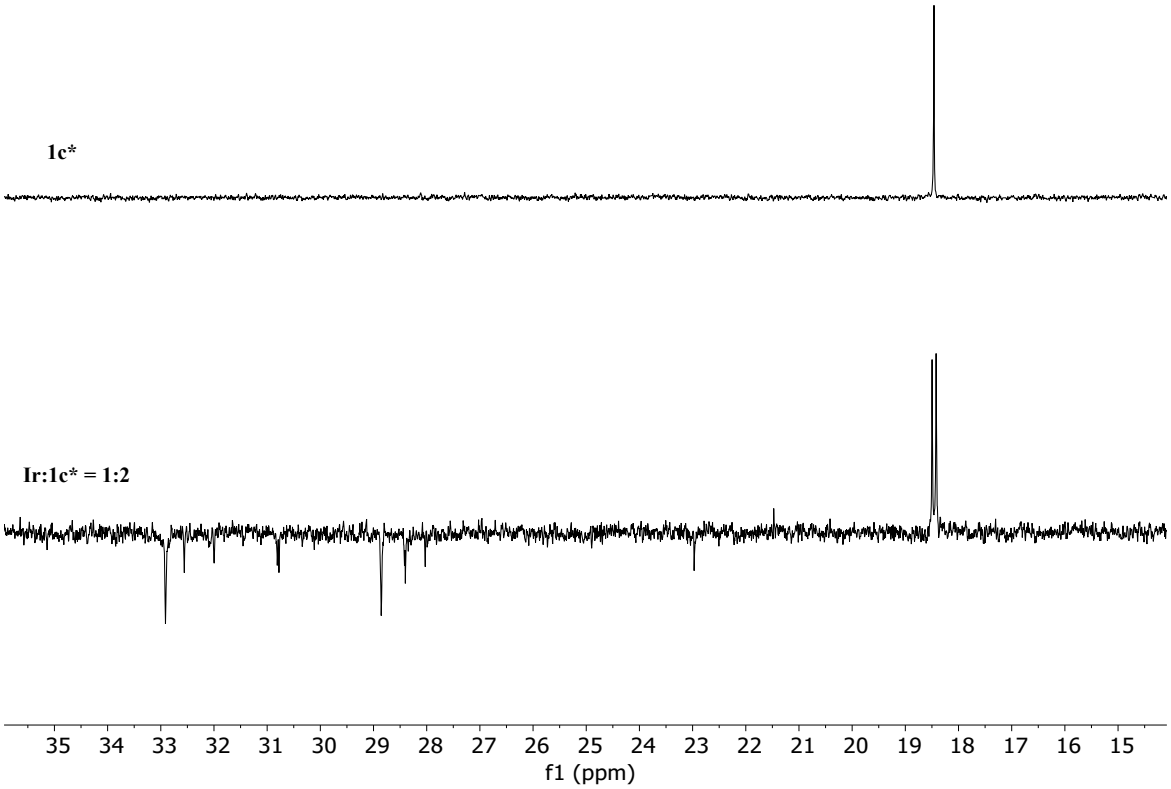

3.4.19. Ir:1p:1c*, ^{1}H NMR in CD_2Cl_2

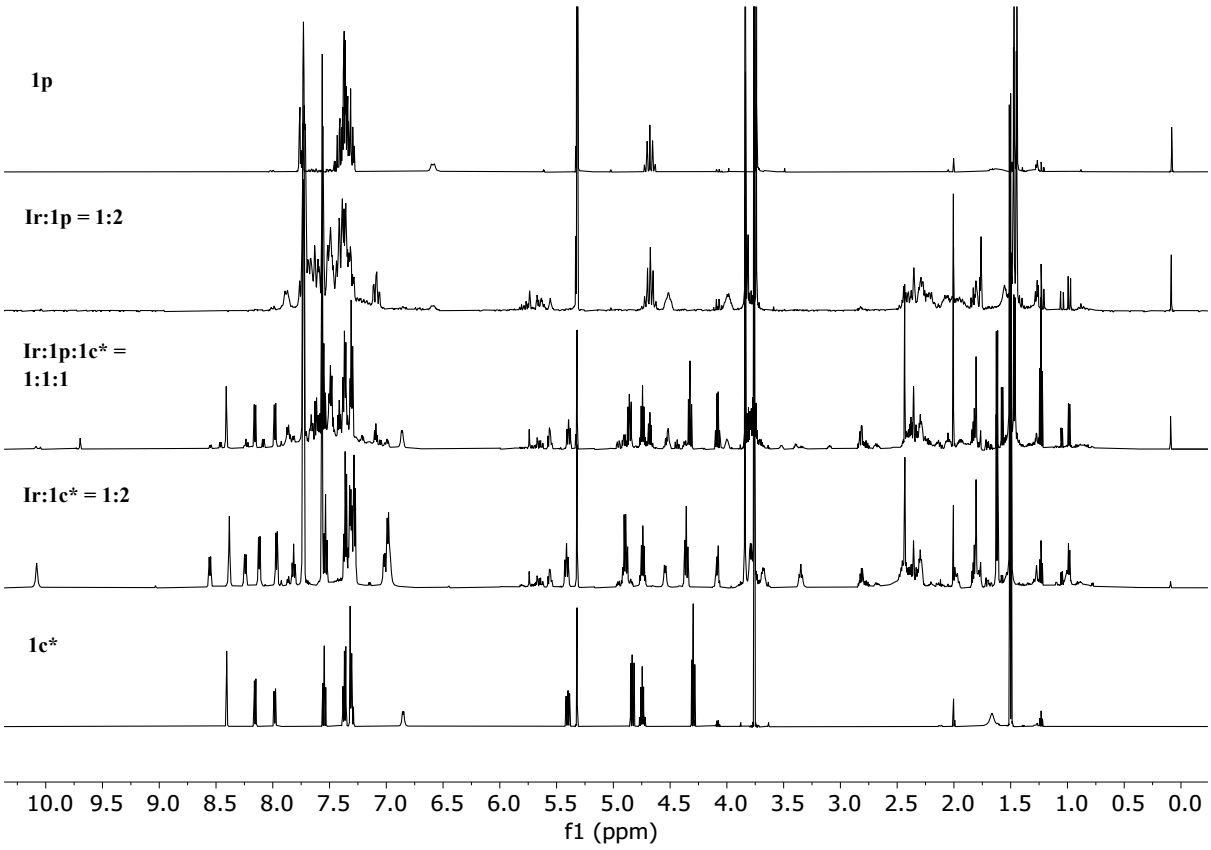

Aromatic group area of Ir:**1c**, ^{1}H NMR in CD_2Cl_2

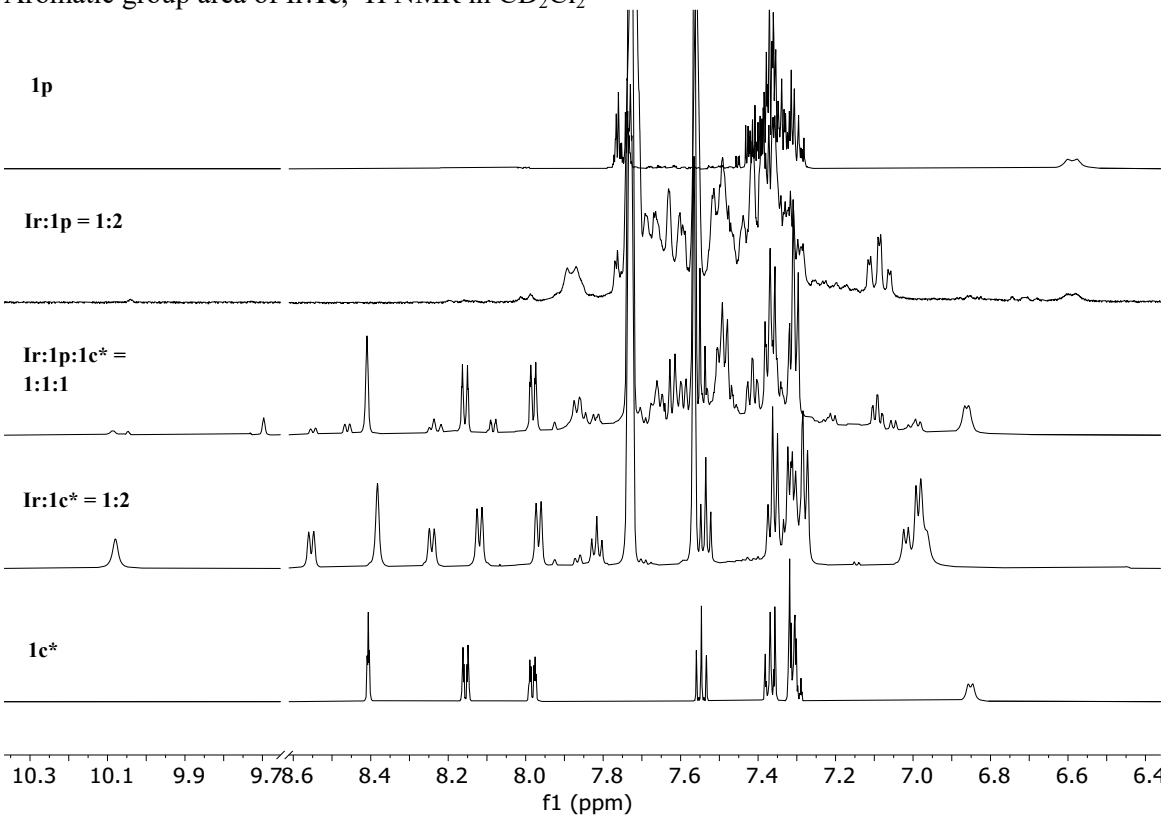

Functional group area

a) Lowered peak intensity

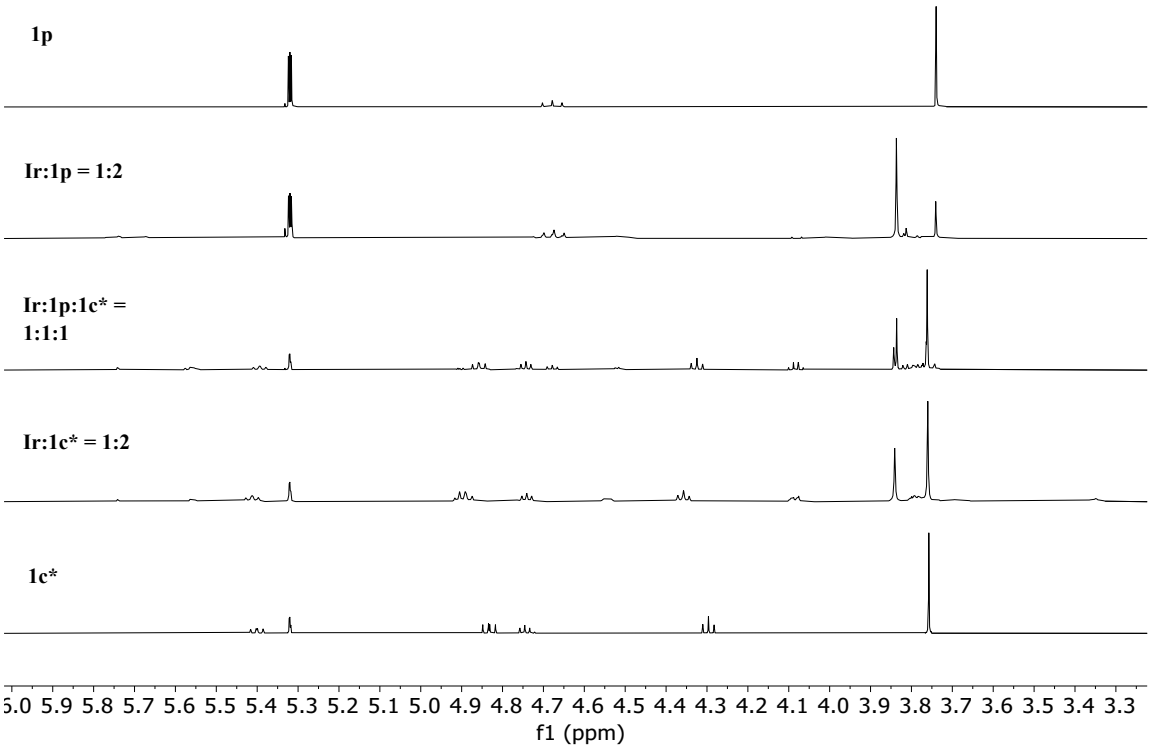

b) Increased peak intensity

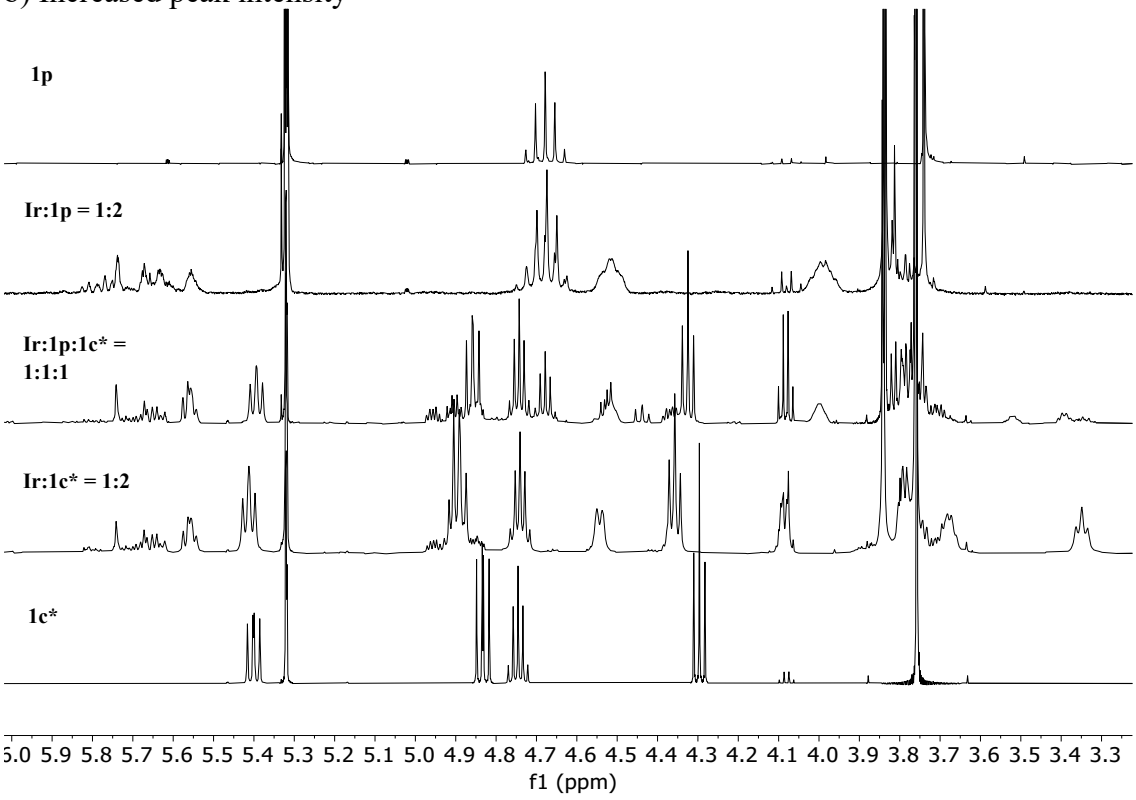

Aliphatic group area

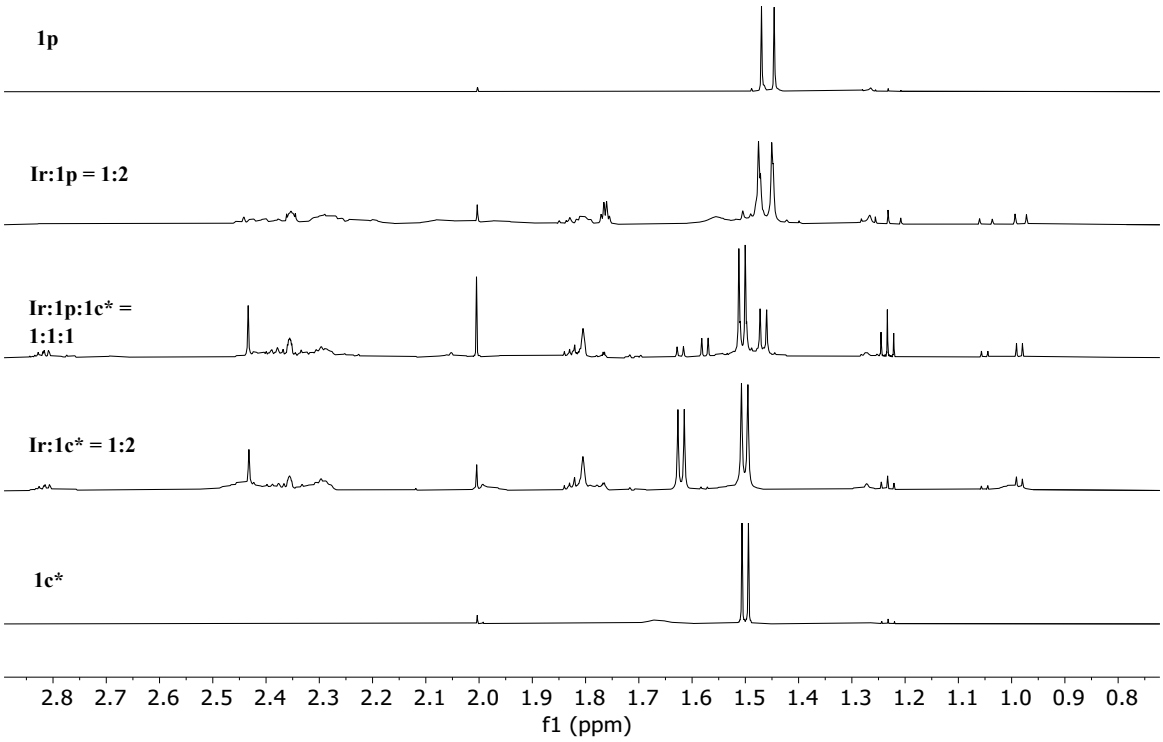

3.4.20. Ir:1p:1c*, ^{31}P NMR in CD_2Cl_2

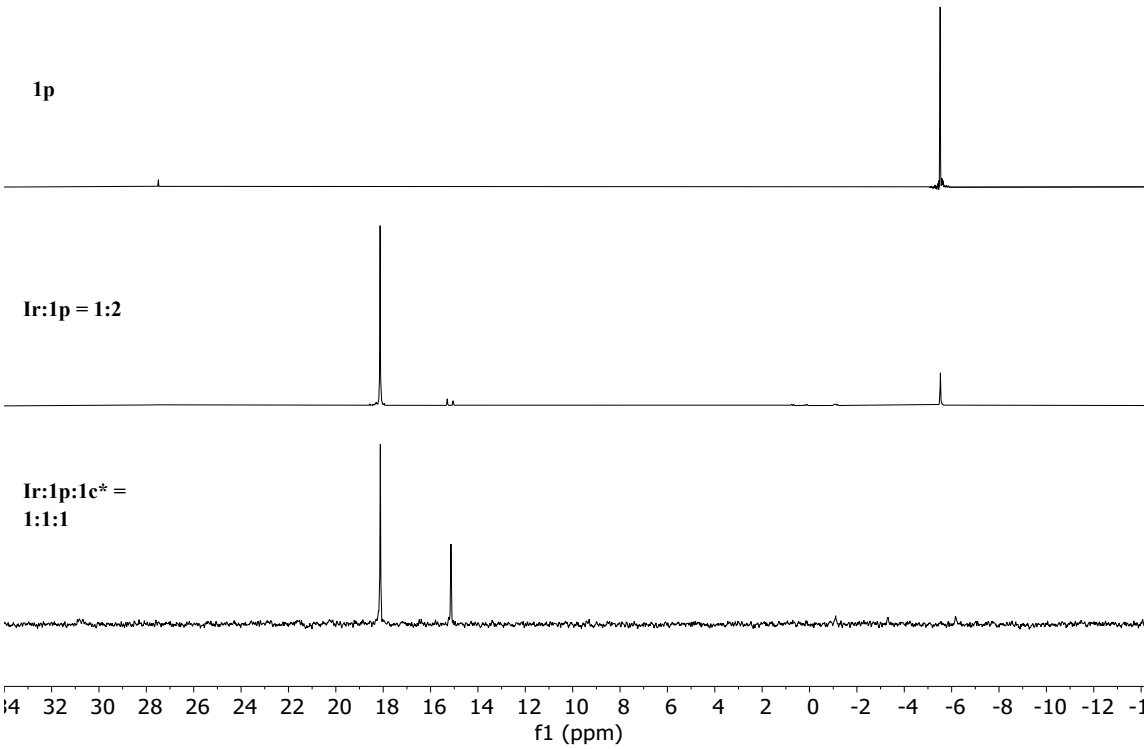

3.4.21. Ir:1p:1c*, ^{13}C NMR in CD_2Cl_2

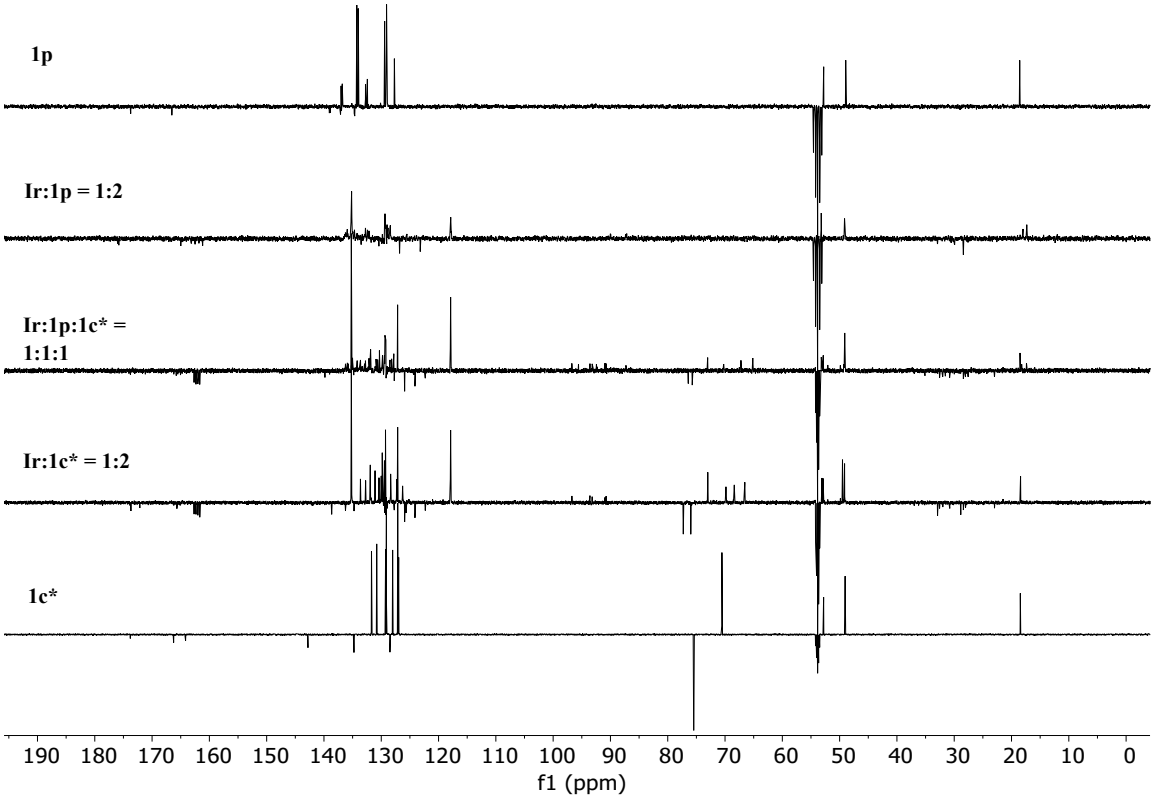

Amide/ester group area

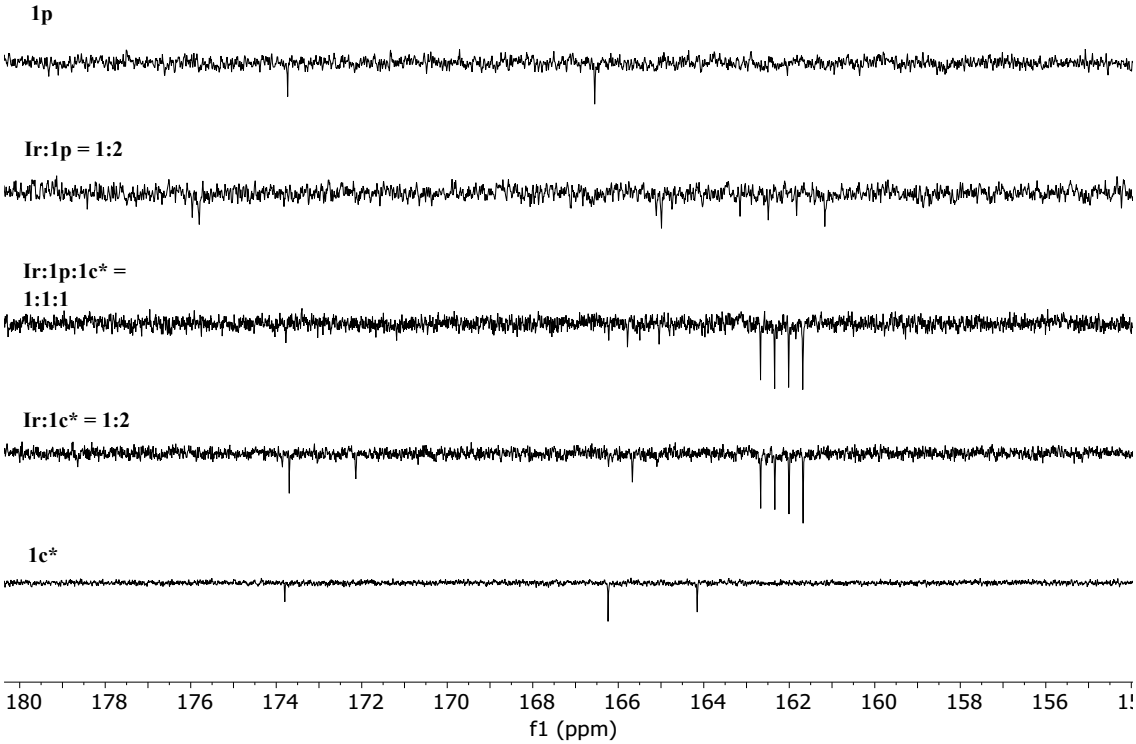

Aromatic group area

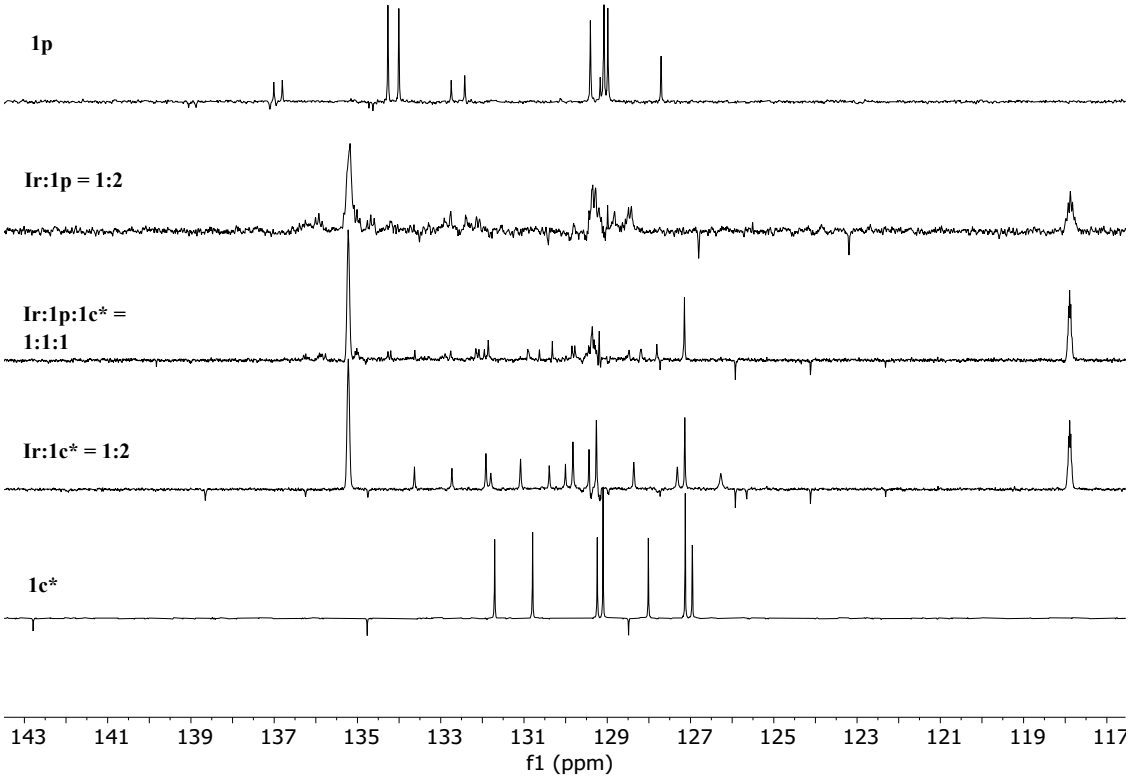

110ppm-80ppm

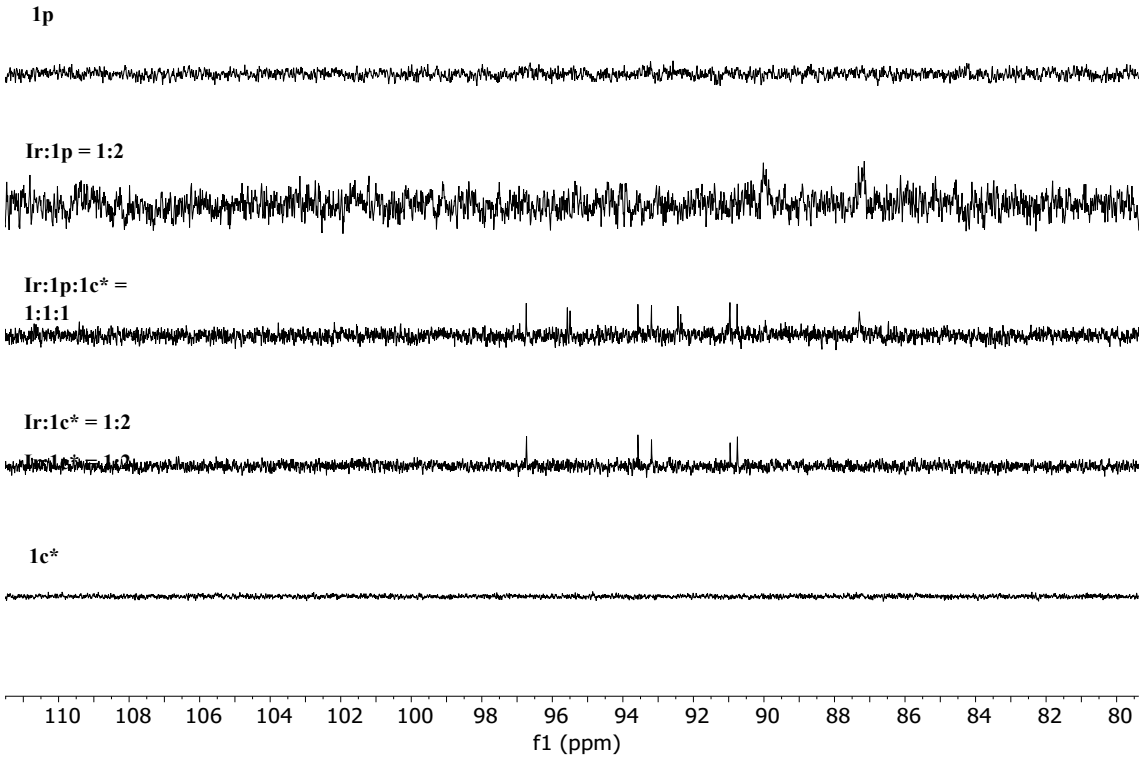

Functional group area

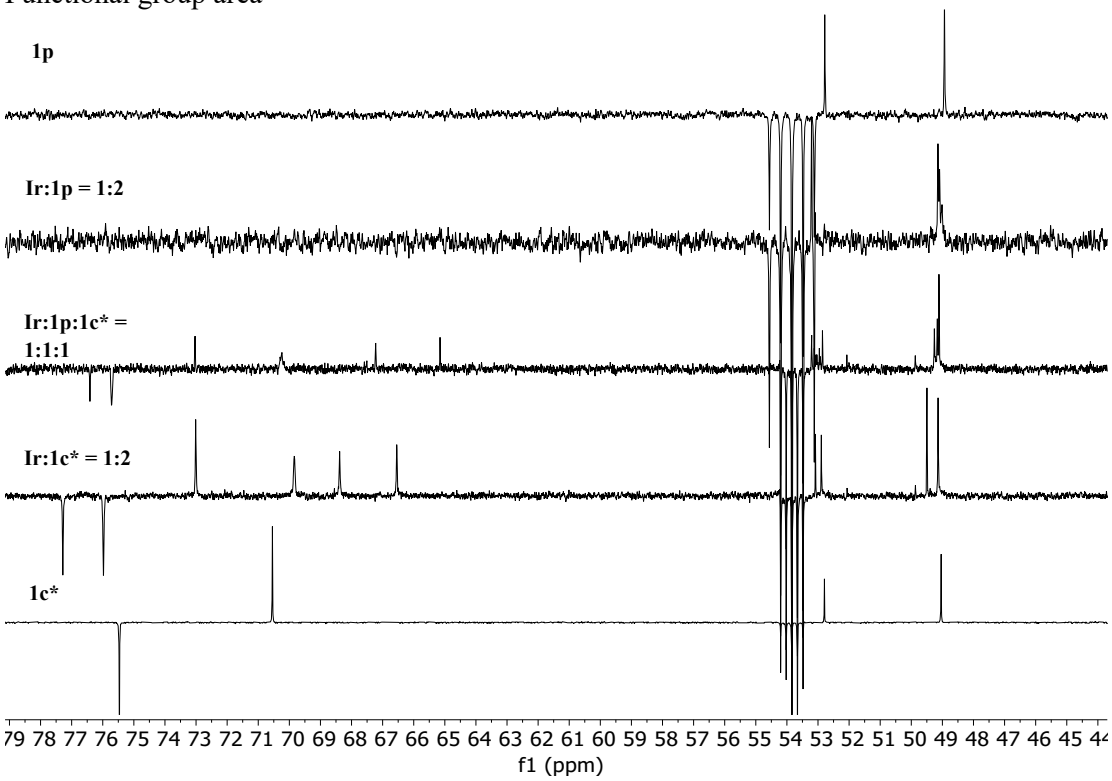

Aliphatic group area

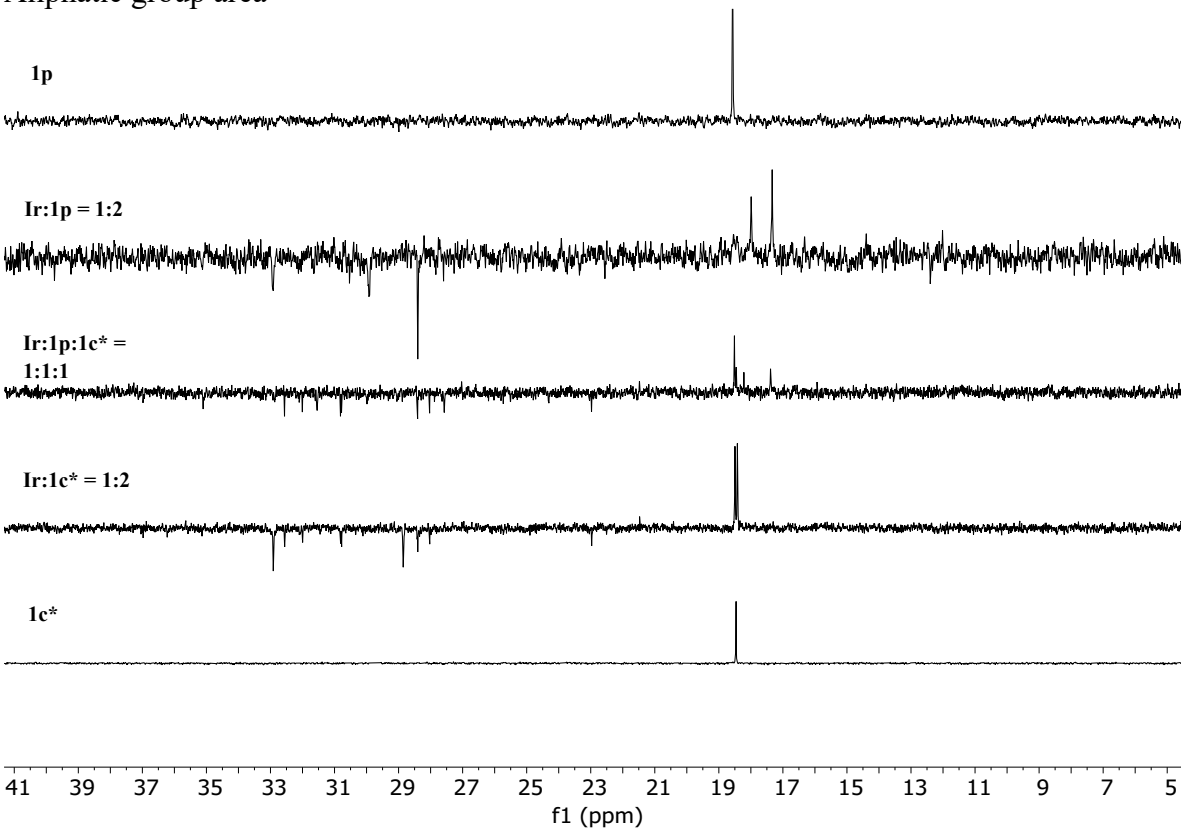

3.4.22. Rh:1p, ^{1}H NMR in CD_2Cl_2

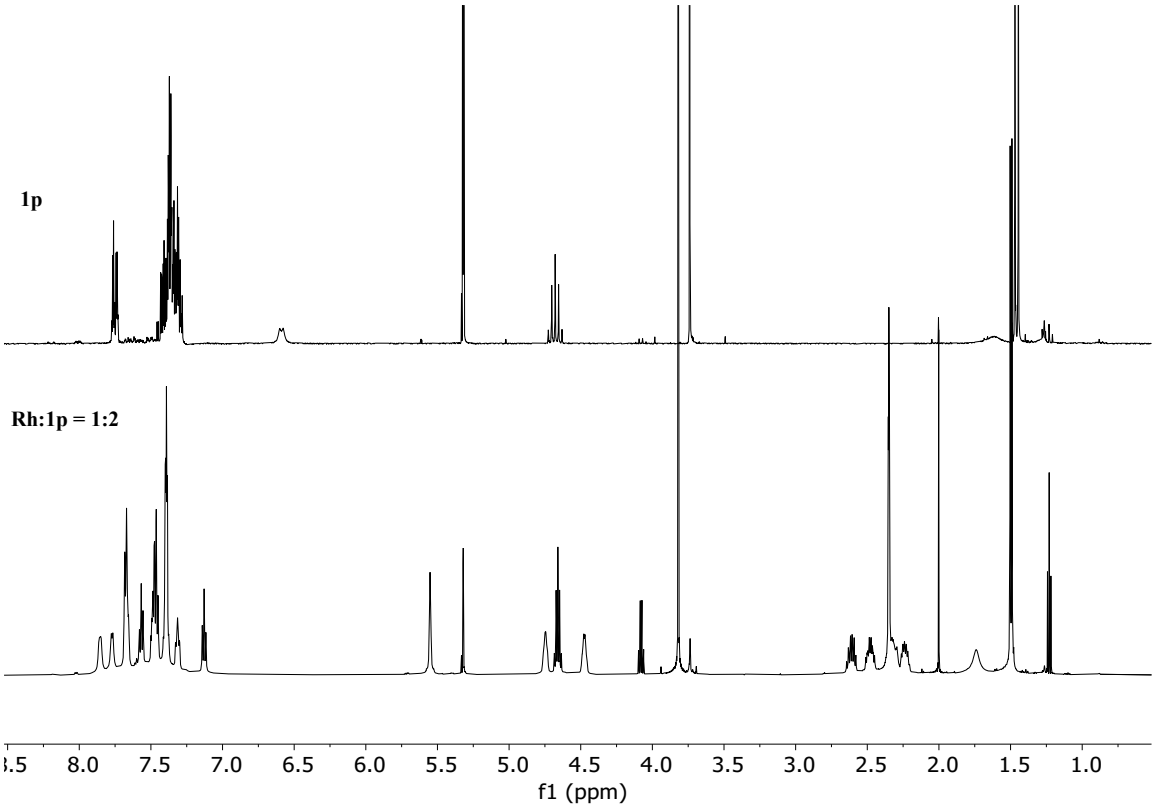

Aromatic group area of Rh:**1p**, ^{1}H NMR in CD_2Cl_2

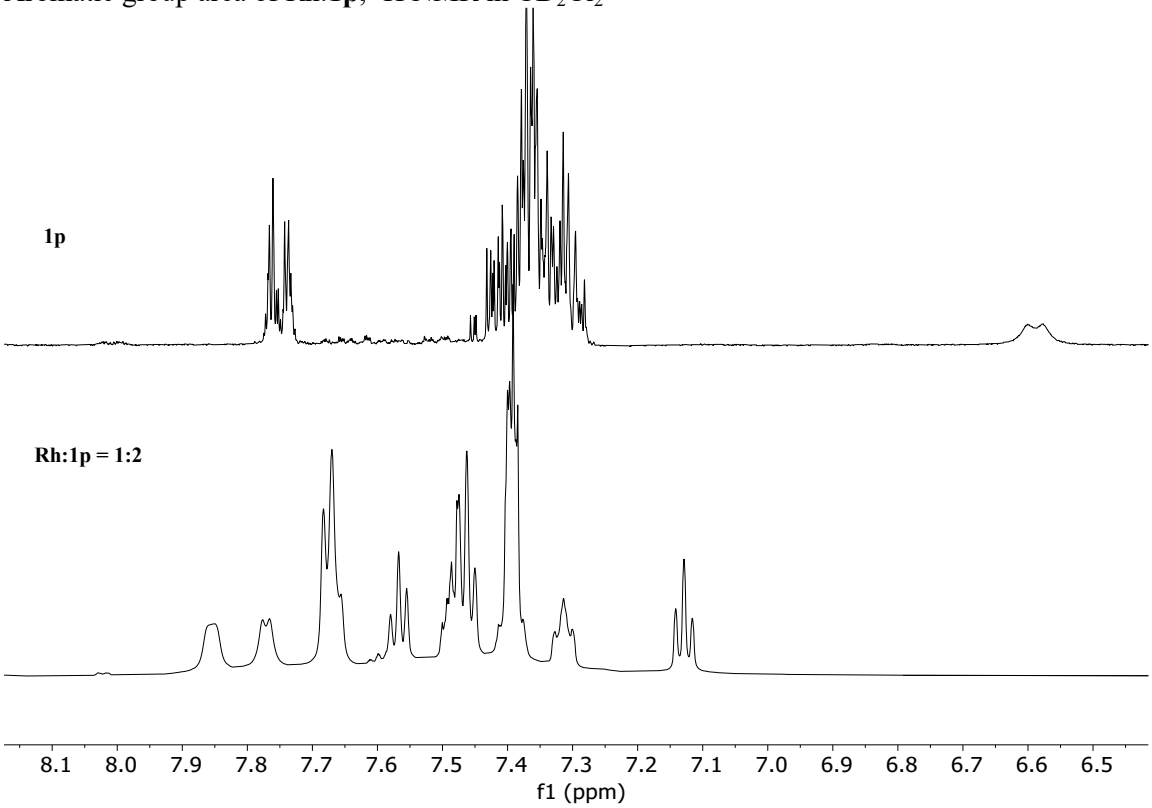

Functional group area

a) Lowered peak intensity

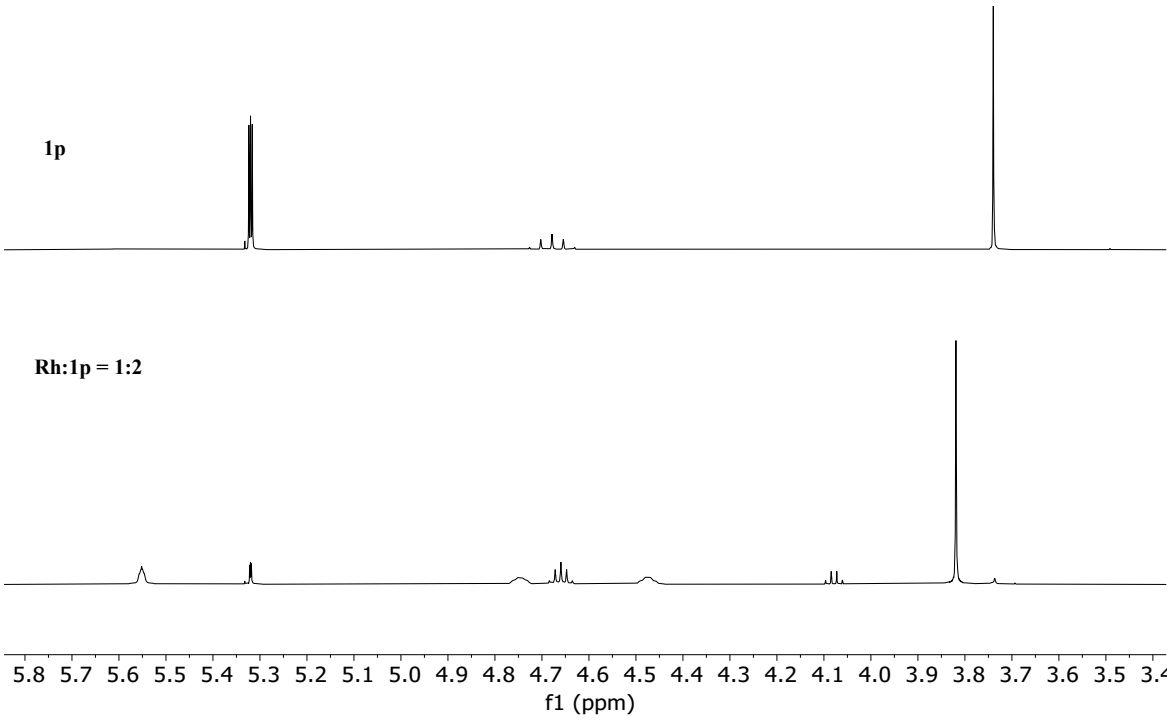

b) Increased peak intensity

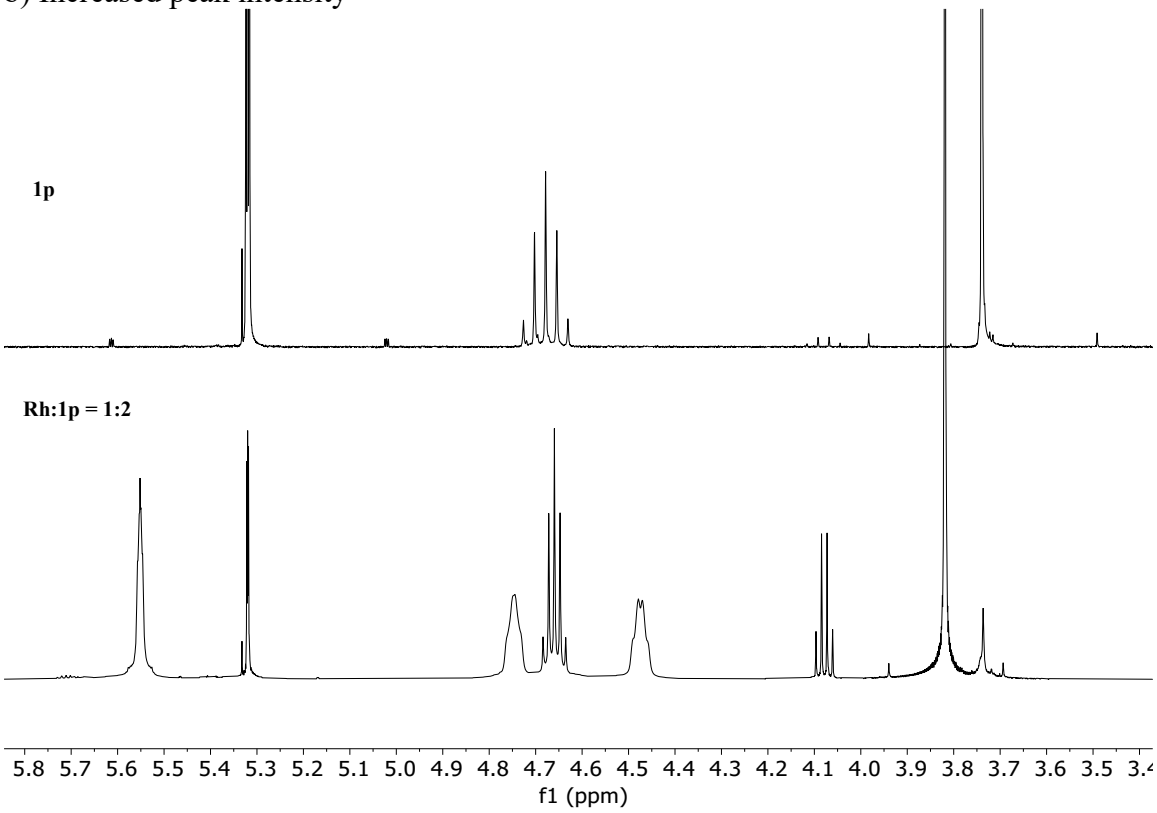

Aliphatic group area

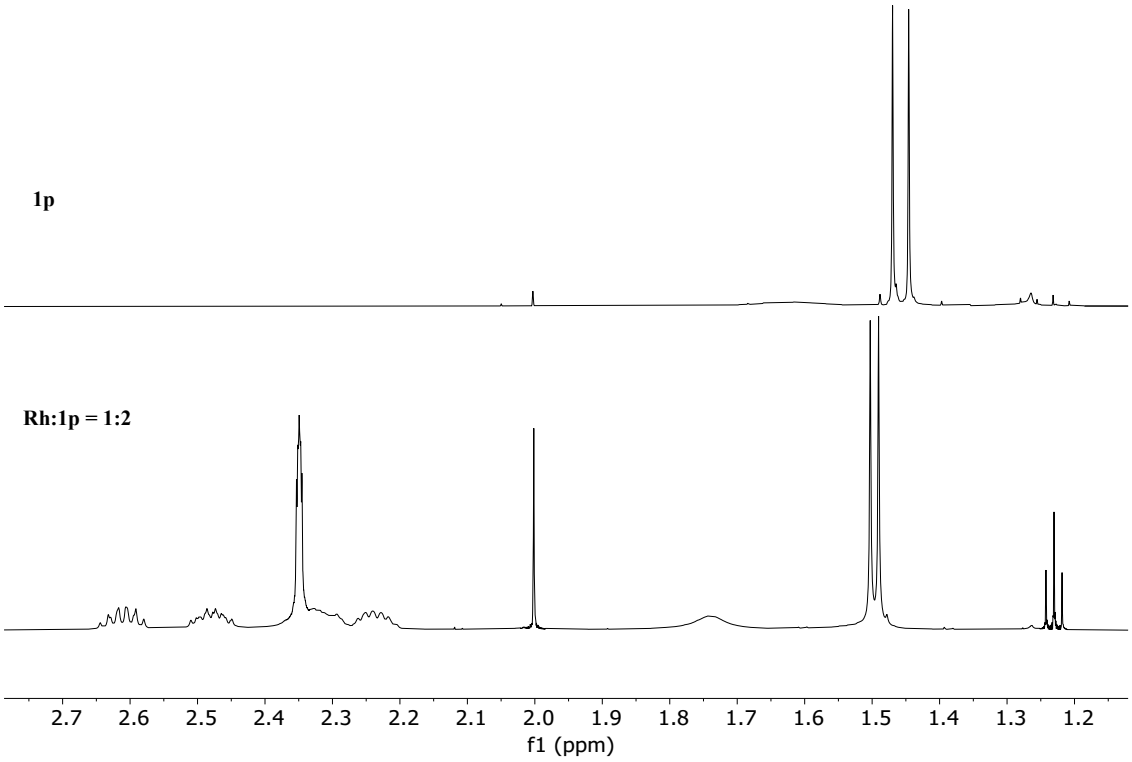

3.4.23. Rh:1p, ^{31}P NMR in CD_2Cl_2

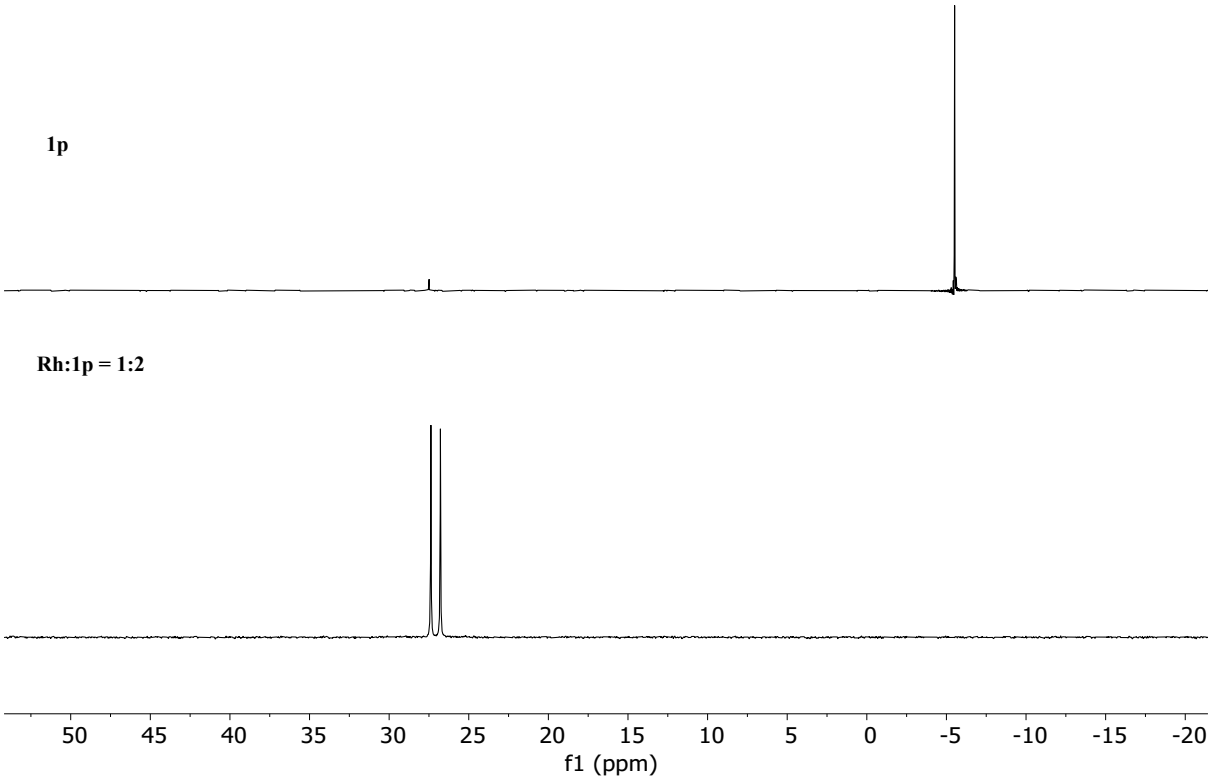

3.4.24. Rh:1p, ^{13}C NMR in CD_2Cl_2

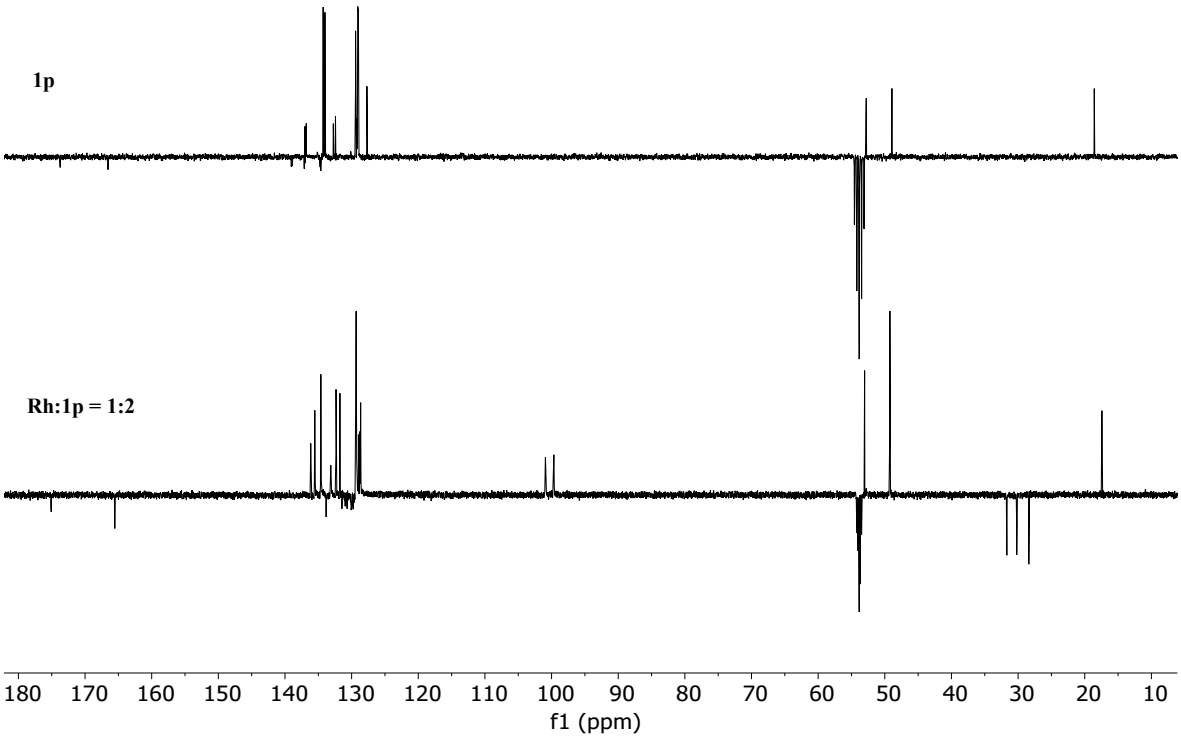

Amide/ester group area

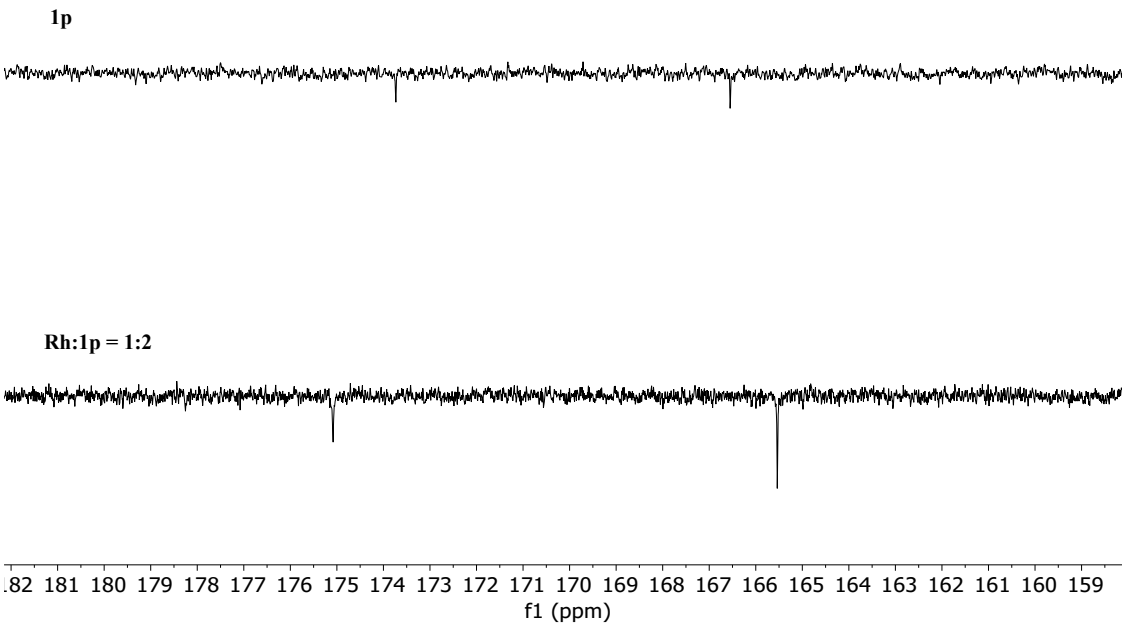

Aromatic group area

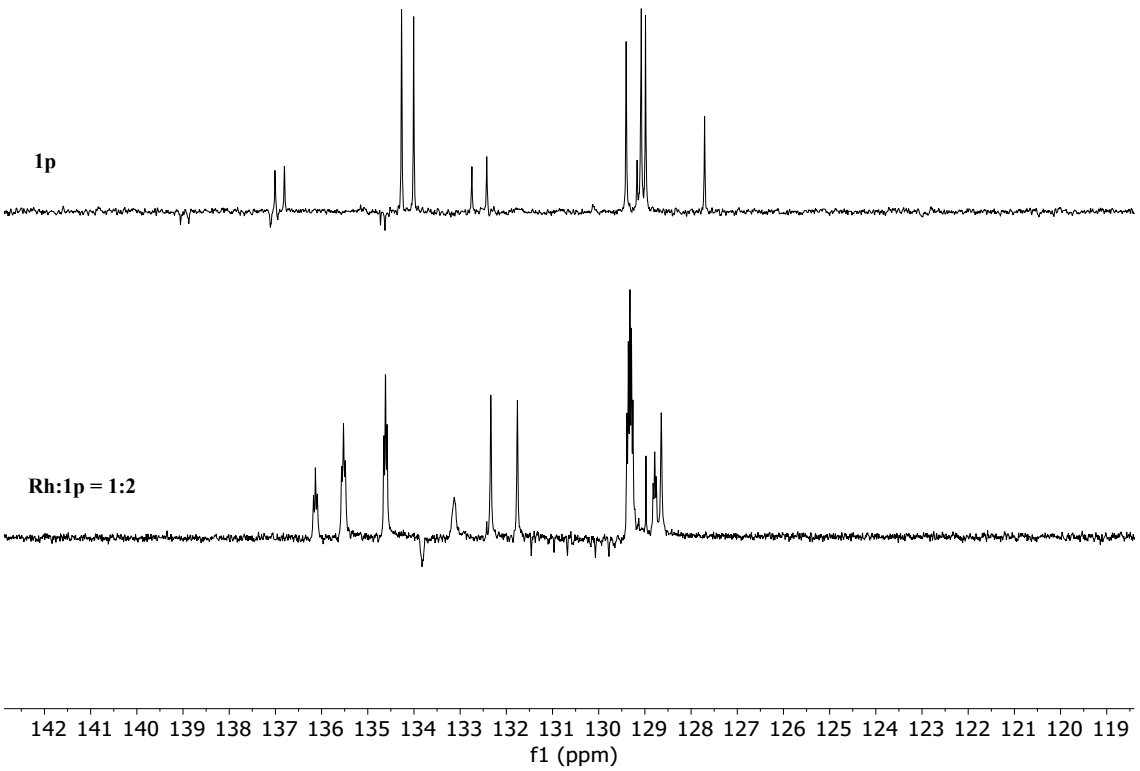

110ppm-80ppm

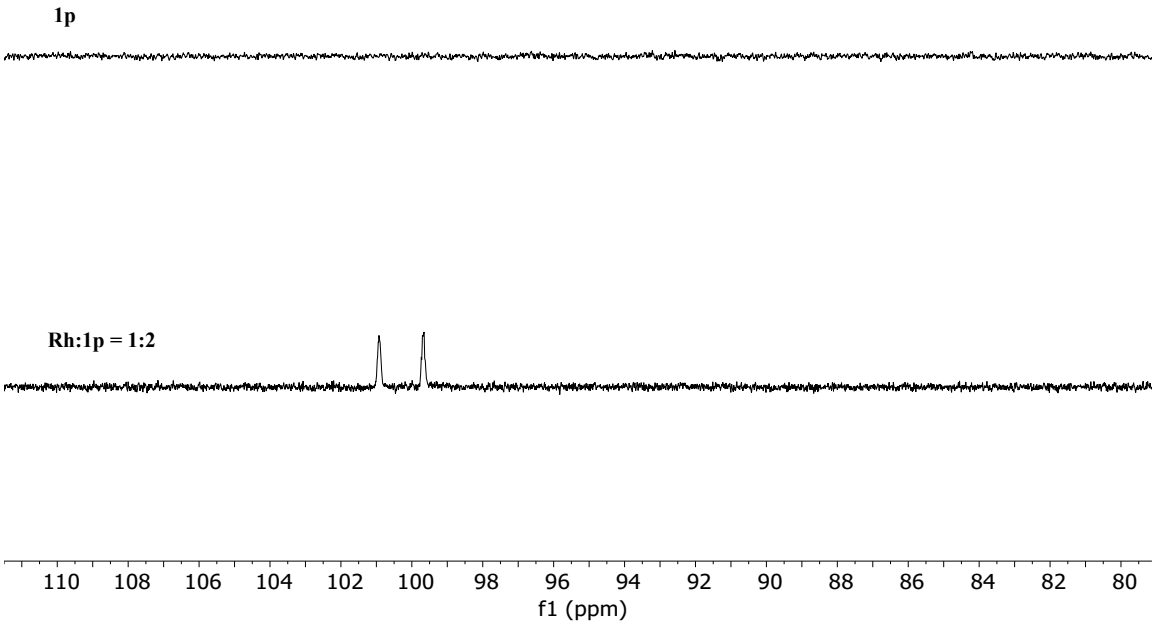

Functional group area

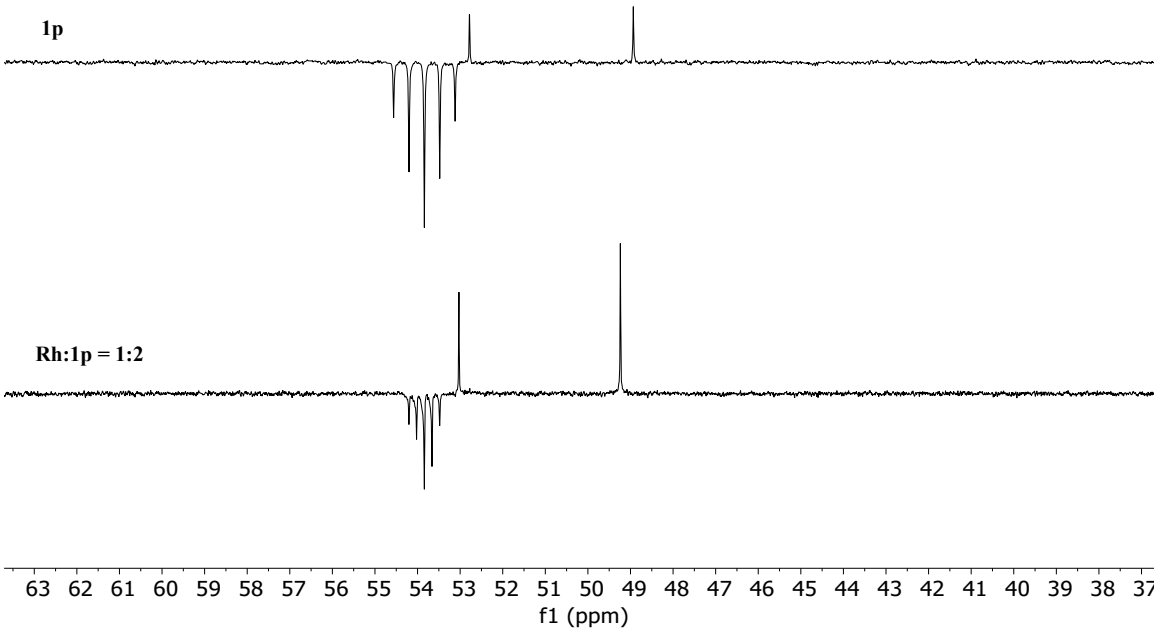

Aliphatic group area

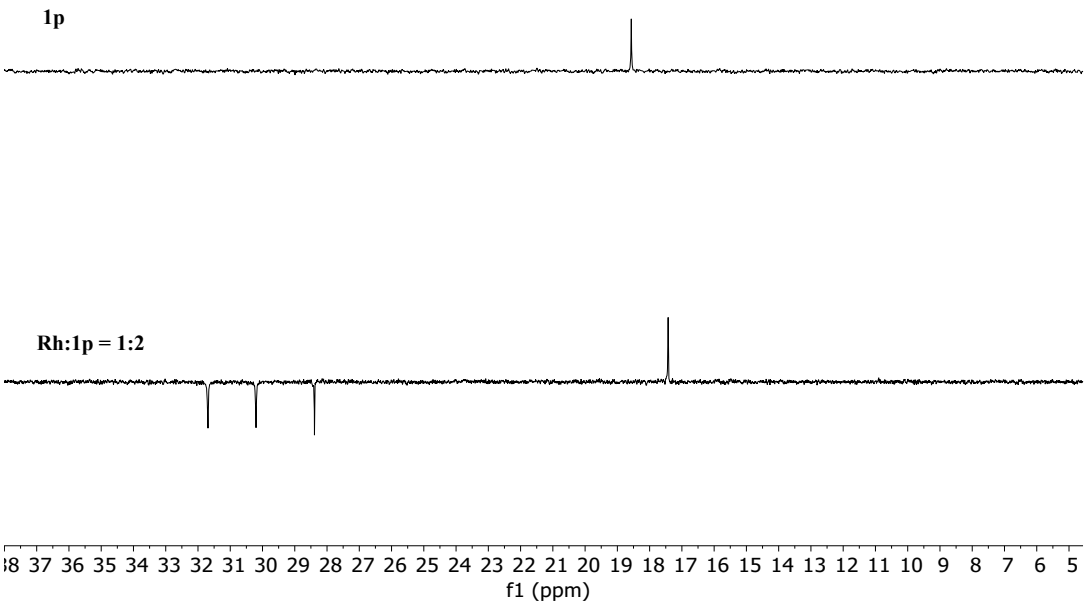

3.4.25. Rh:1c*, ^{1}H NMR in CD_2Cl_2

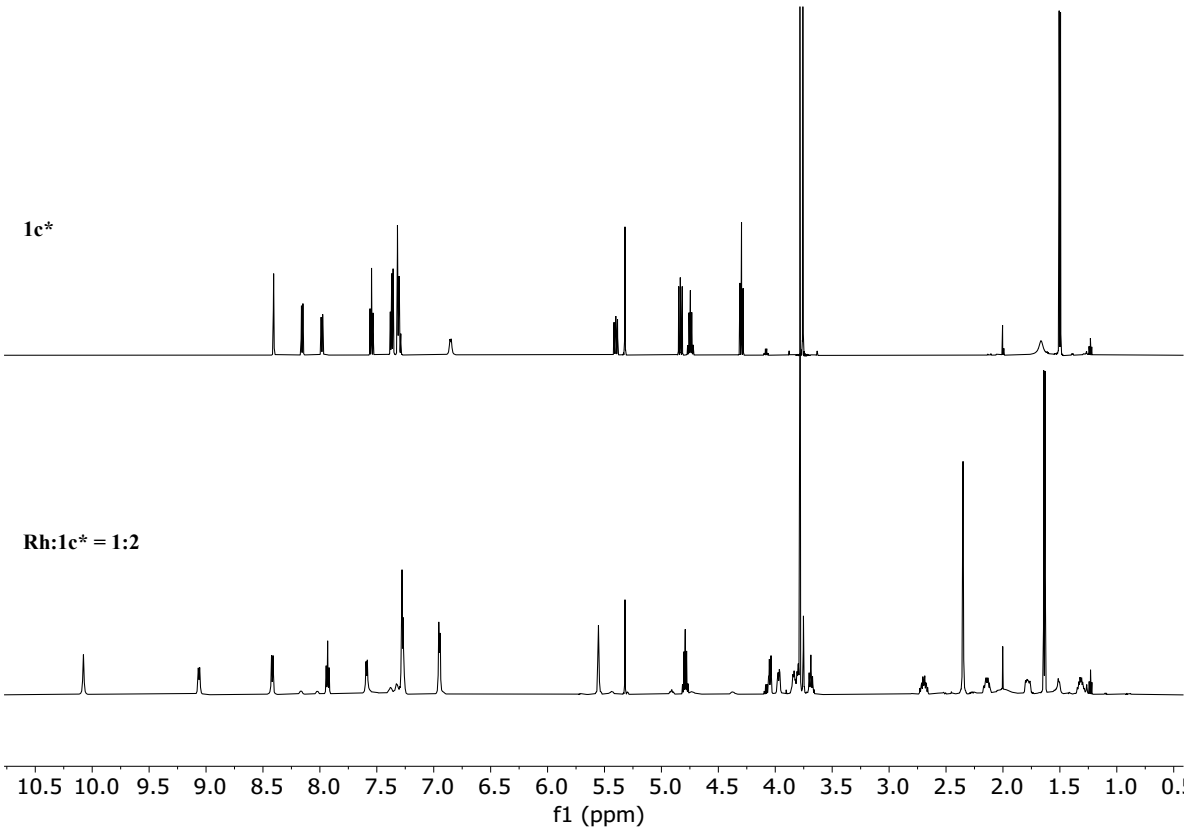

Aromatic group area of Rh:**1p**, ^{1}H NMR in CD_2Cl_2

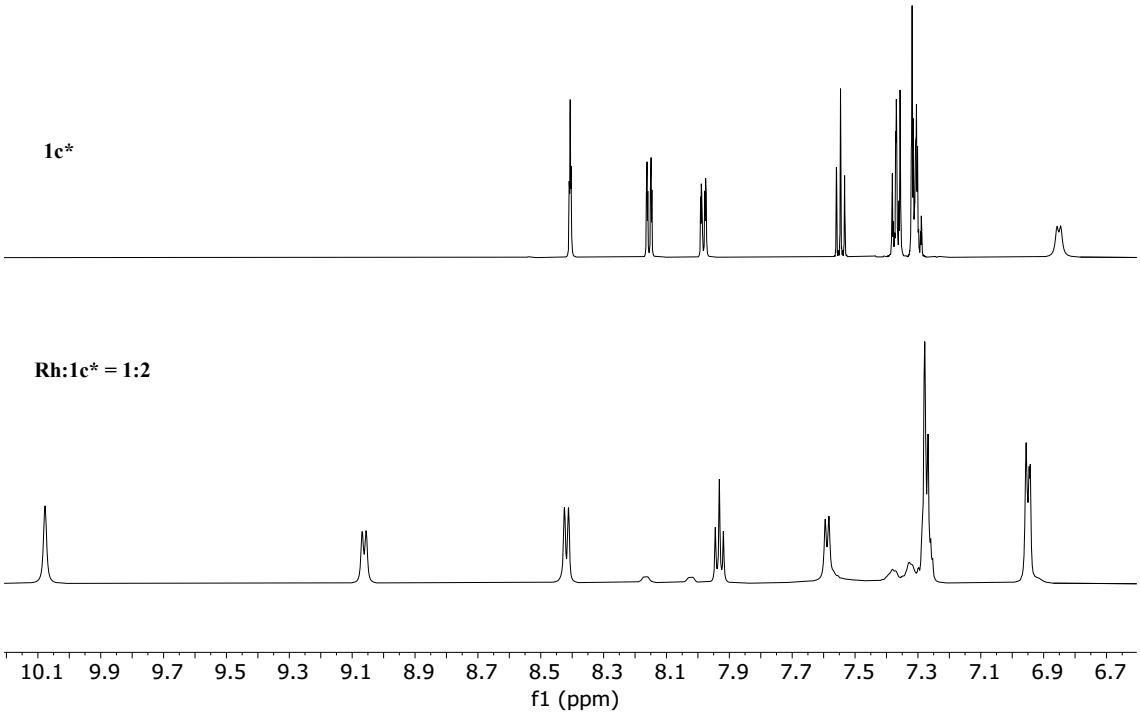

Functional group area
a) Lowered peak intensity

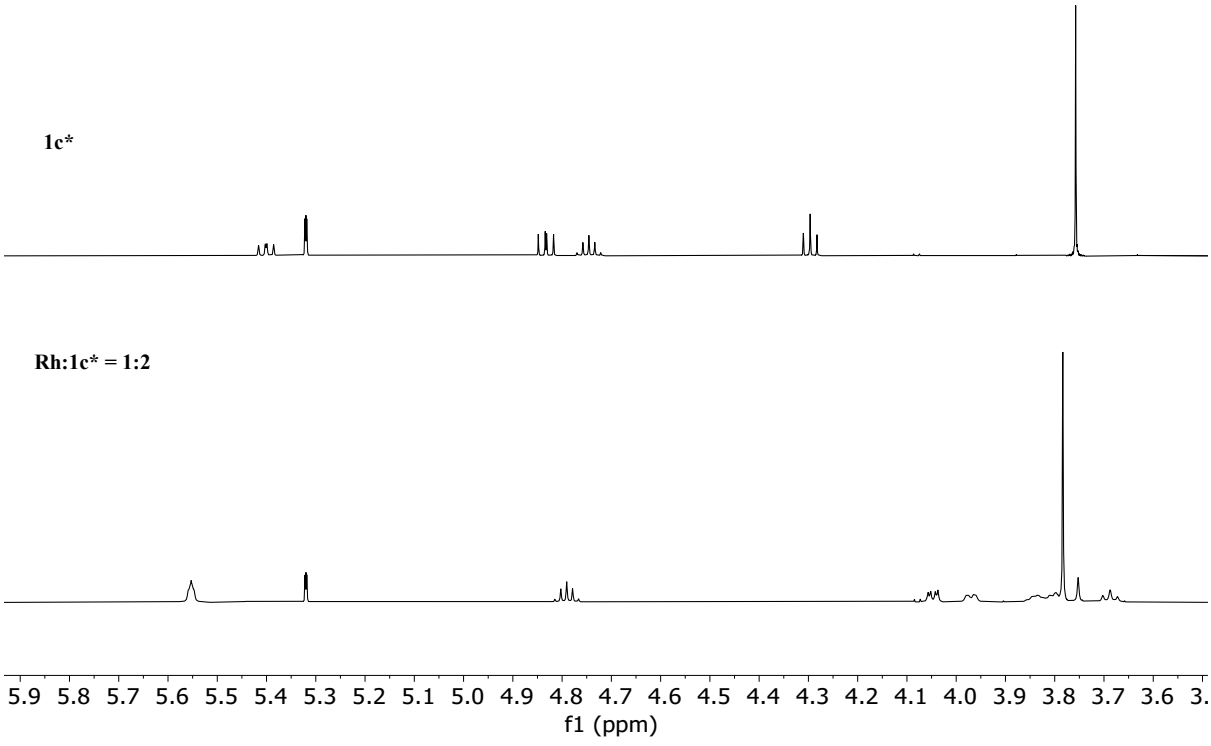

b) Increased peak intensity

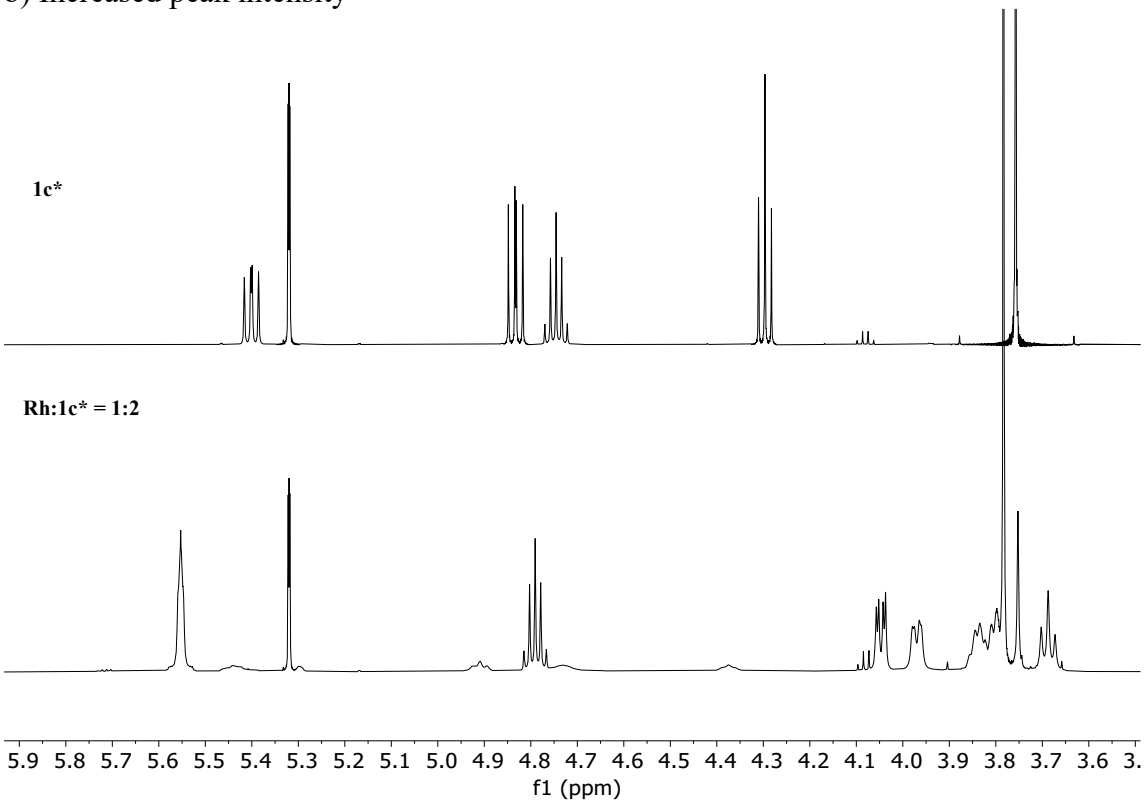

Aliphatic group area

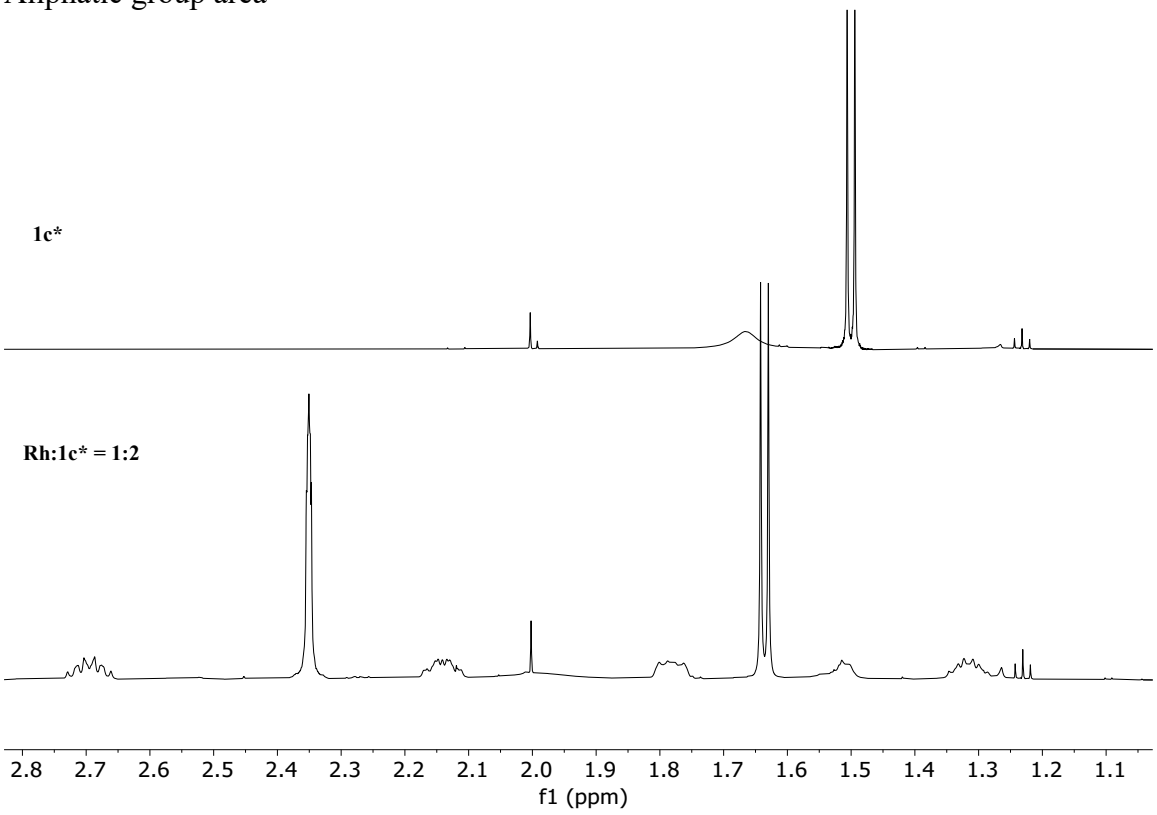

3.4.26. Rh:1c*, ^{13}C NMR in CD_2Cl_2

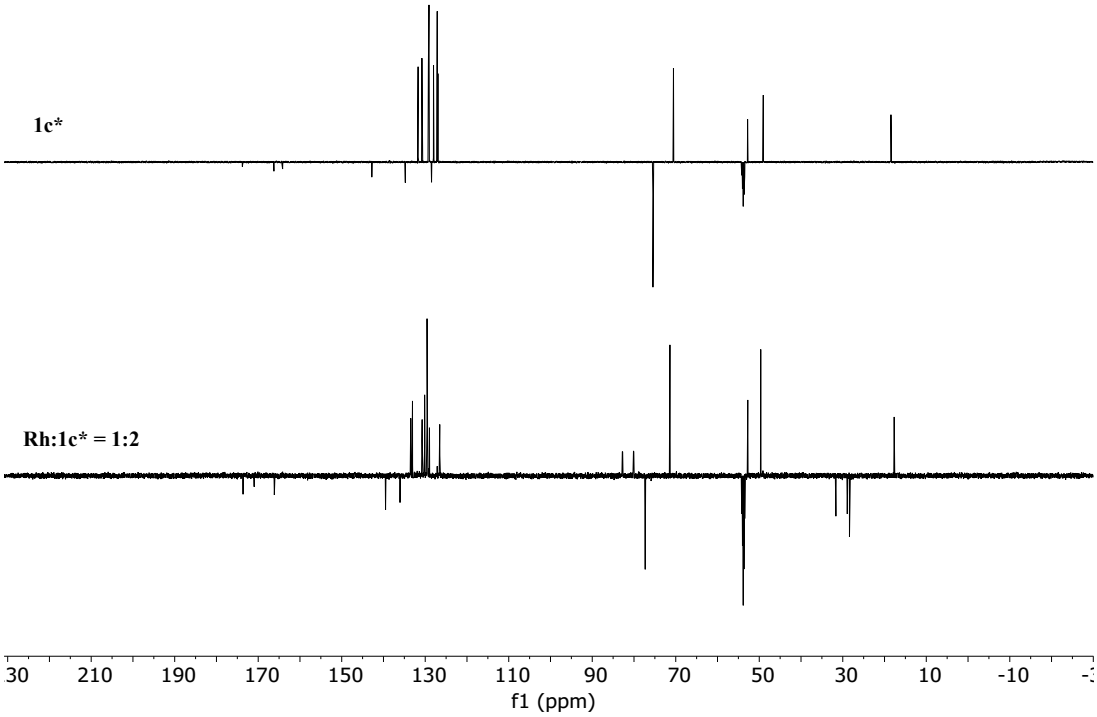

Amide/ester group area

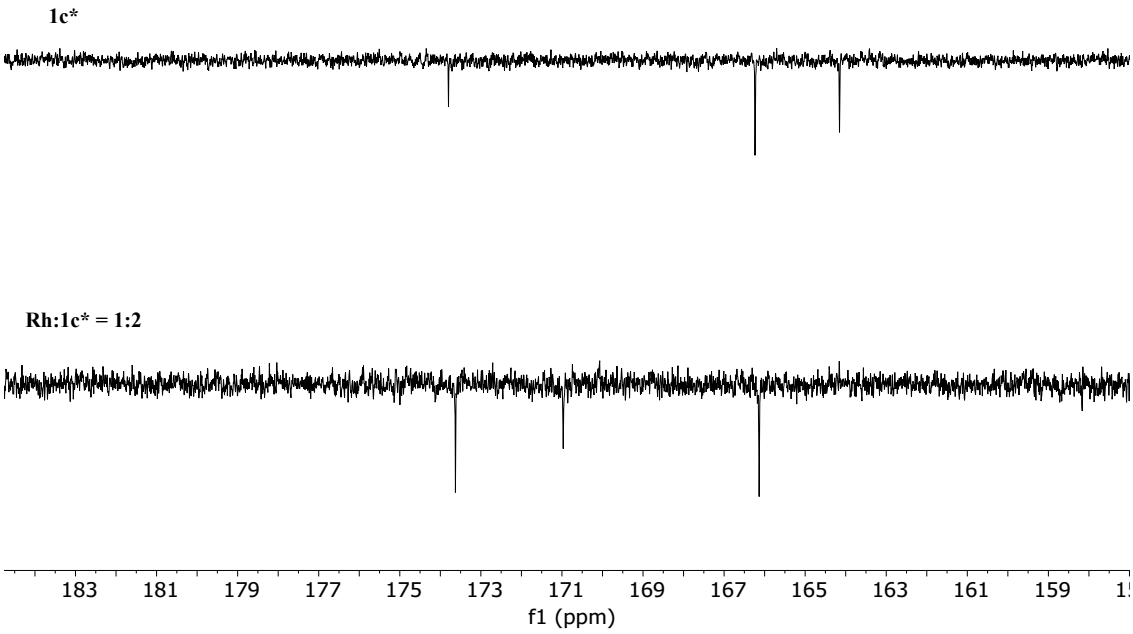

Aromatic group area

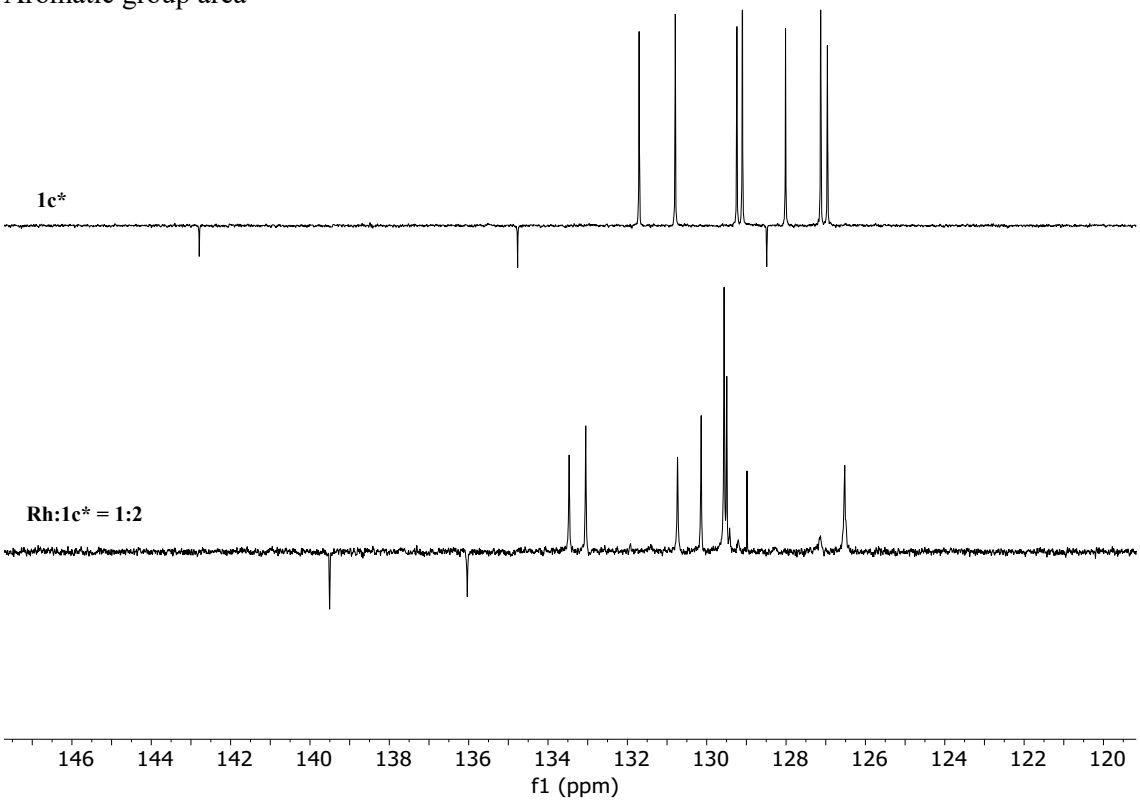

110ppm-80ppm

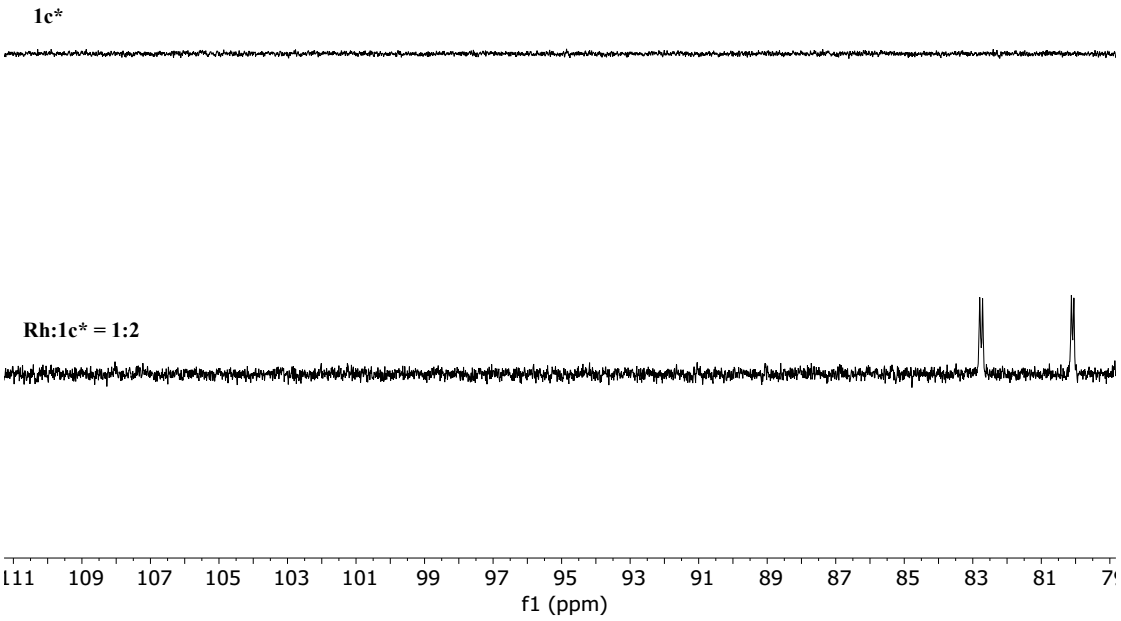

Functional group area

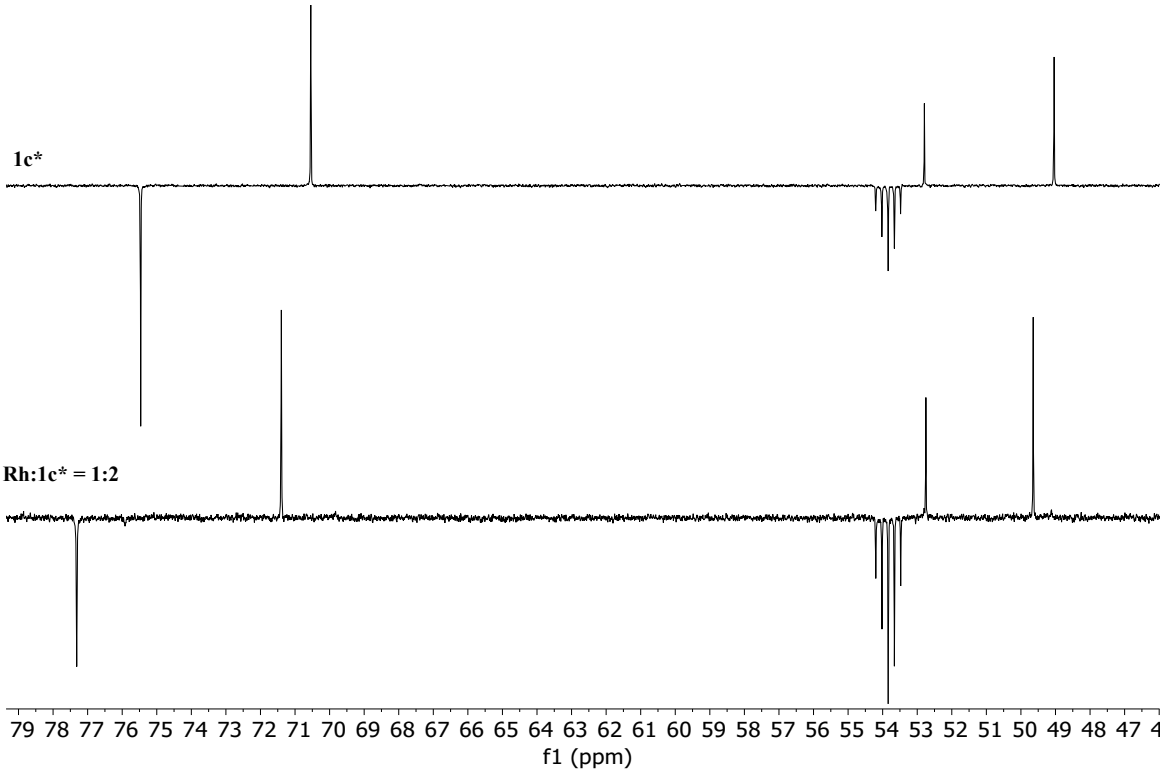

Aliphatic group area

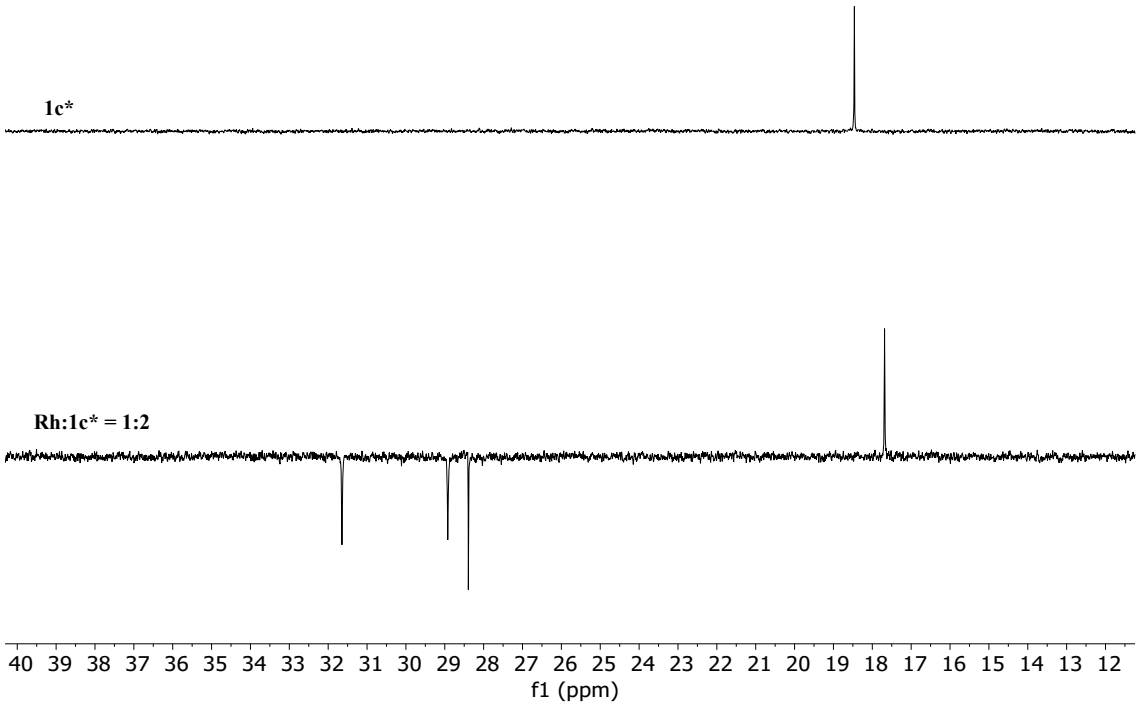

3.4.27. Rh:1p:1c*, ^{1}H NMR in CD_2Cl_2

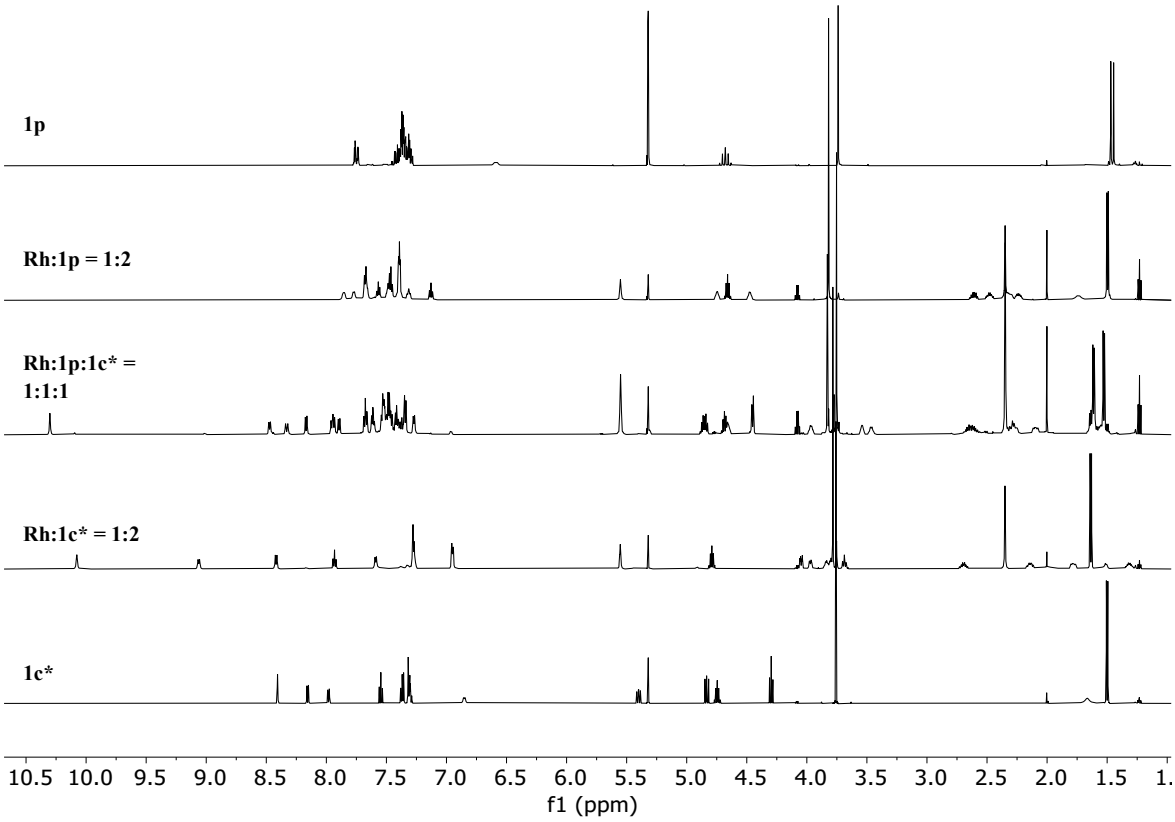

Aromatic group area of Rh:**1p**, ^{1}H NMR inCD_2Cl_2

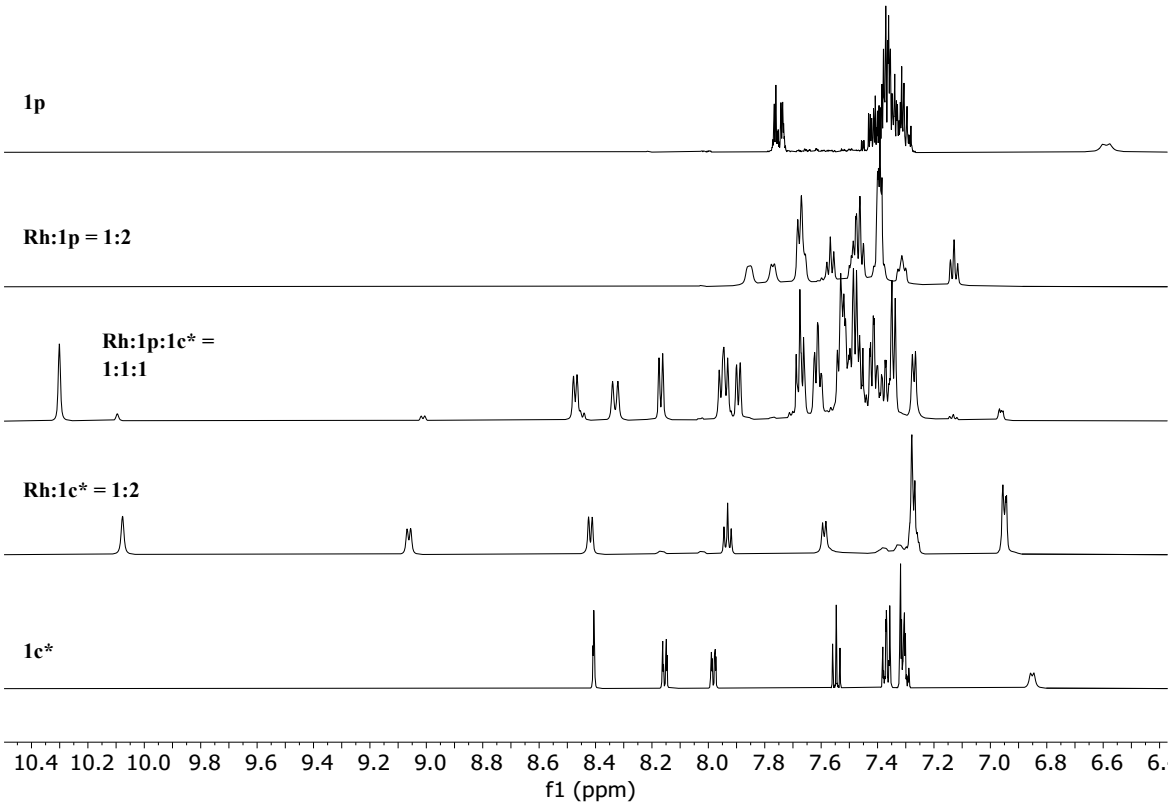

Functional group area
a) Lowered peak intensity

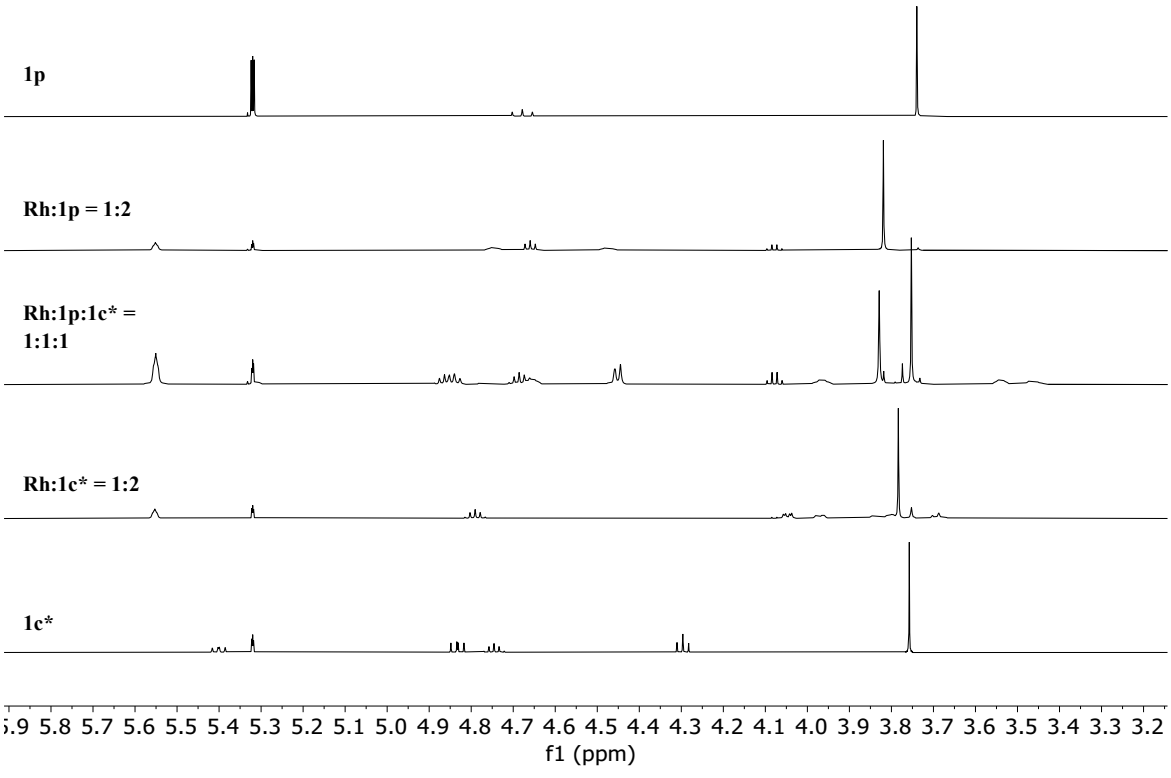

b) Increased peak intensity

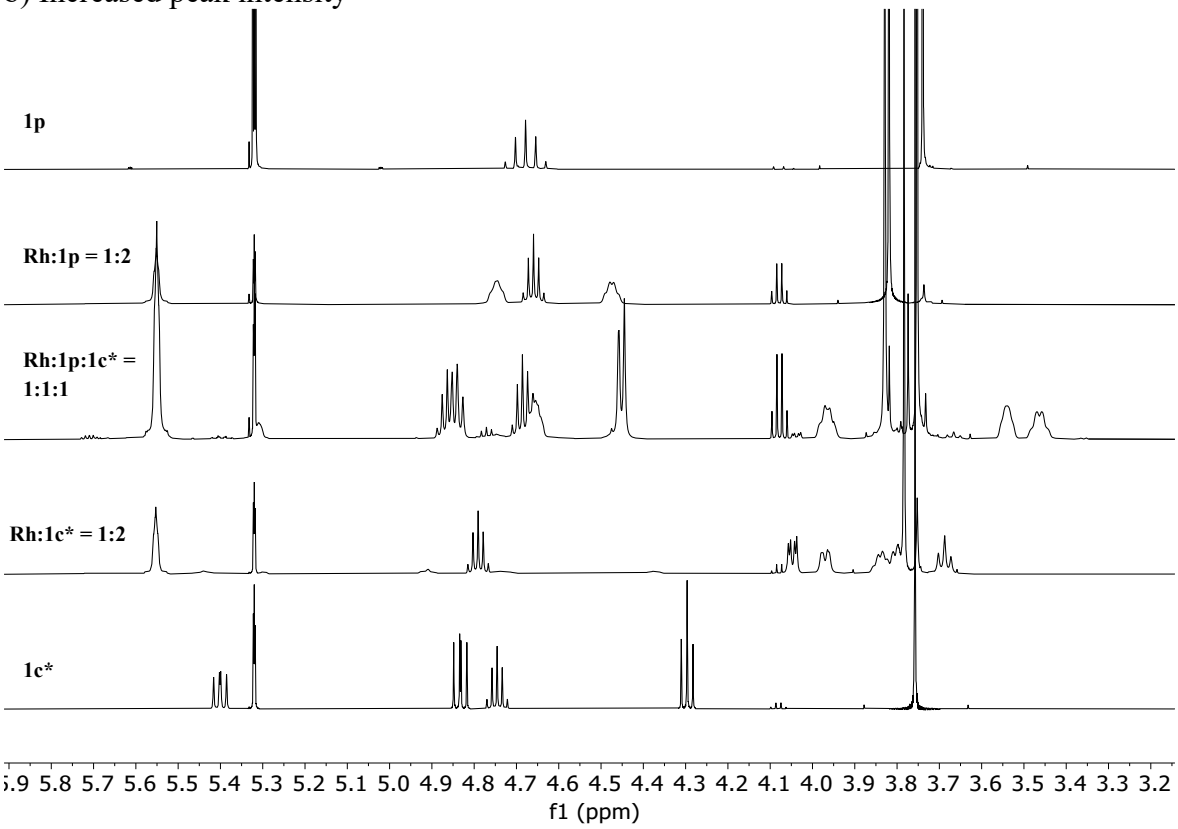

Aliphatic group area

a) Lowered intensity

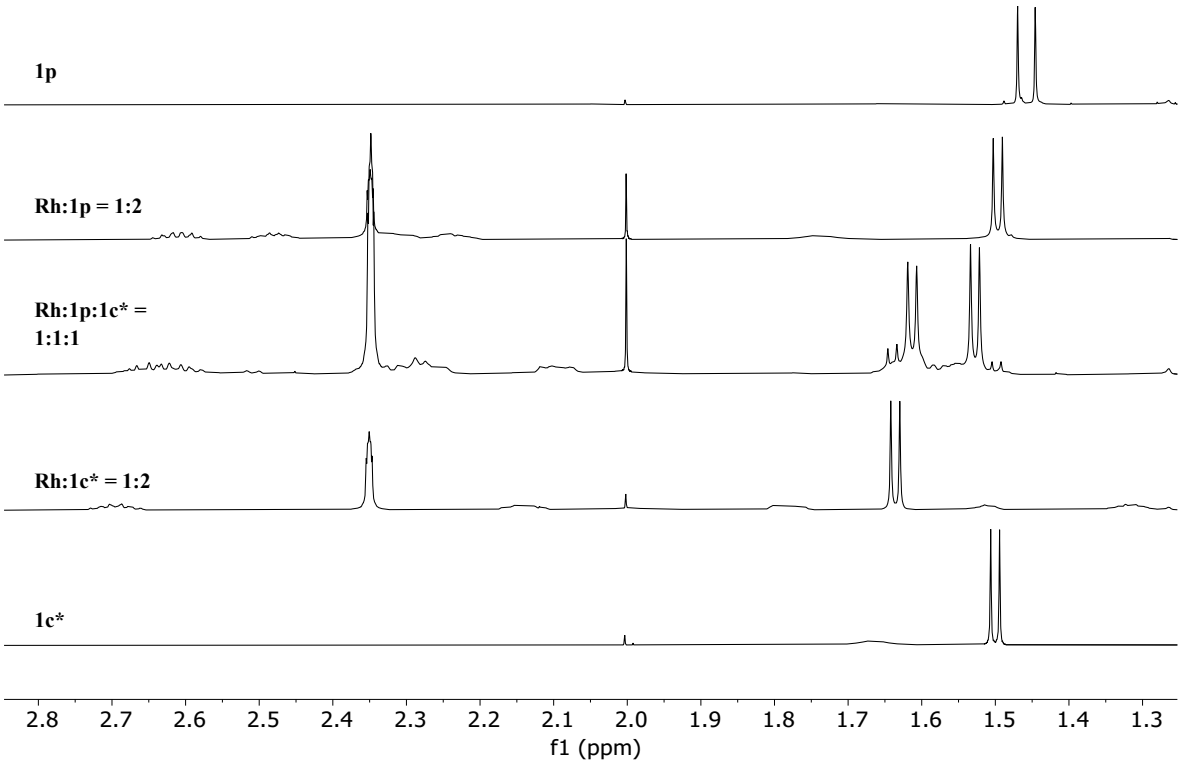

b) Increased intensity

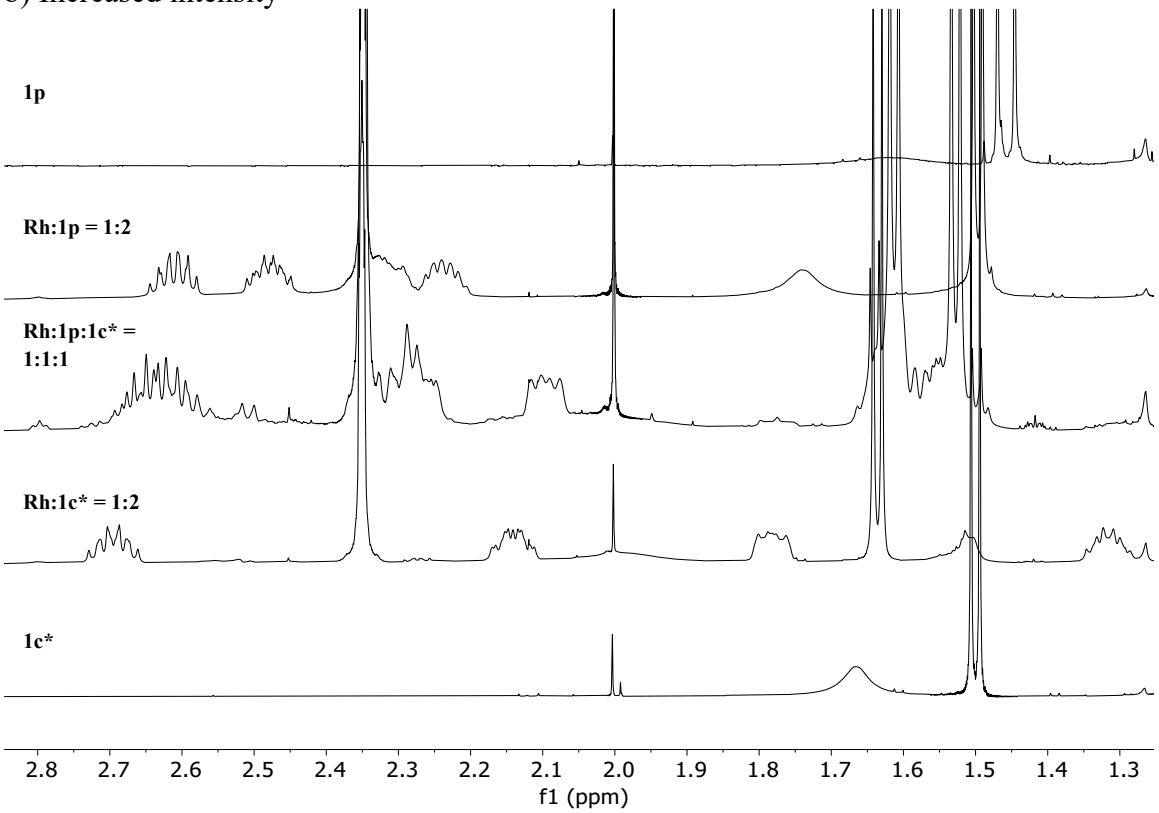

3.4.28. Rh:1p:1c*, ^{31}P NMR inCD_2Cl_2

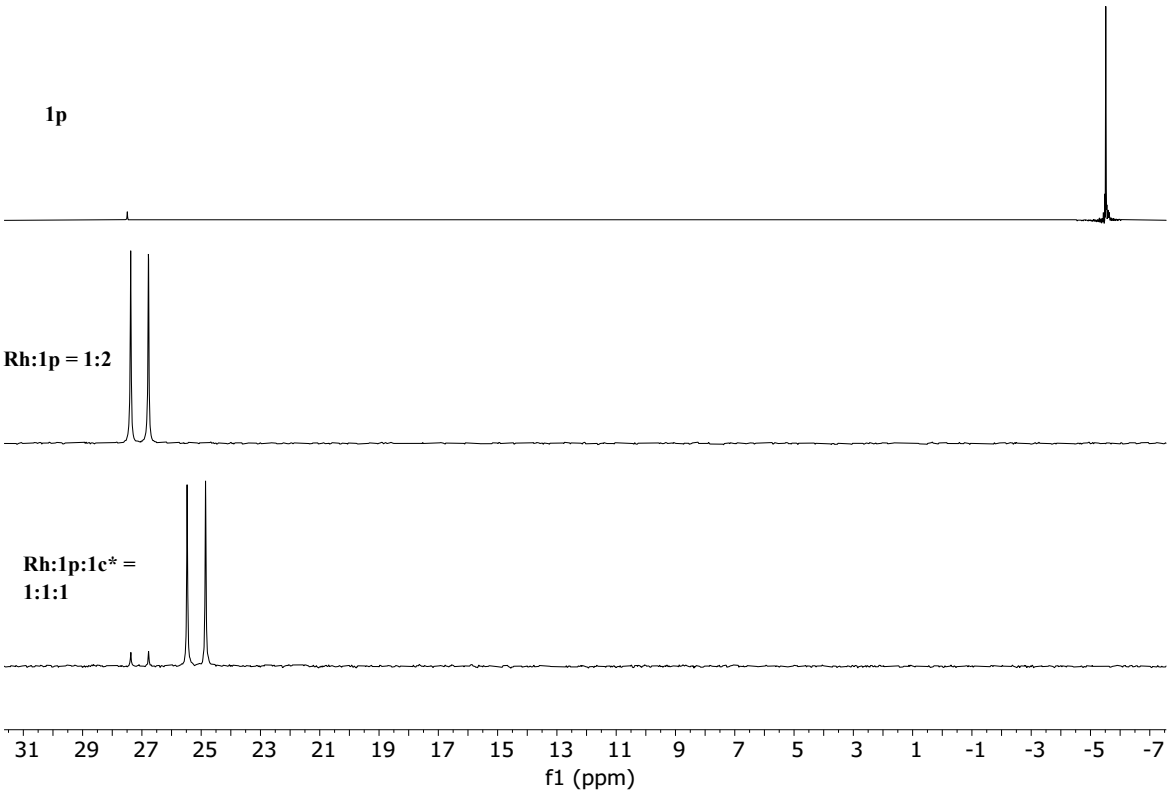

3.4.29. Rh:1p, ^{13}C NMR in CD_2Cl_2

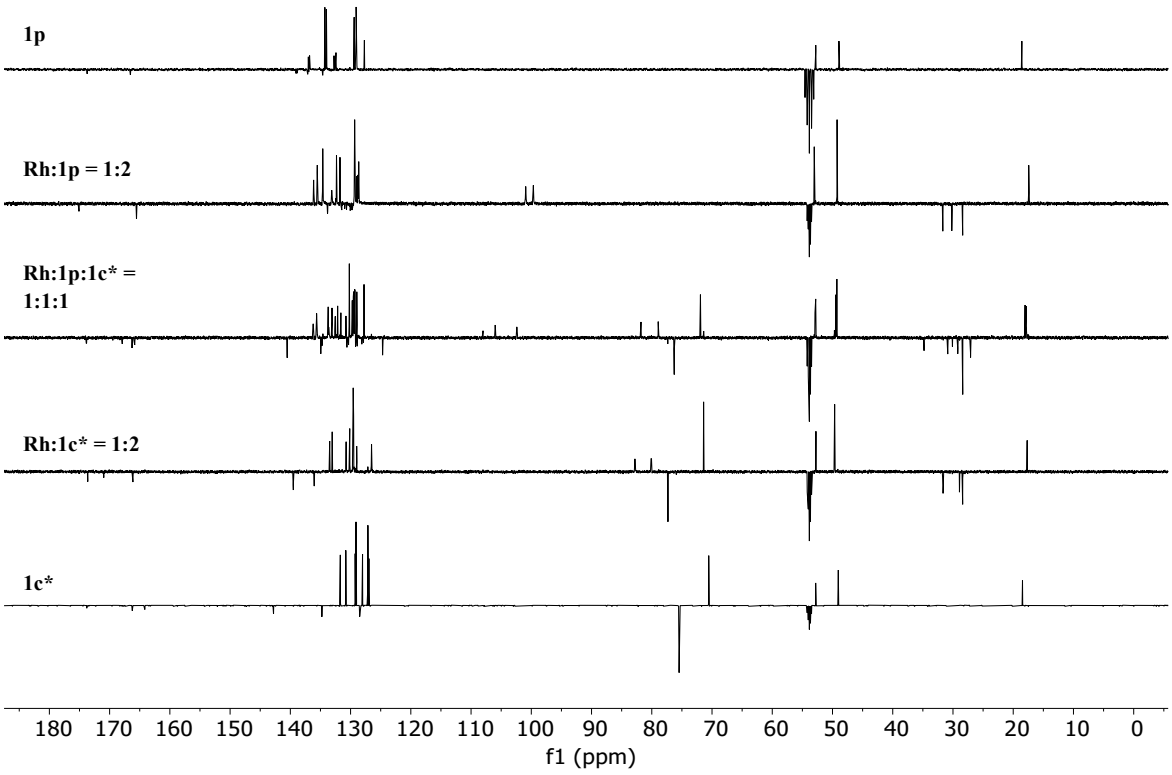

Amide/ester group area

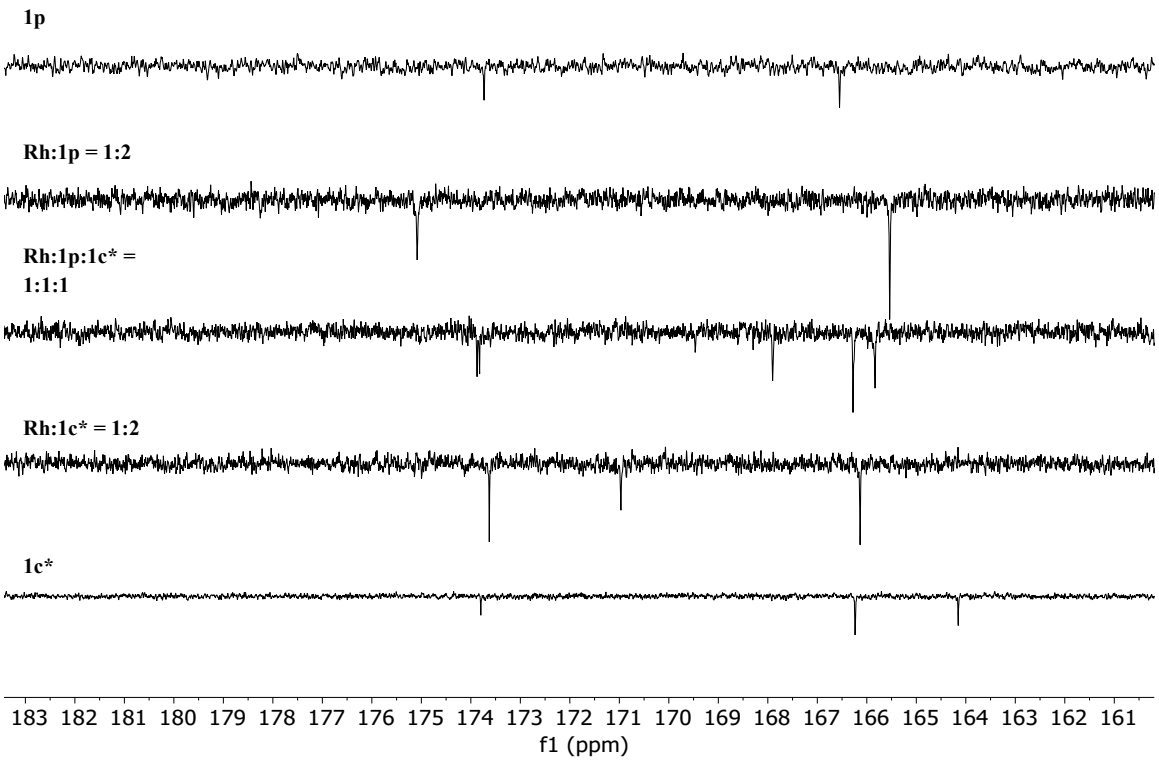

Aromatic group area

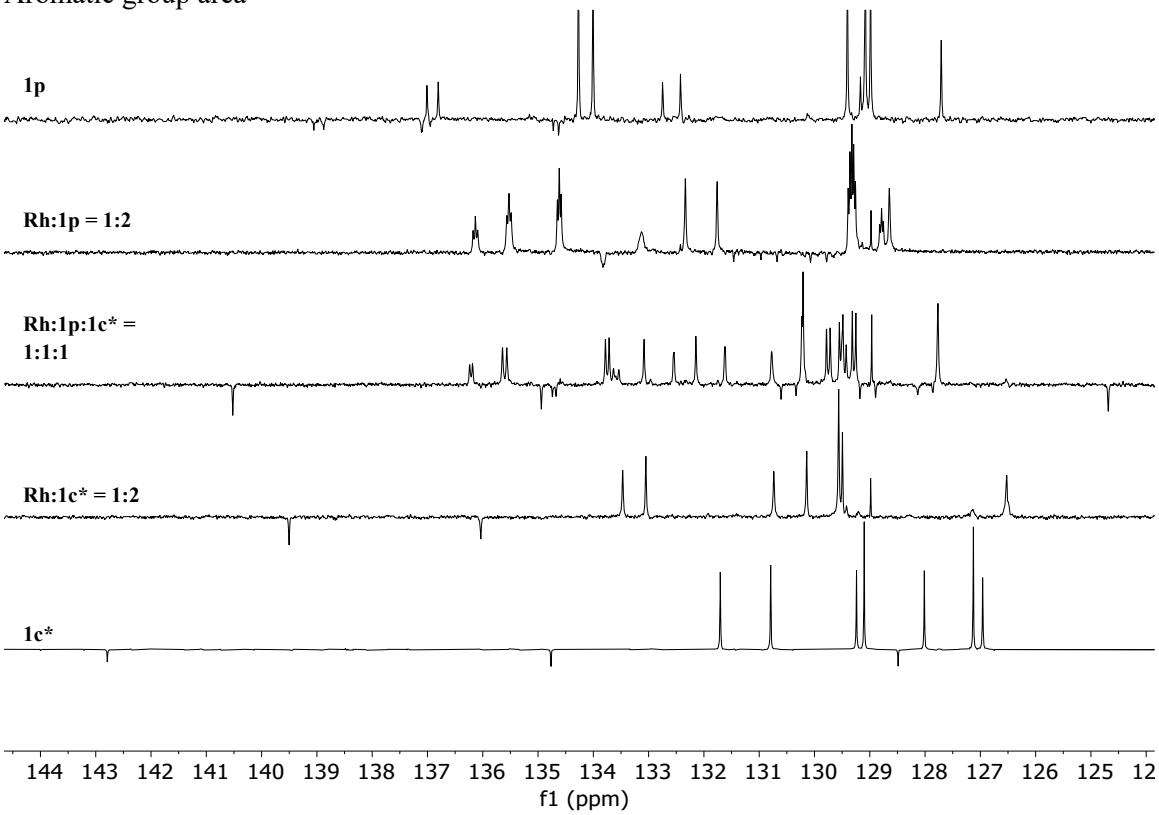

110ppm-80ppm

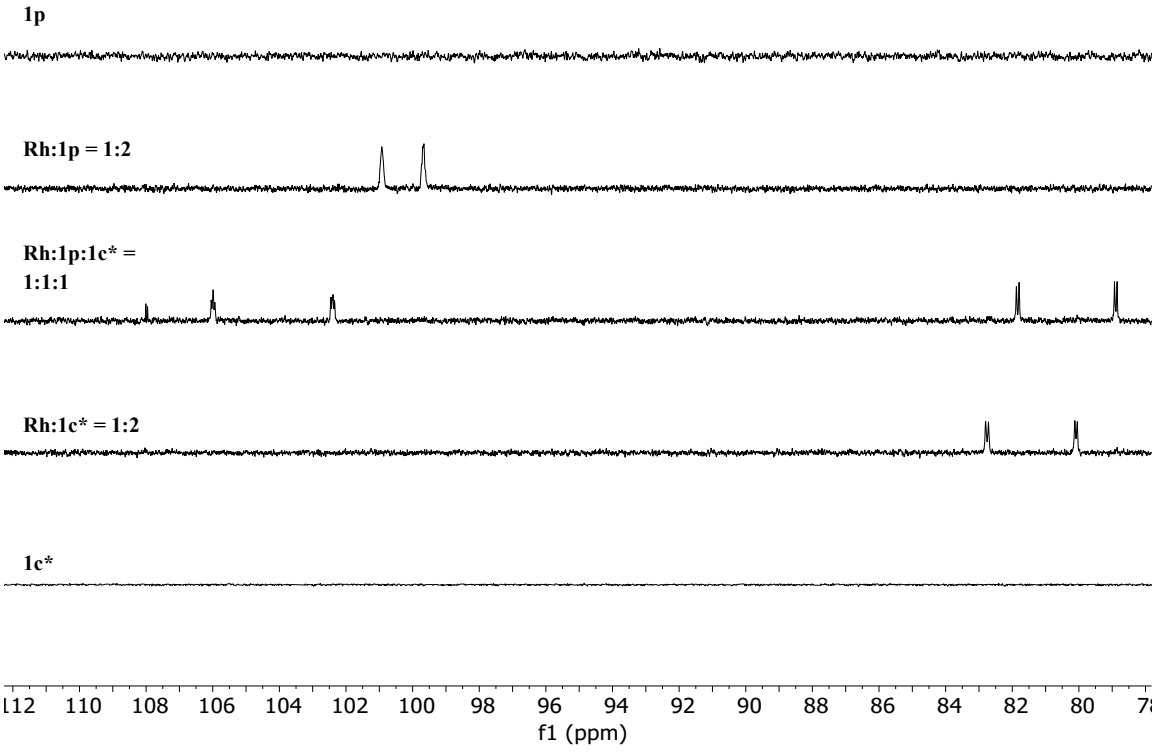

Functional group area

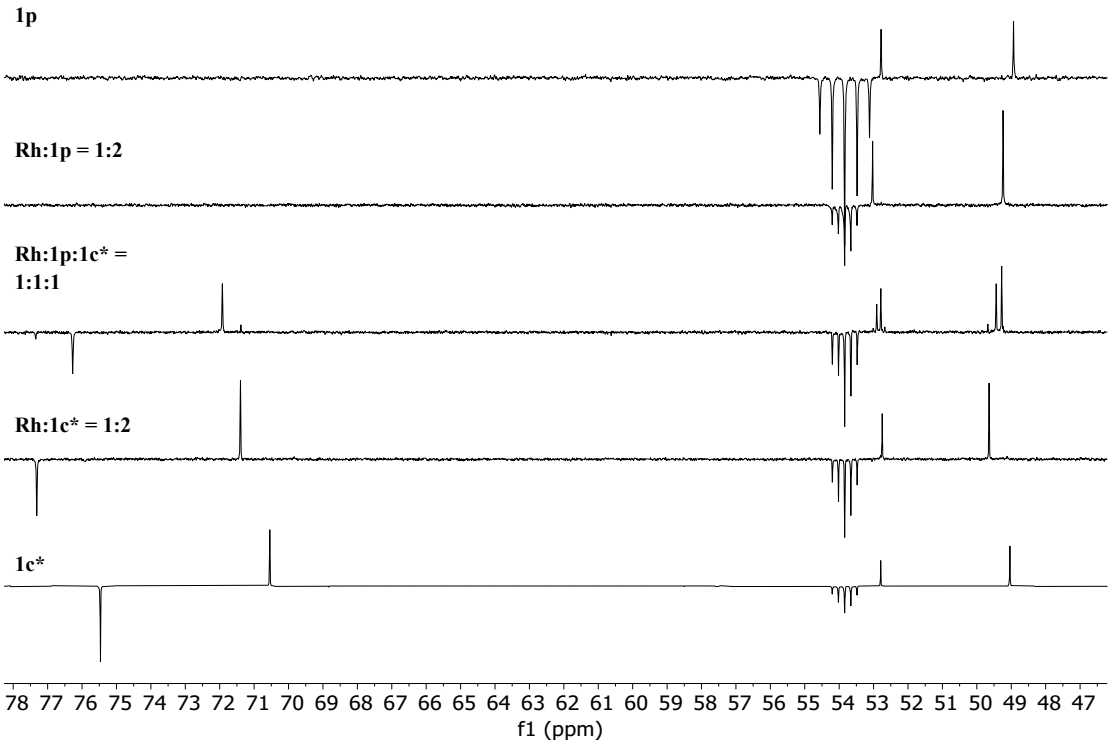

Aliphatic group area

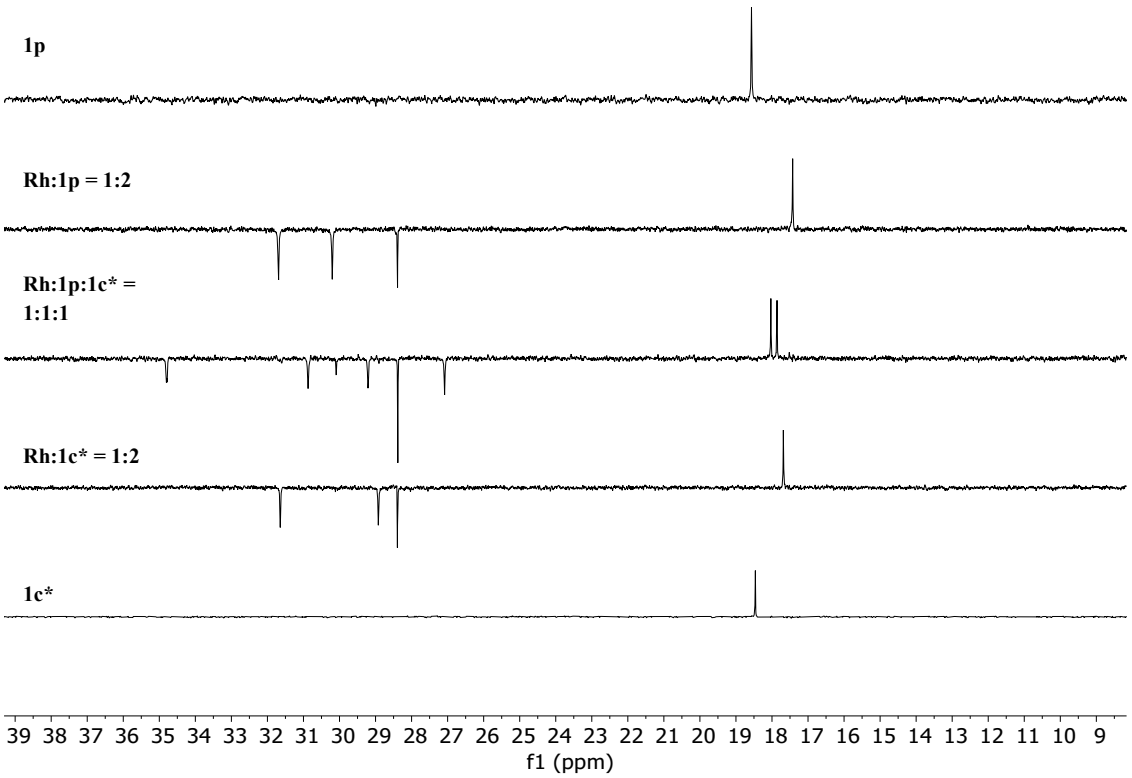

3.4.30. Rh:1p:TPPH$_3$, ^{1}H NMR in CD_2Cl_2

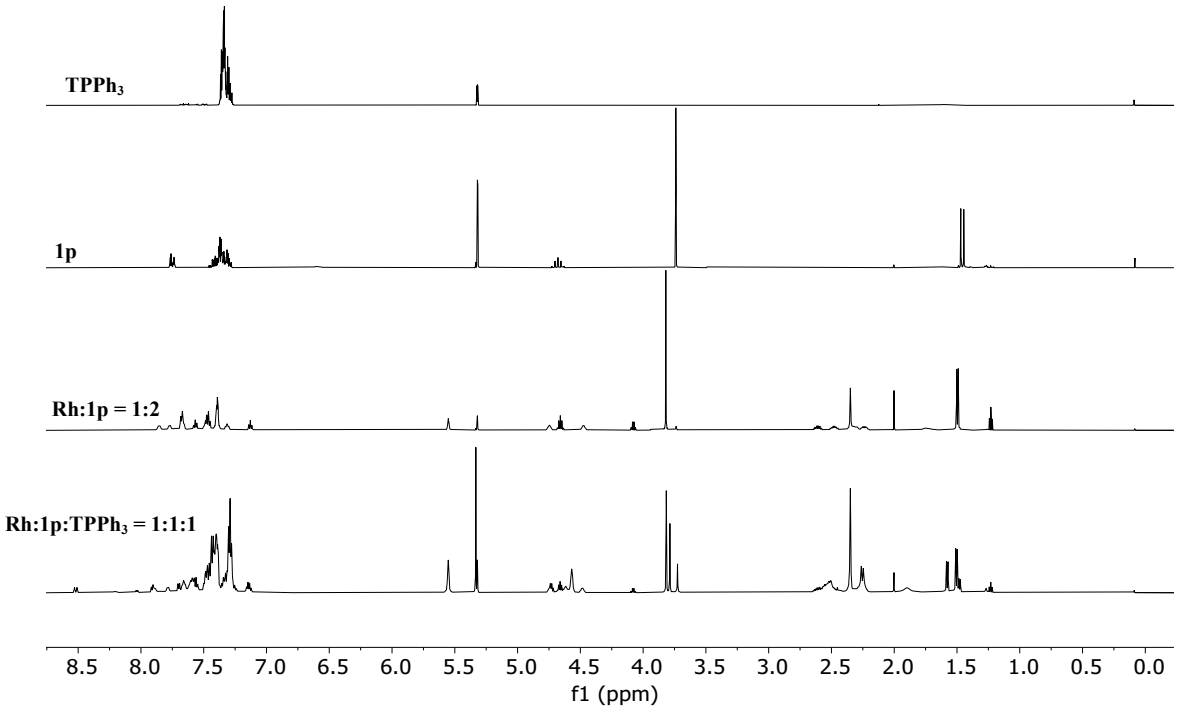

Aromatic group area of Rh:**1p**, ^{1}H NMR inCD_2Cl_2

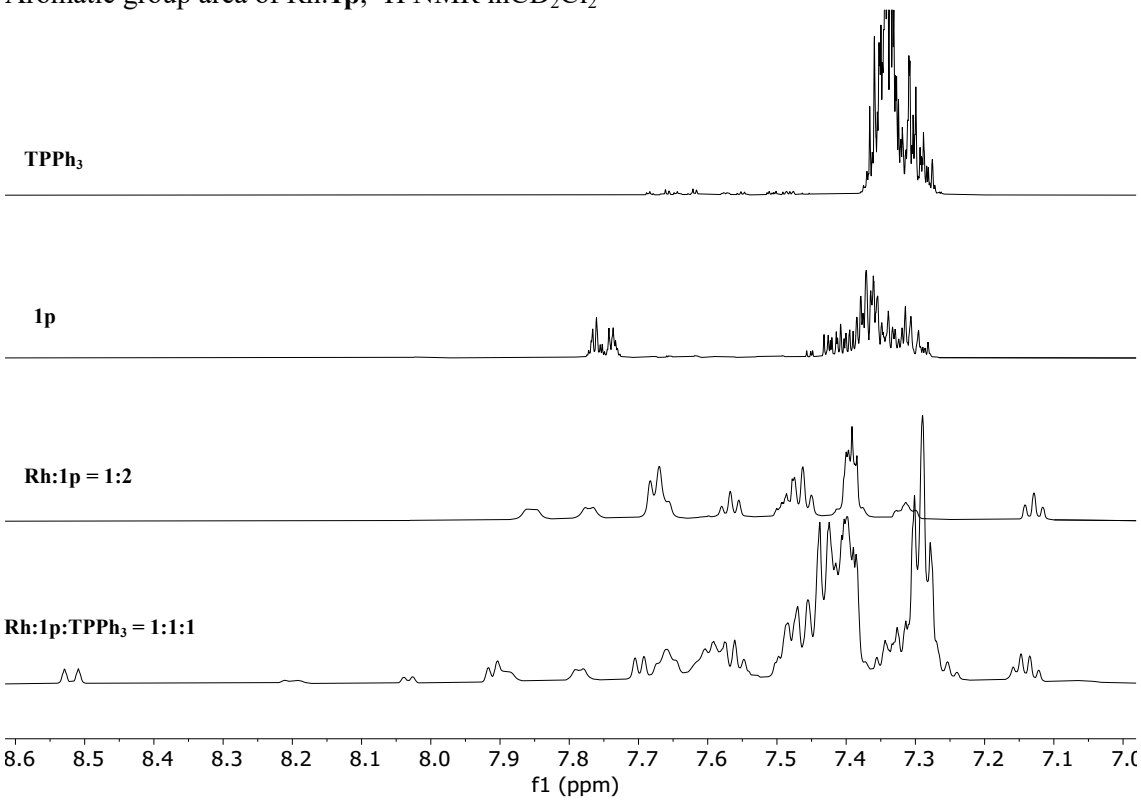

Functional group area

a) Lowered peak intensity

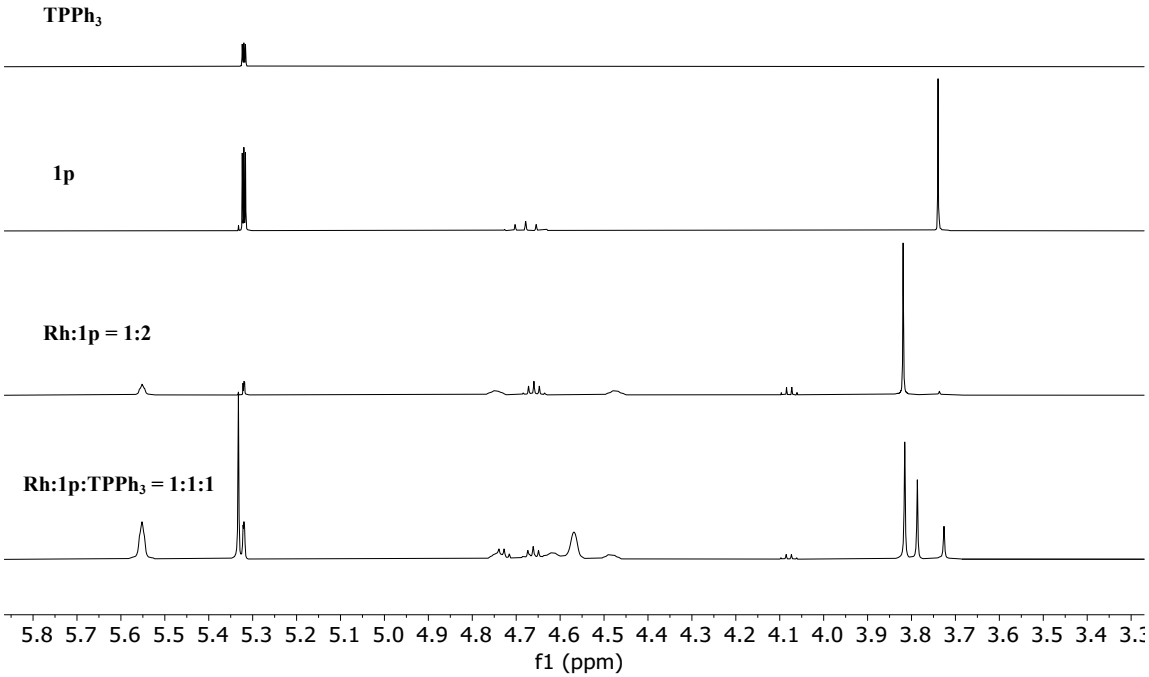

b) Increased peak intensity

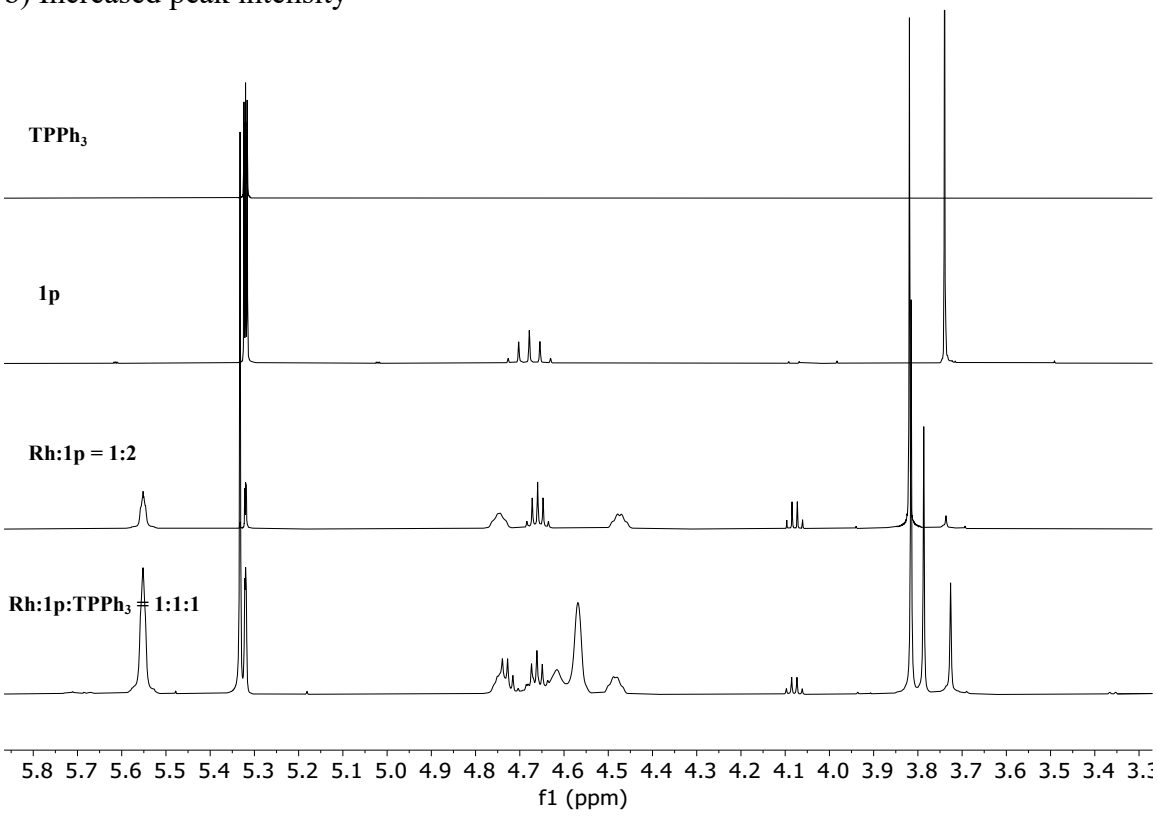

Aliphatic group area

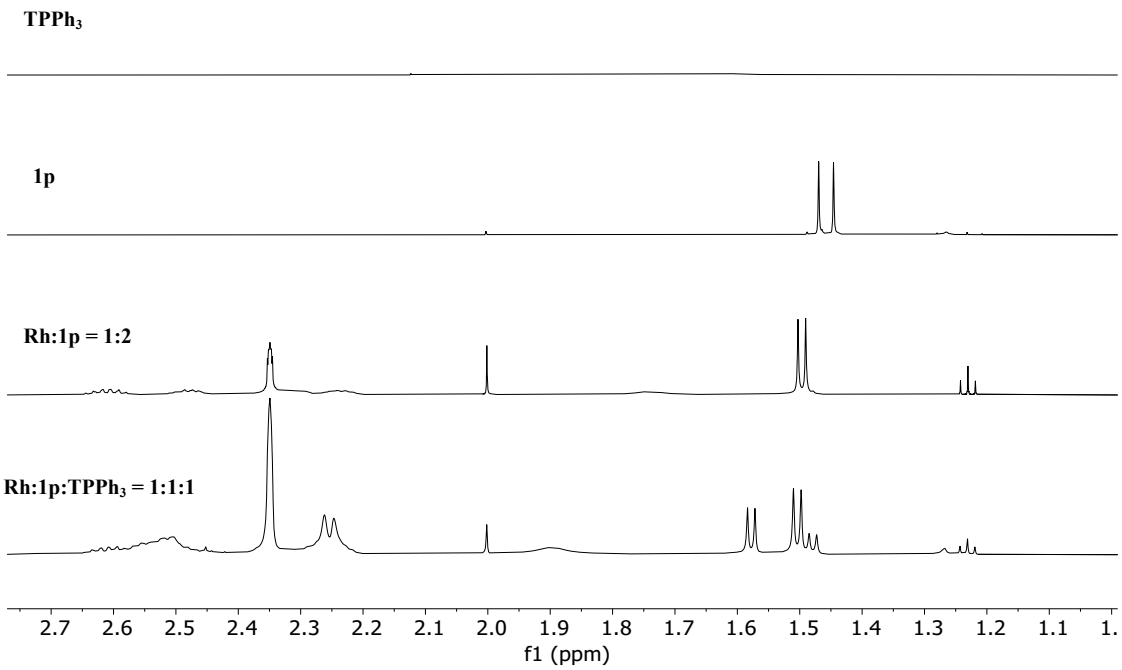

3.4.31. Rh:1p:TPPH$_3$, ^{31}P NMR in CD_2Cl_2

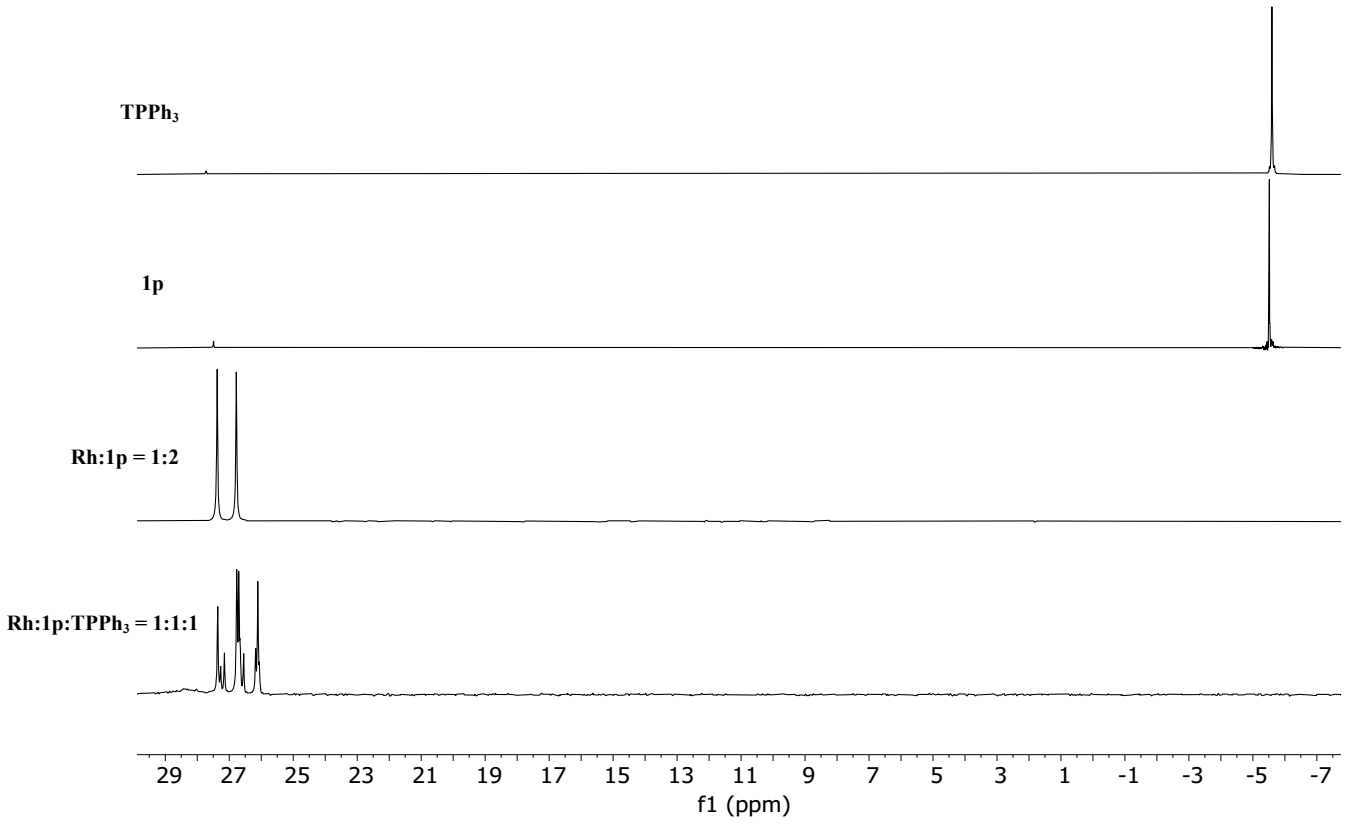

Metal complex and oxidized phosphorus region of chemical shifts

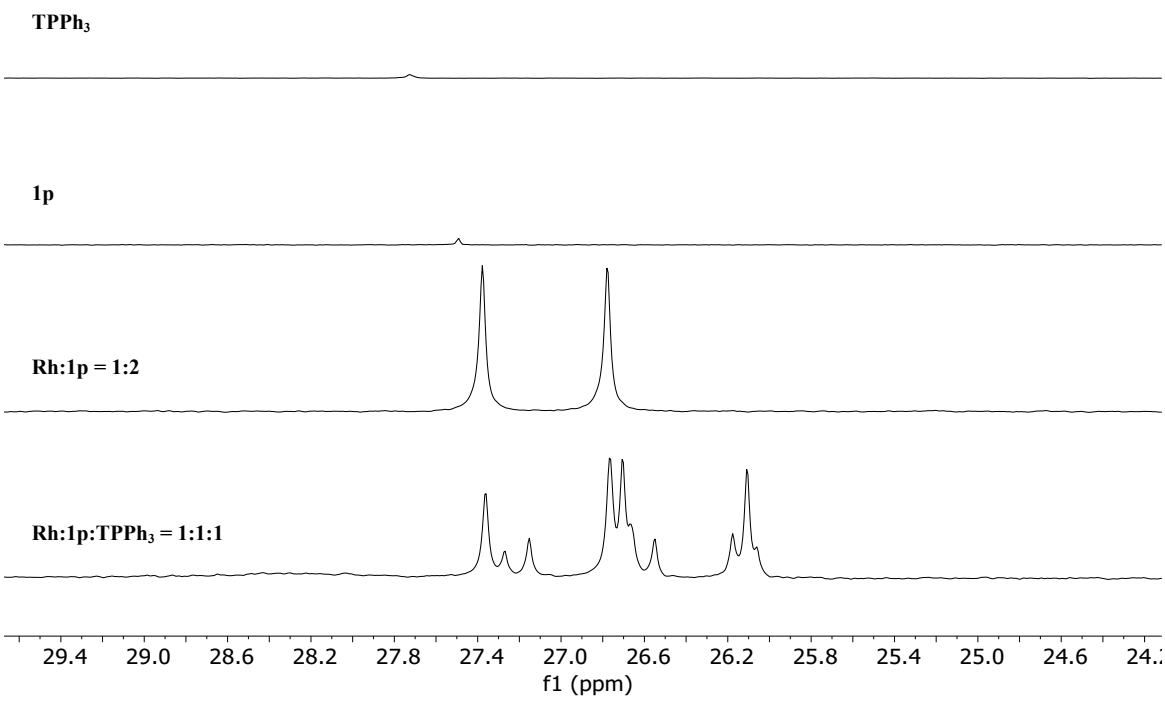

3.5. NMR spectra of hydrogenation and hydroformylation compounds

3.5.1. Methyl-*α*-acetamidocinnamate, ^{1}H NMR in $CDCl_3$

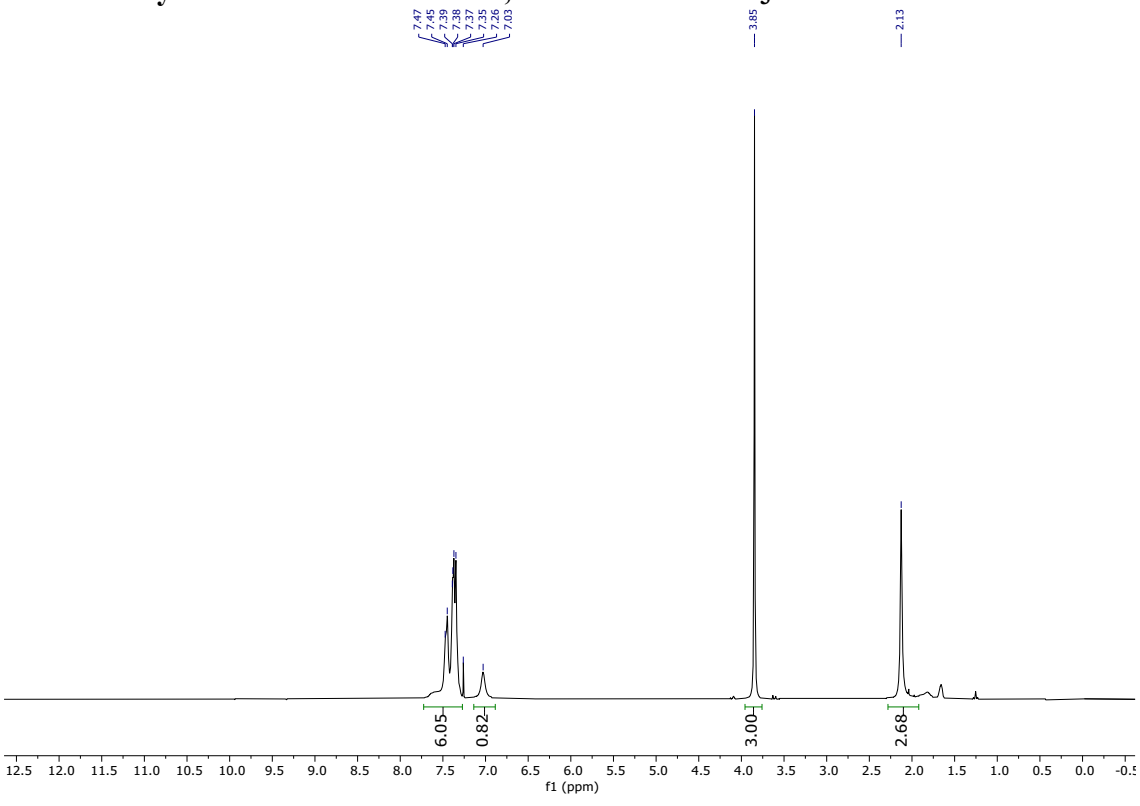

3.5.2. Alcoholic product mixture of hydroformylation of styrene, ^{1}H NMR in $CDCl_3$

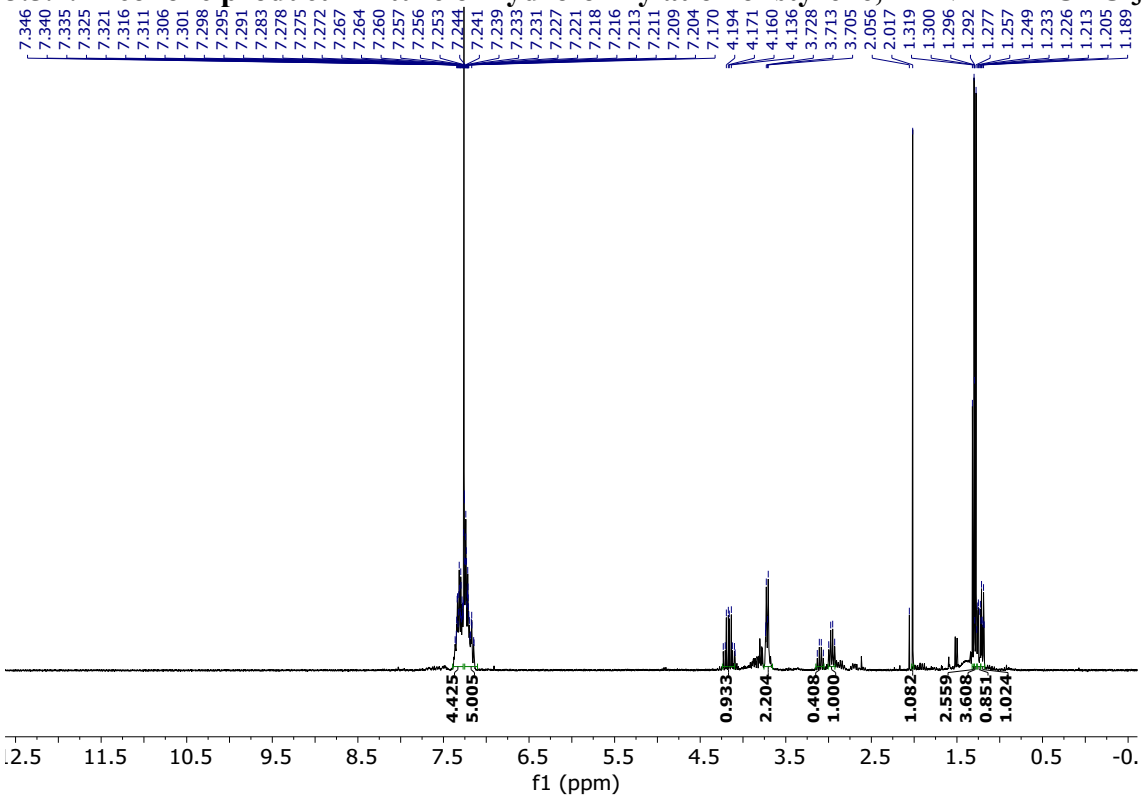

3.5.3. Alcoholic product mixture of hydroformylation of octene, ^{1}H NMR in $CDCl_3$

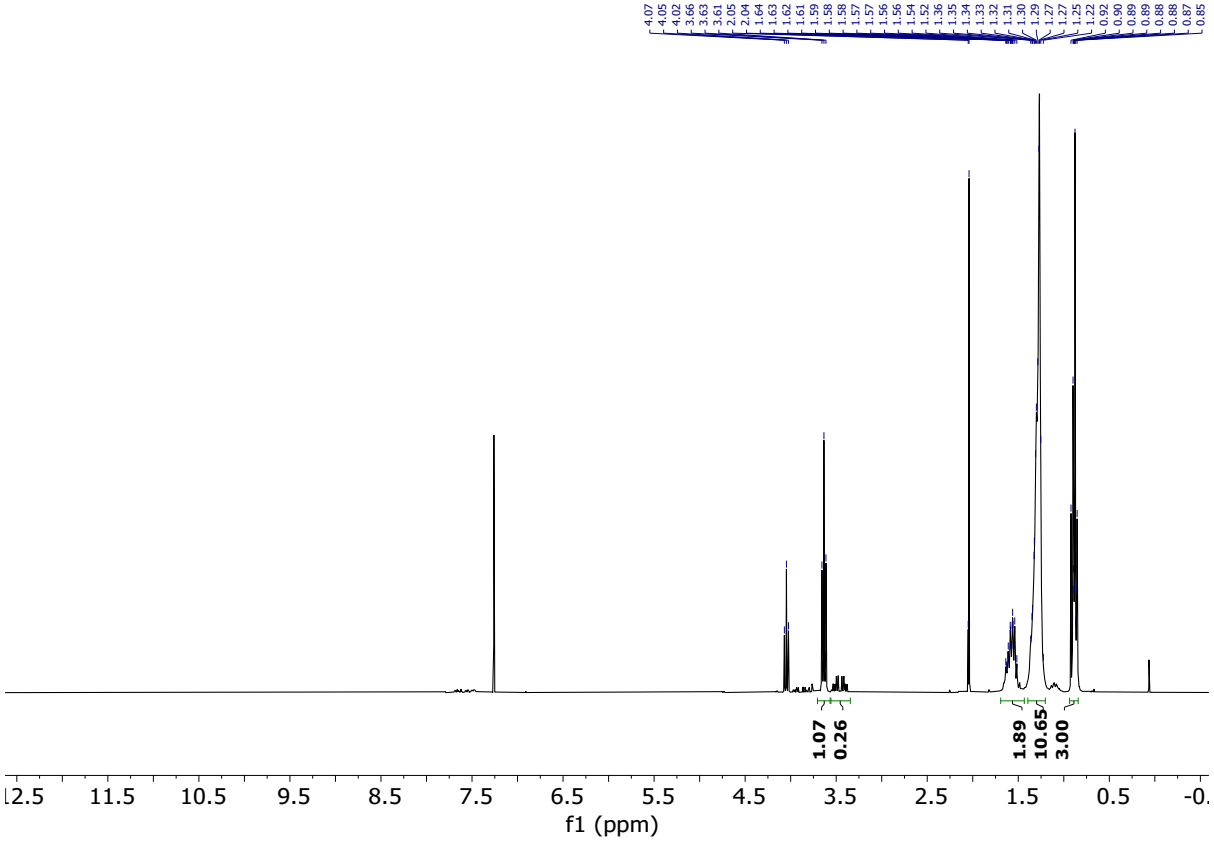

3.6. 1p/1b ligand mixture NMR spectra

3.6.1. ^{1}H NMR in CD_2Cl_2

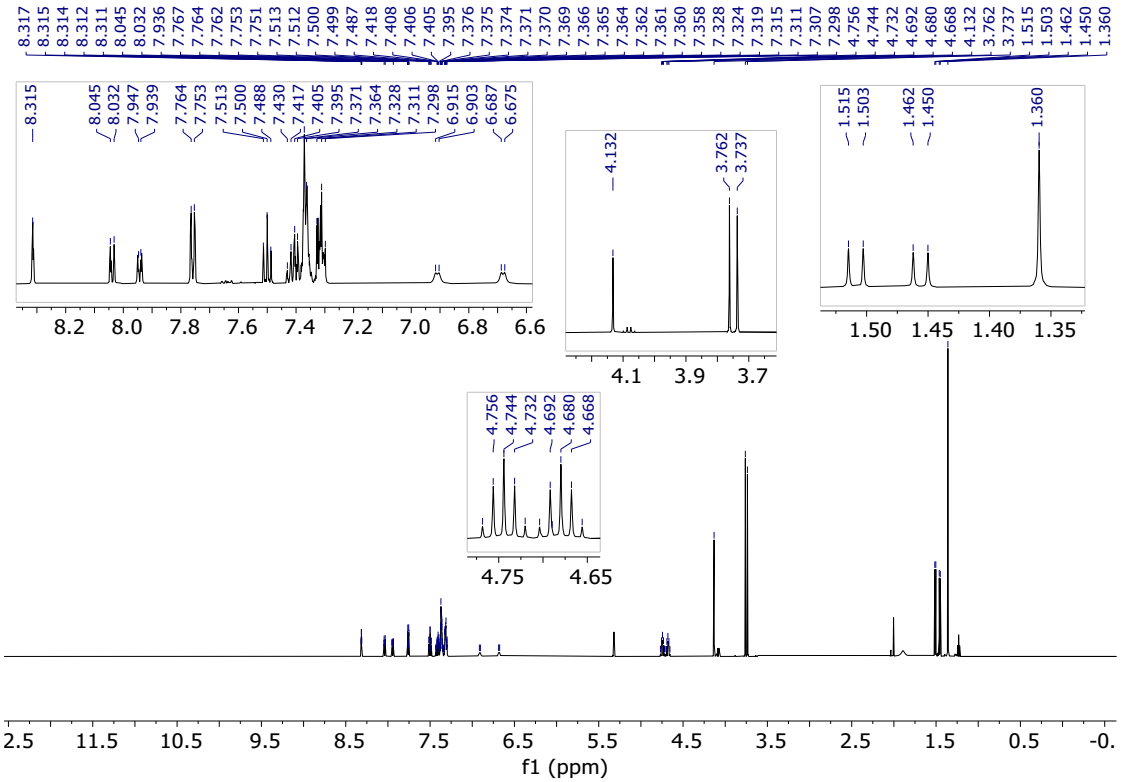

3.6.2. ^{31}P NMR in CD_2Cl_2

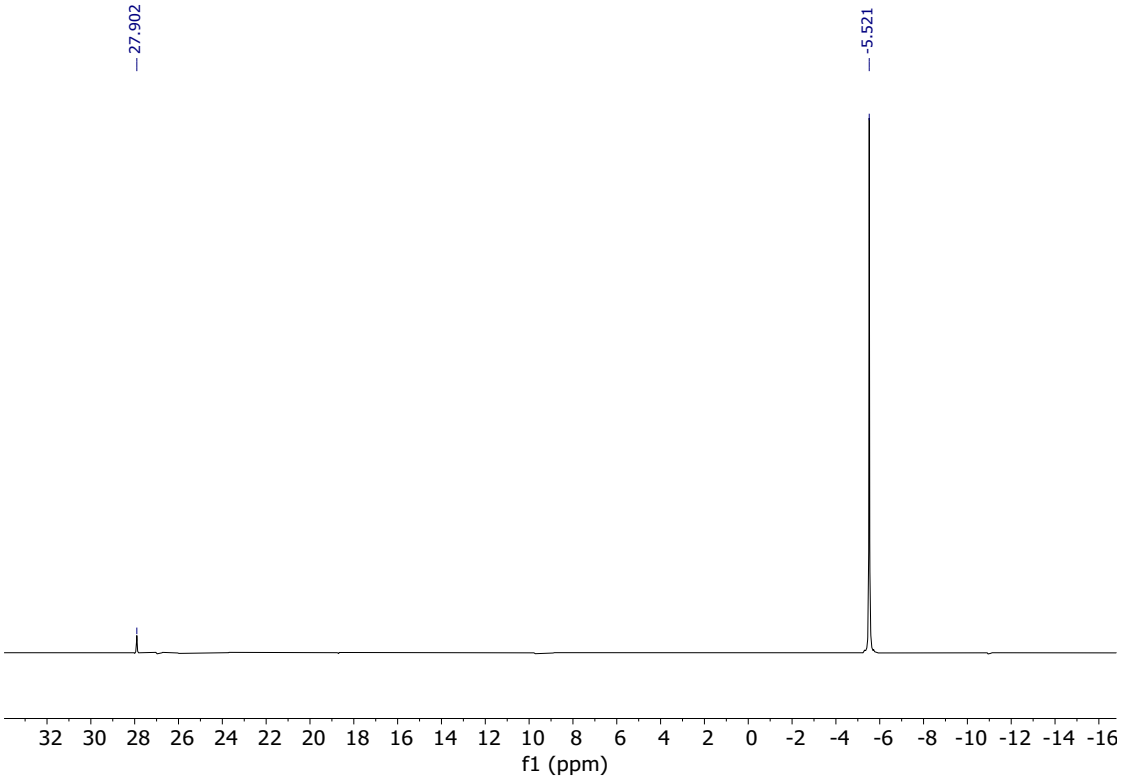

3.6.3. Overlapped ^{1}H NMR spectra of 1p, 1b and 1p/1b mixture inCD_2Cl_2

a) whole spectra

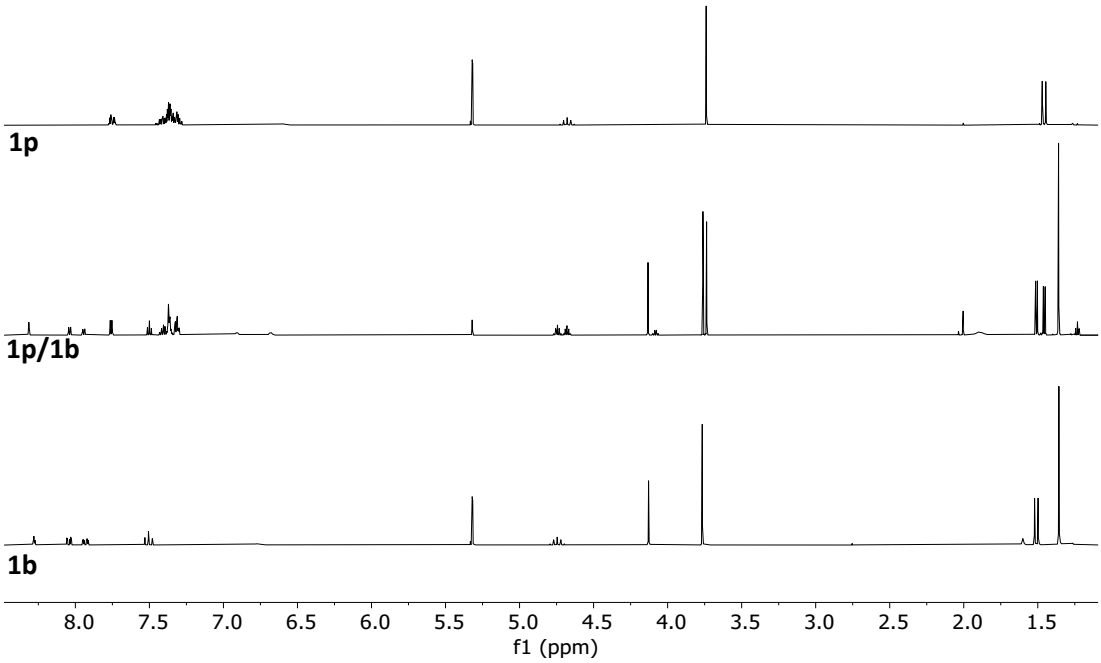

b) aromatic region

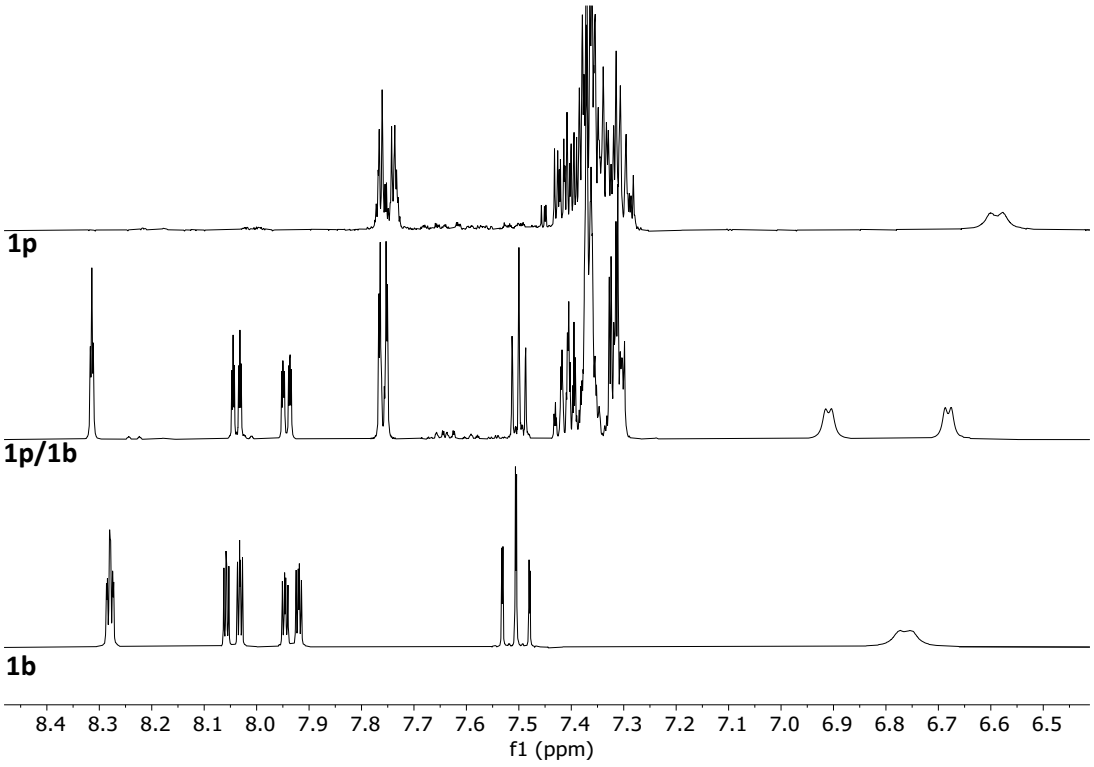

c) Functional group region

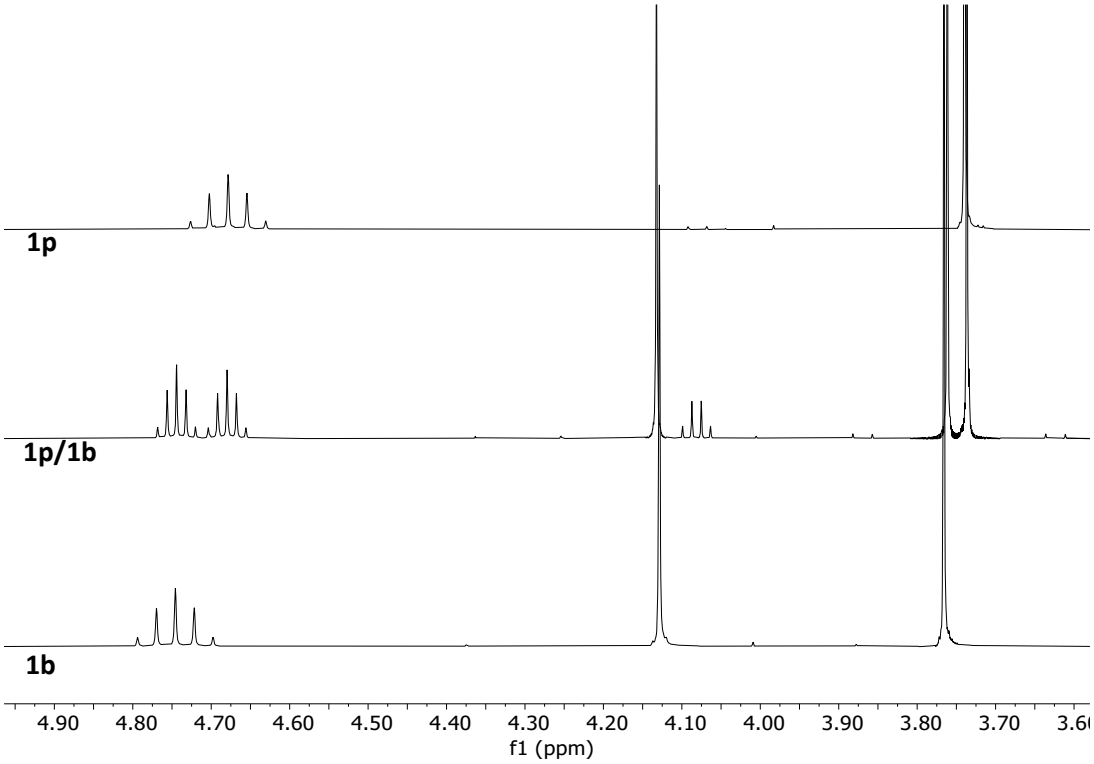

d)Aliphatic group region

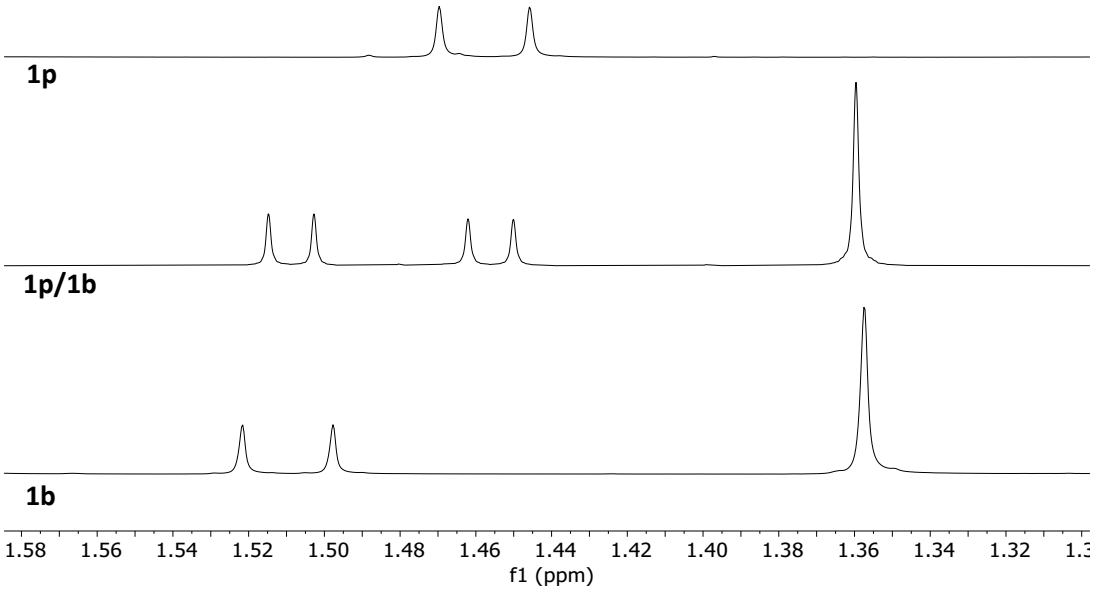

3.7. Rh:1c=1:2 Overlapped ^{1}H NMR spectra: 1st day (black) and 7th day (red) (CD_2Cl_2)*

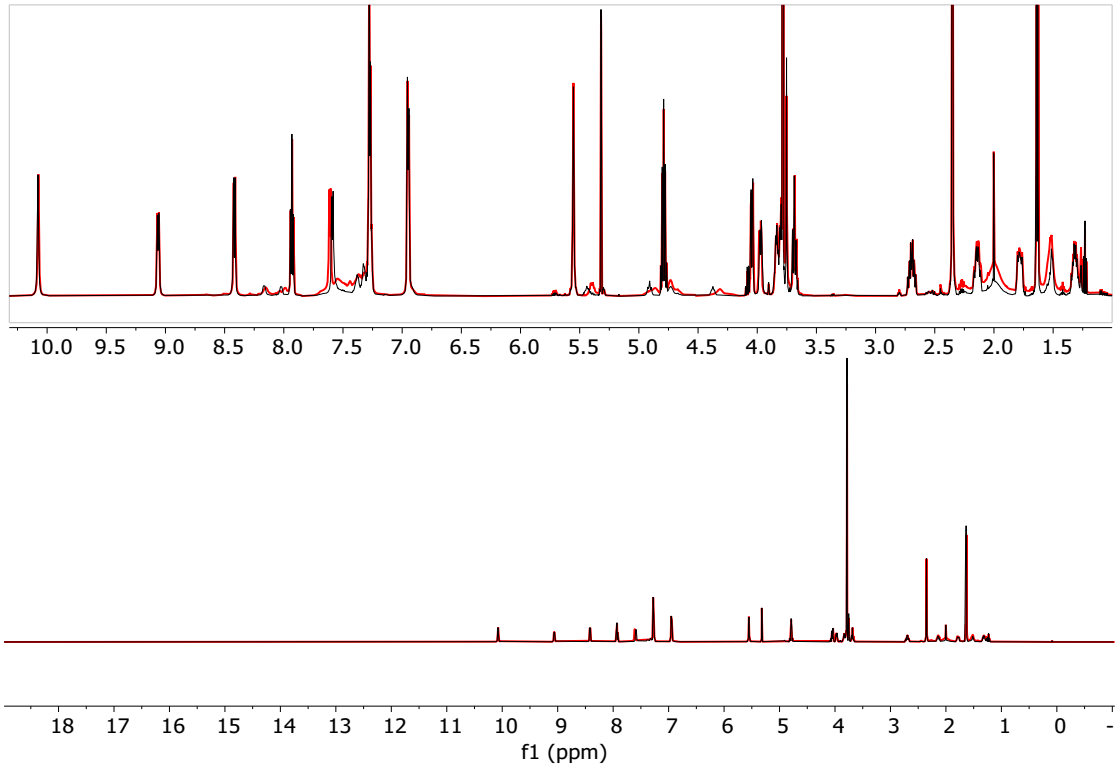

3.8. Ir:1c=1:2 Overlapped ^{1}H NMR spectra: 1st day (black) and 7th day (red) (CD_2Cl_2)

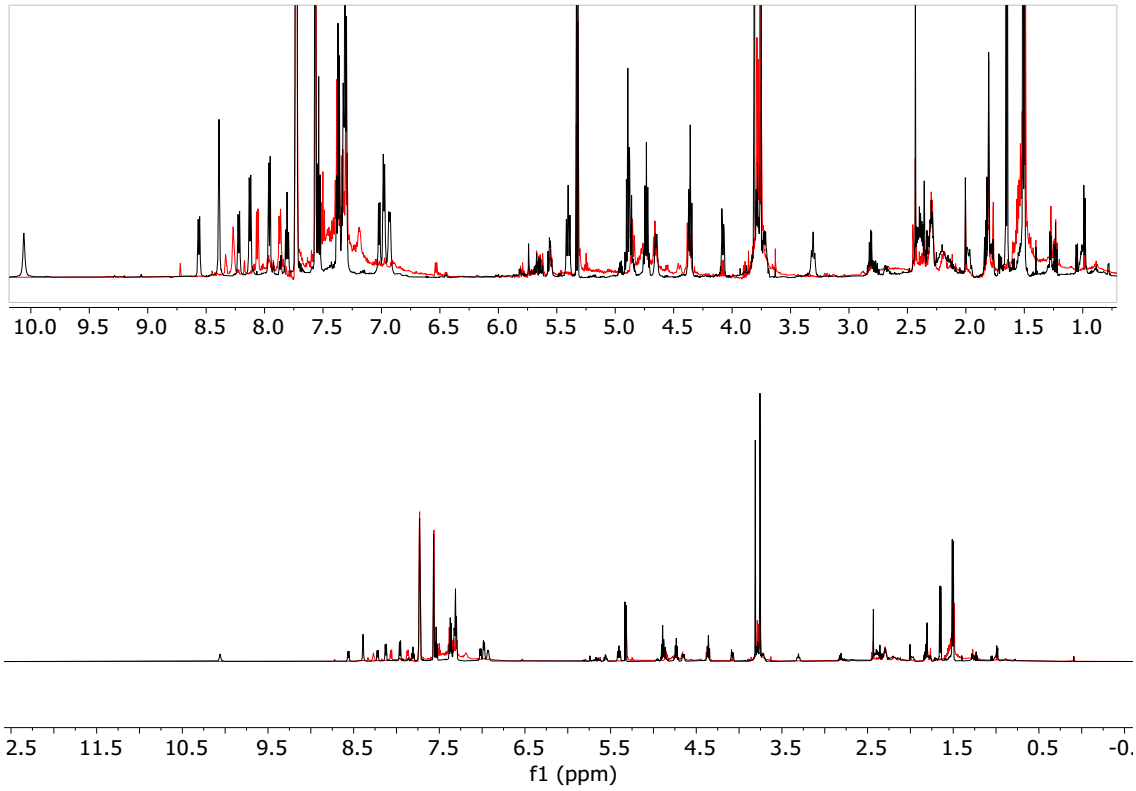

3.9. Rh:1c=1:1 (red, c(Rh)=0.008 M, c(1c*)=0.008 M) and Rh:1c*=1:2 (black, c(Rh)=0.025M, c(1c*)=0.05M) overlapped ^1H NMR in CD_2Cl_2*

a)whole spectra

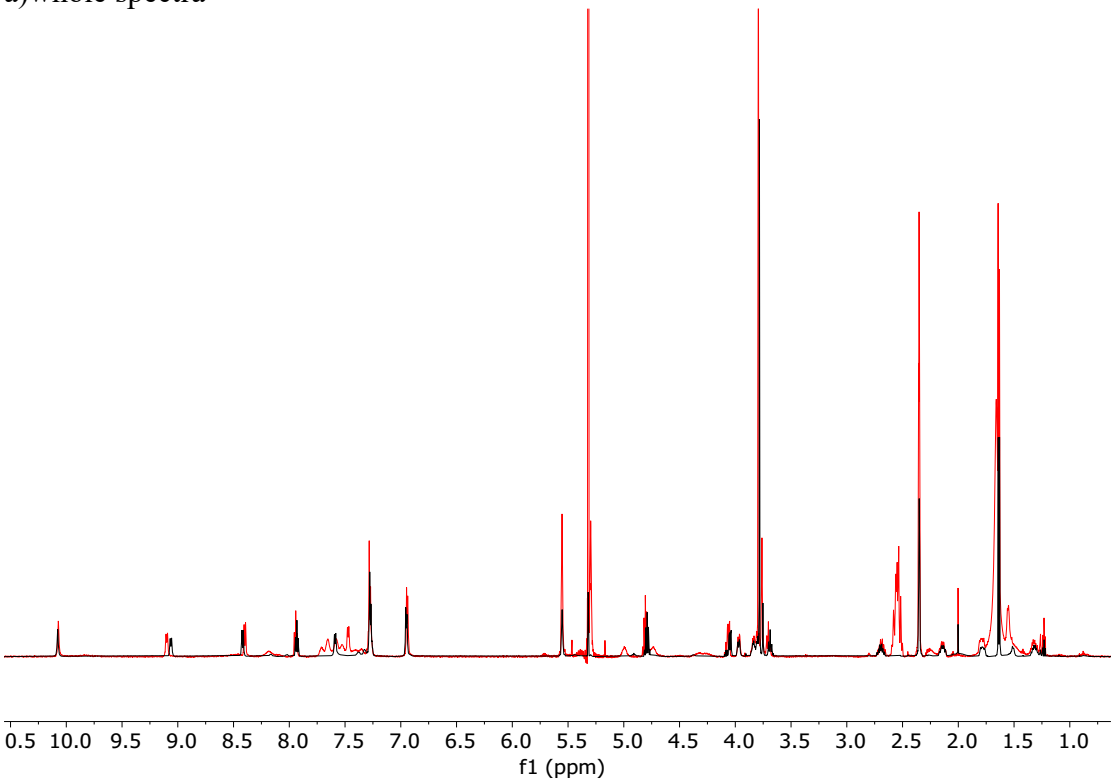

b) aromatic region

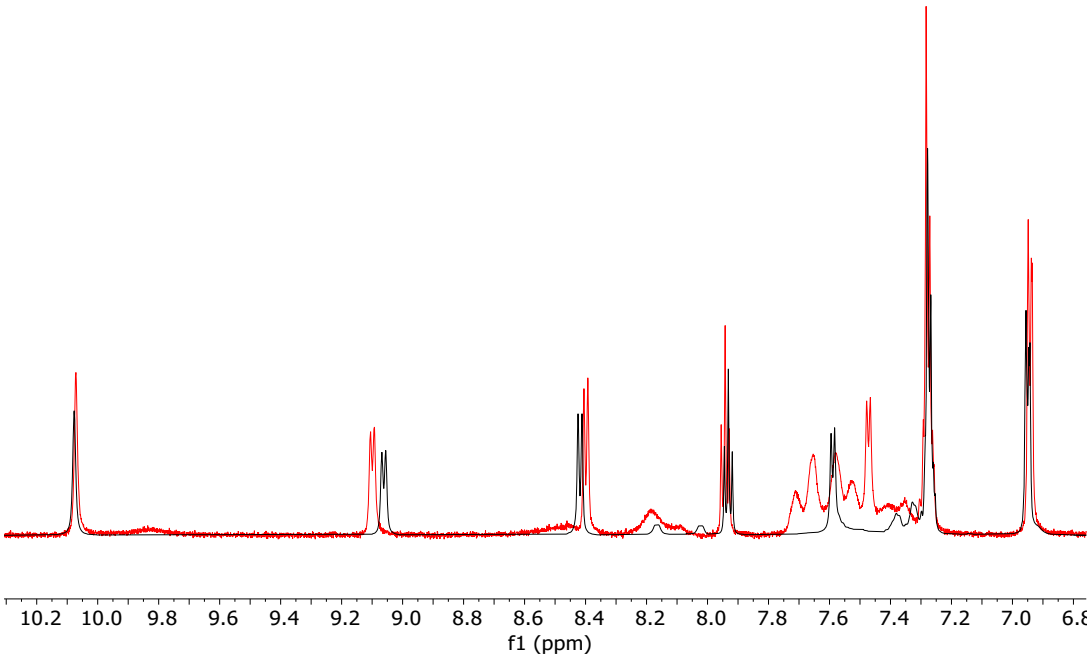

c) functional group area

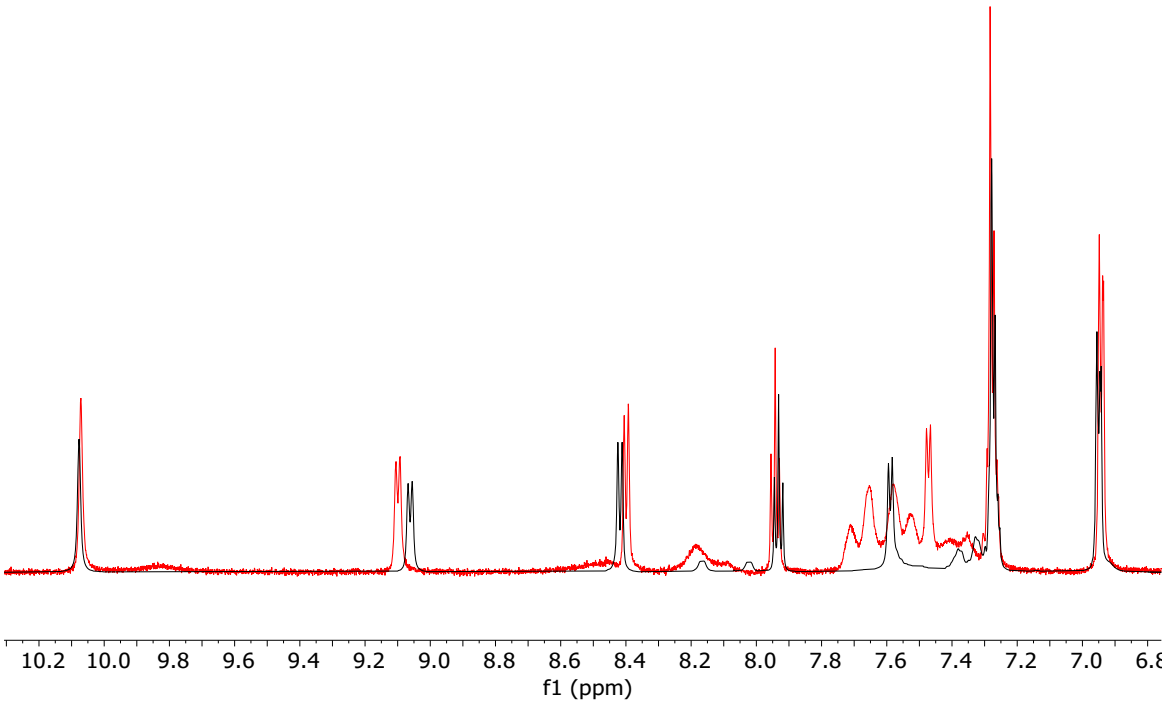

d)Aliphatic group region

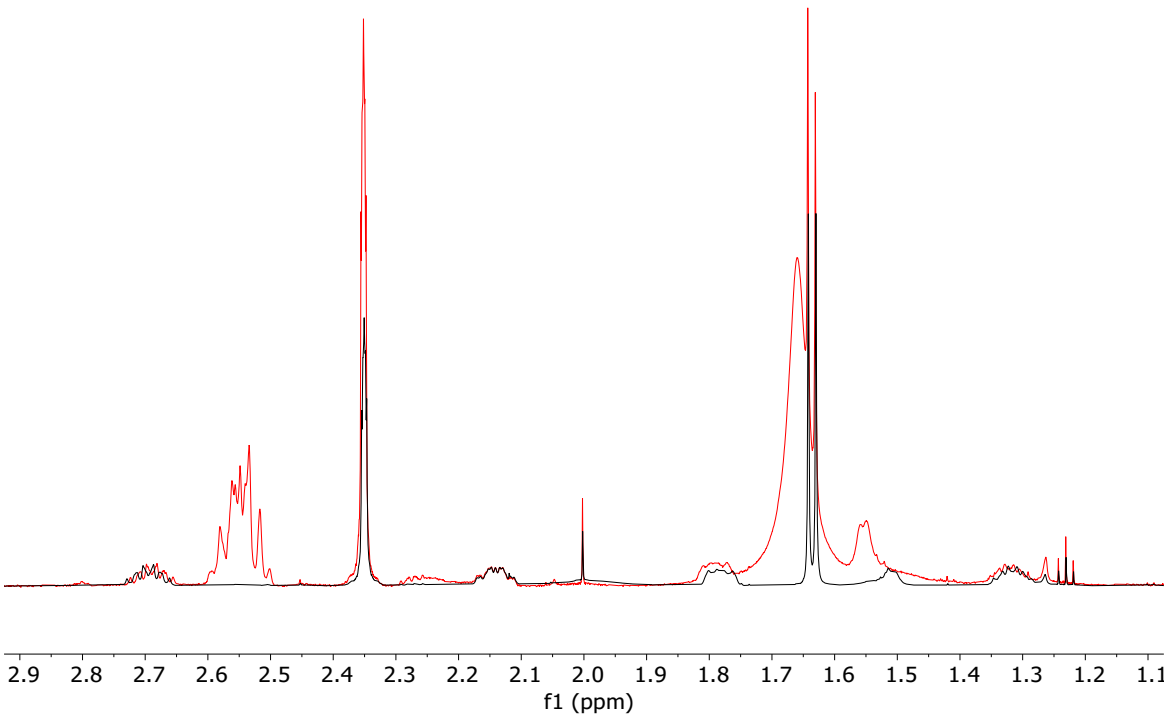

4. UV-VIS Spectra

Several concentrations, namely *c*(M) = 0.03, 0.38mM and 3.49 mM, have been recorded for several precatalytic complexes. In almost all cases, the absorbance in the UV region was too high for the detector sensitivity at concentrations of 0.38 mM and above. These higher concentrations, however, have been recorded to obtain higher absorbance value of peaks in the visible region of the spectra.
Formation of the homoleptic iridium **1p** precatalyst complex as well as time necessary to establish equilibrium was screened by measuring UV-VIS absorbance every 5 minutes immediately after injection of one equivalent of iridium precursor to the solution of ligands. Approximately 45 minutes was necessary for the reaction to reach a plateau in the case of Ir : **1p** = 1 : 2, i.e. for the *in situ* formation of the complex to reach equilibrium. Upon injection of the **1b** solution with the iridium precursor very negligible changes occurred in the spectrum.

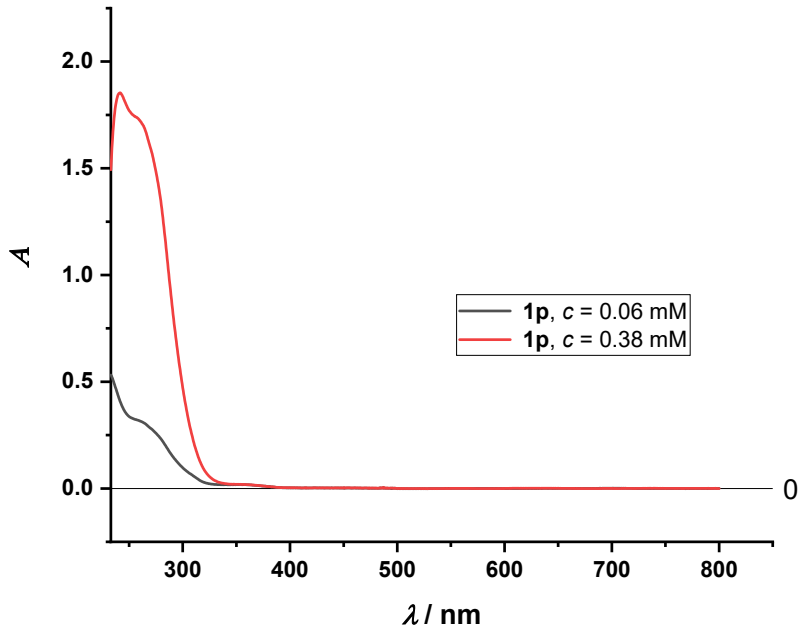

Figure S4. UV-Vis (CH_2Cl_2) of ligand **1p** solution.

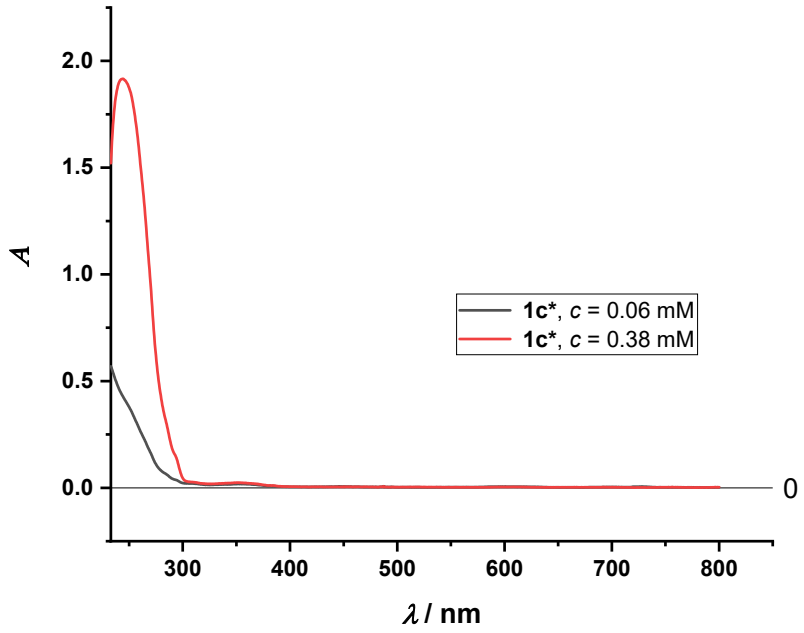

Figure S5. UV-Vis (CH_2Cl_2) of ligand **1c*** solution.

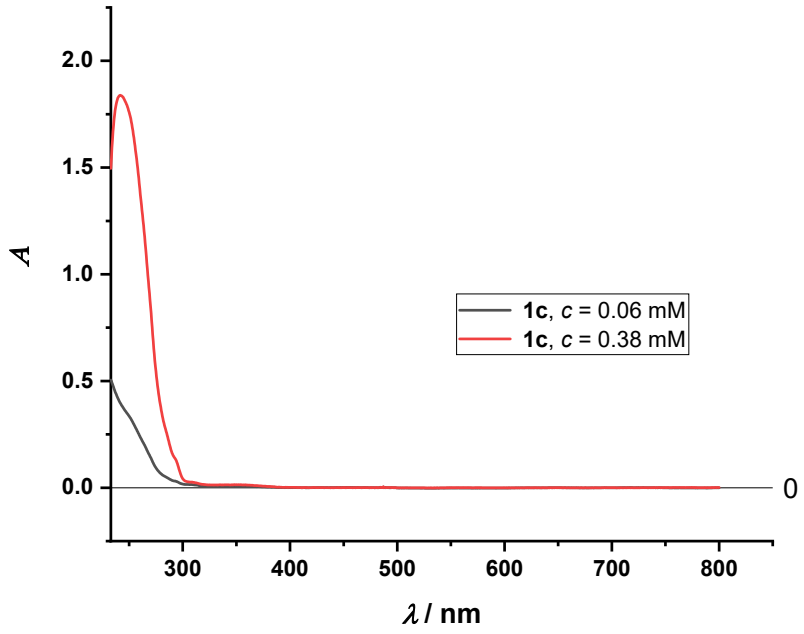

Figure S6. UV-Vis (CH_2Cl_2) of ligand **1c** solution.

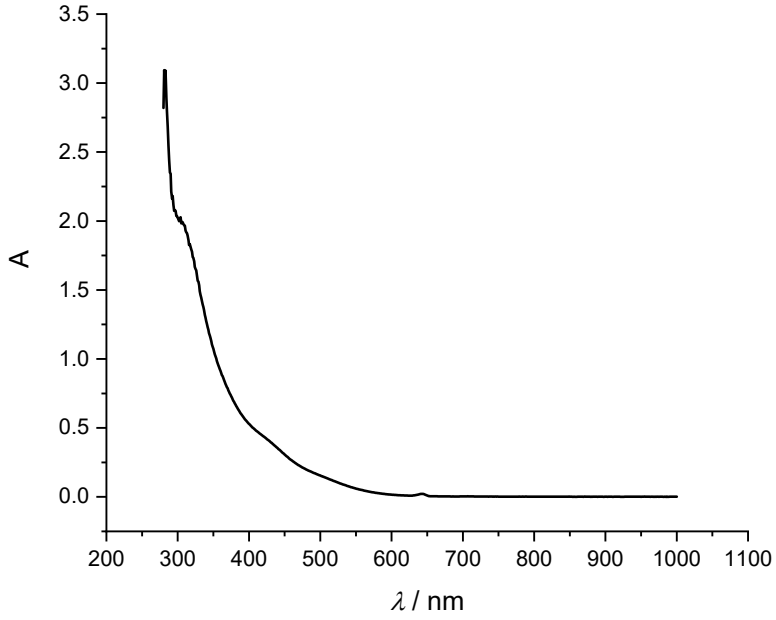

Figure S7. UV-Vis (CH_2Cl_2) of complex [Ir(COD)2]BArF solution. c(Ir) = 3.49mM.

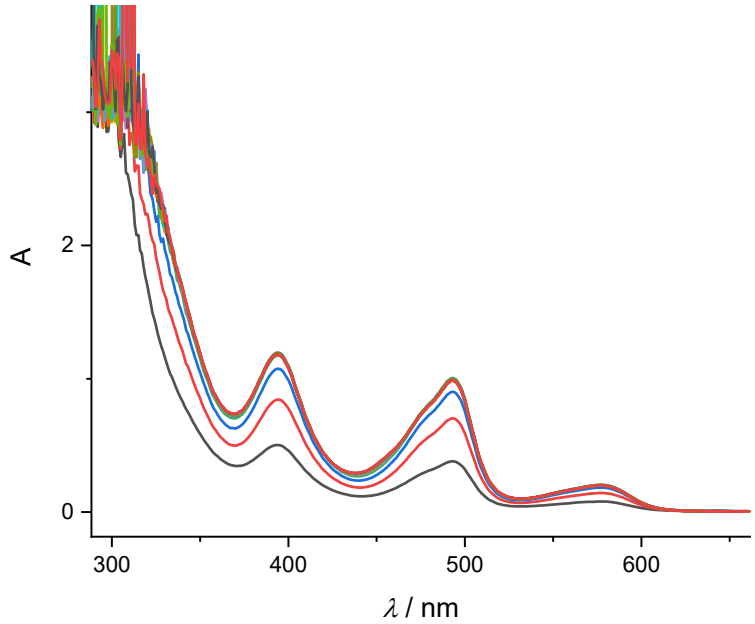

Figure S8. UV-Vis (CH_2Cl_2) of ligand **1p** and complex [Ir(COD)2]BArF solution recorded over a period of 60 minutes after injecting the metal precursor to the ligand solution. *c*(Ir) = 3.49 mM, Ir : **1p** = 1 : 1.

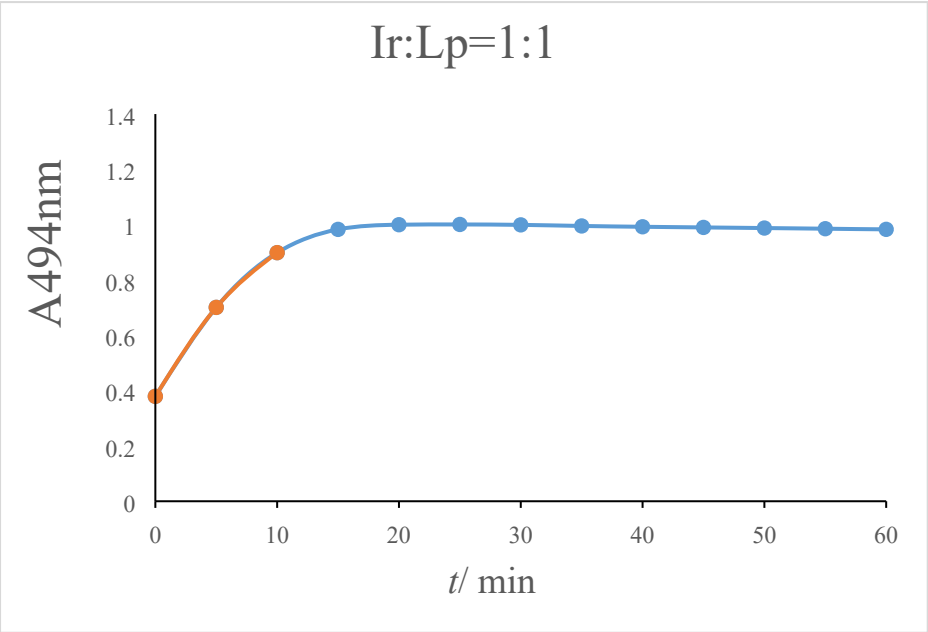

Figure S9. Change of abosrbance at 494 nm with time (CH_2Cl_2) of ligand **1p** and complex [Ir(COD)2]BArF solution.

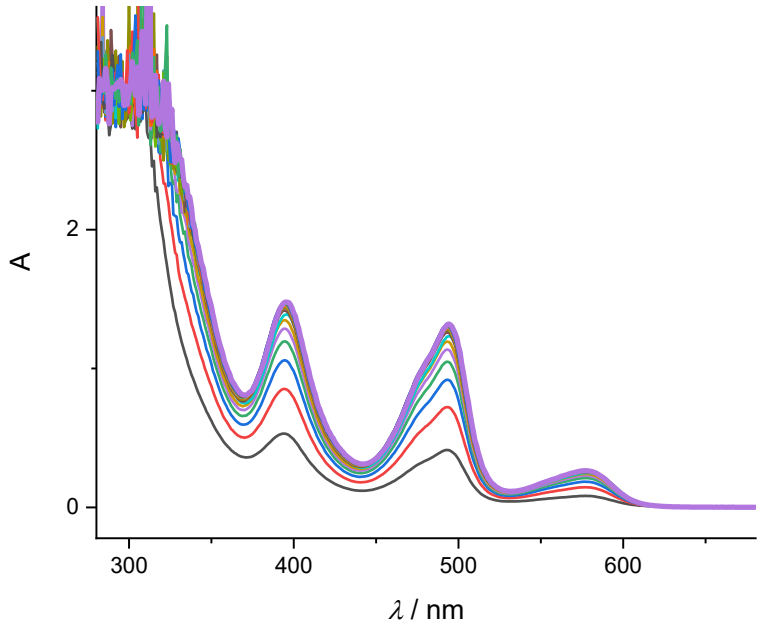

Figure S10. UV-Vis (CH_2Cl_2) of ligand **1p** and complex [Ir(COD)2]BArF solution recorded over a period of 60 minutes after injecting the metal precursor to the ligand solution. c(Ir) = 3.49 mM, Ir : **1p** = 1 : 2.

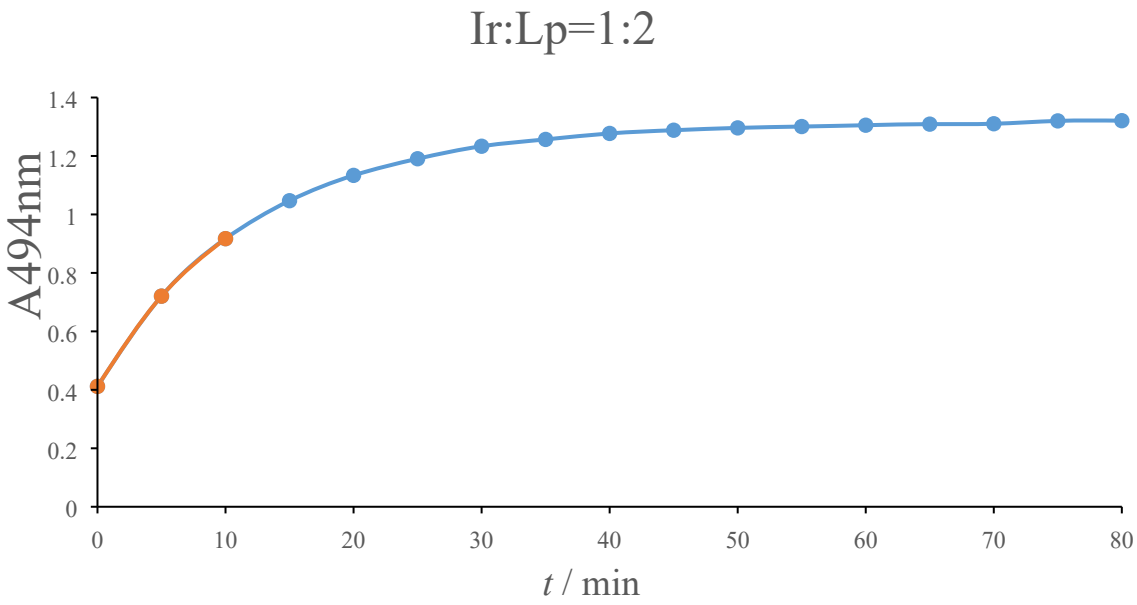

Figure S11.Change of abosrbance at 494nm with time (CH_2Cl_2) of ligand **1p** and complex [Ir(COD)2]BArF solution.

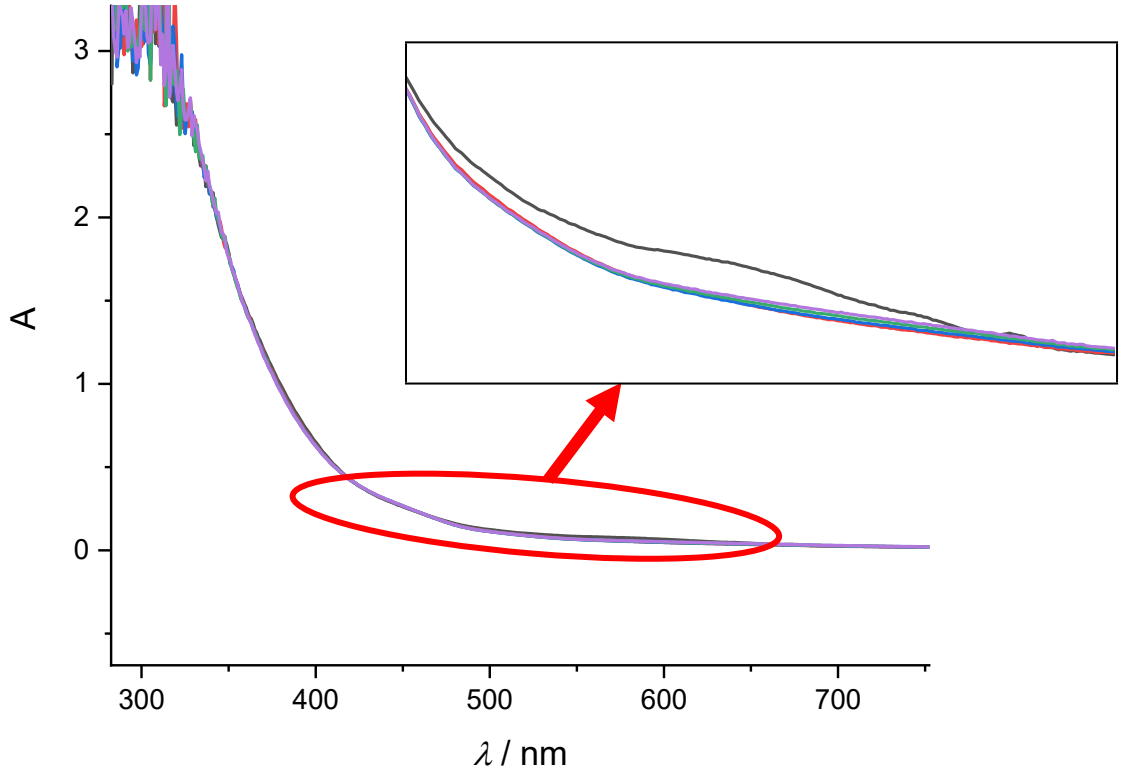

Figure S12.UV-Vis (CH_2Cl_2) of ligand **1b** and complex [Ir(COD)2]BArF solution recorded over a period of 60 minutes after injecting the metal precursor to the ligand solution. c(Ir) = 3.49 mM, Ir : **1b** = 1 : 2.

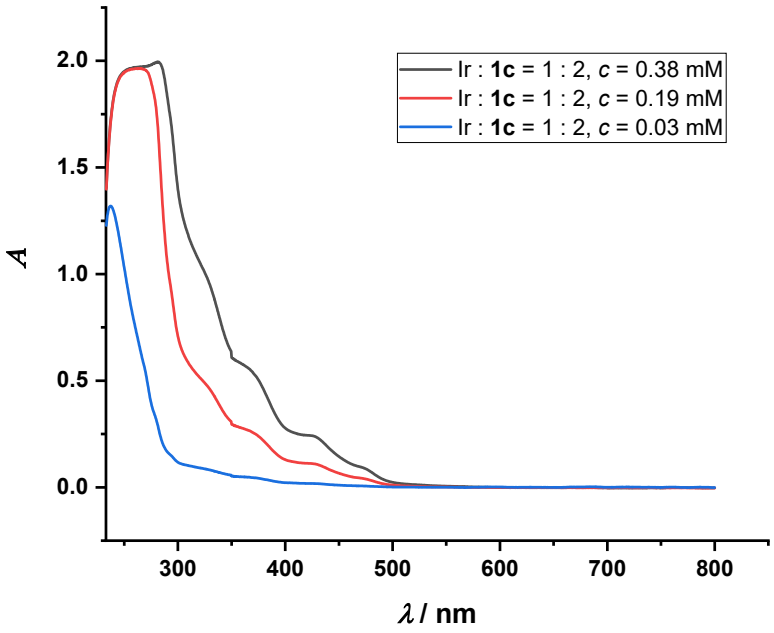

Figure S13. UV-Vis (CH_2Cl_2) of ligand **1c** and complex $[Ir(COD)_2]BArF$ solution Ir : **1c** = 1 : 2.

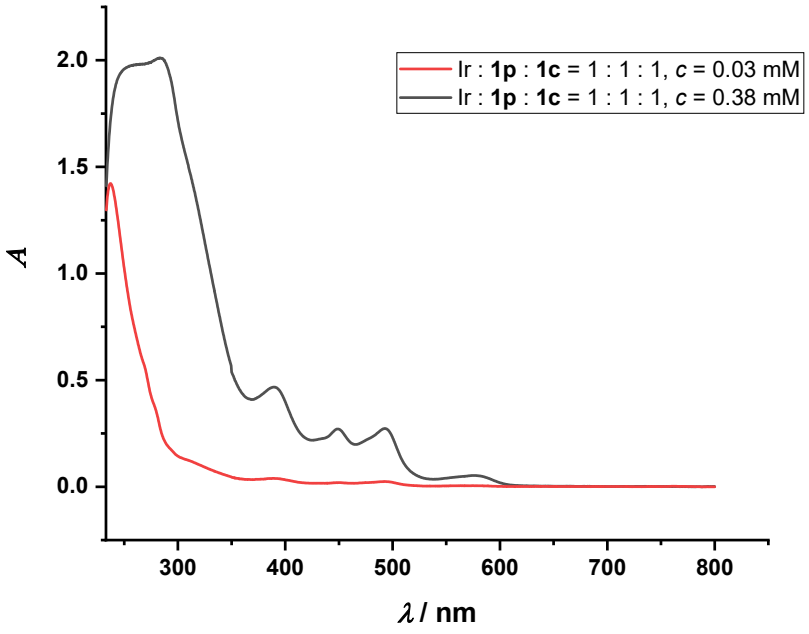

Figure S14. UV-Vis (CH_2Cl_2) of ligand **1p** and **1c** and complex $[Ir(COD)_2]BArF$ solution Ir : : **1p** : **1c** = 1 : 1 : 1.

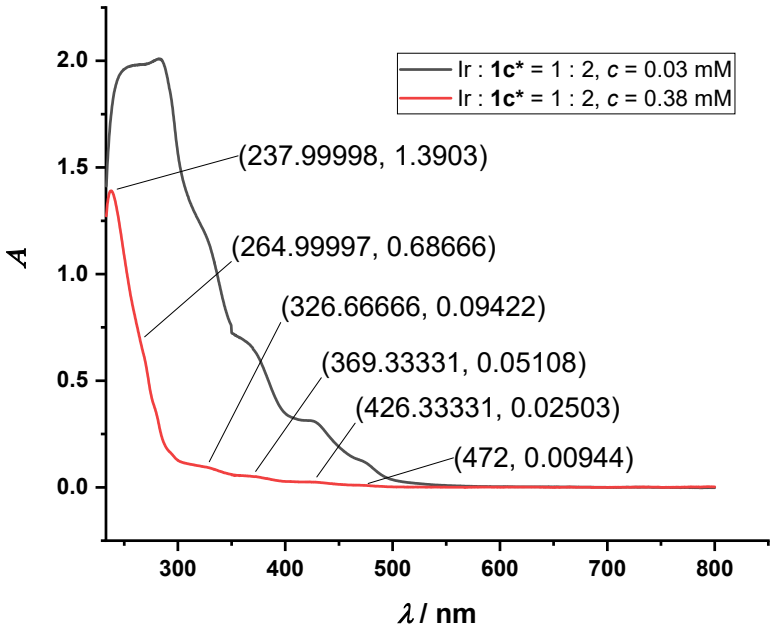

Figure S15. UV-Vis (CH_2Cl_2) of ligand **1c*** and complex $[Ir(COD)_2]BArF$ solution Ir : **1c*** = 1 : 2.

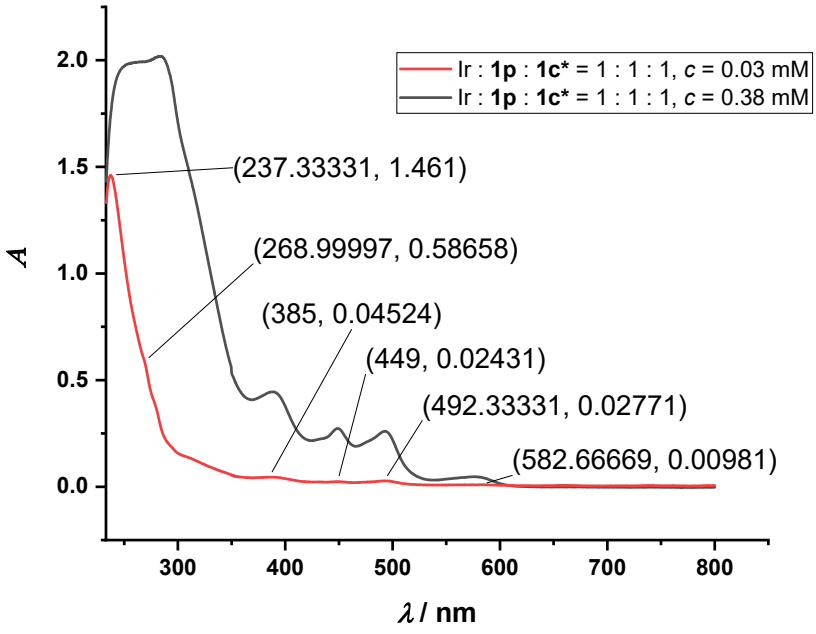

Figure S16. UV-Vis (CH_2Cl_2) of ligand **1p** and **1c*** and complex $[Ir(COD)_2]BArF$ solution Ir : : **1p** : **1c*** = 1 : 1 : 1.

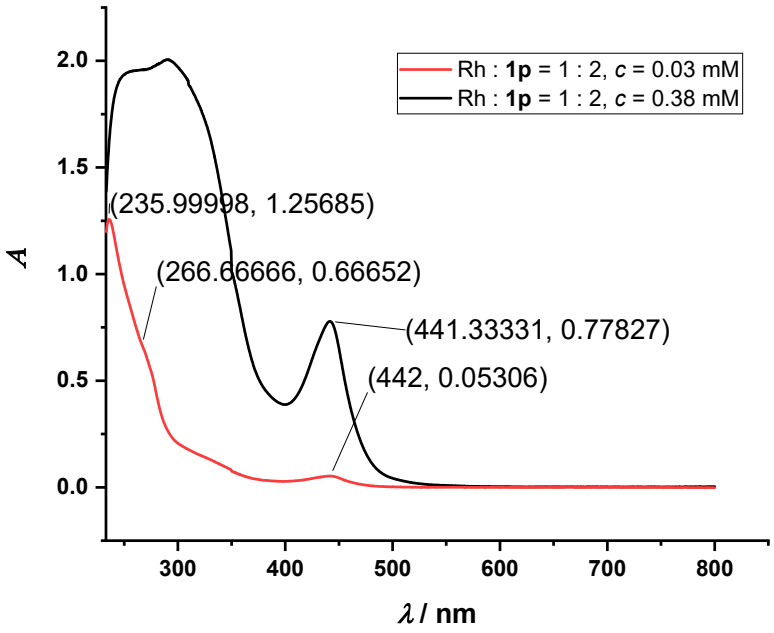

Figure S17. UV-Vis (CH_2Cl_2) of ligand **1p** and complex $[Rh(COD)_2]BF_4$ solution Rh : **1p** = 1 : 2.

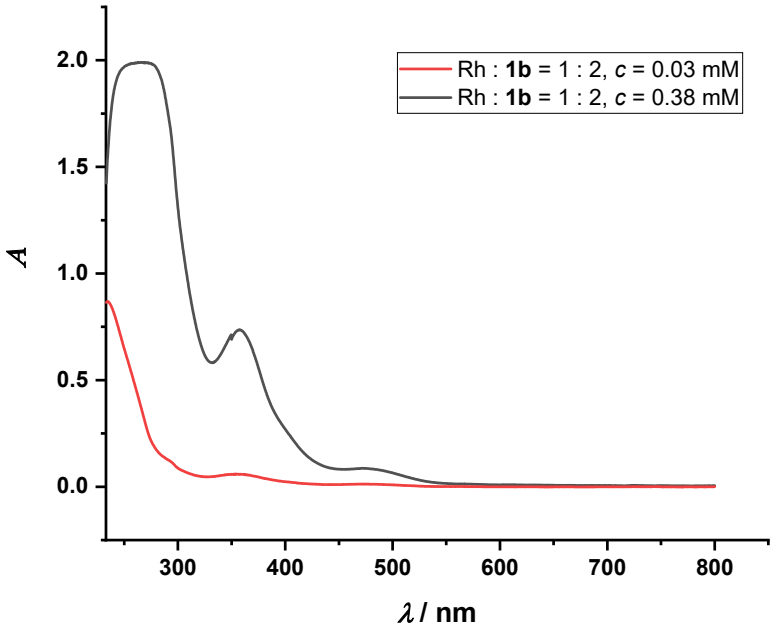

Figure S18. UV-Vis (CH_2Cl_2) of ligand **1b** and complex $[Rh(COD)_2]BF_4$ solution Rh : **1b** = 1 : 2.

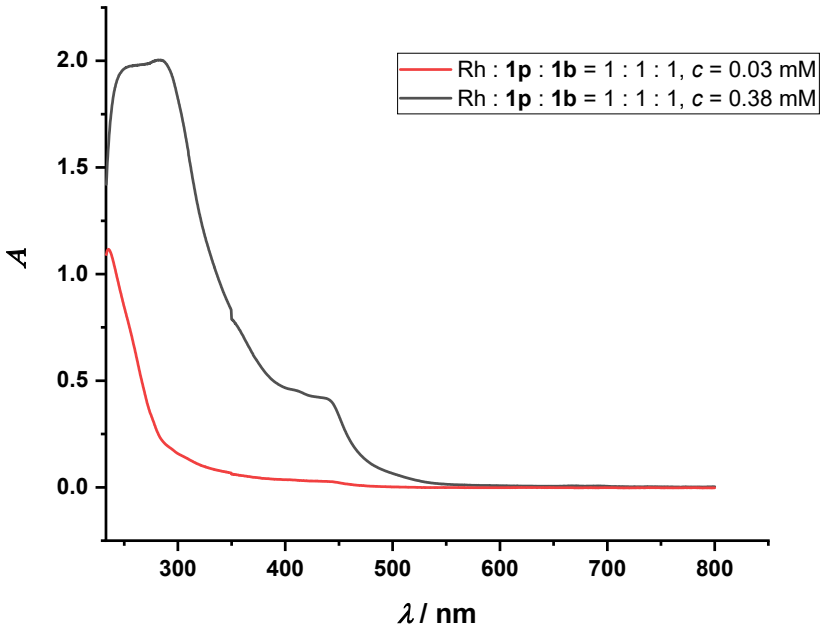

Figure S19. UV-Vis (CH_2Cl_2) of ligand **1p** and **1b** and complex $[Rh(COD)_{2]}BF_4$ solution Rh : **1p** : **1b** = 1 : 1 : 1.

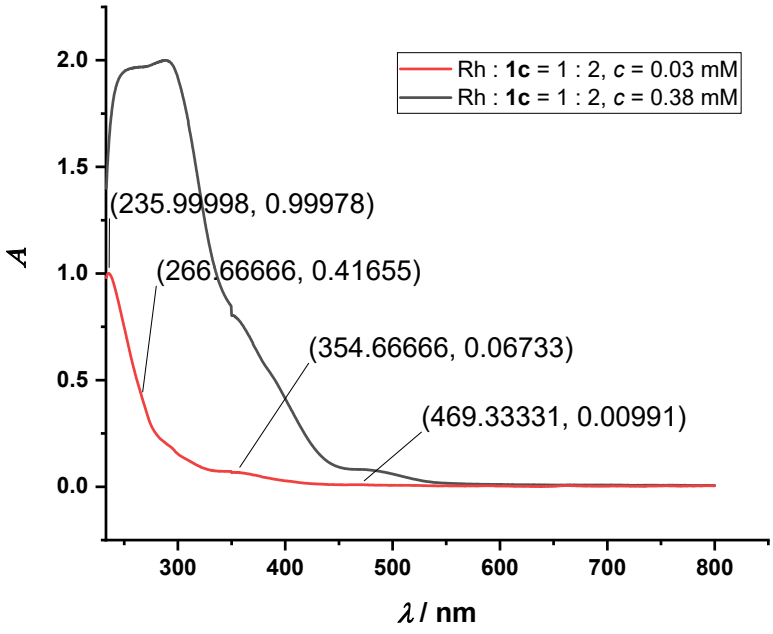

Figure S20. UV-Vis (CH_2Cl_2) of ligand **1c** and complex $[Rh(COD)_{2]}BF_4$ solution Rh : **1c** = 1 : 2.

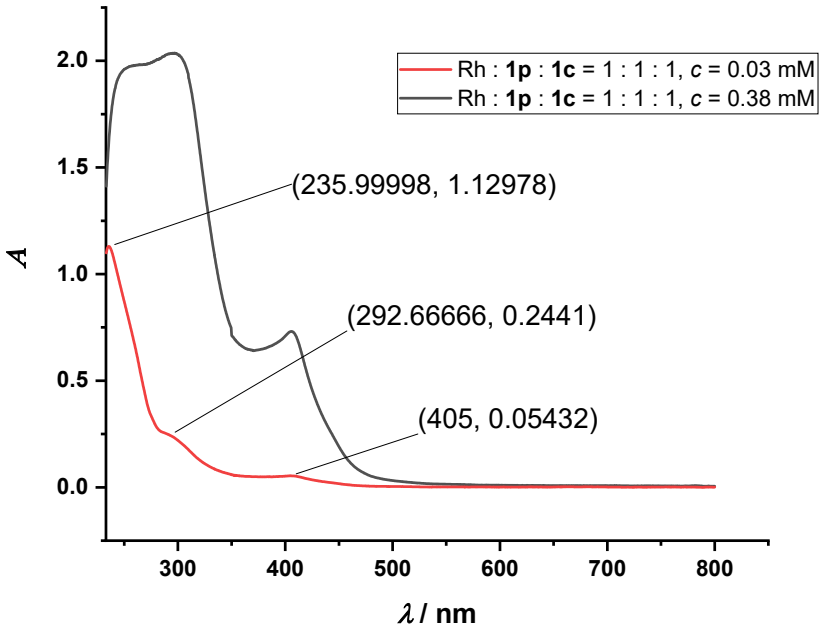

Figure S21. UV-Vis (CH_2Cl_2) of ligand **1p** and **1c** and complex $[Rh(COD)_2]BF_4$ solution Rh : **1p** : **1c** = 1 : 1 : 1.

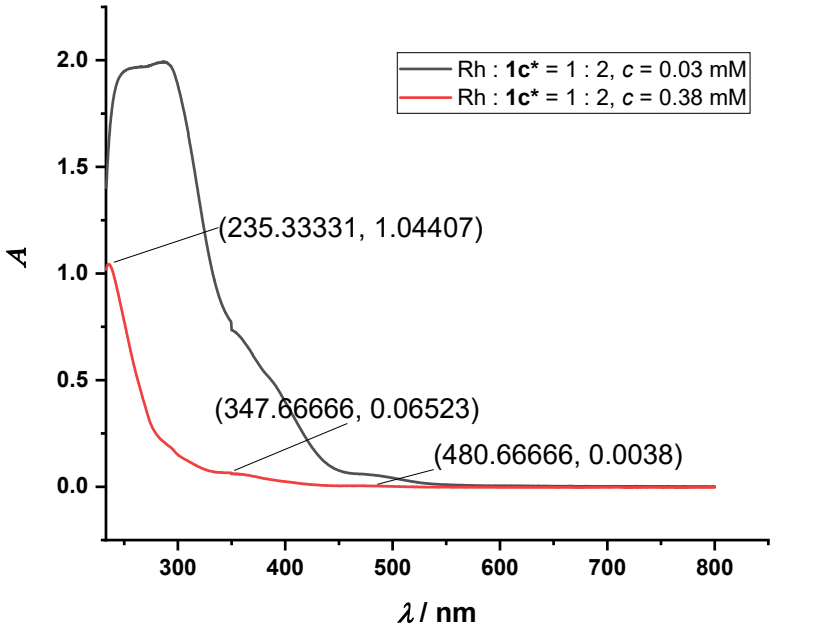

Figure S22. UV-Vis (CH_2Cl_2) of ligand **1c*** and complex $[Rh(COD)_2]BF_4$ solution Rh : **1c*** = 1 : 2.

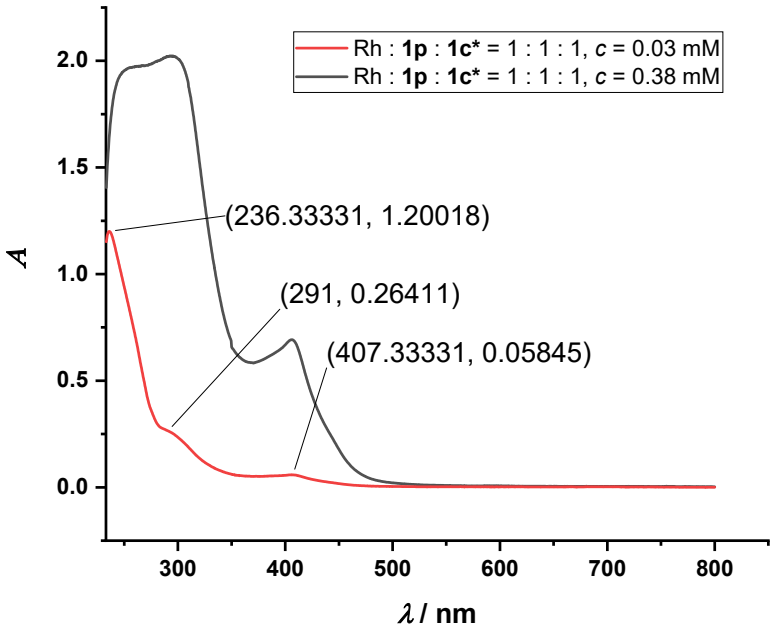

Figure S23. UV-Vis (CH_2Cl_2) of ligand **1p** and **1c*** and complex $[Rh(COD)_2]BF_4$ solution Rh : **1p** : **1c*** = 1 : 1 : 1.

5. CD Spectra

Several concentrations, namely *c*(M) = 0.03, 0.38mM and 3.49 mM, have been recorded for several precatalytic complexes. In almost all cases, the ellipticity in the UV region was too high for the detector sensitivity at concentrations of 0.38 mM and above. These higher concentrations, however, have been recorded to obtain higher ellipticity value of peaks in the visible region of the spectra.

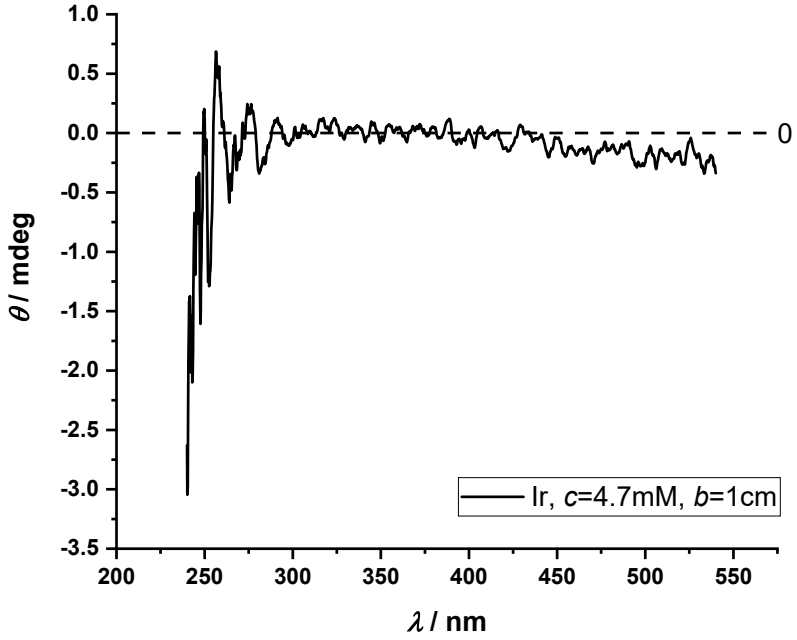

Figure S24. CD (CH_2Cl_2) of $[Ir(COD)_2]$BArF solution.

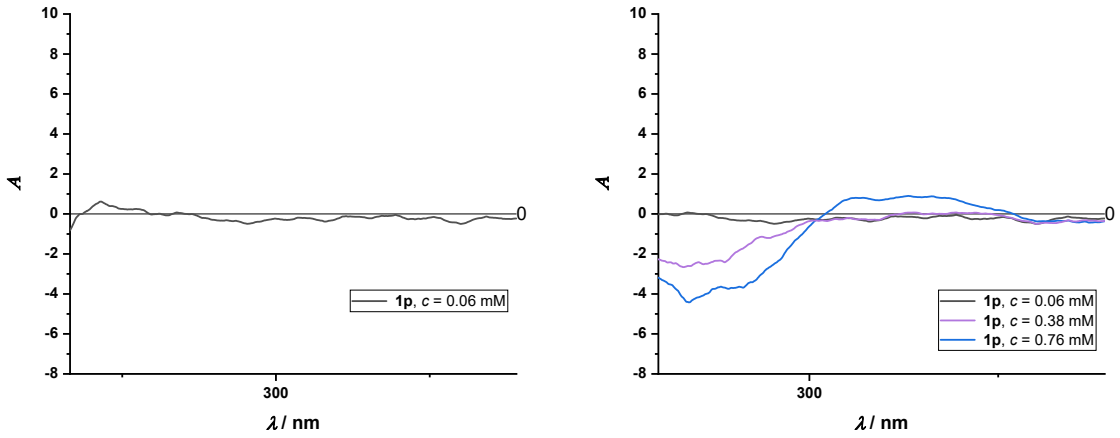

Figure S25. CD (CH_2Cl_2) of **1p** solution.

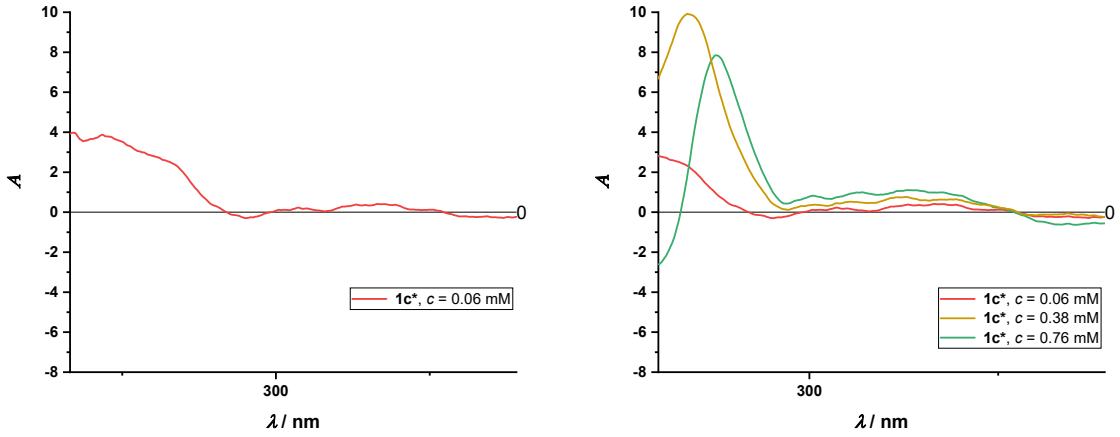

Figure S26. CD (CH_2Cl_2) of **1c*** solution.

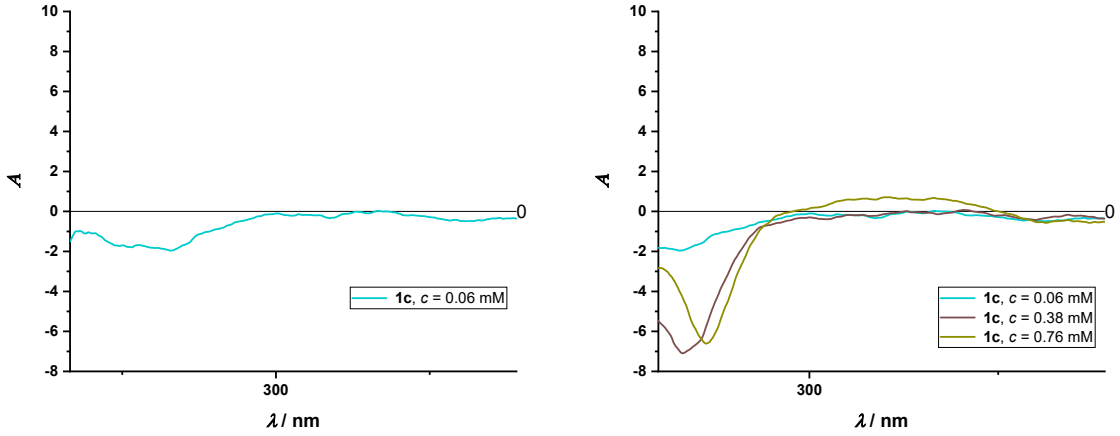

Figure S27. CD (CH_2Cl_2) of **1c** solution.

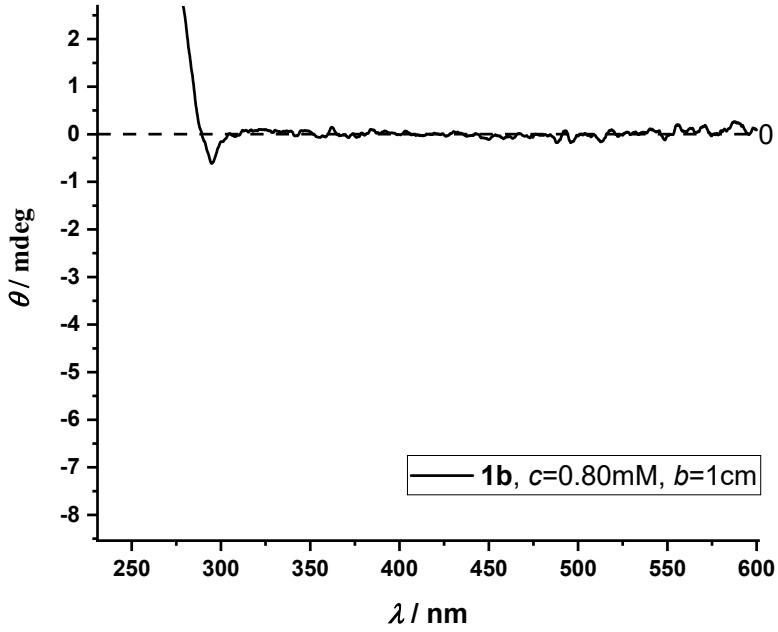

Figure S28. CD (CH_2Cl_2) of **1b** solution.

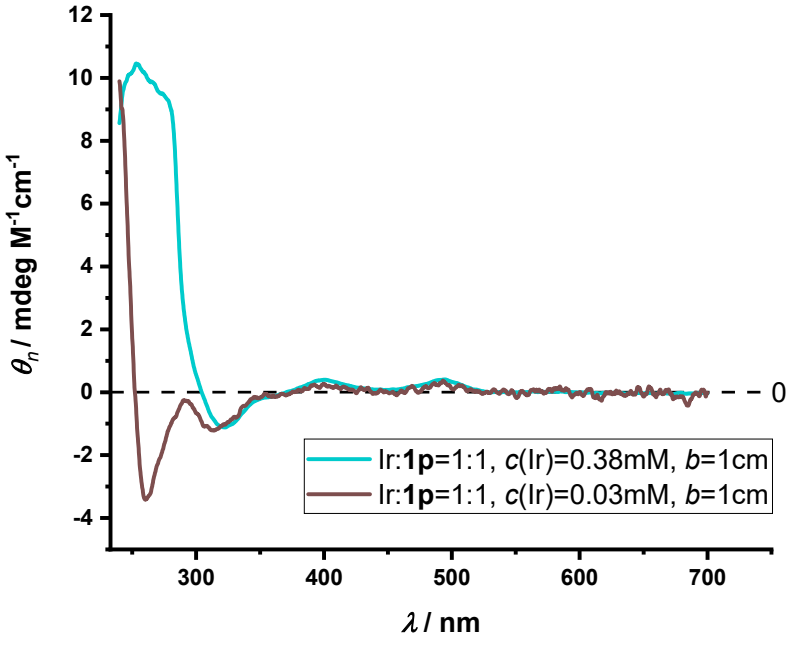

Figure S29. Normalized CD spectrum (CH_2Cl_2) of Ir:**1p**= 1:1 solution. $\theta_n = \theta/(c(\mathrm{Ir})\cdot b\cdot 32982)$.

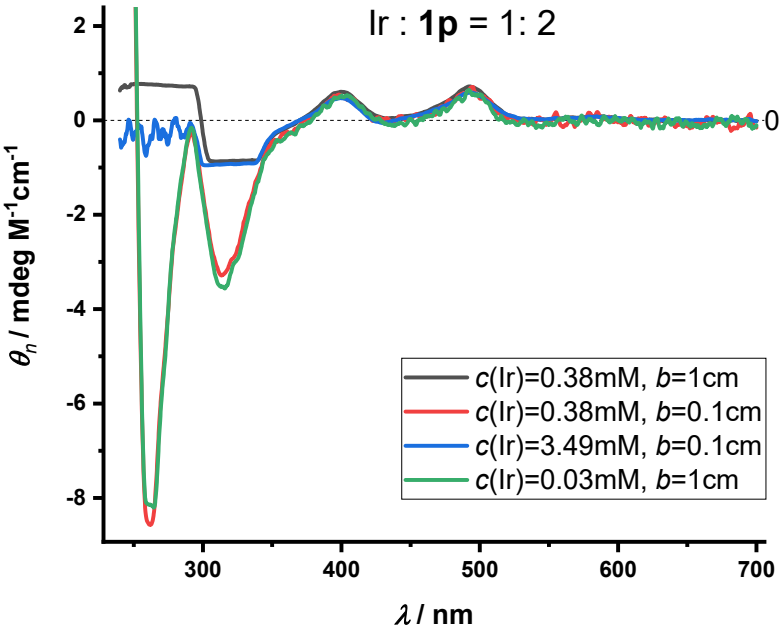

Figure S30. Normalized CD spectra (CH_2Cl_2) of Ir:**1p**= 1:2 solution. $\theta_n = \theta/(c(\mathrm{Ir})\cdot b\cdot 32982)$.

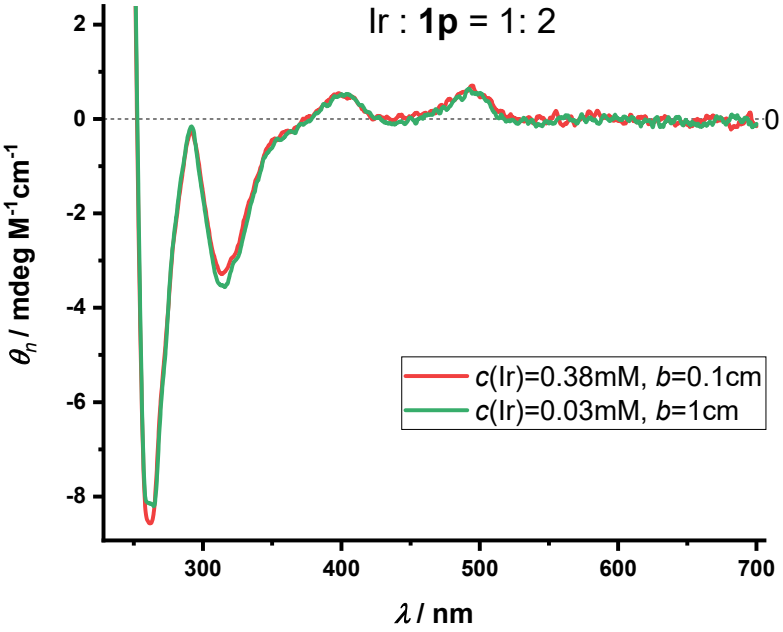

Figure S31. Normalized CD spectra (CH_2Cl_2) of Ir:**1p**= 1:2 solution; UV region. $\theta_n = \theta/(c(\mathrm{Ir})\cdot b\cdot 32982)$.

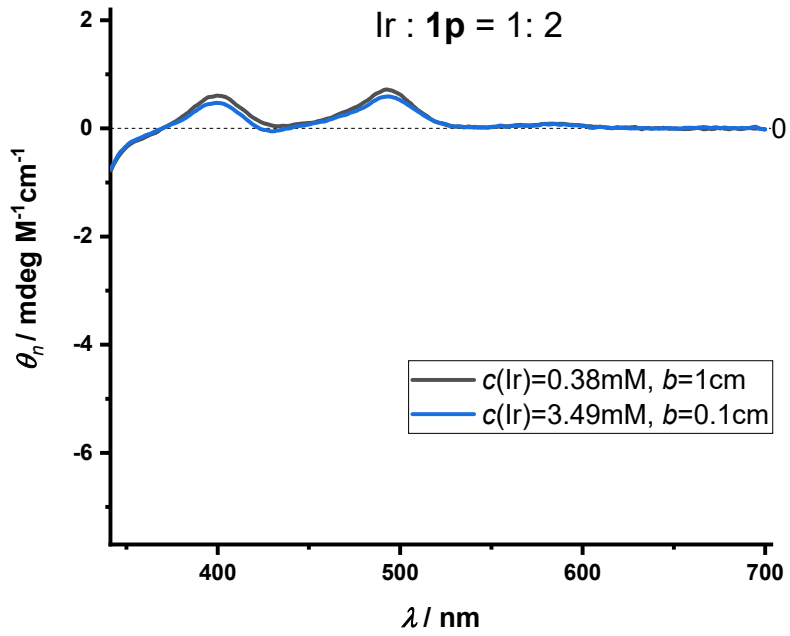

Figure S32. Normalized CD spectra (CH_2Cl_2) of Ir:**1p**= 1:2 solution; VIS region. $\theta_n = \theta/(c(\mathrm{Ir})\cdot b\cdot 32982)$

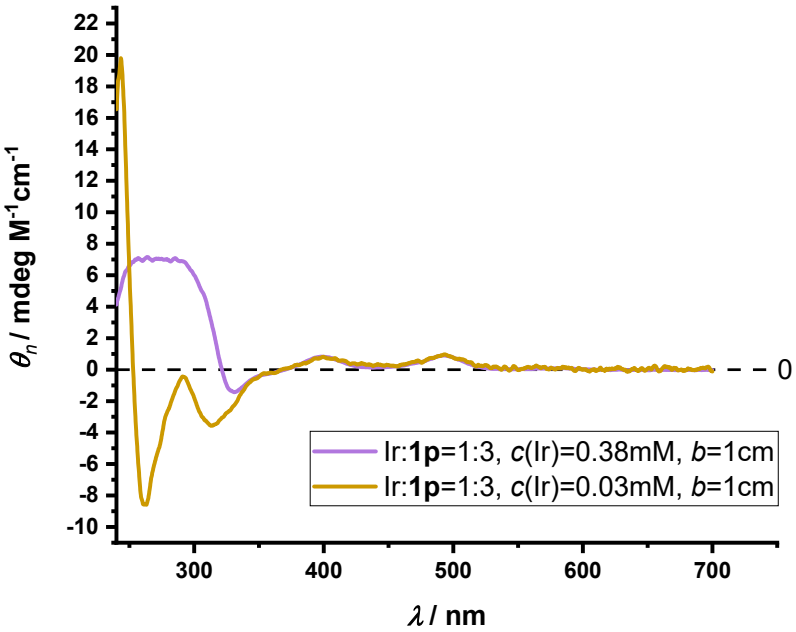

Figure S33. Normalized CD spectra (CH_2Cl_2) of Ir:**1p**= 1:3 solution. $\theta_n = \theta/(c(\mathrm{Ir})\cdot b\cdot 32982)$

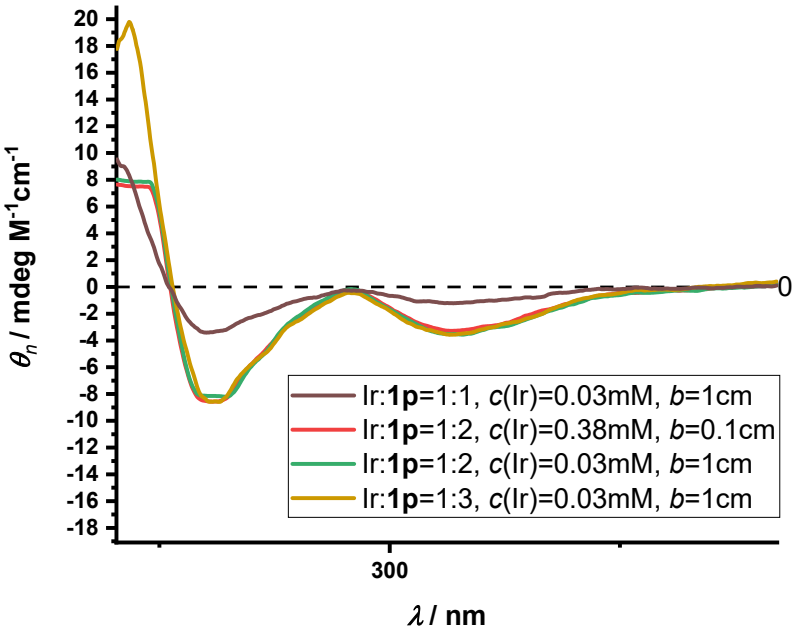

Figure S34. Normalized CD spectra (CH_2Cl_2) of Ir:**1p**= 1:1, 1:2 and 1:3 solutions, UV-area. $\theta_n = \theta/(c(\mathrm{Ir})\cdot b\cdot 32982)$

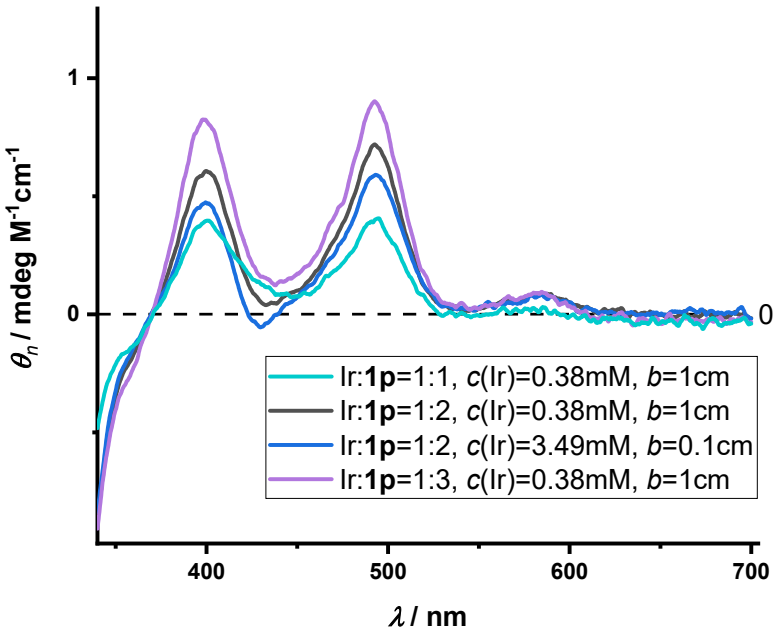

Figure S35. Normalized CD spectra (CH_2Cl_2) of Ir:**1p**= 1:1,1:2 and 1:3 solutions, VIS-area. $\theta_n = \theta/(c(\mathrm{Ir})\cdot b\cdot 32982)$.

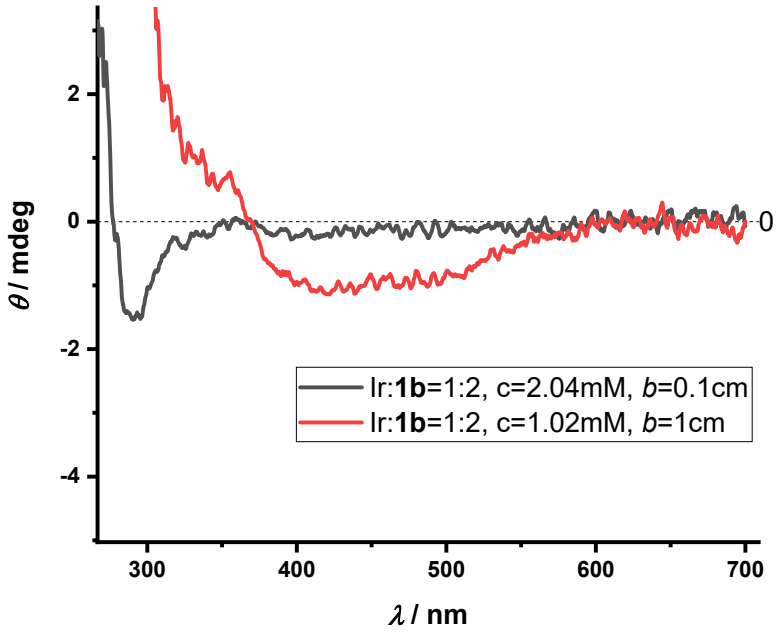

Figure S36. CD spectra (CH_2Cl_2) of Ir:**1b**= 1:2 solution

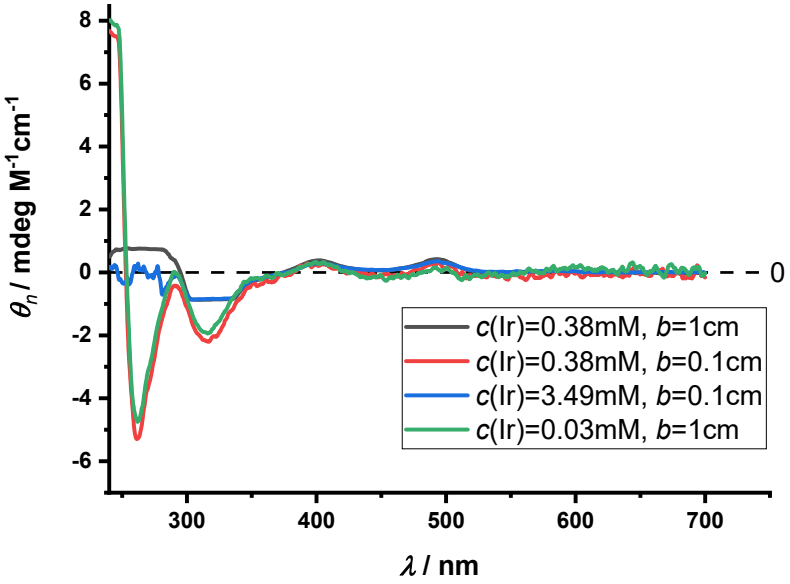

Figure S37. Normalized CD spectra (CH_2Cl_2) of Ir:**1p**:**1b**= 1:1:1 solution. $\theta_n = \theta/(c(\mathrm{Ir})\cdot b\cdot 32982)$.

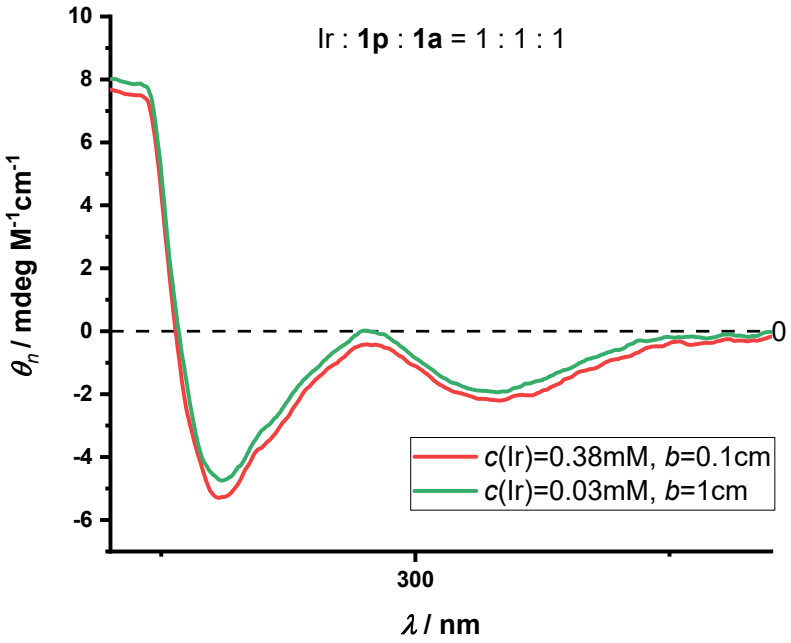

Figure S38. Normalized CD spectra (CH_2Cl_2) of Ir:**1p**:**1b**= 1:1:1 solution, UV-area. $\theta_n = \theta/(c(\mathrm{Ir})\cdot b\cdot 32982)$.

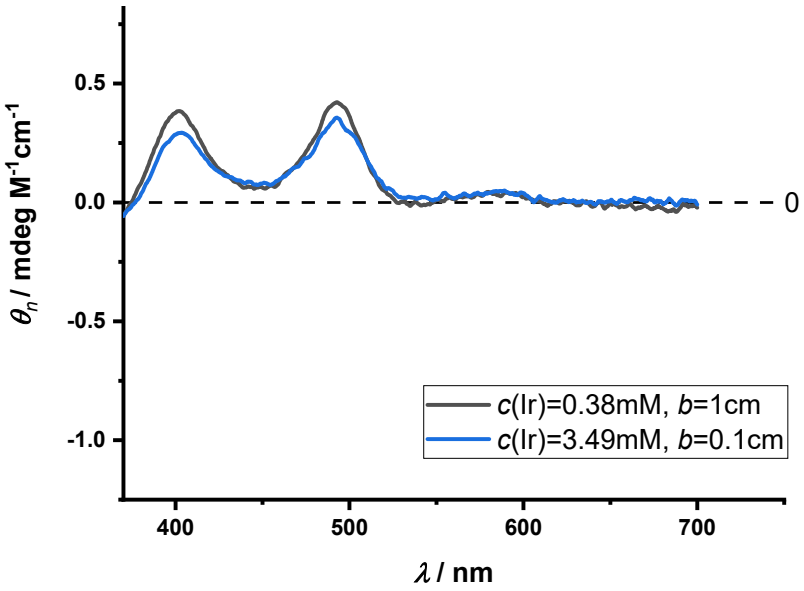

Figure S39. CD (CH_2Cl_2) of Ir:**1p**:**1b**= 1:1:1 solution, VIS-area. $\theta_n = \theta/(c(\mathrm{Ir})\cdot b\cdot 32982)$.

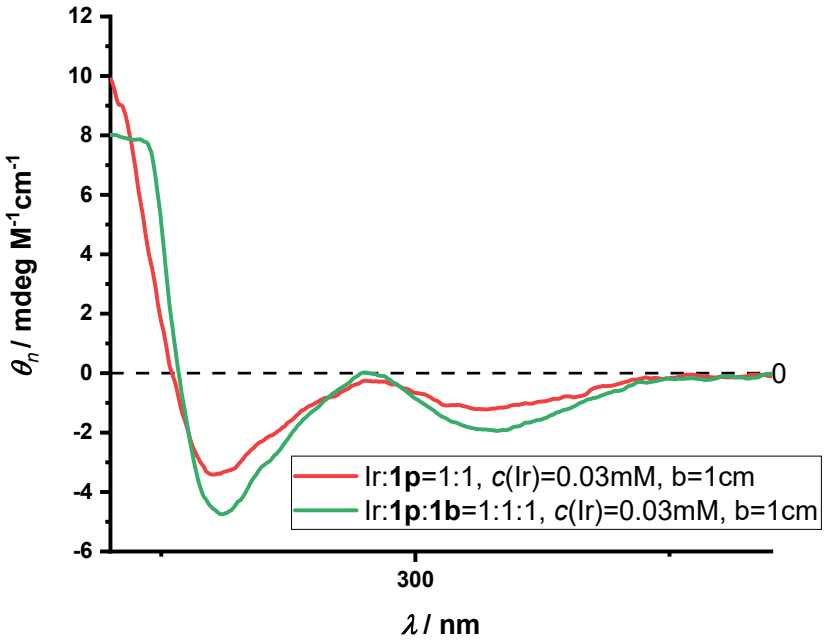

Figure S40. Overlapped normalized CD spektra of (CH_2Cl_2) of Ir:**1p**= 1:1 and Ir:**1p**:**1b**= 1:1:1 solution. UV area. $\theta_n = \theta/(c(\mathrm{Ir})\cdot b\cdot 32982)$.

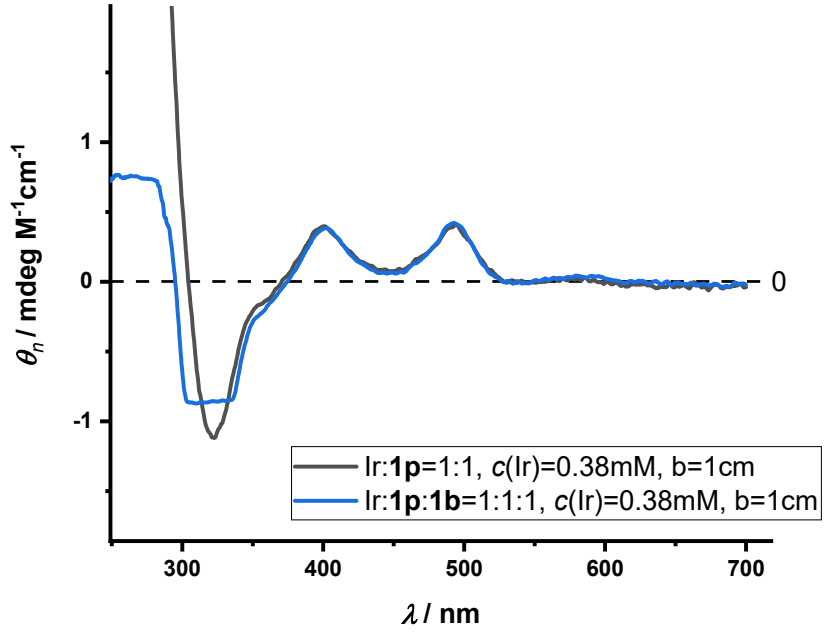

Figure S41. Normalized CD spektra of (CH_2Cl_2) of Ir:**1p**= 1:1 and Ir:**1p**:**1b**= 1:1:1 solution.VIS area. $\theta_n = \theta/(c(\mathrm{Ir})\cdot b\cdot 32982)$.

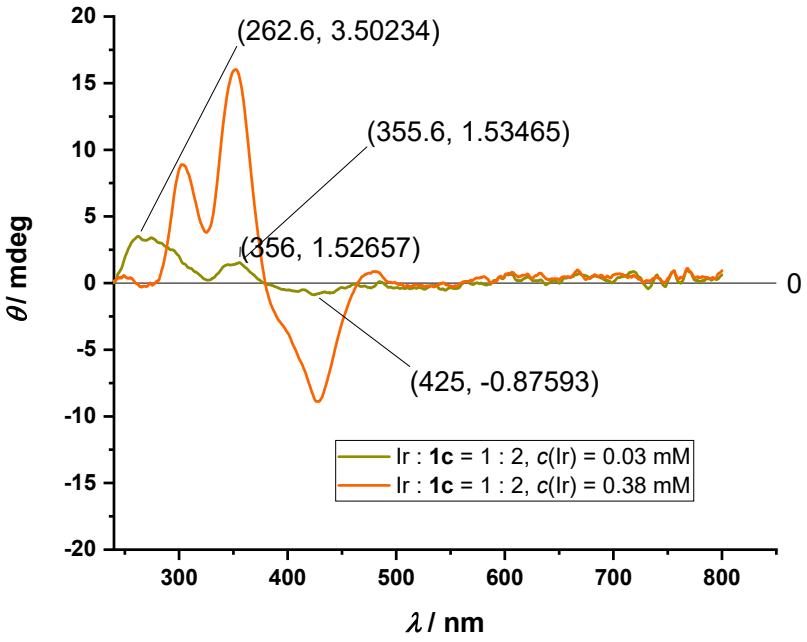

Figure S42. CD spectrum (CH_2Cl_2) of Ir : **1c** = 1 : 2 solutions.

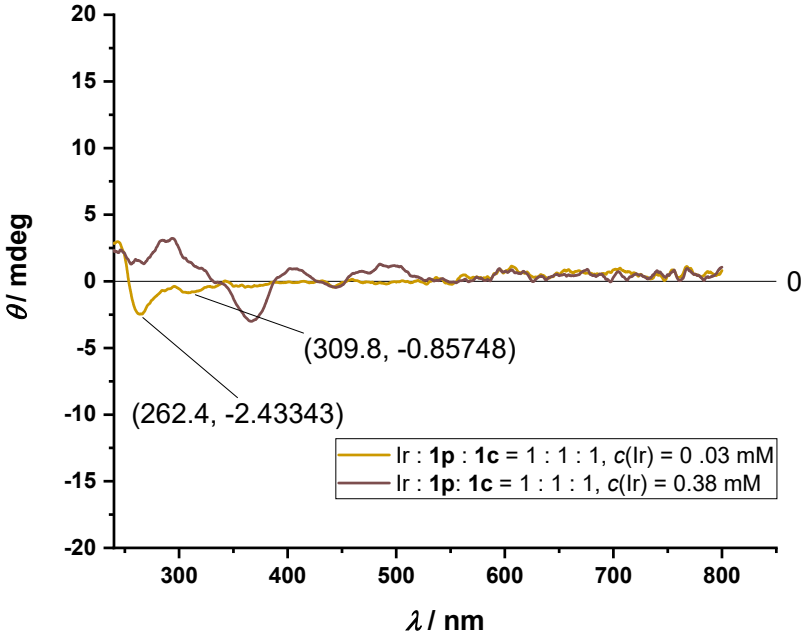

Figure S43. CD spectrum (CH_2Cl_2) of Ir : **1p** : **1c** = 1 : 1 : 1 solutions.

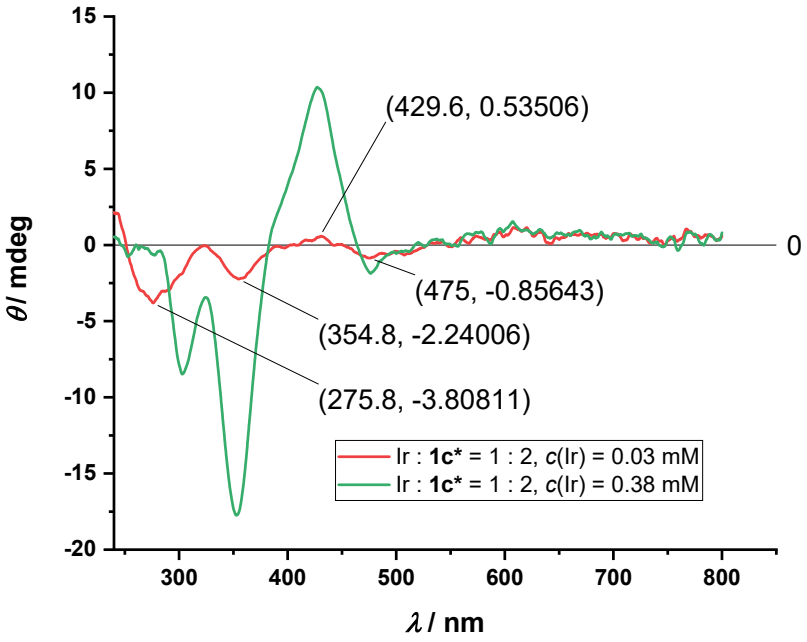

Figure S44. CD spectrum (CH_2Cl_2) of Ir : **1c*** = 1 : 2 solutions.

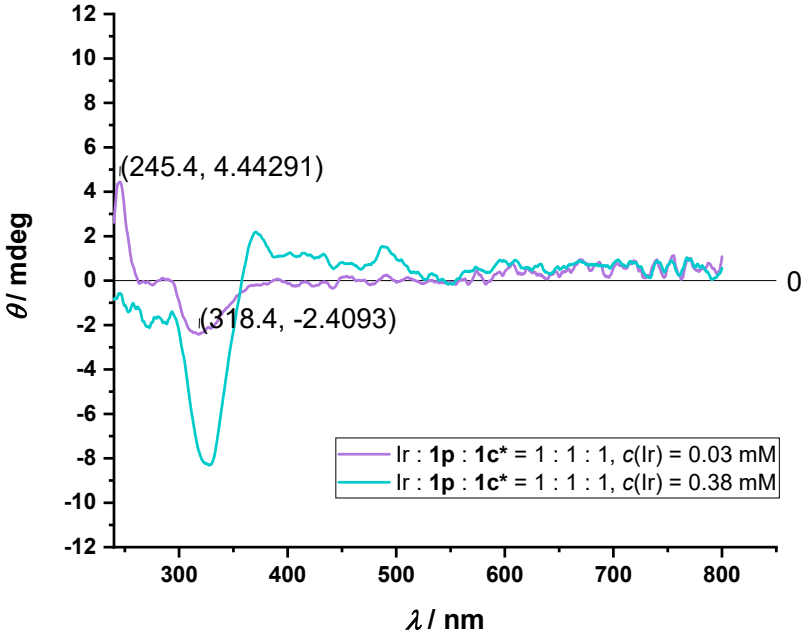

Figure S45. CD spectra (CH_2Cl_2) of Ir:**1p** : **1c***= 1:1 : 1 solutions.

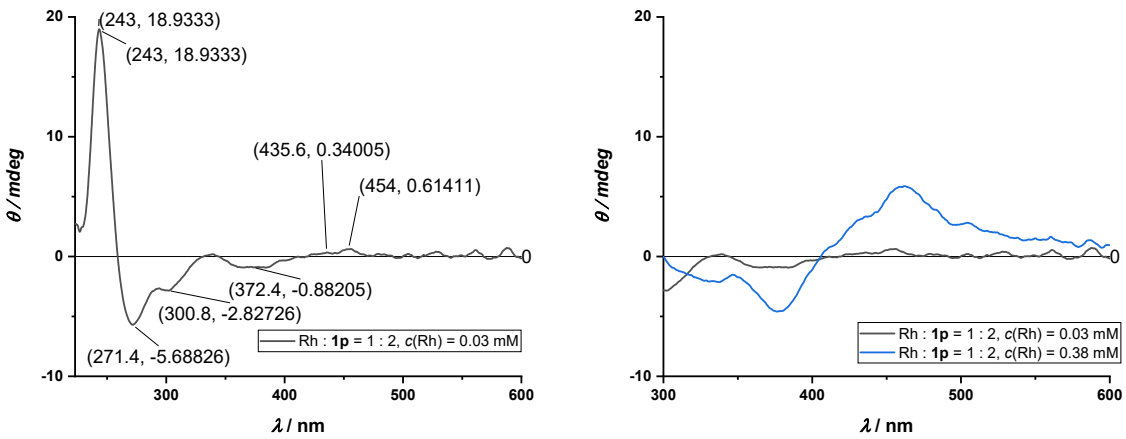

Figure S46. CD spectrum (CH_2Cl_2) of Rh : **1p** = 1 : 2 solutions.

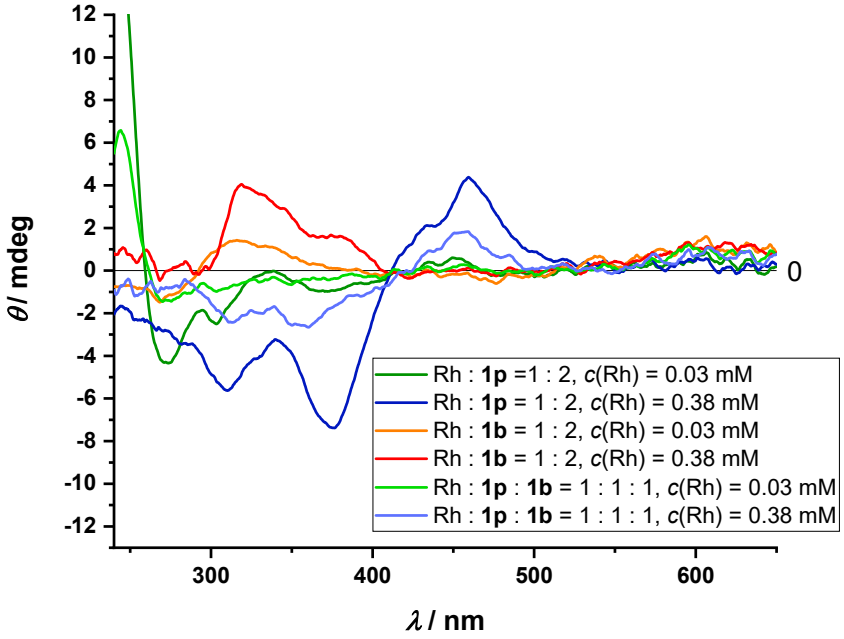

Figure S47. CD spectrum (CH_2Cl_2) of $[Rh(COD)_2]BF_4$ and **1p** and **1b** ligand solutions.

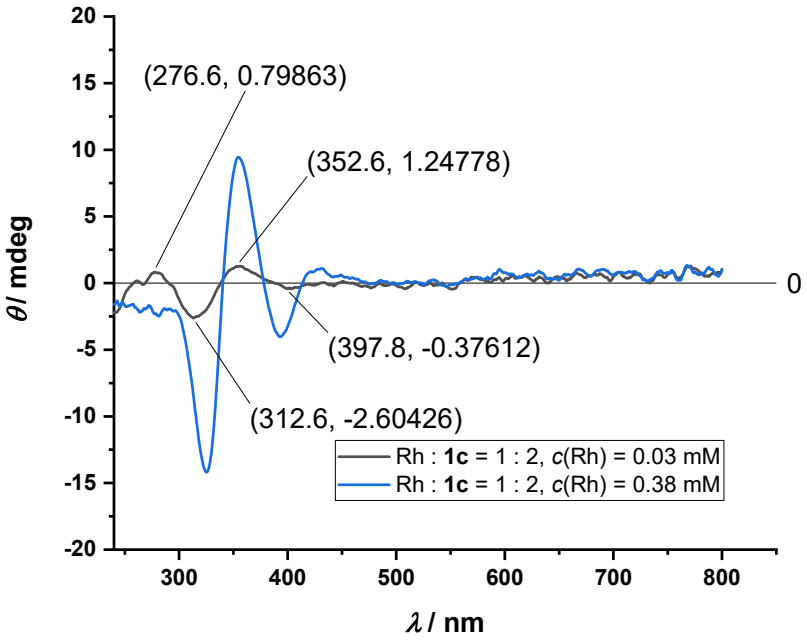

Figure S48. CD spectrum (CH_2Cl_2) of Rh : **1c** = 1 : 2 solutions.

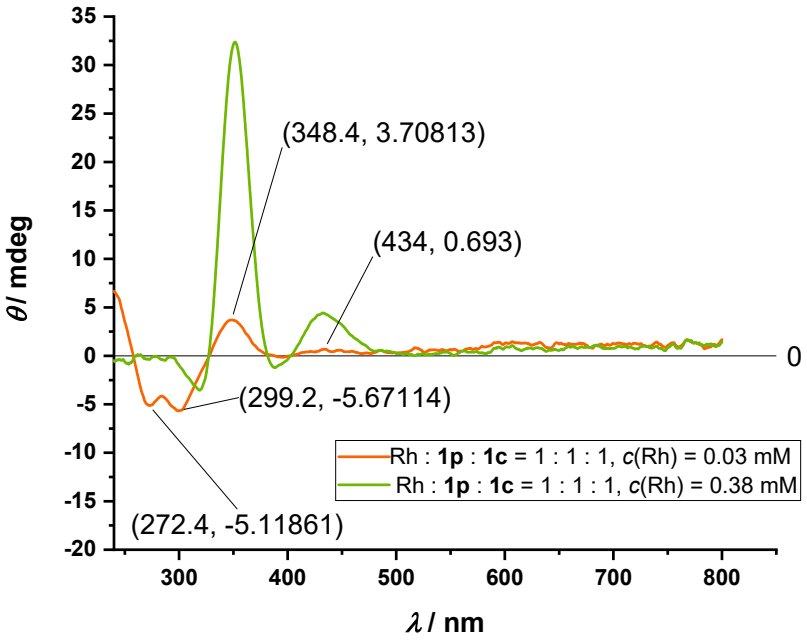

Figure S49. CD spectrum (CH_2Cl_2) of Rh : **1p** : **1c** = 1 : 1 : 1 solutions.

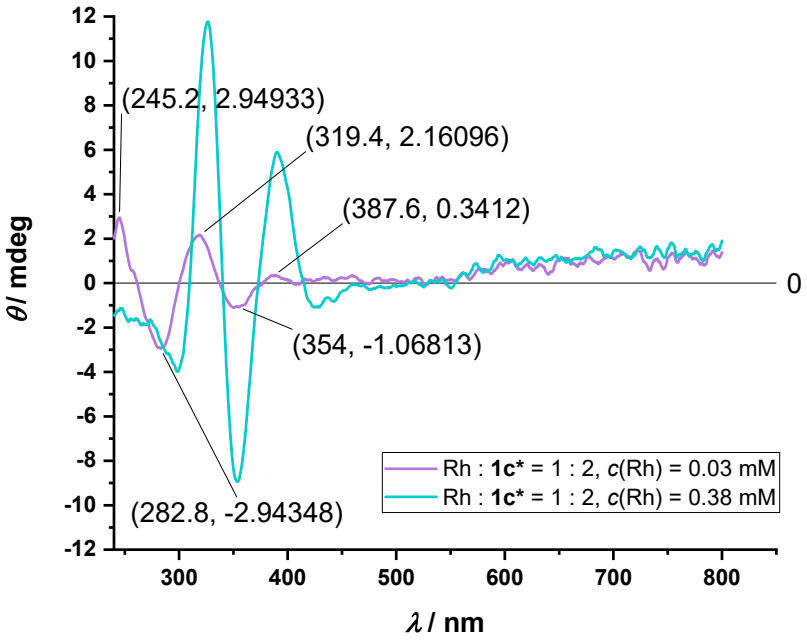

Figure S50. CD spectrum (CH_2Cl_2) of Rh : **1c*** = 1 : 2 solutions.

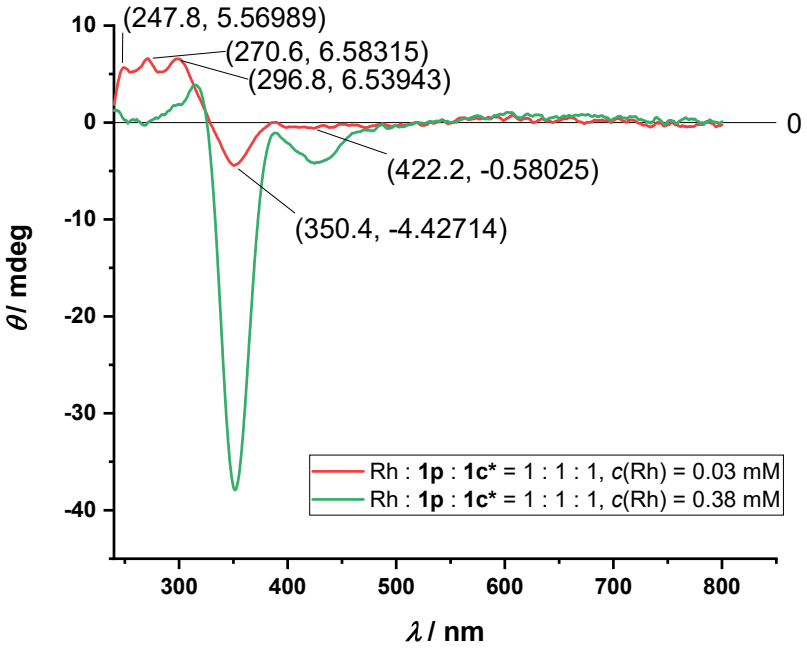

Figure S51. CD spectrum (CH_2Cl_2) of Rh : **1p** : **1c*** = 1 : 1 : 1 solutions.

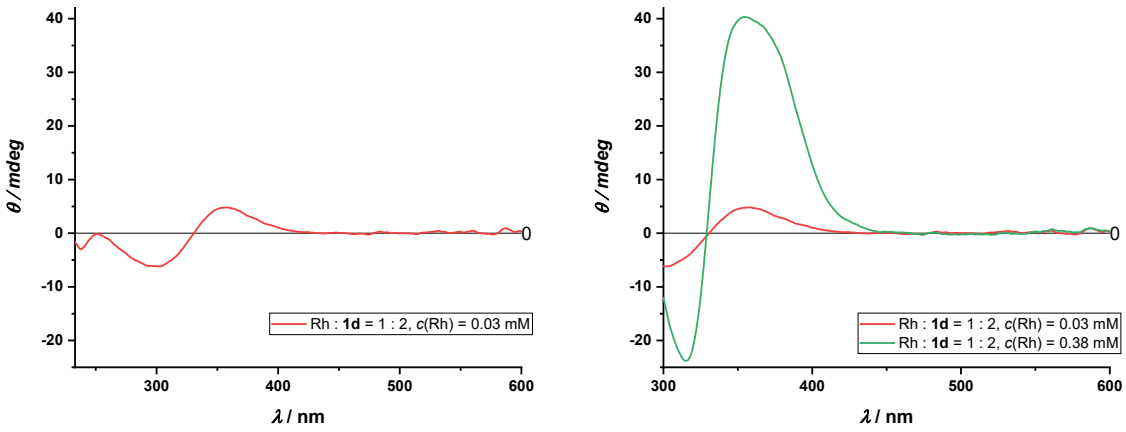

Figure S52. CD spectrum (CH_2Cl_2) of Rh : **1d** = 1 : 2 solutions.

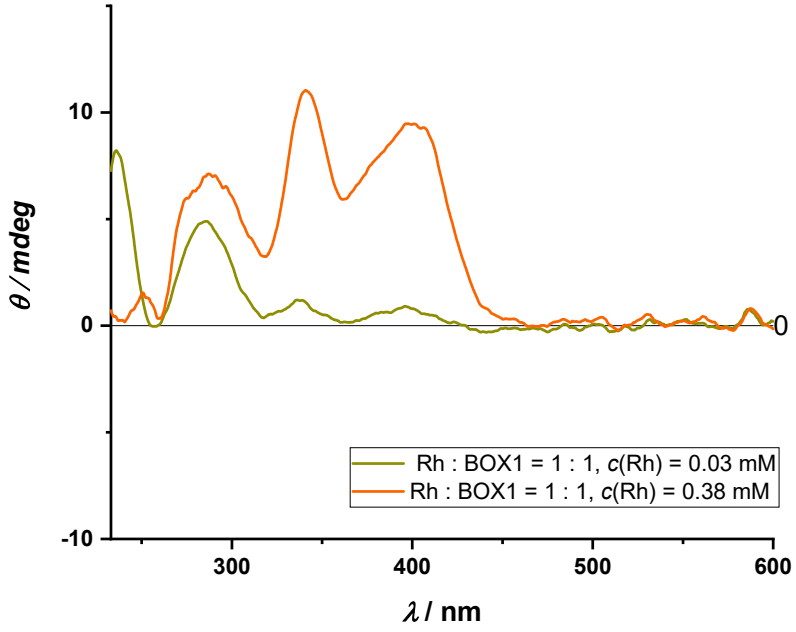

Figure S53. CD spectrum (CH_2Cl_2) of Rh : BOX1 = 1 : 1 solutions. BOX1 = (−)-2,2′-Isopropylidenebis[(4S)-4-phenyl-2-oxazoline]. Ligand BOX1 is a commercially available ligand. CD spectra of precatalytic complex with rhodium have been recorded for purpose of comparison with our complexes.

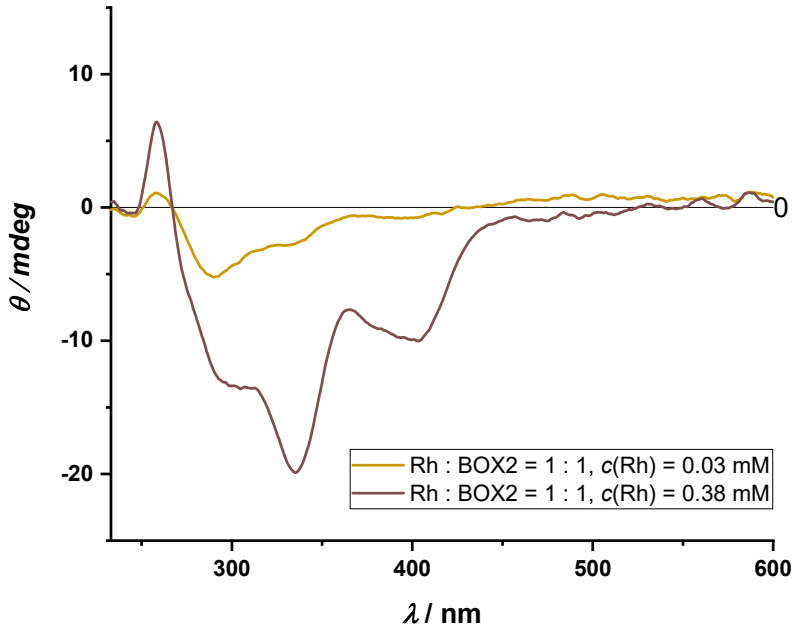

Figure S54. CD spectrum (CH_2Cl_2) of Rh : BOX2 = 1 : 1 solutions. BOX2 = (+)-2,2'-Isopropylidenebis[(4R)-4-benzyl-2-oxazoline]. Ligand BOX1 is a commercially available ligand. CD spectra of precatalytic complex with rhodium have been recorded for purpose of comparison with our complexes.

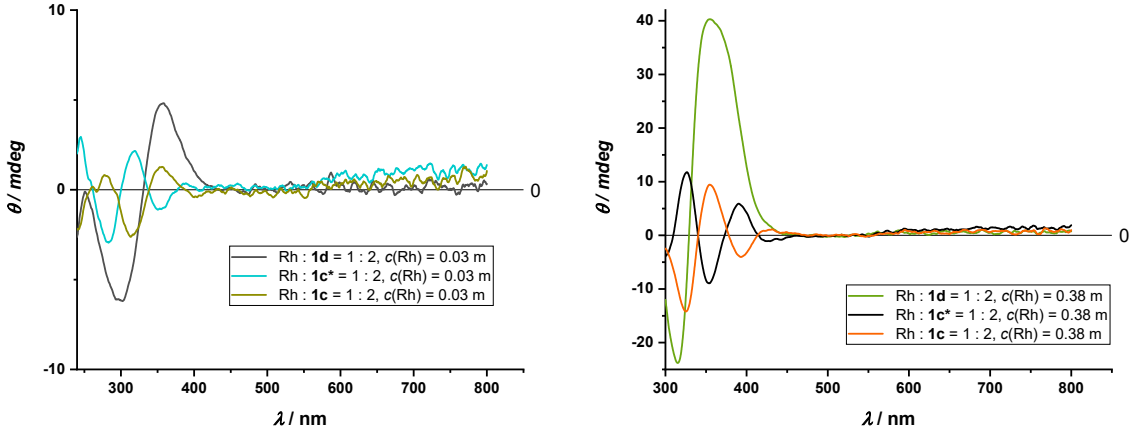

Figure S55. CD spectrum (CH_2Cl_2) of Rh : 1**c** = 1 : 2, Rh : 1**c*** = 1 : 2 and Rh : 1**d** = 1 : 2 solutions.

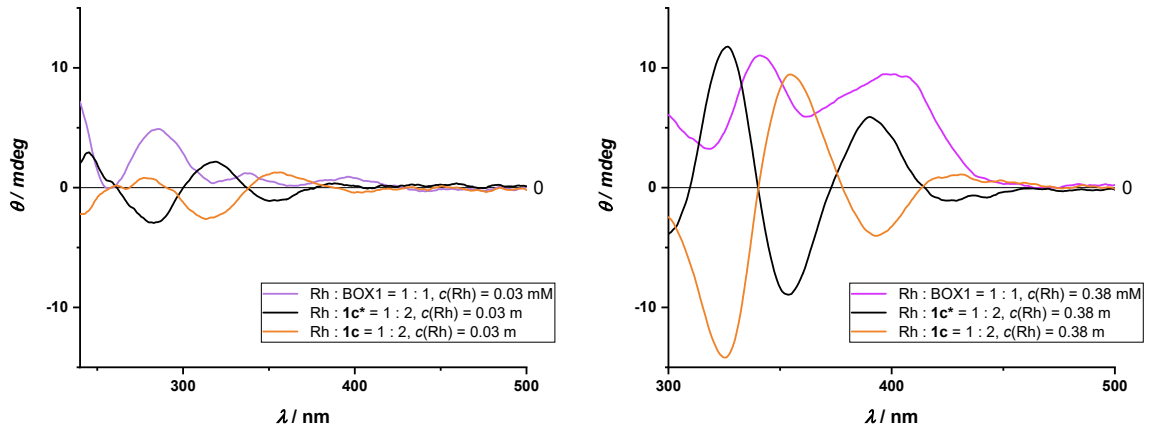

Figure S56. CD spectrum (CH_2Cl_2) of Rh : 1**c** = 1 : 2, Rh : 1**c*** = 1 : 2 and Rh : BOX1 = 1 : 1 solutions. BOX1 = (−)-2,2′-Isopropylidenebis[(4S)-4-phenyl-2-oxazoline]. Ligand BOX1 is a commercially available ligand. CD spectra of precatalytic complex with rhodium have been recorded for purpose of comparison with our complexes.

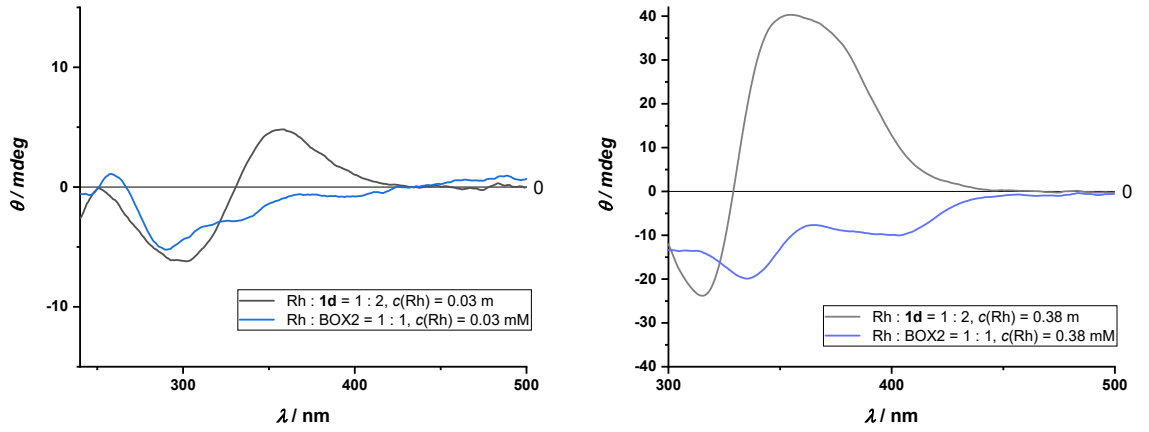

Figure S57. CD spectrum (CH_2Cl_2) of Rh : 1**d** = 1 : 2 and Rh : BOX2 = 1 : 1 solutions. BOX2 = (+)-2,2'-Isopropylidenebis[(4R)-4-benzyl-2-oxazoline]. Ligand BOX1 is a commercially available ligand. CD spectra of precatalytic complex with rhodium have been recorded for purpose of comparison with our complexes.

6. Catalysis, optimization of reaction conditions.

Asymmetric hydrogenation and hydroformylation procedures.
All catalytic reactions were carried out in a stainless steel autoclave with an inset rack suitable for up to 8 reaction vessels (4 mL) with teflon small stirring magnets. In a typical experiment, a reaction vessel is injected with metal precursor and ligand dissolved in dry dichloromethane in argon atmosphere and stirred for 60 minutes in the appropriate solvent. The desired substrate is added to the reaction mixture by dissolving in a small amount of reaction solvent and injecting into the vessel, which is then placed in an autoclave. The autoclave is filled twice with nitrogen and three times with hydrogen. Finally, hydrogenation is carried out under a pressure of 20 bar H_2 and room temperature, or hydroformylation under a pressure of 10 bar H_2 and 10 bar CO and an elevated temperature of 40 °C. At the end of the reaction, the gas is released from the autoclave and then the reaction vessels are handled further. The reaction mixture is diluted with ethyl acetate and filtered through a short column of silica gel (5 cm). The hydroformylation products are further transformed into the corresponding alcohols (reaction with $NaBH_4$, at 0 °C, stirring overnight). Conversion was determined by GC and GC-MS measurement, and enantiomeric excess by GC on a chiral column. The absolute configuration of the products was determined according to the known order of elution under the given conditions.

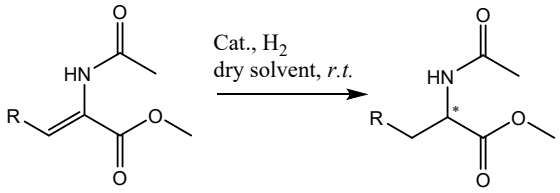

Scheme S4. Catalytic asymmetric hydrogenation.

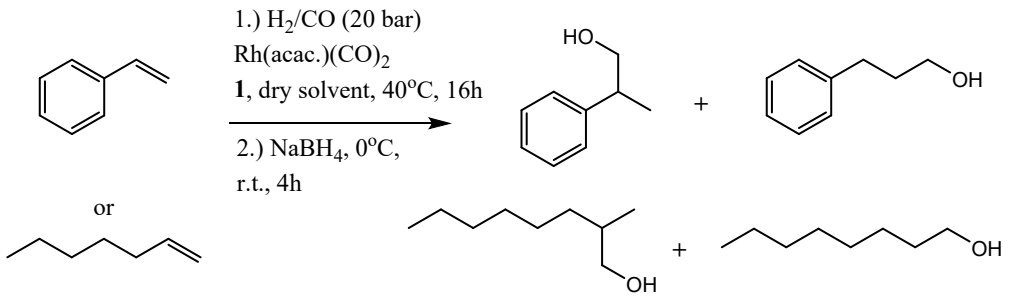

Scheme S5. 1.) Catalytic asymmetric hydroformylation, 2.) transformation of products into corresponding alcohols.

Table S2. Blank tests

Entry	Metal precursor	Ligand(*S*)	M:L_1(:L_2)	*t* / h	Conversion / %	e.e. / %
1	-	**1p**	**1 : 2.2**	16	0	-
2	[Ir(COD)2]BArF	-	-	3	0	-
3	[Ir(COD)2]BArF	**PPh_3, H-A-OMe**	**1 : 2.2 : 2.2**	16	14	0
4	$Rh(COD)_2BF_4$	-	-	3	0	-
5	$Rh(COD)_2BF_4$	**PPh_3**	**1 : 2.2**	16	>99	0

Table S3. Solvent screening

		[Ir(COD)2]BArF		**$Rh(COD)_2BF_4$**	
Entry	Solvent	Conversion / %	e.e. / %	Conversion / %	e.e. / %
6	CH_2Cl_2	>99	84 (*S*)	>99	70 (*S*)
7	*i*-PrOH	<5	-	>99	8 (*S*)
8	toluene	7	64 (*S*)	>99	38 (*S*)
9	THF	22	-	>99	0
10	*t*-BuOAc	6	12 (*S*)	>99	10 (*S*)
11	MeCN	0	-	4	4 (**R**)
12	CF_3CH_2OH	<5	31 (*S*)	>99	58 (*S*)
13	C_6H_5Cl	<5	-	>99	39 (*S*)
14	$CHCl_3$	<5	70 (*S*)	>99	85 (*S*)

Substrate: methyl-*α*-acetamidocinnamate (MAC), Ligand: **1p,** M : **1p** = 1 : 2.2, catalyst loading= 1 mol%, c(cat.)=0,067 mM, (0.0001mmol/1.5mL), p (H_2)= 20 bar, *t* = 16 h, r.t.

Table S4. Catalyst loading and ratio optimization

						[Ir(COD)2]BArF		**$Rh(COD)_2BF_4$**	
Entry	M:**1p**	Catalyst loading	*T* / °C	*p*(H_2) / bar	*t* / h	Conversion / %	e.e. / %	Conversion / %	e.e. / %
15	**1 : 0.55**	0.05 mol%	-5	20	3	n.a.	n.a.	18	66 (*S*)
16	**1 : 1.1**	1 mol%	r.t.	20	16	>99	82 (*S*)	>99	74 (*S*)
17		0.5 mol%	r.t.	20	3	61	82 (*S*)	n.a.	n.a.
18		0.2 mol%	r.t.	20	3	traces	-	>99	72 (*S*)
19			0	20	3	n.a.	n.a.	>99	72 (*S*)
20		0.05 mol%	-5	20	3	n.a.	n.a.	91	64 (*S*)
21	**1 : 1.5**	1 mol%	r.t.	20	16	>99	82 (*S*)	>99	66 (*S*)
22				20	3	>99	80 (*S*)	n.a.	n.a.
23a	**1 : 2.2**	1 mol%	r.t.	20	16	>99	84 (*S*)	>99	70 (*S*)
23b			r.t.	10	16	>99	74 (*S*)	>99	55 (*S*)
24		0.5 mol%	r.t.	20	3	47	82 (*S*)	n.a.	n.a.
25		0.2 mol%	r.t.	20	3	traces	-	>99	72 (*S*)
26			0	20	3	n.a.	n.a.	>99	70 (*S*)
27		0.05 mol%	-5	20	3	n.a.	n.a.	96	68 (*S*)
28	**1 : 3**	1 mol%	r.t.	20	16	21	82 (*S*)	>99	66 (*S*)
29				20	3	20	82 (*S*)	>99	70 (*S*)

Substrate:
methyl-*α*-acetamidocinnamate (MAC),Ligand: **1p,** p (H_2)= 20 bar, solvent: CH_2Cl_2,for 1 mol% cat. loading, c(cat.)=0,067 mM (0.0001mmol/1.5mL)

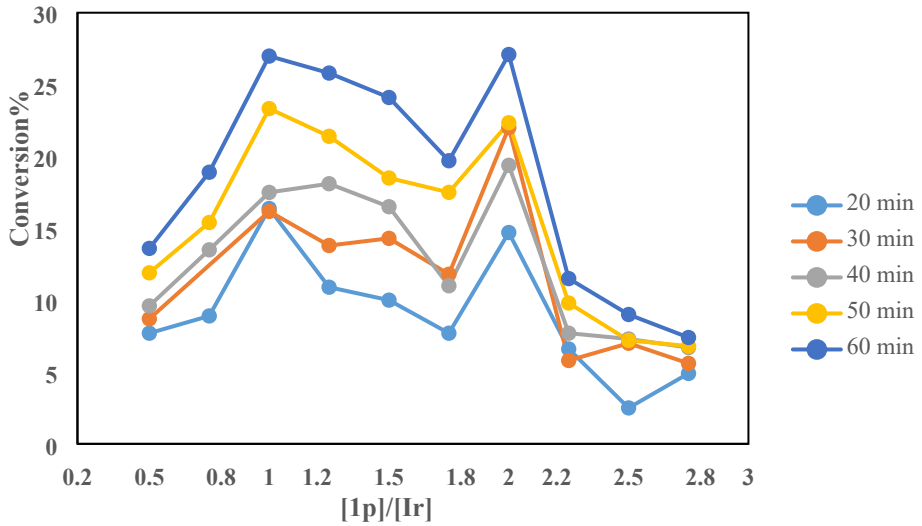

Graph S1. Ligand to metal ratio optimization for catalysis.

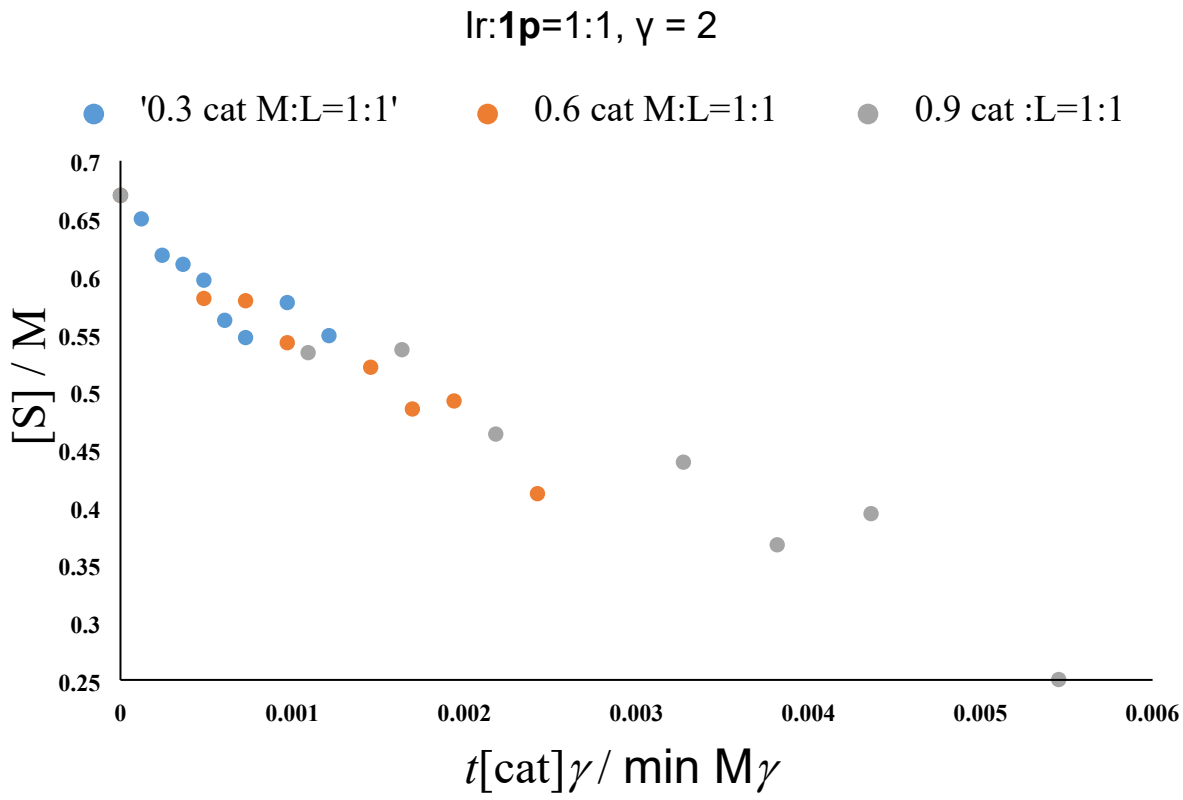

Graph S2. Concentration experiments.

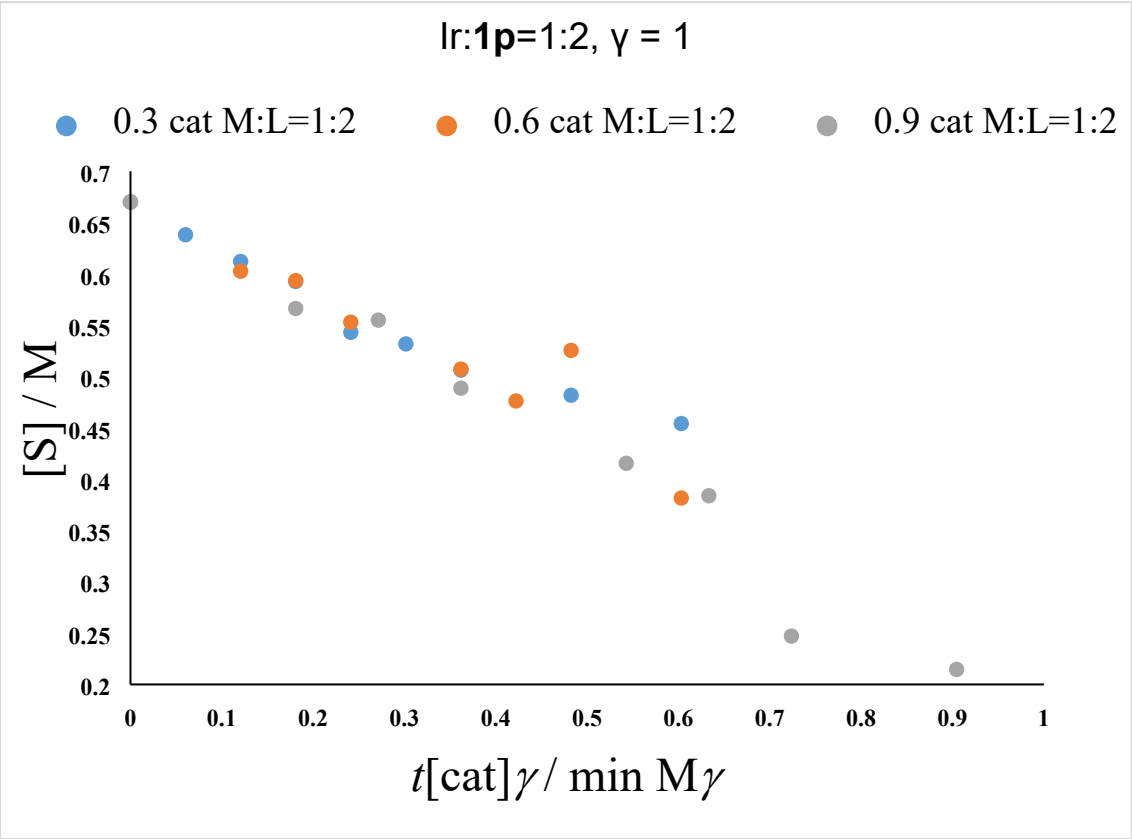

Graph S3. Concentration experiments.

Table S5. Catalysis with ligand mixtures

							[Ir(COD)2]BArF		$Rh(COD)_2BF_4$	
Entry	Ligands	M:L_1:L_2	Catalyst loading	*T* / °C	$p(H_2)$/ bar	*t* / h	Conversion / %	e.e. / %	Conversion / %	e.e. / %
30	**1b**	**1 : 2.2**	1 mol%	r.t.	20	3	0	0	n.a.	n.a.
31	**PPh_3, 1p**	**1 : 1.1 : 1.1**	1 mol%	r.t.	20	3	>99	64 (*S*)	>99	56 (*S*)
32	**PPh_3, 1b**	**1 : 1.1 : 1.1**	1 mol%	r.t.	20	16	>99	-	n.a.	n.a.
33a	**1p , 1b**	**1 : 1.1 : 1.1**	1 mol%	r.t.	20	16	72	70 (*S*)	>99	72 (*S*)
33b				r.t.	10	16	>99	70 (S)	>99	55 (S)
34			0.5 mol%	r.t.	20	3	16	74 (*S*)	>99	70 (*S*)
35			0.2 mol%	r.t.	20	3	traces	-	>99	72 (*S*)
36				0	20	3	n.a.	n.a.	>99	72 (*S*)
37			0.05 mol%	-5	20	3	n.a.	n.a.	86	64 (*S*)
38		**1 : 1.5 : 1.5**	1 mol%	r.t.	20	16	89	80 (*S*)	>99	72 (*S*)
39			1 mol%	r.t.	20	3	52	78 (*S*)	n.a.	n.a.
40		**1 : 1.1 : 2.2**	1 mol%	r.t.	20	16	39	65 (*S*)	n.a.	n.a.
41	**1p , 1c**	**1 : 1.1 : 1.1**	1 mol%	r.t.	20	16	92	64 (*S*)	>99	70 (*S*)
42	**1p , 1c**	**1 : 1.5 : 1.5**	1 mol%	r.t.	20	16	>99	78 (*S*)	>99	68 (*S*)
43	**1p , 1c***	**1 : 1.1 : 1.1**	1 mol%	r.t.	20	5	71	85(*S*)	>99	71 (*S*)
44	**1p , 1d**	**1 : 1.1 : 1.1**	1 mol%	r.t.	20	16	91	62 (*S*)	>99	72 (*S*)
45	**1p , 1d**	**1 : 1.5 : 1.5**	1 mol%	r.t.	20	16	>99	78 (*S*)	>99	68 (*S*)

Substrate: methyl-*α*-acetamidocinnamate (MAC) c(MAC)= 6.7 mM, p (H_2)= 20 bar, solvent: CH_2Cl_2, for 1 mol% cat. loading, c(cat.)=0.067 mM (0.0001mmol/1.5mL) ; c=0.034 mM (0.5%mmol); c=0.013 mM (0. 2%mmol); c=0.003 mM (0.05%mmol)
-rhodium reactions - too fast!

Table S6. Substrate scope

			[Ir(COD)2]BArF		$Rh(COD)_2BF_4$	
Entry	R	*t*/h	Conversion / %	e.e. / %	Conversion / %	e.e. / %
46	phenyl	16	>99	84 (*S*)	>99	70 (*S*)
47	4-Cl-phenyl	16	>99	82 (*S*)	>99	64
48	Tiophen-2-yl	16	28	44 (*S*)		n.a.
49	Tiophen-3-yl	16	>99	82 (*S*)	>99	65 (*S*)
50	Naphth-2-yl	16	>99	78 (*S*)	>99	62 (*S*)

Ligand: **1p,** M : L_p = 1 : 2.2, catalyst loading= 1 mol%, c(cat.)=0,067 mM(0.0001mmol/1.5mL), p(H_2)= 20 bar, solvent: CH_2Cl_2, r.t.

Table S7. Hydroformylation reactions

Asymmetric hydroformilation

Entry	Substrate	Solvent	Conversion[a]/ %	b : l	e.e.%
1	styrene	chlorobenzene	75	98:2	-
2	1-octene	chlorobenzene	35	7:93	-
3	1-octene	toluene	94	18:82	-
4	1-octene	hexane	60[b]	13:87	-
5	1-octene	CH_2Cl_2	77	20:80	-
6	1-octene	THF	79	25:75	-

[a] as determined from GC-MS

[b] catalyst did not dissolve

7. Gas chromatography**, characteristic examples.**

7.1. Hydrogenation Substrates

7.1.1. Methyl α-acetamidocinnamate

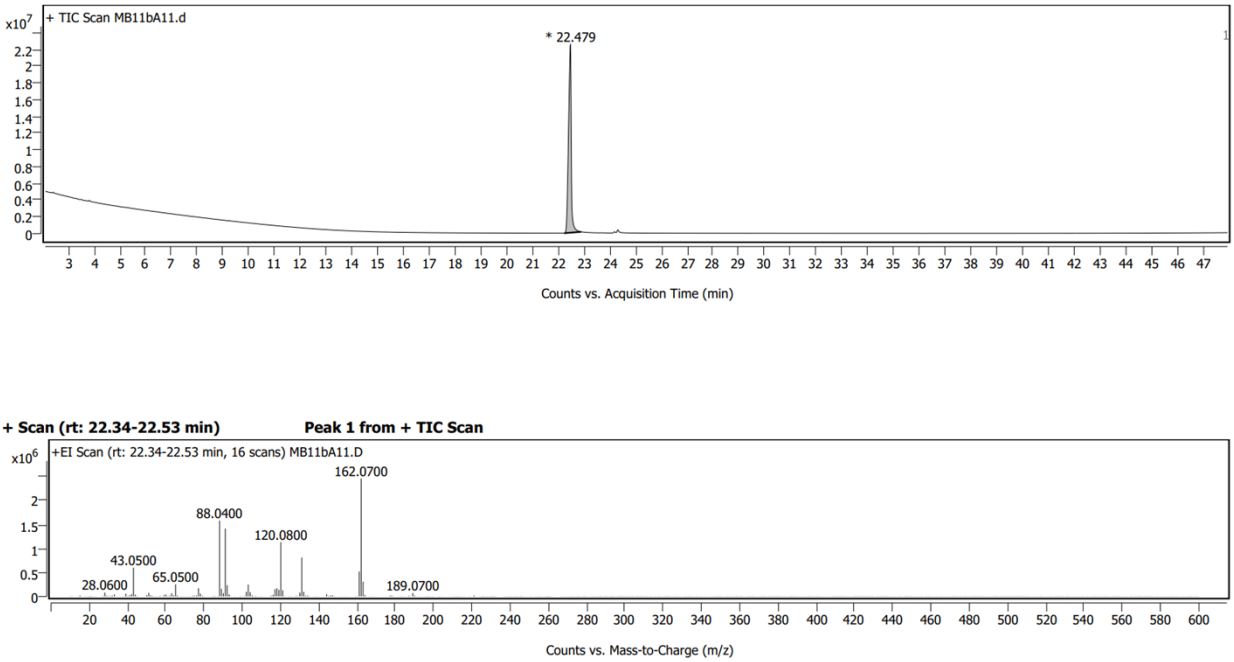

Figure S58. Typical GC-MS spectra of the methyl α-acetamidocinnamate hydrogenation product.

a)

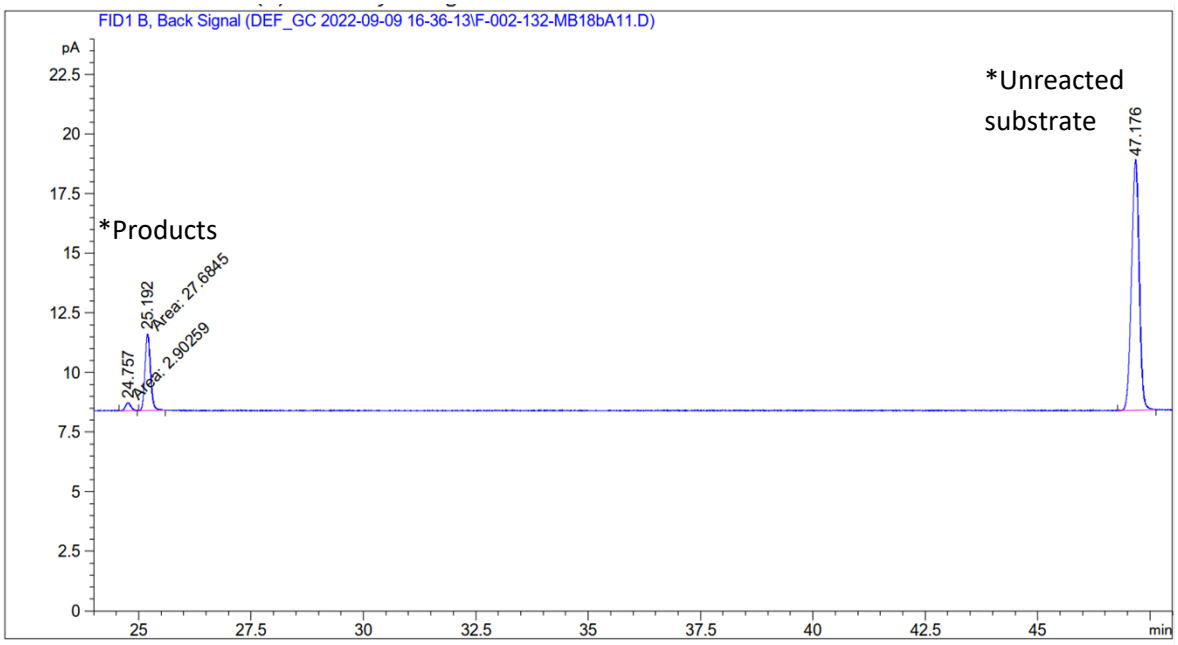

b)

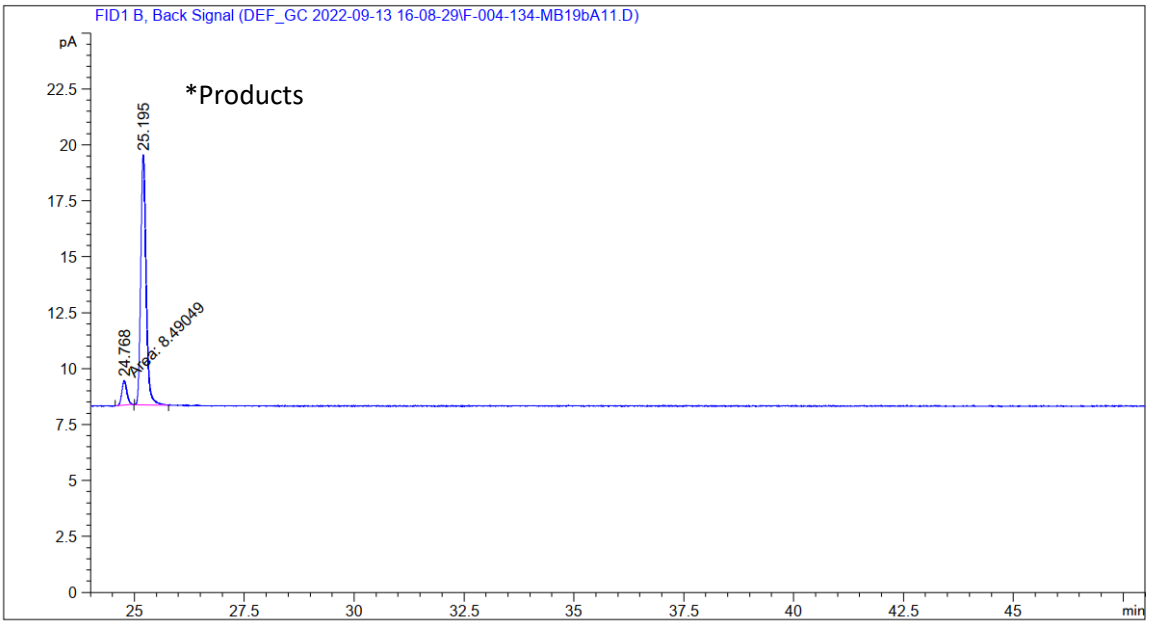

Figure S59. Typical chiral GC spectrum of the methyl α-acetamidocinnamate hydrogenation product with: a) incomplete conversion, b) complete conversion.

Table S8. Typical Chiral GC spectrum data of the methyl α-acetamidocinnamate hydrogenation product with complete conversion.

Peak #	RetTime [min]	Type	Width [min]	Area [pA*s]	Height [pA]	Area %
1	24.768	MM	0.1310	8.49049	1.08062	8.19484
2	25.195	BB	0.1254	95.11728	11.16572	91.80516

7.1.2. Methyl α-acetamido-3-(4-chlorophenyl)acrylate

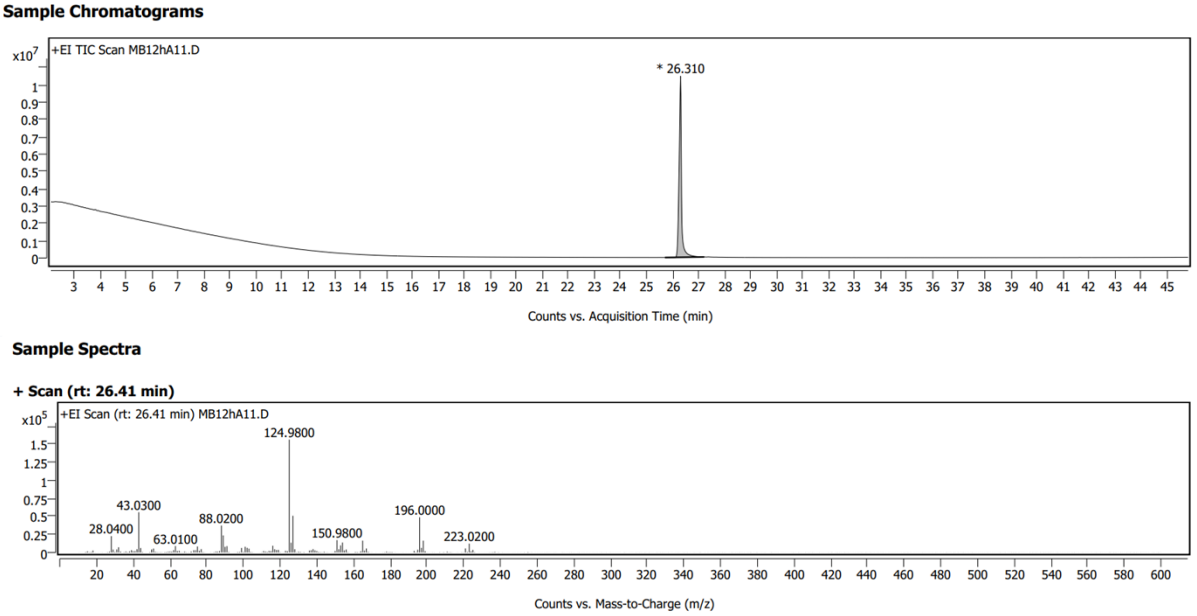

Figure S60. Typical GC-MS spectra of the methyl α-acetamido-3-(4-chlorophenyl)acrylate hydrogenation product.

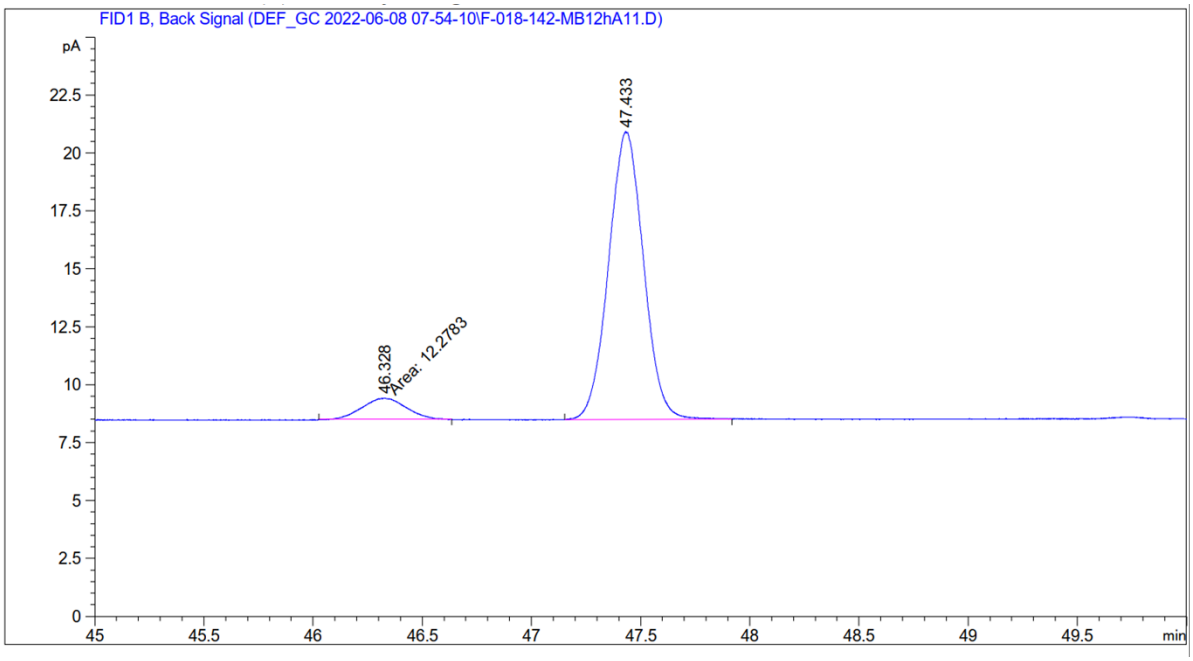

Figure S61. Typical chiral GC spectrum of the methyl α-acetamido-3-(4-chlorophenyl)acrylate hydrogenation product with: a) incomplete conversion, b) complete conversion.

Table S9. Typical Chiral GC spectrum data of the methyl α-acetamido-3-(4-chlorophenyl)acrylate hydrogenation product with complete conversion.

Peak #	RetTime [min]	Type	Width [min]	Area [pA*s]	Height [pA]	Area %
1	46.328	MM	0.2272	12.27833	9.00872e-1	8.16828
2	47.433	BB	0.1438	138.03896	12.41189	91.83172

7.1.3. Methyl α-acetamido-3-(thiophen-2-yl)acrylate

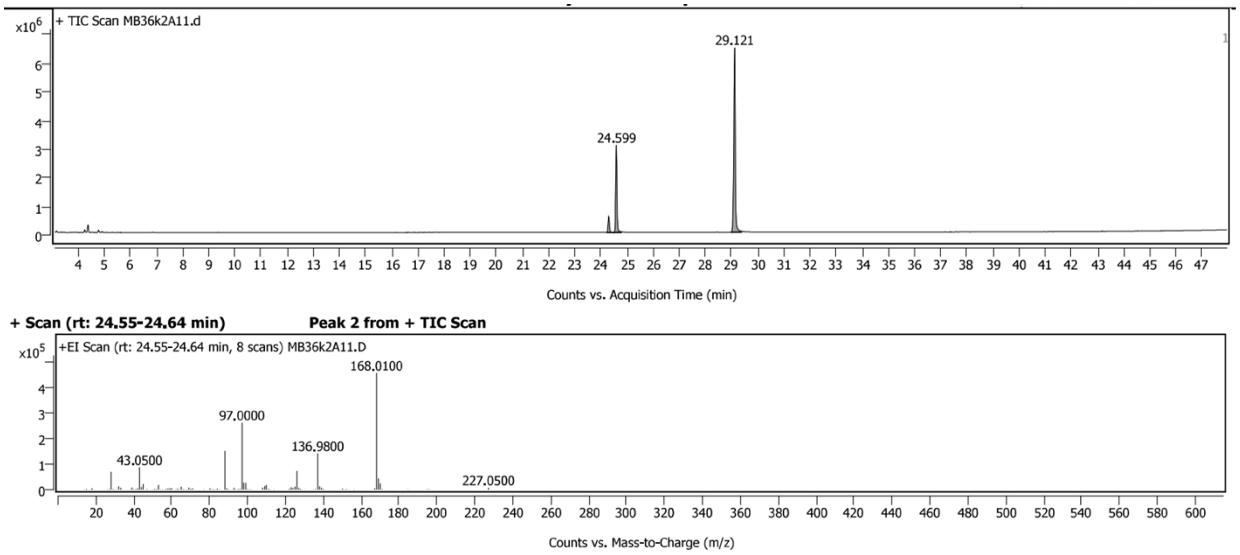

Figure S62. Typical GC-MS spectra of the methyl α-acetamido-3-(thiophen-2-yl)acrylate hydrogenation product.

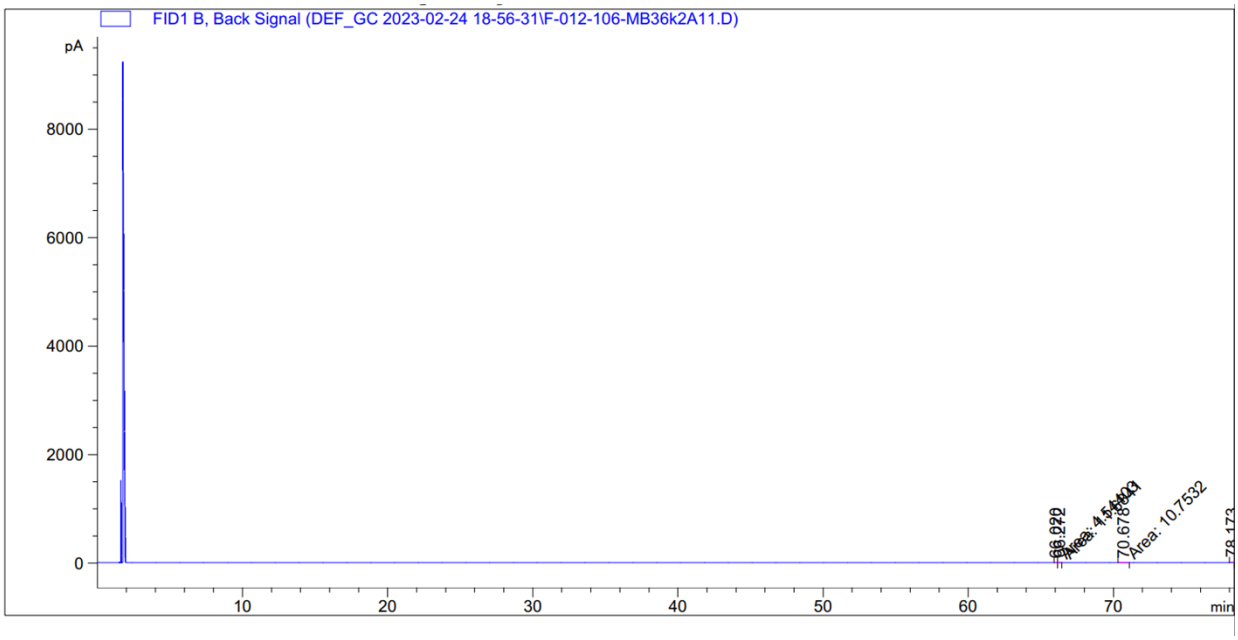

Figure S63. Typical chiral GC spectrum of the methyl α-acetamido-3-(thiophen-2-yl)acrylate hydrogenation product with: a) incomplete conversion, b) complete conversion.

Table S10. Typical Chiral GC spectrum data of the methyl α-acetamido-3-(thiophen-2-yl)acrylate hydrogenation product with complete conversion.

Peak #	RetTime [min]	Type	Width [min]	Area [pA*s]	Height [pA]	Area %
1	66.020	MM	0.0844	4.54403	8.96965e-1	6.92920
2	66.272	MM	0.0764	11.68406	2.54819	17.81705
3	70.678	MM	0.3296	10.75321	5.43820e-1	16.39760
4	78.173	BBA	0.1224	38.59667	4.87521	58.85616

7.1.4. Methyl α-acetamido-3-(thiophen-3-yl)acrylate

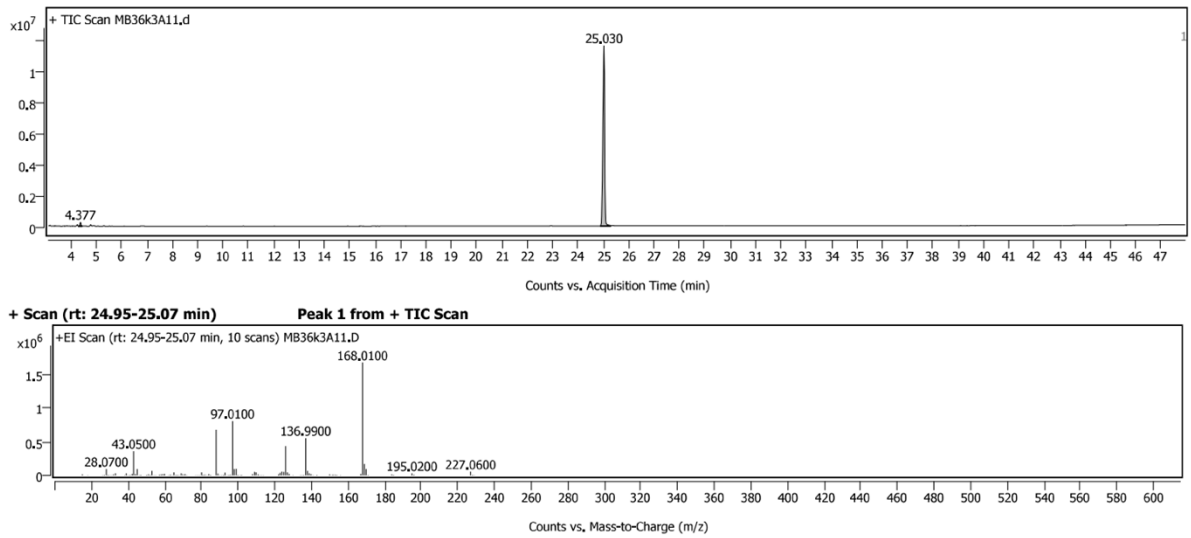

Figure S64. Typical GC-MS spectra of the methyl α-acetamido-3-(thiophen-3-yl)acrylate hydrogenation product.

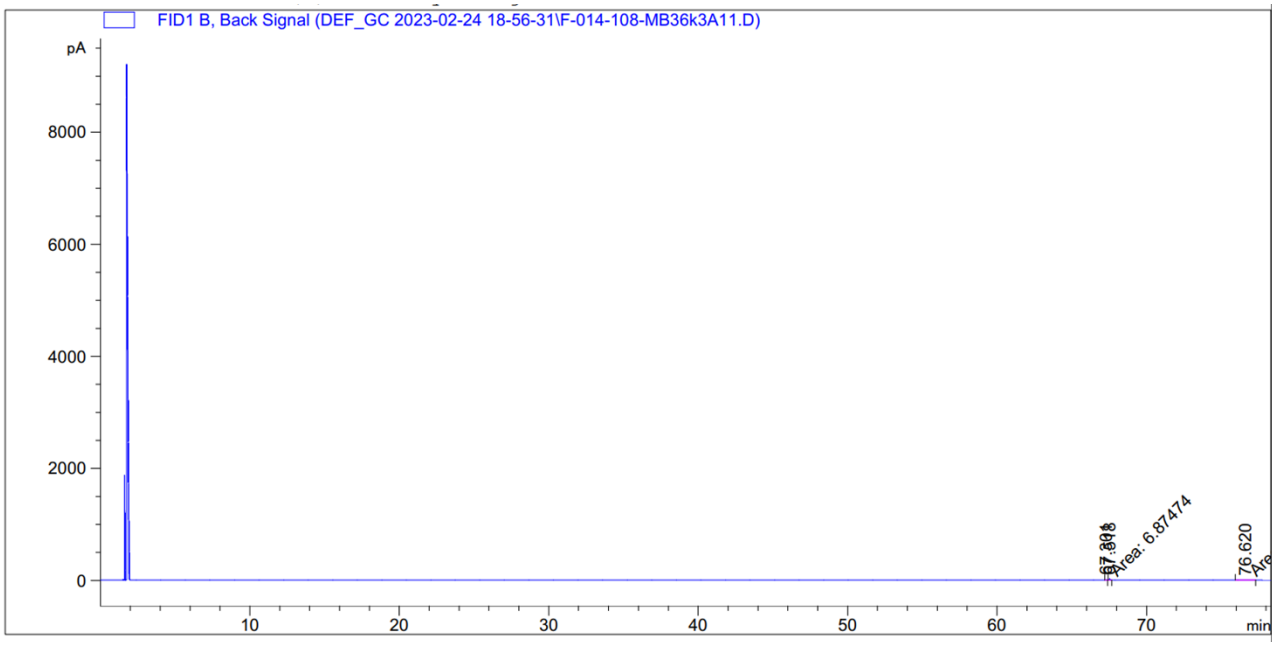

Figure S65. Typical chiral GC spectrum of the methyl α-acetamido-3-(thiophen-3-yl)acrylate hydrogenation product with: a) incomplete conversion, b) complete conversion.

Table S11. Typical Chiral GC spectrum data of the methyl α-acetamido-3-(thiophen-3-yl)acrylate hydrogenation product with complete conversion.

Peak #	RetTime [min]	Type	Width [min]	Area [pA*s]	Height [pA]	Area %
1	67.301	MM	0.0667	6.87474	1.71837	6.30804
2	67.518	BB	0.0574	67.06234	17.62988	61.53420
3	76.620	MM	0.6324	35.04677	9.23633e-1	32.15776

7.1.5. Methyl α-acetamido-3-(naphth-2-yl)acrylate

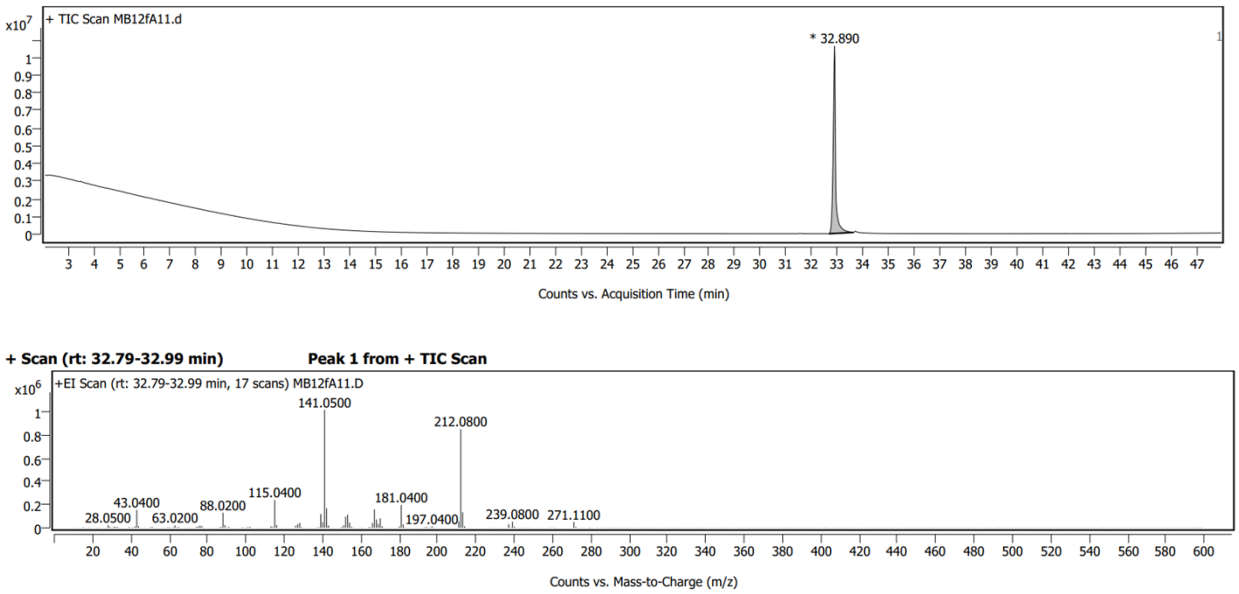

Figure S66. Typical GC-MS spectra of the methyl α-acetamido-3-(naphth-2-yl)acrylate hydrogenation product.

7.2. Hydroformylation Substrates

7.2.1. Styrene

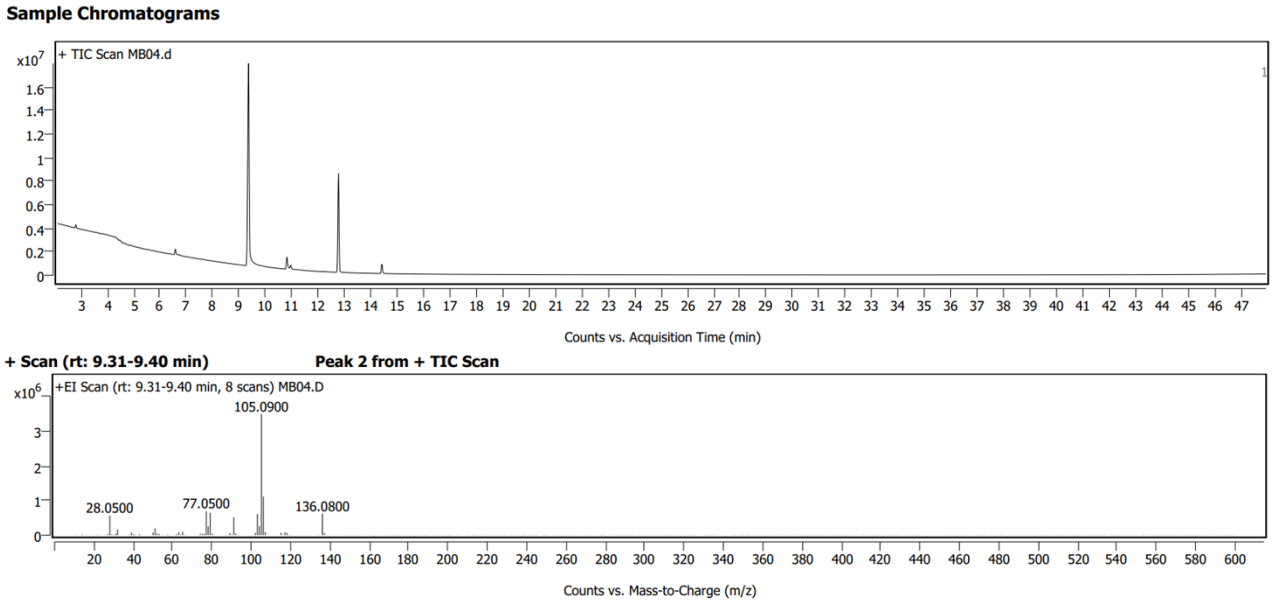

Figure S69. Typical GC-MS spectra of styrene hydroformylation alcoholic product.

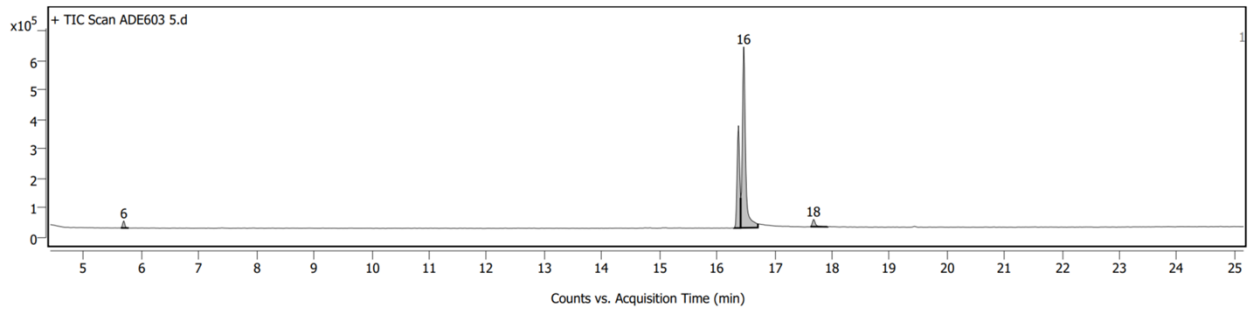

Graph S60. Typical chiral GC spectrum of styrene hydroformylation alcoholic product.

Table S13. typical Chiral GC spectrum data of styrene hydroformylation alcoholic product.

Peak	RT	Area	Area %	Area Sum %	Height	Type	Saturated	Width	FWHM	SNR	RI
1	5.69	63036.83	2.57	1.7	23805.92			0.137	0.043		
2	16.375	1084348.32	44.13	29.31	346489.83			0.117	0.051		
3	16.466	2457215.55	100	66.42	612451.28			0.3	0.054		
4	17.678	95160.36	3.87	2.57	24340.74			0.3	0.054		

7.2.2. 1-octene

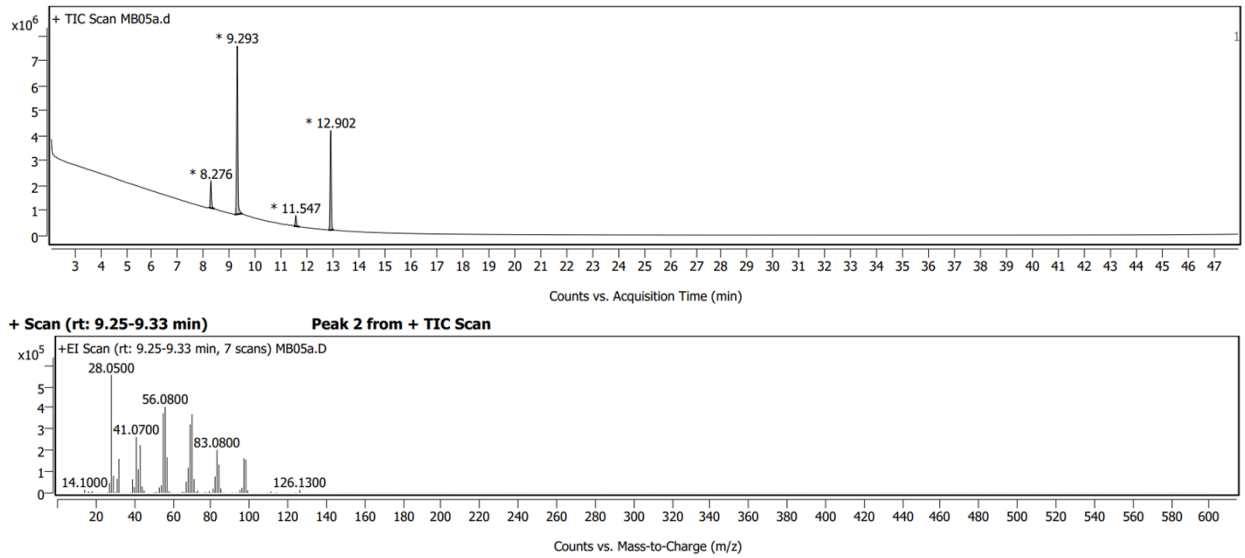

Figure S70. Typical GC-MS spectra of 1-octene hydroformylation alcoholic product.

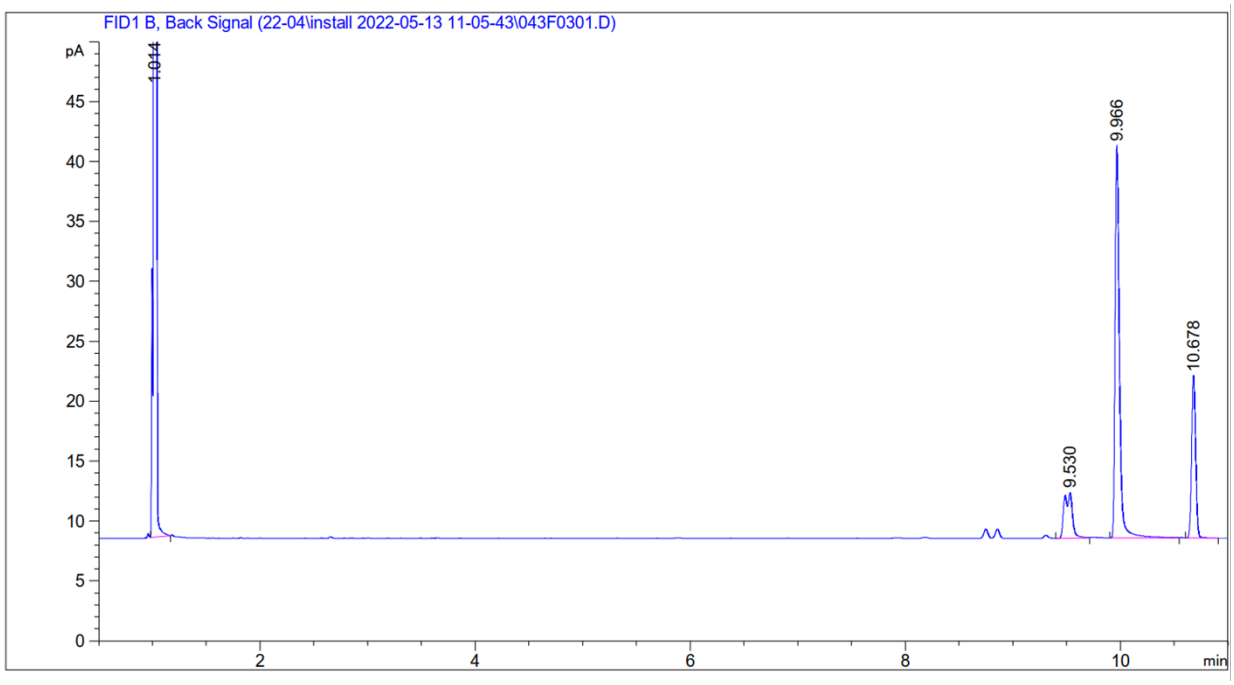

Figure S71. Typical chiral GC spectrum of 1-octene hydroformylation alcoholic product.

Table S14. Typical Chiral GC spectrum data of 1-octene hydroformylation alcoholic product.

Peak #	RetTime [min]	Type	Width [min]	Area [pA*s]	Height [pA]	Area %
1	1.014	BB	0.0191	2.29133e4	1.89683e4	99.35924
2	9.530	BB	0.0710	19.84587	3.79712	0.08606
3	9.966	BB	0.0420	92.53233	32.72927	0.40125
4	10.678	BB	0.0415	35.38796	13.51752	0.15345

8. HRMS(ESI)

ESI-TOF-HRMS of **1p**.

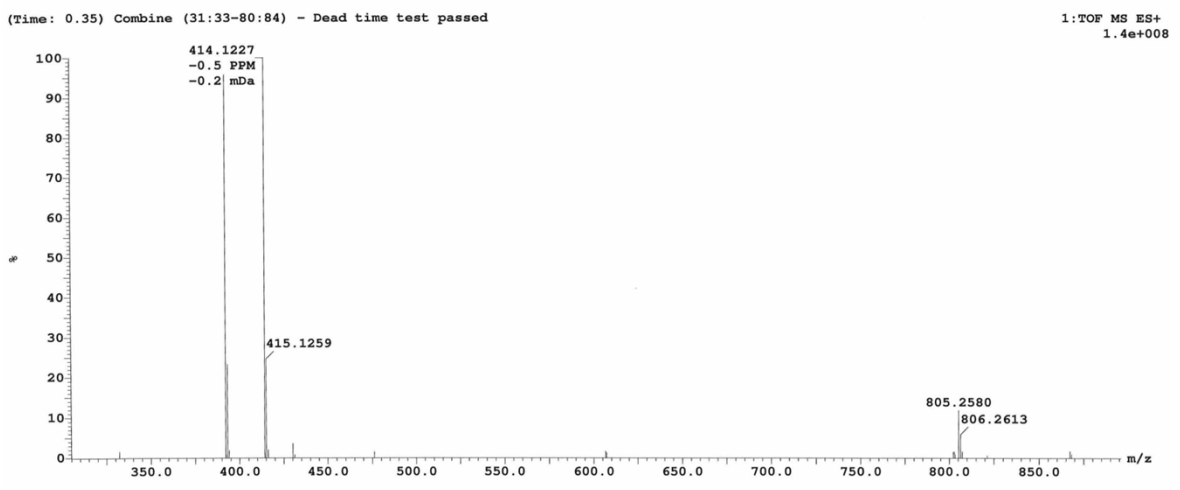

ESI-TOF-HRMS of **1a**.

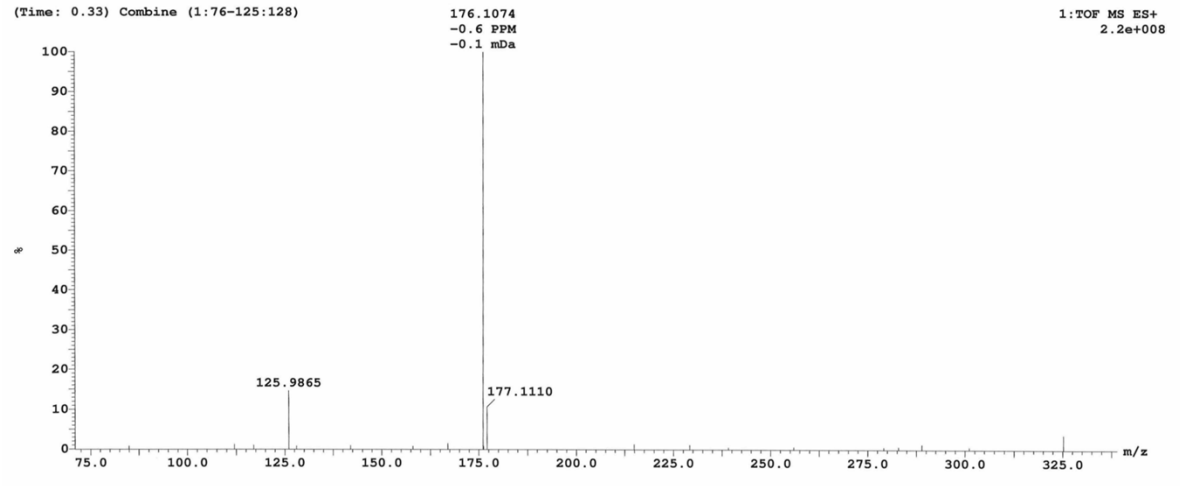

ESI-TOF-HRMS of **1b**.

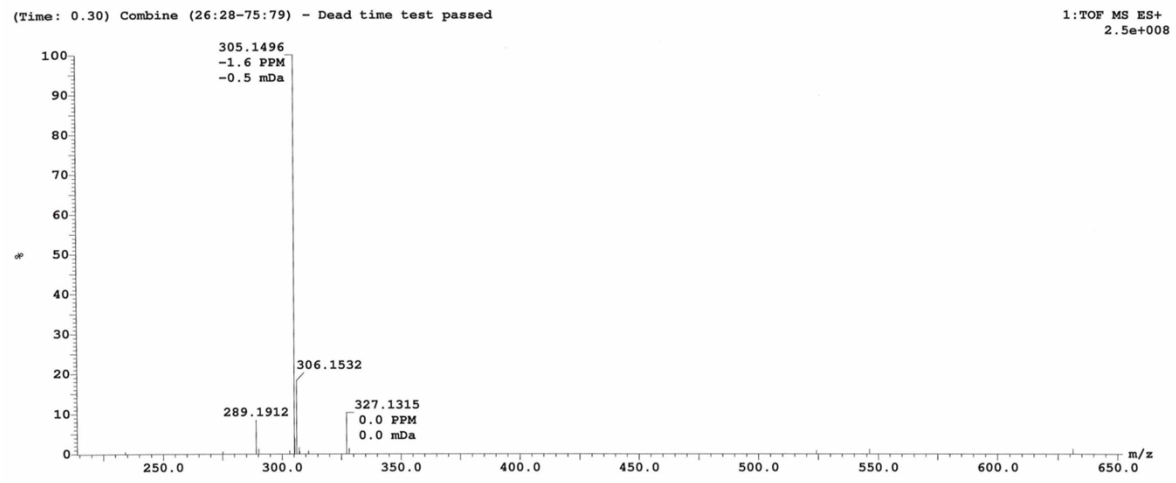

ESI-TOF-HRMS of **1c**.

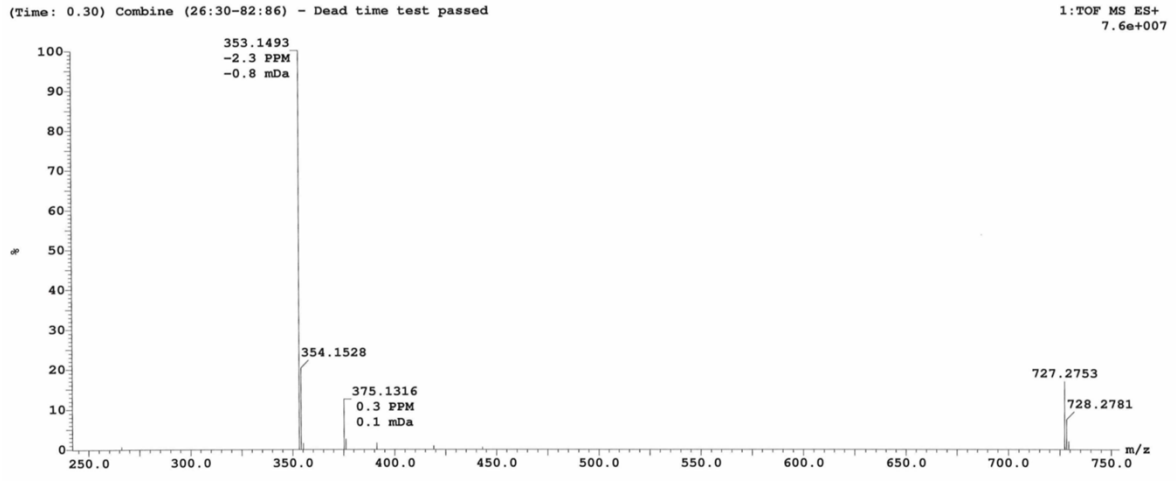

ESI-TOF-HRMS of **1c***.

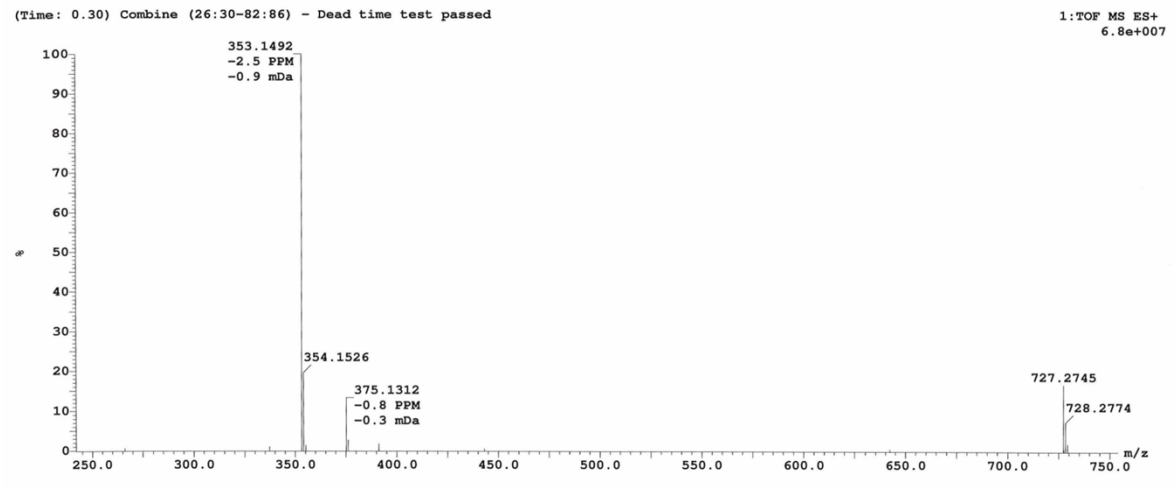

ESI-TOF-HRMS of **1d**.

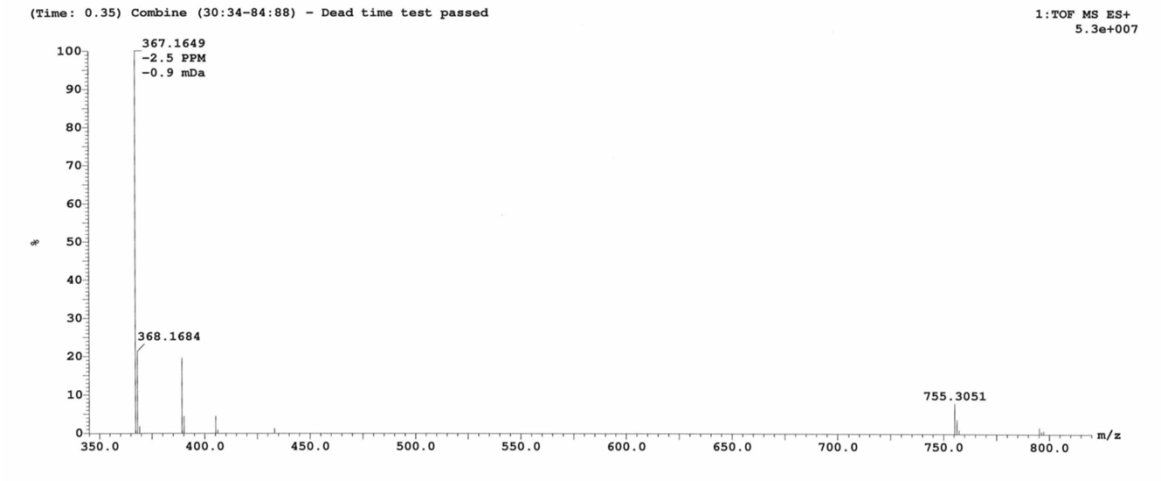

9. X-ray diffraction

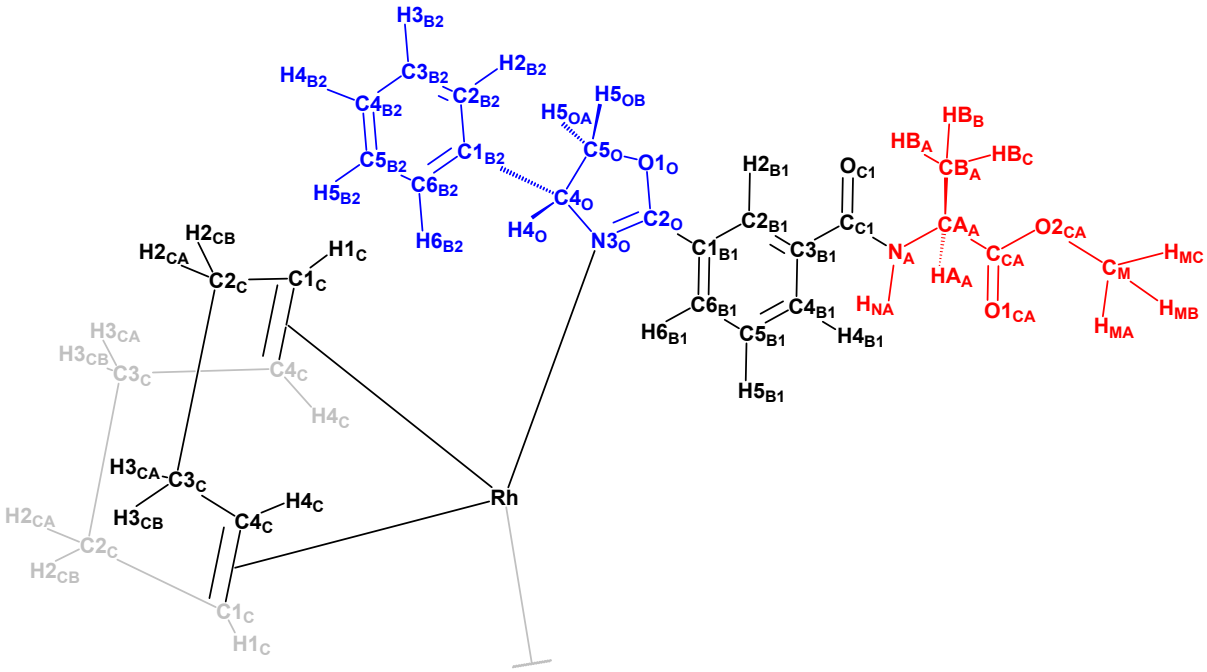

Figure S71. Atom labeling scheme in accordance with the atom labels found in the crystal structure of [Rh(**1c***)$_2$]BF$_4$. The greyed out parts of the molecule are C_2-symmetric with rest of the molecule, bear the same atom labels and are partially left out from the scheme for clarity.

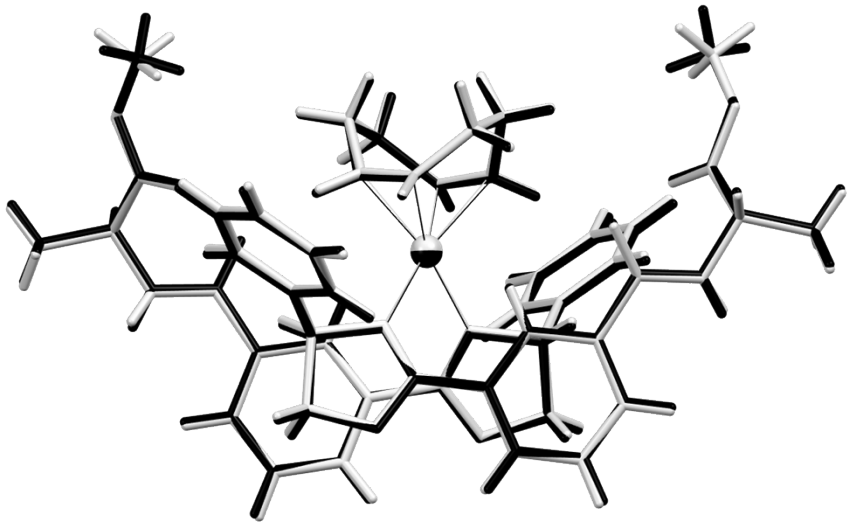

Figure S72. The overlapped structures of the two crystallographically independent metal complex molecules contained in the asymmetric unit of the obtained crystal structure [Rh(**1c***)$_2$]BF$_4$.

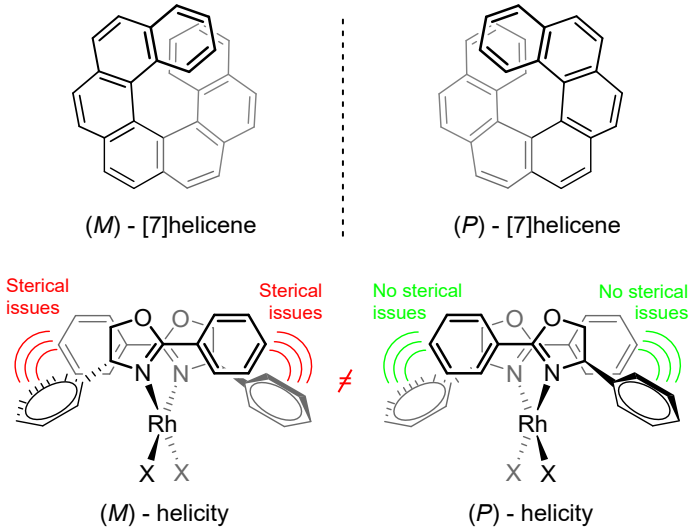

Figure S73. Helical chirality determination in two rhodium structures in a similar fashion as for (*M*)- and (*P*)-[7]helicene. The two subtypes are diastereoisomeric for our complexes due to the incorporated (4*S*)-phenyl-containing and alanine chiral centers.

Table S15. Experimental data for the X-ray diffraction study.

Compound	**[Rh(1c*)$_2$COD]BF$_4$**
Instrument	XtaLAB Synergy
Temperature (K)	293(2)
Formula	$[C_{48}H_{52}N_4O_8Rh][BF_4]$
F_w (g mol^{-1})	1002.65
Crystal system	Monoclinic
Space group	*I*2
a (Å)	20.5437(4)
b (Å)	10.4027(4)
c (Å)	30.6083(9)
α (°)	90
β (°)	106.710(3)
γ (°)	90
V (Å^3)	6265.1(3)
Z	4
Z'	1 (1/2+1/2)
D_{calc} (g cm^{-3})	1.063
F(000)	2072
Reflections collected	27698
Independent reflections	10689
R_{init}	0.0287
Reflections observed	9566
Parameters	606
R_1 [$I > 2\sigma(I)$][a]	0.0346
wR_2 (all data) [b]	0.1010
Goof, *S*[c]	1.110
Maximum/minimum electron density (e Å^3)	0.617/-0.528
Solv. area (Å^3)	2046
El. In solv. area (SQUEEZE)	473

[a] $R_1 = \Sigma||F_o| - |F_c||/\Sigma|F_o|$. [b] $wR_2 = \{\Sigma[w(F_o^2 - F_c^2)^2]/\Sigma[w(F_o^2)^2]\}^{1/2}$. [c] $S = \{\Sigma[w(F_o^2 - F_c^2)^2]/(n - p)\}^{1/2}$ where n is number of reflections and p is the total number of parameters refined.

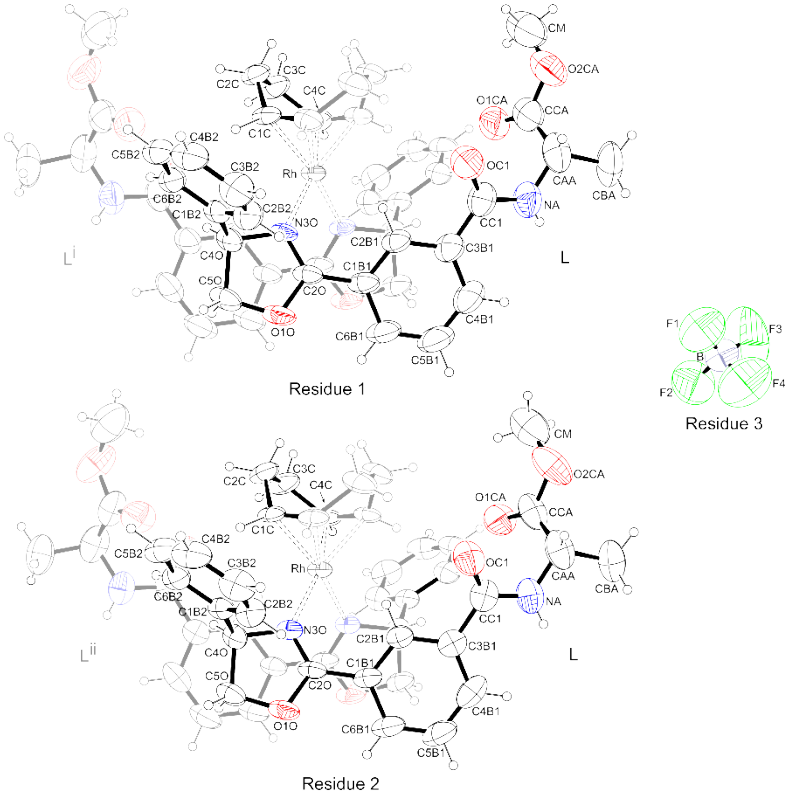

Figure S74. ORTEP-3[4] molecular structure of **[Rh(1c*)$_2$COD]**BF_4 with atom numbering scheme and 30% ellipsoid probability level. The asymmetric unit of the structure consists of three residues (two C_2-symetric $[Rh(L)_2COD]^+$ complexes and a $[BF_4]^-$ anion) and only symmetry-unique atoms are labeled, C_2 symmetry related ligands **1c***^{i}, **1c***^{ii} and atoms from COD groups are not labeled and they are shown in the lighter tone. Symmetry codes (i): -*x*, *y*, -*z*; (ii): 1-*x*, *y*, -*z*.

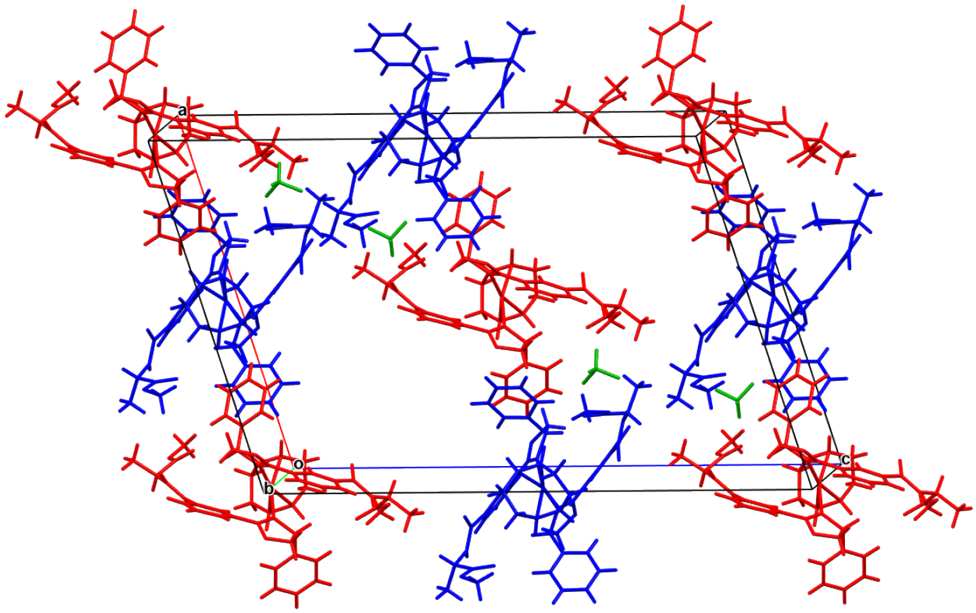

Figure S75. Crystal packing in **[Rh(1c*)$_2$COD] BF$_4$**.[5] Symmetry independent residues 1 and 2 ([Rh(**1c***)$_2$COD]$^+$ complexes) are red and blue, respectively, and [BF$_4$]$^-$ anions are green.

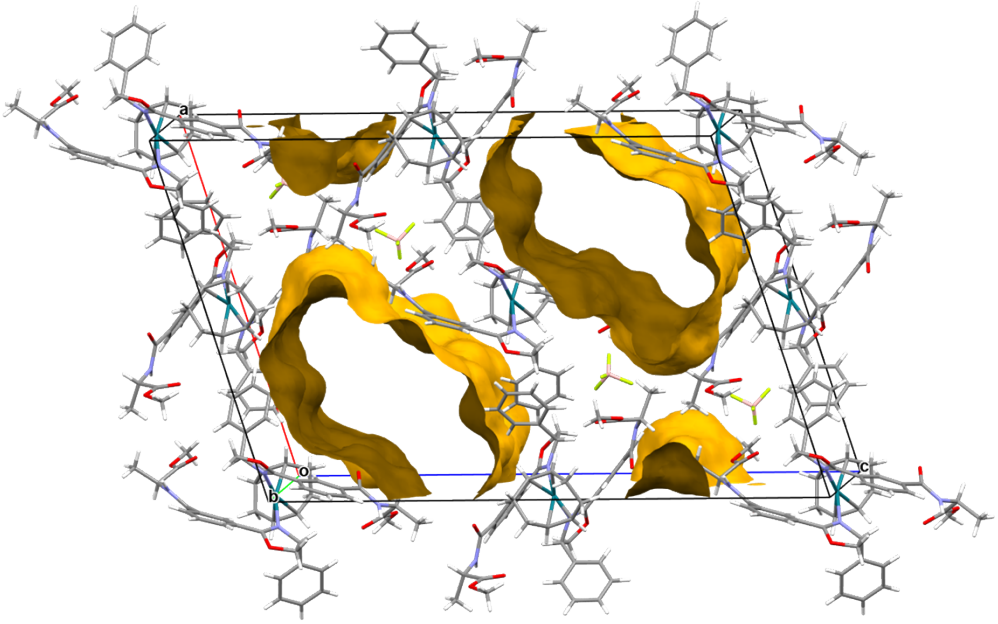

Figure S76. Voids in the crystal packing of **[Rh(1c*)$_2$COD] BF$_4$**.[5] Electron density inside voids, disorderly populated by solvent molecules, is accounted in calculated structure factors by SQEEZE procedure of program PLATON.[6]

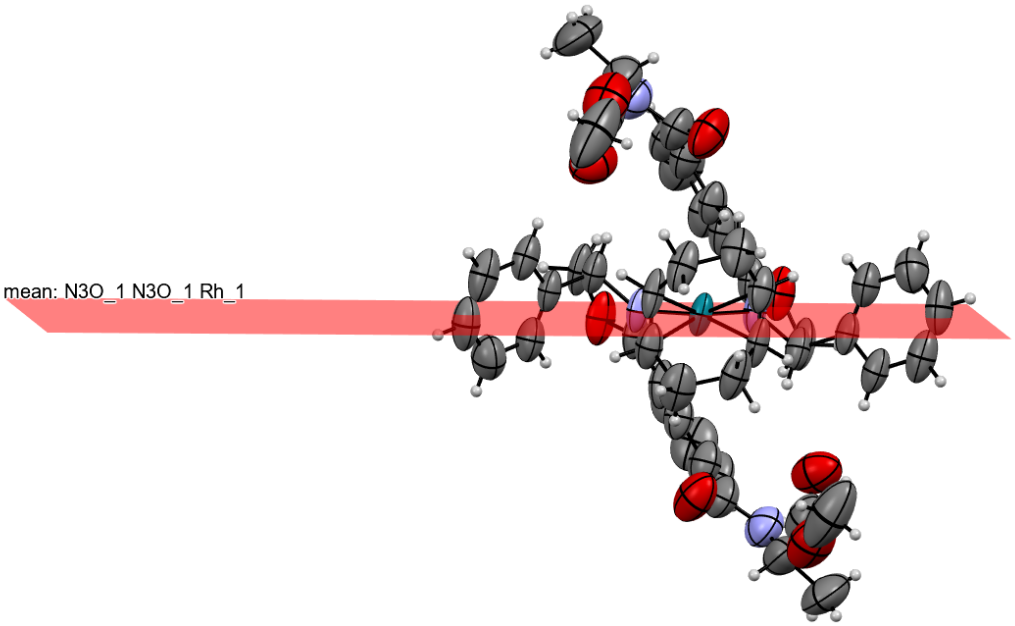

a)

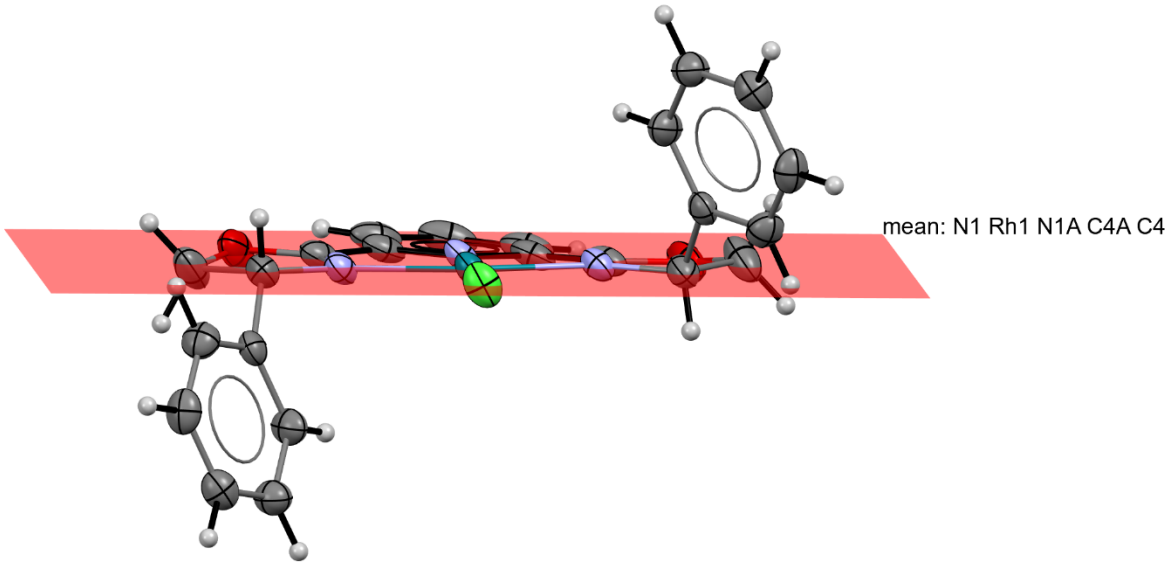

b)

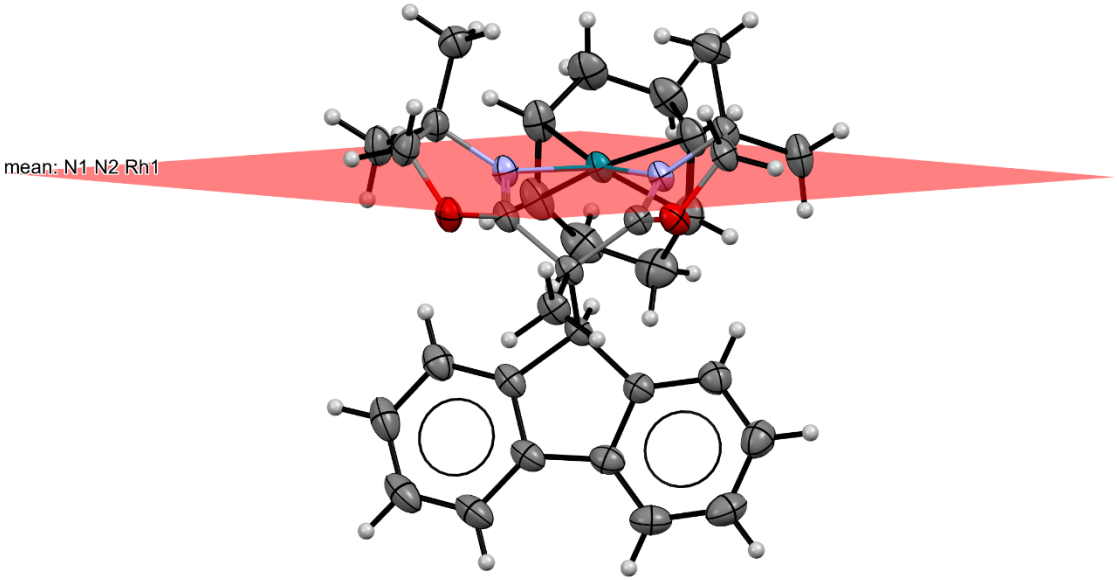

c)

Figure S77. Difference between the placement of two monodentate **1c*** ligands in **[Rh(1c*)$_2$COD] BF$_4$** (a) and bisoxazoline ligands (b, CSD code: BOTFIC; and c, CSD code: LIJJOG)[7,8] around the rhodium atom and the corresponding square-planar coordination planes.

10. References

1 Z. Kokan, Z. Glasovac, M. Majerić Elenkov, M. Gredičak, I. Jerić and S. I. Kirin, *Organometallics*, 2014, **33**, 4005–4015.

2 M. Bakija, B. Perić and S. I. Kirin, *New J. Chem.*, 2024, **48**, 8702–8719.

3 G. Xu, Q. Luo, S. Eibauer, A. F. Rausch, S. Stempfhuber, M. Zabel, H. Yersin and O. Reiser, *Dalton Trans.*, 2011, **40**, 8800.

4 L. J. Farrugia, *J Appl Crystallogr*, 1997, **30**, 565–565.

5 C. F. Macrae, P. R. Edgington, P. McCabe, E. Pidcock, G. P. Shields, R. Taylor, M. Towler and J. Van De Streek, *J Appl Crystallogr*, 2006, **39**, 453–457.

6 A. L. Spek, *Acta Crystallogr C Struct Chem*, 2015, **71**, 9–18.

7 G. L. Parker, S. Lau, B. Leforestier and A. B. Chaplin, *Eur J Inorg Chem*, 2019, **2019**, 3791–3798.

8 B. M. Schmidt, H.-A. Ho, K. Basemann, A. Ellern, T. L. Windus and A. D. Sadow, *Organometallics*, 2018, **37**, 4055–4069.